



HAL
open science

Synthesis of 1,3-diene-based block copolymers by nitroxide-mediated polymerization for application as robust joining between composite matrices

Adrien Métafiot

► To cite this version:

Adrien Métafiot. Synthesis of 1,3-diene-based block copolymers by nitroxide-mediated polymerization for application as robust joining between composite matrices. Materials. Université de Lyon, 2018. English. NNT : 2018LYSEI076 . tel-02063291

HAL Id: tel-02063291

<https://theses.hal.science/tel-02063291>

Submitted on 11 Mar 2019

HAL is a multi-disciplinary open access archive for the deposit and dissemination of scientific research documents, whether they are published or not. The documents may come from teaching and research institutions in France or abroad, or from public or private research centers.

L'archive ouverte pluridisciplinaire **HAL**, est destinée au dépôt et à la diffusion de documents scientifiques de niveau recherche, publiés ou non, émanant des établissements d'enseignement et de recherche français ou étrangers, des laboratoires publics ou privés.



INSA

N° d'ordre NNT : 2018LYSEI076

THÈSE de DOCTORAT de L'UNIVERSITÉ DE LYON
opérée au sein de
l'Institut National des Sciences Appliquées de Lyon
et de
l'Université McGill

École Doctorale N° 34
Matériaux de Lyon

Spécialité de doctorat : Matériaux polymères

Soutenue publiquement le 19/10/2018 par :

Adrien Métafiot

Synthesis of 1,3-Diene-based Block Copolymers by Nitroxide-Mediated Polymerization for Application as Robust Joining between Composite Matrices

Devant le jury composé de :

Nom, prénom grade/qualité établissement/entreprise Président.e (à préciser après la soutenance)

Gigmes, Didier	Directeur de Recherche CNRS	Université Aix Marseille	Rapporteur
Fretigny, Christian	Directeur de Recherche CNRS	ESPCI	Rapporteur
Duchet, Jannick	Professeur des Universités	INSA Lyon	Examinatrice
Defoort, Brigitte	Docteur HDR	ArianeGroup	Examinatrice
Mortaigne, Bruno	Docteur	DGA – Ministère de la défense	Examinateur

Gérard, Jean-François	Professeur des Universités	INSA Lyon	Directeur de thèse
Maric, Milan	Professeur	Université McGill	Invité
Hubert, Pascal	Professeur	Université McGill	Invité

Département FEDORA – INSA Lyon - Ecoles Doctorales – Quinquennal 2016-2020

SIGLE	ECOLE DOCTORALE	NOM ET COORDONNEES DU RESPONSABLE
CHIMIE	CHIMIE DE LYON http://www.edchimie-lyon.fr Sec. : Renée EL MELHEM Bât. Blaise PASCAL, 3e étage secretariat@edchimie-lyon.fr INSA : R. GOURDON	M. Stéphane DANIELE Institut de recherches sur la catalyse et l'environnement de Lyon IRCELYON-UMR 5256 Équipe CDFA 2 Avenue Albert EINSTEIN 69 626 Villeurbanne CEDEX directeur@edchimie-lyon.fr
E.E.A.	ÉLECTRONIQUE, ÉLECTROTECHNIQUE, AUTOMATIQUE http://eedea.ec-lyon.fr Sec. : M.C. HAVGOUDOUKIAN ecole-doctorale.eea@ec-lyon.fr	M. Gérard SCORLETTI École Centrale de Lyon 36 Avenue Guy DE COLLONGUE 69 134 Écully Tél : 04.72.18.60.97 Fax 04.78.43.37.17 gerard.scorletti@ec-lyon.fr
E2M2	ÉVOLUTION, ÉCOSYSTÈME, MICROBIOLOGIE, MODÉLISATION http://e2m2.universite-lyon.fr Sec. : Sylvie ROBERJOT Bât. Atrium, UCB Lyon 1 Tél : 04.72.44.83.62 INSA : H. CHARLES secretariat.e2m2@univ-lyon1.fr	M. Philippe NORMAND UMR 5557 Lab. d'Ecologie Microbienne Université Claude Bernard Lyon 1 Bâtiment Mendel 43, boulevard du 11 Novembre 1918 69 622 Villeurbanne CEDEX philippe.normand@univ-lyon1.fr
EDISS	INTERDISCIPLINAIRE SCIENCES-SANTÉ http://www.ediss-lyon.fr Sec. : Sylvie ROBERJOT Bât. Atrium, UCB Lyon 1 Tél : 04.72.44.83.62 INSA : M. LAGARDE secretariat.ediss@univ-lyon1.fr	Mme Emmanuelle CANET-SOULAS INSERM U1060, CarMeN lab, Univ. Lyon 1 Bâtiment IMBL 11 Avenue Jean CAPELLE INSA de Lyon 69 621 Villeurbanne Tél : 04.72.68.49.09 Fax : 04.72.68.49.16 emmanuelle.canet@univ-lyon1.fr
INFOMATHS	INFORMATIQUE ET MATHÉMATIQUES http://edinformaths.universite-lyon.fr Sec. : Renée EL MELHEM Bât. Blaise PASCAL, 3e étage Tél : 04.72.43.80.46 Fax : 04.72.43.16.87 informaths@univ-lyon1.fr	M. Luca ZAMBONI Bât. Braconnier 43 Boulevard du 11 novembre 1918 69 622 Villeurbanne CEDEX Tél : 04.26.23.45.52 zamboni@maths.univ-lyon1.fr
Matériaux	MATÉRIAUX DE LYON http://ed34.universite-lyon.fr Sec. : Marion COMBE Tél : 04.72.43.71.70 Fax : 04.72.43.87.12 Bât. Direction ed.materiaux@insa-lyon.fr	M. Jean-Yves BUFFIÈRE INSA de Lyon MATEIS - Bât. Saint-Exupéry 7 Avenue Jean CAPELLE 69 621 Villeurbanne CEDEX Tél : 04.72.43.71.70 Fax : 04.72.43.85.28 jean-yves.buffiere@insa-lyon.fr
MEGA	MÉCANIQUE, ÉNERGÉTIQUE, GENIE CIVIL, ACOUSTIQUE http://edmega.universite-lyon.fr Sec. : Marion COMBE Tél : 04.72.43.71.70 Fax : 04.72.43.87.12 Bât. Direction mega@insa-lyon.fr	M. Jocelyn BONJOUR INSA de Lyon Laboratoire CETHIL Bâtiment Sadi-Carnot 9, rue de la Physique 69 621 Villeurbanne CEDEX jocelyn.bonjour@insa-lyon.fr
ScSo	ScSo* http://ed483.univ-lyon2.fr Sec. : Viviane POLSINELLI Brigitte DUBOIS INSA : J.Y. TOUSSAINT Tél : 04.78.69.72.76 viviane.polsinelli@univ-lyon2.fr	M. Christian MONTES Université Lyon 2 86 Rue Pasteur 69 365 Lyon CEDEX 07 christian.montes@univ-lyon2.fr

*ScSo : Histoire, Géographie, Aménagement, Urbanisme, Archéologie, Science politique, Sociologie, Anthropologie

DEDICATION

To Francky, Sylv, Mich, Moune, René, Mic and Laura.

ACKNOWLEDGEMENTS

Foremost, I would like to express my sincere gratitude to my direct research co-supervisor, **Prof. Milan Marić**, for his continuous and valuable guidance during the PhD project. I am grateful to him for his confidence that helped foster my professional development. I convey also my deep gratitude to my thesis director, **Prof. Jean-Francois Gérard**, and my thesis co-supervisor, **Prof. Pascal Hubert**, for their advice and support throughout the entire project.

I want to thank **Dr. Brigitte Defoort**, my industrial supervisor, and **Dr. Audrey Menochet**, co-supervising the project as well. During the entire project, they have been flexible and tolerant regarding the lines of research, entrusting me a high degree of autonomy, for which I am grateful. I want to also address my thanks to **Mr. Philippe Briant**, director of the composite materials laboratory at ArianeGroup, who accepted my application and trusted me from the beginning of the doctoral thesis. I would like to acknowledge the generous financial support from **ArianeGroup** and the French Defense Procurement Agency (**Direction Générale de l'Armement, DGA**). I am grateful to **Mr. Bruno Mortaigne**, my DGA supervisor, for his guidance and his encouragement. I also thank the **Association Nationale de la Recherche et de la Technologie (ANRT)** for its financial contribution.

I would like to thank **Prof. Jason Robert Tavares**, **Prof. Martine Dubé** and **PhD candidate David Brassard** as well for their relevant advice during these three years. It was a real pleasure to share our research projects.

I want to thank my current and past colleagues here at McGill University, namely **Omar, Faezeh, Saeid, Roya, Sharmaine, Marwan, Faraz, Kelly, Simon, Marlon** and **Kevin** for the humorous and enlightening talks. I want to also thank **Yara, Kuan, Léa, Laura** and **Lysandre** which I have had the chance to mentor and train. Their hard work and enthusiasm resulted in contributions to valuable projects.

I thank the center for Self Assembled Chemical Structures (CSACS) from McGill University for the use of their equipment and specifically **Petr Fiurasek** for all his help and training. I also thank **Mary Sullivan** and **Noah Macy** of Arkema for their aid in obtaining the BlocBuilder alkoxyamine initiator and SG1 used in this doctoral thesis. My thanks also go out to **Lou Cusmich, Frank Caporuscio** and **Ranjan Roy**, members of the McGill Chemical Engineering Department technical staff, and **Lisa Volpato**, the store-keeper, without whom the successful completion of this project would not have been possible.

Finally, I want to address my sincerest thanks to **Laura** for her unwavering support. I also thank **Vachette, Rose, Archange** and **Moune** for their kind words of encouragement and for having graciously looked after me over the past years. I spare an affectionate thought for my beloved **Mic** and **René**.

ABSTRACT

The aim of this study was to produce a novel thermoplastic elastomer (TPE), used as a tough and stable joining between composite matrices. Having typically thermo-reversible crosslinks, TPE can be processed as thermoplastics and exhibit elastic behavior similar to that of chemically crosslinked elastomers in a certain temperature range. Nitroxide-mediated polymerization (NMP) was selected to synthesize linear styrenic block copolymer TPE. β -Myrcene (*My*) was first considered to manufacture the soft elastomeric segment poly(β -myrcene) P(*My*) (glass transition temperature $T_g \sim -77$ °C). NMP of *My* at 120 °C in bulk using succinimidyl ester-functionalized BlocBuilder™ alkoxyamine (NHS-BB) was well-controlled, allowing styrene (S) chain-extension from *cis*-1,4-P(*My*) macroinitiator. The resulting P(*My-b-S*) diblock copolymers, exhibiting relatively low number-average molar mass ($M_n < 50$ kg.mol⁻¹), showed limited stress-strain behavior (ultimate tensile strength $\sigma_B < 1.1$ MPa, elongation at break $\varepsilon_B < 16\%$). Meanwhile, the introduction of functional groups into the soft segment was implemented to subsequently aid the adhesive bonding / welding process between the TPE and the considered polar thermoplastic composites. Well-tailored epoxide functionalized P(*My*) were thereby synthesized by *My*/glycidyl methacrylate (GMA) nitroxide-mediated copolymerization. BlocBuilder-terminated poly(ethylene-*co*-butylene)-(SG1)₂ (SG1 = chain-end nitroxide group) difunctional initiator was used to produce S-*My*-S triblock copolymers with $M_n = 56-66$ kg.mol⁻¹, which exhibited improved extensibility ($\sigma_B < 0.8$ MPa, $\varepsilon_B < 200\%$). Poly(styrene) PS blocks were then substituted by higher T_g blocks, namely poly(isobornyl methacrylate) P(IBOMA) to enhance the toughness and the service temperature of the candidate TPE. Micro-phase separated IBOMA-*My*-IBOMA type triblocks exhibited improved mechanical properties ($\sigma_B = 3.9$ MPa, yield strength $\sigma_Y = 5.0$ MPa, $\varepsilon_B = 490\%$) associated with an extended upper service temperature of about 140 °C. However, *My*-based TPE did not satisfy the ArianeGroup mechanical requirements at room temperature, which prompted us to replace P(*My*) by poly(isoprene) (PI), which has much lower entanglement molar mass compared to P(*My*). Well-defined and active 1,4-PI-(SG1)₂ macroinitiators were first chain-extended with S, leading to self-assembled S-I-S triblocks ($M_n = 95-109$ kg.mol⁻¹, molar fraction of S in the copolymer $F_S = 0.30-0.49$, dispersity $\mathcal{D} = 2.11-2.29$). With $F_S = 0.38$, S-I-S showed $\sigma_B = 4.1 \pm 0.2$ MPa and $\varepsilon_B = 380 \pm 60$ %. IBOMA-I-IBOMA type copolymer was then produced ($M_n = 94$ kg.mol⁻¹, $\mathcal{D} = 1.76$, $F_{IBOMA} = 0.35$) and improved stress-strain properties were obtained at room temperature ($\sigma_B = 11.4 \pm 0.6$ MPa and $\varepsilon_B = 1360 \pm 210$ %). Lastly, hydrogenation of I-based block copolymers was performed at normal pressure and resulted mostly in an enhanced thermal stability, a greater tensile stress at break and a reduced elongation at break.

Key-words: thermoplastic elastomer, nitroxide-mediated polymerization, β -myrcene, isoprene.

RÉSUMÉ

L'objectif de ce projet fut consacré à la synthèse d'un élastomère thermoplastique (TPE) innovant, utilisable en tant que joint entre des matrices composites. La polymérisation radicalaire contrôlée par des radicaux nitroxyde (NMP) fut choisie afin de produire des TPE copolymères à blocs de type styrénique. Le β -myrcène (My) fut dans un premier temps sélectionné pour synthétiser le bloc souple poly(β -myrcène) $P(My)$. La NMP du My en masse à 120 °C en utilisant l'amorceur BlocBuilder™ fonctionnalisé avec l'ester succinimidyl (NHS-BB) fut très bien contrôlée, permettant l'extension de chaîne du macro-amorceur *cis*-1,4- $P(My)$ avec du styrène (S). Les copolymères diblocs $P(My-b-S)$ obtenus ayant une masse molaire moyenne en nombre modérée ($M_n < 50 \text{ kg}\cdot\text{mol}^{-1}$) montrèrent un comportement fragile en test de traction uniaxiale (résistance à la rupture en traction $\sigma_B < 1,1 \text{ MPa}$, allongement à la rupture en traction $\varepsilon_B < 16\%$). L'incorporation d'unités fonctionnelles au sein du segment souple fut réalisée en parallèle via la NMP du My avec du méthacrylate de glycidyle (GMA) afin de favoriser possiblement le processus de soudage / collage entre le TPE et les composites thermoplastiques envisagés. Un amorceur bifonctionnel, le poly(éthylène-*co*-butylène)-(SG1)₂ (SG1 = groupe nitroxyde), permit par la suite de synthétiser des copolymères triblocs $S-My-S$ ayant une plus haute masse molaire moyenne $M_n = 56-66 \text{ kg}\cdot\text{mol}^{-1}$ et une plus grande extensibilité ($\sigma_B < 0,8 \text{ MPa}$, $\varepsilon_B < 200\%$). Les segments PS furent remplacés par des segments ayant une température de transition vitreuse (T_g) plus élevée, à savoir des blocs poly(méthacrylate d'isobornyle) $P(IBOMA)$ afin d'augmenter la résistance mécanique et la température de service du TPE candidat. Des triblocs de type $IBOMA-My-IBOMA$, dont les domaines furent micro-structurés, montrèrent de meilleures propriétés mécaniques ($\sigma_B = 3,9 \text{ MPa}$, contrainte à la limite d'élasticité $\sigma_Y = 5,0 \text{ MPa}$, $\varepsilon_B = 490\%$) et une température de service maximale d'environ 140 °C. Toutefois, ces TPE à base de My ne satisfirent pas le cahier des charges industriel à température ambiante, ce qui nous poussa à substituer le bloc flexible $P(My)$ par du poly(isoprène) PI, ayant une masse molaire d'enchevêtrement bien plus faible. Des macro-amorceurs 1,4-PI bien définis et actifs furent d'abord étendus avec du styrène, ce qui permit d'obtenir des triblocs $S-I-S$ auto-assemblés ($M_n = 95-109 \text{ kg}\cdot\text{mol}^{-1}$, fraction molaire en styrène $F_S = 0,30-0,49$, dispersité $\mathcal{D} = 2,11-2,29$). $\sigma_B = 4,1 \pm 0,2 \text{ MPa}$ et $\varepsilon_B = 380 \pm 60 \%$ furent mesurés pour un $S-I-S$ ayant $F_S = 0,38$. Un tribloc de type $IBOMA-I-IBOMA$ fut par la suite synthétisé ($M_n = 94 \text{ kg}\cdot\text{mol}^{-1}$, $\mathcal{D} = 1,76$, $F_{IBOMA} = 0,35$) et montra de meilleures propriétés en contrainte-déformation ($\sigma_B = 11,4 \pm 0,6 \text{ MPa}$, $\varepsilon_B = 1360 \pm 210 \%$). Enfin, des copolymères à blocs à base d'isoprène furent hydrogénés à pression ambiante en utilisant l'agent diimide, ce qui permit notamment d'améliorer la stabilité thermique et la résistance à la rupture de ces matériaux.

Mots clés : élastomère thermoplastique, polymérisation contrôlée par des nitroxydes, β -myrcène, isoprène.

NOMENCLATURE

AA	Acrylic acid
AFM	Atomic force microscopy
Al ₂ O ₃	Basic alumina
ASTM	American section of the international association for testing materials
ATRP	Atom transfer radical polymerization
B	Butadiene
BB	BlocBuilder™ (2-([<i>tert</i> -butyl[1-(diethoxyphosphoryl)-2,2-dimethyl propyl] amino]oxy)-2-methylpropionic acid) alkoxyamine
<i>t</i> BuA	<i>tert</i> -Butyl acrylate
CaH ₂	Calcium hydride
CDCl ₃	Deuterated chloroform
CH ₂ Cl ₂	Methylene chloride
CHCl ₃	Chloroform
Co	Co-monomer
CTE	Coefficient of thermal expansion
DCC	<i>N,N'</i> -Dicyclohexylcarbodiimide
DLS	Dynamic light scattering
DMSO	Dimethyl sulfoxide
DSC	Differential scanning calorimetry
FR	Fineman-Ross
GMA	Glycidyl methacrylate
GPC	Gel permeation chromatography
HMPMA	2-Hydroxy-3-morpholinopropyl methacrylate
HSP	Hansen solubility parameter
I	Isoprene
IBOMA	Isobornyl methacrylate
ID	Experimental identification
KT	Kelen-Tudos
M	Monomer
MA	Maleic anhydride
MeOH	Methanol
Me-THF	2-Methyltetrahydrofuran
MHS	Mark-Houwink-Sakurada
MMA	Methyl methacrylate
<i>My</i>	β -Myrcene
NHS	<i>N</i> -Hydroxysuccinimide
NHS-BB	2-Methyl-2-[<i>N-tert</i> -butyl- <i>N</i> -(1-diethoxyphosphoryl)-2,2-dimethylpropyl]-aminoxy]- <i>N</i> -propionyloxysuccinimide
NLLS	Non-linear least-squares procedure
NMP	Nitroxide-mediated polymerization

NMR	Nuclear magnetic resonance
P [•]	Propagating (macro)radical
PB	Poly(butadiene)
PEB	Poly(ethylene- <i>co</i> -butylene) copolymer
P(GMA)	Poly(glycidyl methacrylate)
PI	Poly(isoprene)
P(IBOMA)	Poly(isobornyl methacrylate)
P(MMA)	Poly(methyl methacrylate)
P(<i>My</i>)	Poly(β -myrcene)
PRE	Persistent radical effect
PS	Poly(styrene)
P-SG1 (or P-N)	Dormant alkoxyamine-terminated species
RAFT	Reversible addition-fragmentation transfer polymerization
RDRP	Reversible-deactivation radical polymerization
S	Styrene
SAXS	Small-angle X-ray scattering
SG1	<i>N-tert</i> -Butyl- <i>N</i> -[1-diethylphosphono-(2,2-dimethylpropyl)] nitroxide
TEM	Transmission electron microscopy
TEMPO	2,2,6,6-Tetramethyl-1-piperidinyloxy radical
TGA	Thermogravimetric analysis
THF	Tetrahydrofuran
TIPNO	2,2,5-Trimethyl-4-phenyl-3-azahexane-3-nitroxide
TPE	Thermoplastic elastomer

Symbols in arabic letters

Đ	Dispersity
DP (or DP _n)	Average degree of polymerization
<i>E</i>	Young's modulus (MPa)
<i>f</i> _{YY,0}	Initial YY molar feed composition
<i>F</i> _{YY}	Molar composition of YY in the final copolymer
<i>k</i>	Boltzmann's constant (J.K ⁻¹)
<i>k</i> _c	Rate of recombination (L.mol ⁻¹ .s ⁻¹)
<i>k</i> _d	Dissociation rate constant (s ⁻¹)
<i>k</i> _p	Propagation rate constant (L.mol ⁻¹ .s ⁻¹)
<i>K</i>	Equilibrium constant (mol.L ⁻¹)
<i>K</i> _{P(YY)} , α _{P(YY)}	Mark-Houwink-Sakurada (MHS) parameters for the polymer P(YY) (<i>K</i> in dL.g ⁻¹)
LV or <i>F</i> _{SG1}	Living molar fraction of chains terminated by a SG1 unit (mol%)
<i>M</i> _e	Entanglement molecular weight (kg.mol ⁻¹)
<i>M</i> _n	Number-average molecular weight (kg.mol ⁻¹)
<i>M</i> _{n,GPC}	Number-average molecular weight directly measured by GPC (kg.mol ⁻¹)
<i>M</i> _{n,MHS}	Corrected <i>M</i> _{n,GPC} value using MHS coefficients (kg.mol ⁻¹)

$M_{n,theo}$	Target number-average molecular weight at $X = 100\%$ ($\text{kg}\cdot\text{mol}^{-1}$)
$M_{n,theo,X}$	Target number-average molecular weight at conversion X ($\text{kg}\cdot\text{mol}^{-1}$)
M_{YY}	Molecular weight of component YY ($\text{g}\cdot\text{mol}^{-1}$)
m_v	Mass of the empty vial (g)
m_{v+p}	Mass of the vial containing the polymer after drying (g)
m_{v+p+s}	Mass of the vial containing the reaction solution (g)
M_w	Weight-average molecular weight ($\text{kg}\cdot\text{mol}^{-1}$)
N_a	Avogadro constant (mol^{-1})
N_c	Number of chains per volume unit
R	Ideal gas constant ($\text{J}\cdot\text{mol}^{-1}\cdot\text{K}^{-1}$)
R^2	Squared linear regression coefficient
r_{YY}	Copolymer reactivity ratio for YY
t	Reaction time (min)
T	Temperature ($^{\circ}\text{C}$)
T_b	Boiling point ($^{\circ}\text{C}$)
T_d	Decomposition temperature ($^{\circ}\text{C}$)
T_g	Glass transition temperature ($^{\circ}\text{C}$)
T_{room} (or RT)	Room temperature ($^{\circ}\text{C}$)
V_m	Molar volume ($\text{cm}^3\cdot\text{mol}^{-1}$)
$v_{P(YY)}$	Volume fraction of $P(YY)$
w_{YY}	Mass fraction of YY
X_{grav}	Gravimetric conversion (%)
X_{NMR}	Conversion determined by proton nuclear magnetic resonance (%)
X_{YY}	YY Individual conversion (%)
z	Lattice coordination number
Z_{ave}	Z-Average diameter (nm)

Greek symbols

δ	Nuclear magnetic resonance signal (ppm)
δ_D, δ_P and δ_H	Hansen solubility parameters ($\text{MPa}^{1/2}$)
δ_{YY}	Solubility parameter of YY ($\text{MPa}^{1/2}$)
$\Delta\beta_{YY}$	Difference between the expansion coefficients of the rubbery and glassy states of polymer $P(YY)$ (K^{-1})
ΔG_m	Gibbs free energy (J)
ε_B	Tensile elongation at break (%)
ρ	Density ($\text{g}\cdot\text{cm}^{-3}$)
σ_B	Tensile strength at break (MPa)
σ_Y	Yield stress (MPa)
σ_{100}	Tensile strength at 100% elongation (MPa)
χ_{AB}	Flory-Huggins interaction parameter for the system A-B

TABLE OF CONTENTS

Acknowledgements.....	i
Abstract.....	iii
Résumé.....	iv
Nomenclature.....	v
Table of contents.....	ix
Résumé substantiel de la thèse.....	1
Main introduction.....	18
Introduction générale.....	22
Technological objectives.....	26
Main objectives of the research project.....	33
Thesis outline.....	39
Part I. Literature review	43
A. Introduction	45
B. From thermoset to thermoplastic elastomers (TPE)	47
B.1. Elasticity and thermoset elastomers	47
B.1.1. What is an elastomer?	47
B.1.2. Thermoset elastomers	49
B.2. Block copolymer TPE	52
B.2.1. Physical crosslinks	53
B.2.2. TPE microstructure	54
B.2.3. Micro(nano)-phase separation	55
B.2.4. Advantages / disadvantages of block copolymer TPE	58
C. Styrenic block copolymer TPE	60
C.1. Factors influencing the properties	60
C.1.1. Introduction	60
C.1.2. Effects of the elastomer type	61
C.1.3. Effects of average molar mass and hard blocks content	64
C.1.4. Influence of the hard segment nature	66

C.2. Hydrogenation of the elastomeric block.....	69
C.2.1. Introduction.....	69
C.2.2. Hydrogenation processes.....	70
C.2.3. Properties of hydrogenated poly(diene)s.....	72
C.3. Commercial styrenic block copolymer TPE.....	76
C.3.1. Industrial producers and applications.....	76
C.3.2. Styrenic TPE.....	78
D. Synthesis of styrenic block copolymer TPE.....	81
D.1. Living ionic polymerization.....	81
D.1.1. Anionic polymerization.....	81
D.1.2. Cationic polymerization.....	82
D.1.3. Drawbacks of living ionic polymerization.....	82
D.2. Reversible-deactivation radical polymerizations (RDRP).....	85
D.2.1. Control of the macromolecular architecture by RDRP.....	85
D.2.2. Block copolymer TPE by RAFT and ATRP.....	86
D.2.3. Focus on nitroxide-mediated polymerization (NMP).....	87
<i>References</i>	89

Part II. β -Myrcene-based copolymers by nitroxide-mediated controlled radical polymerization (NMP).....

Chapter 1. <i>Optimization of the β-myrcene nitroxide-mediated polymerization (NMP) and synthesis of well-defined β-myrcene / styrene block copolymers</i>.....	97
1.1. Preface.....	97
1.2. Abstract.....	97
1.3. Introduction.....	98
1.4. Results and discussion.....	101
1.4.1. NMP of β -myrcene: Determination of appropriate polymerization experimental conditions.....	101
1.4.2. Synthesis of poly(β -myrcene- <i>block</i> -styrene) diblock copolymers.....	113
1.4.3. Synthesis of styrene- β -myrcene-styrene triblock copolymers.....	118
1.4.4. β -Myrcene / styrene statistical copolymerization.....	121
1.4.5. Thermal analysis of the synthesized NMP-based polymers.....	130
1.5. Conclusion.....	134

1.6. References.....	135
Chapter 2. <u>Functionalization of poly(β-myrcene) by β-myrcene / glycidyl methacrylate nitroxide-mediated copolymerization</u>	141
2.1. Preface.....	141
2.2. Abstract.....	141
2.3. Introduction.....	142
2.4. Results and discussion.....	144
2.4.1. Attempts to copolymerize β -myrcene with various functional monomers by NMP.....	144
2.4.2. β -Myrcene/glycidyl methacrylate statistical copolymerization.....	149
2.4.3. Poly(β -myrcene – block – 2 – hydroxy – 3-morpholinopropylmethacrylate) amphiphilic diblock copolymer.....	166
2.5. Conclusion.....	169
2.6. References.....	170
Chapter 3. <u>Replacement of poly(styrene) by poly(isobornyl methacrylate) as the rigid domain of the β-myrcene-based block copolymers</u>	175
3.1. Preface.....	175
3.2. Abstract.....	175
3.3. Introduction.....	176
3.4. Results and discussion.....	179
3.4.1. β -Myrcene / isobornyl methacrylate copolymerization by NMP.....	179
3.4.2. Isobornyl methacrylate - β -myrcene - isobornyl methacrylate triblock copolymers by NMP.....	195
3.5. Conclusion.....	203
3.6. References.....	204
Part III. Synthesis by NMP and characterization of isoprene-based triblock copolymers	209
Chapter 4. <u>Synthesis of isoprene-based triblock copolymers by NMP</u>	211
4.1. Preface.....	211
4.2. Abstract.....	212

4.3. Results and discussion.....	213
4.3.1. Preparation of SG1-terminated poly(isoprene) PI-(SG1) ₂	213
4.3.2. NMP-based styrene-isoprene-styrene triblock copolymers.....	218
4.3.3. Hydrogenation of NMP-based styrene-isoprene-styrene triblock copolymers.....	224
4.3.4. NMP-based isobornyl methacrylate – isoprene – isobornyl methacrylate type triblock copolymer.....	229
4.4. Conclusion.....	234
4.5. References.....	235
Chapter 5. <u>Characterization of commercial styrenic triblock copolymers</u>	239
5.1. Preface.....	239
5.2. Abstract.....	239
5.3. Results.....	240
5.3.1. Commercial S-I-S from <i>Sigma-Aldrich</i> [®]	240
5.3.2. Commercial SEBS from <i>Kraton</i> [®]	245
5.4. Conclusion.....	248
General conclusion.....	251
Conclusion générale.....	256
Perspectives.....	260
Perspectives.....	264
Appendices.....	269
a. Appendix for Chapter 1.....	269
a.1. Experimental section.....	269
a.2. Supporting information.....	273
b. Appendix for Chapter 2.....	288
b.1. Experimental section.....	288
b.2. Supporting information.....	292
c. Appendix for Chapter 3.....	306
c.1. Experimental section.....	306
c.2. Supporting information.....	311

d. Appendix for Chapter 4: Experimental section.....	324
e. Appendix for Chapter 5: Experimental section.....	326

RÉSUMÉ SUBSTANTIEL DE LA THÈSE

Leader mondial de l'accès à l'espace, **ArianeGroup**, anciennement Airbus Safran Launchers (ASL), est une coentreprise détenue à parts égales par Airbus et Safran. ArianeGroup conçoit des solutions innovantes et compétitives en matière de systèmes de lancement et d'applications spatiales civiles et militaires pour des clients institutionnels, commerciaux et industriels. Maître d'œuvre de la famille de lanceurs européens Ariane et des missiles de la force de dissuasion océanique française, cette société est experte dans l'ensemble du cycle de vie d'un lanceur spatial : conception, développement, production, exploitation et commercialisation via la filiale Arianespace. ArianeGroup produit et exploite le lanceur Ariane 5 et développe le futur lanceur Ariane 6, dont elle est autorité de conception.

Les lanceurs fabriqués par ArianeGroup sont formés d'un réservoir de propergol solide appelé corps de propulseur et de viroles appelées jupettes. La liaison entre les jupettes et le réservoir, sollicitée majoritairement par des forces de cisaillement, doit être assurée par un joint souple. Un matériau élastomère répond à cette demande. Les jupettes et le réservoir utilisés actuellement sont des composites thermodurcissables tout comme l'élastomère commercial actuellement employé. L'assemblage entre le réservoir, l'élastomère et les jupettes est réalisé par collage, sur la base de colles polymérisant à chaud, en étuve, positionnées entre l'élastomère et les composites. Cette liaison flexible repose donc sur des matières thermodurcissables, ce qui est problématique d'un point de vue économique principalement. La vulcanisation préliminaire du caoutchouc via l'utilisation d'une presse à haute température et haute pression, l'insertion de résines adhésives et le collage réalisé dans un autoclave géant pendant des cycles de longues durées à hautes températures, constituent des étapes très coûteuses et sont directement liées à l'utilisation de matrices polymère réticulées chimiquement.

Un assemblage réservoir / élastomère / jupettes entièrement thermoplastique est ainsi considéré par ArianeGroup pour la prochaine génération de lanceurs. Pour cela, la société envisage de produire le réservoir et les jupettes à base d'un thermoplastique renforcé par des fibres de carbone. De plus, la substitution du caoutchouc thermodurcissable commercial par un élastomère thermoplastique (TPE), par définition ``physiquement`` réticulé, est une priorité. Le passage d'une structure thermodurcissable à une structure thermoplastique présente plusieurs avantages pour ArianeGroup : pas d'étape de vulcanisation du TPE, vraisemblablement bien moins cher que l'élastomère commercial et pouvant être stocké indéfiniment ; réalisation de l'assemblage final par soudage, une technique efficace et rapide, permettant d'obtenir une liaison souple plus robuste que celle réalisée par collage ; nul besoin de colles qui ont une durée de conservation limitée.

Alors que des projets parallèles d'ArianeGroup étudient la possibilité d'identifier un TPE commercial permettant de réaliser cette liaison flexible, **cette thèse doctorale fut dédiée à la synthèse et la caractérisation d'un TPE original**, satisfaisant le cahier des charges industriel. Les spécifications se basent sur les caractéristiques du caoutchouc commercial actuellement utilisé. En matière de propriétés mécaniques, un comportement en contrainte-élongation du TPE semblable aux traditionnels caoutchoucs vulcanisés est exigé à température ambiante. De plus, l'abattement (pourcentage de pertes) des propriétés mécaniques avec la température ne doit pas être conséquent. Par ailleurs, ce nouveau TPE doit être conforme à la réglementation REACH, disposer d'une longue durée de vie et ses propriétés ne doivent pas être affectées lors de contacts avec certains solvants. L'assemblage réservoir / TPE / jupettes mis en place par la suite devra être stable et robuste avec une haute résistance à la rupture en tension uni-axiale, un module de cisaillement à 100% d'allongement significatif ainsi qu'une rupture cohésive de la liaison. Une liaison par soudage étant privilégiée, le TPE doit supporter des cycles de quelques minutes à des températures de l'ordre de 240-280 °C. Toutefois, une caractérisation de la liaison par collage est également considérée, ce qui implique une stabilité de la performance mécanique du TPE à 160-180 °C pendant plusieurs heures. Quel que soit la technique d'assemblage utilisée, le TPE ne doit pas fluer ni se dégrader et avoir ses propriétés inchangées une fois inséré entre les matrices composites.

Compte tenu de l'ampleur de ce domaine de recherche consacré à la synthèse de TPE, des axes furent privilégiés en amont du projet. La synthèse de TPE copolymères à blocs de type styrénique par « nitroxide-mediated polymerization » (NMP, innocuité envers l'environnement, absence de toxicité, aisée à mettre en œuvre et forte expertise du laboratoire à l'Université McGill), polymérisation radicalaire contrôlée basée sur le piégeage réversible des chaînes en croissance par des nitroxydes, fut envisagée. Les TPE considérés correspondent idéalement à des copolymères triblocs formés de la manière suivante : un bloc central souple (poly(β -myrcène) P(My) ou poly(isoprène) PI) conférant les propriétés d'élastomère aux polymères synthétisés (déformation réversible et important allongement à la rupture), deux blocs poly(styrène) PS identiques et rigides venant s'ajouter de part et d'autre du segment souple, augmentant la tenue mécanique dont la résistance à la rupture. Bien que ces triblocs de type S-My-S et S-I-S furent ciblés initialement, des modifications furent entreprises afin d'essayer de répondre au mieux au cahier des charges d'ArianeGroup.

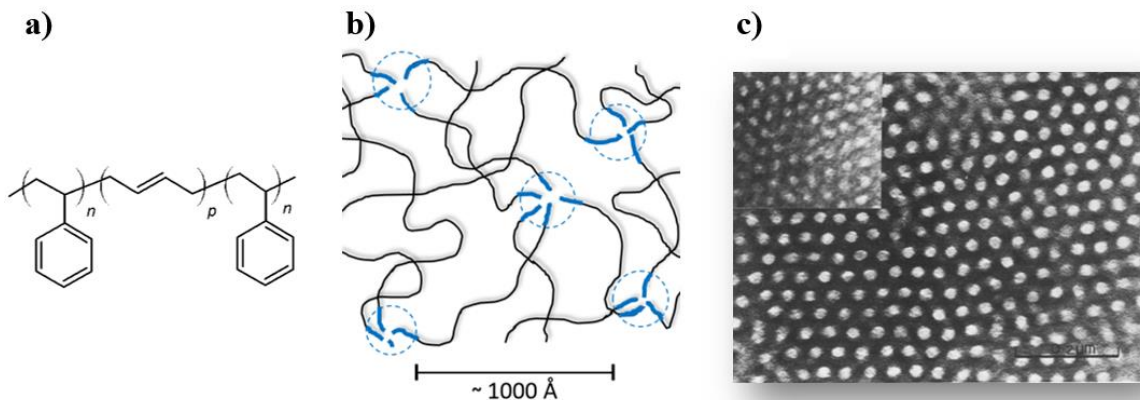
Trois grandes parties composent l'étude bibliographique. Dans un premier temps (B), les élastomères vulcanisés traditionnels (matrice réticulée chimiquement) et les TPE de type copolymère à blocs (matrice réticulée physiquement) sont présentés et comparés. Cette section vise à répondre à la question suivante : Quels sont les avantages de remplacer l'élastomère thermodurcissable par un TPE pour l'application ciblée ? La grande majorité des élastomères exploités industriellement sont des

thermodurcissables qui obtiennent leurs propriétés d'élastomère et de haute tenue mécanique après vulcanisation (réticulation irréversible des chaînes du polymère en présence de soufre à haute pression et à haute température). Malgré entre autres leur excellente résistance aux produits chimiques et à la température, les élastomères thermodurcissables présentent des inconvénients non négligeables : mélangeage préliminaire avec des agents de réticulation, des stabilisateurs et d'autres additifs; vulcanisation; temps de cycle de fabrication relativement longs; impossibilité de remise en œuvre (déchets rarement réutilisés)...De plus, étant chimiquement réticulés, ces caoutchoucs ne peuvent pas être utilisés dans des procédés novateurs comme le soudage où la matrice polymère doit être fondue ou du moins ramollie (dans le domaine de l'écoulement caoutchoutique). Il est ainsi légitime de s'orienter vers de nouveaux types d'élastomères haute-performances disposant de propriétés intrinsèques aussi intéressantes que celles des caoutchoucs traditionnels, tout en étant pas réticulés chimiquement.

Entre les thermoplastiques à la mise en œuvre aisée mais aux propriétés élastiques restreintes, et les élastomères vulcanisés aux propriétés élastiques remarquables, mais à la mise en œuvre plus complexe, des matériaux intermédiaires ont fait leur apparition, les élastomères thermoplastiques (TPE). Ils offrent une combinaison de propriétés particulières : des propriétés mécaniques comparables aux caoutchoucs thermodurcissables mais limitées à un domaine de températures modérées, inférieures aux températures de ramollissement des domaines rigides ; facilité de mise en œuvre des thermoplastiques, sans vulcanisation ; facilité de recyclage des déchets. Les TPE de type copolymères à blocs, constitués d'une phase souple (PI par exemple) généralement prédominante et d'une phase rigide (PS par exemple) reliées entre elles par des liaisons covalentes, peuvent être vus comme des matériaux de substitution prometteurs aux élastomères vulcanisés. Des nœuds de réticulation physiques, qui peuvent se définir comme des liaisons intermoléculaires non-covalentes et thermoréversibles, sont formés par la phase rigide, qui une fois dans le domaine de l'écoulement caoutchoutique à haute température, permet la mise en œuvre du TPE.

Alors que les caoutchoucs vulcanisés ne peuvent être joints à d'autres surfaces polymère que par collage ou par fixation mécanique, la possibilité de joindre les TPE dans le domaine de l'écoulement caoutchoutique ou à l'état fondu par soudage à haute température apparaît avantageux. Le soudage ne fait pas appel à des matériaux tiers dans la liaison et permet à deux pièces assemblées de reconstituer une structure monolithique. On retrouve dans la liaison de deux pièces soudées des caractéristiques proches de celles des matériaux constituant ces pièces. Le soudage est un procédé rapide et contrôlé qui s'impose dans beaucoup de domaines où il est nécessaire d'obtenir une liaison mécanique forte et durable sur des pièces en série. Alors que les temps de cycle pour un procédé par collage peuvent durer plusieurs heures au minimum, quelques minutes au maximum suffisent généralement pour obtenir une soudure robuste.

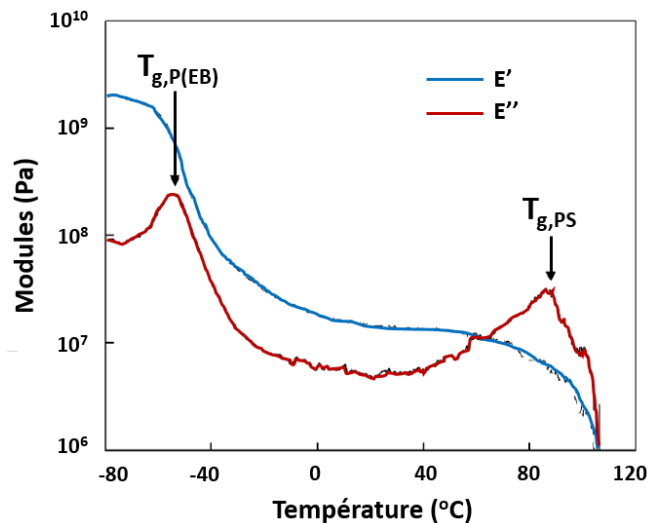
La deuxième partie de la revue de la littérature (C) se consacre aux propriétés des TPE copolymères à blocs linéaires de type styrénique, famille de TPE ciblée pour ce projet doctoral. Ce sont généralement des triblocs de type [bloc rigide – bloc souple – bloc rigide] tels que S-I-S et S-B-S (B = butadiène). Les propriétés de ces copolymères séquencés dépendent principalement de la nature et de la longueur du segment souple et des segments rigides ainsi que du rapport phase souple / phase rigide. La nature des blocs rigides est par exemple primordiale et influencera principalement les propriétés mécaniques et thermiques de ces TPE. L'une des principales faiblesses de ces TPE est que leur température de service maximale est plus ou moins équivalente à la température de transition vitreuse (T_g) des blocs rigides. Ces derniers étant en grande majorité des segments PS, ces TPE commencent à s'écouler à 95 °C environ. Le remplacement des blocs PS par des blocs plus rigides ayant une T_g plus élevée, tels que le poly(α -méthyl-*p*-méthyl styrène) P(MMS) ($T_g \sim 183$ °C) ou le poly(méthacrylate d'isobornyle) P(IBOMA) ($T_g \sim 190$ °C), permet d'augmenter considérablement la température de service du TPE ainsi que leur résistance en traction aux petites (< 100%) et aux grandes déformations (> 100%).



a) Structure du copolymère tribloc poly(styrène-*bloc*-butadiène-*bloc*-styrène) (abrégé S-B-S). **b)** Représentation schématique d'une morphologie possible des copolymères triblocs de type SBS où les blocs poly(styrène) minoritaires (bleu) forment des sphères rigides au sein d'un domaine poly(butadiène) flexible et continu (noir). **c)** Cliché obtenu par MET (microscopie électronique en transmission) d'un copolymère tribloc S-B-S dans lequel les blocs PS adoptent une morphologie de sphères.

L'hydrogénation du segment souple des TPE est également une modification chimique d'intérêt. Il s'agit de saturer le bloc flexible en faisant réagir du dihydrogène avec les doubles liaisons C=C.

L'hydrogénation des triblocs S-I-S et S-B-S mène donc respectivement au S-EP-S (EP = éthylène/propylène) et au S-EB-S (EB = éthylène/butylène). L'utilisation à haute pression d'un catalyseur homogène (complexe à base de cobalt ou de nickel par exemple) ou hétérogène (palladium sur CaCO_3 par exemple) est majoritaire bien que très dangereuse (H_2 gazeux, catalyseur pyrophorique, haute pression, haute inflammabilité du mélange...). L'hydrogénation à pression ambiante en utilisant le diimide est une technique beaucoup plus sûre et tout aussi efficace. Elle fut optimisée pour la saturation des homopolymères PI et PB en présence du *p*-toluènesulfonyl hydrazide, en tant que générateur d'agents diimide, et de tripropylamine afin d'éliminer les réactions secondaires dégradant le polymère. Les poly(diène)s hydrogénés possèdent typiquement des températures de service (+ 10 à + 40 °C) et de dégradation (+ 30 à + 90 °C) supérieures, un module de conservation E' et une résistance en tension plus élevés que les polymères originaux insaturés. La meilleure stabilité thermique et la plus grande tenue mécanique de ces triblocs de type styrénique ayant leur segment souple hydrogéné est donc d'intérêt pour la problématique industrielle.



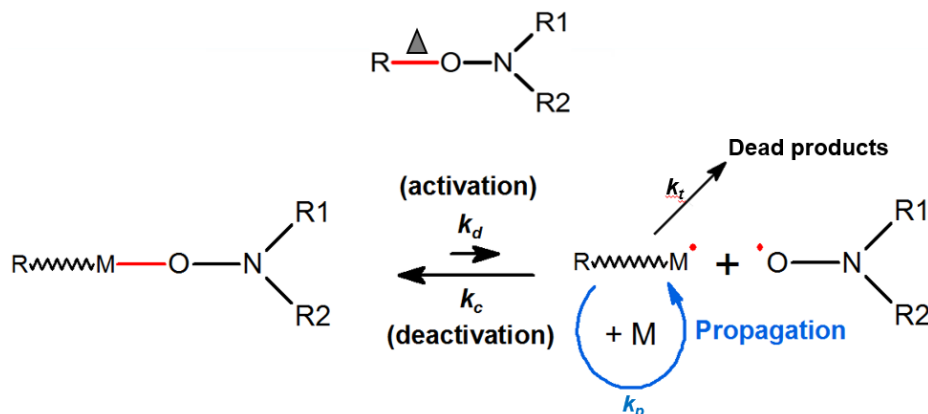
Variations du module de conservation (E' , courbe bleue) et du module de perte (E'' , courbe rouge) en fonction de la température (1 Hz, $5\text{ °C}\cdot\text{min}^{-1}$) pour un copolymère tribloc S-EB-S commercial (*Kraton*TM G1651 E), possédant 31.5 m% de styrène. À $T < T_{g,P(EB)}$ (température de transition vitreuse de la séquence éthylène/butylène), état vitreux du S-EB-S ; à $T_{g,P(EB)} < T < T_{g,PS}$, plateau caoutchoutique (température de service de l'élastomère thermoplastique) ; à $T > T_{g,PS}$, écoulement visqueux permettant la mise en œuvre du matériau.

Bien que la thèse porte essentiellement sur la synthèse de ces TPE, il est important de connaître des produits similaires disponibles sur le marché, utilisables comme références. S-I-S, S-B-S et sa version hydrogénée S-EB-S constituent la grande majorité des TPE de type styrénique commerciaux produits entre autres par les compagnies *Kraton*, *Dexco*, *S&E Specialty Polymers* et *Dynasol*. Les S-I-S et S-B-S de *Kraton*, contenant une minorité de blocs rigides (15-34 m% S), présentent des propriétés en traction uniaxiale satisfaisantes (résistance à la rupture en traction $\sigma_B = 28-33$ MPa, allongement à la rupture en traction $\epsilon_B = 880-1300\%$) à température ambiante bien qu'ils ne semblent pas assez résistants pour supporter des procédés d'assemblage à $T \geq 160$ °C (résistance en traction à 300% d'allongement $\sigma_{300} \leq 4,1$ MPa et indice de fluidité à chaud IFC relativement élevé à 200 °C). Malgré un allongement à la rupture en traction inférieur mais acceptable ($\geq 500\%$), Les S-EB-S de *Kraton* (29-57 m% S) s'avèrent plus intéressants puisqu'ils disposent d'une plus grande résistance à la traction ($\sigma_{300} = 4,8-7,9$ MPa) et d'une plus grande résistance au fluage (IFC ≤ 5 g/10min à 230 °C). Un S-EB-S fonctionnalisé possédant environ 2 m% d'unités anhydride maléique est également produit chez *Kraton*. Il pourrait ainsi être testé dans le procédé d'assemblage par soudage (ou par collage) afin de savoir si les groupes polaires encouragent l'adhésion avec les matrices composites considérées pour l'application industrielle.

La troisième et dernière partie de l'état de l'art (D) s'intéresse aux différentes techniques de polymérisation utilisées pour produire des TPE copolymères à blocs de type styrénique. La polymérisation anionique fut, dans un premier temps, présentée. Il s'agit aujourd'hui de la seule méthode utilisée industriellement pour la production d'élastomères thermoplastiques à base de styrène et de diènes (S-I-S et S-B-S principalement), par addition séquentielle ou par couplage. La polymérisation cationique peut être également utilisée pour la préparation de triblocs S-iB-S (iB = isobutylene) notamment. Par rapport au procédé anionique, les blocs rigides peuvent être formés à partir de différents types de monomères (α -méthyl styrène, *para*-chloro styrène...). Bien que ces techniques ioniques soient très efficaces, les conditions expérimentales sont exigeantes (absence d'impuretés, d'eau et d'oxygène) et de nombreuses étapes préliminaires sont nécessaires (dégazage, distillation des solvants et monomères...). De plus, les monomères portant un groupement fonctionnel sont difficilement polymérisables du fait de leur incompatibilité avec les ions et contre-ions formés durant la polymérisation.

Par conséquent, la synthèse contrôlée de copolymères à blocs à base de diènes par voie radicalaire, ne nécessitant pas des conditions expérimentales exigeantes et s'adressant à une large gamme de monomères, s'avère prometteuse. Trois techniques majeures de polymérisation radicalaire contrôlée furent développées : par transfert de chaîne réversible par addition-fragmentation (RAFT), par transfert d'atomes (ATRP) et en présence de nitroxydes (NMP). La préparation d'élastomères thermoplastiques via ces trois procédés radicalaires est alors présentée dans cette revue de la littérature, mettant en avant la

prédisposition de la technique NMP à polymériser de manière contrôlée les diènes tels que l'isoprène ou le butadiène.



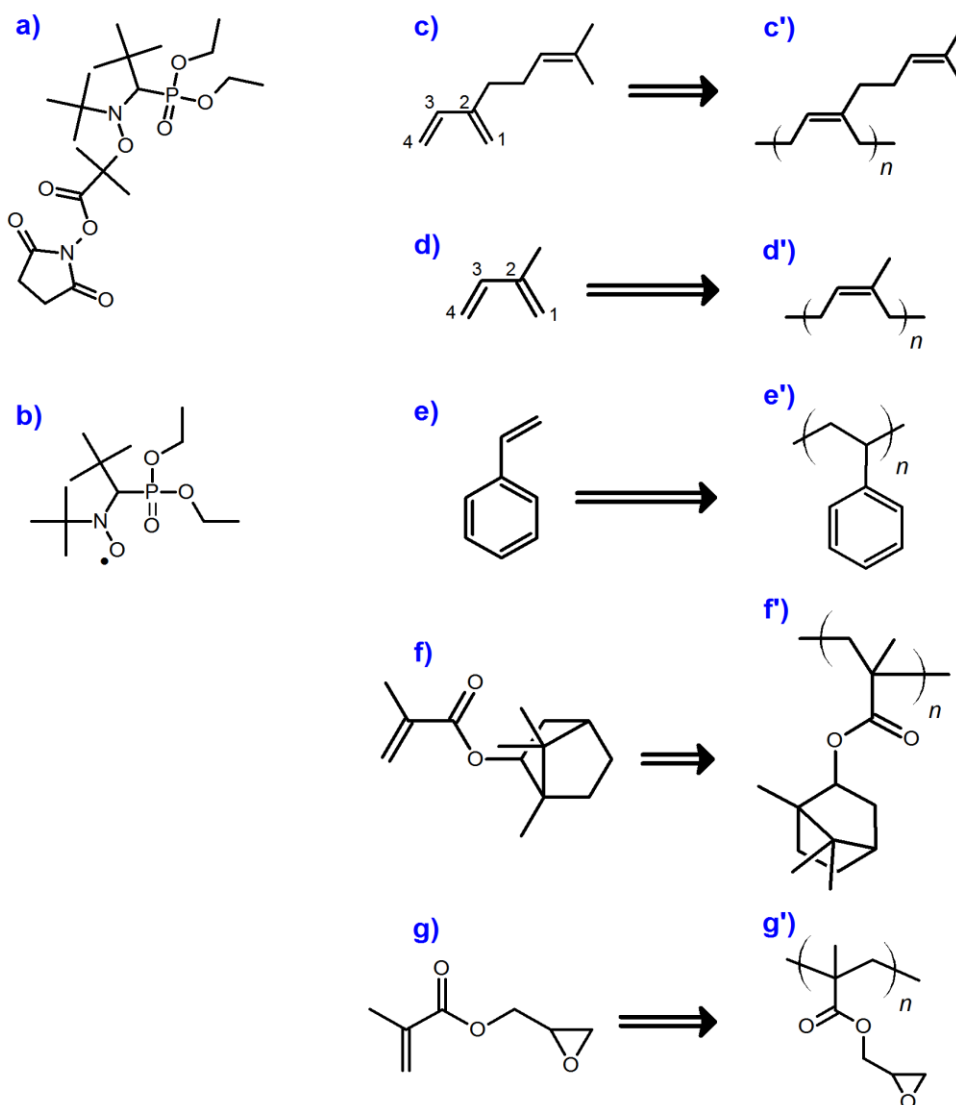
Structure des alcoxyamines de formule générale RONR_1R_2 (**haut**) possédant une liaison covalente C-O thermolabile. Son homolyse forme le radical alkyle R^\bullet , permettant d'amorcer la polymérisation, et le radical nitroxyde stable $\text{R}_1\text{R}_2\text{NO}^\bullet$, permettant de contrôler la polymérisation en désactivant de manière réversible le bout de chaîne du macroradical en croissance. Schéma cinétique simplifié de la technique NMP (**bas**), présentant l'équilibre dynamique entre une faible concentration d'espèces actives et une haute concentration d'espèces dormantes (M = monomère(s), k_d = constante de vitesse de l'homolyse de la liaison C-O (dissociation), k_c = constante de vitesse de recombinaison entre $\text{R}(\text{M})_n^\bullet$ et le nitroxyde $\text{R}_1\text{R}_2\text{NO}^\bullet$, k_p = constante de vitesse de propagation, k_t = constante de vitesse de recombinaison entre radicaux $\text{R}(\text{M})_n^\bullet$ (terminaison irréversible)).

L'étude expérimentale débuta en choisissant de synthétiser le poly(β -myrcène) P(My) en tant que segment souple du TPE candidat. Le β -myrcène (My, 7-méthyl-3-méthylène-octa-1,6-diène) est un monoterpène qui peut être extrait d'huiles essentielles de plusieurs plantes de la famille des lauracées par exemple. My fut sélectionné puisqu'il s'agit d'un diène conjugué possédant une structure voisine à celle de l'isoprène, tout en ayant l'avantage d'avoir une température d'évaporation élevée ($T_b = 167^\circ\text{C}$). Ce monomère naturellement renouvelable et non-volatil est par conséquent adapté à la polymérisation radicalaire contrôlée en utilisant un simple montage à reflux.

L'optimisation de la polymérisation radicalaire contrôlée par des radicaux nitroxyde (NMP) de My fut tout d'abord nécessaire afin de synthétiser un élastomère à l'architecture maîtrisée (dispersité $\text{Đ} = \text{M}_w/\text{M}_n$ relativement faible, croissance linéaire des chaînes avec la conversion X). La nature de l'amorceur

(BlocBuilder™ commercial abrégé BB et BlocBuilder™ fonctionnalisé avec l'esther succinimidyl, abrégé NHS-BB), le choix du milieu réactionnel (masse, 1,4-dioxane, toluène), la température ($T = 110-130\text{ °C}$), la masse molaire moyenne en nombre ciblée ($M_{n,theo} = 20-50\text{ kg.mol}^{-1}$, correspondant au produit entre la masse molaire de My et le rapport molaire entre la concentration de monomère et celle d'amorceur) ainsi que l'influence de l'ajout supplémentaire de radicaux nitroxyde SG1• (4,9 et 11,7 mol% par rapport à l'amorceur) furent évalués. La polymérisation de My à 120 °C en masse, amorcée par NHS-BB sans radicaux nitroxyde supplémentaires et ciblant $M_{n,theo} \leq 30\text{ kg.mol}^{-1}$, fut considérée optimale. En effet, ces conditions expérimentales donnèrent les résultats les plus satisfaisants avec une évolution linéaire de M_n en fonction de X ($M_n/M_{n,theo} \sim 90\%$ en moyenne) et \bar{D} relativement faible ($< 1,30$) jusqu'à environ 70% de conversion. Une microstructure de type *cis*-1,4 fut prédominante ($> 80\text{ mol}\%$) avec une minorité d'unités 1,2 et 3,4 (5-10 mol% pour chacune). Ce polydiène synthétisé par NMP montra une température de transition vitreuse égale à -77 °C ainsi qu'une température maximale de dégradation (T_{dec} , 50% de perte de masse) de 385 °C . Afin de vérifier le caractère actif des bouts de chaînes du $P(My)$, idéalement terminé par des unités nitroxyde thermiquement labiles, une extension de chaîne de ce macro-amorceur $P(My)$ avec du styrène fut réalisée dans 50 m% de toluène. L'addition du bloc rigide poly(styrène) PS fut confirmée par chromatographie d'exclusion stérique (SEC, augmentation uniforme de M_n) et par résonance magnétique nucléaire du proton ($^1\text{H NMR}$, détection des pics correspondant aux protons aromatiques et aliphatiques du PS). Différents diblocs $My-S$ furent synthétisés ($M_n = 33,7-49,0\text{ kg.mol}^{-1}$, $\bar{D} = 1,33-1,88$, fraction molaire en styrène incorporé $F_S = 0,27-0,62$) et leurs propriétés en traction-élongation furent évaluées à température ambiante. Une extensibilité très limitée ($\epsilon_B < 16\%$) accompagnée d'une grande fragilité ($\sigma_B < 1,1\text{ MPa}$) de ces copolymères diblocs furent observées. Deux principales raisons pouvaient expliquer ces propriétés mécaniques en deçà des attentes : la longueur de chaîne moyenne relativement faible des diblocs ($M_n < 50\text{ kg.mol}^{-1}$) et surtout du segment souple $P(My)$ ($M_n \leq 30,4\text{ kg.mol}^{-1}$) ; une structure dibloc qui ne favorise pas de manière optimale la réticulation physique du réseau polymère puisque les chaînes flexibles ne sont attachées aux chaînes rigides que par un seul bout. Afin d'augmenter le M_n de ce TPE et d'obtenir une structure tribloc $S-My-S$, permettant à chaque segment souple d'être physiquement confiné entre deux phases rigides, un amorceur bifonctionnel fut préparé. Il s'agit du macro-amorceur téléchélique poly(éthylène-*ran*-butylène) terminé par des groupes nitroxyde SG1 à ses deux bouts de chaîne et abrégé PEB-(SG1)₂. Ce dernier fut synthétisé par estérification de son homologue PEB-(OH)₂ terminé par des groupes hydroxyle, suivi d'une addition intermoléculaire radicalaire en utilisant l'alcoxyamine commerciale BlocBuilder™. La préparation d'un segment souple $P(My)-(SG1)_2$ bien défini, ayant une masse molaire moyenne ($M_n = 44,6-59,3\text{ kg.mol}^{-1}$) supérieure à celle des précédents blocs $P(My)-SG1$ monofonctionnels ($M_n \leq 30,4\text{ kg.mol}^{-1}$), fut optimisée en utilisant l'amorceur PEB-(SG1)₂ en masse à 120 °C pendant 5 à 6 h. Suite à l'extension de chaîne de ces macro-amorceurs $P(My)-(SG1)_2$ avec du styrène,

des triblocs S-My-S furent obtenus ($M_n = 50,0-72,2 \text{ kg}\cdot\text{mol}^{-1}$, $\bar{D} = 1,72-2,41$, $F_S = 0,18-0,25$). Bien que ces triblocs montrèrent des allongements à la rupture en traction ($\varepsilon_B = 164-195\%$) largement supérieurs à ceux mesurés pour les diblocs My-S, leur résistance mécanique ($\sigma_B < 0,8 \text{ MPa}$) ne s'est pas améliorée. Par conséquent, ces copolymères à base de β -myrcène ne répondirent pas au cahier des charges industriel.

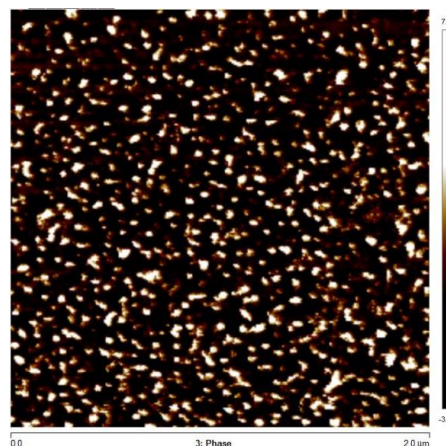


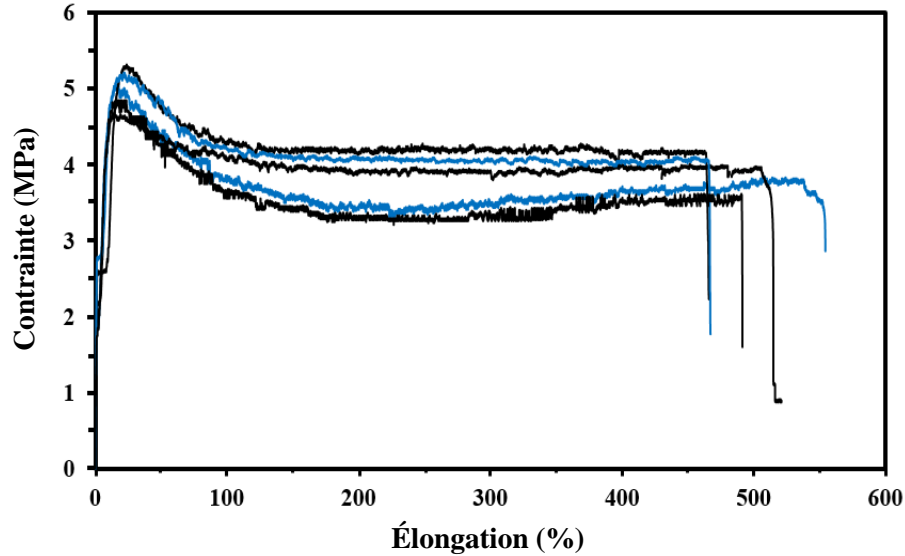
Structures **(a)** de l'alkoxyamine NHS-BB, **(b)** du radical nitroxyde SG1 \cdot , des monomères **(c)** β -myrcène (*My*), **(d)** isoprène (I), **(e)** styrène (S), **(f)** méthacrylate d'isobornyle (IBOMA) et **(g)** méthacrylate de glycidyle (GMA) et des polymères **(c')** *cis*-1,4-poly(β -myrcène) (*cis*-1,4-P(*My*)), **(d')** *cis*-1,4-poly(isoprène) (*cis*-1,4-PI), **(e')** poly(styrène) (PS), **(f')** poly(méthacrylate d'isobornyle) (P(IBOMA)) et **(g')** poly(méthacrylate de glycidyle) P(GMA).

En parallèle de cette étude, nous nous sommes penchés sur **la fonctionnalisation du segment souple P(My)**. En effet, la capacité du TPE à assurer la liaison entre deux matériaux composites est un objectif essentiel du projet doctoral. Si l'assemblage se réalise par collage (utilisation de composites thermodurcissables portant des groupes fonctionnels réactifs), la modification du TPE permettrait l'adhésion par liaisons covalentes de ce dernier avec la matrice thermodurcissable par exemple. Dans le cas d'un soudage (utilisation de composites thermoplastiques ayant une matrice relativement polaire), l'ajout d'unités fonctionnelles au sein du TPE candidat pourrait augmenter la miscibilité à l'interface avec les composites via la formation de liaisons intermoléculaires et favoriserait donc le processus d'inter-diffusion des chaînes macromoléculaires de part et d'autre de la surface de contact. Il fut envisagé de copolymériser *My* avec un monomère fonctionnel par NMP afin d'obtenir en une seule étape un segment élastomère portant des groupes polaires. La copolymérisation de *My* avec l'anhydride maléique (MA) ne fut pas concluante, possiblement due à une réaction secondaire de type *Diels-Alder*. De même, la copolymérisation par NMP de *My* avec l'acrylate de *tert*-butyle (*t*BuA) ne fut pas contrôlée, probablement causée par une réaction secondaire de type ``back-biting`` (réaction de transfert intramoléculaire) engendrant de nombreuses ramifications au sein des chaînes polymère. Toutefois, la synthèse contrôlée par NMP de copolymères P(*My-co*-MMA) (MMA = méthacrylate de méthyle) avec des valeurs M_n proches de celles prédites et $\mathcal{D} \leq 1,32$ nous poussa à étudier la copolymérisation de *My* avec un autre ester méthacrylique portant un groupe fonctionnel, à savoir le méthacrylate de glycidyle (GMA) possédant une fonction époxyde. La copolymérisation du couple *My*/GMA par NMP à 120 °C en masse, amorcée par NHS-BB, fut entreprise pour une fraction molaire initiale en GMA ($f_{GMA,0}$) comprise entre 0,10 et 0,90 par rapport à *My*. Les rapports de réactivité, déterminés par les méthodes de Fineman-Ross ($r_{My} = 0,80 \pm 0,31$, $r_{GMA} = 0,71 \pm 0,15$), Kelen-Tudos ($r_{My} = 0,48 \pm 0,12$, $r_{GMA} = 0,53 \pm 0,18$) et par une technique non-linéaire des moindres carrés résolvant l'équation de Mayo-Lewis ($r_{My} = 0,49 \pm 0,13$, $r_{GMA} = 0,50 \pm 0,13$) indiquèrent la nature statistique de cette copolymérisation. D'un point de vue cinétique, quel que soit $f_{GMA,0}$, la polydispersité des chaînes fut relativement faible ($\mathcal{D} \leq 1,55$) et M_n évolua linéairement avec la conversion X ($M_n/M_{n,theo} > 70\%$ en moyenne) et ceci même à $X > 80\%$. L'extension de chaîne réussie de ces copolymères statistiques P(*My-stat*-GMA) avec *My*, GMA et S témoigna d'une synthèse contrôlée par NMP, permettant de conserver en bout de chaîne le groupe nitroxyde thermiquement labile (fraction molaire $> 70\%$, mesurée par ^{31}P NMR). L'insertion d'unités époxyde dans le segment P(*My*) ouvre la porte à de multiples modifications possibles. L'ouverture quantitative des cycles époxyde d'un dibloc P(*My-b*-GMA) via de la morpholine fut dans cette étude effectuée, afin de produire un dibloc amphiphile P(*My-b*-HMPMA) capable de s'auto-assembler en micelles dans l'eau (taille moyenne Z , $Z_{ave} = 120-130$ nm à $T = 45-65$ °C et pour une concentration $[P(My-b-HMPMA)] \leq 0,7$ mg.ml $^{-1}$).

Les propriétés mécaniques à température ambiante non concluantes des triblocs S-My-S nous poussèrent dans un premier temps à **remplacer les blocs PS par des blocs P(IBOMA)** (IBOMA = méthacrylate d'isobornyle). P(IBOMA) ayant une T_g (~ 190 °C) bien supérieure à celle du poly(styrène) (~ 100 °C), une plus grande tenue mécanique combinée à une plus haute température de service maximale étaient attendues. Des triblocs à base de My et de IBOMA furent ainsi synthétisés, dans des conditions très similaires à celles utilisées pour la synthèse des triblocs S-My-S (préparation du macro-amorceur P(My) via PEB-(SG1)₂ et extension de chaîne avec IBOMA et une petite quantité de My ou S en tant que comonomère). Deux T_g distinctes ($T_{g,1} = -64$ à -58 °C, $T_{g,2} = +179$ à $+181$ °C) furent détectées par calorimétrie différentielle à balayage (DSC), correspondant respectivement aux domaines souple et rigide, ce qui laissa supposer d'une organisation des blocs P(My) et P(IBOMA) en masse. La micro-séparation de phase fut confirmée par microscopie de force atomique (AFM, préparation de films par évaporation lente de dichlorométhane), montrant la présence de potentielles nano-structures à base de sphères/cylindres de P(IBOMA) dans une matrice continue de P(My) (triblocs ayant $M_n = 51$ kg.mol⁻¹, $\bar{D} = 1,91$, $F_{IBOMA} = 0,28$, voir figure ci-dessous). Alors que les triblocs S-My-S se décomposèrent à $T = 435-445$ °C, la dégradation thermique des triblocs de type IBOMA-My-IBOMA s'effectua en deux étapes. Une première perte de masse fut visible par analyse thermogravimétrique (TGA) à $T = 240-310$ °C, correspondant vraisemblablement au détachement des groupes isobornyle de la macromolécule, suivi d'une seconde perte de masse à $T = 370-380$ °C, correspondant à la scission des chaînes principales. Une température de service maximale d'environ 140 °C fut déterminée par analyse dynamique mécanique (DMA), indiquant une plus grande stabilité de la performance mécanique de ce matériau en comparaison aux TPE à base de styrène qui perdent leurs propriétés, c'est-à-dire s'écoulent, généralement à partir de 90 °C. Enfin, un tribloc de type IBOMA-My-IBOMA ($M_n = 95$ kg.mol⁻¹, $\bar{D} = 2,23$ et $F_{IBOMA} = 0,36$) fut testé mécaniquement et montra de meilleures propriétés en traction-élongation que les précédents copolymères S-My-S avec $\sigma_B = 3,9 \pm 0,2$ MPa (limite d'élasticité à $5,0 \pm 0,2$ MPa), $\epsilon_B = 490 \pm 30$ % et un module d'Young $E = 2,32 \pm 0,3$ MPa (figure ci-dessous).

Image de phase ($2 \mu\text{m} \times 2 \mu\text{m}$) obtenue par microscopie à force atomique (AFM) en mode *Tapping* de la surface d'un copolymère tribloc expérimental de type IBOMA-My-IBOMA ($M_n = 51$ kg.mol⁻¹, $\bar{D} = 1,91$, $F_{IBOMA} = 0,28$). Le domaine sombre représente la phase continue P(My).





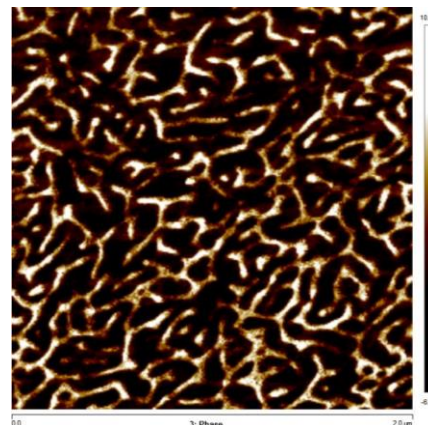
Cinq courbes contrainte-élongation (température ambiante, 10 mm.min⁻¹) d'un copolymère tribloc expérimental de type IBOMA-*My*-IBOMA ($M_n = 95 \text{ kg.mol}^{-1}$, $\bar{D} = 2,23$ et $F_{\text{IBOMA}} = 0,36$). $\sigma_B = 3,9 \pm 0,2 \text{ MPa}$, $\varepsilon_B = 490 \pm 30 \%$ et $E = 2,32 \pm 0,3 \text{ MPa}$ furent déterminés.

Bien que la substitution des segments PS par P(IBOMA), plus rigides, donna des résultats encourageants, le développement par NMP de triblocs à base de *My* ne permit pas de satisfaire les exigences du cahier des charges. La principale lacune fut une résistance à la rupture en traction trop faible ($\sigma_B \leq 3,9 \text{ MPa}$). Ces faibles propriétés mécaniques peuvent s'expliquer principalement par la masse molaire entre nœuds d'enchevêtrement élevée du P(*My*) ($M_{e,P(My)} = 22\text{-}31 \text{ kg.mol}^{-1}$), causant une faible densité d'enchevêtrement de la matrice souple entre les domaines rigides. La difficulté de synthétiser par NMP des triblocs de très haute masse molaire moyenne ($M_n < 110 \text{ kg.mol}^{-1}$ dans notre étude) est également une raison qui peut être avancée. Il fut ainsi décidé de **remplacer le segment central P(*My*) par un segment souple poly(isoprène) PI** présentant trois avantages majeurs : masse molaire entre enchevêtrements bien plus faible ($M_{e,PI} = 4\text{-}6 \text{ kg.mol}^{-1} \ll M_{e,P(My)}$) ; synthèse et caractérisation de PI et de TPE à base d'isoprène abondamment rapportées dans la littérature ; disponibilité commerciale de TPE de type styrénique à base d'isoprène, pouvant être utilisables comme références. La chimie de l'isoprène par voie radicalaire étant similaire à celle du β -myrcène, l'expérience acquise lors la synthèse du P(*My*) par NMP fut adoptée.

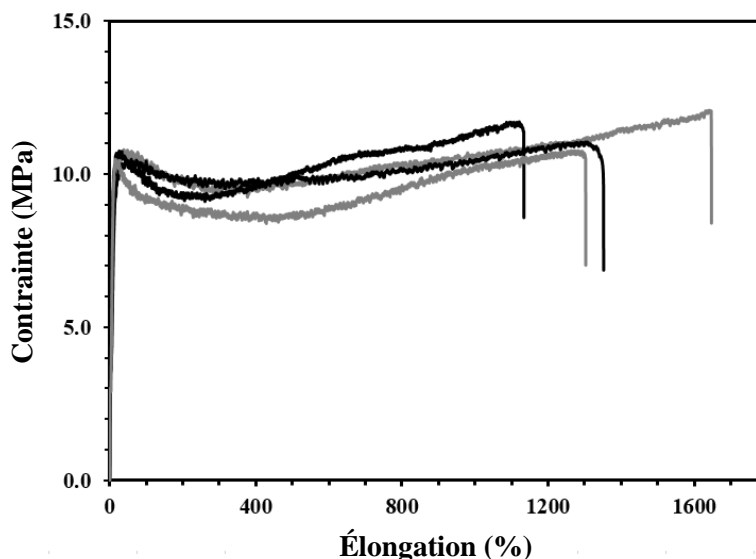
Tout d'abord, **la synthèse du poly(isoprène) par NMP fut optimisée** pour produire un segment souple de haute masse molaire moyenne et terminé par des groupes nitroxyde en bouts de chaîne

(poly(isoprène) nitroxy-téléchélique, permettant par la suite de pouvoir ajouter deux blocs rigides identiques). La polymérisation de l'isoprène amorcée par PEB-(SG1)₂ dans un réacteur pressurisé à 115 °C dans 50 v% de pyridine pendant 13-16 h donna les résultats les plus intéressants. Dans ces conditions et en ciblant une masse molaire théorique relativement élevée à 100% de conversion ($M_{n,theo} \sim 145 \text{ kg.mol}^{-1}$), la polymérisation fut contrôlée pour $X < 30\%$, se traduisant par un faible écart entre les masses molaires expérimentales et théoriques et une dispersité inférieure à 1,60. La synthèse de PI ayant $M_n = 51\text{-}56 \text{ kg.mol}^{-1}$ et $\mathcal{D} = 1,48\text{-}1,64$ fut effective. De plus, le fractionnement de ce segment flexible par précipitation en utilisant le couple de solvants benzène / méthanol permit d'éliminer les chaînes courtes irréversiblement terminées et conduisit principalement à une plus grande longueur de chaîne moyenne ($M_n = 54\text{-}61 \text{ kg.mol}^{-1}$, $\mathcal{D} = 1,47\text{-}1,59$). Une T_g égale à -60 °C et une température de dégradation maximale T_{dec} sous atmosphère d'azote voisine de 390 °C furent mesurées pour ces PI, constitués d'environ 80-85 mol% d'addition 1,4 (unités *cis*-1,4 > 65 mol%). Le caractère « vivant » du macro-amorceur PI permit de produire différents **triblocs S-I-S** ($M_n = 95\text{-}109 \text{ kg.mol}^{-1}$, $\mathcal{D} = 2,11\text{-}2,29$, $F_S = 0,30\text{-}0,49$) par extension de chaîne avec du styrène en masse à 115 °C pendant 1 à 2 h environ. Deux T_g furent détectées par DSC : $T_{g,1}$ de -61 à -65 °C (domaine PI souple) et $T_{g,2}$ de 102 à 104 °C (domaines PS rigides). Une séparation de phase possiblement cylindrique ou lamellaire à l'échelle du micromètre fut observée par AFM pour un S-I-S ayant $F_S = 0,30$ (voir figure ci-dessous). $T_{dec} \sim 420 \text{ °C}$ fut déterminée sous N₂ ($\sim 400 \text{ °C}$ sous air) pour un de ces S-I-S, ce qui est satisfaisant vis-à-vis de la problématique industrielle. Alors que le tribloc S-I-S contenant $F_S = 0,49$ ($M_n = 103 \text{ kg.mol}^{-1}$, $\mathcal{D} = 2,11$) fut rigide ($\sigma_B = 10,8 \pm 1,2 \text{ MPa}$, $E = 2,6 \pm 0,7 \text{ MPa}$) mais peu extensible ($\epsilon_B = 21 \pm 7 \%$), le S-I-S ayant $F_S = 0,38$ ($M_n = 108 \text{ kg.mol}^{-1}$, $\mathcal{D} = 2,18$) montra une plus grande ductilité ($\sigma_B = 4,1 \pm 0,2 \text{ MPa}$, $E = 1,2 \pm 0,6 \text{ MPa}$ et $\epsilon_B = 380 \pm 60 \%$). Comme attendu, leur température de service maximale se limita généralement à 90-100 °C, comme indiqué par DMA, par la chute du module de conservation à $T > T_{g,PS}$. Par conséquent, bien qu'ayant des propriétés mécaniques supérieures à leurs homologues à base de *My*, ces triblocs S-I-S manquèrent de résistance à la traction à $T = 100\text{-}160 \text{ °C}$.

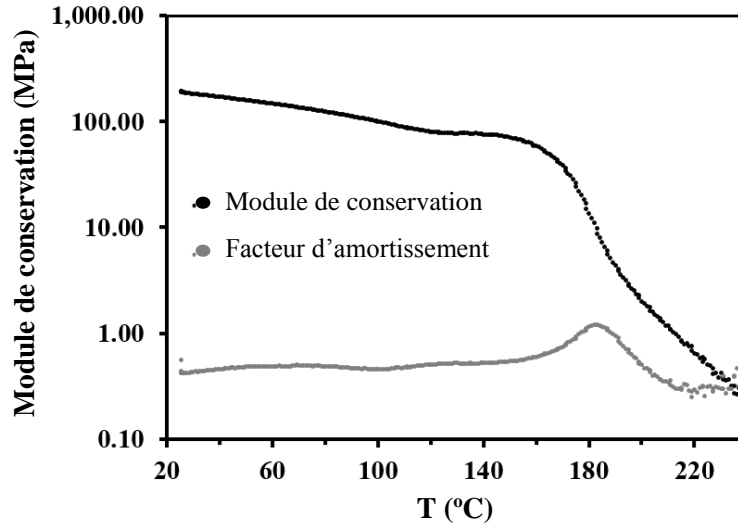
Image de phase (2 μm x 2 μm) obtenue par microscopie à force atomique (AFM) en mode *Tapping* de la surface d'un copolymère tribloc expérimental S-I-S ($M_n = 94,6 \text{ kg.mol}^{-1}$, $\mathcal{D} = 2,29$, $F_S = 0,30$). Le domaine sombre représente la phase continue PI.



Afin de combler ces lacunes, un **tribloc de type IBOMA-I-IBOMA** fut développé ($M_n = 94$ kg.mol⁻¹, $\bar{D} = 1,76$ et $F_{IBOMA} = 0,35$) de la même manière. Bien que sa morphologie à l'échelle microscopique ne fût pas clairement identifiée par AFM, la température de transition vitreuse de la phase souple fut clairement détectée par DSC à -63 °C ainsi que celle du domaine rigide à environ 182 °C. Comme observé préalablement dans le cas des copolymères à base de β -myrcène et de méthacrylate d'isobornyle, la décomposition de ce tribloc de type IBOMA-I-IBOMA se réalisa en deux principales étapes ($T_{d,1} = 265-345$ °C, perte du cycle isobornyle ; $T_{d,2} = 345-500$ °C, dégradation de la chaîne principale) sous atmosphère inerte. Ce tribloc fut ensuite analysé quant à ses propriétés mécaniques et rhéologiques. Une importante extensibilité ($\epsilon_B = 1360 \pm 210$ %) associée à une bonne résistance mécanique ($\sigma_B = 11,4 \pm 0,6$ MPa) furent mesurées (figure ci-dessous). Ces résultats peuvent s'expliquer par l'existence d'enchevêtrements dans les blocs souples ($M_{n,PI} = 53$ kg.mol⁻¹ ~ 10 $M_{e,PI}$) combinée à la rigidité des unités IBOMA. La réponse mécanique dynamique de ce tribloc en torsion sur une large plage de température permet de mettre en évidence une température de service maximale de l'ordre de 160 °C. Au-delà de cette température, une chute du module de conservation intervient (figure ci-dessous). Ce tribloc à base d'isoprène et de méthacrylate d'isobornyle fut ainsi le copolymère synthétisé par NMP le plus concluant, compte tenu de son comportement en traction uni-axiale et de sa potentielle haute température de service maximale. La dégradation thermique précoce de ce dernier à partir d'environ 250 °C reste toutefois problématique et son comportement mécanique à haute température ne fut pas évalué.



Quatre courbes contrainte-élongation (température ambiante, 10 mm.min⁻¹) d'un copolymère tribloc expérimental de type IBOMA-I-IBOMA ($M_n = 94$ kg.mol⁻¹, $\bar{D} = 1,76$ et $F_{IBOMA} = 0,35$). $\sigma_B = 11,4 \pm 0,6$ MPa, $\epsilon_B = 1360 \pm 210$ % et $E = 3,5 \pm 1,1$ MPa furent déterminés.



Variations du module de conservation (noir) et du facteur d'amortissement (gris) en fonction de la température (0.15 Hz, 1% d'élongation, 5 °C.min⁻¹) d'un copolymère tribloc expérimental de type IBOMA-I-IBOMA ($M_n = 94 \text{ kg.mol}^{-1}$, $D = 1.76$ et $F_{IBOMA} = 0,35$).

Dans le but d'augmenter principalement la résistance en traction et la température de dégradation du TPE candidat, **des essais d'hydrogénation** furent effectués sur des triblocs expérimentaux et de référence à base d'isoprène et de styrène. Il fut question de saturer le segment central PI. Cette modification chimique fut réalisée dans des conditions ``douces`` à pression ambiante, sans catalyseur ni dihydrogène. Spécifiquement, les S-I-S furent dissous dans du solvant *p*-xylène et chauffés à 125 °C pendant 3 h avec du *p*-toluène sulfonylhydrazide, générateur de l'agent diimide, et du tributyle amine. La conversion des unités isoprène en unités éthylène/propylène fut de 67-77 mol% (¹H NMR). Alors que la stabilité thermique des copolymères hydrogénés ne fut que légèrement améliorée sous air, en comparaison aux homologues insaturés, une augmentation plus importante de la température de dégradation fut constatée sous atmosphère inerte (N₂). Les propriétés mécaniques à température ambiante furent également affectées par l'hydrogénation du segment souple. σ_B et E furent augmentés de 30-55% et de 300-440% respectivement, indiquant une plus grande résistance en traction et dureté de ces S-I-S partiellement saturés. Toutefois, ces derniers montrèrent un allongement à la rupture en traction plus faible (par exemple, ϵ_B diminuant de 4700% à 3300% environ pour un S-I-S de référence après hydrogénation). Des analyses de spectrométrie mécanique dynamique ont été menées afin de déterminer l'influence de cette réaction chimique sur le comportement thermo-mécanique de ces matériaux. Le module de conservation E' d'un matériau de

référence S-I-S hydrogéné fut supérieur, que cela soit à l'état caoutchoutique ($T < T_{g,PS}$) ou dans un état tel que la température soit supérieure à $T_{g,PS}$. De plus, la baisse du module de conservation à $T > 90$ °C fut beaucoup plus modérée, indiquant une plus grande résistance thermique.

Enfin, **trois TPE de référence furent caractérisés**. Il s'agissait de deux triblocs S-I-S de *Sigma-Aldrich*[®] (S₄-I-S₄, $M_n = 98 \text{ kg.mol}^{-1}$, $\bar{D} = 1,29$, $F_S \sim 0,08$ et S₈-I-S₈, $M_n = 97 \text{ kg.mol}^{-1}$, $\bar{D} = 1,25$, $F_S \sim 0,16$) et d'un tribloc SEBS de *Kraton*[®] ($M_n = 88 \text{ kg.mol}^{-1}$, $\bar{D} = 1,16$, $F_S = 0,48$), synthétisés industriellement par polymérisation anionique. L'objectif était d'évaluer le potentiel de certains triblocs commerciaux de type styrénique, différents en composition (S₄-I-S₄ et S₈-I-S₈) et en structure (S-I-S et SEBS), vis-à-vis des propriétés exigées en contrainte-taux d'extension à température ambiante. Malgré une extensibilité remarquable ($\epsilon_B = 4250 \pm 230$ %), les matériaux S₄-I-S₄ manquèrent de résistance à la traction pour l'application recherchée ($\sigma_B = 7,5 \pm 0,6$ MPa), du fait d'une fraction molaire en styrène relativement faible (~ 8 mol%). Les propriétés mécaniques du S₈-I-S₈, contenant deux fois plus d'unités styrène, se rapprochèrent d'avantage des exigences d'ArianeGroup avec $\sigma_B = 12,7 \pm 0,7$ MPa et $\epsilon_B = 3740 \pm 140$ %, bien que manquant encore de résistance mécanique. Cela permet de rendre compte qu'une fraction molaire en styrène supérieure à 20% doit être ciblée pour cette famille de TPE. Pour les essais mécaniques de ces S-I-S de référence, l'entrée en plasticité est suivi d'une phase de durcissement, provoquant un accroissement significatif de la résistance à la rupture. Un tel comportement, caractéristique des élastomères thermoplastiques, ne fut pas observé pour les S-I-S préparés par NMP, ce qui pourrait s'expliquer par une distribution en masses molaires plus large ($\bar{D} = 2,18-2,29$, c'est-à-dire la présence de chaînes courtes fragilisant le copolymère) en comparaison à celle des produits de référence ($\bar{D} \leq 1,29$). Il peut également être avancé qu'une plus haute polydispersité des chaînes ne favorise pas une séparation nette des phases, se traduisant par des propriétés mécaniques inférieures aux attentes. Pour finir, un SEBS commercial (version hydrogénée du S-B-S) ayant une haute fraction molaire en styrène (48 mol%) montra des caractéristiques mécaniques à température ambiante très intéressantes avec $\sigma_B = 25,0 \pm 2,1$ MPa, $\sigma_{100} = 4,6 \pm 0,4$ MPa, $\epsilon_B = 730 \pm 40$ % et $E = 0,6 \pm 0,1$ MPa. Il commença à se dégrader (5% de perte de masse) à 260 °C sous air et à 340 °C sous N₂. Des essais TGA en condition isotherme indiquèrent que ce tribloc ne se décompose pas à $T \leq 275$ °C sous atmosphère inerte. Toutefois, une diminution importante de son module de conservation G' à $T > 60$ °C fut constatée, laissant supposer une perte non négligeable de ses propriétés mécaniques à haute température.

Différents copolymères à blocs de type styrénique furent ainsi préparés par NMP dans des conditions expérimentales simples, au cours de ce projet de recherche doctoral. L'influence de la nature du segment élastomère fut évaluée : les triblocs S-My-S montrèrent un comportement fragile en traction ($\sigma_B < 1$ MPa, $\epsilon_B < 200\%$) alors que de meilleures propriétés mécaniques furent déterminées pour les triblocs S-I-

S constitués d'une phase souple PI bien plus enchevêtrée ($\sigma_B = 2,8-4,1$ MPa, $\varepsilon_B = 380-450$ %). L'influence de la nature des blocs rigides fut également étudiée : le remplacement des blocs PS traditionnels par des blocs P(IBOMA) plus rigides permit d'augmenter considérablement la résistance en traction et l'extensibilité du copolymère tribloc. $\varepsilon_B \sim 1350\%$ et une température de service maximale d'environ 150 °C furent ainsi mesurés pour le copolymère tribloc de type IBOMA-I-IBOMA. Son insuffisante résistance mécanique ($\sigma_B \sim 11$ MPa) associée à son instabilité thermique (début de la dégradation à 220 °C sous air et 265 °C sous azote) furent toutefois préjudiciables pour l'application industrielle.

En continuité avec l'étude réalisée pour cette thèse, les futurs travaux pourraient se consacrer à l'optimisation des copolymères à blocs à base d'isoprène synthétisés par NMP afin de satisfaire entièrement le cahier des charges d'ArianeGroup. Le copolymère tribloc de type IBOMA-I-IBOMA, qui montra les caractéristiques mécaniques les plus intéressantes, pourrait être utilisé en tant que référence et modifié de la manière suivante :

- Synthèse de PI en milieu dispersé afin de préparer un segment souple de plus haute masse molaire moyenne et avec une dispersité plus faible (amélioration des propriétés en traction uniaxiale attendue du fait d'une phase souple plus enchevêtrée et contenant moins de chaînes courtes).
- Remplacement de P(IBOMA) par un polymère au moins aussi rigide mais plus stable thermiquement tel que le poly(α -méthylène- γ -butyrolactone) P(MBL) (augmentation de la température de dégradation).
- Hydrogénation du bloc PI central (plus grande résistance en traction et stabilité thermique).

MAIN INTRODUCTION

Thermoplastic elastomers (TPE) have been defined by the International Institute of Synthetic Rubber Producers as: “*Polymers, polymer blends or compounds which, above their melt temperatures, exhibit thermoplastic character that enables them to be shaped into fabricated articles and which, within their design temperature range, possess elastomeric behavior without crosslinking during fabrication. This process is reversible and the product can be reprocessed and remolded.*”

The development of thermoplastic materials having essentially elastic properties started in the early 1930's with the invention of plasticization of poly(vinyl chloride) (PVC) at the B. F. Goodrich Company¹. This invention led to further interest in flexible plastics and eventually to the preparation of blends of PVC and butadiene-acrylonitrile rubber (NBR)^{2,3}. The PVC/NBR blends, when properly formulated, have a rubber-like behavior and bridge the gap between liquid plasticized PVC and conventional cured elastomers. Thus, they can be considered as the precursors of TPE, as we know them today. A breakthrough occurred with the discovery of the basic diisocyanate polyaddition reaction⁴ in 1937, which was first applied to produce polyurethane fibers and then to the development of some elastomeric polyurethanes at DuPont and ICI companies⁵⁻⁷. The work at DuPont focused on elastic fibers and eventually led to the invention of elastic linear copolyesters, prepared by melt-ester interchange between two melt copolymerized polymers⁸. These synthetic elastomers had higher strength than vulcanized natural rubbers and exhibited a faster elastic recovery. They were used to make fibers by extrusion or spinning from solutions and can be considered as the first types of TPE⁹.

The global consumption of TPE is expected to grow from 4.2 million tons in 2015 to nearly five and a half million tons in 2020¹⁰. This can be explained by the ability of TPE to be processed as thermoplastic materials while possessing the physical and mechanical properties of vulcanized elastomers. Industries increasingly use TPE due to the significant cost savings arising from the TPE ability to be processed on machinery designed for thermoplastics. Conventional rubbers, whether natural or synthetic ones, are thermosetting materials that must undergo a chemical crosslinking reaction during molding or extrusion, denoted curing or vulcanization. Due to this reaction, they are not processable using conventional thermoplastic equipments. The thermoplastic molding and extrusion processes used for TPE, on the other hand, do not involve the crosslinking. Furthermore, TPE processing scrap, reject parts or end of life products can be easily reprocessed, whereas most thermosetting elastomers end up as land fill.

In addition to the advent of TPE as affordable substitute materials to traditional thermoset rubbers, the increased use of high-performance thermoplastic composites, especially in some sectors of the

aerospace industry, is apparent. Thermoplastics provide several important advantages over thermosets when used in composite materials, most notably better impact damage resistance, high damage tolerance, good fatigue resistance, higher fracture toughness, higher operating temperatures, low storage cost and infinite shelf life. Thermoplastic composites offer several processing benefits over thermoset composites as well. They are reprocessable, repairable, and reformable, which together provide ease of fabrication and cost-effectiveness. Thermoplastic composites can also be deformed to complex shapes and then cooled to solidify in shorter times than required by thermoset composites, which have relatively lengthy manufacturing times due to slow cure kinetics of the thermoset resins. The group of thermoplastics that are mostly used in aircraft composite structures currently are called polyketones, and includes poly(etherketone) (PEK), poly(etherketoneketone) (PEKK) and, the most common poly(etheretherketone) (PEEK).

This promising replacement of thermoset materials by thermoplastics, offering a larger process window, prompts engineers to rethink the joining between aerospace structures.

The research project proposed and funded by ArianeGroup for this doctoral thesis falls within the context discussed above, where the substitution of traditional thermoset materials by thermoplastics has become a major issue of the aerospace industry. One of the key activity of ArianeGroup is devoted to the manufacture of launchers which consist of a tank joined with skirts by a soft junction. The tank and the skirts are currently thermoset composites whereas the soft junction is a thermoset rubber. The joining is operated by adhesive bonding using a specific resin. Such a thermoset-based soft junction remains problematic, mostly from an economical point of view. The vulcanization of the rubber, the use of a resin and the adhesive bonding performed in an autoclave during long cycle processing times are, to name but a few, detrimental. Taking mostly into account the economical disadvantages of using thermosets and performing long and multi-step processes, ArianeGroup is studying the development of a thermoplastic-based tank/rubber/skirt assembly. Indeed, for the next-generation of launchers, ArianeGroup examines the production of tank and skirts in thermoplastic composites and the replacement of the traditional thermoset rubber used for the flexible junction by a thermoplastic elastomer. This complete change from thermoset composites and rubber to thermoplastic composites and elastomer will allow the formation of the final assembly by welding, a promising and cost-efficient joining technique.

Exclusive to thermoplastic materials, welding (or thermal bonding) has great potential for the joining, assembly, and repair of composite components. This process involves heating and melting the polymer on the bond surfaces of the components and then pressing these surfaces together for polymer

solidification and consolidation. Welding allows short processing cycles and offers additional advantages including reduced surface preparation requirements, reprocessing, recyclability and improved integrity/durability. Suitable for joining thermoplastic composites directly with each other, this technique is also appropriate for assembling thermoplastic composites with thermoplastic elastomers.

Due to the difficulties to find a suitable commercial thermoplastic elastomer, this work aimed to develop experimentally a novel thermoplastic elastomer exhibiting properties similar to those of the current thermoset rubber. Furthermore, the weldability of the synthesized thermoplastic elastomer directly with the substitute thermoplastic composite or indirectly by using an in-between thermoplastic layer was a prominent requirement.

This doctoral work was, to a large majority, focused on the synthesis of a novel thermoplastic elastomer in order to replace the current vulcanized rubber. A specific controlled radical polymerization, termed nitroxide-mediated polymerization, was selected to produce styrenic triblock copolymer thermoplastic elastomers. Poly(β -myrcene), a bio-sourced elastomer, was first considered as the elastomeric mid-segment before being substituted by poly(isoprene).

This manuscript is divided into three main parts: (I) State of the art; (II) a first experimental section devoted to the synthesis of β -myrcene-based copolymers by nitroxide-mediated polymerization (NMP); (III) a second experimental section mainly focused on the synthesis by NMP, the characterization and the hydrogenation of isoprene-based triblock copolymers. The literature review (I) is first dedicated to thermoset rubbers and TPE to understand the will from industrials to take advantage of technologies based on thermoplastics. Styrenic block copolymer TPE, considered in this research, are then introduced more specifically as well as the polymerization processes applicable to synthesize them. The second part (II) includes three chapters. The first chapter presents the synthesis of β -myrcene/styrene (*My/S*) copolymers by NMP and concludes with the achievement of *S-My-S* triblock copolymers. The second chapter is devoted to the functionalization of P(*My*) by nitroxide-mediated copolymerization of *My* with epoxy-functional glycidyl methacrylate (GMA). The introduction of polar groups into the TPE aimed to possibly encourage the subsequent welding with relatively polar thermoplastic composites initially considered for this project. The third chapter focuses on the synthesis of *My/isobornyl methacrylate* (IBOMA) copolymers by NMP. The objective was to replace PS outer blocks by higher glass transition segments such as P(IBOMA) to enhance the toughness and the service temperature of the candidate TPE. The last major part (III) includes two final chapters. The fourth chapter is dedicated to the synthesis of isoprene-based triblock copolymers by NMP whereas the fifth chapter deals with the characterization of commercial styrenic block copolymer TPE. In these two last chapters, the partial hydrogenation of experimental and commercial TPE's PI segment is detailed as well.

- (1) Semon W. L., *US Patent* 1 929 453, B. F. Goodrich Co., **1933**.
- (2) Henderson D. E., *US Patent* 2 330 353, B. F. Goodrich Co., **1943**.
- (3) Wolfe J. R. In *Thermoplastic Elastomers: A Comprehensive Review*; Legge N. R., Holden G., Schroeder H. E., eds.; Hanser Publishers: Munich, **1987**; Chapter 6.
- (4) Bayer O., Siefken W., Rinke H., Orthner R., Schild H., *German Patent* 738 981, I. G. Farben, **1937**.
- (5) Christ A. E., Hanford W. E., *US Patent* 2 333 639, DuPont, **1940**.
- (6) *British Patents* 580 524 (**1941**) and 574 134 (**1942**), ICI Ltd.
- (7) Hanford W. E., Holmes D. F., *US Patent* 2 284 896, DuPont, **1942**.
- (8) Snyder M. D., *US Patent* 2 632 031, DuPont, **1952**.
- (9) *US Patent* 2 629 873, DuPont, **1954**.
- (10) Thermoplastic Elastomers Market Size, Industry Share Report, Global Market Insights, **2016**.

INTRODUCTION GÉNÉRALE

Les élastomères thermoplastiques (TPE) ont été définis par l'Institut International des Producteurs de Caoutchoucs Synthétiques comme: *``Des polymères, des mélanges de polymères ou des formulations de polymères qui, au-dessus de leur température de fusion (ou de la température de transition vitreuse du domaine rigide), se comportent comme des thermoplastiques, ce qui permet de les mettre en forme aisément, et montrent, lorsqu'ils sont utilisés dans leur température de service, un comportement élastique semblable aux caoutchoucs thermodurcissables traditionnels alors qu'ils ne sont pas réticulés. N'ayant donc pas de réseau chimiquement réticulé, les élastomères thermoplastiques peuvent être remis en œuvre et remoulés.``*

Le développement de matériaux thermoplastiques ayant des propriétés élastiques débuta dans les années 1930 avec la plastification du polychlorure de vinyle (PVC) par la compagnie B. F. Goodrich¹. Cette invention mena par la suite à la préparation de mélanges à base de PVC et de caoutchouc du type copolymère butadiène-acrylonitrile (NBR)^{2,3}. Cela permit d'obtenir un matériau intermédiaire entre le PVC plastifié et les élastomères vulcanisés traditionnels. Les mélanges PVC / NBR peuvent ainsi être considérés comme les précurseurs des TPE, comme nous les connaissons aujourd'hui. La découverte de la réaction de polyaddition en utilisant du diisocyanate en 1937 constitua une avancée majeure dans le développement des TPE⁴. Cette technique de polymérisation fut employée chez Dupont et ICI afin de synthétiser des fibres de polyuréthane ayant des propriétés similaires à celles d'élastomères vulcanisés⁵⁻⁷. Cela conduisit par la suite à la synthèse d'élastomères de type copolyester, ayant une résistance en traction supérieure aux caoutchoucs vulcanisés et une reprise élastique aux temps courts^{8,9}. Ces matériaux furent ainsi considérés comme étant les premiers TPE.

La consommation mondiale de TPE devrait progresser de 4,2 millions de tonnes en 2015 à environ cinq millions et demi de tonnes en 2020¹⁰. L'intérêt des TPE s'explique par leur capacité à être mis en œuvre comme des matériaux thermoplastiques tout en ayant des propriétés physiques et mécaniques aussi intéressantes que celles des élastomères thermodurcissables. Ils permettent donc une grande flexibilité dans leur procédé de fabrication et de mise en œuvre. Aujourd'hui, le secteur industriel utilise de plus en plus les TPE puisqu'ils s'adaptent directement aux machines traditionnelles mise en service pour les thermoplastiques. Qu'il soit naturel ou synthétique, l'élastomère conventionnel est un thermodurcissable qui est vulcanisé. La vulcanisation est une réaction réalisée durant le moulage ou l'extrusion et permettant la réticulation chimique et permanente du caoutchouc. Du fait de cette réaction, l'élastomère ne peut plus être remis en forme. Bien que la durée de la réaction de vulcanisation dépende de nombreux paramètres, il faut compter entre quelques minutes et plusieurs heures afin de conduire à un réseau tridimensionnel

efficace. En comparaison, les procédés de moulage et d'extrusion utilisés pour les TPE, ne nécessitant pas d'étape de réticulation, peuvent être réalisés très rapidement. Une vingtaine de secondes peut être suffisant, ce qui se traduit par des profits non-négligeables. De plus, la possibilité de recycler les TPE est un atout considérable. Les déchets, rebuts ou articles en fin de vie à base de TPE peuvent être aisément remis en œuvre alors que les élastomères thermodurcissables en fin de cycle se retrouvent bien souvent dans les décharges.

C'est dans ce contexte que la problématique industrielle étudiée pour cette thèse prend toute sa place. Leader mondial de l'accès à l'espace, ArianeGroup conçoit des solutions innovantes et compétitives en matière de système de lancement et d'applications spatiales civiles et militaires. Ses activités couvrent l'ensemble du cycle de vie d'un lanceur spatial : conception, développement, production, exploitation et commercialisation. ArianeGroup produit et exploite le lanceur Ariane 5, le plus fiable du marché commercial, et développe le futur lanceur Ariane 6.

Le projet de recherche proposé et financé par ArianeGroup pour cette thèse doctorale s'inscrit parfaitement dans une logique de remplacement des matériaux thermodurcissables traditionnels par des thermoplastiques. Cela représente un enjeu majeur de l'industrie aéronautique. L'une des activités clés d'ArianeGroup est consacrée à la fabrication de lanceurs. Ces derniers sont constitués d'un corps de propulseur (réservoir de propergol solide) et de viroles (appelées jupettes). La liaison entre les jupettes et le réservoir, sollicitée principalement en cisaillement, est assurée par un élastomère. Aujourd'hui, les jupettes et le réservoir sont des composites thermodurcissables. L'élastomère est également un polymère thermodurcissable. La liaison flexible entre ces structures est réalisée par collage, sur la base d'une colle spécifique polymérisant à chaud, en étuve. Un tel assemblage reposant sur des matières thermodurcissables est problématique, d'un point de vue économique principalement. La vulcanisation du caoutchouc, l'insertion de la colle et le collage réalisé dans un autoclave pendant des cycles de longues durées, constituent par exemple des étapes très coûteuses et sont directement liées à l'utilisation de matrices polymère réticulées chimiquement. ArianeGroup envisage alors le développement d'un assemblage réservoir / élastomère / jupettes entièrement thermoplastique. En effet, pour la génération future de ses lanceurs, ArianeGroup souhaiterait fabriquer le réservoir et les jupettes en composite thermoplastique et remplacer l'élastomère vulcanisé assurant la flexibilité de la liaison par un TPE. Ce changement total de composites et d'élastomères thermodurcissables à des composites et des élastomères thermoplastiques permettrait de réaliser l'assemblage final par soudage, une technique efficace et économique.

À la différence des autres procédés d'assemblage, le soudage ne s'applique qu'aux thermoplastiques. Seuls ceux-ci possèdent des caractéristiques rhéologiques suffisantes, lors de la fusion (pour les semi-cristallins) ou du ramollissement (pour les amorphes), pour permettre une interpénétration

des couches superficielles nécessaire à leur liaison. La réalisation d'une liaison par soudage permet d'obtenir d'un point de vue industriel une robustesse supérieure aux technologies de collage. La moindre sensibilité à l'environnement et à la pollution ainsi qu'un cycle de réalisation plus rapide sont des atouts fondamentaux.

En raison des difficultés à identifier un élastomère thermoplastique commercial satisfaisant le cahier des charges fixé par ArianeGroup, cette thèse avait pour objectif de développer en laboratoire un élastomère thermoplastique (TPE) permettant de rivaliser avec l'actuel caoutchouc thermodurcissable. La capacité de ce nouvel élastomère à se souder directement aux composites thermoplastiques envisagés ou indirectement via l'insertion d'un matériau thermoplastique intermédiaire constituait une exigence industrielle importante.

La polymérisation radicalaire contrôlée par des nitroxydes (NMP) fut sélectionnée afin de produire un TPE de type styrénique. Le poly(β -myrcène) P(My), un élastomère biosourcé de la famille des polyterpènes, fut d'abord envisagé en tant que segment souple du TPE avant d'être remplacé par le poly(isoprène) PI.

Ce manuscrit se divise en trois grandes parties : (I) état de l'art ; (II) première partie expérimentale consacrée à la synthèse de copolymères à base de β -myrcène (My) par NMP ; (III) seconde partie expérimentale qui se concentre sur la synthèse par NMP et la caractérisation de copolymères à blocs à base d'isoprène. L'état de l'art (I) introduit dans un premier temps les élastomères thermodurcissables et thermoplastiques puis se focalise plus précisément sur les TPE copolymères à blocs de type styrénique envisagés dans cette étude. La deuxième section (II) comporte trois chapitres. Le premier chapitre évoque la synthèse de copolymères β -myrcène/styrène (My/S) par NMP, permettant notamment d'obtenir des copolymères triblocs S-My-S. Le deuxième chapitre présente la fonctionnalisation du poly(β -myrcène) P(My) par la copolymérisation radicalaire contrôlée par des radicaux nitroxyde du β -myrcène avec le méthacrylate de glycidyle, un monomère vinylique portant un groupe époxyde. L'incorporation d'unités réactives au sein du TPE avait pour but d'encourager le soudage ultérieur de l'élastomère avec les composites thermoplastiques relativement polaires. Le troisième chapitre se concentre sur la synthèse contrôlée de copolymères My/IBOMA (IBOMA = méthacrylate d'isobornyle) par NMP. L'objectif était ici de remplacer les segments poly(styrène) PS par des blocs P(IBOMA) plus rigides ayant une température de transition vitreuse plus élevée et permettant ainsi d'augmenter la résistance à la rupture et d'élargir la température de service du TPE candidat. La troisième grande partie (III) de ce manuscrit comprend deux chapitres finaux. Le quatrième chapitre est consacré à la synthèse de triblocs à base d'isoprène par NMP alors que le cinquième chapitre se focalise sur la caractérisation de TPE de référence de type styrénique.

L'hydrogénation partielle du segment souple poly(isoprène) de copolymères triblocs expérimentaux et de référence est également présentée dans ces deux derniers chapitres.

- (1) Semon W. L., *US Patent* 1 929 453, B. F. Goodrich Co., **1933**.
- (2) Henderson D. E., *US Patent* 2 330 353, B. F. Goodrich Co., **1943**.
- (3) Wolfe J. R. In *Thermoplastic Elastomers: A Comprehensive Review*; Legge N. R., Holden G., Schroeder H. E., eds.; Hanser Publishers: Munich, **1987**; Chapter 6.
- (4) Bayer O., Siefken W., Rinke H., Orthner R., Schild H., *German Patent* 738 981, I. G. Farben, **1937**.
- (5) Christ A. E., Hanford W. E., *US Patent* 2 333 639, DuPont, **1940**.
- (6) *British Patents* 580 524 (**1941**) and 574 134 (**1942**), ICI Ltd.
- (7) Hanford W. E., Holmes D. F., *US Patent* 2 284 896, DuPont, **1942**.
- (8) Snyder M. D., *US Patent* 2 632 031, DuPont, **1952**.
- (9) *US Patent* 2 629 873, DuPont, **1954**.
- (10) Thermoplastic Elastomers Market Size, Industry Share Report, Global Market Insights, **2016**.

TECHNOLOGICAL OBJECTIVES

■ Introduction

Equally owned by Airbus and Safran, ArianeGroup is a world leader in access to space, providing innovative and competitive solutions for civil and military launch systems and space applications. ArianeGroup is an expert in the most cutting-edge technologies, from all aspects of complete propulsion systems right down to the individual items of equipment and materials. One of the core businesses of ArianeGroup is dedicated to the production of launchers in thermoset composites, made by winding processes. In such a process, a stationary mandrel rotates, while a carriage arm travels horizontally up and down the length of the mandrel. As the mandrel turns, the rovings wrap around it to form a composite layer over the mandrel's surface. Before encountering the mandrel, the fibers are impregnated in a resin, which later solidifies with the fiber to create the final composite material.

The launchers are composed of a tank (vessel) in a composite joined with skirts by a soft junction. Both the tank and the skirts are made of composite materials and undergo different deformations, as depicted in Figure 1. They must support the weight of the launcher. Moreover, the tank exhibits deformations in diameter (radial deformation) and in height. The tank can be deformed under pressure. Accordingly, an elastomeric junction has to be used to transmit mostly shearing forces generated by these deformations. Such a joint is termed ``shearing ply``.

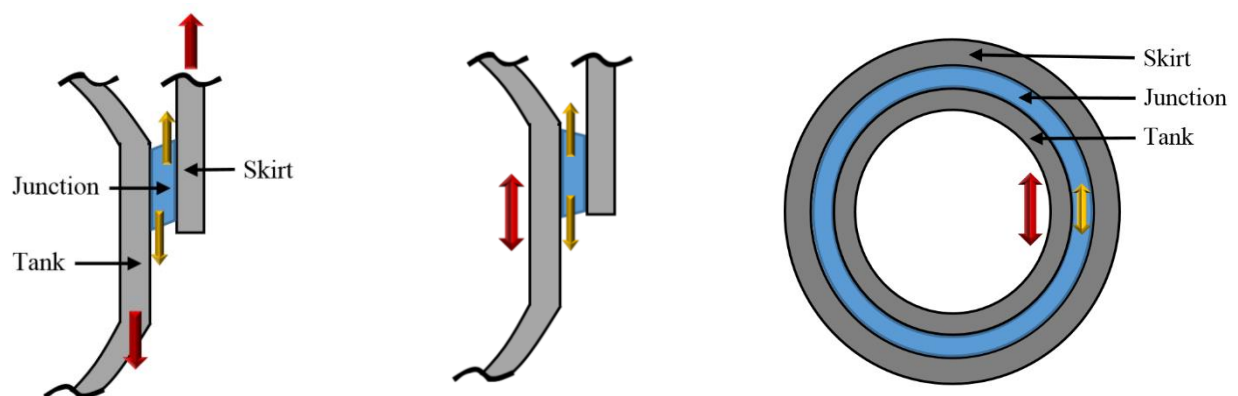


Figure 1. Shearing forces (yellow arrows) generated through the flexible junction due to tank and skirt deformations (red arrows) caused by the weight of the launcher (**left**) and due to tank deformations in diameter (**middle**) and height (**right, top view**).

■ Current tank-skirt assembly

The tank and the skirts are presently thermoset composites and a commercial thermoset is used as the elastomeric joint. The assembly tank/rubber/skirt is implemented by using a specific adhesive, as represented in [Figure 2](#). Accordingly, the joining technique used is an adhesive bonding of thermosets: the adhesive is placed between the parts to be bonded (adherends) where it serves as the material that joins the parts and transmits the load through the joint. This technology relies on the covalent bonding at the interface via chemical reactions.

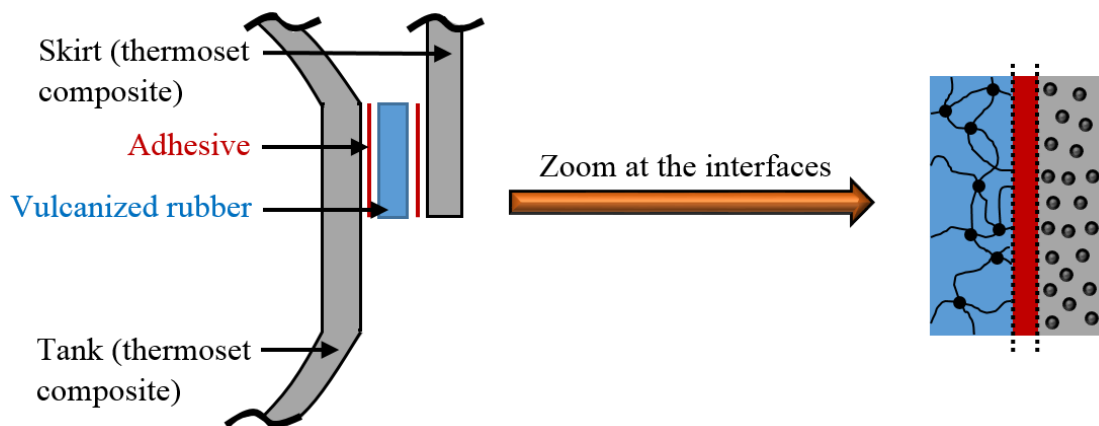


Figure 2. Schematic of the current assembly performed by ArianeGroup using a specific adhesive to implement the adhesive bonding. The illustration on the right shows rubber/adhesive and adhesive/thermoset composite interfaces where covalent bonding occurred (the black solid circles represent crosslinking points whereas the grey solid circles correspond to the reinforcement components of the thermoset composite).

This assembly requires critical steps which lead to increasing costs. First, vulcanization, in a specific press at high temperature and pressure, must be implemented to crosslink the rubber. Then, the assembly tank/adhesive/rubber/adhesive/skirt to bond is placed in a giant autoclave to proceed to the curing (hardening) of the adhesive. The use of an adhesive bonding technology to make the joint is detrimental due to the long assembly times. Moreover, the limited service life of the adhesive and the storage of the elastomer are non-negligible issues. Indeed, the rubber before vulcanization has a use-by date due to its reactivity (UV hardening / brittleness).

■ **First technological challenge: replacement of the thermoset rubber by a thermoplastic elastomer**

The substitution of the current vulcanized rubber by a thermoplastic elastomer (TPE) would give significant benefits: no vulcanization step; reduction of the cost of the raw material (potentially ten times cheaper); versatility of the process based on that of thermoplastics and thus versatility of the joining technique; and unlimited storage.

The substitute TPE must exhibit inherent properties as good as those of the current thermoset rubber. Consequently, TPE specifications are required as indicated in Table 1. It must be noted that the TPE will be used under usual atmospheric conditions.

Mechanical properties of the TPE	Mechanical properties of the assembly	Service conditions	Health and safety
Similar to the stress-strain properties of the thermoset rubber used currently	Satisfactory tensile strength at break and high shear modulus at 100% elongation	Continuous service temperature = 10 to 40 °C	REACH compliance
		Maximum service temperature = 80 °C	
	Minimal loss of the mechanical properties with temperature	Life time > 20 years	
	Type of failure = Cohesive fracture	Hygrometry: Relative humidity = 35 to 65 % (short periods at 100 %)	
		No mechanical damage with diestone and 1,1,1-trichloroethane	

Table 1. Main industrial requirements for the candidate TPE and the resulting assembly. REACH is the European Regulation on Registration, Evaluation, Authorization and Restriction of Chemicals, came into effect in 2007.

The TPE stress-strain properties desired by ArianeGroup were targeted after uniaxial tensile tests, and must be highly reproducible, and performed on the specific thermoset rubber currently used. The Young's modulus of the TPE at 100 % elongation will be important to determine since it will affect directly the thickness of the joint: the lower the modulus, the thinner the joint. A life time of minimum 20 years is mostly due to the very long period for assembling a launcher.

Even though the major aim of replacing the thermoset rubber by a TPE is to allow the implementation of a more robust and cost-effective joining technique, it must be noted that the TPE will be first joined to the tank and skirt by adhesive bonding, as currently performed. Indeed, this joining process as well as the subsequent characterization, using a by double lap shear configuration for instance, is optimized in the ArianeGroup facilities. This means that the TPE must be robust (capability of preserving its properties) at elevated temperatures since an adhesive bonding would necessitate to heat at 160-180 °C for more than 10 hours.

■ **Second technological challenge: Joining of the assembly tank / TPE / skirts by welding**

Even though the substitution of the thermoset rubber by a suitable TPE would constitute a major advance, the main technological breakthrough consists of the development of a new cost-effective and robust joining technique to assemble the tank, the TPE and the skirts. For future launchers, ArianeGroup studies manufacturing of tank and skirts in thermoplastic composites instead of thermoset composites. Specific matrices reinforced with carbon nanotubes or carbon fibers are thus considered.

Thermoplastic composite technology intends to achieve improved properties and low-cost processes compared to composites containing a chemically crosslinked matrix. The use of thermoplastic-based composites and elastomer for this assembly represents a major advantage since processing, joining or shaping can be done using standard techniques used for thermoplastics in the melt state. Taking the advantage of handling thermoplastics, the production of welded structures is possible. The process of welding involves heating and melting the polymer on the bonded surfaces of the components and then pressing these surfaces together for polymer solidification and consolidation. This is an affordable method and the structures have typically a higher strength in comparison to adhesive bonding. The limited shelf lives and working lives of adhesives, the rigorous surface preparation and the lengthy cure times caused by adhesive bonding are eliminated by using a welding technique.

A resistive welding process is mainly studied. Resistance welding uses an electrically resistive element or implant, such as metal mesh or carbon strip, between the joint elements. An electrical current is applied to the resistive implant to increase the temperature of the implant due to resistance heating. The temperature of the implant increases at the interface, melts the polymer around the implant, and creates a weld under the application of pressure. Figure 3 shows a possible welding configuration.

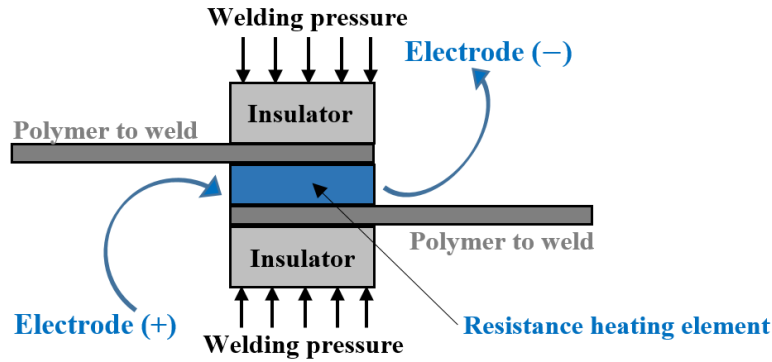


Figure 3. Schematic of a resistance welding process for a lap shear coupon.

Resistance welding can be used to weld most thermoplastic-based materials. The process is reasonably fast, simple, cheap, and clean. Since the implant remains in the bond, material compatibility between the implant and joint elements is important. To obtain a good quality weld, the resistance of the heating element should be determined to adjust the level of power input during the process. Also, controlling the heating/cooling rates improve the weld quality and mechanical performance of the weld. Resistance welding has great potential for welding high-performance continuous fiber thermoplastic composites especially for aerospace applications. Thermal insulation, input energy, welding time, fiber orientation, and type of heating element are the parameters that influence the quality and performance of the resistance welded parts.

Obviously, the direct welding between the TPE and the thermoplastic composites would be ideal. This can be performed in principle by using the considered composites as electrically resistive elements since they contain carbon nanotubes or carbon fibers (network of conductive particles) having a concentration higher than the percolation threshold. Such a welding would lead to a tank / TPE / skirt assembly without any additional intermediary layers, as depicted in [Figure 4a](#). However, the use of a thermoplastic composite exhibiting a high processing temperature imposes stringent thermal requirements for the welding, which would require temperatures that would probably degrade the TPE. The addition of another thermoplastic composite, situated between the TPE and the tank/skirts, can therefore be envisioned for the resistive welding process. This intermediate material, requiring a lower processing temperature and fully miscible with the thermoplastic composite considered initially, would impose lower thermal requirements. Such an assembly is depicted in [Figure 4b](#).

The failure of a resistance-welded joint can be dominated by one of the following failure modes: interfacial failure, cohesive failure of the heating element, tearing of the heating element, and tearing of the laminate. ArianeGroup would like a cohesive fracture at the TPE / thermoplastic composite interface where the failure occurs through the heating element.

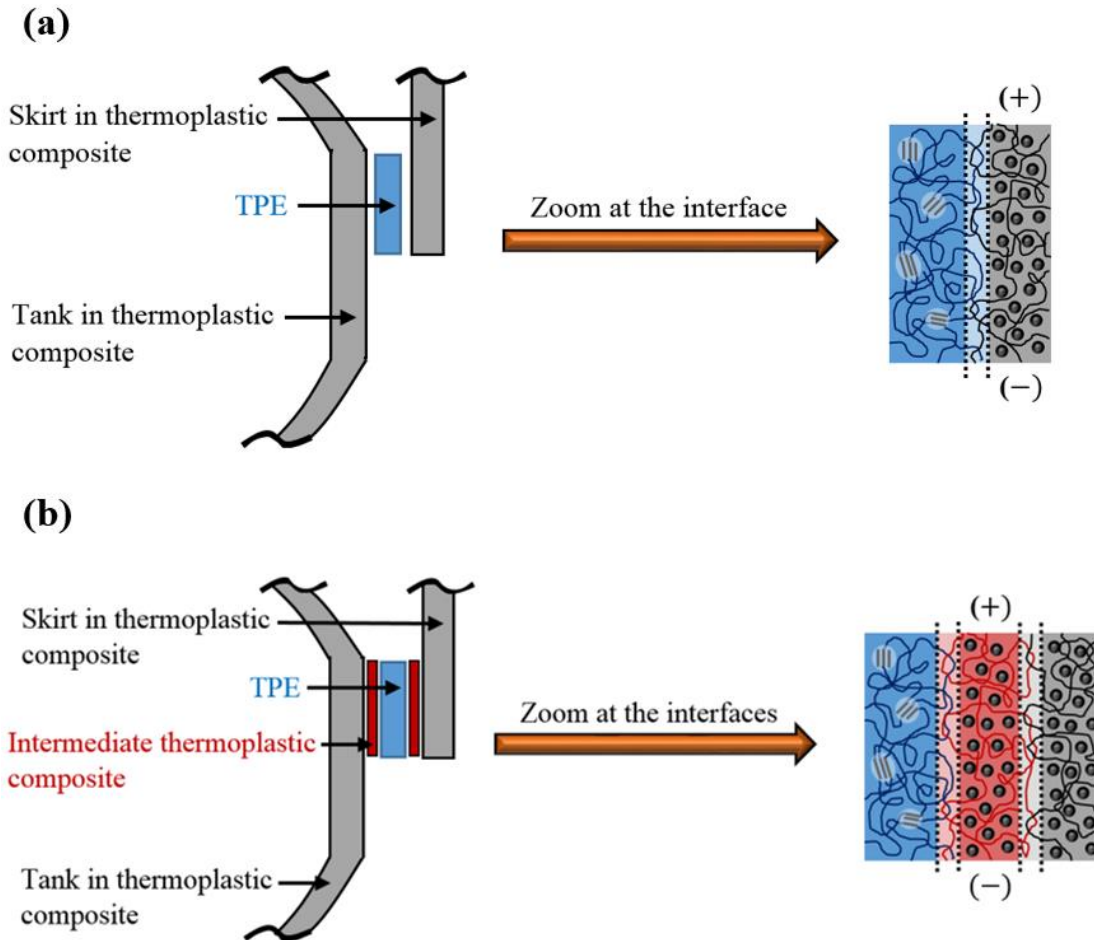


Figure 4. The new thermoplastic-based tank (grey) / TPE (blue) / skirt (grey) assembly could be welded directly using a specific thermoplastic composite as the resistance heating element **(a)** or indirectly via the use of in-between thermoplastic composite layers (red) used as resistance heating elements **(b)**. The illustrations on the right show **(a)** TPE / thermoplastic composite interface where interdiffusion of the chains occurred (TPE arbitrarily represented by spherical hard domains in a continuous soft matrix; the grey solid circles correspond to the reinforcement components of the thermoplastic composite) and **(b)** TPE / intermediate composite and intermediate composite / thermoplastic composite interfaces.

■ Objectives of the thesis

This research project aimed to synthesize a novel thermoplastic elastomer capable of providing a tough and robust joining between the tank and the skirts of the launcher. This TPE must exhibit stress-strain properties comparable to these of traditional thermoset rubbers at room temperature. Moreover, a limited decrease of its mechanical properties at high temperature is desired (continuous service temperature = 10-

40 °C, maximum service temperature = 80 °C). This new TPE must be REACH compliant, with a life time of 20 years at least. Its mechanical properties do not have to be affected by contact with diestone and 1,1,1-trichloroethane.

Whatever the joining technique considered for assembling the TPE with the tank and the skirts (adhesive bonding or welding), the assembly must be stable and robust with a high tensile strength at break as well as an elevated shear modulus at 100% elongation. The cohesive fracture of the connection is also required. In the case where adhesive bonding is implemented, the candidate TPE would be heated at 160-180 °C for more than 10 hours to be effectively assembled with the adhesive. If welding is applied, significantly shorter processing time would be needed (a few minutes possibly) but higher temperature may be applied (240-280 °C). In any case, the TPE must not degrade nor flow at the joining temperature. In addition, it must be capable of preserving its properties after the bonding step.

MAIN OBJECTIVES OF THE RESEARCH PROJECT

■ Introduction

Many independent routes could have been considered for this doctoral thesis to produce a thermoplastic elastomer (TPE) satisfying ArianeGroup specifications. Due to time constraints and in order to follow a relevant route, privileged axes were selected for the following key points of the research: method of synthesis (anionic, radical, cationic...) ; type (block copolymer, rubber/plastic blend...) and nature (styrenic, polyurethane, polyester, polyamide...) of the TPE ; composition (monomers and their respective molar fraction) and morphology (spherical, cylindrical, lamellar...) of the TPE ; solutions to enhance the TPE properties (thermal stability, service temperature, mechanical behavior, weldability...). This part aims to outline the major directions chosen during this research project. Please note that no references have been added in this section purposely since each scientific point is developed and detailed more exhaustively in the next parts, particularly in the state of the art.

■ Polymerization technique

Nitroxide-mediated controlled radical polymerization (NMP), a reversible-deactivation radical polymerization (RDRP), was selected. A controlled radical polymerization was thereby preferred to another polymerization technique, such as a living ionic polymerization process, since it does not require stringent process conditions. Moreover, the difficulty to polymerize functional monomers by living ionic polymerization was a hurdle for this project since the functionalization of the candidate TPE was envisioned to enhance its joining properties. In contrast to reversible addition-fragmentation chain transfer (RAFT) polymerization and atom transfer radical polymerization (ATRP), two other RDRP processes, purely organic systems can be employed when using NMP. NMP does not require the use of sometimes unpleasant sulfur chemistry that is associated with the chain transfer agents used in RAFT. NMP systems, comprising radical initiator / nitroxide or alkoxyamine with or without additional nitroxide, are also typically simpler initiating systems compared to ATRP initiating systems, which require, at minimum, activated halide, metal halide, and ligand, but often include other additives to facilitate the polymerization. An additional advantage that NMP offers over ATRP and RAFT is in the ability to control the polymerization of conjugated 1,3-diene monomers, a first essential step to produce the desired TPE. For some time, NMP was the only RDRP method that could be used to prepare homopolymers and block copolymers of 1,3-dienes such as isoprene

and 1,3-butadiene. It was thus possible to rely on several publications reporting isoprene and butadiene polymerizations by NMP. Lastly, being co-supervised by Prof. Maric, it also appeared crucial for me to perform NMP in order to take advantage of his expertise in this specific field. The presence of commercial nitroxides and alkoxyamines in his laboratories and the competence of his research team to synthesize well-tailored monofunctional and difunctional initiators for NMP was beneficial as well. It must be added that NMP under homogeneous conditions in bulk or in organic solvents was favored. Even though promising, NMP in dispersed media (mostly water) was not implemented because of the time it might have required to find the optimal recipe.

In conclusion, NMP was essentially chosen for its simplicity to implement, its robustness for controlling the polymerization of 1,3-dienes and the knowledge of Prof. Maric's laboratories for this nitroxide-based RDRP system.

■ Type and class of TPE

Block copolymer TPE were targeted in this thesis since, as mentioned previously, a controlled radical polymerization was selected, which appeared totally adequate to synthesize well-tailored block copolymers. Thermoplastic vulcanizates (TPV) using dynamic vulcanization, polyamide elastomers synthesized by esterification and polycondensation, copolyester elastomers (COPE) manufactured by transesterification or even reactor thermoplastic polyolefins (RTPO) produced by catalytic copolymerization of olefins, were for instance disregarded. More specifically, styrenic block copolymers (SBC) were chosen considering the large variety of vinyl monomers being polymerizable by NMP and leading to the achievement of flexible, hard or even functional blocks. A triblock structure was desired since it allows generally the TPE to have higher tensile strength compared to a similar diblock copolymer, in which the rubber chains are attached to a rigid chain at only one end and are therefore not physically cross-linked. Moreover, a plethora of styrenic triblock copolymers, reported in the literature or available commercially, can be used as references. Most of them satisfy the ArianeGroup mechanical requirements at room temperature, which is a good starting point. While exhibiting typically low upper service temperature limit, modifications of the SBC in the laboratory were planned to enhance its thermal robustness as discussed below. Even though investigated by RDRP, TPE with graft (hard segments are chemically bonded to the elastomer-like main chain as pendant chains), star (rigid arms and rubbery core) or brush (glassy backbone and rubbery brushes for example) topologies were not considered.

From an experimental viewpoint, a difunctional initiator (Di-I) was favored to prepare triblock copolymers. It can be used to make the rubbery segment. This way, since the two chain ends are ideally

capped by a nitroxide moiety, the flexible block synthesized can be subsequently used as a macro-initiator to polymerize a second batch of monomer(s) in order to add two outer rigid blocks.

■ Composition and morphology of TPE

Two conjugated 1,3-diene monomers were selected to produce the flexible middle block, namely β -myrcene (*My*, 7-methyl-3-methylene-octa-1,6-diene) and isoprene (*I*, 2-methylbuta-1,3-diene). *My* was first used as an isoprene substitute building block. *My* exhibits two valuable features in comparison to isoprene: it is a natural renewable compound with low volatility (boiling point, $T_b = 167\text{ }^\circ\text{C}$) meaning that pressurized equipment is not needed to handle it. After receiving high-pressure reactors, isoprene ($T_b = 34\text{ }^\circ\text{C}$), more common for the synthesis of block copolymer TPE, was handled. Well-controlled isoprene NMP was previously studied by Hawker for instance or more recently by Harrison, which constitutes a major advantage for our research. Butadiene was disregarded for this study due to its subzero boiling point ($T_b = -4\text{ }^\circ\text{C}$) making the polymerization more demanding and its similarity with isoprene monomer. About the subsequent addition of the two outer hard blocks, poly(styrene) PS was first selected as a reference since it is used in a large majority of styrenic block copolymers. Furthermore, the NMP of styrene was comprehensively studied by Georges, Hawker, Charleux and Gigmes amongst others.

Micro-phase separation is expected due to the immiscible polymer segments of the TPE. The preparation of TPE showing a spherical morphology (hard blocks forming discrete minority spheres embedded in a rubbery matrix) was selected due to their isotropic nature. Indeed, since the spherical domains are randomly dispersed, the stress-strain behavior exhibits isotropic mechanical property. In that case, triblock copolymers having about 10-20 mol% of hard blocks were targeted (arbitrary percentages since it mostly depends on the nature of the segments used). However, higher hard blocks content going up to 40 mol% were also envisioned (cylindrical, gyroid or lamellar morphologies assumed) to increase the hardness of the TPE if needed.

■ Solutions to enhance TPE properties

After achieving optimized NMP-based styrenic triblock copolymers, modifications can be performed so that the industrial requirements can be satisfied. First, the functionalization of the TPE can be implemented since this latter is supposed to be welded to relatively polar thermoplastic composites. The goal was thus to increase the miscibility at the welding interface to favor chains inter-diffusion. Even if an adhesive bonding is first processed with thermoset composites, the incorporation of functional units into the TPE could be valuable to promote covalent bonding at the interface. Considering the distinct advantage

of NMP about its robustness to readily add functional groups, it was decided to perform the TPE polar modification by copolymerizing directly the diene monomer with glycidyl methacrylate (GMA), carrying an epoxide group.

Secondly, poly(styrene) blocks (glass transition temperature, $T_g \sim 100\text{ }^\circ\text{C}$) initially considered can be substituted to higher T_g hard blocks to improve the tensile stress and the service temperature of the TPE. This latter characteristic is of great interest for ArianeGroup since the candidate TPE must maintain its mechanical performance until $80\text{ }^\circ\text{C}$ and support welding process and adhesive bonding process temperatures ($T > 160\text{ }^\circ\text{C}$). Poly(isobornyl methacrylate) P(IBOMA) ($T_g \sim 190\text{ }^\circ\text{C}$) can be considered as a hard component substitute although several other hard segments could be used by NMP such as poly(α -methylene- γ -butyrolactone) P(MBL) ($T_g \sim 190\text{-}200\text{ }^\circ\text{C}$).

The active feature of NMP-based polymers is based on the reversible capping of the active chain-end radical with a nitroxide leaving group. At the end of the synthesis, chain-ends should thus be ideally terminated by a thermally labile nitroxide moiety. Removing the nitroxide groups after synthesis, which will prevent their liberation during subsequent heating processes (extrusion, injection, welding, adhesive bonding, hydrogenation...), can enhance thermal stability. Accordingly, this step appeared necessary for our optimized TPE. Many efficient strategies have been reported to remove the terminal nitroxide and can be directly applied in our situation. Lastly, a second post-polymerization process termed hydrogenation was envisioned regarding the soft poly(diene) middle block. Achieving a TPE having a saturated mid-segment could improve its resistance to the thermal and oxidative degradations. Moreover, higher TPE tensile strength can be expected after hydrogenation, which can be valuable for this industrial problematic.

■ **Conclusion:** We proposed to perform NMP in bulk or in organic solvents using a difunctional initiator to synthesize linear styrenic triblock copolymers, exhibiting ideally a spherical nano-phase separation. Poly(β -myrcene) or poly(isoprene) were considered as constituting the elastomeric middle block (60-90 mol% of the TPE) whereas two outer poly(styrene) blocks were envisioned to provide rigidity (10-40 mol% of the TPE), as depicted in [Figure 5](#) below. Four chemical modifications were planned to improve the candidate TPE properties: functionalization of the poly(diene) segment by adding glycidyl methacrylate units (encouraging the joining process); replacement of PS blocks by higher T_g hard blocks (increasing the tensile stress and broadening the service temperature); nitroxide removal (thermal stability enhancement); hydrogenation of the soft block (higher tensile stress and degradation temperature). [Figure 6](#) shows schematically these various modifications.

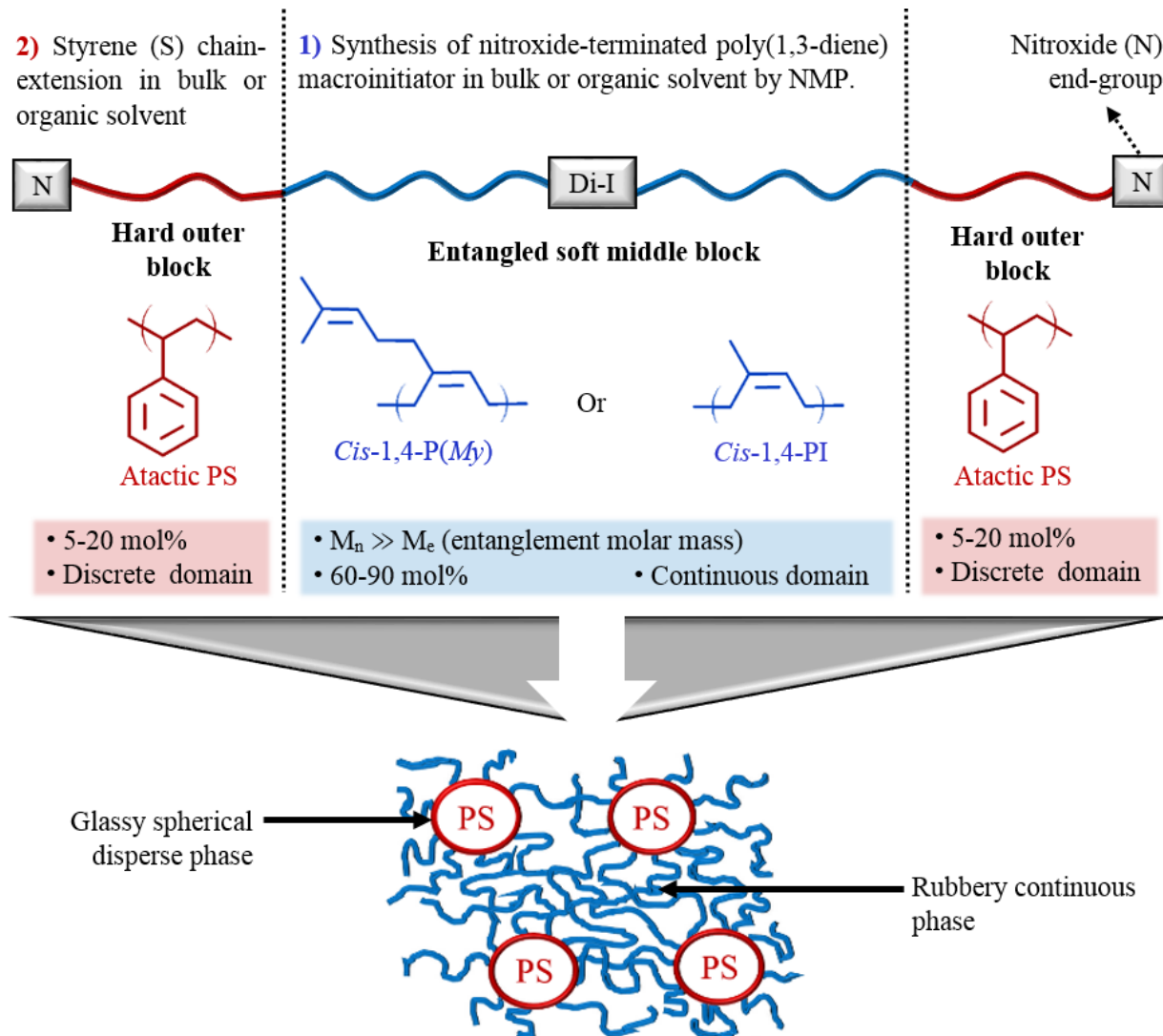


Figure 5. Summary outline of the linear styrenic triblock thermoplastic elastomer envisioned for this thesis. The difunctional initiator Di-I used corresponds to a dialkoxyamine. According to NMP mechanism when all the suitable parameters are met, nitroxide groups (N) are attached to the two TPE chain ends. The schematic at the bottom represents the expected nano-phase separation of the TPE, where PS rigid spheres act as physical crosslinks.

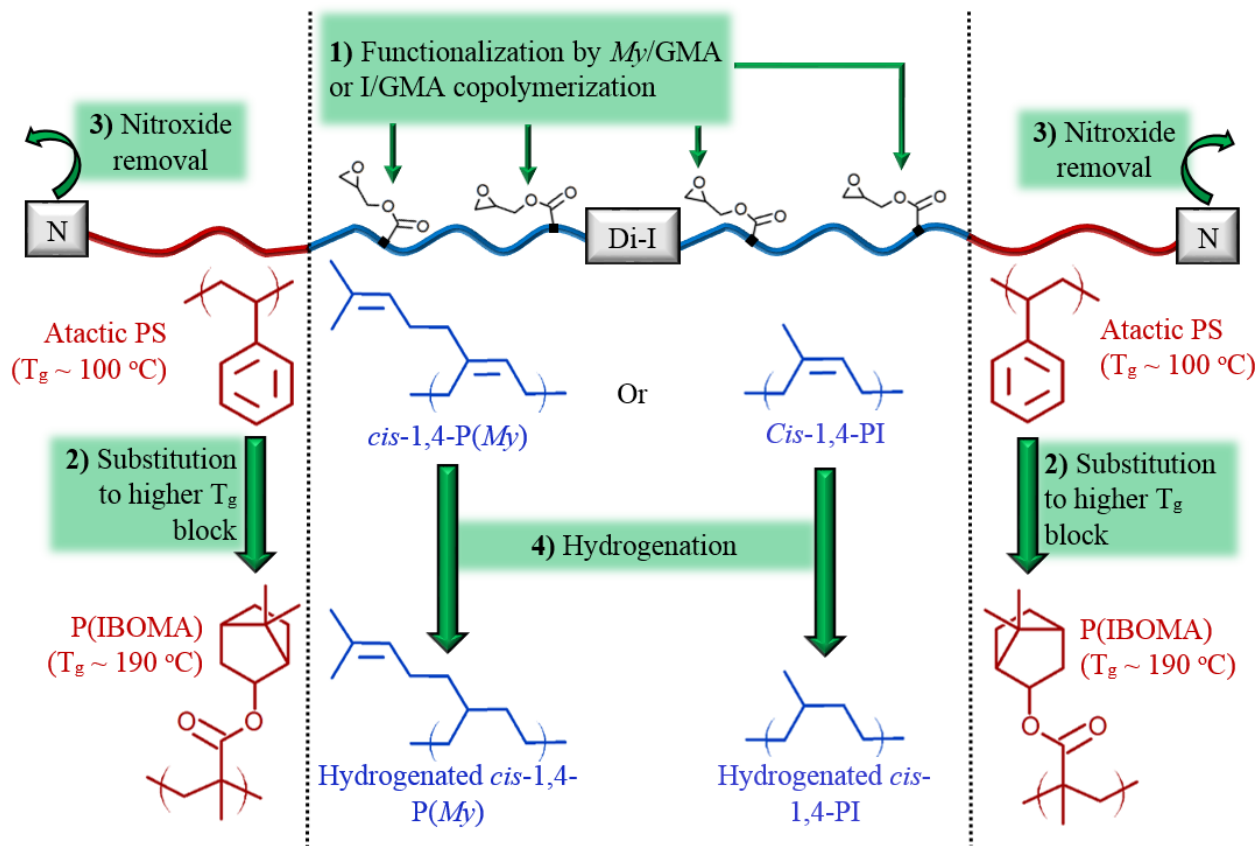


Figure 6. Summary outline of the different ways considered in this thesis to improve TPE properties. The notations from 1) to 4) correspond to the chronological order to perform the modifications. Poly(isobornyl methacrylate) P(IBOMA) is mentioned herein as an example to replace the PS outer blocks.

THESIS OUTLINE

■ A collaborative project

This industrial thesis (thèse CIFRE-défense), done from January 2015 to December 2017, was predominantly financed by ArianeGroup with a financial assistance from the French government via the French Defense Procurement Agency (Direction Générale de l'Armement, DGA). Dr. Brigitte Defoort, from the composite materials laboratory at ArianeGroup, coordinated the project. M. Bruno Mortaigne was my DGA responsible. Dr. Jean-François Gérard, professor and former research director at INSA Lyon and currently chairman of the European Polymer Federation (EPF), was my thesis director. Prof. M. Maric and Prof. P. Hubert, respectively from the Departments of Chemical and Mechanical Engineering at McGill University, were my thesis co-supervisors. Even though solely registered at "Institut National des Sciences Appliquées (INSA) de Lyon", as a PhD student, I spent time at McGill University as a visiting PhD candidate under the supervision of Prof. M. Maric, to synthesize and characterize polymers. The laboratories of Prof. P. Hubert were also used to implement mechanical tests. I also worked at the laboratory "Ingénierie des Matériaux Polymères (IMP)" from INSA Lyon under the supervision of Prof. Gérard to review the literature and characterize the polymer materials.

It must be added that this research was explored jointly with another ArianeGroup project led by PhD candidate David Brassard from Polytechnique Montreal and co-supervised by Prof. J. R. Tavares from Polytechnique Montreal and Prof. M. Dubé from ETS (École de Technologie Supérieure) Montreal. This second project falls totally within our industrial issue since David Brassard aims to develop a welded flexible junction between two filament wound thermoplastic composite parts, while focusing mostly on the welding process. This junction is composed of a thermoplastic elastomer welded to the composite components. David Brassard uses an extra electrically conductive nanocomposite heating element for the resistance welding process implemented.

■ Structure of the PhD manuscript

Following these introductory sections (pages 1-41), three main parts constitute this thesis. The first part (pages 43-92) reviews the literature relevant to the industrial problematic with an emphasis on the thermoplastic elastomers targeted for this research project and their synthesis. The second and third parts present, in the form of chapters, the experimental work led throughout the doctoral thesis in chronological order. To alleviate the chapters, the respective appendices containing the experimental sections along with the supporting information are given at the end of the PhD manuscript (pages 269-328). Please note that at the beginning of each chapter appears a preface, specially added for the PhD manuscript, to make the transition from the previous chapter to the new chapter. It explains concisely the reasons that prompted us to lead the study in question. It must be noted that the references are gathered at the end of each chapter (or part, in the case of the literature review).

The second part (pages 95-207) clusters all the experimental studies based on the use of poly(β -myrcene) P(*My*) as the soft block of the candidate TPE. Whatever the status of the chapters (published, submitted or not submitted), they are all written in a paper-based format:

- **Chapter 1** (pages 97-139), a manuscript published in the journal *Macromolecules*, details the optimized synthesis by nitroxide-mediated polymerization of well-defined P(*My*) leading to the achievement of β -myrcene / styrene (*My*/S) block copolymers (first year of the PhD, 2015). It sums up the preliminary attempts to achieve satisfactory *My*-based thermoplastic elastomers (TPE), using poly(styrene) PS hard blocks. Please note that the section 1.4.3 regarding the synthesis of S-*My*-S triblock copolymers was not present in the original publication and was added to the PhD manuscript.

- **Chapter 2** (pages 141-172), a manuscript published in the *Journal of Polymer Science, Part A: Polymer Chemistry*, presents the well-controlled nitroxide-mediated copolymerization of *My* with glycidyl methacrylate (GMA). Led in parallel with the experiments presented in Chapter 1, this study aimed to functionalize the soft middle block (herein P(*My*)) of the candidate TPE in order subsequently to encourage the adhesive bonding or welding process with the relatively polar thermoplastic composite.

- **Chapter 3** (pages 175-207), a manuscript which will be soon submitted to the journal *Polymer Chemistry*, introduces the synthesis of β -myrcene / isobornyl methacrylate (*My*/IBOMA) copolymers by NMP (second year of the PhD, 2016). The goal was to produce enhanced *My*-based block copolymers by replacing PS segments by P(IBOMA) hard blocks exhibiting a higher glass transition temperature.

Since *My*-based copolymers were not satisfying ArianeGroup requirements, the substitution of P(*My*) by poly(isoprene) (PI) as the rubbery component was undertaken. The third part (pages 209-249), corresponding to the work led during the second half of the doctoral thesis, is devoted to the synthesis of isoprene-based triblock copolymers as well as the characterization of commercial thermoplastic elastomers mostly based on isoprene. Unlike the previous chapters, which were more academic, these sections are more technical and industrially oriented. They are thereby purposely more concise and results-based. Two chapters are introduced:

- **Chapter 4** (pages 211-237) is dedicated to the achievement of linear isoprene-based triblock copolymers by NMP. S-I-S triblocks exhibiting various molar fractions of styrene unit were first synthesized and characterized. The incomplete hydrogenation of the PI mid-segment was performed. PS blocks were then replaced by P(IBOMA) blocks to produce isoprene-based triblocks exhibiting higher upper service temperature, tensile strength at break and elongation at break.

- **Chapter 5** (pages 239-249) details the characterization and the hydrogenation of some commercial styrenic block copolymers, allowing comparative study with the experimental NMP-based block copolymers synthesized.

Finally, a general conclusion summing up the work conducted over this research project and the recommendations for future work are given (pages 251-267).

PART I. LITERATURE REVIEW

A. Introduction

Thermoplastic elastomers (TPE) combine the functional properties of comparable thermoset elastomers with the manufacture advantages of thermoplastics. They are defined as *“a family of rubber-like materials that, unlike conventional vulcanized rubbers, can be processed and recycled like thermoplastic materials”* (ASTM D1566). These materials of interest are highlighted in this state of the art, organized according to the industrial problematic. Three main sections constitute the literature review.

The first section (B, pages 47-59) is dedicated to the thermoset elastomers and block copolymer TPE and highlights the industrial benefits of using thermoplastic polymers in order mainly to implement advantageous joining processes. After defining the notion of elasticity, the state of the art introduces the traditional thermoset elastomers, used massively in the industry, and their main shortcomings. A focus on nitrile rubber (NBR), a commercial vulcanized elastomer currently used by ArianeGroup to provide the tough joining in question between thermoset composites, is supplied as well. Block copolymer TPE, which can be seen as a way of substitution of the vulcanized rubbers, are then presented. This transition from thermoset to thermoplastic polymers follows the desire of ArianeGroup to replace thermoset elastomer/composite by thermoplastic materials. It should be noted that three major types of TPE exist, namely: block copolymers; rubber/plastic blends; dynamically vulcanized rubber/plastic alloys denoted as thermoplastic vulcanisates. This literature review is intentionally focused on the block copolymer TPE, to narrow down the scope of the research area and to be in line with the industrial project. The concept of physical crosslinks, the phase structure and the phase separation of these copolymers are introduced to understand their peculiar thermoreversible networks. Furthermore, the main advantages of block copolymer TPE over thermoset rubbers are given to support the desired changeover from conventional thermosets to new thermoplastics exhibiting similar properties. Eventually, joining techniques, corresponding to one of the main industrial key issue, are presented for thermosets and thermoplastics. The possibility to perform welding (or thermal bonding) for thermoplastics, a promising method offering many advantages over the other joining processes, is underlined.

The second section (C, pages 60-80) focuses on the general properties of styrenic block copolymers (SBC), the family of TPE selected for this project. It is first of importance to know how to optimize the formulation of these materials to achieve the desired properties. The influences of the nature of the poly(diene) middle block, the average chain length and the styrene fraction over the characteristics of these

TPE are thus discussed. Moreover, the glass transition temperature (T_g) of PS blocks limiting the upper service temperature of styrenic block copolymers, the substitution of the typical PS segments by higher T_g hard blocks is then presented. After synthesis, post-polymerization modifications of styrenic TPE can be envisioned as well to strengthen its properties. Hydrogenation of the poly(diene) midsegment, introduced subsequently, allows the resulting TPE to be mostly more stable thermally and tougher. Considering that the candidate TPE has to support welding or adhesive bonding process at $T > 160$ °C, such an enhancement could be valuable. Eventually, attention is paid to directly available commercial SBC, which can be used as references for the experimental block copolymers synthesized in laboratory.

The last section (D, pages 81-88) of this literature review is devoted to the various polymerization techniques used to make styrenic block copolymer TPE. Living anionic polymerization, proceeding by formation of carbanions at the polymer chain ends, was first introduced. Applied industrially, it is the most robust and effective technique to manufacture well-defined styrenic TPE such as SBS and SIS. Living cationic polymerization, allowing the synthesis of well-defined poly(isobutylene), poly(styrene) and poly(styrene) derivatives, can also be employed to prepare some interesting block copolymers. Despite the excellent results obtained from living ionic polymerizations, several main constraints appear regarding our industrial project: the stringent and demanding experimental conditions required combined; the non-negligible number of preliminary steps to follow prior to the polymerization; the difficulty to polymerize functional monomer. Accordingly, the use of a reversible-deactivation radical polymerization (RDRP), which does not require demanding experimental conditions and can be apply to a large range of monomers, is promising. The synthesis of block copolymer TPE via the three main RDRP processes, namely atom-transfer radical polymerization (ATRP), reversible addition-fragmentation chain transfer (RAFT) and nitroxide-mediated polymerization (NMP) are presented. Due to its capability to control effectively 1,3-diene monomers and its simplicity of implementation, NMP appears to be an appropriate synthesis method for the industrial problematic.

B. From thermoset to thermoplastic elastomers (TPE)

B.1. Elasticity and thermoset elastomers

Please note that the terms ‘*elastomer*’ and ‘*rubber*’ are mentioned herein in the exact same way as a polymer showing the property of ‘viscoelasticity’ (colloquially ‘elasticity’, defined below).

B.1.1. What is an elastomer?

Considered as the most versatile of engineering materials, elastomers are an important class of polymers exhibiting randomly distributed chains connected by crosslinks. They behave very differently from plastics and metals, particularly in the way they deform and recover under load. Elastomers consist of relatively long polymer chains, which by their high degree of flexibility and mobility allow a significant deformation¹.

One of the most important property of an elastomer is its elasticity which can be defined as the ability of the rubber to return to its original shape and size after being stretched, compressed, twisted or bent². Elastic deformation lasts only as long as a deforming force is applied and disappears once the force is removed. When a stress is applied, the configuration of the chains may be changed rapidly due to the high mobility of the elastomer. Thanks to the crosslinking of the network (formation of a three-dimensional structure from a linear polymer by a chemical or physical method)³, the macromolecules are prevented from flowing relative to each other under stress. On removal of the external force, the rubber is rapidly restored to its original dimensions, with essentially no residual or non-recoverable strain. Without the crosslinks, the applied stress would result in a permanent deformation. It is of importance to underline that the response of the rubbery polymer is intramolecular. The force is transmitted to the chains through the linkages at their extremities. The chains exhibit then a different conformation and act like an individual spring, according to Hooke’s Law⁴. The elastomer undergoes immediate, linear and reversible high strain to an applied force. The extensibility is caused by uncoiling of the random molecular coils (high entropy) into more linear conformations (lower entropy). The limit to elastic response is reached when the macromolecules are fully extended (one conformation resulting in a minimal entropy)⁵. A representation of the two different conformations is depicted in [Figure 7](#).

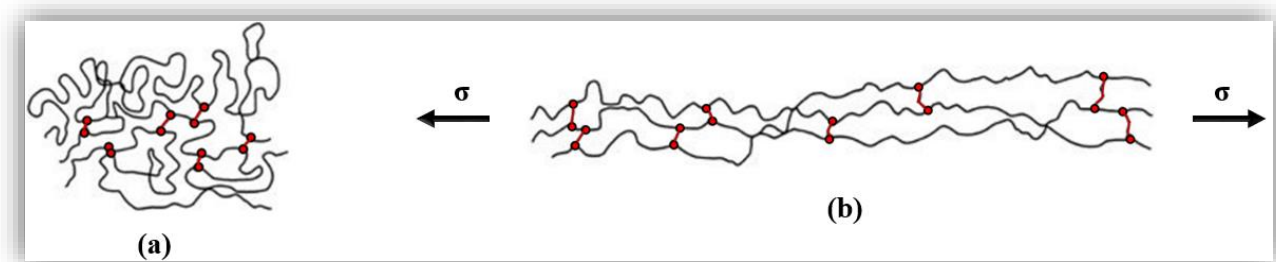


Figure 7. Schematic of crosslinked (in red) elastomer macromolecules **(a)** unstretched (random coil structure) and **(b)** under uniaxial tensile stress.

Another essential feature of an elastomer is its excellent resilience. Resilience as applied to elastomers is essentially their capacity to return rapidly to their original shape after temporary deflection. It indicates thereby the speed of recovery, unlike compression set, which measures the degree of recovery. When an elastomer is deformed, an energy input is involved, part of which is not returned when it regains its original shape. This part of the energy which is not returned is dissipated as heat in the elastomer. The ratio of energy returned to energy applied to produce the deformation is defined as the material's resilience⁶. Furthermore, reversibility and immediate response are obtained with macromolecules that have flexible chains with weak intermolecular forces. The large reversible strain must be rapid which means the restraining intermolecular forces must be minimal. Consequently, polar groups and hydrogen bonding groups are not desirable if a polymer is to be an elastomer. Steric hindrance via bulky pendant groups or rigid intra-chain groups has to be minimal as well to encourage the uncoiling. The arrangement of the macromolecules and their configuration is also of importance. The amorphous nature of the elastomer results from the irregularity of the chains due to the difference in geometrical arrangement. Formation of unstrained random coils means that the elastomer must be non-crystalline since any regular crystal structures would be unable to contribute to elastomeric properties. These latter are optimized with the *cis* configuration although the motion of the bonded carbon atoms is limited by the double bond. The *trans* configuration favors a regular planar zig-zag conformation that may crystallize⁵.

The majority of elastomers have a number of other interesting features such as: low permeability to air, gases, water and steam; good electrical and thermal insulation; good mechanical properties; ability to adhere to various fibers, metals and plastics. It should be added that rubbers with improved or specific properties can be produced to meet a wide variety of service conditions by adequate selection of compounding ingredients. This combination of properties is the reason elastomers are used in a large number of engineering needs in fields dealing mainly with sealing, shock absorbing, vibration damping, and electrical and thermal insulation⁵.

Historically, most elastomer components were manufactured using vulcanization, which prompts us to introduce the family of the thermoset elastomers.

B.1.2. Thermoset elastomers

Most types of elastomers are thermosets. It consists of single-phase materials, without the dual hard and soft phases, which can be polymerized as homopolymers or random copolymers/terpolymers. The structure is amorphous, exclusive of crystalline domains, which means that these rubbery materials undergo a glass transition temperature, but no melting point.

Thermoset elastomers gain most of their strength after vulcanization, an irreversible crosslinking of their polymer chains that occurs when the compound is subjected to pressure and heat in the presence of sulphur⁷. The polymer is traditionally crosslinked after molding or shaping to fix molecules into their positions. A thermoset elastomer typically consists of a rubber-like polymer containing a reinforcing filler, a plasticizing agent, one or more stabilizers, a crosslinking agent, commonly sulfur, several accelerators which increase the rate of crosslinking, and additives as needed. The crosslinking reaction is a rate limiting step in the manufacturing process to form conventional thermoset rubber articles. Much of the attention paid to forming these articles has focused on developing the formulations, known as compounds. These compounds must achieve the performance requirements and also chemically react in sufficiently controlled fashion to crosslink as quickly as possible at the time desired in the processing, but not prior⁷. The vulcanization of *cis*-1,4-poly(isoprene) is illustrated in [Figure 8](#).

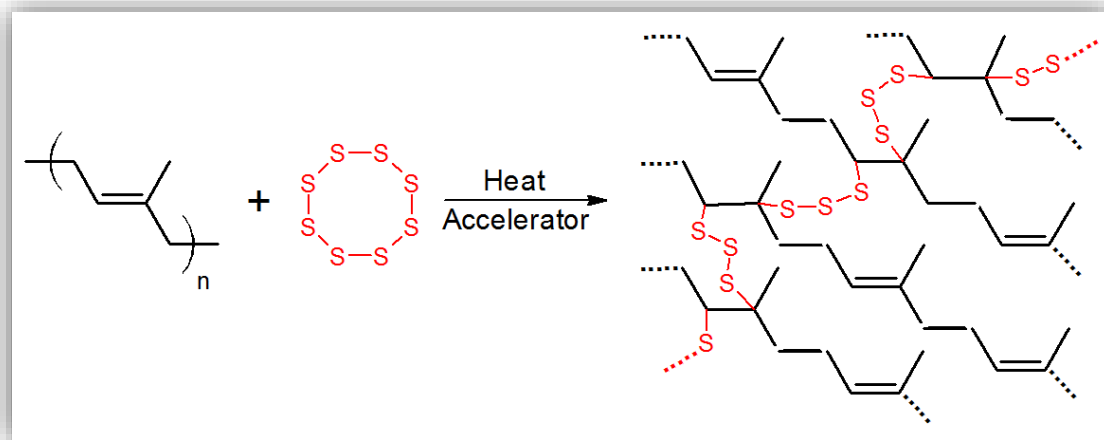


Figure 8. Brief synthetic route of the vulcanization of *cis*-1,4-poly(isoprene) using sulfur curing agent S₈ generating disulphide covalent bonds between the flexible macromolecular chains.

Some well-known thermoset elastomers can be cited. Natural rubber (NR, *cis*-1,4-polyisoprene), obtained from *Hevea brasiliensis* tree, is regularly used after compounding with vulcanizing agents, antioxidants and fillers. NR has high abrasion or wear resistance, electrical resistance, chemical resistance to acids, alkalies and alcohols and damping or shock absorbing properties. It is applied extensively in manufacturing truck tires, off-the-road giant tires and aircraft tires⁸. Styrene-butadiene thermoset rubber (SBR) is an appropriate material for automobile tires thanks to its excellent abrasion resistance⁵. Ethylene-propylene-diene monomer (EPDM) thermoset elastomer is a synthetic rubber having outstanding heat, ozone and weather resistance due to its stable, saturated polymer backbone structure. EPDM is mainly used as a standard lining material for steam hoses, automotive weather-stripping and seals, radiator, electrical insulation and roofing membrane⁵. The structures of NR, SBR and EPDM are shown in Figure 9.

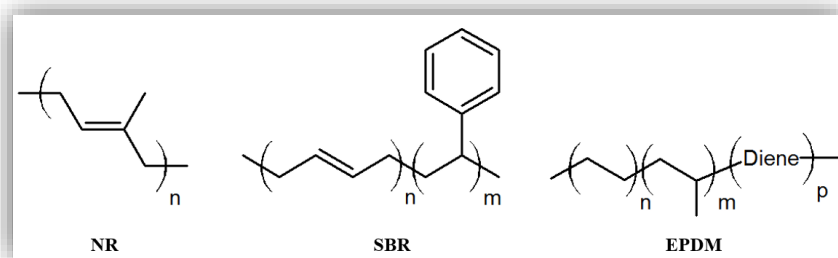


Figure 9. Repetitive units of natural rubber (NR) homopolymer and styrene-butadiene (SBR) and ethylene-propylene-diene monomer (EPDM) copolymers.

More attention can be paid to acrylonitrile–butadiene rubber (or nitrile-butadiene rubber, NBR) since it is the synthetic thermoset elastomer currently used by ArianeGroup to assemble the soft junction as discussed above in the industrial issue part. Typical cure for NBR is performed using sulfur. With the combination of accelerators, a service temperature ranging from 125 to 135 °C can be reached. The butadiene segment imparts elasticity and low temperature flexibility. It contains unsaturated bonds that are the site for crosslinking such as vulcanization. It is also the main attack site for heat, chemicals and oxidation. On the other hand, the acrylonitrile segment imparts hardness, tensile strength, abrasion resistance, and heat resistance among other things. By reason of polarity, the acrylonitrile content determines basic properties such as oil resistance or solvent resistance. That is the reason why appropriate acrylonitrile content has to be selected so that balanced properties are achieved. Commonly, this rubber contains between 34 and 40 mol% of acrylonitrile repetitive units, as an industrial standard. This gives the most versatile compound performance for oil swell and low temperature properties. The major advantages

of NBR are a high resistance to petroleum oils, mineral oils, vegetable oils, aliphatic hydrocarbons and many acids in addition to good elongation properties, excellent tensile strength as well as adequate resilience and compression set. Its limitations are its cost and its slow decay on contact with ozone, sunlight and weathering. Moreover, it has poor resistance to ketones, esters, aldehydes, chlorinated and aromatic hydrocarbons. Nitrile rubber is widely used in automotive industry as automotive seals and gaskets, which subject to contact with hot oils. It is used as automotive water handling applications and in fuel and oil handling hose as well. In healthcare industry, its resilience makes it a perfect material for non-latex gloves⁹. Table 2 below sums up the main properties of industrial NBR containing between 18 and 50 mol% of acrylonitrile units¹⁰⁻¹².

Properties	NBR
Physical	
Specific gravity (g.cm ⁻³)	1.0 to 1.4
Refractive index	1.54
Mechanical	
Elongation at break (%)	350 to 600
Tensile strength at break (MPa)	3.5 to 27
Hardness, shore A	30 to 95
Young's Modulus at 300% elong. (MPa)	62 to 68
Thermal	
Minimum service T (°C)	- 50 to - 20
Minimum T for continuous use, static (°C)	- 40
Maximum service T (°C)	+ 100 to + 120
Maximum for continuous use, static (°C)	+ 120
Brittle point (°C)	- 60 to 0
Glass transition T (°C)	- 38 to - 2

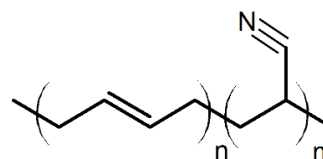


Table 2. Some physical, mechanical and thermal characteristics of NBR exhibiting an acrylonitrile content ranging from 18 to 50 mol%¹⁰⁻¹² (industrial sources: RobinsonTM Rubber Products Company; K.C. Seals Inc.). The structure of NBR is given to the right of the table.

Thermoset rubbers offer distinct performance advantages over similar thermoplastic polymers thanks to their permanent crosslinked structure. High chemical resistance and thermal stability associated with excellent creep/set resistance are generally exhibited by these vulcanized materials. However, some non-negligible shortcomings appear when handling thermoset polymers. The permanent state brought about by crosslinking and the need to perform a crosslinking reaction on elastomers are disadvantages for their

applications¹³. Thermoset rubbers require mixing of curatives, stabilizers, process aids and other additives. The part-to-part consistency is not optimal due to the compound difference that can be caused by the variations in weighing and metering of the various components. On the other hand, little to no compounding or mixing is required for thermoplastics. The thermoset rubber process includes several steps such as mixing, shaping and vulcanization, which can make the operation costly and reduce the reproducibility of the fabrication. The processing operation for a thermoset has longer cycle times due to the type of process involved (compression molding) and the need for vulcanization. Typically, thermoset process cycle times are measured in minutes whereas thermoplastic ones are in seconds. Consequently, the production rate for thermoplastic materials, whose process uses less energy, is much greater. While a thermoplastic scrap can be reground and reprocessed with no significant loss in performance, a vulcanized rubber cannot be reprocessed. It must be ground to a powder or crumb form to be recycled and then only be used as a filler material. It is traditionally treated as scrap and must be disposed of as waste since thermoset rubber process scrap has limited reuse capability. This limitation has been a source of economic and environmental concern for conventional thermoset rubber. Expanded thermoset rubber goods pose an end-of-life disposal concern given their lack of recyclability. Since more scrap is produced in thermoset rubber processing, the production cost is made higher by the loss of material and disposal cost of the scrap¹⁴.

In direct connection with the industrial problematic, another major inconvenient can be mentioned: some thermoplastic processes, such as bloc molding, thermoforming and heat welding, are not possible with thermoset rubbers. In the manufacturing of aerospace composite structures, thermal bonding or welding has great potential for the joining and offers many advantages over other joining techniques. However, this method cannot be applied to thermoset materials since they cannot melt. It follows that thermoset and vulcanized rubber components can only be joined using adhesive bonding or mechanical fastening methods¹⁵.

Taking these shortcomings into account, it is legitimate to look for high-performance rubbers which are not chemically crosslinked and exhibiting properties as good as those of vulcanized rubbers.

B.2. Block copolymer TPE

Please note that the following literature review only focuses on block copolymer thermoplastic elastomers (TPE).

B.2.1. Physical crosslinks

Polymers having a significant average chain length generate entanglements by molecular intertwining with a spacing in the bulk state depending on the particular macromolecular structure. A polymer melt with a high degree of polymerization can thus exhibit transient rubber-like behavior even in the absence of any permanent intermolecular bonds¹⁶. In a crosslinked elastomer, many of these entanglements are permanently locked in and, at high enough degree of crosslinking, they may be regarded fully equivalent to crosslinks, contributing to the elastic response of the material. Generally, a network is obtained by linking of polymer chains together. The chemical and permanent crosslinking of elastomers, mostly via vulcanization, was discussed above. Physical crosslinks, which can be defined as non-covalent and thermo-reversible intermolecular bonds holding polymer chains together in network under some conditions but not under others, can be generated as well. Physical crosslinks interconnect polymer chains using interactions other than covalent bonding, such as hydrogen bonding, hydrophobic interaction, ionic bonding, and coordination bonding. The key parameter is temperature. The bonds are strong at low temperatures, but the materials can flow at higher temperatures due to the disappearance of these physical crosslinks. These latter can be mostly formed in three distinct polymeric networks:

- Partially crystalline polymers for which the crystalline regions are embedded in the amorphous matrix and serve as physical crosslinks. For instance, the crystalline regions in low density polyethylene can behave in this way. The flexible chains surrounding the crystallites impart extensive deformability to the material¹⁷.

- Ionomer formation where ionic groups such as sodium methacrylate may be introduced along a polymer chain. At a level of about 5 mol%, a segregation takes place with the ionic groups forming small ionic domains¹⁸.

- Two-phase block copolymers comprising of a major proportion of a soft segment, affording the flexible elastomeric nature, and a minor proportion of a hard segment, providing both physical cross-link sites and filler reinforcement characteristics¹⁹.

This latter polymeric network is characteristic of a large group of polymers denoted as block copolymer thermoplastic elastomers (TPE). They can be defined as block copolymers with thermos-reversible crosslinks which can be processed as thermoplastics (by melt processing) and exhibiting elastic behavior similar to that of chemically crosslinked conventional elastomers in a certain temperature range²⁰. Attention can be now paid to the peculiar structure of block copolymer TPE.

B.2.2. TPE microstructure

Block copolymer thermoplastic elastomers (TPE) display phase-separated morphologies. One phase displays hard behaviour at ambient temperature whereas the other is an elastomer exhibiting a sub-zero glass transition temperature (T_g). The phases are bonded chemically by block polymerization. The hard phase gives these TPE their strength and leads to physical crosslinks. Without the physical crosslinking, the elastomer phase would be free to flow under stress and the polymer would be practically unusable. On the other hand, the elastomer phase provides flexibility and elasticity to the system. When the hard phase is melted or dissolved in a solvent, the material can flow and can be processed by usual thermoplastic processing. The individual polymers constituting the respective phases retain most of their characteristics so that each phase exhibits its specific T_g or crystalline melting temperature (T_m). T_g and T_m are the temperatures at which the particular elastomer goes through transitions in its physical properties²¹. Figure 10a shows briefly the measurement of the flexural modulus *versus* temperature for block copolymer TPE. There are three distinct regions:

- Below the glass transition of the elastomeric phase, the copolymer is stiff and brittle since both the phases are glassy.

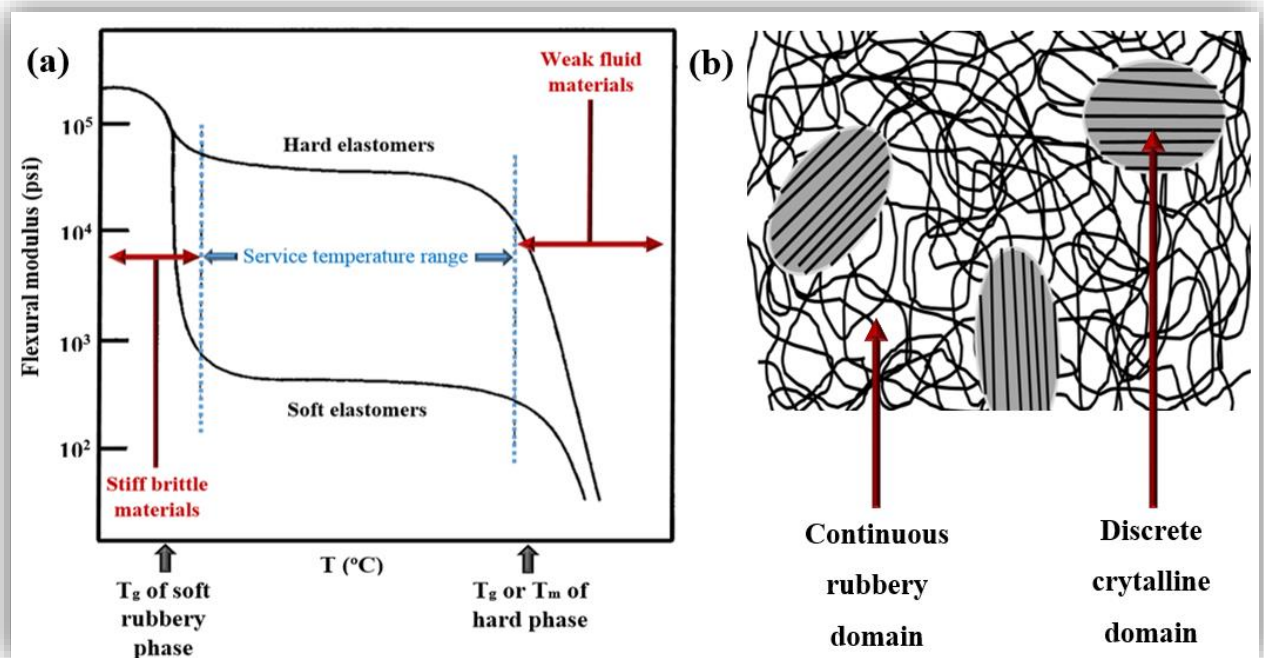


Figure 10. (a) General trends of flexural modulus (stiffness) of a typical block copolymer TPE in dependence of temperature and (b) schematic of the morphology of a block copolymer TPE.

- Above its T_g , the elastomeric phase softens, and the material is elastic, resembling a conventional vulcanized rubber.

- As the temperature increases, the modulus stays relatively constant (a region referred to as “rubbery plateau”) until the point where the hard phase softens or melts. At this point, the material becomes a viscous fluid. Above the crystalline melt temperature or the glass transition temperature of the rigid domain, the block copolymer chains are no longer locked into position and all the chains are free to flow.

Accordingly, the service temperature range lies usually between the T_g of the elastomeric phase (lower service temperature) and the T_g (or T_m) of the hard phase (upper service temperature). A simple representation of the structure of a block copolymer TPE is given in [Figure 10b](#). The hard crystalline regions act as physical crosslinks and the soft rubbery phase provides the overall flexibility of these copolymers. The rubbery phase does not crystallize with the rigid blocks and form a continuous domain of softer chains. These flexible macromolecules are held together by the crystalline domains, which allow to lock the copolymer chains in specific locations. When these copolymers are deformed, the hard blocks remain crystalline and do not deform. The soft rubbery phase is easily deformed and provides elastic behavior. The recovery of these materials is good as long as the domains are not strained too greatly, and the temperatures are well below the T_g (or T_m) of the hard segments²².

B.2.3. Micro(nano)-phase separation

To obtain valuable mechanical properties in a two-component polymeric system, the two components must not be totally incompatible nor fully soluble (homogeneous phase). Most of systems are compatible to the extent that a minimum degree of mixing is apparent or interfacial bonding is generated directly, such as in graft or block copolymers. The polymer incompatibility is due to the very small entropy gained after mixing different sorts of macromolecules. In the limit of high average molecular weight, only polymer pairs with zero or negative heats of mixing form one phase. Generally, materials mix to form a single-phase system if the free energy of mixing (ΔG_m) is negative. ΔG_m can be expressed in terms of enthalpy of mixing (ΔH_m) and entropy of mixing (ΔS_m):

$$\Delta G_m = \Delta H_m - T\Delta S_m$$

where T is the temperature. Phase separation occurs if $\Delta G_m > 0$, thus, $\Delta H_m > T\Delta S_m$. It has to be considered that ΔH_m for hydrocarbon polymers is almost always positive because of the lack of strongly interacting

groups. ΔH_m increases as the structures of the two polymers forming the segments become less alike. The temperature and the entropy of mixing will always be positive, $-T\Delta S_m$ will always be negative. Nonetheless, $-T\Delta S_m$ will tend to zero as the average molecular weights of the blocks become high and/or as the temperature decreases. Accordingly, it appears obvious that three main parameters favor phase separation: blocks with highly different structures; blocks with high average molecular weight; low temperature^{23,24}.

Unlike blend of polymers, where the different polymers can separate at macroscopic scale, the separation occurs at the microscopic (or nanoscopic) scale for block copolymers. This is explained by the covalent bond linking the blocks of different polymers, which forces them to regroup in smaller domains. The two (or more) distinct and incompatible segments provide unique solid state and solution features to block copolymers, which can then be used for a variety of applications. The microphase separation in block copolymers gives rise to formation of various types of microdomains, including spherical, cylindrical, lamellar, and others. The phase behavior of undiluted A-B diblock copolymers is essentially determined by three factors: the overall degree of polymerization N ; the architectural constraints and the composition of the diblock (overall volume fraction of the segment A); the A–B segment–segment Flory–Huggins interaction parameter χ_{AB} ²⁵. While the first two parameters are controlled by the polymerization conditions and affect the translational and configurational entropy, χ_{AB} is determined by the selection of the monomers A and B. χ_{AB} has a temperature dependence given by:

$$\chi_{AB} = \alpha / T + \beta$$

where α and β are constant depending on composition and architectural constraints of the block copolymer²⁵. At equilibrium, the block copolymer macromolecules are in the lowest free energy configuration. Increasing χ_{AB} by lowering the temperature encourages a reduction of the contact between A and B. If N is high enough, it is accomplished with some loss of translational and configurational entropy by local compositional ordering. Such local segregation is referred to as *microphase separation* in the block copolymer. Alternatively, if χ_{AB} or N is low enough, the entropic factor will be predominant, resulting in a compositionally disordered phase. Since the entropic and enthalpic contributions to free energy density scale respectively as N^{-1} and χ_{AB} , the product $\chi_{AB} N$, termed the reduced interaction parameter or lumped interaction parameter, imposes the block copolymer phase state. When $\chi_{AB} N$ is higher than a specific value for the considered system, the microphase separated structure evolve below which the system is in the disordered state. This phenomenon is called order-disorder transition (ODT)²⁶. As the temperature is raised above a certain critical value, the microdomain structure disappears completely, giving rise to a disordered homogeneous phase. The temperature at which the microdomain structure completely disappears is referred

to as the order-disorder transition temperature (T_{ODT}). This transition is depicted in [Figure 11](#) for a symmetric A-B diblock copolymer.

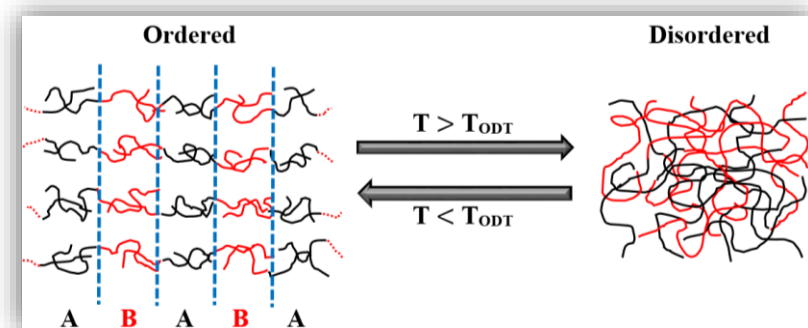


Figure 11. Schematic illustration of the thermally reversible order-disorder transition for a symmetric A-B diblock copolymer ($F_A = 0.50$). Accordingly, a lamellar morphology represents the ordered phase at $T < T_{ODT}$.

For a symmetric A-B diblock copolymer (i.e., $F_A = 0.5$), the transition occurs when $\chi_{AB} N \approx 10.5$. At sufficiently large values of $\chi_{AB} N$, different ordered structures are obtained and are represented in the form of a phase diagram ([Figure 12](#)). For $\chi_{AB} N \ll 10.5$, the copolymer melt is disordered and homogeneous and the A-B interaction is sufficiently low that the individual chains assume unperturbed Gaussian statistics. At $\chi_{AB} N \approx 10.5$, a weak demixing between the blocks A and B is apparent. The repulsion between the blocks is strong enough that phase separation occurs. This regime is called *weak segregation limit* and the copolymers showing this behavior are characterized by a widened interface due to a phase mixing. As the value of $\chi_{AB} N$ is greater than 10, nearly pure A and B domains are formed. The chain conformation is no longer Gaussian but rather perturbed. This regime is termed as *strong segregation limit* and is caused by the higher immiscibility of the two different segments resulting in a reduced interface. The stretching of the chains is increased²⁶.

A variety of structures develop in block copolymers upon microphase separation. This phenomenon is due to two main effects. First, dissimilar blocks tend to segregate because of their inherent chemical incompatibility. The spatial extent of phase separation is, however, limited by the connectivity of the blocks dictated by the architecture of the macromolecules. As a compromise of both the effects, periodic microstructures evolve. The geometry of the microphase separated structure is, therefore, very sensitive to the chemical nature and molecular structure of the copolymer as well as its total composition²⁶.

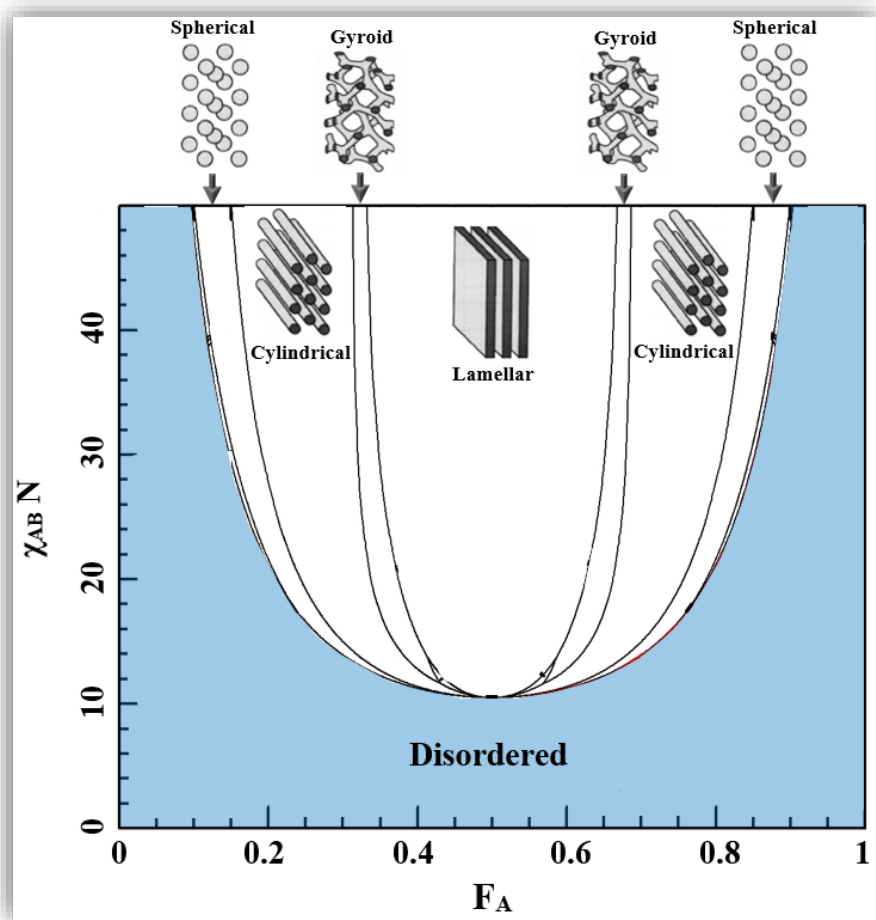


Figure 12. Theoretical phase diagram for a linear A-B block copolymer as a function of $\chi_{AB}N$ and volume fraction of block A (F_A). The schematic diagrams of the ordered lamellar, gyroid, cylindrical and spherical morphologies observed in A-B diblock copolymer systems, showing the domain occupied by the short minority block (the remaining space is filled by the majority block), are given as well.

After investigating the phase structure and the phase separation of these particular block copolymers, it is of interest to explore their specific features compared to thermosets exhibiting similar properties in order to consider block copolymer TPE as replacement materials.

B.2.4. Advantages / disadvantages of block copolymer TPE

Block copolymer TPE offer some valuable advantages in comparison to vulcanized rubbers. First of all, the process required is easier with fewer steps. Indeed, TPE rely on processing techniques used for

thermoplastics, more effective and less costly. Consequently, the final cost of the finished material is lower. The process has also shorter fabrication times (injection molding, rapid and highly economical, is generally used for thermoplastics) which allows to reduce finished part costs as well. Since molding cycles for TPE last usually several seconds as opposed to minutes for conventional thermoset rubbers, the productivity is significantly increased. It can be thus stated that the thermoplastic process uses typically less total energy (lower energy consumption) due to shorter molding cycles and simpler processing. Secondly, since the majority of TPE is supplied fully formulated and ready for fabrication, compounding or mixing are rarely required, with no need to add reinforcing agents, stabilizers or cure systems. Hence, batch-to-batch variations in weighting and metering components are absent, leading to improved consistency in both raw materials and fabricated articles. The simple formulations used combined with straightforward processes allow a better-quality control and closer tolerances of finished parts. Furthermore, the more important reproducibility and consistency of properties of TPE resins result in reduced quality control costs. It can be noted that TPE processes are adequate for high speed automation and amenable to robotic assistance while thermoset rubber processing is usually much more laborious. The possibility of reusing scrap in the same fashion as with thermoplastics is an important benefit as well. The TPE scrap can be reused as a regrind frequently producing materials having the same properties as the virgin material (minimal loss in performance). Lastly, a paramount advantage of TPE over conventional rubbers is the possibility to use specific thermoplastic processes such as blow molding, heat welding and thermoforming^{14,20}.

Nonetheless, some detriments have to be mentioned when handling block copolymer TPE. The upper service temperature of these latter is limited due to the glass transition (or melting) of the hard phase. This inherent property limits the use of block copolymer TPE to service temperatures well below their upper glass transition temperature or melting point. Moreover, the raw materials to synthesize the TPE can be expensive and thus the cost of TPE materials are generally higher than the thermoset rubbers. TPE have lower temperature resistance, thermal stability, chemical resistance and worse form recovery (high compression set) after being under load. Although it is a common step for thermoplastic polymers, drying prior to processing is required for TPE whereas it is mostly never performed for vulcanized materials¹⁴.

Although some shortcomings such as the relatively low heat resistance and thermal stability can be raised when using TPE, a major advantage is that processing, joining or shaping can be done using standard techniques used for thermoplastics in the melt state.

C. Styrenic block copolymer TPE

C.1. Factors influencing the properties

C.1.1. Introduction

Styrenic block copolymers are defined by a specific polymeric structure consisting of multiple blocks of poly(styrene) (PS) connected by segments that are essentially in rubbery state. They exhibit mostly A–B–A triblock structures, where A is a PS segment and B is an elastomeric segment. This latter soft segment is usually a polydiene, such as poly(butadiene) (PB) or poly(isoprene) (PI). Please note that the more convenient and more widely used nomenclatures for these copolymers are S–B–S and S–I–S. These polymers form two separated phases as discussed previously, retaining many of the properties of the respective homopolymers. Accordingly, they exhibit high strength combined with elastomeric characteristics without the use of vulcanization chemicals. Styrenic block copolymers have two distinct glass transition temperatures (T_g). At room temperature, PS is rigid and strong whereas the flexible phase is elastic and can be extended. The PS phase is typically present in a minority and therefore consists of separate regions. These glassy domains are attached to the ends of elastomeric chains and create multifunctional junction points similar to chemical crosslinks (the elastomeric midsegments are tied together in a three-dimensional network). However, these crosslinks are of a physical nature and are therefore less stable thermally. At ambient temperature, these triblock thermoplastics behave in many ways like vulcanized rubbers. At $T > T_{g,PS} \approx 100$ °C, PS domains soften, the network becomes weaker, and eventually the material is capable of flowing. Likewise, the domains totally lose their strength when the material is dissolved in a solvent (styrenic block copolymers can typically be dissolved in solvents in which both respective homopolymers are soluble). When the polymer is cooled down or the solvent is evaporated, the domains harden and the network regains its original integrity²⁰. Most of the currently used hard and soft segments of TPE based on styrenic copolymers with their respective T_g are given in [Figure 13](#).

It has to be added that branched styrenic block copolymers with the structure (S-E)_nX (E = elastomeric segment; x = junction point with a functionality of *n*) have similar properties. However, structures exhibiting only one rigid segment such as I-S-I or B-S-B are not capable of forming continuous networks because only one end of each polydiene chain is terminated by a polystyrene block and the resulting materials are weak with no resemblance to conventional vulcanized rubber²².

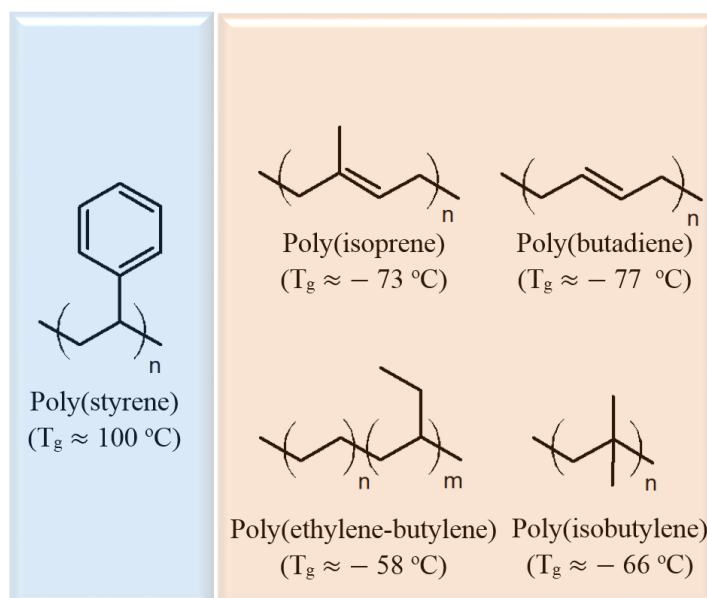


Figure 13. Hard blocks (blue background) A and soft blocks (orange background) B of conventional A-B-A styrenic triblock copolymers. Their T_g is approximated since it depends on the regio- and stereo-selectivity as well as the average molecular weight of the segments.

Commercially, several flexible midsegments, namely PB, PI, poly(ethylene-butylene) P(EB), poly(ethylene-propylene) P(EP), poly(isobutylene) P(IB) and poly(ethylene-ethylene-propylene) P(EEP), have been used in association with the two PS outer segments. Styrenic block copolymers are the largest volume and one of the lowest priced commercial TPE²⁰.

C.1.2. Effects of the elastomer type

Since styrenic TPE consist of two incompatible phases at service temperature, the final properties of these polymers are influenced by the properties of the individual phases and the interface. It is therefore necessary to consider several factors. As regards styrenic block copolymers, the constituents' nature (soft and hard segments), their molecular weight and relative molar fraction are crucial parameters to optimize in order to obtain valuable TPE characteristics.

The change in the styrenic TPE center-block results in difference in properties. Poly(butadiene) PB and poly(isoprene) PI have one double bond in the original monomer unit, which are prone to a chemical attack and limit the thermal and oxidative resistance of the SIS and SBS block copolymers. In contrast, poly(ethylene-*co*-butylene) P(EB) is saturated and SEBS copolymers are much more stable than the former.

The modulus of these block copolymers should be inversely proportional to the molecular weight between the entanglements (M_e)²⁷. Some values of M_e for various possible elastomeric segments²⁸ are given in [Table 3](#). The M_e for P(EB) can be assumed to be similar to that for poly(ethylene-*co*-propylene).

Poly(diene)	M_e (g.mol ⁻¹)
Poly(ethylene- <i>co</i> -butylene) ^(a)	1 700
<i>Cis</i> -1,4-poly(butadiene) ^(b)	2 930
<i>Cis</i> -1,4-poly(isoprene) ^(c)	3 890
3,4-Poly(isoprene) ^(d)	5 960
1,4-Poly(myrcene) ^(e)	22 100
3,4-Poly(myrcene) ^(f)	31 100

Table 3. Entanglement molar masses of some poly(diene)s²⁸. **(a)** Random copolymer with 7 ethyl branches per 100 backbone carbons. **(b)** 96 % *cis*-content. **(c)** 100 % *cis*-content, natural rubber. **(d)** 75 % 3,4 and 25 % 1,2. **(e)** 0 % 3,4-content. **(f)** 64 % 3,4-content.

In comparison, SIS copolymers have much lower viscosity than SBS copolymers since the PI chains have much higher entanglement molecular weight than the PB chains. On the other hand, SBS copolymers display a much higher elastic modulus and better low temperature properties. Thus, most SIS copolymers are traditionally used in hot-melt pressure sensitive adhesives while SBS copolymers are mainly used in footwear and asphalt modification. Due to a more entangled elastomeric continuous phase, SBS typically exhibits higher tensile stress than SIS having a similar composition. This is illustrated in [Figure 14](#) which compares tensile properties at room temperature of SBS and SIS samples having similar M_{ns} and styrene contents²⁹. Although SBS samples shown slightly reduced elongations at break, mainly due to their greater hardness, compared to SIS triblocks, SBS tensile stresses at break were significantly higher than those of SIS polymers.

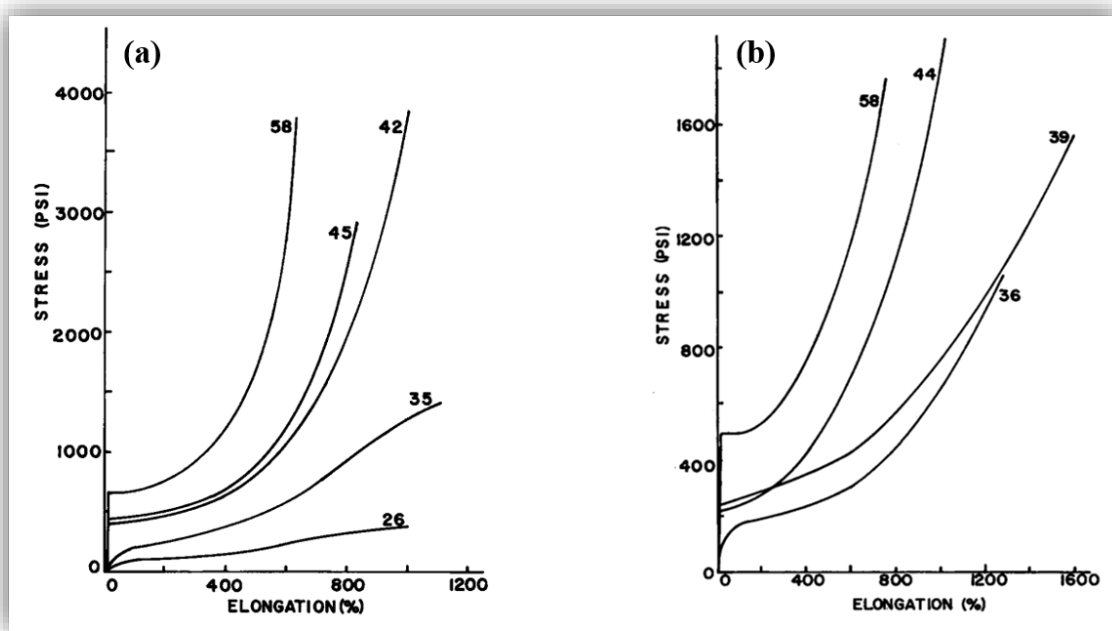


Figure 14. Stress-strain curves for (a) SBS triblock copolymers ($M_n = 18\text{-}64\text{-}18 \text{ kg}\cdot\text{mol}^{-1}$) and (b) SIS triblock copolymers ($M_n = 20\text{-}60\text{-}20 \text{ kg}\cdot\text{mol}^{-1}$) both prepared anionically using dilithium adducts of isoprene as initiators (5 inches/min cross-head speed, room temperature). Numbers on curve are the styrene contents of the polymers²⁹.

Polymer	δ_D	δ_P	δ_H	δ
Poly(styrene) PS	21.3	5.8	4.3	22.5
Poly(butadiene) PB	17.5	2.3	3.4	18.0
poly(isoprene) PI	16.6	1.4	- 0.8	16.7
Poly(ethylene) PE	15.1	- 4.2	2.0	15.8

Table 4. Hansen' solubility parameters data for PS, PB, PI and PE^{30,31}. δ_D = Dispersion forces contribution, δ_P = Polar forces arising from dipole moments contribution, δ_H = Hydrogen-bonds between molecules contribution, $\delta = (\delta_D^2 + \delta_P^2 + \delta_H^2)^{0.5}$.

The soft segment type also influences the driving force for phase separation and hence the physical properties. Table 4 gathers Hansen solubility parameters for PS, PI, PB, and P(EB)^{30,31}. The lower solubility parameters for isoprene *versus* butadiene means that better phase separation between the soft and the hard

domains can be theoretically achieved at lower weight percentage of styrene. Hydrogenation of the diene phase reduces the solubility parameters of the elastomer phase and allows the formation of a stronger phase separation. Therefore, SEBS can be copolymerized for phase separation with less styrene blocks M_n while still obtaining a good phase separation, compared to unsaturated SIS and SBS TPE³².

C.1.3. Effects of average molar mass and hard blocks content

The condition for complete miscibility of two substances is that the Gibbs free energy of mixing (ΔG_M) be favorable, that is, negative. On the other hand, if ΔG_M is positive, phase separation will occur. In the case of block copolymers, a positive value of the free energy of mixing means that separate domains will be formed. The free energy of mixing can be expressed as $\Delta G_M = \Delta H_M - T\Delta S_M$ where ΔH_M is the enthalpy of mixing, ΔS_M is the entropy of mixing, and T is the absolute temperature. For styrene-diene block copolymers, the enthalpy of mixing is positive because there are no strongly interacting groups and it increases as the two polymers forming the segments become less alike. T and ΔS_M will always be positive and consequently the product ($T\Delta S_M$) will always be negative. This term will approach zero, however, as the molar masses of the segments become large and/or as T decreases^{23,24}. Thus, the domain formation will be favored by the following conditions:

- High degree of structural difference between the segments
- High average molar masses of the segments
- Low temperature

Based on this approach, the values of critical molar masses and temperatures for domain formations have been developed and can be predicted quite well. Findings reported from studies^{33,34} are:

- SBS triblock copolymer with PS end-segments having M_n of 7 kg.mol⁻¹ changes to a one-phase system at about 150 °C.
- Similar block copolymers with PS end-segments having M_n of 10 kg.mol⁻¹ and greater appear to be separated at temperatures up to 200 °C.
- The critical molar mass for domain formation in SBS appears to be about 7 kg.mol⁻¹.

Styrenic TPE must also exhibit a highly entangled elastomeric phase to be mechanically valuable. The physical chain entanglements contribute mainly to the network density and to the stress at small elongations. The soft block should thereby have a molar mass which is at least several times higher than the molar mass between entanglements M_e (Table 3 above). Highly entangled poly(diene)s show ductile

fracture due to the energetically favorable shear yielding deformation mechanism. Low entanglement density of the soft phase likely leads to a brittle fracture behavior of the styrenic TPE.

SB become harder and stiffer as the proportion of the hard styrene segments is increased. The stress–strain behavior of otherwise similar block copolymers with a wide range of polystyrene contents shows a family of stress–strain curves, as it can be seen in [Figure 14](#). As the styrene content increases, the products change from soft, weak, rubbery materials to strong elastomers, then to leathery materials, and finally to hard, glassy thermoplastics. As the content of styrene is increased, the morphology of the polystyrene changes from spheres to cylinders, both dispersed in the continuous elastomer phase. When the volume fractions of both components are about equal, the two form alternating lamellae. As the styrene content increases, a continuous polystyrene phase forms in which either cylinders or spheres of the elastomer are dispersed³⁵. This latter situation is illustrated in [Figure 15](#), showing various morphologies of S-rich P(I-*b*-S) diblock copolymers where PS forms (in an unusual way) the continuous domain³⁶. SBC mechanical behavior are mainly governed by their microphase separated structures. Accordingly, the styrene fraction must be wisely selected.

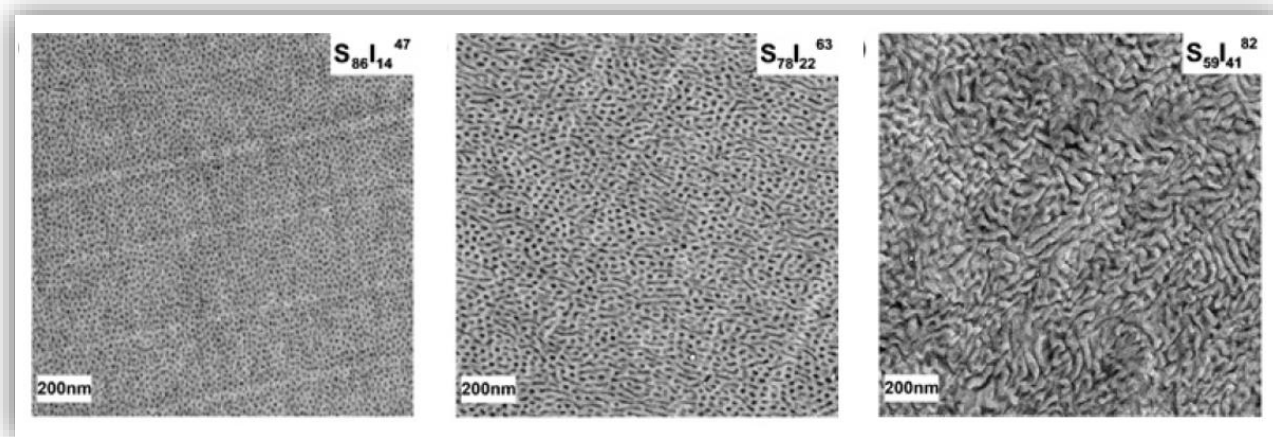


Figure 15. Transmission electron micrographs (TEM) after compression molding of P(I-*b*-S) diblock copolymers exhibiting a fraction of styrene of 86 wt% (left, spherical morphology), 78 wt% (middle, cylindrical morphology) and 59 wt% (right, lamellar morphology). The bright phase corresponds to the PS phase and the dark one to the PI phase³⁶.

C.1.4. Influence of the hard segment nature

As many applications benefit from low-cost styrenic block copolymers (SBC), high-temperature applications and other advanced consumptions of SBC, such as in tire rubber, are largely limited by the relatively low glass transition temperature (T_g) of poly(styrene) PS. When the service conditions approach 95°C, softening of PS domains dramatically reduces the tensile stress of these thermoplastic elastomers (TPE). One major research interest is thereby to increase their upper service temperature. These efforts mainly explored anionic polymerization of polymers with higher glass transition temperatures³⁷. [Table 5](#) below gives some hard segments allowing to increase the upper limit service temperature of SBC.

Some examples can be detailed in order to understand the effects of adding rigid segments having a $T_g > 100$ °C. Attention can be first paid to the substitution of PS blocks with poly(α -methyl- p -methyl styrene) P(MMS) end blocks in styrenic TPE. P(MMS)-P(My)-P(MMS) triblock (P(My) = 1,4-poly(β -myrcene) in majority) was synthesized by sequential anionic polymerization⁴⁰. To elucidate thermal behavior along with viscoelastic properties, this triblock was subjected to dynamic mechanical analysis (DMA) and compared to a conventional PS-PI-PS triblock, as shown in [Figure 16a](#). The PS-PI-PS sample has an elastic modulus of approximately 1 MPa between -40 and +90 °C, at which point the modulus drops due to softening of the PS phase, as expected (black trace). On the other hand, the rubbery plateau (also around 1 MPa) for P(MMS)-P(My)-P(MMS) extends to 160 °C before a drop in the modulus is observed at the softening point of the P(MMS) blocks. This suggests that this latter TPE may well have an attractively high service temperature. A similar observation was reported by Jérôme *et al.* when comparing by DMA hydrogenated or not P(MMA)-PB-P(MMA) (PB = poly(butadiene)) and P(IBOMA)-PB-P(IBOMA) triblocks ([Figure 16b](#)) made by sequential anionic polymerization⁴². P(IBOMA)-PB-P(IBOMA) and hydrogenated P(MMA)-PB-P(MMA) have a comparable G' up to about 90 °C. At higher temperatures, G' of hydrogenated P(MMA)-PB-P(MMA) starts to decrease rapidly, whereas it persists up to 160 °C for the sample having P(IBOMA) hard outer segments. Substitution of P(MMA) outer blocks by P(IBOMA) results in a substantial increase in the upper service temperature, in agreement with a much higher T_g for P(IBOMA) (190 °C, by DSC) compared to that of P(MMA).

Furthermore, a higher tensile stress is typically observed for styrenic TPE replacing PS hard blocks by higher T_g blocks. Stress-strain data for PS-PI-PS and P(MS)-PI-P(MS) triblocks, synthesized using 1,4-dilithio-1,1,4,4-tetraphenylbutane as the initiator³⁹, are shown in [Figure 17](#). It is readily apparent that the P(MS)-PI-P(MS) block polymer exhibited a markedly higher tensile strength than the PS-PI-PS sample of equivalent composition. Thus, it would seem that end blocks with glass transition temperatures higher than polystyrene enhance the tensile strength of the material.

Hard block type	T _g (°C)	Structure
Poly(styrene) derivatives		
Poly(<i>tert</i> -butyl styrene) ³⁸ P(<i>t</i> BS)	~ 130	
Poly(α -methyl styrene) ³⁹ P(MS)	~ 173	
Poly(α -methyl- <i>p</i> -methyl styrene) ⁴⁰ P(MMS)	~ 183	
Poly(<i>p</i> -adamantyl styrene) ⁴¹ P(AdmS)	~ 203	
Poly(methacrylate) derivatives		
Poly(<i>tert</i> -butyl methacrylate) ⁴² P(<i>t</i> BMA)	~ 116	
Poly(methyl methacrylate) ⁴² P(MMA)	~ 120	
Poly(isobornyl methacrylate) ⁴² P(IBOMA)	~ 202	
Rigid conjugated poly(diene)s		
Poly(1,3-cyclohexadiene) ⁴³ P(CHD)	~ 140-150	
Poly(benzofulvene) ⁴⁴ P(BF)	~ 140-195	

Table 5. Examples of hard segments as PS substitutes in styrenic TPE. Regarding the structure of PS derivatives, the blue bonds correspond to the added groups in comparison to PS. 1,4-addition (left repetitive unit) and 1,2-addition (right repetitive unit) are depicted in P(CHD) and P(BF) structures. Note that the synthesis of these hard blocks was mostly performed by anionic polymerization.

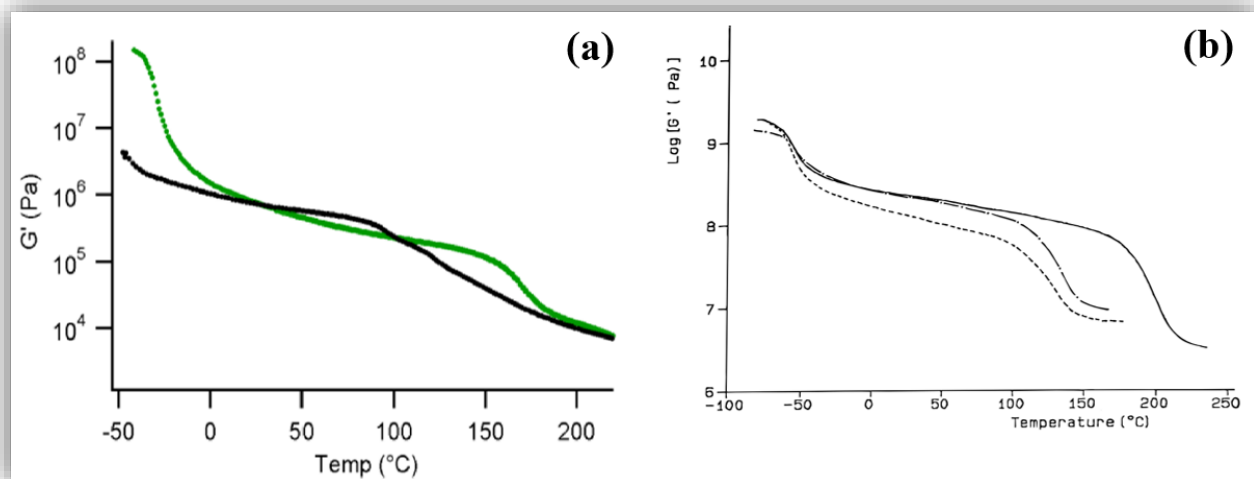


Figure 16. (a) Elastic moduli (G') of PS-PI-PS ($M_n = 23\text{-}164\text{-}23 \text{ kg}\cdot\text{mol}^{-1}$, black solid curve) versus P(MMS)-P(My)-P(MMS) ($M_n = 36\text{-}168\text{-}36 \text{ kg}\cdot\text{mol}^{-1}$, green solid curve) with $\omega = 1 \text{ rad}\cdot\text{s}^{-1}$, an initial strain of 10 % and a $3 \text{ }^{\circ}\text{C}\cdot\text{min}^{-1}$ temperature range rate⁴⁰ and (b) G' of P(IBOMA)-PB-P(IBOMA) ($M_n = 20\text{-}55\text{-}20 \text{ kg}\cdot\text{mol}^{-1}$, solid curve (—)), hydrogenated P(MMA)-PB-P(MMA) ($M_n = 25\text{-}80\text{-}25 \text{ kg}\cdot\text{mol}^{-1}$, discontinuous curve (- · -)) and P(MMA)-PB-P(MMA) ($M_n = 25\text{-}80\text{-}25 \text{ kg}\cdot\text{mol}^{-1}$, dashed curve (---)) at 1 Hz ⁴².

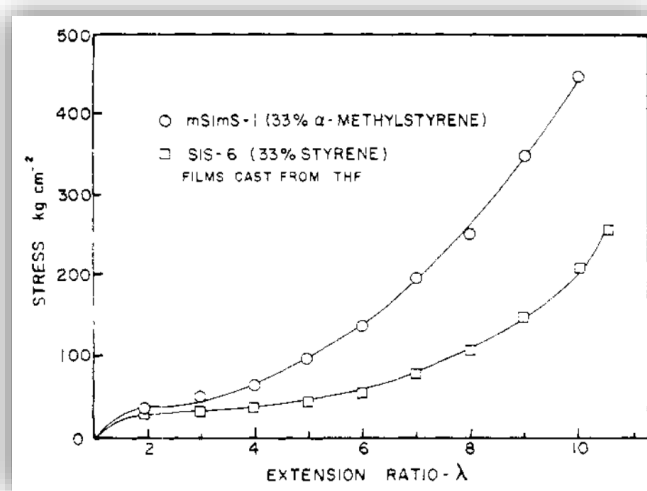


Figure 17. Stress-strain curves of PS-PI-PS ($M_n = 20\text{-}87\text{-}20 \text{ kg}\cdot\text{mol}^{-1}$, open square) and P(MS)-PI-P(MS) ($M_n = 21\text{-}85\text{-}21 \text{ kg}\cdot\text{mol}^{-1}$, open circles) cast films (tetrahydrofuran used) at $20 \text{ }^{\circ}\text{C}$ and at $5 \text{ cm}\cdot\text{min}^{-1}$ (crosshead speed)³⁹.

It might be added that the interaction coefficient between P(MS) and PI is virtually the same as that of PS and PI. Hence, the amount of phase blending in these two triblock polymers studied should be nearly identical. It can be assumed that the effectiveness of the glassy domains (the sites of stress concentration) is greatly dependent on the degree of phase separation. Thus, the better the phase separation, i.e., the less the glassy domains are diluted by the rubbery component, the greater is the energy absorbed prior to the disintegration of these domains.

C.2. Hydrogenation of the elastomeric block

Please note that this section is only devoted to the hydrogenation of elastomers, such *cis*-1,4-poly(isoprene) or *cis*-1,4-poly(butadiene), as well as the hydrogenation of the soft segment of styrenic block copolymers. Accordingly, hydrogenated styrene/isoprene triblock means herein that only the poly(isoprene) segment was saturated for instance. Even though the hydrogenation of hard blocks such as poly(styrene) is well-known, it is not the purpose of this review.

C.2.1. Introduction

Chemical modifications of unsaturated polymers have received a great deal of attention for many years. Today, the hydrogenation of polymers is perhaps the most widely practiced post-polymerization chemical reaction. Hydrogenation is a chemical reaction between molecular hydrogen (H₂) and another compound, usually in the presence of a catalyst such as nickel (Ni), palladium (Pd) or platinum (Pt). This process is generally conducted to reduce or saturate compounds. Hydrogenation of unsaturated polymers can provide an alternate route to a variety of unique and useful elastomers and thermoplastics with specific structures and properties. Hydrogenation processes are directly affected by the nature of the catalyst, purity of substrates, temperature, pressure, contaminants in the substrate, instability of intermediates and solvents. Many polymers with new monomer sequence distributions and compositions, difficult or impossible to prepare directly through conventional polymerizations, can be easily obtained via hydrogenation. Moreover, hydrogenated poly(diene)s have normally enhanced resistance to oxidative and thermal degradations in comparison to the parent unsaturated polymers. Hydrogenated polymers are produced and available commercially, and have also been used as well-defined substrates, providing a basis for the study of a variety of important aspects of polymer physical behavior, including spectral analysis of polymeric

hydrocarbons, the effect of local chain microstructure on rheological behavior, crystallization and melting properties as well as polymer–polymer phase mixing⁴⁵.

C.2.2. Hydrogenation processes

The predominant means of hydrogenation of poly(diene)s has been their combination with molecular hydrogen in the presence of a soluble transition metal catalysts. These reactions are commonly run in organic solvents at relatively high dilution (10-30 % polymer) in a stirred pressure reactor at moderate temperatures. A class of complexes known collectively as Ziegler-type catalysts, cobalt (Co) and nickel (Ni) complexes (particularly the hydrocarbon soluble 2-ethylhexanoate and acetylacetonate complexes) activated with organo-lithium (Li) or organo-aluminum (Al) compounds, are probably the most extensively studied and commercially utilized regarding homogeneous catalytic hydrogenation. These catalysts are effective in the saturation of poly(butadiene) PB and poly(isoprene) PI homopolymers (including natural rubber) and in block or random copolymers with styrene (S), and can be optimized for a given polymer with respect to the ratio of transition metal to the Li- or Al-activating species^{46,47}. [Figure 18](#) depicts the saturation of butadiene units in a styrenic block copolymer via Ziegler-based hydrogenation. A noticeable drawback with the commercial use of the Zeigler-type catalysts is that the residual metal has to be removed before use. Heterogeneous catalytic hydrogenation can be implemented as well. Transition metal catalysts using a variety of inorganic supports have found utility in the hydrogenation of the polymers containing isolated alkenes such as those encountered in poly(diene)s and metathesis-derived polymers. Conditions are known in which high levels of saturation can be achieved without chain degradation. Palladium (Pd) on CaCO₃ is known to have good activity for PI- and PB-based polymers without bringing about chain cleavage⁴⁷.

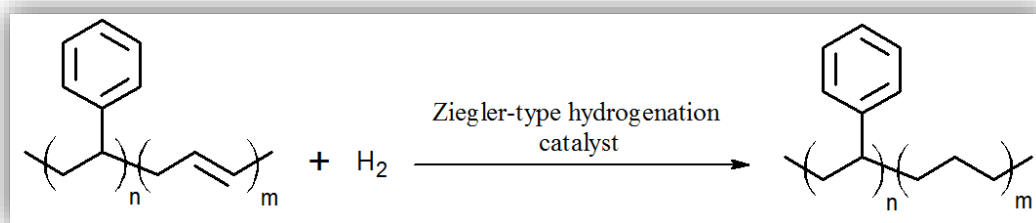


Figure 18. Selective saturation of styrene-butadiene block copolymer using a Ziegler-type hydrogenation catalyst. This latter is formed by combination of a group 8-10 transition metal pre-catalyst and a trialkylaluminium co-catalyst in a hydrocarbon solvent such as benzene.

Industrially, the hydrogenation is efficiently performed using these two catalytic techniques. However, these reactions remain highly hazardous. The primary hazard associated with any form of hydrogen is obviously producing a flammable mixture, leading to a fire or detonation when exposed to air, oxygen or sparks. Use of hydrogen, pyrophoric catalyst, flammable solvents and generation of in situ unstable intermediates are the main safety concerns when hydrogenations are run. Substrate impurities, the wrong choice of catalyst, contaminated hydrogen (carbon dioxide, carbon monoxide and hydrocarbons) and low concentration of catalyst are major contributing factors for the runaway reactions. Proper handling of catalysts is critical due to high reactivity before and after introducing hydrogen. Existence of any impurity or colored impurity in substrate can inhibit the catalyst activity resulting in partial reduction of the substrate and occasionally in a run-away reaction. Substrates should be completely purified prior to subjecting them to hydrogenations. Hydrogenation reactions are largely exothermic in nature and can eventually increase overall pressure inside the vessel. Moreover, on a laboratory scale, the equipment required to perform hydrogenations at moderate to high hydrogen pressure is often not readily available. Lastly, catalytic hydrogenation reactions are expensive methods due to the use of costly H₂ gas and metal catalysts and the need of a high pressure reactor^{48,49}.

Ambient pressure hydrogenations are the safest among all hydrogenations. The hydrogenation of carbon-carbon double bonds (C=C) using chemical ways has also been developed. The most largely performed of these techniques relies on the chemistry of the reactive intermediate diimide (HN=NH), a reactive species that can transfer hydrogen to alkene or alkyne functional groups. These methods are in wide use in laboratory settings, because they allow for efficient saturation of olefins without the need for expensive high-pressure reactors and are tolerant of a variety of functional groups. A stoichiometric excess of the diimide must be provided to result in a complete saturation. The required excess is due to disproportionation of diimide. The diimide hydrogenation is briefly showcased in [Figure 19](#). Hydrogenation of poly(diene)s with the diimide-based reagent termed *p*-toluenesulfonylhydrazide (TSH) has been reported, including specifically the saturation of PI and PI block copolymers and PB. It was found by the researchers that acid by-products from the TSH degradation reaction can react with incompletely hydrogenated polymers, generating chain cleavage and the incorporation of a fragment of the TSH onto the polymer chain. The use of amine tripropyl amine (TPA) associated with the TSH reagent in refluxing *o*-xylene was found to suppress the contribution of side reactions during the saturation of PB and its copolymers. Even though it improved the integrity of hydrogenated PI, it did not give complete saturation in one treatment. In addition, the complete elimination of chain degradation chemistry was not apparent for PI. This effective TSH / TPA couple technique has since been used to hydrogenate a large range of alkene-containing polymers, where its convenience and tolerance of functional groups is of interest and has recently been

extended to hydrogenate alkynes. With no need of high pressure, H₂ gas and catalyst, this method is straightforward and safe^{50,51}.

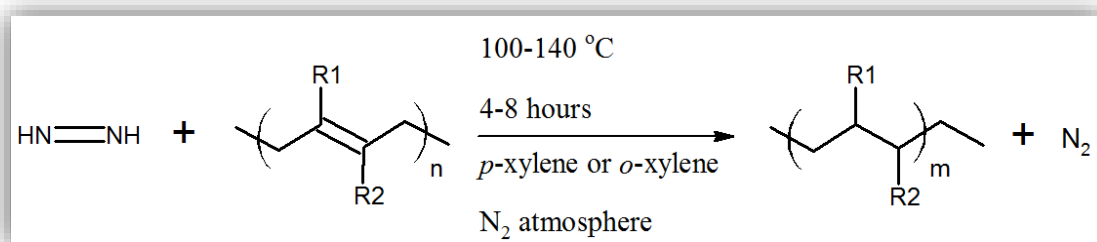


Figure 19. Use of diimide to hydrogenate poly(diene) using typical experimental conditions. To avoid the protonation of the unsaturated poly(diene) during the diimide hydrogenation, the reaction must be run in the presence of a high boiling point tertiary amine (tri-*n*-propylamine and tributylamine are commonly used).

C.2.3. Properties of hydrogenated poly(diene)s

The main enhancement of hydrogenated poly(diene)s compared to their original unsaturated polymers is undoubtedly their better thermal stability. This latter can be measured by thermogravimetric analysis (TGA) by determining for instance the temperature at which weight loss is most apparent ($T_{\text{deg,max}}$). $T_{\text{deg,max}}$ of hydrogenated natural rubber and hydrogenated synthetic *cis*-1,4-poly(isoprene) samples increased with increasing the degree of hydrogenation⁵². This can be explained in that a weak π -bond within the original elastomers was converted to a stronger C-H σ -bond by the hydrogen molecule. Similar observations were reported for *cis*-1,4-poly(butadiene) and *trans*-1,4-poly(2,4-hexadiene) for instance⁵³, as summarized in [Table 6](#).

It must be added that the glass transition temperature (T_g) is different after hydrogenation as well. Regarding PI samples, while the degree of hydrogenation of the natural rubber increased from 0 to 85.8 %, the T_g increased from -63.8 to -60.0 °C⁵². This can be explained by the replacement of amorphous segments of poly(isoprene) by crystalline ethylene-propylene units in the polymer structure. A similar shift in T_g was observed for hydrogenated synthetic *cis*-1,4-poly(isoprene)⁵⁴. A similar trend was also reported for methyl methacrylate/butadiene triblock copolymer having its poly(butadiene) midsegment hydrogenated and exhibiting $T_g = -52.0$ °C whereas its original counterpart had a lower $T_g = -61.0$ °C⁵⁵.










Polymer	DH (%)		T _{deg,max} (°C)
Natural rubber	0		381.7
	85.8		465.9
Synthetic <i>cis</i> -1,4-poly(isoprene)	0		386.0
	89.7		464.0
<i>Cis</i> -1,4-poly(butadiene)	0		440
	> 99		470
Trans-1,4-poly(2,4-hexadiene)	0		345
	> 98		435

Table 6. Maximum degradation temperature (T_{deg,max}) for various poly(diene)s and their hydrogenated counterparts (DH = Degree of hydrogenation)^{52,53}.

Dynamical mechanical analysis also showed a marked increase of the storage modulus E' (indicating the stiffness of the elastomer) of hydrogenated *cis*-1,4-poly(isoprene) compared to the parent unsaturated PI, as given in [Figure 20a](#). At $T < T_{g,PIs} \approx -40$ °C, natural rubber exhibits $E' \sim 200$ MPa whereas its hydrogenated counterpart (hydrogenation degree, HD = 85.8 %) is significantly stiffer ($E' \sim 430$ MPa). Even after the glass transition (increase of mobility and deformation of the polymer chains with increasing temperature), E' remains higher for hydrogenated PI. The higher E' of hydrogenated natural rubbers can be explained in that the replacement of the ethylene/propylene segments by hydrogenation of the isoprene unit in the polymer chain tends to decrease the mobility and the free volume of the polymer⁵². Such a trend of greater E' (or G') with hydrogenation degree, confirmed for PI, cannot be generalized for other poly(diene)s. The storage modulus for methyl methacrylate/butadiene, isobornyl methacrylate/butadiene and *tert*-butyl methacrylate/butadiene triblocks having their poly(butadiene) midsegment hydrogenated were lower compared to the original copolymers in the glassy region, whereas the reverse situation was observed in the rubbery plateau region⁵⁵. A similar observation was reported by Saito and coworkers regarding hydrogenated styrene-*block*-styrene-*co*-butadiene-*block*-styrene (S-SB-S, hydrogenation of the butadiene units)⁵⁶, as depicted in [Figure 20b](#). Interestingly, all these studies showed that hydrogenated elastomers or thermoplastic elastomers were stiffer in the rubbery plateau, at $T > T_g$.

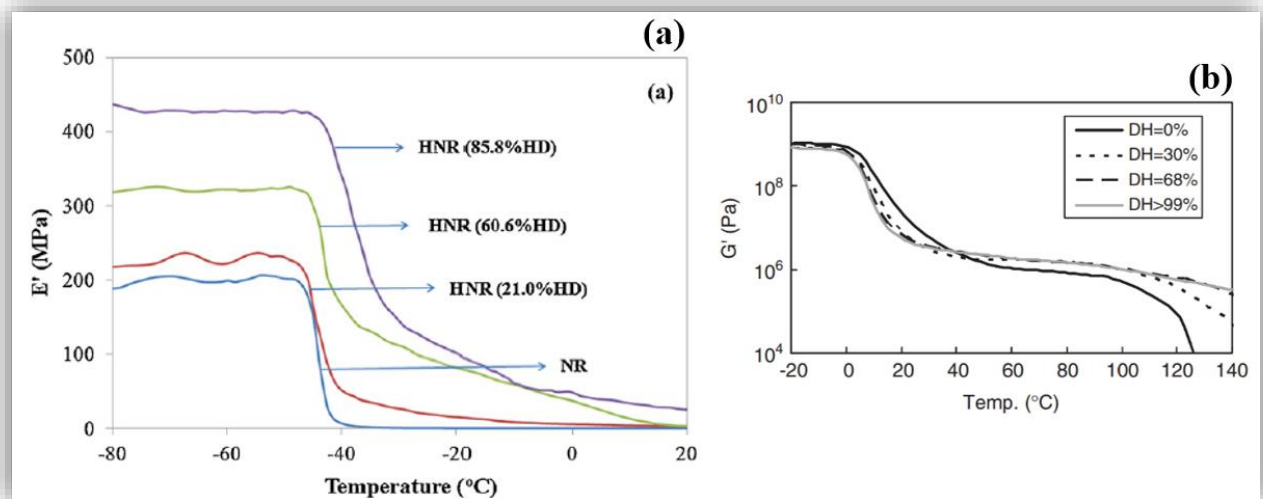


Figure 20. Temperature dependence of storage modulus (E' or G') for (a) natural rubber (NR) and hydrogenated natural rubber (HNR) exhibiting different hydrogenation degrees (HDs)⁵² and for (b) styrene-*block*-styrene-*co*-butadiene-*block*-styrene S-SB-S triblock copolymer and its hydrogenated counterparts (poly(butadiene) middle block exhibiting various degree of hydrogenation (DH))⁵⁶.

It is of interest to note that hydrogenated styrenic TPE generally show a higher upper service temperature as seen in [Figure 20b](#). While G' of S-SB-S triblock starts to drop at $T \sim 90$ $^{\circ}\text{C}$, fully hydrogenated S-SB-S still has a high G' at 140 $^{\circ}\text{C}$. This can be explained by the much stronger phase separation of hydrogenated TPE with a greater incompatibility, a greater difference in solubility parameters between the hydrogenated soft midblock and PS hard blocks.

The effect of hydrogenation on the mechanical properties of elastomers or thermoplastic elastomers is of great interest as well. Stress-strain curves of a series of hydrogenated S-SB-S triblock copolymers with various degrees of hydrogenation (DH) and equivalent PS contents are given in [Figures 21a and 21b](#). The modulus of the initial slope increased with increased DH ([Figure 21b](#)), whereas the tensile elongation at break decreased with increased DH ([Figure 21a](#)). In the hydrogenated S-SB-S with high DH, a sharp increase in stress was observed in high-strain regions and in low-strain regions after increasing DH. The tensile stress at break for highly hydrogenated S-SB-S (DH > 99 %) doubled the tensile stress at break for neat S-SB-S (DH = 0 %). The sharp increase in stress and the high strength at break point are behaviors similar to the behaviors of cross-linked rubbers. These results indicate that hydrogenated S-SB-S strengthens with increasing DH, although the content of the hard PS outer block segment did not change. A study of the phase behavior was led by the research team to understand the variation in stress-strain

properties with the DH. TEM and SAXS results indicated that the microphase structure expands with increasing DH owing to an increased incompatibility between the PS and hydrogenated SB block segments. Figures 21c and 21d show schematic illustrations of phase-separated structure for hydrogenated S-SB-S with different DH. Accordingly, the enhancement of the mechanical properties can be attributed to the increased segregation of the microphase structure with increasing DH⁵⁶.

Similar results were obtained regarding *tert*-butyl styrene/isoprene (TBS/I) star block copolymers. While neat samples exhibited very high elongations up to 3 000 % combined with very low tensile strength (0.5 MPa maximum), the hydrogenation of about 90 % of the isoprene units produced samples having reduced ultimate elongations (< 700 %) but significantly greater tensile stresses at break (> 25 MPa). The change in solubility parameter that occurred when PI segment was hydrogenated to poly(ethylene-*co*-propylene) presumably caused the rejection of hard P(TBS) from the rubber phase to yield discrete domains of P(TBS). Accordingly, it can be assumed that hydrogenation allowed the thermoplastic elastomer to perfect its phase separation to provide improved elastomeric properties⁵⁷.

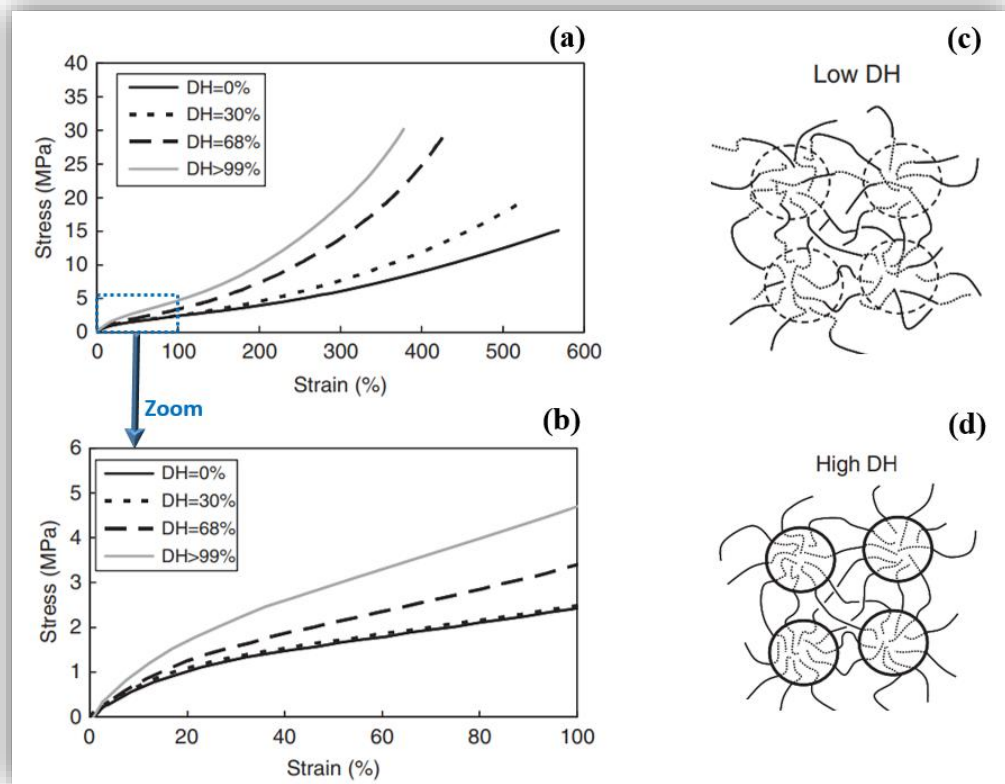


Figure 21. Stress-strain curves for hydrogenated S-SB-S in (a) the high-strain regions and (b) low-strain region, and schematic illustrations of (c) ambiguous phase separation for weakly hydrogenated S-SB-S and (d) strong phase separation for highly hydrogenated S-SB-S⁵⁶.

C.3. Commercial styrenic block copolymer TPE

C.3.1. Industrial producers and applications

The first commercial styrenic thermoplastic elastomers deriving their properties from an ABA block copolymer structure were poly(styrene)-*block*-poly(isoprene)-*block*-poly(styrene) PS-PI-PS (or SIS) and poly(styrene)-*block*-poly(butadiene)-*block*-poly(styrene) PS-PB-PS (or SBS) introduced in 1965 at an ACS Rubber Division Meeting at Shell Development Company. Initial applications were in molded shoe soles, hot melt adhesives and injection molded rubber goods. To further extend the range of applications, these polymers were made more stable by full hydrogenation in the early 1970s. Fully hydrogenated styrenic block copolymers exhibited poor resistance to oils, leading to the introduction of polymers with selectively hydrogenated rubber blocks. Through selective hydrogenation of the flexible segment, SBS became SEBS (styrene-ethylene/butylene-styrene triblock) and SIS became SEPS (styrene-ethylene/propylene-styrene triblock). A more recent development, although not yet commercialized, is styrenic block copolymers with an isobutylene mid-segment (S-iB-S). A wide range of triblock, diblock and star architectures were introduced in the 1970s with styrene contents ranging typically from 10 to 50 %. In 1998, worldwide production of styrenic TPE from more than 20 manufacturers was more than 10⁶ tons^{58,59}. The major current manufacturers and the trade names of their products are listed in Table 7. It is of interest to note that only anionic polymerization was applied to synthesize commercial styrenic TPE.

SBC differ from other TPE in at least two major ways. First, both hard and soft domains are amorphous, and thus pure SBC are soluble in common solvents such as toluene. Secondly, in their various end uses, these polymers are always compounded with large amounts of other ingredients. These latter can be other polymers, oils, fillers and resins. In the majority of their applications, the styrenic block copolymers comprise less than 50 % of the final product.

Injection molding and extrusion are performed to shape compounded products. Products based on SBS are generally compounded with PS, hydrocarbon oils and fillers. In those based on SEBS, poly(propylene) PP often replaces PS since PP gives better solvent resistance and increases the upper service temperature. Footwear, wire and cable insulation, automotive and pharmaceutical items can be given as typical applications

Company	Trade name	Type	Applications
Kraton	<i>Kraton</i> [®] D	SBS, SIS, SIBS ^(a)	Hot melt spray, diaper adhesives, elastic films.
	<i>Kraton</i> [®] FG	Functionalized SEBS ^(b)	Impact modifiers in nylon and polyesters.
	<i>Kraton</i> [®] G	SEBS, SEP(S) ^(c)	Soft, strong compounds for handles and grips, elastic components in diapers, oil gels.
	<i>Cariflex</i> [®] IR	I ^(d)	Gloves, medical products, tackifiers, paints.
Dexco	<i>Vector</i> [®]	SIS, SBS	Hot melt pressure sensitive adhesives, photopolymer plate applications, hygiene.
	<i>Taipol</i> [®]	SBS, SEBS	Compounding, plastic modification.
INEOS	<i>K-Resin</i> [®]	SBS	Packaging, toys, medical components.
Styrolution	<i>Styroflex</i> [®]	SBS	Flexible films, medical tubes, stretch hoods.
Zeon	<i>Quintac</i> [®]	SIS	Grades for hot melt pressure sensitive adhesive.
Fina	<i>Finaprene</i> [®]	SB, SBS	Improve the general adhesion of the compounds, reduce the blend viscosity.
S&E Specialty Polymers	<i>Tufprene</i> [®]	SBS, SEBS	Molding and over-molding, footwear, gaskets, toys.
Asahi	<i>Asaprene</i> [®]	SBS	Adhesives component, asphalt modifier.
Dynasol	<i>Calprene</i> [®]	SBS, SEBS	Bitumen application, footwear.
	<i>Solprene</i> [®]	SBS, SSBR ^(e)	Elastomeric modifier for asphalt mixtures for paving and roofing applications.
Enichem	<i>Europrene Sol T</i> [®]	SBS	Compounding for both footwear and technical applications, toughening agent in polymer modification and plastic recycling.
Firestone	<i>Stearon</i> [®]	SB, SBS	Grafting and melt blending plastic applications, non-woven hot melt adhesives.
Kuraray	<i>Septon</i> [®]	SEP, SEPS ^(c) , SEBS, SEEPS	Tapes, cold seal food packaging, reactive adhesives, toys and sporting goods.
J-VON	<i>Hercuprene</i> [®]	PP / EPDM blends	Flexible material for appliances, hose and tubing, connectors, insulation.
Saint-Gobain	<i>C-Flex</i> [®]	Not specified	Pharmaceutical and biopharmaceutical applications for fluid processing.
Teknor Apex	<i>Elexar</i> [®]	Not specified	Wire and cable jacketing and insulation, electrical connectors and plugs.
Chi Mei	<i>Kibiton</i> [®]	SBS	Shoe soles, toys, asphalt modifications, mechanical products, adhesive agents.

Table 7. Main producers and trade names of styrenic TPE and the respective industrial applications^{58,59,60}. **(a)** SIBS = Styrene-isoprene/butadiene-styrene. **(b)** SEBS with grafted maleic anhydride. **(c)** SEPS = Styrene-ethylene/propylene-styrene. **(d)** synthetic poly(isoprene) products. **(e)** Solution-polymerized styrene-butadiene rubber (SSBR).

Styrenic TPE are extensively used in adhesives, sealants and coatings. Tackifying and reinforcing resins are used to obtain a desirable balance of properties. Oils and fillers can also be added. SBC-based adhesives and sealants can be applied either from solvents or as hot melts. A major application is in pressure sensitive hot melt adhesives. SIS triblocks are softer and stickier and so they are typically employed to formulate adhesives of this type. SBC blending with thermoplastics or other polymeric materials can be also mentioned. Styrenic TPE are compatible with a wide variety of other polymers. Blends with many other thermoplastics have enhanced impact resistance amongst others⁶⁰.

C.3.2. Styrenic TPE

Although this doctoral thesis was mostly dedicated to the synthesis of a novel styrenic triblock copolymer, some commercial styrenic block copolymers can be explored and used as benchmark materials. In this section, only products from *Kraton*[®] company were investigated since *Kraton*[®] is specialized in the production of high-performance styrenic TPE and detailed technical data sheets are provided. Nine commercial *Kraton*[®] are detailed herein and consist of linear SIS, SBS, SEBS and functionalized SEBS triblock TPE, as summarized in [Table 8](#).

First of all, it can be noticed that all these *Kraton*[®] triblocks satisfied ArianeGroup stress-strain properties at room temperature (tensile strength at break > 15 MPa, Tensile elongation at break > 400 %). However, important differences must be mentioned according to the nature of the elastomeric mid-segment and the composition of the TPE. SIS *Kraton*[®] polymers are high performance TPE with a combination of high strength, low hardness and low viscosity for easy processing as a melt or in solution. They are the lowest viscosity and hardness of all the styrenic TPE. For samples D1161 B and D1164 P presented in the [Table](#), this is highlighted by their relatively low modulus at 300 % elongation (≤ 3.1 MPa). Moreover, their melt flow index at 200 °C ranging from 8.0-19 g/10min indicate that these materials significantly soften and flow at such a temperature. It can thus be assumed that these linear SIS should not be thermally robust enough to support welding process or adhesive bonding process at $T > 160$ °C.

SBS *Kraton*[®] are versatile with a combination of high strength, wide range of hardness and low viscosity. Although similar to SIS samples, SBS are typically harder, which is mainly due to the more entangled poly(butadiene) matrix (lower entanglement molar mass compared to poly(isoprene)). For the industrial problematic, SBS appear more interesting due to their both greater modulus at 300 % elongation and stress at break, in comparison to SIS *Kraton*[®]. Moreover, their melt flow index at 200 °C is significantly lower than that of SIS exhibiting a similar composition, which is valuable for our technological issue.

Trade name	Type	300 % modulus (MPa)	Stress at break ^(a) (MPa)	Elongation at break ^(a) (%)	Melt flow Index (g/10min)
<i>Kraton</i> [®] D1161 B	Linear SIS (15 wt% S)	0.9	28	1300	8.5-19 (200 °C)
<i>Kraton</i> [®] D1164 P	Linear SIS (29 wt% S)	3.1	28	1000	8.0-15 (200 °C)
<i>Kraton</i> [®] D1101 A	Linear SBS (31 wt% S)	2.9	33	880	< 1 (200 °C)
<i>Kraton</i> [®] D1191 E	Linear SBS (34 wt% S)	4.1	30	1100	< 1 (200 °C)
<i>Kraton</i> [®] G1650 E	Linear SEBS ^(b) (29 wt% S)	5.6	35	500	5 (230 °C)
<i>Kraton</i> [®] G1652 H	Linear SEBS ^(b) (30 wt% S)	4.8	31	500	5 (230 °C)
<i>Kraton</i> [®] A1536 H	Linear SEBS ^(b) (40 wt% S)	6.4	> 34	660	7 (260 °C)
<i>Kraton</i> [®] A1535 H	Linear SEBS ^(b) (57 wt% S)	7.9	28	> 600	< 1 (230 °C)
<i>Kraton</i> [®] FG1901 G	MA-grafted SEBS ^(c) (30 wt% % S, 2 wt% MA)	Not specified	34	500	14-28 (230 °C)

Table 8. Some properties of linear *Kraton*[®] triblocks. **(a)** Typical properties determined on film cast from toluene solution. **(b)** SEBS samples correspond to fully hydrogenated SBS TPE. **(c)** MA = Maleic anhydride.

SEBS *Kraton*[®] are the strongest, the most highly dilutive and the most compatible with polyolefins and mineral oils of all the styrenic TPE. They are second generation styrenic block copolymers with a hydrogenated midblock (ethylene/butylene copolymer) and are intended for use where UV resistance, high service temperature and processing stability are essential. Four linear SEBS triblocks are presented in the

Table above exhibiting various weight fractions of styrene unit (29-57 wt% S). SEBS *Kraton*[®] have a relatively limited extensibility (elongation at break = 500-660 %) and a comparable tensile stress at break (28-35 MPa) compared to SIS and SBS *Kraton*[®]. SEBS are tougher due to the hydrogenated midsegment. For similar S weight fractions (29-34 wt% S), SEBS exhibit a higher modulus at 300 % elongation and an improved resistance to flow (only 5 g/10min at 230 °C) in comparison with SBS and SIS samples. While keeping similar stress-strain properties, richer-S SEBS (40-57 wt% S) have a relatively high modulus at 300 % elongation (6.4-7.9 MPa) and a highly limited flowing at high temperatures (230-260 °C). Furthermore, although not indicated in the material data sheets, it can be assumed that SEBS *Kraton*[®] exhibit enhanced thermal stability and service temperature since it consists of fully hydrogenated SBS (see section C.2.3).

Lastly, a functionalized SEBS *Kraton*[®] termed FG1901 G is mentioned as well. It is of interest to find commercial styrenic TPE carrying functional units since such a polar modification could encourage adhesive bonding process or welding process with composite matrices as regards the industrial project. FG1901 G consists of a linear SEBS triblock with maleic anhydride (MA) grafted onto the rubbery midblock (1.0-2.0 wt% MA). MA-grafting improves the adhesion to nylon, poly(ester), ethylene vinyl alcohol, aluminum, steel, glass and many other substrates. It is very efficient impact modifier in nylon and poly(ester)s for making super tough engineering thermoplastic materials. FG1901 G exhibit sufficient stress-strain properties even though it appears to flow more easily at 230 °C compared to a similar SEBS (G1652 H).

In conclusion, SIS and SBS *Kraton*[®] appear to be decent reference materials for mechanical properties at room temperature although an apparent lack of hardness. SEBS *Kraton*[®] look more advantageous for our project, being tougher and more robust thermally (maintenance of the mechanical performance with temperature). The major drawback of these commercial SBC is presumably their poor thermal robustness especially at $T > 90$ °C when PS hard blocks start softening.

D. Synthesis of styrenic block copolymer TPE

D.1. Living ionic polymerization

Ionic polymerization is the most studied approach for the formation of styrenic block copolymers (SBC). It consists of a controlled/living chain polymerization that have ionic species as the active polymerization centers. Because of the differences in reactivity between carbanions and carbocations, different monomer classes are suitable for anionic and cationic polymerizations, although there is some overlap⁶¹.

D.1.1. Anionic polymerization

Anionic polymerization proceeds by formation of carbanions at the polymer chain ends as the active center and is a well-established method for the synthesis of tailored block copolymers. In industrial practice, this method is used to prepare several important classes of block copolymers including the SBC. The anionic polymerization of styrene and diene monomers is the typical example of a controlled block copolymer synthesis. These polymerizations are typically initiated by an organolithium species and proceed in the absence of chain termination or transfer. Under the appropriate conditions, these polymerizations are living and can be used for the formation of a variety of block copolymers with prescribed molecular weights, narrow molecular weight distributions, and well-defined block lengths. The solvents usually used are inert hydrocarbons, such as cyclohexane or toluene. Anionic polymerization methods are used for the preparation of the commercially important S-I-S and S-B-S triblock copolymers. More generally, a large majority of the styrenic block copolymer TPE commercially available are made by anionic polymerization. This synthesis can be accomplished by either sequential addition of monomers (polymerization starts at one end of the molecule and continues to the other end) or by chain coupling (polymerization starts at each end of the molecule and then the reactive chains are joined together by a coupling or linking agent). The preferred initiator for the sequential and coupling polymerization methods is *sec*-butyllithium because it initiates the polymerization very readily (initiation rate high in comparison to the rate of the subsequent polymerization). Styrenes and dienes make up the group of monomers most used for the preparation of block copolymers by anionic polymerization. Although there are only a handful of commercially available styrenes (styrene, alpha-methyl styrene...) and dienes (isoprene, butadiene...), by changing the synthetic conditions, changes in the diene polymerization *regio*- and *stereo*-selectivity can lead to changes in the polymer properties^{61,62}.

For example, the glass transition temperature of poly(butadiene) can be tuned by altering the fraction of the 1,2-content along the polymer backbone⁶³. In this way, the physical properties of the corresponding block copolymers can be systematically modified.

D.1.2. Cationic polymerization

Cationic polymerization (sometimes referred to as carbocationic polymerization) is used to polymerize monomers that cannot be polymerized anionically, although it can only be employed for a limited range of monomers. The most used monomers are styrenes, vinyl ethers, and isobutylene. In comparison to the anionic approach, the initiating systems in controlled cationic polymerization are often more complex. For preparing triblock copolymer, F-R-F difunctional initiators are used, where F represents a functional group such as chlorine, hydroxyl or methoxy group and R is a hydrocarbon moiety. In addition to the initiating species, a “co-initiator” is often used to modify the naturally high reactivity of the propagating cationic species. By decreasing the reactivity of the propagating center in cationic polymerization, side reactions such as chain transfer to monomer and chain termination can be significantly reduced⁶⁴.

A fairly recent development in the synthesis of SBC is the living cationic polymerization producing well-defined poly(styrene-*block*-isobutylene-*block*-styrene) (S-*i*B-S). The process is typically carried out at $T = -80\text{ }^{\circ}\text{C}$ in a moderately polar solvent. TiCl_4 or BCl_3 are used as co-initiators⁶⁵. Even though only P(*i*B) can comprise the center elastomeric block via this approach, various outer hard blocks can be inserted. In contrast to anionically prepared SBC, the styrenic block can be made up from α -methyl styrene, para-methyl styrene, para-tertiary-butyl styrene, para-chloro styrene, and other monomers⁶⁶. The high T_g values of these substituted styrenes and others mean a higher upper service temperature than the analog S-*i*B-S and S-EB-S block copolymers. Cationic polymerization using multifunctional initiators opens the possibilities to synthesize a variety of SBC as well, such as multi-arm star block copolymers and arborescent block copolymers comprising a dendritic (tree-like) P(*i*B) core carrying multiple PS outer blocks. The multiarm starblock copolymers are alternatives to linear block copolymers because their superior combination of and processing properties, including high combined with lower viscosities at similar molecular weights⁶⁷.

D.1.3. Drawbacks of living ionic polymerization

Without any doubt, living ionic polymerization, and more importantly anionic polymerization, is the most robust and effective technique to manufacture well-defined styrenic block copolymers. However, considering our industrial issue, two limiting factors can be mentioned.

First, the experimental conditions are stringent and demanding. Oxygen, water, or any other impurity must be completely eliminated to prevent undesirable reaction of the highly reactive propagating species. Even a concentration at the part per million level of these impurities can markedly affect the polymerization. The anionic polymerization high vacuum technique is the best method for the synthesis of model macromolecules even though it is a demanding, time-consuming method leading to a limited quantity of products. A high vacuum line (10^{-5} to 10^{-9} mbar) is typically composed of a high-quality mechanical vacuum pump (pressure reduced to 10^{-2} - 10^{-3} mbar), a mercury or oil diffusion pump (pressure down to about 10^{-5} mbar), a liquid nitrogen trap, an upper glass tube rig and a lower glass tube rig and stopcocks, as shown in [Figure 22a](#). A glass cutter and a hand torch are also necessary tools for making reactors. Moreover, prior to the polymerization, numerous steps are paramount.

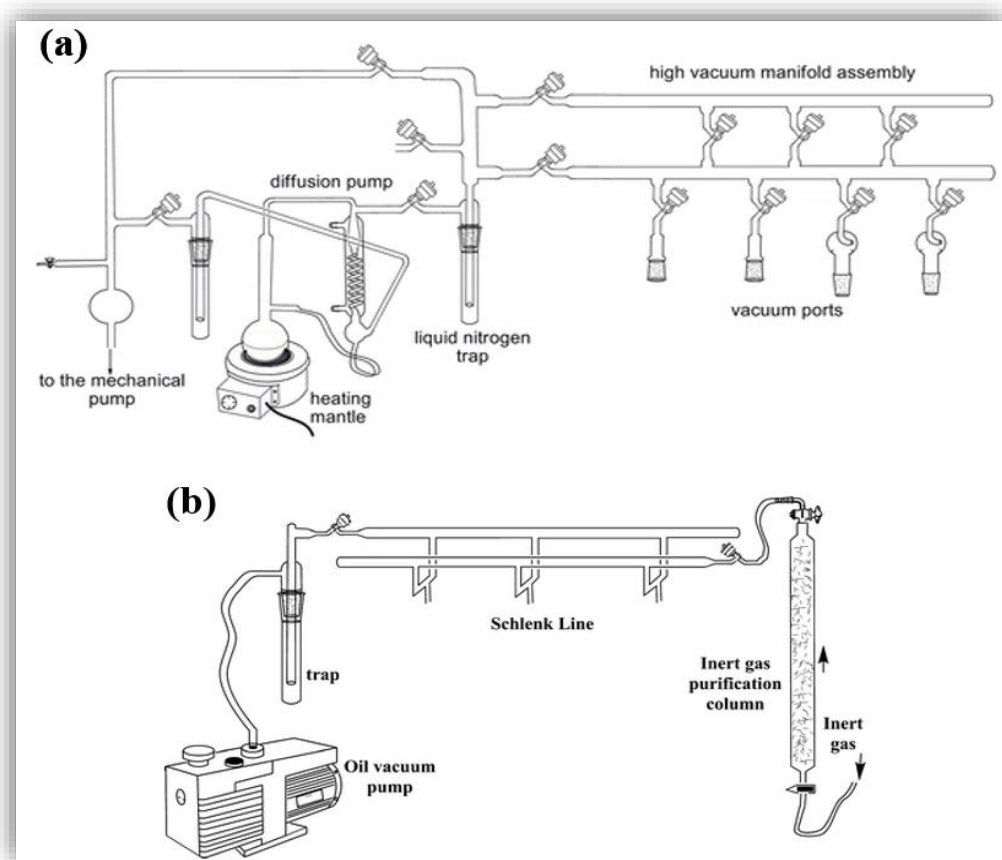


Figure 22. General representation of (a) a high vacuum line⁶⁸ and (b) a Schlenk line⁶⁹.

Degassing (mainly oxygen via freeze-thaw cycles), distillation of liquids (solvents, monomers...), dilution (concentrated reagent diluted with purified solvent) and ampoullization (collection of small quantities of solvent additives or alcohols) are common procedures. The initiator, such as *sec*-butyllithium (*sec*-BuLi), has to be dried over CaH₂ on the vacuum line, degassed thoroughly and distilled into a calibrated ampoule. Solvents and monomers have to be carefully purified as well. Benzene can be taken as an example. It is purified by stirring over concentrated sulfuric acid for a week in a conical flask inside a fume hood. Then, benzene is transferred carefully into a round-bottom flask containing finely grounded CaH₂ and a magnetic stir bar, attached to the vacuum line, and degassed. It is left for reaction of CaH₂ with and water present overnight. Then the benzene is again degassed and distilled into a calibrated cylinder containing polystyryllithium (PSLi) made from *n*-BuLi and styrene⁶⁸. In comparison with the high vacuum techniques, the Schlenk technique is a bit simpler to perform allowing anionic polymerization reactions to be carried out under inert gas condition in a commercially available Schlenk flask. The Schlenk method is also more amenable to carrying out reactions on a larger scale, whereas polymerizations carried out under high vacuum conditions with break seal techniques are usually conducted on the scale of about 10 g or less⁶⁹. A schematic of a Schlenk line is given in [Figure 22b](#).

A second disadvantage of the living ionic polymerization is that functionalized monomers are difficult to polymerize because the functional moieties are rarely compatible with the ions and counterions formed during the polymerization. Living anionic polymerization of acrylates and methacrylates for example is not so straightforward because of the serious side reactions derived from the functional groups in the polar monomers. In addition, exothermic rapid propagation and partially aggregated propagating species often cause broadening of the molecular weight distribution. Recently, a number of novel polymerization systems for (meth)acrylate monomers have been developed to overcome such drawbacks in controlling macromolecular architectures by suitably selecting the initiator, counter cation, solvent, additive, and polymerization temperature. One of the most striking examples is the binary initiator system of a bulky organolithium and LiCl in THF at -78 °C. More generally, this polymerization method has been incompatible with most of useful reactive functional groups, since the propagating chain ends of anionic living polymers are highly basic and extremely nucleophilic. It has been thus very difficult to polymerize functional monomers containing acidic or electrophilic substituents, such as OH, COOH, and CHO groups, under the anionic condition. It has to be noted that anionic polymerization of functional monomers has greatly progressed in the last three decades by mostly introducing the concept of protective groups. Poly(4-hydroxystyrene) was for instance produced anionically by protecting the acidic phenolic OH group with a bulky *tert*-butyldimethylsilyl group⁷⁰.

D.2. Reversible-deactivation radical polymerizations (RDRP)

D.2.1. Control of the macromolecular architecture by RDRP

Ionic polymerization is the most efficient method to produce well-defined block copolymers with generally an excellent control of the dispersity of the polymer chains lower than 1.1. Nevertheless, as discussed above, this kind of polymers is difficult to prepare (no oxygen, no moisture, high purity of monomers...) and quite a few monomers (styrene, butadiene, methyl methacrylate...) are consequently involved in industrial processes.

Such precise macromolecular synthesis employs concepts of living polymerization, in which the contribution of chain breaking reactions is minimized and the apparent simultaneous growth of all chains can be achieved via nearly instantaneous initiation. A combination of fast initiation and an absence of termination seemingly conflicts with the fundamental principles of radical polymerization, which proceeds via slow initiation and in which all chains are essentially dead at any given instant. However, the development of several controlled/living radical systems, termed reversible-deactivation radical polymerizations (RDRP), utilizing an intermittent formation of active propagating species has recently been realized concurrent with similar developments in ionic polymerization systems. A number of RDRP methods have been developed and the three most promising are: nitroxide-mediated polymerization (NMP), atom transfer radical polymerization (ATRP) and degenerative transfer with alkyl iodides, methacrylate macromonomers, and dithioesters via reversible addition-fragmentation chain transfer (RAFT) polymerization. To extend the lifetime of the propagating chains, each of these methods relies on establishing a dynamic equilibrium between a low concentration of active propagating chains and a predominant amount of dormant chains that are unable to propagate or terminate⁷¹. Radicals are reversibly trapped in a deactivation/activation process, as shown in [Figure 23](#).

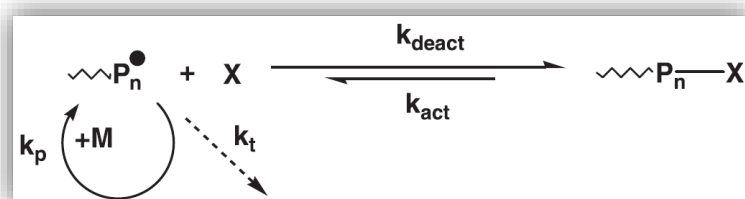


Figure 23. Illustration of the deactivation/activation process in RDRP⁷¹.

This approach relies on the persistent radical effect (PRE), which is a peculiar kinetic feature which provides a self-regulating effect in RDRP systems. Propagating radicals $P\bullet$ are rapidly trapped in the deactivation process (with a rate constant of deactivation, k_{deact}) by species X, which is typically a stable radical such as a nitroxide (by NMP). The dormant species are activated (with a rate constant, k_{act}) either spontaneously/thermally, in the presence of light, or with an appropriate catalyst (as in ATRP) to reform the growing centers. Consequently, while all chains are terminated in the conventional radical process, the terminated chains constitute a small fraction of all the chains ($\sim 1-10\%$) as a result of the greater number of growing chains in a RDRP process. The remaining chains are dormant species, capable of reactivation, functionalization, and chain extension to form block copolymers for instance⁷².

D.2.2. Block copolymer TPE by RAFT and ATRP

Various block copolymer TPE were achieved via RAFT. For instance, a series of well-controlled S-*n*BuA-S triblock (*n*BuA = *n*-butyl acrylate) copolymers ($M_n = 77-338 \text{ kg.mol}^{-1}$, $\bar{D} = 1.41-3.19$) were prepared by emulsion polymerization with a carefully designed amphiphilic macro-RAFT agent. The ultimate tensile strength reached 10 MPa with an elongation at break of 500% at the PS composition of 40-50 wt %⁷³. The RAFT of *N*-aryl itaconimide and dialkyl itaconate, which were generated from naturally derived itaconic acid, was also investigated⁷⁴. It allowed the production of well-defined polymers with controlled M_n and relatively low \bar{D} (≤ 1.59) and enabled block copolymerization to realize a novel, bio-based thermoplastic elastomer consisting of hard itaconimide and soft itaconate segments. The AFM images of the copolymer revealed a typical microphase-separated structure with co-continuous lamellae and/or cylinder morphologies. A last study can be mentioned. A series of poly(1-adamantyl acrylate)-*b*-poly(tetrahydrofurfuryl acrylate)-*b*-poly(1-adamantyl acrylate) triblock copolymers ($M_n = 47-201 \text{ kg.mol}^{-1}$, $\bar{D} = 1.66-3.03$) was prepared by RAFT and a strong microphase separation behavior was demonstrated⁷⁵. $E = 1.5-52.4 \text{ MPa}$, $\sigma_B = 1.1-2.6 \text{ MPa}$ and $\varepsilon_B = 240-803\%$ were measured for these all-acrylic-based TPE. The elasticity of these triblock copolymers was also demonstrated by the results of hysteresis experiments at around 250% deformation (residual strain of about 65% was observed after the deformation).

RAFT limitations include the lack of commercial availability and stability of many transfer agents, the removal of dithioester and some other end groups required due to their color, toxicity, and potential odor, and the difficulty associated with end-functionalization. Another shortcoming, directly linked to our industrial problematic, is that little has been reported on RAFT polymerizations of diene monomers. Lebreton *et al.* reported on RAFT polymerization of butadiene using various fluorinated dithiobenzoates as RAFT agents⁷⁶. Jitchum and Perrier reported on RAFT polymerization of isoprene with a decent control⁷⁷.

The main difficulty lies with the high polymerization temperatures that are required to obtain acceptable rates of fragmentation and perhaps to the stability of the RAFT agents.

The synthesis of well-defined B-A-B type triblock copolymer TPE via ATRP was attempted as well. Three examples can be cited. Wang and coworkers developed S-B-S ($M_n = 19 \text{ kg.mol}^{-1}$, $\bar{D} = 2.16$) and S-E-S (E = ether, $M_n < 13 \text{ kg.mol}^{-1}$, $\bar{D} = 1.34\text{-}1.58$) by the combination of the end-group transformation of prefabricated hydroxyl-terminated oligomers and ATRP⁷⁸. The hydroxyl-terminated oligomers, such as poly(ether) diol, poly(ester) diol and hydroxyl-terminated poly(butadiene), were reacted with chloroacetyl chloride to form α,ω -bichloroacetyl oligomers, used then as macro-initiator in the bulk polymerization of styrene. Poly(MMA-*b*-LMA-*b*-MMA) triblock (LMA = lauryl methacrylate, $M_n = 84 \text{ kg.mol}^{-1}$, $\bar{D} = 1.14$) by a two-stage ATRP in bulk at 35 °C using a complex as a catalyst and an initiator. The resulting triblock consists of a rubbery middle block ($T_{g,P(LMA)} \sim -65 \text{ °C}$) and glassy end blocks ($T_{g,P(MMA)} = 90\text{-}105 \text{ °C}$)⁷⁹. Lastly, the ATRP of MMA initiated by a α,ω -dibromo poly(*n*-butyl acrylate) P(*n*BuA) in the presence of $\text{NiBr}_2(\text{PPh}_3)_2$ led to P(MMA-*b*-*n*BuA-*b*-MMA) triblock copolymer ($M_n = 89\text{-}94 \text{ kg.mol}^{-1}$, $\bar{D} = 1.19\text{-}1.23$, $F_{\text{MMA}} = 0.22\text{-}0.23$)⁸⁰.

The main disadvantage of performing ATRP can be the use of a transition metal complex, which must often be removed from the final product, and a suitable ligand. More specifically for our project, ATRP of dienes remains a challenge since diene monomers can competitively displace ligands and generate less redox-active complexes. These competitive complex formation processes are especially important for low ppm copper processes. To overcome these issues, it is necessary to prepare more stable complexes (speciation) but with preserved activity and dynamics. Furthermore, high-molecular weight polymers are usually difficult to access by ATRP due to outer sphere electron transfer processes, involving oxidation or reduction radicals, as well as β -H elimination reactions⁸¹.

D.2.3. Focus on nitroxide-mediated polymerization (NMP)

In comparison to other RDRP processes, the NMP of diene monomers was well-reported. The NMP of conjugated dienes such as butadiene (B)^{82,83} and more importantly isoprene (I)⁸⁴ was studied from the early times of the technique by both the groups of Georges and Boutevin in both cases with 2,2,6,6-tetramethylpiperidiny-1-oxy (TEMPO), a stable free nitroxide. Well-defined homopolymers and copolymer architectures based on either B or I could be achieved using the 2,2,5-trimethyl-4-phenyl-3-azahexane-3-oxyl nitroxide (TIPNO), demonstrating the ability of the technique to provide high molar mass PB with low polydispersity indexes. Worth mentioning are block and random copolymers based on

associations of 1,3-dienes with functionalized vinyl monomers, including styrene, acrylate and methacrylate derivatives using TIPNO⁸⁵⁻⁸⁹. The controlled radical copolymerization of chloroprene or I with dimethyl 1,3-butadiene-1-phosphonate in the presence of TEMPO was later investigated, in a bimolecular initiating system⁹⁰. The living polymerization of bicyclic dienes was also studied with the aim of preparing thermally cross-linkable block copolymers⁹¹. *N-tert*-butyl-*N*-[1-diethylphosphono-(2,2-dimethylpropyl)] nitroxide (SG1) also demonstrated some great ability to control the polymerization of I⁹²⁻⁹⁴. In particular, Nicolas and co-workers reported on the effects of temperature, initiator concentration, initiator structure and solvent on the preparation of PI from a range of SG1-based initiators containing primary, secondary or tertiary homolytic initiating groups with various functionalities⁹³. Control over I polymerizations using acid-functionalized alkoxyamines was poor compared to polymerizations employing the corresponding *N*-hydroxysuccinimide (NHS)-ester alkoxyamines, which also opened the door to efficient functionalization. Accordingly, an important advantage that NMP offers over ATRP and RAFT polymerizations is in the ability to control effectively the polymerization of 1,3-dienes.

Moreover, it is today acknowledged that NMP is the easiest RDRP process, employing purely organic systems⁷¹. The latter, comprising radical initiator/nitroxide or alkoxyamine with or without additional nitroxide, are also typically simpler initiating systems compared to ATRP initiating systems, which require activated halide, metal halide, and ligand, but include traditionally additional additives to facilitate the polymerization. In comparison to RAFT polymerization, NMP does not require the use of sometimes unpleasant sulfur chemistry⁷¹.

References

- (1) Deepalekshmi, P.; Visakh, P. M.; Mathew, A. P.; Chandra, A. K.; Thomas, S. Advances in Elastomers: Their Blends and Interpenetrating Networks-State of Art, New Challenges and Opportunities. In *Advances in Elastomers I: Blends and Interpenetrating Networks*; Visakh, P. M., Thomas, S., Chandra, A. K., Mathew, A. P., Eds.; Springer-Verlag: Berlin, **2013**; 1-10.
- (2) Edwards, S. F. The Theory of Rubber Elasticity. *The British Polymer Journal* **1977**, 140-143.
- (3) Braun, D.; Cherdrón, H.; Rehahn, M.; Ritter, H.; Voit, B. Modification of Macromolecular Substances. In *Polymer Synthesis: Theory and Practice*; Braun, D., Cherdrón, H., Rehahn, M., Ritter, H., Voit, B., Eds.; Springer: Berlin, **2001**; 329-380.
- (4) Atkins, P.; De Paula, J. Materials 1: Macromolecules and Self-Assembly. In *Atkins' Physical Chemistry*; Atkins, P., De Paula, J., Eds.; Oxford University Press: New York, **2010**; 659-694.
- (5) Shanks, R. A.; Kong, I. General Purpose Elastomers: Structure, Chemistry, Physics and Performance. In *Advances in Elastomers I: Blends and Interpenetrating Networks*; Visakh, P. M., Thomas, S., Chandra, A. K., Mathew, A. P., Eds.; Springer-Verlag: Berlin, **2013**; 11-46.
- (6) Cowie, J. M. G. The Elastomeric State. In *Polymers: Chemistry and Physics of Modern Materials, 2nd Edition*; Cowie, J. M. G., Ed.; Nelson Thornes Ltd: Cheltenham, **1991**; Chapter 14, 304-320.
- (7) Rajesh Babu, R.; Shibulal, G. S.; Chandra, A. K.; Naskar, K. Compounding and Vulcanization. In *Advances in Elastomers I: Blends and Interpenetrating Networks*; Visakh, P. M., Thomas, S., Chandra, A. K., Mathew, A. P., Eds.; Springer-Verlag: Berlin, **2013**; 83-136.
- (8) Sunder, J. Morphology and Mechanical Properties of Natural Rubber/Polyolefin Blends. In *Elastomer Technology Handbook*; Cheremisinoff, N. P., Ed.; CRC Press: Boca Raton, **1993**; 381-398.
- (9) Bhattacharjee, S.; Bhowmick, A. K.; Avasthi, B. Properties and Degradation of Nitrile Rubber. In *Elastomer Technology Handbook*; Cheremisinoff, N. P., Ed.; CRC Press: Boca Raton, **1993**; 518-555.
- (10) Schweitzer, P. A. Nitrile Rubber (NBR, BUNA-N). In *Encyclopedia of Corrosion Technology, Second Edition, Revised and Expanded*; Schweitzer, P. A., Ed.; Marcel Dekker, Inc.: New York, **2004**; 415-418.
- (11) Nagdi, K. Composition and Properties of 30 Rubber Types. In *Rubber as an Engineering Material: Guide for Users*; Nagdi, K., Ed.; Hanser Publishers: Munich, **1993**; Chapter 1.
- (12) Thorn, A. D.; Robinson, R. A. Compound Design. In *Rubber Products Manufacturing Technology*; Bhowmick, A. K., Hall, M. M., Benarey, H. A., Eds.; Marcel Dekker, Inc.: New York, **1994**; 1-94.
- (13) Krejsa, M. R.; Koenig, J. L. The Nature of Sulfur Vulcanization. In *Elastomer Technology Handbook*; Cheremisinoff, N. P., Ed.; CRC Press: Boca Raton, **1993**; 475-494.
- (14) Payne, M. T.; Rader, C. P. Thermoplastic Elastomers: A Rising Star. In *Elastomer Technology Handbook*; Cheremisinoff, N. P., Ed.; CRC Press: Boca Raton, **1993**; 557-594.
- (15) Messler, R. W. Joining of Polymers. In *Joining of Materials and Structures: From Pragmatic Process to Enabling Technology*; Messler, R. W., Ed.; Elsevier: Oxford, **2004**; 621-648.
- (16) Gent, A. N. Rubber Elasticity: Basic Concepts and Behavior. In *Science and Technology of Rubber, Second Edition*; Mark, J. E., Erman, B., Eirich, F. R., Eds.; Academic Press: San Diego, **1994**; 1-22.
- (17) Geil, P. H. *Polymer Single Crystals*; Wiley-Interscience: New-York, **1963**.
- (18) Kinsey, R. H. Ionomers, Chemistry and New Developments. *Appl. Polym. Symp.* **1969**, 11 (77).
- (19) Hsieh, H. L.; Farrar, R. C. Polymers, Rubbers, Synthetic (Block Copolymers). In *Encyclopedia of Chemical Processing and Design*; McKetta, J. J., Cunningham, W. A., Eds.; Marcel Dekker, Inc.: New York, **1992**; 32-66.
- (20) Drobny, J. G. Introduction. In *Handbook of Thermoplastic Elastomers*; Drobny, J. G., Ed.; William Andrew Inc.: Norwich, **2007**; 1-8.
- (21) Whelan, T. Dictionary. Alphabetic. In *Polymer Technology Dictionary*; Whelan, T., Ed.; Chapman & Hall: London, **1994**; 438-450.
- (22) Kear, K. E. Developments in Thermoplastic Elastomers. In *Rapra Review Reports*; Humphreys, S., Ed.; Rapra Technology Limited: Shrewsbury, **2003**; 3-6.
- (23) Flory, P. *Principles of polymer chemistry*; George Fisher Baker non-resident lectureship in chemistry at Cornell University; New Cornell University Press: New York, **1953**.
- (24) Odian, G. *Principles of Polymerization*, 4th ed.; John Wiley & Sons: Hoboken, NJ, **2004**; 812.
- (25) Flory, P. *Principles of Polymer Chemistry*; Cornell University Press: Ithaca, New York, **1975**.

- (26) Bates, F. S. Block Copolymer Thermodynamics: Theory and Experiment. *Annu. Rev. Phys. Chem.* **1990**, *41*, 525-57.
- (27) Costa, F. R.; Dutta, N. K.; Choudhury, N. R.; Bhowmick, A. K. Thermoplastic Elastomers. In *Current Topics in Elastomers Research*; Bhowmick, A. K., Ed.; CRC Press: Boca Raton, **2008**; 101-164.
- (28) Fetters, L. J.; Lohse, D. J.; Colby, R. H. Chain Dimensions and Entanglement Spacings. In *Physical Properties of Polymers Handbook, 2nd Edition*; Mark, J. E., Ed.; Springer: New York, **2007**; 447-454.
- (29) Cunningham, R. E.; Auerbach, M. Preparation and Stress-Strain Properties of SBS and SIS Block Polymers made with Dilithium Initiators. *J. Appl. Polym. Sci.* **1972**, *16*, 163-173.
- (30) Hansen, C. M. *Hansen Solubility Parameters, A User's Handbook*, 2nd ed.; CRC Press: New York, **2007**; 32-43.
- (31) Camacho, J.; Diez, E.; Diaz, I.; Ovejero, G. Hansen Solubility Parameters: From Polyethylene and Poly(vinyl acetate) Homopolymers to Ethylene-Vinyl acetate Copolymers. *Polym. Int.* **2017**, *66*, 1013-1020.
- (32) Morton, M. Morphology and Structure-Property Relations of ABA Triblock Copolymers. In *Anionic Polymerization: Principles and Practice*; Morton, M., Ed.; Academic Press: New York, **1983**; 201-213.
- (33) Chung, C. I.; Gale, J. C. Newtonian Behavior of a Styrene-Butadiene-Styrene Block Copolymer. *J. Polym. Sci., Polym. Phys. Ed.* **1976**, *14* (6), 1149-1156.
- (34) Gouinlock, E. V.; Porter, R. S. Linear Dynamic Mechanical Properties of an SBS Block Copolymer. *Polym. Eng. Sci.* **1977**, *17* (8), 535-543.
- (35) Drobny, J. G. Introduction. In *Handbook of Thermoplastic Elastomers*; Drobny, J. G., Ed.; William Andrew Inc.: Norwich, **2007**; 161-178.
- (36) Haenelt, T. G.; Georgopoulos, P.; Abetz, C.; Rangou, S.; Alisch, D.; Meyer, A.; Handge, U. A.; Abetz, V. Morphology and Elasticity of Polystyrene-*block*-polyisoprene Diblock Copolymers in the Melt. *Korea-Australia Rheology Journal* **2014**, *26* (3), 263-275.
- (37) Wang, W.; Lu, W.; Kang, N.-G.; Mays, J.; Hong, K. Thermoplastic Elastomers based on Block, Graft, and Star Copolymers. In *Elastomers*; Cankaya, N., Ed.; InTechOpen: **2017**; 97-120.
- (38) Fetters, L. J.; Firer, E. M.; Dafauti, M. Synthesis and Properties of Block Copolymers. 4. Poly(*p*-*tert*-butylstyrene-*diene-p*-*tert*-butylstyrene) and Poly(*p*-*tert*-butylstyrene-*isoprene-styrene*). *Macromolecules* **1977**, *10* (6), 1200-1207.
- (39) Fetters, L. J.; Morton, M. Synthesis and Properties of Block Polymers. I. Poly- α -methylstyrene-polyisoprene-poly- α -methylstyrene. *Macromolecules* **1969**, *2* (5), 453-458.
- (40) Bolton, J. M.; Hillmyer, M. A.; Hoyer, T. R. Sustainable Thermoplastic Elastomers from Terpene Derived Monomers. *ACS Macro Letters* **2014**, *3* (8), 717-720.
- (41) Kobayashi, S.; Kataoka, H.; Ishizone, T.; Kato, T.; Ono, T.; Kobukata, S.; Ogi, H. Synthesis and Properties of New Thermoplastic Elastomers containing Poly[4-(1-adamantyl) styrene] Hard Segments. *Macromolecules* **2008**, *41* (14), 5502-5508.
- (42) Yu, J. M.; Dubois, P.; Jérôme, R. Poly[alkyl methacrylate-*b*-butadiene-*b*-alkyl methacrylate] Triblock Copolymers: Synthesis, Morphology, and Mechanical Properties at High Temperatures. *Macromolecules* **1996**, *29* (26), 8362-8370.
- (43) Imaizumi, K.; Ono, T.; Natori, I.; Sakurai, S.; Takeda, K. Microphase-separated Structure of 1,3-Cyclohexadiene / Butadiene Triblock Copolymers and its Effect on Mechanical and Thermal Properties. *Journal of Polymer Science Part B: Polymer Physics* **2001**, *39* (1), 13-22.
- (44) Wang, W.; Schlegel, R.; White, B. T.; Williams, K.; Voyloy, D.; Steren, C. A.; Goodwin, A.; Coughlin, E. B.; Gido, S.; Beiner, M.; Hong, K. High temperature Thermoplastic Elastomers Synthesized by Living Anionic Polymerization in Hydrocarbon Solvent at Room Temperature. *Macromolecules* **2016**, *49* (7), 2646-2655.
- (45) McManus, N. T.; Rempel, G. L. Chemical Modification of Polymers: Catalytic Hydrogenation and Related Reactions. *J. Macromol. Sci., Part C* **1995**, *35* (2), 239-285.
- (46) Mohammadi, N. A.; Rempel, G. L. Homogeneous Catalytic Hydrogenation of Polybutadiene. *J. Mol. Cat.* **1989**, *50* (3), 259-275.
- (47) Esneault, C. P.; Hahn, S. F.; Meyers, G. F. Development of Elastomers Based on Fully Hydrogenated Styrene-Diene Block Copolymers. In *Developments in Block Copolymer Science and Technology*; Hamley, I. W., Ed.; John Wiley & Sons: Chichester, **2004**; 341-362.
- (48) Adkins, H. Hazards in Catalytic Hydrogenation at Elevated Temperatures and Pressures. *J. Am. Chem. Soc.* **1931**, *53* (7), 2808-2809.
- (49) Parker, D. K. Emulsion Polymers (Noncatalytic Diimide Hydrogenation). In *Polymeric Materials Encyclopedia, 12 Volume Set*; Salamone, J. C., Ed.; CRC Press: New York, **1996**; 2048-2053.
- (50) Hahn, S. F. An Improved Method for the Diimide Hydrogenation of Butadiene and Isoprene Containing Polymers. *J. Polym. Sci., Part A: Polym. Chem.* **1992**, *30*, 397-408.
- (51) Wu, Z.; Papandrea, J. P.; Apple, T.; Interrante, V. Cross-Linkable Carbosilane Polymers with Imbedded Disilacyclobutane Rings Derived by Acyclic Diene Metathesis Polymerization. *Macromolecules* **2004**, *37*, 5257-5264.

- (52) Piya-areetham, P.; Prasassarakich, P.; Rempel, G. L. Organic Solvent-Free Hydrogenation of Natural Rubber Latex and Synthetic Polyisoprene Emulsion Catalyzed by Water-Soluble Rhodium Complexes. *Journal of Molecular Catalysis A: Chemical* **2013**, 372, 151-159.
- (53) Hsieh, H. L.; Yeh, H. C. Polymers from Hydrogenated Polydienes prepared with Neodymium Catalysts. In *Advances in Elastomers and Rubber Elasticity*; Lal, J., Mark, J. E., Eds.; Springer: New York, **1986**; pp 197-220.
- (54) Hinchiranan, N.; Prasassarakich, P.; Charmondusit, K.; Rempel, G.L. Hydrogenation of Synthetic *cis*-1,4-Polyisoprene and Natural Rubber Catalyzed by [Ir(COD)py(PCy₃)PF₆]. *J. Appl. Polym. Sci.* **2006**, 100, 4219-4233.
- (55) Yu, J. M.; Yu, Y.; Dubois, P.; Teyssié, P.; Jérôme, R. Synthesis and Characterization of Hydrogenated Poly[alkylmethacrylate(*b*-styrene)-*b*-butadiene-*b*-(styrene-*b*-) alkylmethacrylate] Triblock and Pentablock Copolymers. *Polymer* **1997**, 38 (12), 3091-3101.
- (56) Araki, Y.; Shimizu, D.; Hori, Y.; Nakatani, K.; Saito, H. Mechanical Properties and Microphase Structure of Hydrogenated S-SB-S Triblock Copolymers. *Polymer Journal* **2013**, 45, 1140-1145.
- (57) Hoover, J. M.; Ward, T. C.; McGrath, J. E. Hydrogenated Star Block Copolymers of Butylstyrene, Isoprene and Divinylbenzene. In *Advances in Polyolefins: The World's Most Widely Used Polymers*; Seymour, R. B., Cheng, T. C., Eds.; Springer: New York, **1987**; 89-96.
- (58) Holden, G.; Wilder, C. R. Thermoplastic Styrenic Block Copolymers. In *Handbook of Elastomers, 2nd Edition, Revised and Expanded*; Bhowmick, A. K., Stephens, H., Eds.; Marcel Dekker, Inc.: New York, **2001**; 321-386.
- (59) Bening, R. C.; Korcz, W. H.; Handlin, D. L. Styrenic Block Copolymer Elastomers. In *Modern Styrenic Polymers: Polystyrenes and Styrenic Copolymers*; Scheirs, J., Priddy, D., Eds.; John Wiley & Sons, Ltd: Chichester, **2003**; 465-480.
- (60) Holden, G. Thermoplastic Elastomers and Their Applications. In *Applied Polymer Science: 21st Century*; Craver, C., Carraher, C., Eds.; Elsevier: Oxford, **2000**; 231-256.
- (61) Theodosopoulos, G.; Pitsikalis, M. Block Copolymers by Anionic Polymerization: Recent Synthetic Routes and Developments. In *Anionic Polymerization: Principles, Practice, Strength, Consequences and Applications*; Hadjichristidis, N., Hirao, A., Eds.; Springer: Tokyo, **2015**; 541-550.
- (62) Hsieh, H. L.; Quirk, R. P. Commercial Applications of Anionically Prepared Polymers. In *Anionic Polymerization: Principle and Practical Applications*; Hsieh, H. L., Quirk, R. P., Eds.; Marcel Dekker: New York, **1996**; 475-532.
- (63) He, T.; Li, B.; Ren, S. Glass Transition Temperature and Chain Flexibility of 1,2-Polybutadiene. *J. Appl. Polym. Sci.* **1986**, 31 (3), 873-884.
- (64) Aoshima, S.; Kanaoka, S. A Renaissance in Living Cationic Polymerization. *Chem. Rev.* **2009**, 109 (11), 5245-5287.
- (65) Storey, R. F.; Baugh, D. W.; Choate, K. R. Poly(styrene-*b*-isobutylene-*b*-styrene) Block Copolymers Produced by Living Cationic Polymerization: I. Compositional Analysis. *Polymer* **1999**, 40 (11), 3083-3090.
- (66) Kanaoka, S.; Eika, Y.; Sawamoto, M.; Higashimura, T. Living Cationic Polymerization of *p*-Chlorostyrene and Related Para-Substituted Styrene Derivatives at Room Temperature. *Macromolecules* **1996**, 29 (5), 1778-1783.
- (67) Kaszas, G.; Puskas, J.; Kennedy, J. P.; Hager, W. G. J. Polyisobutylene-containing Block Polymers by Sequential Monomer Addition. II. Polystyrene-polyisobutylene-polystyrene Triblock Polymers: Synthesis, Characterization, and Physical Properties. *J. Polym. Sci., Part A: Polym. Chem.* **1991**, 29, 427-435.
- (68) Ratkanthwar, K.; Hadjichristidis, N.; Mays, J. W. High Vacuum Techniques for Anionic Polymerization. In *Anionic Polymerization: Principles, Practice, Strength, Consequences and Applications*; Hadjichristidis, N., Hirao, A., Eds.; Springer: Tokyo, **2015**; 19-60.
- (69) Ratkanthwar, K.; Zhao, J.; Zhang, H.; Hadjichristidis, N.; Mays, J. W. Schlenk Techniques for Anionic Polymerization. In *Anionic Polymerization: Principles, Practice, Strength, Consequences and Applications*; Hadjichristidis, N., Hirao, A., Eds.; Springer: Tokyo, **2015**; 3-18.
- (70) Ishizone, T.; Goseki, R. Living Anionic Addition Polymerization. In *Encyclopedia of Polymeric Nanomaterials*; Kobayashi, S., Mullen, K., Eds.; Springer: Berlin, **2014**; 1-18.
- (71) Braunecker, W. A.; Matyjaszewski, K. Controlled/Living Radical Polymerization: Features, Developments, and Perspectives. *Prog. Polym. Sci.* **2007**, 32, 93-146.
- (72) Matyjaszewski, K.; Spanswick, J. Controlled/Living Radical Polymerization. *Materials Today* **2005**, 26-33.
- (73) Luo, Y.; Wang, X.; Zhu, Y.; Li, B. -G.; Zhu, S. Polystyrene-block-poly(*n*-butyl acrylate)-block-polystyrene Triblock Copolymer Thermoplastic Elastomer Synthesized via RAFT Emulsion Polymerization. *Macromolecules* **2010**, 43, 7472-7481.
- (74) Satoh, K.; Lee, D. -H.; Nagai, K.; Kamigaito, M. Precision Synthesis of Bio-Based Acrylic Thermoplastic Elastomer by RAFT Polymerization of Itaconic Acid Derivatives. *Macromol. Rapid Commun.* **2013**, 35 (2), 161-167.
- (75) Lu, W.; Wang, Y.; Wang, W.; Cheng, S.; Zhu, J.; Xu, Y.; Hong, K.; Kang, N. -G.; Mays, J. All Acrylic-based Thermoplastic Elastomers with High Upper Service Temperature and Superior Mechanical Properties. *Polym. Chem.* **2017**, 8, 5741-5748.

- (76) Lebreton, P.; Ameduri, B.; Boutevin, B.; Corpart, J. -M. Use of Original ω -Perfluorinated Dithioesters for the Synthesis of Well-Controlled Polymers by Reversible Addition-Fragmentation Chain Transfer (RAFT). *Macromol. Chem. Phys.* **2002**, *203* (3), 522-537.
- (77) Jitchum, V.; Perrier, S. Living Radical Polymerization of Isoprene via the RAFT Process. *Macromolecules* **2007**, *40* (5), 1408-1412.
- (78) Wang, X. -S.; Luo, N.; Ying, S. -K.; Liu, Q. The Synthesis of ABA Block Copolymers of 'Living'/Controlled Radical Polymerization using Hydroxy-terminated Oligomers as Precursors. *Eur. Polym. J.* **2000**, *36* (1), 149-156.
- (79) Chatterjee, D. P.; Mandal, B. M. The ATRP Synthesis of the Potential Thermoplastic Elastomer Poly(methyl methacrylate)-b-(lauryl methacrylate)-b-(methyl methacrylate) Unrealized by Ionic Polymerization. *Macromol. Symp.* **2006**, *240*, 224-231.
- (80) Moineau, G.; Minet, M.; Teyssié, P.; Jérôme, R. Synthesis of Fully Acrylic Thermoplastic Elastomers by Atom Transfer Radical Polymerization (ATRP), 2: Effect of the Catalyst on the Molecular Control and the Rheological Properties of the Triblock Copolymers. *Macromol. Chem. Phys.* **2000**, *201*, 1108-1114.
- (81) Matyjaszewski, K. Atom Transfer Radical Polymerization (ATRP): Current Status and Future Perspectives. *Macromolecules* **2012**, *45* (12), 4015-4039.
- (82) Pradel, J. L.; Ameduri, B.; Boutevin, B. Use of Controlled Radical Polymerization of Butadiene with AIBN and Tempo for the Determination of the NMR Characteristics of Hydroxymethyl Groups. *Macromol. Chem. Phys.* **1999**, *200*, 2304-2308.
- (83) Pradel, J. L.; Ameduri, B.; Boutevin, B. Controlled Radical Polymerization of 1,3-Butadiene. II. Initiation by Hydrogen Peroxide and Reversible Termination by Tempo. *J. Polym. Sci., Part A: Polym. Chem.* **2000**, *38*, 3293-3302.
- (84) Keoshkerian, B.; Georges, M.; Quinlan, M.; Veregin, R.; Goodbrand, B. Polyacrylates and Polydienes to High Conversion by a Stable Free Radical Polymerization Process: Use of Reducing Agents. *Macromolecules* **1998**, *31*, 7559-7561.
- (85) Benoit, D.; Harth, E.; Fox, P.; Waymouth, R. M.; Hawker, C. J. Accurate Structural Control and Block Formation in the Living Polymerization 1,3-Dienes by Nitroxide-Mediated Procedures. *Macromolecules* **2000**, *33*, 363-370.
- (86) Cheng, C.; Qi, K.; Khoshdel, E.; Wooley, K. L. Tandem Synthesis of Core-Shell Brush Copolymers and their Transformation to Peripherally Cross-linked and Hollowed Nanostructures. *J. Am. Chem. Soc.* **2006**, *128*, 6808-6809.
- (87) Wegrzyn, J. K.; Stephan, T.; Lau, R.; Grubbs, R. B. Preparation of Poly(ethylene oxide)-block-poly(isoprene) by Nitroxide Mediated Free Radical Polymerization from PEO Macroinitiators. *J. Polym. Sci., Part A: Polym. Chem.* **2005**, *43*, 2977-2984.
- (88) Sundararaman, A.; Stephan, T.; Grubbs, R. B. Reversible Restructuring of Aqueous Block Copolymer Assemblies through Stimulus Induced Changes in Amphiphilicity. *J. Am. Chem. Soc.* **2008**, *130*, 12264-12265.
- (89) Cai, Y.; Aubrecht, K. B.; Grubbs, R. B. Thermally Induced Changes in Amphiphilicity Drive Reversible Restructuring of Assemblies of ABC Triblock Copolymers with Statistical Polyether Blocks. *J. Am. Chem. Soc.* **2010**, *133*, 1058-1065.
- (90) Ajellal, N.; Thomas, C. M.; Carpentier, J. -F. Controlled Radical Polymerization of Conjugated 1,3-Dienes with Methyl 1,3-Butadiene-1-phosphonate. *Polymer* **2008**, *49*, 4344-4349.
- (91) Luo, K.; Rzaev, J. Living Radical Polymerization of Bicyclic Dienes: Synthesis of Thermally Cross-linkable Block Copolymers. *Macromolecules* **2009**, *42*, 9268-9274.
- (92) Matsuoka, H.; Suetomi, Y.; Kaewsaiha, P.; Matsumoto, K. Nanostructure of a Poly(acrylic acid) Brush and its Transition in the Amphiphilic Diblock Copolymer Monolayer on the Water Surface. *Langmuir* **2009**, *25*, 13752-13762.
- (93) Harrisson, S.; Couvreur, P.; Nicolas, J. SG1 Nitroxide-Mediated Polymerization of Isoprene: Alkoxyamine Structure/Control Relationship and α,ω -chain-end Functionalization. *Macromolecules* **2011**, *44*, 9230-9238.
- (94) Harrisson, S.; Couvreur, P.; Nicolas, J. Use of Solvent Effects to Improve Control over Nitroxide-Mediated Polymerization of Isoprene. *Macromol. Rapid Commun.* **2012**, *33*, 805-810.

**PART II. β -Myrcene-based copolymers
by nitroxide-mediated
controlled radical
polymerization (NMP)**

Chapter 1. Optimization of the β -myrcene nitroxide-mediated polymerization (NMP) and synthesis of well-defined β -myrcene / styrene block copolymers

1.1. Preface

Pending the acquisition of high pressure reactors to polymerize isoprene (low boiling point), β -myrcene (*My*), a non-volatile 1,3-diene, was first considered as a promising building block for making the flexible segment of the thermoplastic elastomer. This chapter presents an article published in the journal *Macromolecules* (Métafiot, A.; Kanawati, Y.; Gérard, J. -F.; Defoort, B.; Maric, M. Synthesis of β -Myrcene-Based Polymers and Styrene Block and Statistical Copolymers by SG1 Nitroxide-Mediated Controlled Radical Polymerization. *Macromolecules* **2017**, *50*, 3101-3120). It details first the optimized controlled polymerization of β -myrcene by nitroxide-mediated polymerization. The subsequent synthesis of *My*-S diblock and S-*My*-S triblock copolymers (S = styrene) was made possible by the active feature of the well-defined P(*My*) elastomeric segment.

1.2. Abstract

Nitroxide-mediated polymerization (NMP) of β -myrcene (*My*) at 120 °C in bulk using unimolecular SG1-based succinimidyl ester-functionalized BlocBuilder™ (BB) alkoxyamine resulted in low dispersity ($\mathcal{D} = 1.1-1.4$) poly(myrcene)s P(*My*)s with high SG1 chain end fidelity. The polymerizations also showed the number-average molecular weights (M_n) increased almost linearly with conversion. SG1-terminated P(*My*) macroinitiators were cleanly chain-extended with styrene (S) and the S-rich P(*My*-*b*-S) diblock copolymers exhibited two distinct glass transition temperatures (T_{gs}), indicative of micro-phase separation. P(*My*-*b*-S) diblocks showed brittle stress-strain behavior, plausibly due to relatively low M_n . *My*/S mixtures, with initial S molar feed compositions $f_{s,0} = 0.10-0.94$ were also statistically copolymerized ($M_n = 8.2-19.8$ kg.mol⁻¹, $\mathcal{D} \leq 1.37$ and monomodal distributions). Copolymer reactivity ratios were $r_s = 0.25 \pm 0.04 / 0.34 \pm 0.19$ and $r_{My} = 1.88 \pm 0.12 / 2.19 \pm 0.07$ using Fineman-Ross and Kelen-Tüdös methods. The statistical P(*My*-*stat*-S) copolymers displayed a range of T_{gs} (− 77 to + 30 °C) depending on *My* molar fraction. *My*-rich and S-rich P(*My*-*stat*-S)s were then successfully chain-extended with both S and *My*.

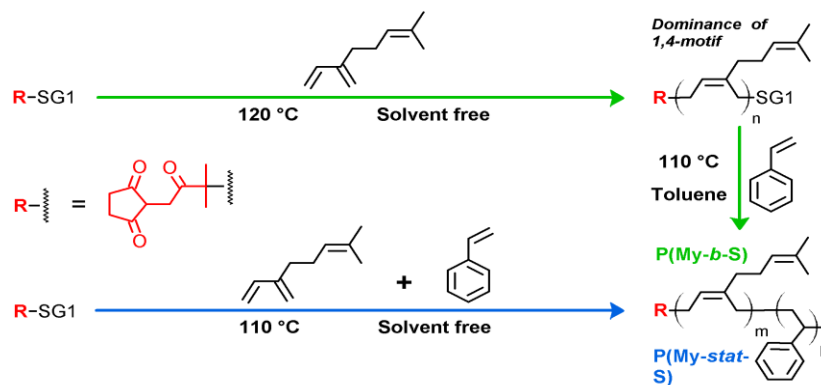


Table of contents graphic. Synthesis of P(My), P(My-stat-S) and P(My-b-S) polymers by NMP.

1.3. Introduction

Terpenes are hydrocarbons that contain one or more carbon–carbon double bonds and share the same elementary unit as isoprene. They are a class of important bio-derived compounds^{1,2} and have been known for hundreds of years as components of essential oils obtained from leaves, flowers, and fruits of many plants³. Among the vast members of the terpene family, β -myrcene (7-methyl-3-methylene-octa-1,6-diene, abbreviated *My*) particularly is an interesting “renewable” monomer, as it is a component of the bay, ylang–ylang, wild thyme, lemon grass, and juniper berry essential oils³. It is an acyclic monoterpene with a highly active conjugated diene structure that can be polymerized by classical polymerization methods. Based upon its relatively low cost³ and ease of isolation^{4,8}, *My* has been studied quite extensively as a starting material for polymers. Similar to other 1,3-dienes, such as butadiene and isoprene, *My* also forms rubbery polymers when polymerized. It is either used in small amounts as an additive to adjust elastomeric properties, or as a main component in poly(myrcene)s P(*My*)s³. For instance, the syntheses of styrene/ β -myrcene (*S/My*) copolymers and *My*-based composites showed that the use of *My* improved the mechanical properties of poly(styrene)-based plastics⁹. Likewise, Cawse and coworkers incorporated hydroxyl-functionalized P(*My*) into a poly(urethane) leading to improved stress-strain behavior and impact properties¹⁰. Hence, *My*, either as a homopolymer or when copolymerized with another monomer, can provide a wide latitude of polymer properties. *My*'s polymerization was comprehensively studied by conventional free radical polymerization¹¹⁻¹⁶. Coordination polymerization was also applied to this acyclic conjugated diene. For example, Loughmari and Georges et al. reported stereoselective polymerization of *My* utilizing a lanthanide-based catalyst¹⁷. Living or quasi-living ionic polymerizations of *My* have been explored as well. For instance, Sivola et al reported the synthesis of living P(*My*)s via anionic

polymerization initiated by *n*-butyllithium (*n*-BuLi)¹⁸. This approach allows manufacturing tailor-made macromolecules with precise and pre-determined molar masses, compositions, topologies and functionalities. P(*My*-*b*-S) triblock copolymer, which could be used as a thermoplastic elastomer, was made in this way by Quirk et al^{19,20}. Hoyer and Hillmyer reported a similar polymer combined with bio-based α -methyl-*p*-methylstyrene prepared by the dehydrogenation of limonene²¹. In spite of these successful outcomes by living anionic polymerization, this technique exhibits one main disadvantage which is the requirement of stringent reaction conditions, especially the use of chemically ultrapure reagents as well as the absolute removal of air and of traces of water²². Polymer chemists have long desired to develop polymerization processes that combine the control of microstructure typified by ionic polymerization but with the ease of industrial implementation typified by other types of polymerization such as free radical or addition polymerization.

The advances in macromolecular synthesis in the last two decades provided a game-changing synthetic tool to easily achieve complex macromolecular architectures: reversible-deactivation radical polymerization (RDRP)²³⁻²⁷. In comparison to living anionic and cationic polymerizations, RDRP differs by its relative ease-of-use since only dissolved oxygen has to be eliminated, it can polymerize a wide variety of vinylic monomers by a radical mechanism that are not possible ionically, and the latitude in process conditions possible (bulk, solution, emulsion, dispersion, etc.)²⁸. The three major families of RDRP are nitroxide-mediated polymerization (NMP)^{25,26,29}, atom transfer radical polymerization (ATRP)^{24,30-32} and reversible addition fragmentation transfer polymerization (RAFT)^{23,33-35}.

RDRP applied to *My* is a great opportunity to produce high value-added polymers with a segment based on renewable monomers. Surprisingly enough, RDRP-based P(*My*) has not been synthesized and characterized prior to 2015. Very recently, the first RDRP of *My* was successfully performed by RAFT³⁶. However, NMP has so far never been applied for *My* polymerization, whereas this process exhibits some advantages: NMP does not rely on sulfur-based chain transfer agents like RAFT does or metallic ligands that ATRP required, which may contaminate polymers for some applications^{37,38}. NMP is historically the first and represents perhaps the easiest RDRP technology to apply as the initiators and mediators are directly available from commercial sources. Although the synthesis of this poly(terpene) by NMP has not been studied yet, other 1,3-diene monomers were polymerized in a controlled manner. Indeed, isoprene and butadiene were successfully polymerized by NMP. The achievement of relatively broad molecular weight distribution NMP-based polyisoprenes ($\bar{D} = M_w/M_n$, dispersity of 1.36-1.53) with the use of TEMPO, the first-generation stable nitroxide, was reported in the late 1990s^{39,40}. Hawker and co-workers used then a TIPNO-based initiator⁴⁶, 2,2,5-trimethyl-3-(1-phenylethoxy)-4-phenyl-3-azahexane to produce polyisoprenes and polybutadienes with relatively high number-average molar masses ($M_n > 80\ 000\ \text{g}\cdot\text{mol}^{-1}$) and narrow molecular weight distributions ($\bar{D} < 1.3$)⁴¹. Grubbs et al synthesized a well-defined

poly(isoprene) sample ($\bar{D} = 1.28$) using 2,2-dimethyl-3-(1-phenylethoxy)-4-phenyl-3-azapentane alkoxyamine produced by the addition of two equivalents of 1-phenylethyl radical to 2-methyl-2-nitrosopropane⁴². They also reported the NMP of isoprene using a poly(ethylene oxide)-alkoxyamine macroinitiator, resulting in diblock copolymers with narrow molecular weight distributions ($\bar{D} < 1.20$) characteristic of living chain growth processes⁴³. The discovery of more labile second-generation initiators exhibiting a lower energy C-ON bond homolysis^{44,45} such as 2,2,5-trimethyl-4-phenyl-3-azahexane-N-oxyl (TIPNO)⁴⁶ and [*tert*-butyl[1-(diethoxyphosphoryl)-2,2-dimethylpropyl]amino] nitroxide, termed DEPN or SG1⁴⁷ (Figure 1,1) allowed controlled polymerizations at lower temperatures. One of the most predominant alkoxyamine unimolecular initiators based on SG1 is 2-([*tert*-butyl[1-(diethoxyphosphoryl)-2,2-dimethylpropyl]amino]oxy)-2-methylpropionic acid termed BlocBuilder™ (BB, Figure 1,2). Initiators containing the SG1 moiety have high dissociation rate constants⁴⁵ giving excellent control over the homopolymerizations of 1,3-dienes⁴⁸ and many other monomers such as acrylates⁴⁹⁻⁵². Harrison and coworkers reported for the first time the NMP of isoprene from a range of SG1-based initiators⁵³. Well-controlled poly(isoprene)s were obtained without addition of extra SG1. At higher conversions, the dispersity of all synthesized poly(isoprene)s approached 1.1.

Given the positive results achieved previously with isoprene and butadiene using BlocBuilder™ type initiators, the NMP-based *My* chemistry appears very promising. Furthermore, *My* exhibits two valuable features in comparison to isoprene and butadiene: It is a natural renewable compound with low volatility (boiling point $T_b = 167\text{ °C}$)³, meaning that pressurized equipment is not needed to handle it.

In the present study, we report first the effects of target number-average molecular weight ($M_{n,theo}$), reaction medium, temperature and additional SG1 free nitroxide on the control of NMP of *My*. A BlocBuilder™-modified initiator, the succinimidyl ester terminated NHS-BlocBuilder (NHS-BB, Figure 1,3)⁵⁴⁻⁵⁷ was used during this study and the relevance of this choice is explained below in the discussion. The optimized reaction conditions were used to chain-extend cleanly P(*My*)-SG1 macroinitiator with a fresh batch of S. Thermal and stress-strain properties of the resulting P(*My*-*b*-S) diblock copolymer were also investigated. Further, NHS-BB initiated the copolymerization of *My* and S via NMP was studied in terms of reactivity ratios and the resulting glass transition temperatures of the copolymers. To the best of our knowledge, this paper is the first comprehensive kinetic investigation of the nitroxide-mediated (co-)polymerization of *My* leading to well-defined P(*My*) homopolymers, P(*My*-*b*-S) diblock copolymers and P(*My*-*stat*-S) statistical copolymers.

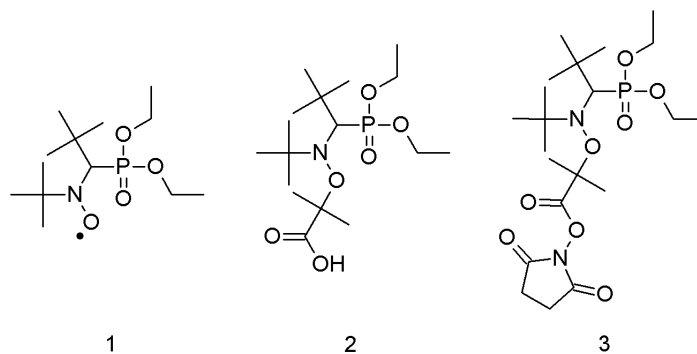


Figure 1. Structure of the *N-tert-butyl-N*-[1-diethylphosphono-(2,2-dimethylpropyl)] nitroxide (SG1, **1**), of the 2-([*tert-butyl*[1-(diethoxyphosphoryl)-2,2-dimethylpropyl]amino]oxy)-2-methylpropionic acid alkoxyamine (BlocBuilder™, BB, **2**) and of the succinimidyl ester terminated NHS-BlocBuilder alkoxyamine (**3**).

1.4. Results and discussion

1.4.1. NMP of β -myrcene: Determination of appropriate polymerization experimental conditions.

The experimental conditions of the various *My* polymerizations performed and the characterization of the resulting poly(myrcene)s P(*My*)s at the end of the experiments are summarized Table 1 and Table 2 respectively.

■ Choice of NHS-BlocBuilder (NHS-BB) as controlling alkoxyamine.

SG1-based initiators such as BlocBuilder™ (BB) or NHS-BB⁵⁴ have lower activation energy and much higher dissociation rate constants (k_d) compared to TEMPO-based initiators⁶². As a result, they can be activated at lower temperatures and allow controlled polymerizations of a wider range of monomers, such as methacrylates, 1,3-dienes and styrenic monomers. However, the use of additional SG1 nitroxide is needed to further reduce the reaction rate and produce well-defined polymers when polymerizing non-styrenic monomers initiated by BlocBuilder™^{50,52,63,64}. In comparison, the higher dissociation rate (~ 15 times) and slightly lower activation energy (~ 0.9 times) of NHS-BB, both measured at 120 °C in *tert-butyl* benzene, lead to rapid initiation and quick release of the SG1 rate moderator⁵⁴. Such intrinsic features permit

polymerizations to be done without any added free nitroxide at the onset of the polymerization. The NHS-BB was thus used to effectively control the homopolymerization of isoprene in bulk at 115 °C ($\bar{D} \leq 1.15$ and $M_n = 2.4 \text{ kg}\cdot\text{mol}^{-1}$ after 16 h)⁵³ and styrene (S) in bulk at 120 °C ($\bar{D} \leq 1.35$ and $M_n = 21.2 \text{ kg}\cdot\text{mol}^{-1}$ after 150 min)⁵⁴ without aid of additional SG1 nitroxide. Accordingly, the NHS-functionalized alkoxyamine is predicted to be effective in obtaining well-defined P(*My*) without additional SG1 free radical.

NHS-BB-initiated P(*My*) (experiment *My*-6) and BB-initiated P(*My*) (experiment *My*-6') were synthesized under the same experimental conditions (Table 1) in order to deem the effectiveness of BlocBuilder™ and NHS-BB to control the homopolymerization of *My*. As Figure 2.a indicates, the kinetic plots were linear with respect to reaction time. Interestingly, k_p/k_t increased when using BB ($7.2 \pm 0.4 \cdot 10^{-5} \text{ s}^{-1}$, Table 2) instead of NHS-BB ($4.3 \pm 0.7 \cdot 10^{-5} \text{ s}^{-1}$, Table 2). A similar evolution of M_n with conversion can be noticed for both experiments with M_n increasing linearly with conversion up to about 40% and slightly plateauing afterwards as shown in Figure 2.b. However, a major difference can be observed regarding \bar{D} values. Dispersity for polymerization *My*-6 initiated by NHS-BB remained lower than 1.3 whereas broader molecular weight distribution values were measured for *My*-6' initiated by BB ($1.42 \leq \bar{D} \leq 1.46$ for $X_{My} > 0.15$, Figure 2.b). Accordingly, NHS-BB initiator appeared to be slightly more efficient than BlocBuilder™ initiator to control *My* homopolymerization at 120 °C in bulk. The improvement when using NHS-BB may be due to the faster establishment of the equilibrium between dormant and propagating species, which might occur at $X_{My} = 0.15$ -0.25 as indicated by the narrower \bar{D} values ($\bar{D} = 1.24$ -1.25 for $0.08 < X_{My} < 0.15$ and $\bar{D} = 1.15$ -1.18 for $0.22 < X_{My} < 0.30$). Accordingly, NHS-BB was privileged for the study of the NMP of *My*.

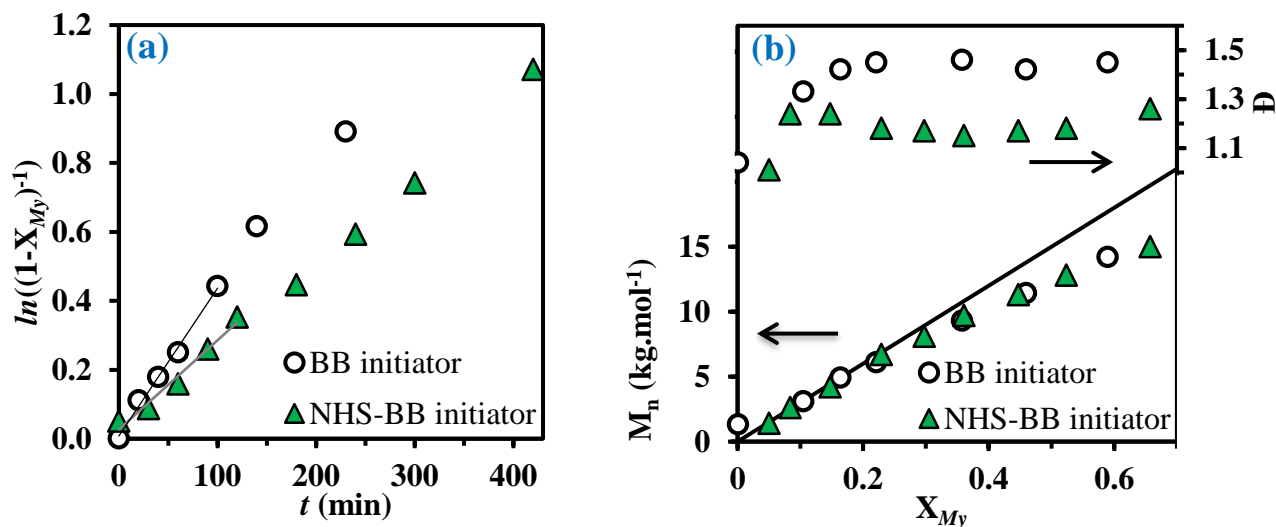


Figure 2. (a) Semi-logarithmic kinetic plots of $\ln((1-X_{My})^{-1})$ ($X_{My} = My$ conversion) versus reaction time t and (b) M_n and \bar{D} versus X_{My} for polymerization *My*-6 (solid green triangle) and *My*-6' (open circle) initiated by NHS-BB and BB respectively.

Table 1. Experimental conditions for *My* polymerizations for 7 h initiated by BB or NHS-BB.

ID	[BB] ₀ (M)	[NHS- BB] ₀ (M)	[SG1] ₀ (M)	<i>r</i> ^(a)	[<i>My</i>] ₀ (M)	Solvent ^(b)	[Solvent] ₀ (M)	T (°C)	<i>M_{n,theo}</i> (kg.mol ⁻¹)
<i>My</i> -1	0	0.020	0	0	3.01	Toluene	4.56	110	20.5
<i>My</i> -2	0	0.014	0	0	3.04	Toluene	4.54	110	29.6
<i>My</i> -3	0	0.008	0	0	2.94	Toluene	4.53	110	50.1
<i>My</i> -4	0	0.015	0	0	3.29	1,4- dioxane	5.12	100	29.8
<i>My</i> -5	0	0.026	0	0	5.81	-	0	110	30.4
<i>My</i> -6	0	0.025	0	0	5.61	-	0	120	30.6
<i>My</i> -6 ^(c)	0.026	0	0	0	5.83	-	0	120	30.5
<i>My</i> -7	0	0.026	0	0	5.75	-	0	130	30.1
<i>My</i> -8	0	0.027	0.001	0.049	5.87	-	0	120	29.6
<i>My</i> -9	0	0.026	0.003	0.117	5.80	-	0	120	30.4

a) Initial molar concentration ratio of SG1 free nitroxide to NHS-BB initiator = $r = [\text{SG1}]_0 / [\text{NHS-BB}]_0$.

b) Solution polymerizations done in 50 wt% solvent *versus* initial masses of *My* and NHS-BB.

c) Experiment *My*-6' has been run for 230 min.

■ Kinetic order and apparent rate constant of *My* polymerization by NMP.

The semi-logarithmic kinetic plots of $\ln((1-X_{My})^{-1})$ (X_{My} = *My* conversion) *versus* time are illustrated in Figure 3. All *My* polymerizations obeyed first order kinetics as described by Equation 4 and generated good fits to linear kinetic plots until 300 min polymerization. A loss of linearity was apparent at $X_{My} > 0.3$.

$$\ln([M]_0 / [M]_t) = \ln([M]_0 / ([M]_0(1-X_{My}))) = k_p \times [P'] \times \text{time} \quad (4)$$

Table 2. Molecular characterization, kinetic data and selectivity of P(*My*) synthesized with BB or NHS-BB.

ID	$X_{My}^{(a)}$	$M_n^{(b)}$ (M)	$\mathcal{D}^{(b)}$	$k_p K^{(c)}$ (10^5 s^{-1})	1,4-content ^(d) (%)	<i>Cis</i> -1,4-content ^(e) (%)	1,2-content ^(d) (%)
<i>My</i> -1	0.56	7.5	1.35	1.9 ± 0.4	89.7	72.6	7.4
<i>My</i> -2	0.43	12.8	1.58	2.5 ± 0.5	87.6	-(g)	8.6
<i>My</i> -3	0.83	9.6	1.43	1.2 ± 0.9	81.2	66.8	11.2
<i>My</i> -4	0.40	8.6	1.32	1.4 ± 0.8	90.9	-(g)	4.0
<i>My</i> -5	0.41	8.2	1.19	1.6 ± 0.4	-(g)	-(g)	-(g)
<i>My</i> -6	0.66	14.9	1.26	4.3 ± 0.7	80.3	88.7	9.3
<i>My</i> -6'	0.59	14.2	1.45	7.2 ± 0.4	80.5	-(g)	8.2
<i>My</i> -7	0.45	3.8	1.27	1.2 ± 0.6	82.4	-(g)	9.2
<i>My</i> -8	0.60	12.9	1.30	$0.2 \pm 0.03^{(f)}$	83.2	73.2	9.4
<i>My</i> -9	0.80	13.4	1.46	$0.3 \pm 0.06^{(f)}$	82.1	81.5	9.7

a) *My* conversion (X_{My}) determined gravimetrically and via ^1H NMR (average value).

b) M_n and M_w determined by GPC calibrated with PS standards in tetrahydrofuran (THF) at 40 °C and converted to P(*My*) using MHS constants.

c) $k_p K$ corresponding to the product of the propagation rate constant k_p and the equilibrium constant K derived from the slopes $k_p[P^*]$ ($[P^*]$ = concentration of propagating macro-radicals) taken from the semi-logarithmic kinetic plots of $\ln((1-X_{My})^{-1})$ versus time in the linear region from 0 min to 120 min (0 min to 100 min for *My*-6' ; squared linear regression coefficient = $R^2 \geq 0.95$ for every experiment). $k_p K$'s estimated from $k_p[P^*]$ and $r = [\text{SG1}]_0 / [\text{NHS-BB}]_0$ (Equation 6). Error bars derived from the standard errors in the slope from the linear fits of $\ln((1-X_{My})^{-1})$ versus time.

d) Regioselectivity determined by ^1H NMR in CDCl_3 . 3,4-content% not mentioned and calculated as follows: 3,4-content% = $100 - 1,4\text{-content}\% - 1,2\text{-content}\%$.

e) Stereoselectivity determined by ^{13}C NMR in CDCl_3 . *trans*-1,4-content% not mentioned and calculated as follows: *trans*-1,4-content% = $100 - cis\text{-}1,4\text{-content}\%$.

f) $k_p[P^*] = (3.2 \pm 0.6) \times 10^{-5} \text{ s}^{-1}$ for *My*-8 ; $k_p[P^*] = (2.6 \pm 0.5) \times 10^{-5} \text{ s}^{-1}$ for *My*-9.

g) ^1H and ^{13}C NMR peaks not clearly detectable.

In Equation 4, $[M]_0$ and $[M]_t$ are concentrations of monomer at time zero and a subsequent later time t , respectively, k_p is the propagation rate constant and $[P^*]$ is the concentration of propagating macro-radicals. It can be first noted that almost every trend line fitted to data at the early stages of the polymerization has a positive y-intercept, suggesting the presence of polymers at the commencement of the reaction. This can be explained by the arbitrary $t = 0$ min chosen when $T = 100$ °C, which is relatively high compared to the NHS-BB decomposition temperature < 70 °C. For every experiment, the straight kinetic trend at $X_{My} < 0.3$ revealed a steady $[P^*]$ established by balancing the rates of activation and deactivation via the SG1 free nitroxide mediator. This illustrates thereby the expected persistent radical effect (PRE)²² based on the dynamic equilibrium between low $[P^*]$ chains and a predominant concentration of dormant chains. However, deviations from the linear trends are observed after the initial stages of the polymerizations, especially when a solvent was used ($My-1$, $My-2$ and $My-3$ in Figure 3.a and $My-4$ in Figure 3.b). This is explained by a change in the concentration of active propagating species $[P^*]$ ²². A downward curvature, as clearly observed for experiment $My-2$ after 200 min ($X_{My} > 0.3$), suggests a decrease in $[P^*]$ which may be caused by irreversible termination reactions resulting in an increase of the concentration of the persistent radical. On the other hand, an upward curvature, as seen for experiments $My-1$, $My-2$ and $My-4$, suggests an increase of $[P^*]$ which may be caused by a slower initiation. This latter assumption would suggest that NHS-BB's dissociation rate constant is slightly lower in toluene and 1,4-dioxane than in bulk. In any case, these significant kinetic deviations starting even at moderate conversions ($X_{My} \sim 30\%$) suggest that other undesirable processes occurred. The thermal self-initiation of My^{75} and its relatively low purity level (≤ 10 mol% of impurities including limonene and isomers and dimers of My among others) might alter the persistent radical concentration as well.

The slopes, calculated from four to five sample points taken in the linear region, from the kinetic plots reveal the apparent rate constant in terms of the product of k_p with $[P^*]$, $k_p[P^*]$. For the systems studied here, the $k_p[P^*]$ values were all obtained during the early stages of the polymerization, where the number-average molecular weight (M_n) increased linearly with conversion (first 120 min of the reaction). From these values, k_pK can be estimated from Equation 5 and Equation 6, where K is the equilibrium constant, $[SG1^*]$ is the concentration of free nitroxide ($[SG1^*] = [SG1^*]_0$ is assumed in the early stages of the polymerization due to a high initial SG1 concentration), $[P-SG1]$ is the concentration of dormant alkoxyamine terminated species which is assumed to be equal to the initial concentration of NHS-BB, $[NHS-BB]_0$ (generally the case in the early stages of the polymerization) and r is the ratio of the initial molar concentration of SG1 free nitroxide to NHS-BB, $[SG1]_0/[NHS-BB]_0$.

$$K = ([P^*] \times [SG1^*]) / [P-SG1] \quad (5)$$

$$k_p K \cong (k_p \times [P^*] \times [SG1^*]_0) / [NHS-BB]_0 = k_p \times [P^*] \times r \quad (6)$$

Table 2 summarizes the experimental $k_p K$ values for the various polymerizations led. Without additional SG1, all $k_p K$ values are in the same order of magnitude, namely 10^{-5} s^{-1} , regardless $M_{n,theo}$ from 20 to 50 $\text{kg}\cdot\text{mol}^{-1}$ ($DP = [My]_0 / [NHS-BB]_0$ from 147 to 367), the reaction medium (in bulk or in solution) and the temperature (110 to 130 °C). When adding additional SG1 free nitroxide in the feed (*My*-8 and *My*-9), the polymerization has, by contrast, a $k_p K$ about an order of magnitude lower (10^{-6} s^{-1}). It was expected since SG1 free radical acts as a rate moderator, slowing the reaction down⁶⁵. However, a clear increase of the polymerization rate at the final stages of the polymerization was observed for the experiment *My*-9 with 11.7 mol% of additional SG1 relative to NHS-BB. This may be explained by a slower initiation process in the presence of a significant amount of SG1 free nitroxide, giving rise then to a higher $[P^*]$. Interestingly, induction periods may be apparent for some polymerizations such as experiment *My*-3. Indeed, at the beginning of this reaction ($t < 100 \text{ min}$), very low X_{MyS} , almost plateauing, were observed. This can presumably be explained by the role of the SG1 nitroxide trapping the radicals generated at the early stages of the reaction until SG1 reached its equilibrium concentration with the dormant species. At this point, the induction time is terminated and followed by the controlled NMP (at $t > 100 \text{ min}$ for experiment *My*-3, X_{MyS} increased linearly with time as initially expected). $k_p K$ values corresponding to NMP-based polymerization of isoprene in bulk at 115°C without additional SG1 are in the same range, from 0.4 to $1.4 \times 10^{-5} \text{ s}^{-1}$ ⁵³. These relatively slow NMP-based polymerizations of 1,3-diene monomers compared to styrenic and methacrylate monomers which exhibit higher k_p ^{44,66-68}, was previously noted by Hawker et al regarding the NMP of isoprene and butadiene initiated by a TIPNO-based initiator⁴¹.

■ Influence of alkoxyamine concentration.

Attention was first paid to the theoretical number-average molecular weight ($M_{n,theo} = M_{My} \times DP$) in order to know if high molecular weight $P(My)$ samples could be achieved by simply increasing the monomer/initiator initial molar ratio. Therefore, various amounts of NHS-BB alkoxyamine were used to prepare $P(My)$ s by heating *My* at 110 °C for 7 h in 50 wt% toluene, allowing to target three different $M_{n,theo}$ at quantitative conversion (*My*-1, *My*-2 and *My*-3 in Table 1). $P(My)$ s with M_n ranging from 7.5 to 12.8 $\text{kg}\cdot\text{mol}^{-1}$ and dispersities of 1.35-1.68 (Table 2) were synthesized. M_n were on average 87%, 83% and 51% of $M_{n,theo}$ during the polymerizations ($M_n/M_{n,theo}$ average values from 0 to 7 h) as regards the experiments *My*-1, *My*-2 and *My*-3 respectively (Figure 4.a). Accordingly, deviations from the theoretical molar masses are higher with increasing target $M_{n,theo}$. Besides, the lowest \bar{D} were obtained when targeting the lowest

$M_{n,theo}$ (\bar{D} of 1.14-1.35, Figure 4.a) confirming that irreversible termination reactions and/or some chain-transfer reactions⁶⁹ to M_y or $P(M_y)$ or toluene solvent are more prevalent as $M_{n,theo}$ increasing, generating the likely loss of control. In the ideal case of a controlled/living radical polymerization, fast initiation as compared to propagation and fast exchange between active (P^* in low concentration) and dormant species ($P-SG1$ in our situation) allow all chains to begin to grow at the same time and the reaction to be free of irreversible termination and transfer reactions. This results in a linear increase of M_n with X_{M_y} while \bar{D} stays narrow (< 1.3).

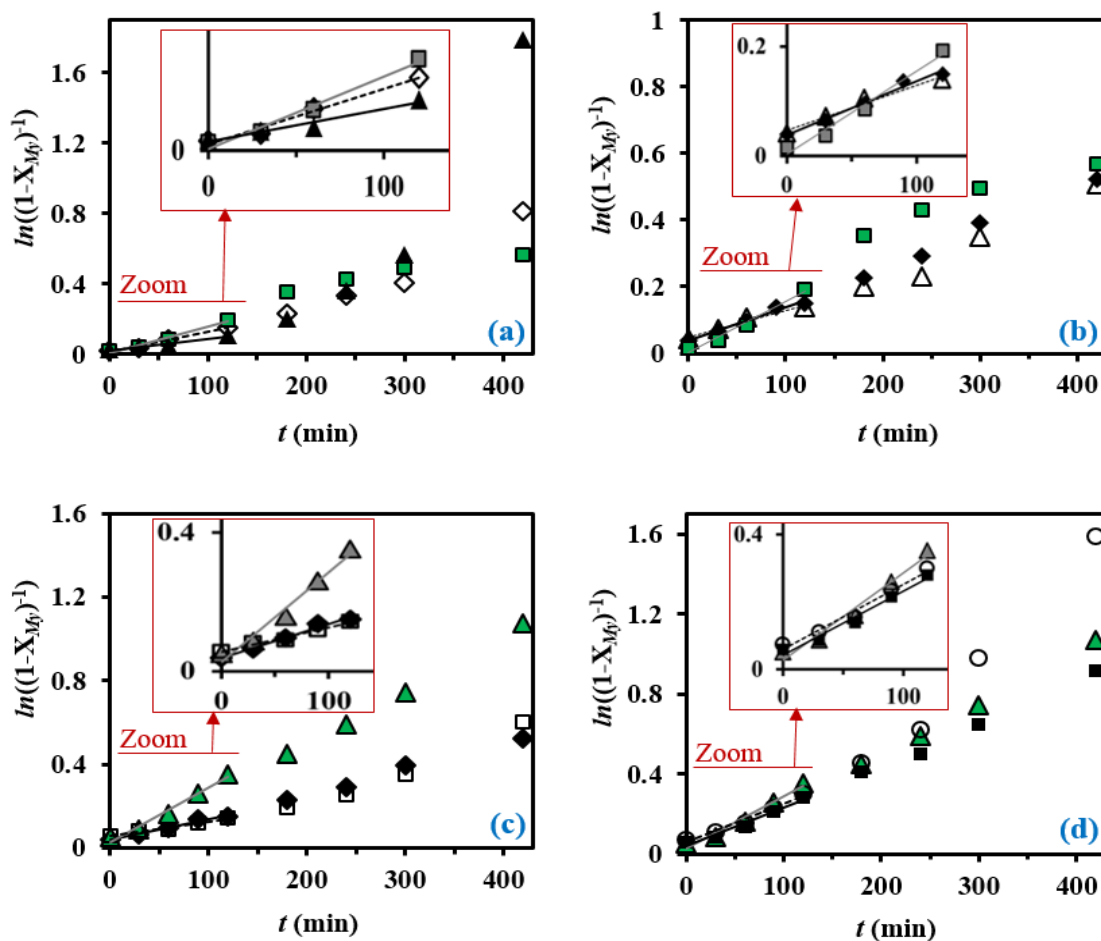


Figure 3. Semi-logarithmic kinetic plots of $\ln((1-X_{M_y})^{-1})$ ($X_{M_y} = M_y$ conversion) versus polymerization time t for M_y polymerizations initiated by NHS-BB. **a) Influence of $M_{n,theo}$:** M_y -1 with $M_{n,theo} = 20.5$ $\text{kg}\cdot\text{mol}^{-1}$ (\diamond), M_y -2 with $M_{n,theo} = 29.6$ $\text{kg}\cdot\text{mol}^{-1}$ (\blacksquare) and M_y -3 with $M_{n,theo} = 50.1$ $\text{kg}\cdot\text{mol}^{-1}$ (\blacktriangle); **b) Influence of the reaction medium:** M_y -2 in toluene (\blacksquare), M_y -4 in 1,4-dioxane (\triangle) and M_y -5 in bulk (\blacklozenge); **c) Influence of temperature:** M_y -5 at 110 °C (\blacklozenge), M_y -6 at 120 °C (\blacktriangle) and M_y -7 at 130 °C (\square); **d) Influence of additional SG1:** M_y -6 with no additional SG1 (\blacktriangle), M_y -8 with $[\text{SG1}]_0 / [\text{NHS-BB}]_0 = 0.049$ (\blacksquare) and M_y -9 with $[\text{SG1}]_0 / [\text{NHS-BB}]_0 = 0.117$ (\circ). The straight lines indicate linear fits to the experimental data during the initial stages of the polymerization (0 to 120 min). All experimental ID and characterization of experiments are listed in Table 1 and Table 2.

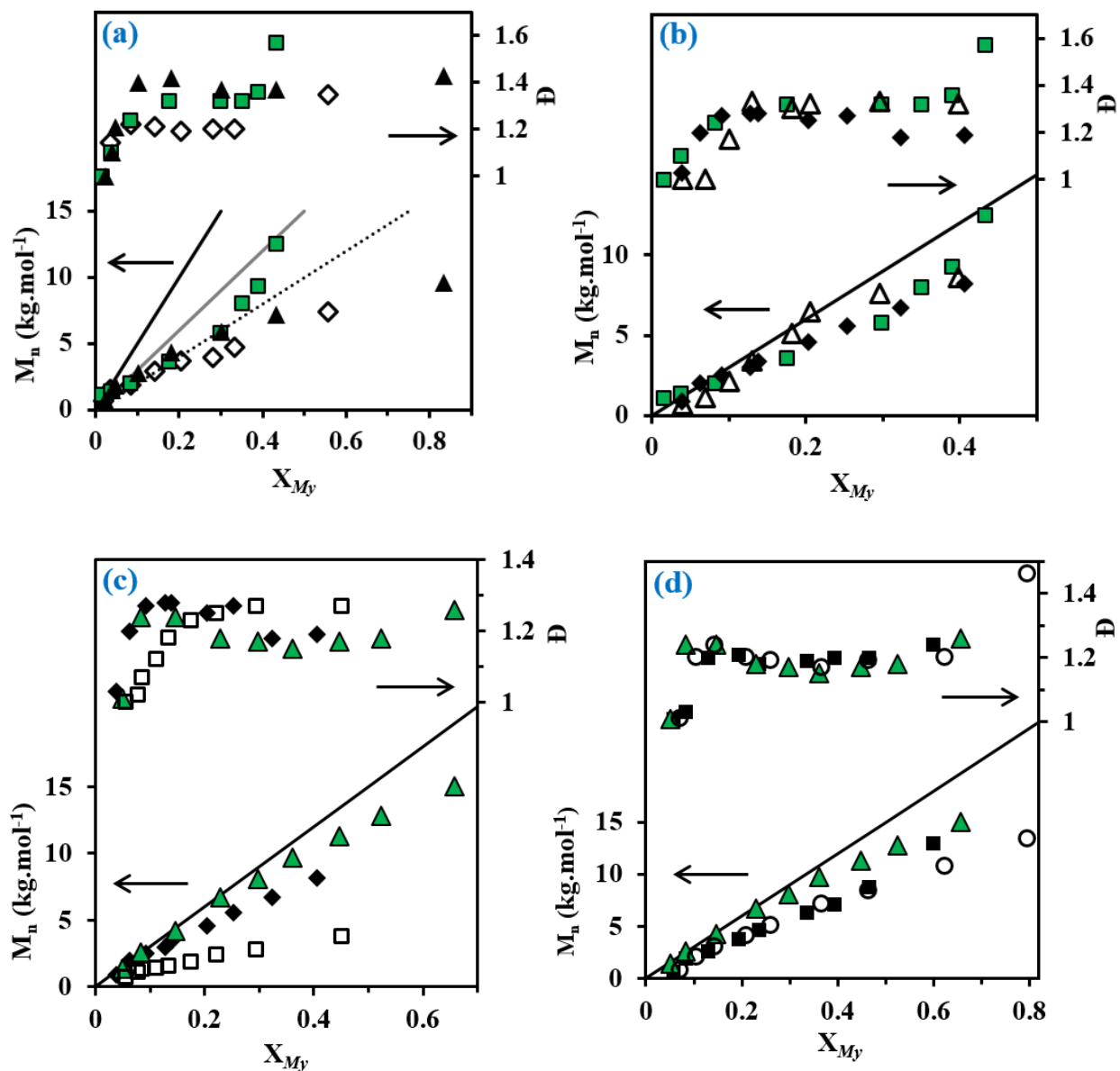


Figure 4. M_n determined by GPC relative to PS standards in THF and corrected with appropriate MHS coefficients and \bar{D} versus conversion for the various M_y polymerizations initiated by NHS-BB. **a) Influence of $M_{n,theo}$:** M_y-1 with $M_{n,theo} = 20.5 \text{ kg.mol}^{-1}$ (\diamond), M_y-2 with $M_{n,theo} = 29.6 \text{ kg.mol}^{-1}$ (\blacksquare) and M_y-3 with $M_{n,theo} = 50.1 \text{ kg.mol}^{-1}$ (\blacktriangle); **b) Influence of the reaction medium:** M_y-2 in toluene (\blacksquare), M_y-4 in 1,4-dioxane (\triangle) and M_y-5 in bulk (\blacklozenge); **c) Influence of temperature:** M_y-5 at $110 \text{ }^\circ\text{C}$ (\blacklozenge), M_y-6 at $120 \text{ }^\circ\text{C}$ (\blacktriangle) and M_y-7 at $130 \text{ }^\circ\text{C}$ (\square); **d) Influence of additional SG1:** M_y-6 with no additional SG1 (\blacktriangle), M_y-8 with $[\text{SG1}]_0 / [\text{NHS-BB}]_0 = 0.049$ (\blacksquare) and M_y-9 with $[\text{SG1}]_0 / [\text{NHS-BB}]_0 = 0.117$ (\circ). The straight lines indicate the theoretical M_n ($M_{n,theo}$) versus conversion based on the monomer to initiator ratio for the particular experiment. All experimental ID and characterization of experiments are listed in Table 1 and Table 2.

The rate of polymerization was almost unaffected with the increase of the NHS-BB concentration, k_pK staying around $2.0 \cdot 10^{-5} \text{ s}^{-1}$. An increase of the k_pK with lower $M_{n,theo}$ could have been expected as those polymerizations may have a reduced probability of irreversible termination reactions compared to polymerizations with higher target M_n ⁶³. Moreover, in such a situation with a lower $M_{n,theo}$, the equilibrium may not strongly favour the alkoxyamine such that the instantaneous chain radical concentration is not low enough to avoid bimolecular termination reactions. Accordingly, bimolecular termination events may be more apparent, resulting in an increase of the overall polymerization rate until the steady state predicted by the PRE is reached. Harrison and al reported⁵³ an increase of the rate of isoprene polymerization in a nonlinear manner with the concentration of BlocBuilderTM, the rate of reaction being proportional to $[\text{BlocBuilder}^{\text{TM}}]^{0.42}$.

A target number-average molecular weight of $30 \text{ kg}\cdot\text{mol}^{-1}$ ($DP = [My]_0 / [\text{NHS-BB}]_0 = 220$) is thereafter chosen since it allowed achieving relatively high average chain length $P(My)$ with a decent degree of control.

▣ Influence of the reaction medium.

The presence of a solvent, due to its polarity and its viscosity for instance, can induce drastic changes for both k_d ⁷⁰ and k_c (rate of recombination)⁷¹ of the initiator. A loss of control can be generated by chain-transfer reactions to the solvent as highlighted by Charleux and coworkers for the NMP of acrylic acid in 1,4-dioxane^{64,72}. On the other hand, the solvent can also improve the control of the NMP. Harrison and al reported better control of isoprene polymerization by SG1-based NMP when using 1,4-dioxane and pyridine instead of bulk, due to a disruption of intramolecular hydrogen bonding within the alkoxyamine initiator and stabilization of the SG1 free nitroxide⁷³. Accordingly, it is of interest to determine the influence of the reaction medium, which may play a significant role on the NMP of My .

The polymerization of My , mediated by NHS-BB, was carried out at $110 \text{ }^\circ\text{C}$ in toluene (50 wt%) and in bulk, and at $100 \text{ }^\circ\text{C}$ in 1,4-dioxane (50 wt%) due to its lower boiling point ($T_{b,1,4\text{-dioxane}} = 101 \text{ }^\circ\text{C}$), while keeping $M_{n,theo}$ constant around $30 \text{ kg}\cdot\text{mol}^{-1}$ ($My-2$, $My-5$ and $My-4$ respectively in Table 1). No change in the overall rate of polymerization was observed as k_pK values were not significantly different and the final conversion was around 0.4, regardless of the reaction medium (Table 2). The molecular weights for each experiment followed the same trend with a linear increase of up to 20% conversion and a slight plateau at higher conversions (Figure 4.b) indicating presumably the occurrence of irreversible termination reactions. Interestingly, narrower molecular weight distributions were obtained when performing My polymerization in bulk ($\mathcal{D} \leq 1.27$, Figure 4.b). The slightly higher \mathcal{D} obtained for the two

solution polymerizations might be explained by the extra contribution of chain-transfer side reactions to toluene and 1,4-dioxane.

Accordingly, *My* polymerization in bulk gave satisfactory results in terms of control compared to that in solution using 1,4-dioxane and toluene. Bulk polymerization of *My* was thus applied for further studies.

■ Determination of the appropriate polymerization temperature.

A third series of *My* NMPs was undertaken, varying only one experimental parameter, namely the reaction temperature, ranging from 110 °C to 130 °C (*My*-5, *My*-6 and *My*-7 in Table 1). This was made possible through the low volatility of this monoterpene ($T_{b,My} = 167$ °C). Increasing the temperature from 110 °C to 120 °C more than doubled the k_pK value with significantly greater conversions (~ 1.7 times on average) during the experiment (Table 2). Therefore, an increase in the overall rate of polymerization, as expected by the Arrhenius equation⁷⁴, was observed. Furthermore, contrary to what one might think, this was not accompanied by a loss of control over the polymerization. Indeed, M_n increased linearly with X_{My} with slight discrepancies at the final stages. M_n values were on average 90% of the theoretical ones while \bar{D} remained below 1.3 (Figure 4.c). Unexpectedly, polymerization at 130 °C was not faster than that at 120 °C. Its overall rate of polymerization was very close to that of the polymerization performed at 110 °C (Figure 3.c). Besides, despite low $\bar{D} \leq 1.3$, significant deviations from the predicted line were observed regarding the average molecular weights (Figure 4.c). This marked loss of control occurring from the early stages of the experiment may be due to irreversible termination reactions, which were becoming more frequent at higher temperature.

Consequently, a reaction temperature of 120 °C (experiment *My*-6) was deemed satisfactory since it provides a polymerization at least as controlled as at 110 °C combined with a higher overall rate of reaction. Similarly, 115 °C was the optimized reaction temperature of the SG1-based NMP of isoprene for a control polymerization at an acceptable rate of reaction⁵³. The GPC traces for *My*-6 are given in Figure 5 and exhibit a monomodal shift of relatively narrow peaks taken at different points in the polymerization. A second and minor population of longer P(*My*) chains can be generally detected at the early stages of the polymerization as observed at $t = 1$ h. This higher M_n peak, generally observed for almost every *My* polymerization led, appeared at the commencement of the reaction ($t < 60$ min), remained constant (no clear shift to lower elution volumes) to become not detectable by GPC at the last stages of the experiment. A negligible fraction of high M_n P(*My*) was therefore obtained at the end of the reactions compared to the amount of well-controlled polydiene chains. This may be due to *My* auto-initiation increasing the amount of propagating radicals that would not necessarily be reversibly terminated by the SG1 and therefore would

not be controlled (deviation from the initial stoichiometry with $[P^*] > [SG1^*]$). Although auto-polymerization should be moderated by the equilibrium established by the PRE, My auto-polymerization is likely significantly faster than My NMP making the mediation by SG1 more complicated. It should be noted that the presence of a high M_n peak was likewise observed at the early stages of most of the My polymerizations performed such as experiment My -10-S (Figure 6.a) and experiment My /S-50 at 1 h (Figure 9). Lastly, a GPC measurement of commercial My used (grade $\geq 90\%$, stored at 4-5 °C to prevent early polymerization) indicated the absence of any polymers. The assumption that high M_n P(My) could be already present before polymerization does not appear relevant, auto-polymerization being inhibited at low T and impurities consisting mainly in monomers and dimers. Since the 1950s, My is known to polymerize spontaneously at elevated temperature as other conjugated dienes whereas its loss by auto-polymerization at T_{room} was estimated to one third after three months without inhibitor⁷⁵.

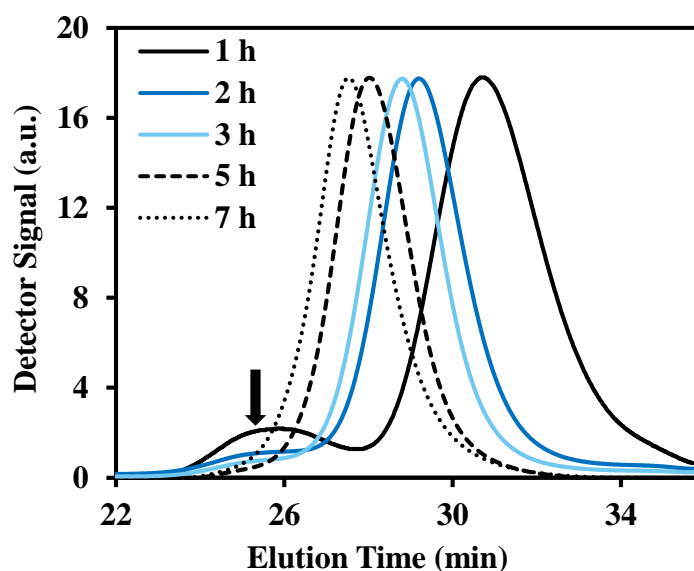


Figure 5. Normalized GPC traces of P(My) initiated by NHS-BB at 120 °C in bulk targeting $M_{n,theo} = 30 \text{ kg.mol}^{-1}$ at quantitative conversion (experiment My -6). The arrow indicates the peak/shoulder observed at $t = 1 \text{ h}$ corresponding to a minor fraction of high molecular weight P(My) ($M_n = 45.3 \text{ kg.mol}^{-1}$, $\bar{D} = 1.28$) presumably due to My auto-initiation.

▣ Effects of additional SG1 free nitroxide.

The effectiveness of additional SG1 over the control of non-styrenic monomer polymerizations initiated by the BlocBuilder™ initiator was demonstrated. For instance, the control of *tert*-butyl acrylate

polymerization was improved by introducing 5-6% of free nitroxide relative to the BlocBuilder™ initiator, reducing both the overall rate of reaction and the \bar{D} values⁷⁶. In order to know if such a strategy could be efficient for the system *My*/NHS-BB, two extra experiments were undertaken: *My*-8 and *My*-9 with respectively 4.9% and 11.7% of additional SG1 mediator relative to NHS-BB and implemented under the optimized reaction conditions, namely in bulk at 120 °C targeting 30 kg.mol⁻¹ at $X_{My} = 100\%$ (Table 1). The results were compared with experiment *My*-6 where no additional SG1 was used. Adding about 5% of additional SG1 relative to NHS-BB in the feed did not affect the polymerization of *My*, exhibiting nearly identical overall rate of reaction (Figure 3.d) and M_n and \bar{D} values over time not significantly different (Figure 4.d). More surprising, a loss of control seems to be apparent in the late stages of the polymerization ($t > 240$ min, $X_{My} > 0.46$) when around 12% of SG1 free radical was added initially. A loss of linearity was highlighted in the $\ln((1-X_{My})^{-1})$ versus time plot (Figure 3.d) combined with greater deviations of the experimental molar masses from the theoretical ones (Figure 4.d). It might be explained by a higher rate of irreversible termination by β -hydrogen chain-transfer (disproportionation) to SG1, as shown by McHale and coworkers for the system SG1/MMA (methyl methacrylate) when using large excesses of nitroxide⁷⁷. In our case, the percentage of free nitroxide was relatively low and a further analysis would be necessary to clearly identify the possible main chain-end forming event occurring. Another assumption explaining these results for experiment *My*-9 with the highest $r = 0.117$ may be the contribution to extra SG1 nitroxide to high M_n propagating macroradicals resulted from self-initiation of *My*. In that case, higher deviations of the measured M_n from $M_{n,theo}$ can be expected as well without however bringing about a loss of control (linear trend of M_n versus X_{My} , and $\bar{D} < 1.3$ except at the end of the reaction, Figure 4.d).

■ Microstructural features of NMP-based P(*My*).

My is expected to yield P(*My*) polymer with a variety of structural units. Such a substituted diene system can produce units of 1,2-, 3,4-, 1,4-*cis* and 1,4-*trans*. 1,2-, 3,4- and 1,4- isomers were detected by ¹H NMR whereas the signature peaks for 1,4-*cis* and 1,4-*trans* motifs were obtained from ¹³C NMR spectra (see Supporting Information for the spectral assignments of ¹H NMR and ¹³C NMR from typical experiments, Figures S2a and S3a). The analyses were in good accordance with the literature^{21,58}. The proportions of these four different types of microstructure at the end of each polymerization are given in Table 2. It can be concluded that the NMP of *My* initiated by NHS-BB affords a P(*My*) that is 1,4-regular (80 to 90%) with 1,2- (5 to 10%) and 3,4-defects (5 to 10%). This is in agreement with the predominant 1,4-microstructure (96%) of P(*My*) synthesized by RAFT with 2-ethyl-sulfanylthiocarbonylsulfanylpropionic acid ethyl ester chain-transfer agent³⁶. More generally, the 1,4-motif is typically dominant (>

75%) by free radical polymerization^{12,13,15,16} of *My*. Similar proportions of 1,4-addition (81%), 1,3-addition (13%) and 1,2-addition (6%) were determined for the NMP in bulk of isoprene⁵³. Moreover, the NMP-based poly(terpene) exhibits a high *cis*-selectivity, higher than 65%. The coexistence of *cis* and *trans* isomers was qualitatively reported regarding RAFT-based³⁶ and emulsion-based¹⁶ P(*My*)s.

1.4.2. Synthesis of poly(β -myrcene-*block*-styrene) diblock copolymers

■ Chain-extension with styrene (S) from poly(β -myrcene) P(*My*) macroinitiator.

The active feature of NMP-based polymers is enabled due to the nitroxide moieties capped at the chain ends. To investigate the ability of the expected SG1-terminated P(*My*) homopolymer to re-initiate a second batch of monomer, chain-extension experiments were performed using S monomer and three P(*My*) macroinitiators (*My*-10, *My*-11 and *My*-12) exhibiting different degrees of polymerization ($13.2 \text{ kg}\cdot\text{mol}^{-1} < M_n < 30.4 \text{ kg}\cdot\text{mol}^{-1}$). The experimental conditions and results of these experiments are summarized in Table 3 and Table 4, respectively. With a fresh batch of purified styrene, P(*My*) macroinitiator was extended with a poly(styrene) PS block with M_n ranging approximately from 12 to 26 $\text{kg}\cdot\text{mol}^{-1}$. \bar{D} of the diblock copolymers (1.33, 1.83, 1.50 and 1.88) were higher than that of their macroinitiator (1.18, 1.32, 1.32 and 1.38). This broadening of \bar{D} after the chain-extensions can be due to the diffusion of the mediating SG1 radical from the propagating chain end to styrene monomer. Side reactions involving radical crossovers for NMP were reported by Hawker *et al*⁷⁸. This assumption is consistent with the reactivity ratios of *My* and S determined in part C highlighting the shiftless and unprivileged addition of S towards the propagating radical $--My^*$. Besides, irreversible termination and some macroinitiator chains which were not initiated could also have contributed to the loss of control observed during these chain-extensions. The S molar composition of the synthesized P(*My*-*b*-S) copolymers (F_S), measured via ¹H NMR spectroscopy (¹H NMR spectrum of recovered P(*My*-*b*-S) copolymer *My*-11-Sa provided in the Supporting Information, Figure S4a) varied from 27 to 62 mol%.

The GPC chromatograms of the chain-extension experiments are shown in Figure 6. For every experiment, the P(*My*-*b*-S) chain-extended block copolymer (dotted line) shifted to lower elution time compared to its P(*My*) macroinitiator (solid line). These marked shifts demonstrated the increase of M_n with polymerization time. Moreover, the GPC traces of the chain-extended polymers retained generally their monomodal nature, indicating a high level of chain end fidelity. For each experiment, the tails of chain-extended copolymers overlap to some degree with the associated macroinitiator traces. This tailing, partly

due to the presence of “dead” chains from the macroinitiator, was slightly more apparent for the chain-extensions *My*-11-Sa and *My*-12-S where high $M_{n,theo}$ was targeted ($\geq 90 \text{ kg}\cdot\text{mol}^{-1}$) combined, in the case of *My*-11-Sa, with a long reaction time. Under such conditions, irreversible terminations are more prevalent, generating a loss of control which can be also highlighted by the increase of $\mathcal{D} > 1.8$ at the end of these chain-extensions.

In summary, these results confirmed the ability of NMP-based P(*My*) macroinitiator to reinitiate a new batch of styrene and polymerize in a controlled way. Slight tails were observed, likely due to a small portion of inactive macroinitiator as well as the occurrence of irreversible termination events.

■ Tensile properties of P(*My*-*b*-S) diblock copolymer.

Uniaxial tensile testing was performed on the resulting P(*My*-*b*-S) diblock copolymers, with $F_S = 0.27$ - 0.62 , in order to determine their mechanical behavior. Table 4 gives the tensile properties of the various copolymers and Figure 7 illustrates the stress-strain curves of two specimens from experiments *My*-11-Sa ($F_S = 0.47$) and *My*-12-S ($F_S = 0.27$) (all stress-strain curves of the specimens from *My*-11-Sa,

Table 3. Formulations of chain-extensions with purified S using various P(*My*) macro-initiators in 50 wt% toluene solution at 110 °C.

ID	Macroinitiator		Formulation of chain-extension				
	M_n ($\text{kg}\cdot\text{mol}^{-1}$)	\mathcal{D}	[Macroinitiator] ₀ (M)	[S] ₀ (M)	[Toluene] ₀ (M)	$M_{n,theo}^{(a)}$ ($\text{kg}\cdot\text{mol}^{-1}$)	t (min)
<i>My</i> -10-S	13.2	1.18 ^(c)	0.006	3.442	4.812	73	300
<i>My</i> -11-Sa ^(b)	22.8	1.32	0.005	3.242	4.829	90	420
<i>My</i> -11-Sb ^(b)	22.8	1.32	0.005	3.143	4.802	88	140
<i>My</i> -12-S	30.4	1.38	0.004	3.026	4.809	109	120

a) $M_{n,theo}$ corresponding to the targeted number-average molecular weight of the whole P(*My*-*b*-S) diblock copolymer at 100% of S conversion.

b) Same P(*My*) macroinitiator used for these two experiments.

c) Tail observed at about 24 min elution time (Figure 6.a) not integrated for the measurement of the molecular weight distribution.

Table 4. Molecular and mechanical characterization of diblock copolymers after chain-extension with purified S from various P(*My*) macro-initiators at 110 °C in 50 wt% toluene.

ID	X _S ^(a)	F _S ^(b)	M _n ^(c) (kg.mol ⁻¹)	Đ ^(c)	E ^(d) (MPa)	Ultimate tensile strength ^(d) (MPa)	Tensile elongation at break ^(d) (%)
<i>My</i> -10-S	0.34	0.62	33.7	1.33	– ^(e)	– ^(e)	– ^(e)
<i>My</i> -11-Sa	0.38	0.47	49.0	1.83	264 ± 53	0.86 ± 0.19	0.80 ± 0.15
<i>My</i> -11-Sb	0.22	0.39	38.5	1.50	126 ± 70	0.63 ± 0.06	1.57 ± 0.18
<i>My</i> -12-S	0.31	0.27	42.6	1.88	6 ± 4	0.37 ± 0.05	13.94 ± 1.63

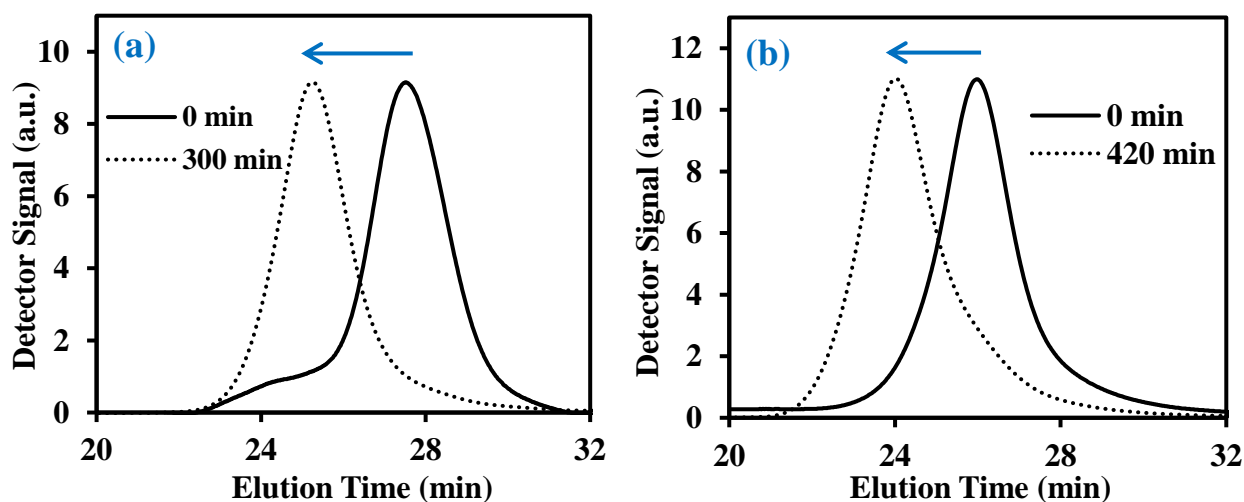
a) S conversion (X_S) determined only by ¹H NMR spectroscopy in CDCl₃.

b) Molar fraction of S in the copolymer (F_S) as determined by ¹H NMR in CDCl₃.

c) M_n and M_w determined by GPC calibrated with PS standards in tetrahydrofuran (THF) at 40 °C. M_n of the P(*My*) segment corrected for each experiment using the appropriate MHS parameters.

d) Young's modulus (E), ultimate tensile strength and tensile elongation at break measured by uniaxial tensile testing via a MTS Insight™ material testing system with a 5 kN load cell at room temperature and a cross-head speed of 1 mm.min⁻¹. 6, 5 and 5 specimens tested for the experiments *My*-11-Sa, *My*-11-Sb and *My*-12-S respectively. Averaged results given with the respective standard deviations.

e) Specimens too brittle to perform tensile testing.



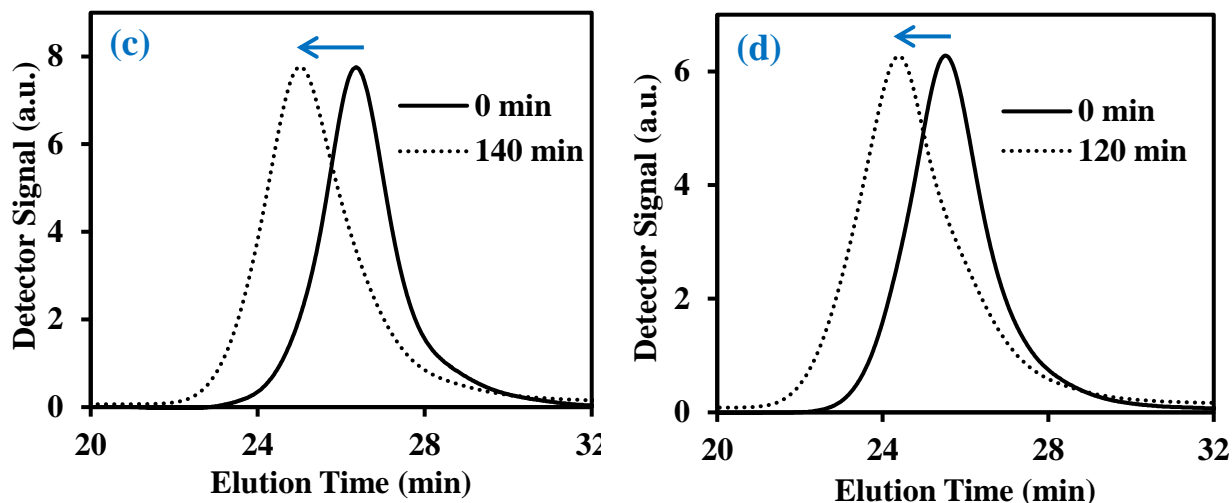


Figure 6. Normalized GPC traces for S chain-extensions from various P(*My*) macroinitiators at 110 °C in 50 wt% toluene. **a)** is the chain extension experiment *My*-10-S; **b)** is the chain extension experiment *My*-11-Sa; **c)** is the chain extension experiment *My*-11-Sb; **d)** is the chain extension experiment *My*-12-S.

My-11-Sb and *My*-12-S samples provided in the Supporting Information, Figures S6a, S7a and S8a).

Regardless of the molar composition of the samples, all stress-strain curves were marked by a linear elastic region, followed by a short failure region. No plastic deformation was observed, resulting in a failure point very close to the yielding point. Every specimen, breaking after reaching their elastic limit, exhibited both brittle behavior with low ultimate tensile strength (< 1.1 MPa, Table S1a in Supporting Information) and low extensibility with poor elongation at break (< 16%, Table S1a in Supporting Information). Materials from experiment *My*-10-S, even more fragile, fractured before performing the mechanical test. As a comparison, isoprene/styrene P(*I-b-S*) triblock copolymer having slightly higher overall M_n (68.5 kg.mol⁻¹) and F_S (0.40) exhibited thermoplastic elastomeric mechanical behavior with significant strength (tensile stress at break > 20 MPa) combined with high elongation at break (> 1000%)⁷⁹. Likewise, butadiene/styrene P(*B-b-S*) triblock sample exhibiting $M_n = 73$ kg.mol⁻¹ and $F_S = 0.40$ had largely better stress-strain properties with tensile stress at break higher than 20 MPa and elongation at break higher than 700%⁸⁰, in comparison to the NMP-based P(*My-b-S*) copolymers. Such a mechanical behavior for P(*I-b-S*) and P(*B-b-S*) triblocks can be in part explained by a highly entangled polydiene matrix forming the flexible rubbery domain. P(*I-b-S*) and P(*B-b-S*) triblock copolymers mentioned above exhibited M_n for the elastomeric block ($M_{n,PI} = 41.1$ kg.mol⁻¹ and $M_{n,PB} = 41.2$ kg.mol⁻¹) largely higher than their respective

entanglement molecular weight ($M_{e,PI} = 4\text{-}6 \text{ kg}\cdot\text{mol}^{-1}$ and $M_{e,PB} = 2\text{-}4 \text{ kg}\cdot\text{mol}^{-1}$)⁸¹, allowing the matrix phase to have a high entanglement density. By contrast, the maximum M_n of the poly(terpene) segment in the $P(My\text{-}b\text{-}S)$ copolymers was $\sim 30.4 \text{ kg}\cdot\text{mol}^{-1}$ (experiment $My\text{-}12\text{-}S$), only slightly higher than $P(My)$ entanglement molecular weight ($M_{e,P(My)} = 22\text{-}31 \text{ kg}\cdot\text{mol}^{-1}$)⁸¹. Although $My\text{-}12\text{-}S$ sample may have been entangled, it is very likely that $My\text{-}11\text{-}Sa$ and $My\text{-}11\text{-}Sb$ samples exhibiting shorter $P(My)$ chains ($M_{n,P(My)} = 22.8 \text{ kg}\cdot\text{mol}^{-1}$) did not form an entangled elastomeric phase. This difference in mechanical behavior between $P(My\text{-}b\text{-}S)$ diblock samples and $P(I\text{-}b\text{-}S)$ / $P(B\text{-}b\text{-}S)$ triblock samples was presumably due to different molecular architectures as well. When the rubbery segment ($P(My)$, PI or PB) is in excess of the rigid segment (PS) so that the rubber forms the continuous phase, the triblock copolymers have generally higher tensile strengths compared to similar diblock copolymers⁸². The rigid segment is aggregated in both cases and both types of block copolymers have the characteristics of a rubber containing rigid fillers. However, the rubber phase acts like it is cross-linked in triblock polymers because both ends of each elastomeric chain are attached to a rigid dispersed phase (entanglements are physically trapped). In the diblock polymer, the rubber chains are attached to a rigid chain at only one end and therefore are not cross-linked. Adhikari studied the influence of the presence of 60 wt% of $P(B\text{-}b\text{-}S)$ diblock chains ($F_S = 0.5$) to linear $P(B\text{-}b\text{-}S)$ triblock copolymers ($F_S = 0.5$) on the mechanical properties of this latter. Although the strain at break values were similar for both types of structures ($\sim 900\%$), $P(B\text{-}b\text{-}S)$ triblock copolymer containing an important amount of $P(B\text{-}b\text{-}S)$ diblock chains exhibited tensile stress at break ($< 15 \text{ MPa}$) significantly lower in comparison to the pure $P(B\text{-}b\text{-}S)$ triblock ($> 30 \text{ MPa}$)⁸³. Therefore, it can be assumed that the poor tensile properties exhibited by the $P(My\text{-}b\text{-}S)$ diblock copolymers were also due their network architecture since only one end of the $P(My)$ chains was anchored to a PS glassy domain. The untrapped $P(My)$ end-blocks were thus able to relax stress by chain reptation, reducing the elastic response of the physical network.

The modulus of elasticity (E), also known as Young's modulus, is defined by the slope of the linear elastic region of the stress-strain curve⁸⁴. As expected, synthesized $P(My\text{-}b\text{-}S)$ Young's modulus, ranging from 10^1 to 10^2 MPa in order of magnitude, is between $P(My)$ Young's modulus ($E_{P(My)} \sim 10^{-3} \text{ MPa}$)¹⁶ and PS Young's modulus ($E_{PS} \sim 10^3 \text{ MPa}$)⁸⁵. This elastic modulus range measured experimentally is in agreement with that of $P(I\text{-}b\text{-}S)$ triblock copolymers ($1 \text{ MPa} < E < 900 \text{ MPa}$) prepared by anionic polymerization and exhibiting an overall M_n of about $100 \text{ kg}\cdot\text{mol}^{-1}$ and $F_S = 0.19\text{-}0.58$ ⁸⁶. Furthermore, it is of interest to note that tensile testing for $P(My\text{-}b\text{-}S)$ samples showed ultimate tensile strength values ranging from 0.4 to 0.9 MPa and elongations at break ranging from 1 to 14% . This suggests that mechanical properties of $P(My\text{-}b\text{-}S)$ block copolymers can be readily tuned based on molar composition. The greater the molar fraction of My , the higher the elongation at break and the lower the Young's modulus and the

ultimate tensile strength as previously reported by Bolton *et al.* for β -myrcene/ α -methyl-*p*-methylstyrene triblock copolymers²¹.

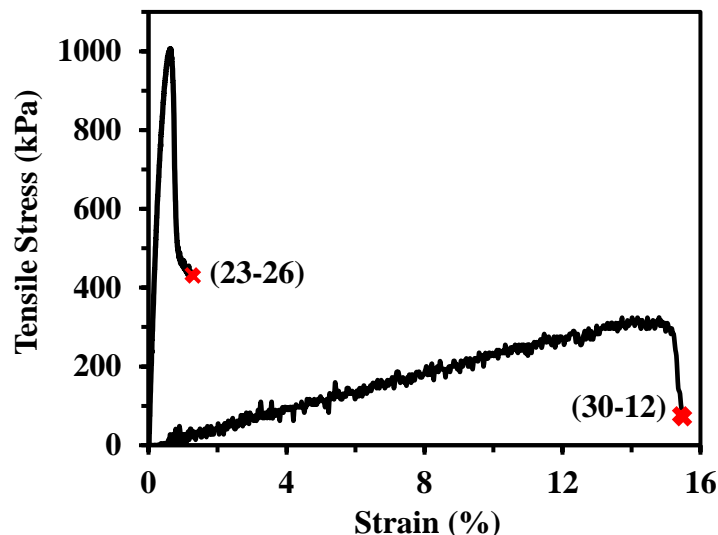


Figure 7. Tensile stress-strain curves of two P(*My-b-S*) diblock copolymer specimens from experiment *My-11-Sa* (specimen 5) with $M_{n,P(My)} = 22.8 \text{ kg}\cdot\text{mol}^{-1}$ and $M_{n,PS} = 26.2 \text{ kg}\cdot\text{mol}^{-1}$ (**23-26**) and from experiment *My-12-S* (specimen 2) with $M_{n,P(My)} = 30.4 \text{ kg}\cdot\text{mol}^{-1}$ and $M_{n,PS} = 12.2 \text{ kg}\cdot\text{mol}^{-1}$ (**30-12**) at room temperature and $1 \text{ mm}\cdot\text{min}^{-1}$. The red crosses denote failure points.

1.4.3. Synthesis of styrene- β -myrcene-styrene triblock copolymers

Varying molecular architecture can dramatically influence the physical properties of block copolymers. It can be assumed that *My-S* diblock copolymers prepared previously exhibited poor mechanical properties since only one end of the rubbery block was anchored to a glassy domain. The synthesis of symmetric *S-My-S* triblock copolymers (all entanglements are ideally physically trapped) by NMP was thereby envisioned. To that end, a poly(ethylene-*stat*-butylene) statistical copolymer capped by a SG1 nitroxide moiety at each end, abbreviated PEB-(SG1)₂ ($M_n = 5.7 \text{ kg}\cdot\text{mol}^{-1}$, $\bar{D} = 1.17$, Ph. 1a, synthesis detailed in Chapter 3) was produced. Then, P(*My*)-(SG1)₂ macro-initiator (Ph. 1b) exhibiting $M_n = 44.6 \text{ kg}\cdot\text{mol}^{-1}$, $\bar{D} = 1.44$ and 88 mol% of 1,4-motif was prepared by mixing 0.185 mmol of the PEB-(SG1)₂ dialkoxyamine with 183 mmol of *My* monomer at 120 °C for 310 min. Lastly, two chain-extensions of P(*My*)-(SG1)₂ (0.045 and 0.049 mmol) with styrene (32.6 and 34.11 mmol) in 50 wt% toluene at 115 °C for 50 and 110 min allowed the achievement of two linear *S-My-S* triblock copolymers: *S*₁₀-*My*-*S*₁₀ ($M_n = 56.4 \text{ kg}\cdot\text{mol}^{-1}$, $\bar{D} = 1.72$, $F_S = 20.4\%$) and *S*₁₆-*My*-*S*₁₆ ($M_n = 65.9 \text{ kg}\cdot\text{mol}^{-1}$, $\bar{D} = 1.86$, $F_S = 32.1\%$, Ph. 1c and 1d), respectively.



Ph. 1. (a) Synthesized telechelic poly(ethylene-*stat*-butylene) difunctional initiator terminated by SG1 groups (PEB-(SG1)₂), (b) P(*My*)-(SG1)₂ macro-initiator obtained from *My* NMP initiated by PEB-(SG1)₂, (c) dry S-*My*-S triblock copolymer (sample S₁₆-*My*-S₁₆) obtained via the S chain-extension from P(*My*)-(SG1)₂ macro-initiator and (d) dog-bone tensile bar specimens (ASTM D638, type V) from sample S₁₆-*My*-S₁₆ shaped by hot press.

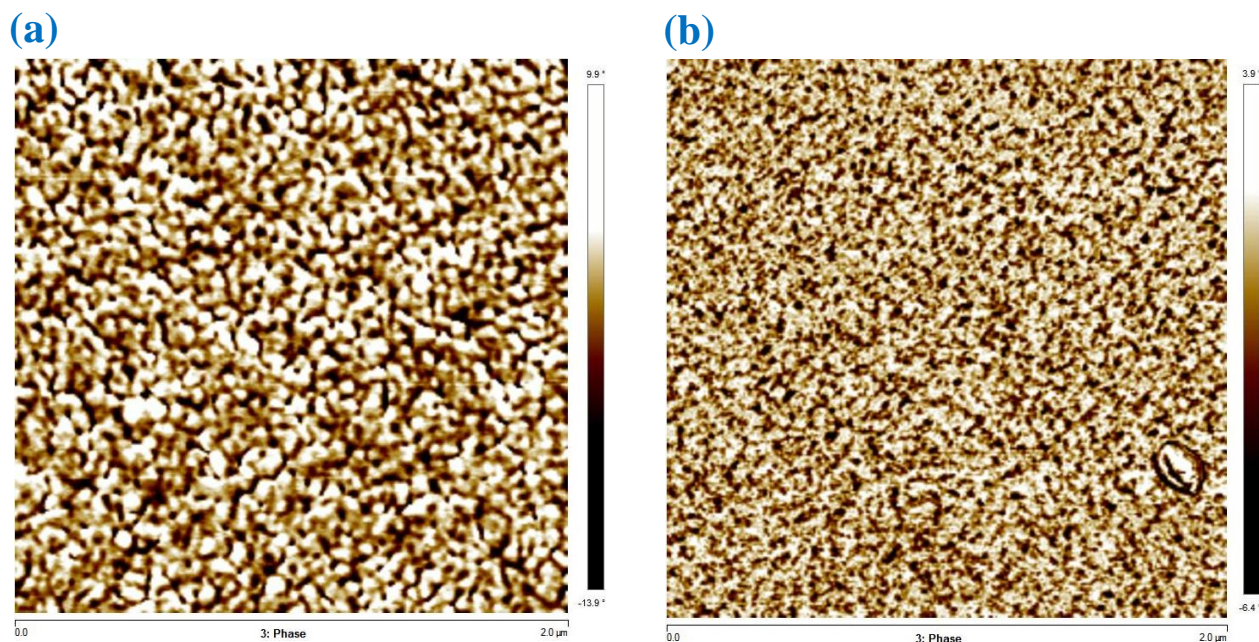


Figure 7. Atomic force microscopy (AFM) phase image (2 μm x 2 μm) under tapping mode of operation of the surface morphology of S-*My*-S triblock copolymers: (a) S₁₆-*My*-S₁₆ and (b) S₁₀-*My*-S₁₀. The dark domain represents the S component (color-coded height scale given to the right of the image).

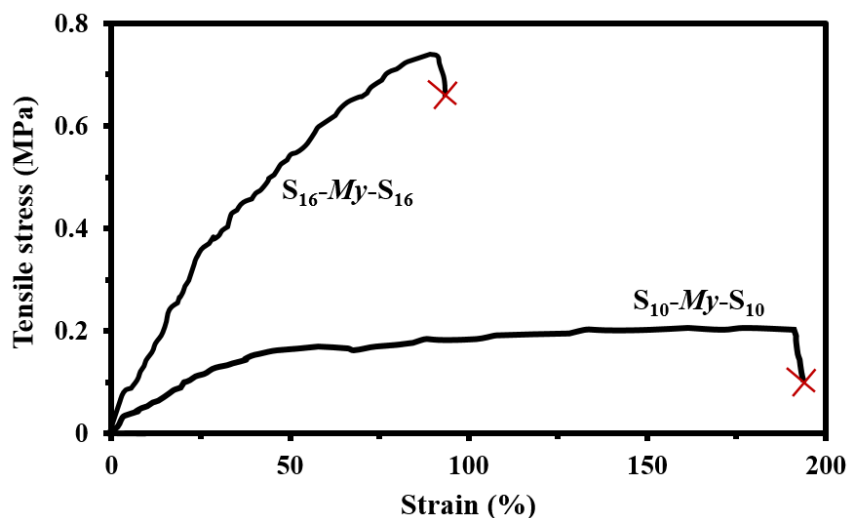


Figure 7''. Tensile stress-strain curves of one $S_{10}\text{-}My\text{-}S_{10}$ specimen and one $S_{16}\text{-}My\text{-}S_{16}$ specimen at room temperature and $1\text{ mm}\cdot\text{min}^{-1}$. The red crosses denote failure points.

Atomic force microscopy (AFM, tapping mode, AFM Bruker Multimode 8 equipped with Nanoscope V controller, scanning speed for image acquisition was 0.5 Hz) was performed to study the micro-phase behavior of the synthesized triblock copolymers. Figure 7' shows AFM phase images (Nanoscope Analysis software, version 1.5) of the samples $S_{10}\text{-}My\text{-}S_{10}$ and $S_{16}\text{-}My\text{-}S_{16}$, initially dissolved in chloroform and spin coated on a silicon wafer. Interestingly, despite a marked disorganization, two phases can be observed for both images with a continuous light domain representing $P(My)$ soft matrix and discrete dark domains corresponding to the rigid PS aggregates. For both cases, the morphology cannot be clearly defined. While the presence of disoriented spheres or cylinders might be seen for $S_{10}\text{-}My\text{-}S_{10}$ (Figure 7'b), a pseudo lamellar structure may have been obtained for the sample $S_{10}\text{-}My\text{-}S_{10}$ possessing a higher fraction of S units (Figure 7'a).

Lastly, uniaxial tensile testing was implemented at room temperature at a cross-head speed of $5\text{ mm}\cdot\text{min}^{-1}$. Figure 7'' gives the representative stress-strain curves of one specimen of the samples $S_{10}\text{-}My\text{-}S_{10}$ and one specimen of the sample $S_{16}\text{-}My\text{-}S_{16}$. Generally, $S_{10}\text{-}My\text{-}S_{10}$ exhibited a tensile strength at break $\sigma_B = 0.28 \pm 0.05\text{ MPa}$ and an elongation at break $\varepsilon_B = 183 \pm 11\%$ while $S_{16}\text{-}My\text{-}S_{16}$ showed $\sigma_B = 0.73 \pm 0.07\text{ MPa}$ and $\varepsilon_B = 89 \pm 8\%$. Compared to the previous $My\text{-}S$ diblocks, a higher extensibility was shown by these NMP-based $S\text{-}My\text{-}S$. A more entangled $P(My)$ matrix (higher entanglement density) may explain this greater capacity to stretch.

1.4.4. β -Myrcene / styrene statistical copolymerization

My/*S* mixtures, with initial *S* molar feed compositions $f_{S,0} = 0.10-0.94$ were copolymerized by NMP in bulk using NHS-BB as initiator and a target molecular weight at full conversion of $M_{n,theo} = 30 \text{ kg}\cdot\text{mol}^{-1}$. Every experiment was performed at 110 °C in order to avoid the auto-initiation of *S* which is negligible below 120 °C⁸⁷. However, auto-initiation pathways involving dimerization of *S* and *My* might occur at 110 °C. Order-of-magnitude estimate of the rate constant for the dimerization of *S* and *My* could be made by inhibition experiments for example. It would allow knowing if any thermal radical generation in the spontaneous *My*/*S* copolymerization (initiation step) occurs. Table 5 indicates the formulations of the various *My*/*S* copolymerizations.

■ Effect of feed composition on copolymer composition.

An investigation of how feed composition controls the copolymer composition was first performed. The compositions of the copolymers (F_S and $F_{My} = 1 - F_S$, Table 6 for the final compositions) were determined by ¹H NMR (see experimental section for full information). The terminal model⁸⁸ was used herein, postulating that the chemical reactivity of a propagating chain depended only on the chemical nature of the active monomer at the chain end.

Extraction of the reactivity ratios was done by linearization of the Mayo-Lewis equation⁸⁹ (eg. the Fineman-Ross (FR) approach⁹⁰) and by the Kelen-Tüdös (KT) approach⁹¹ (equations and experimental data used to determine the reactivity ratios can be found in the Supporting Information). FR and KT plots are shown in Figures 8.a and 8.b respectively and yielded $r_{My} = 1.88 \pm 0.12$ and $r_S = 0.25 \pm 0.04$ ($r_{My} \times r_S = 0.47 \pm 0.11$) via the FR method and $r_{My} = 2.19 \pm 0.07$ and $r_S = 0.34 \pm 0.19$ ($r_{My} \times r_S = 0.74 \pm 0.41$) via the KT method. The errors associated with the experimental data were derived from the standard errors of the slopes from FR and KT plots. Although the KT method is more reliable than the FR method, it is still a linearization. Statistically, a non-linear least-squares fit to the Mayo-Lewis equation is probably the soundest method to determine the desired parameters⁹². Therefore, the reactivity ratios were also determined using a non-linear least-squares fitting of the data. Using the reactivity ratios determined by the KT method as initial guesses, the statistical fit to the data yielded reactivity ratios $r_{My} = 2.90 \pm 1.25$ and $r_S = 0.47 \pm 0.27$ (see Supporting Information), which are consistent compared to those obtained by the other approaches. For all the methods, $r_{My} > 1$ and $r_S < 1$, suggesting that *My* monomer is more reactive than *S* monomer toward both propagating species ($--My^*$ and $--S^*$). The macro-radicals had a marked preference for *My* and the copolymers formed instantaneously were always richer in *My* than *S*.

Table 5. *My*/*S* copolymerization formulations for various compositions at 110 °C in bulk initiated by NHS-BB and targeting $M_{n,theo} = 30 \text{ kg.mol}^{-1}$ at $X = 1.0$.

ID ^(a)	[NHS-BB] ₀ (M)	[<i>My</i>] ₀ (M)	[<i>S</i>] ₀ (M)	<i>f</i> _{S,0}	<i>t</i> (min)
<i>My</i>/S-0	0.026	5.83	0	0	420
<i>My</i>/S-10	0.027	5.44	0.59	0.10	420
<i>My</i>/S-20	0.027	5.00	1.31	0.21	420
<i>My</i>/S-30	0.025	4.54	2.03	0.31	420
<i>My</i>/S-40	0.027	4.04	2.66	0.40	420
<i>My</i>/S-45	0.027	3.77	3.11	0.45	420
<i>My</i>/S-50	0.028	3.50	3.59	0.51	420
<i>My</i>/S-60	0.029	2.91	4.32	0.60	420
<i>My</i>/S-70	0.028	2.28	5.18	0.69	420
<i>My</i>/S-80	0.029	1.59	6.47	0.80	360 ^(b)
<i>My</i>/S-90	0.030	0.83	7.02	0.89	400
<i>My</i>/S-95	0.031	0.43	7.35	0.94	180 ^(b)
<i>My</i>/S-100	0.030	0	8.72	1	150 ^(b)

a) Experimental identification (ID) given by *My*/S-XX where the number abbreviation XX refers to the rounded % initial molar fraction of S in the mixture (*f*_{S,0}).

b) Experiments stopped before 420 min due to a highly viscous reaction medium.

A compositional drift was observed as indicated by the product $r_{My} \times r_S$ being less than unity. In the initial stages of the copolymerization, *My* was incorporated faster, producing a *My*-rich copolymer. When *My* was depleted, more S monomer was added. This specific behavior is highlighted by the difference in copolymer composition between the initial and the final stages of the reaction. For instance, the copolymer was composed of 76 mol% of *My* at 1 h and only of 53 mol% of *My* at 7 h for the experiment *My*/S-50 with *f*_{S,0} = 0.51 (individual *My* and S conversions in the course of the experiment *My*/S-50 provided in the

Table 6. Molecular characterization at the end of the experiments and kinetic data of P(*My-stat-S*) copolymers at 110 °C in bulk initiated by NHS-BB and targeting $M_{n,theo} = 30 \text{ kg}\cdot\text{mol}^{-1}$ at $X = 1.0$.

ID	$F_S^{(a)}$	$X_{My}^{(b)}$	$X_S^{(b)}$	$X_{NMR}^{(b)}$	$M_n^{(c)}$ ($\text{kg}\cdot\text{mol}^{-1}$)	$\mathcal{D}^{(c)}$	$\langle k_p \rangle \langle K \rangle^{(d)}$ (10^5 s^{-1})
My/S-0	0	0.40	0	0.40	8.2	1.19	1.6 ± 0.3
My/S-10	0.08	0.47	0.39	0.46	12.6	1.25	2.2 ± 0.1
My/S-20	0.15	0.44	0.33	0.42	10.0	1.26	1.5 ± 0.3
My/S-30	0.28	0.41	0.37	0.40	8.4	1.24	1.2 ± 0.3
My/S-40	0.38	0.50	0.45	0.48	13.7	1.25	1.8 ± 0.2
My/S-45	0.34	0.40	0.28	0.35	10.0	1.33	1.3 ± 0.2
My/S-50	0.48	0.50	0.45	0.47	11.7	1.19	1.7 ± 0.4
My/S-60	0.31	0.38	0.31	0.34	9.8	1.36	1.1 ± 0.6
My/S-70	0.45	0.54	0.45	0.48	13.9	1.24	1.2 ± 0.3
My/S-80	0.66	0.89	0.95	0.94	13.8	1.33	2.5 ± 0.6
My/S-90	0.83	0.84	0.78	0.79	19.8	1.31	2.0 ± 0.7
My/S-95	0.96	0.81	0.89	0.89	11.0	1.37	4.1 ± 1.1
My/S-100	1	0	0.88	0.88	15.6	1.20	7.5 ± 0.8

a) See notation b) in Table 4.

b) Individual monomer conversions X_{My} and X_S determined by ^1H NMR. Average monomer conversion $X_{NMR} = X_{My}f_{My,0} + X_S f_{S,0}$ (further details in the experimental section).

c) M_n and M_w determined by GPC calibrated with PS standards in THF at 40 °C. Appropriate MHS coefficients and $F_{My} = 1 - F_S$ used to convert molecular weights based on PS to the fraction of *My* incorporated in the P(*My-stat-S*) copolymer.

d) See notation c) in Table 2 ($R^2 \geq 0.94$).

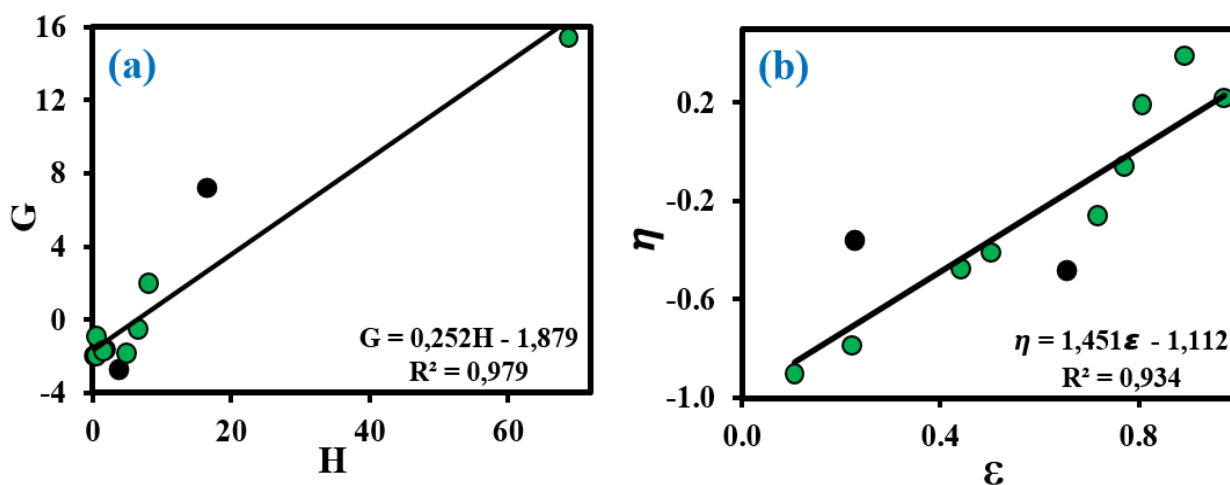
Supporting Information, Figure S9a). The reactivity ratios for *My/S* free radical copolymerization in bulk initiated by azobisisobutyronitrile (AIBN) at 65 °C were also determined, $r_{My} = 1.36$ and $r_S = 0.27$, using a non-linear least-squares method¹⁴. Similar behaviors were observed for isoprene/styrene I/S ($r_I = 1.92$ -

2.02 and $r_S = 0.42-0.54$)^{93,94} and butadiene/styrene B/S ($r_B = 1.35-1.83$ and $r_S = 0.37-0.84$)⁹⁵⁻¹⁰¹ free radical copolymerizations, confirming the more reactive nature of these 1,3-diene monomers compared to S.

The Mayo-Lewis plot is depicted in Figure 8.c and shows that NMP-based P(*My-stat-S*) formed instantaneously was always richer in *My*, regardless the initial *My/S* composition, with no azeotrope observed. A similar trend curve was obtained by Trumbo although the P(*My-stat-S*)s, synthesized by free radical polymerization in bulk at 65 °C in this case, contained a higher fraction of S¹⁴. This is explained by a lower *My* reactivity ratio ($r_{My} = 1.36$)¹⁴ in comparison to that of the SG1-based nitroxide-mediated statistical copolymerization ($r_{My} \geq 1.88$). The possible temperature dependence of *My/S* copolymerization reactivity ratios may explain the difference in P(*My-stat-S*) composition for similar $f_{S,0}$ between Trumbo's copolymers made at 65 °C and NMP-based copolymers made at 110 °C.

■ Effect of feed composition on kinetics.

The initial molar feed composition of S ($f_{S,0}$) not only influences the copolymer composition but also influences the polymerization kinetics. $\langle k_p \rangle \langle K \rangle$ kinetic values for this binary system (the product of the average propagation rate constant $\langle k_p \rangle$ and the average equilibrium constant $\langle K \rangle$) are given in Table 6, which introduces the final molecular characterization of the various copolymers as well (semi-logarithmic plot of overall conversion $\ln((1-X_{NMR})^{-1})$ versus time, M_n versus X_{NMR} plot and \bar{D} versus X_{NMR} plot provided in the Supporting Information, Figures S10a, S11a and S12a respectively). All the GPC chromatograms indicated the distributions were monomodal as illustrated in Figure 9 for the experiment *My/S-50*.



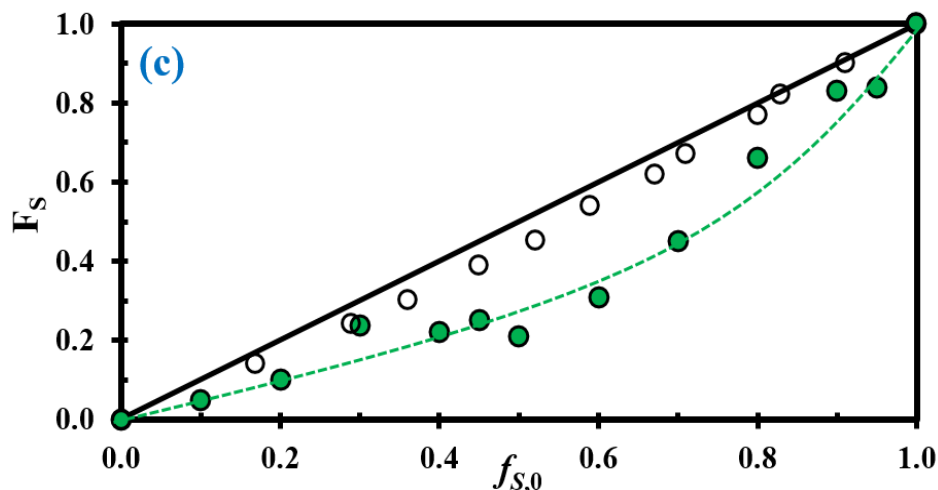


Figure 8. (a) FR and (b) KT plots to determine the binary reactivity ratios (solid black circles corresponding to experimental outliers not taken into account for the calculations) and (c) Mayo-Lewis plot of copolymer composition with respect to S (F_S) *versus* initial styrene feed composition $f_{S,0}$ (experimental data indicated by the solid green circles (•) while the dotted green line is the associated trend line ; open circles (○) refer to the data of Trumbo for M_y/S system using conventional radical copolymerization at 65 °C in bulk initiated by azobisisobutyronitrile (AIBN)¹⁴; The thin straight line indicates the azeotropic composition ($f_{S,0} = F_S$) for M_y and S statistical copolymerizations done in bulk at 110 °C using NHS-BB. See Supporting Information for the full characterization of the samples used.

Furthermore, dispersity *versus* overall conversion plot displayed a Poisson-like distribution ($\bar{D} \approx 1 + 1/DP_n$)¹⁰² for every experiment with relatively broad \bar{D} values at the early stages at $X_{NMR} < 0.20$ ($X_{M_y} < 0.26$ and $X_S < 0.17$) and narrower ones during the subsequent stages of the copolymerization. Such a kinetic feature highlights a rapid initiation with respect to propagation and negligible chain-transfer and termination reactions.

For $f_{S,0} = 0.10$ -0.69, the initial molar composition of the mixture did not significantly affect the copolymerization kinetics. The overall polymerization rate was relatively low with $\langle k_p \rangle / \langle K \rangle = 1.11$ -2.21 10^{-5} s^{-1} and $X_{NMR} \leq 0.52$ ($X_{M_y} \leq 0.56$ and $X_S \leq 0.47$) after 7 h. The first-order kinetic behavior was strongly marked as observed with the linear trend of the $\ln((1 - X_{NMR})^{-1})$ *versus* time curves ($R^2 \geq 0.96$ from 0 to 420 min). This kinetic behavior was closely similar to that of M_y homopolymerization under the same experimental conditions (experiment M_y -5, Table 1 and Table 2). Accordingly, for $f_{S,0} < 0.70$, the copolymerization kinetics was governed by the monoterpene kinetics. Besides, a good control of the reactions was observed with M_n increasing linearly with X_{NMR} and slightly plateauing at higher conversions

(M_n on average 87% of $M_{n,theo}$ at the end of the experiments) and $\mathcal{D} \leq 1.43$ from the onset to the end of these copolymerizations.

For $f_{S,0} = 0.80-0.94$, My/S statistical copolymerizations were faster as indicated in Table 6 by the higher $\langle k_p \rangle \langle K \rangle$ values ($2.03-4.11 \cdot 10^{-5} \text{ s}^{-1}$) and the almost quantitative overall conversions at the end of the experiments ($X_{NMR} \geq 0.80$ with $X_{My} \geq 0.76$ and $X_S \geq 0.81$). This was likely due to the higher homopropagation rate constant for S ($k_{p,S}$) compared to that of My . Homopolymerization of S (experiment $My/S-100$) exhibited $k_p K = 7.46 \cdot 10^{-5} \text{ s}^{-1}$ approximately one order of magnitude greater than that for My homopolymerization ($k_p K = 1.64 \cdot 10^{-5} \text{ s}^{-1}$), under the same reaction conditions. The propagation rate constants for the radical polymerization of S and I initiated by di-*tert*-butyl peroxide at 5 °C were $k_{p,S} = 180 \pm 10 \text{ L}\cdot\text{mol}^{-1}\cdot\text{s}^{-1}$ and $k_{p,I} = 125 \pm 30 \text{ L}\cdot\text{mol}^{-1}\cdot\text{s}^{-1}$ ¹⁰³. Similar trend was reported previously for the radical photopolymerization of S at 60 °C with 2-azobispropane as sensitizer ($k_{p,S} = 176 \text{ L}\cdot\text{mol}^{-1}\cdot\text{s}^{-1}$)¹⁰⁴ and for the emulsion polymerization of I at 60 °C with diisopropyl-benzene monohydroperoxide / tetraethylenepentamine (DIBHP/TEPA) catalyst system ($k_{p,I} = 50 \text{ L}\cdot\text{mol}^{-1}\cdot\text{s}^{-1}$)¹⁰⁵. The lower propagation rate constant reported regarding the free radical polymerization of I compared to that of S is consistent with the kinetic data obtained herein for the NMP of My and S.

The higher overall conversions achieved for $f_{S,0} > 0.70$ resulted in an apparent loss of control. Indeed, non-linear $\ln((1-X_{NMR})^{-1})$ versus time curves combined with higher deviations of experimental average molar masses from the predicted line were observed. M_n were on average 58% of $M_{n,theo}$ at the end of the experiments $My/S-80$, $My/S-90$ and $My/S-95$. It should be first noted that the linear PS standards used for calibrating the GPC might not be very accurate for these statistical copolymers containing $F_{My} = 0.16-0.34$. The differences in hydrodynamic volumes of these copolymers having flexible C6/C8 side chains and that of the PS standards may be apparent. Although corrections were made using Mark-Houwink-Sakurada equation, the only MHS coefficients found for P(My) may not be perfectly appropriate for this study. Indeed, $K_{P(My)}$ and $\alpha_{P(My)}$ were obtained at 30 °C for a broad average molar mass range of 1,4-P(My)s ($M_n = 6.3-55.5 \text{ kg}\cdot\text{mol}^{-1}$) with 10 mol% of 3,4-content. However, such significant deviations cannot be only attributed to the GPC data. It is likely that irreversible termination reactions became more prevalent at high conversions resulting in a loss the SG1 functionality on the chain-end and thus more dead chains. Chain transfer side reactions to monomer, generating monomeric radicals giving rise to a population of very short chains, was well-investigated for the NMP of styrene^{106,107}. Even at a temperature as low as 110 °C, NMP of S in toluene mediated by SG1 generated a significant population of new short chains presumably due to chain transfer to S¹⁰⁸. For this polymerization, it was reported that the total number of chains increased linearly with conversion, resulting in a gradual increase in \mathcal{D} combined to a plateau of $M_n < M_{n,theo}$. Despite of higher overall polymerization rates, My/S copolymerizations for $f_{S,0} > 0.70$ still exhibited relatively narrow molecular weight distributions ($\mathcal{D} \leq 1.37$).

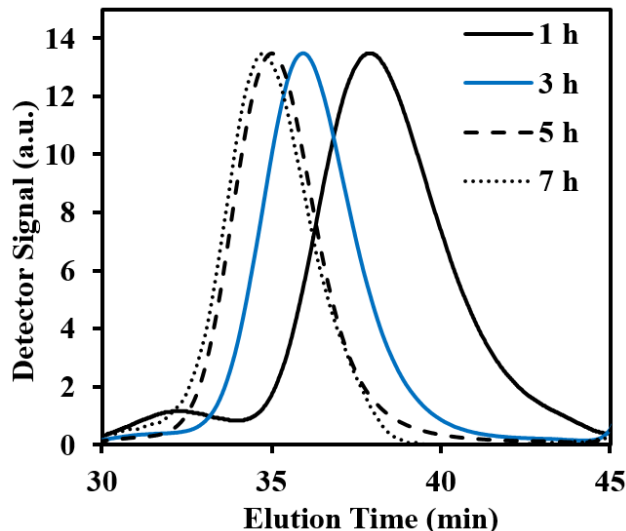


Figure 9. Normalized GPC traces of P(*My-stat-S*) copolymer initiated by NHS-BB at 110 °C in toluene targeting $M_{n,theo} = 30 \text{ kg}\cdot\text{mol}^{-1}$ at quantitative conversion (experiment *My/S-50*).

▣ Active feature of *My*-rich and *S*-rich P(*My-stat-S*) copolymers.

Two different *My/S* statistical copolymers, namely *My/S-07* ($F_S = 0.07$, *My*-rich P(*My-stat-S*)) and *My/S-55* ($F_S = 0.55$, *S*-rich P(*My-stat-S*)), were synthesized under the same previous experimental conditions and their chain end fidelity was studied. Table 7.A gives the molecular characterization of *My/S-07* and *My/S-55* copolymers. *My*-rich P(*My-stat-S*) macroinitiator was shown to have an elevated fraction of chain-end nitroxide groups ($\sim 94 \pm 6 \text{ mol}\%$ SG1 chain-end functionality, standard deviation derived from the difference in M_n value between the GPC result and the corrected M_n using MHS equation) based upon ^{31}P NMR measurements (see Supporting Information, Figure S5a with diethylphosphite as an internal reference, the presence of the phosphorus atom in the SG1 molecule was used as a tracer^{72,109}). It should be noted that the calculation of the fraction of SG1 groups was done by considering similar relaxation times between diethylphosphite and the polymer. This elevated fraction of SG1 groups was mainly due to a slow copolymerization resulting in a low overall conversion and a negligible contribution of side reactions ($M_{n,1}$ was 89% of $M_{n,theo,X1}$ and $\mathcal{D} < 1.3$). *S*-rich P(*My-stat-S*) macroinitiator contained a lower “living” chain fraction ($\sim 72 \pm 5 \text{ mol}\%$), due to a higher overall conversion achieved leading to a slight loss of control ($M_{n,1}$ was 81% of $M_{n,theo,X1}$).

In order to confirm the active feature of these two macroinitiators first characterized spectroscopically, two sets of tests were then performed to evaluate the effectiveness of the expected SG1-capped copolymers to cleanly initiate a second batch of monomer: chain-extensions of *My/S-07* and

Table 7. Chain-extensions of **A)** *My*-rich and *S*-rich P(*My-stat-S*) macro-initiators with **B)** *My* and *S* monomers in 50 wt% toluene or in bulk and **C)** molecular characterization of the resulting chain-extended products.

A. Macroinitiator ^(a)							
ID	$f_{S,0}$	$F_{S,1}$	$F_{SG1}^{(b)}$	X_1	$M_{n,1}$ (kg.mol ⁻¹)	$M_{n,theo,X1}^{(c)}$ (kg.mol ⁻¹)	\bar{D}_1
<i>My/S-07</i>	0.20	0.07	0.94 ± 0.05	0.33	11.7	13.2	1.29
<i>My/S-55</i>	0.79	0.55	0.72 ± 0.04	0.52	16.9	20.8	1.34
B. Formulation of chain-extension							
ID	[Macroinitiator] ₀ (M)	[<i>My</i>] ₀ (M)	[<i>S</i>] ₀ (M)	[Toluene] ₀ (M)	$M_{n,theo}^{(d)}$ (kg.mol ⁻¹)	T (°C)	<i>t</i> (min)
<i>My/S-07-My.a</i>	0.005	2.80	0	4.82	83.7	110	180
<i>My/S-07-My.b</i>	0.010	5.79	0	0	89.0	120	300
<i>My/S-07-S</i>	0.005	0	3.67	4.76	84.0	110	180
<i>My/S-55-My.a</i>	0.006	2.53	0	4.81	75.9	110	180
<i>My/S-55-My.b</i>	0.010	5.41	0	0	90.1	120	300
<i>My/S-55-S</i>	0.006	0	3.31	4.98	75.9	110	180
C. Chain-extended copolymer ^(a)							
ID	X_2	$F_{S,2}$	$M_{n,2}$ (kg.mol ⁻¹)	$M_{n,theo,X2}^{(e)}$ (kg.mol ⁻¹)	\bar{D}_2		
<i>My/S-07-My.a</i>	0.16	0.06	21.0	23.2	1.35		
<i>My/S-07-My.b</i>	0.48	0.02	30.4	48.8	1.59		
<i>My/S-07-S</i>	0.38	0.69	34.5	39.2	1.43		
<i>My/S-55-My.a</i>	0.15	0.37	22.4	25.8	1.44		
<i>My/S-55-My.b</i>	0.57	0.19	40.7	58.6	2.59		
<i>My/S-55-S</i>	0.44	0.80	36.4	42.9	1.60		

a) The indexes “1” and “2” refer respectively to the final features of the P(*My-stat-S*) macroinitiator and the whole chain-extended P(*My-co-S*) copolymer (macroinitiator + P(*My*) or PS segment added).

b) F_{SG1} corresponds to the living molar fraction of macroinitiator chains terminated by a SG1 unit and was measured by ³¹P NMR in CDCl₃.

c) $M_{n,theo,X1}$ corresponds to the predicted $M_{n,1}$ at the respective X_1 measured experimentally and was calculated as follows: $M_{n,theo,X1} = X_1 M_{n,theo,1}$ with $M_{n,theo,1} = 40$ kg.mol⁻¹ at $X = 1.0$.

d) $M_{n,theo}$ corresponds to the targeted number-average molecular weight of the whole chain-extended P(*My-stat-S*) copolymer at $X = 1.0$.

e) $M_{n,theo,X2}$ corresponds to the predicted $M_{n,2}$ of the whole chain-extended P(*My-stat-S*) copolymer (macroinitiator + second block added) at the respective X_2 measured experimentally and was calculated as follows: $M_{n,theo,X2} = X_2 (M_{n,theo} - M_{n,1}) + M_{n,1}$ (= Predicted M_n of the second block added at conversion X_2 + experimental M_n of the macroinitiator).

My/S-55 with *My* (experiments *My*/S-07-*My*.a and *My*/S-55-*My*.a in Table 7.B) and S (experiments *My*/S-07-S and *My*/S-55-S in Table 7.B) monomers at 110 °C in 50 wt% toluene for 3 h. Accordingly, the influence of the composition of P(*My*-*stat*-S) macroinitiators over their ability to polymerize a second batch of monomer was discussed as well as their own versatility to chain-extend *My* and S. The final characterization of the chain-extended products is shown in Table 7.C. *My*-rich macroinitiator *My*/S-07 cleanly chain-extended *My* and S as demonstrated by the low dispersities obtained ($\mathcal{D} \leq 1.43$) and the low deviations of the experimental $M_{n,2}$ values of the chain-extended copolymers from the theoretical ones ($M_{n,2}/M_{n,theo,X2} \geq 88\%$) at the corresponding conversion X_2 . Likewise, successful chain-extensions with *My* and S were performed from S-rich macroinitiator *My*/S-55 even though broader molecular weight distributions ($\mathcal{D} = 1.44$ with *My* and 1.60 with S) were measured than those of the first set of chain-extensions ($\mathcal{D} = 1.35$ and 1.43) and slightly higher deviations of $M_{n,2} \geq 85\%$ of $M_{n,theo,X2}$. This minor loss of control can be directly related to the intrinsic features of the S-rich macroinitiator *My*/S-55 having likely a greater proportion of irreversibly terminated chains relative to the *My*-rich macroinitiator *My*/S-07. Accordingly, the living feature of both *My*-rich and S-rich P(*My*-*stat*-S) macroinitiators was confirmed as also observed by the monomodal nature and the clear shift to the left of the GPC traces corresponding to the chain-extended products (see Supporting Information, Figure S13a). Furthermore, both *My* and S monomers were able to be cleanly added to the macroinitiators with slower *My* chain-extension kinetics as previously highlighted in comparison to *My*/S copolymerization kinetics. Indeed, $X = 0.15$ - 0.16 were achieved after 3 h reaction for each chain-extension with *My* resulting in the addition of relatively short elastomeric block $\leq 9.3 \text{ kg.mol}^{-1}$ (we did not let the polymerization occur for long enough).

Chain-extensions with *My* from *My*/S-07 macroinitiator (experiment *My*/S-07-*My*.b in Table 7.C) and from *My*/S-55 macroinitiator (experiment *My*/S-55-*My*.b in Table 7.C) in bulk at 120 °C for 5 h were then performed in order to increase the polymerization rate. As expected, faster chain-extensions were achieved with $X = 0.31$ at 3h for experiment *My*/S-07-*My*.b and $X = 0.39$ at 3h for experiment *My*/S-55-*My*.b compared to lower $X = 0.15$ - 0.16 at 3 h in toluene at 110°C. Furthermore, the final conversions $X \geq 0.48$ at 5 h (Table 7.C) for the chain-extensions performed in bulk at 120 °C were significantly greater. Interestingly, the number-average degree of polymerization of the bloc added for the chain-extensions *My*/S-07-*My*.b and *My*/S-55-*My*.b more than doubled with a P(*My*) segment added exhibiting $M_n \geq 18.7 \text{ kg.mol}^{-1}$ compared to previous experiments *My*/S-07-*My*.a and *My*/S-55-*My*.a in toluene at 110 °C. Nonetheless, the higher polymerization rate observed for *My* chain-extensions in bulk at 120 °C resulted in a marked loss of control as indicated by the broadening of \mathcal{D} ($\mathcal{D}_2 \geq 1.59$) and significant deviations of experimental molar masses compared to the predicted ones ($M_{n,2}/M_{n,theo,X2} \geq 62\%$). Non-negligible tails, especially for experiment *My*/S-55-*My*.b, can be observed on the GPC traces (see Supporting Information,

Figure S13a), likely due to the presence of “dead” chains from the macroinitiators and irreversible terminations.

1.4.5. Thermal analysis of the synthesized NMP-based polymers

Thermogravimetric analysis (TGA) was first performed to evaluate the thermal stability of the *My*-based polymers. The decomposition temperatures for P(*My*) and PS homopolymers as well as P(*My-b-S*) diblock copolymers are given in Table 8 (TGA thermograms provided in the Supporting Information, Figure S14a). P(*My*) exhibiting $M_n = 30.4 \text{ kg}\cdot\text{mol}^{-1}$ and containing 79% of 1,4-microstructure (*My*-12) showed a single degradation peak at $T_{\text{dec,max}} = 385 \text{ }^\circ\text{C}$ with the sample weight dramatically falling after the onset of decomposition at $T_{\text{dec,1}} \sim 290 \text{ }^\circ\text{C}$, preceded by a first weight loss at $T \sim 195 \text{ }^\circ\text{C}$. This early significant loss of weight ($\sim 35 \%$) can likely be attributed to the presence of unreacted *My* ($T_{\text{b,My}} = 167 \text{ }^\circ\text{C}$) and its impurities such as limonene ($T_{\text{b,My}} = 176 \text{ }^\circ\text{C}$) and volatile isomers and dimers of *My*. Indeed, TGA analysis for the macroinitiator *My*-12 was performed after drying the sample under air flow without any purification step by dissolution / precipitation cycles. Taking the final NMR conversion of 58% into account, it can be assumed that a significant concentration of *My* remained in the P(*My*) matrix. $T_{\text{dec,max}} = 425\text{-}427 \text{ }^\circ\text{C}$ for persulfate (47% 1,4-content) and redox ($\sim 100\%$ 1,4-content) initiated P(*My*)s, which had respectively $M_n = 92.9\text{-}109.8 \text{ kg}\cdot\text{mol}^{-1}$ were previously measured¹⁶. The slightly better thermal stability achieved compared to the NMP-based sample can be mainly explained by the total absence of nitroxide at the polymer chain-end of persulfate and redox initiated P(*My*)s. NMP-based P(*My*) chains prepared herein are in a majority terminated by a nitroxide group. Since the polymer-nitroxide bond is thermally unstable, homolytic cleavage at high temperature can occur, leading to side reactions (backbiting, chain-scission) and resulting in a lower thermal stability¹¹⁰. Moreover, the significantly higher M_n exhibited by persulfate and redox initiated P(*My*)s could have contributed to the higher $T_{\text{dec,max}}$ as well. NHS-BB initiated PS (*My/S*-100) exhibited a two-step degradation pattern with the sample weight gradually falling from $190 \text{ }^\circ\text{C}$, likely due to the evaporation of residual styrene and volatile oligomers, until it reached about $370 \text{ }^\circ\text{C}$, where beyond that the polymer degraded rapidly. PS $T_{\text{dec,max}}$ was $445 \text{ }^\circ\text{C}$, which is consistent with poly(styrene)s of similar molecular weights¹¹¹. Both *My*-11-Sa and *My*-10-S P(*My-b-S*) diblock copolymers showed the same two-step degradation pattern with a slight weight loss from $T \sim 150 \text{ }^\circ\text{C}$ to $T \sim 350 \text{ }^\circ\text{C}$ followed by the main degradation peak. P(*My-b-S*) diblock copolymers, with $T_{\text{dec,max}} = 435\text{-}440 \text{ }^\circ\text{C}$, exhibited a thermal stability similar to that of PS homopolymer.

Differential scanning calorimetry (DSC) measurements were then performed to determine glass transition temperatures (T_g s) for P(*My*), PS and P(*My-b-S*) diblock copolymers. Table 8 shows measured

Table 8. Glass transition temperatures (T_g s) and decomposition temperatures (T_{dec} s) for P(*My*) (*My*-12), PS (*My*/S-100) and P(*My*-*b*-S) diblock copolymers (*My*-10-S, *My*-11-Sa, *My*-11-Sb and *My*-12-S).

ID	F _S	T _g ^(a) (°C)	T _{dec,1} ^(b) (°C)	T _{dec,max} ^(b) (°C)	T _{dec,2} ^(b) (°C)
<i>My</i>-12	0	− 77	290	385	485
<i>My</i>-12-S	0.27	− 63	-	-	-
<i>My</i>-11-Sb	0.39	− 77	-	-	-
<i>My</i>-11-Sa	0.47	− 73 / + 61	140	440	490
<i>My</i>-10-S	0.62	− 70 / + 57	155	435	490
<i>My</i>/S-100	1.0	+ 77	190	445	490

a) T_g (°s) measured by DSC under nitrogen atmosphere at a rate of 10 °C.min⁻¹ using three scans per cycle (heat/cool/heat).

b) $T_{dec,1}$ (onset of decomposition), $T_{dec,max}$ (temperature at which weight loss is most apparent) and $T_{dec,2}$ (end of decomposition) measure by thermogravimetric analysis (TGA) under nitrogen flow at a ramp rate of 10 °C.min⁻¹ (TGA thermograms provided in the Supporting Information).

T_g s (DSC plots with changes in the slope provided in the Supporting Information, Figures S15a and S16a). As expected, P(*My*), as an amorphous elastomer, had a $T_g = -77$ °C much below the ambient temperature and very close to the natural rubber *cis*-1,4-PI, which has T_g around -73 °C¹¹². NMP-based PS exhibiting $M_n = 15.6$ kg.mol⁻¹ had a $T_g = +77$ °C instead of 100-110 °C for atactic PS with $M_n > 100$ kg.mol⁻¹¹¹³. Beyond the critical influence of M_n on T_g , the possible presence of oligomers in the PS matrix, behaving as plasticizers, could play a minor role in lowering the glass transition temperature. S-rich diblock copolymers, namely *My*-10-S and *My*-11-Sa, showed two separated T_g s: a first one at about -70 °C corresponding to the soft P(*My*) block and a second one around $+60$ °C corresponding to the hard PS block. This is illustrated in Figure 10 by the changes in slope of the DSC trace for *My*-11-Sa sample.

This suggests the possible micro-phase separation of these two heterogeneous phases. However, an in-depth analysis of the P(*My*-*b*-S)s phase behavior, including atomic force microscopy (AFM) and small-angle X-ray scattering (SAXS) for example, would demonstrate whether or not a micro-phase separation is apparent and determine the morphology of this latter. It can be noted that the T_g s of these diblocks did not exactly correspond to the T_g s of the respective P(*My*) and PS homopolymers. This might be due to a partial

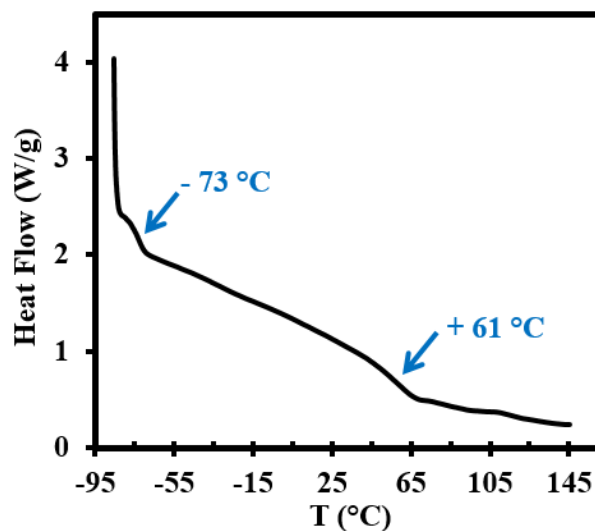


Figure 10. DSC trace (second heating run) of P(*My-b-S*) diblock copolymer *My-11-Sa*. The blue arrows indicate the changes in slope observed. DSC traces of the other P(*My-b-S*) diblock copolymers can be found in the Supporting Information.

miscibility of the two blocks caused by both a relatively low M_n and a vulnerable phase separation taking the structural similarities between *My* and *S* repetitive units into account. Partial mixing of PI and PS blocks were previously observed for P(*I-b-S*) diblocks leading to in-between glass transition temperatures¹¹⁴. Interestingly, for *My*-rich diblock copolymers (*My-11-Sb* and *My-12-S*) with $F_S \leq 0.39$, no second glass transition was observed. The T_g for the PS segment was not visible on the DSC thermograms presumably due to a too low PS content. Similarly, as regards β -myrcene/ α -methyl-*p*-methylstyrene *My*/AMMS triblocks with $F_{AMMS} < 0.35$, even though the T_g for P(*My*) was detectable, no DSC signal corresponding to the T_g of the P(AMMS) outer segments was observed²¹. By contrast, both T_{gs} for P(*I-b-S*) diblock copolymers were visible even for a large fraction of PS ($F_S = 0.78$) and the T_g for PI was not observed only for $F_S = 0.92$ ¹¹⁴.

T_g values were also measured for P(*My-stat-S*) statistical copolymers exhibiting $F_S = 0.08-0.96$, as presented in Figure 11 (DSC traces given in the Supporting Information, Figure S16a). Evidently, as the final molar content of styrene in the copolymer increased, T_g increased due to the pendant aromatic groups of *S* repeat units, providing rigidity and hardness. An exponential trend was observed with liquid rubber P(*My-stat-S*) copolymers achieved for $F_S \leq 0.48$, exhibiting $T_g < -40$ °C. A more significant dependence of T_g on F_S was apparent for *S*-rich copolymers. Indeed, T_{gs} ranged from -9 °C to $+77$ °C for $F_S = 0.66-1.00$. This may be explained by the sequence distribution of *My* repetitive units within the polymer chains.

The propagating species has a clear preference for M_y , even at a low molar fraction of M_y in the final copolymer, and short $P(M_y)$ segments can be formed, resulting in “elastomeric knots” in the matrix. These peculiar connections, exhibiting a high flexibility with long side chains, may significantly disrupt the PS network. Theoretical T_g , $T_{g,th}$, for these copolymers can be predicted by the Fox equation¹¹⁵ (7) where w_{M_y} and w_S are the weight fractions of M_y and S, and T_{g,M_y} and $T_{g,S}$ are the experimental T_g s of $P(M_y)$ and PS homopolymers.

$$1/T_{g,th} = w_{M_y}/T_{g,M_y} + w_S/T_{g,S} \quad (7)$$

Figure 11 also includes the Fox equation predictions of the $P(My-stat-S)$ T_g s. Non-negligible deviations can be noticed from our experimental data and explained by the limitations of the Fox equation in its prediction of the glass transition temperatures. Basically, it is a simple bulk additive relation disregarding the sequence distribution of M_y and S monomer units in the copolymer¹¹⁶. Moreover, the characterized $P(My-stat-S)$ s did not exhibit the same M_n , ranging from 8.2 to 19.8 kg.mol⁻¹. Slight changes in T_g values can thereby be expected, as predicted by the empirical Flory-Fox equation^{117,118}. M_y , containing two isoprene units, is a monoterpene structurally related to the readily available petro-chemical isoprene (I)³. Both $P(M_y)$ and

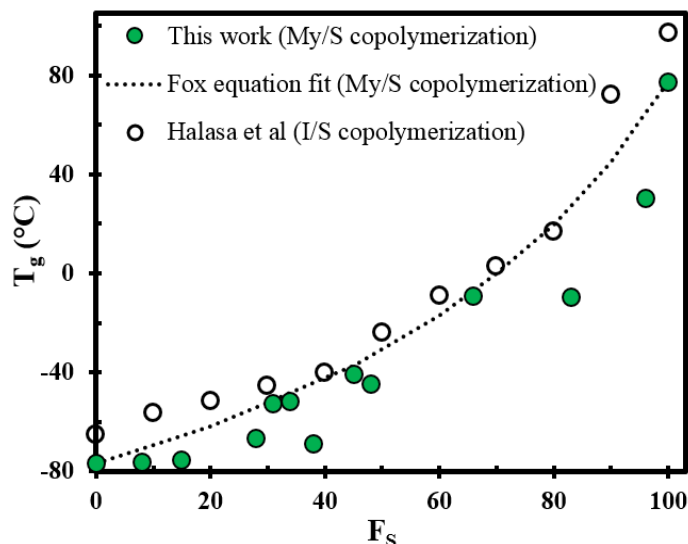


Figure 11. F_S effects on T_g in $P(My-stat-S)$ statistical copolymers (solid green circles). All of the DSC traces are given in the Supporting Information. The Fox equation predictions of the $P(My-stat-S)$ T_g s are represented by the dotted line. The open circles refer to Halasa *et al*'s data for $P(I-ran-S)$ random copolymers produced by anionic polymerization at 65 °C using a catalyst system of various sodium dodecylbenzene sulfonate (SDBS) to *n*-butyllithium (*n*-BuLi) ratios¹²⁰.

poly(isoprene) PI polymers are elastomers, exhibiting a maximum glass transition temperature $T_{g,\infty}$ between -70 and -80 °C¹¹⁹. It is thereby worthwhile to compare the T_g s of P(*My-stat-S*)s with those of P(*I-stat-S*) copolymers. Interestingly, a similar dependence of T_g on F_S was reported by Halasa and coworkers for P(*I-ran-S*) random copolymers¹²⁰ as shown in Figure 11. The higher T_g s measured can be mainly attributed to the higher experimental T_g for PI (-65 °C) than that of P(*My*) (-77 °C) and the greater $M_n > 120$ kg.mol⁻¹ exhibited by the various P(*I-ran-S*) copolymers.

1.5. Conclusion

In this study, the optimized NMP of *My* was accomplished at 120 °C in bulk initiated by the alkoxyamine NHS-BB without requiring additional SG1 free nitroxide. Relatively low apparent rate constant ($k_p K_{My} = 4.3 \cdot 10^{-5} \text{ s}^{-1}$) compared to S homopolymerization by NMP, first-order kinetic behavior (linear trend of $\ln((1-X_{My})^{-1})$ versus time with $R^2 > 0.99$) and M_n increasing linearly with X_{My} (M_n on average 90% of $M_{n,theo}$) were apparent under these experimental conditions when targeting moderate $M_{n,theo} \sim 30$ kg.mol⁻¹ at complete conversion. Resulting *cis*-1,4-rich P(*My*) containing 1,2- and 3,4-defects ($< 20\%$) and exhibiting $\bar{D} < 1.30$ was achieved. Its T_g and decomposition temperature $T_{dec,max}$ were -77 °C and $+385$ °C, respectively. The active feature of the NMP-based P(*My*) macroinitiator was confirmed by subsequent chain-extensions with S leading to well-defined P(*My-b-S*) diblock copolymers, retaining their monomodal nature. S-rich P(*My-b-S*)s showed two separate T_g s, at about -70 °C and $+60$ °C, indicating possibly their micro-phase separation. P(*My-b-S*) diblocks exhibited better thermal stability ($T_{dec,max} = 435\text{-}440$ °C) than P(*My*) and poor strain-stress properties with ultimate tensile strength < 0.9 MPa and tensile elongation at break $< 14\%$. This brittle behavior combined with a low extensibility can be largely explained by a lack of entanglement density due to the experimental P(*My*) $M_n = 13.2\text{-}30.4$ kg.mol⁻¹, lower than or equal the P(*My*) entanglement molecular weight ($M_{e,P(My)} = 22\text{-}31$ kg.mol⁻¹)⁸¹. BlocBuilder-terminated poly(ethylene-*co*-butylene)-(SG1)₂ difunctional initiator was used to produce S-*My*-S triblock copolymers with $M_n = 56\text{-}66$ kg.mol⁻¹, which exhibited improved extensibility ($\sigma_B < 0.8$ MPa, $\epsilon_B < 200\%$). Statistical copolymers from *My* and S were also prepared by NMP with $f_{S,0} = 0.10\text{-}0.94$ at 110 °C in bulk using NHS-BB. The Fineman-Ross approach yielded $r_{My} = 1.88 \pm 0.12$ and $r_S = 0.25 \pm 0.04$ ($r_{My} \times r_S = 0.47 \pm 0.11$) whereas $r_{My} = 2.19 \pm 0.07$ and $r_S = 0.34 \pm 0.19$ ($r_{My} \times r_S = 0.74 \pm 0.41$) were determined by Kelen-Tüdös approach. Well-controlled copolymerizations were performed with resulting P(*My-stat-S*)s exhibiting $M_n = 8.2\text{-}19.8$ kg.mol⁻¹, $\bar{D} < 1.40$ and monomodal distributions as shown by the GPC chromatograms. P(*My-stat-S*)s displayed a glass transition temperature between -77 and $+30$ °C depending on the molar composition of S in the statistical copolymer. The high chain-end fidelity of *My*-rich and S-rich P(*My-stat-S*)s was

confirmed via successful chain-extensions with both *My* and *S*. This investigation thereby presented a robust and simple way to synthesize P(*My*), P(*My-b-S*) and P(*My-stat-S*) by NMP.

1.6. References

- (1) Sylvestre, A. J. D.; Gandini, A. Rosin: Major Sources, Properties and Applications. In *Monomers, Polymers and Composites from Renewable Resources*, 1st ed.; Belgacem, M. N., Gandini, A., Eds.; Elsevier: Oxford, **2008**; pp 67–88.
- (2) Wilbon, P. A.; Chu, F.; Tang, C. Progress in Renewable Polymers from Natural Terpenes, Terpenoids, and Rosin. *Macromol. Rapid Commun.* **2013**, *34* (1), 8–37.
- (3) Behr, A.; Johnen, L. Myrcene as a Natural Base Chemical in Sustainable Chemistry: A Critical Review. *ChemSusChem* **2009**, *2* (12), 1072–1095.
- (4) Goldblatt, L. A.; Palkin, S. Process for Converting Nopinene to Myrcene. U.S. Patent US2420131A, **1947**.
- (5) Savich, T. R.; Goldblatt, L. A. Process for Producing Myrcene from Beta-Pinene. U.S. Patent US2507546, **1950**.
- (6) Wattimena, F. Isomerization of Terpene Compounds. U.S. Patent US4108917A, **1978**.
- (7) Yermakova, A.; Chibiryaev, A. M.; Kozhevnikov, I. V.; Anikeev, V. I. The Kinetics of Thermal Isomerization of β -Pinene and a Mixture of β - and α -Pinenes in Supercritical Ethanol. *J. Supercrit. Fluids* **2008**, *45* (1), 74–79.
- (8) Kolichski, M. B.; Cocco, L. C.; Mitchell, D. A.; Kaminski, M. Synthesis of Myrcene by Pyrolysis of β -Pinene: Analysis of Decomposition Reactions. *J. Anal. Appl. Pyrolysis* **2007**, *80* (1), 92–100.
- (9) Marti, A. New Styrenic Materials, a Natural Alternative to B in ABS; Chalmers University of Technology: **2014**.
- (10) Cawse, J. L.; Stanford, J. L.; Still, R. H. Polymers from Renewable Sources: 5. Myrcene Based Polyols as Rubber-Toughening Agents in Glassy Polyurethanes. *Polymer* **1987**, *28* (3), 368–374.
- (11) Johanson, A. J.; McKennon, F. L.; Goldblatt, L. A. Emulsion Polymerization of Myrcene. *Ind. Eng. Chem.* **1948**, *40* (3), 500–502.
- (12) Cawse, J. L.; Stanford, J. L.; Still, R. H. Polymers from Renewable Sources: 4. Polyurethane Elastomers based on Myrcene Polyols. *J. Appl. Polym. Sci.* **1986**, *31* (6), 1549–1565.
- (13) Cawse, J. L.; Stanford, J. L.; Still, R. H. Polymers from Renewable Sources: 3. Hydroxy-Terminated Myrcene Polymers. *J. Appl. Polym. Sci.* **1986**, *31* (7), 1963–1975.
- (14) Trumbo, D. L. Free Radical Copolymerization Behavior of Myrcene: I. Copolymers with Styrene, Methyl Methacrylate or *p*-Fluorostyrene. *Polym. Bull.* **1993**, *31*, 629–636.
- (15) Choi, S. W.; Ritter, H. Novel Polymerization of Myrcene in Aqueous Media via Cyclodextrin-Complexes. *e-Polymer*. **2007**, DOI: 10.1515/epoly.2007.7.1.527.
- (16) Sarkar, P.; Bhowmick, A. K. Synthesis, Characterization and Properties of a Bio-based Elastomer: Polymyrcene. *RSC Adv.* **2014**, *4*, 61343–61354.
- (17) Loughmari, S.; Hafid, A.; Bouazza, A.; El Bouadili, A.; Zinck, P.; Visseaux, M. Highly Stereoselective Coordination Polymerization of β -Myrcene from a Lanthanide-based Catalyst: Access to Bio-Sourced Elastomers. *J. Polym. Sci., Part A: Polym. Chem.* **2012**, *50* (14), 2898–2905.
- (18) Sivola, A. *n*-Butyllithium-Initiated Polymerization of Myrcene and its Copolymerization with Styrene. *Acta Polytech. Scand.-Chem. Technol. Ser.* **1977**, *134*, 7–65.
- (19) Quirk, R. P.; Huang, T.-L. Alkylolithium-Initiated Polymerization of Myrcene: New Block Copolymers of Styrene and Myrcene. In *New Monomers and Polymers*; Culbertson, B. M., Pittman, Jr., C. U., Eds.; Springer: New York, **1984**; pp 329–355.
- (20) Quirk, R. P. Research on Anionic Triblock Copolymers. In *Thermoplastic Elastomers*, 3rd ed.; Calhoun, A., Holden, G., Kricheldorf, H. R., Eds.; Hanser Gardner Publications: Cincinnati, OH, **2004**; pp 69–91.
- (21) Bolton, J. M.; Hillmyer, M. A.; Hoye, T. R. Sustainable Thermoplastic Elastomers from Terpene-Derived Monomers. *ACS Macro Lett.* **2014**, *3*, 717–720.
- (22) Nicolas, J.; Guillaneuf, Y.; Lefay, C.; Bertin, D.; Gimes, D.; Charleux, B. Nitroxide-Mediated Polymerization. *Prog. Polym. Sci.* **2013**, *38* (1), 63–235.

- (23) Chiefari, J.; Chong, Y.; Ercole, F.; Krstina, J.; Jeffery, J.; Le, T.; Mayadunne, R.; Meijs, G.; Moad, C.; Moad, G.; Rizzardo, E.; Thang, S. Living Free-Radical Polymerization by Reversible Addition-Fragmentation Chain Transfer: The RAFT Process. *Macromolecules* **1998**, *31*, 5559–5562.
- (24) Braunecker, W. A.; Matyjaszewski, K. Controlled/Living Radical Polymerization: Features, Developments, and Perspectives. *Prog. Polym. Sci.* **2007**, *32* (1), 93–146.
- (25) Georges, M. K.; Veregin, R. P. N.; Kazmaier, P. M.; Hamer, G. K. Narrow Molecular Weight Resins by a Free-Radical Polymerization Process. *Macromolecules* **1993**, *26* (11), 2987–2988.
- (26) Veregin, R. P. N.; Georges, M. K.; Kazmaier, P. M.; Hamer, G. K. Free Radical Polymerizations for Narrow Polydispersity Resins: Electron Spin Resonance Studies of the Kinetics and Mechanism. *Macromolecules* **1993**, *26* (20), 5316–5320.
- (27) Wang, J.-S.; Matyjaszewski, K. Controlled/"Living" Radical Polymerization. Atom Transfer Radical Polymerization in the Presence of Transition-Metal Complexes. *J. Am. Chem. Soc.* **1995**, *117* (20), 5614–5615.
- (28) Hadjichristidis, N.; Pispas, S.; Floudas, G. Block Copolymers: Synthetic Strategies, Physical Properties, and Applications; John Wiley & Sons: Hoboken, NJ, **2003**; pp 3–65.
- (29) Solomon, D. H.; Rizzardo, E.; Cacioli, P. New Polymerization Process and Polymers Produced Thereby. Eur. Pat. Appl. 0135280A3, **1985**.
- (30) di Lena, F.; Matyjaszewski, K. Transition Metal Catalysts for Controlled Radical Polymerization. *Prog. Polym. Sci.* **2010**, *35* (8), 959–1021.
- (31) Matyjaszewski, K. Controlled Radical Polymerization: State of the Art in 2008. In *Controlled/Living Radical Polymerization: Progress in ATRP*; Matyjaszewski, K., Ed.; American Chemical Society: Washington, DC, **2009**; pp 3–13.
- (32) Matyjaszewski, K.; Xia, J. Atom Transfer Radical Polymerization. *Chem. Rev.* **2001**, *101* (9), 2921–2990.
- (33) Jitchum, V.; Perrier, S. Living Radical Polymerization of Isoprene via the RAFT Process. *Macromolecules* **2007**, *40* (5), 1408–1412.
- (34) Moad, G.; Barner-Kowollik, C. The Mechanism and Kinetics of RAFT Process: Overview, Rates, Stabilities, Side Reactions, Product Spectrum and Outstanding Challenges. In *Handbook of RAFT Polymerization*; Barner-Kowollik, C., Ed.; Wiley-VCH: Weinheim, **2008**; 51-104.
- (35) Moad, G.; Rizzardo, E.; Thang, S. H. Living Radical Polymerization by the RAFT Process-A Second Update. *Aust. J. Chem.* **2009**, *62* (11), 1402-1472.
- (36) Hilschmann, J.; Kali, G. Bio-based Polymyrcene with Highly Ordered Structure via Solvent Free Controlled Radical Polymerization. *Eur. Polym. J.* **2015**, *73*, 363-373.
- (37) Hawker, C. J.; Bosman, A. W.; Harth, E. New Polymer Synthesis by Nitroxide Mediated Living Radical Polymerizations. *Chem. Rev.* **2001**, *101* (12), 3661-3688.
- (38) Grubbs, R. B. Nitroxide-Mediated Radical Polymerization: Limitations and Versatility. *Polym. Rev.* **2011**, *51*, 104-137.
- (39) Keoshkerian, B.; Georges, M.; Quinlan, M.; Veregin, R.; Goodbrand, B. Polyacrylates and Polydienes to High Conversion by a Stable Free Radical Polymerization Process: Use of Reducing Agents. *Macromolecules* **1998**, *31*, 7559-7561.
- (40) Georges, M. K.; Hamer, G. K.; Listigovers, N. A. Block Copolymer Synthesis by a Nitroxide-Mediated Living Free Radical Polymerization Process. *Macromolecules* **1998**, *31*, 9087-9089.
- (41) Benoit, D.; Harth, E.; Fox, P.; Waymouth, R. M.; Hawker, C. J. Accurate Structural Control and Block Formation in the Living Polymerization of 1,3-Dienes by Nitroxide-Mediated Procedures. *Macromolecules* **2000**, *33* (2), 363-370.
- (42) Grubbs, R. B.; Wegrzyn, J. K.; Xia, Q. One-Step Synthesis of Alkoxyamines for Nitroxide-Mediated Radical Polymerization. *Chem. Commun.* **2005**, 80-82.
- (43) Wegrzyn, J. K.; Stephan, T.; Lau, R. N.; Grubbs, R. B. Preparation of Poly(ethylene oxide)-*block*-Poly(isoprene) by Nitroxide-Mediated Free Radical Polymerization from PEO Macroinitiators. *J. Polym. Sci., Part A: Polym. Chem.* **2005**, *43* (14), 2977-2984.
- (44) Bertin, D.; Gignes, D.; Marque, S. R. A.; Tordo, P. Kinetic Subtleties of Nitroxide Mediated Polymerization. *Chem. Soc. Rev.* **2011**, *40*, 2189-2198.
- (45) Bertin, D.; Gignes, D.; Marque, S. R. A.; Tordo, P. Polar, Steric, and Stabilization Effects in Alkoxyamines C-ON Bond Homolysis: A Multiparameter Analysis. *Macromolecules* **2005**, *38* (7), 2638-2650.
- (46) Benoit, D.; Chaplinski, V.; Braslau, R.; Hawker, C. J. Development of a Universal Alkoxyamine for "Living" Free Radical Polymerizations. *J. Am. Chem. Soc.* **1999**, *121* (16), 3904-3920.
- (47) Grimaldi, S.; Finet, J.-P.; Le Moigne, F.; Zeghdaoui, A.; Tordo, P.; Benoit, D.; Fontanille, M.; Gnanou, Y. Acyclic *beta*-Phosphonylated Nitroxides: A New Series of Counter-Radicals for "Living"/Controlled Free Radical Polymerization. *Macromolecules* **2000**, *33*, 1141-1147.

- (48) Luo, K.; Rzaev, J. Living Radical Polymerization of Bicyclic Dienes: Synthesis of Thermally Cross-Linkable Block Copolymers. *Macromolecules* **2009**, *42* (23), 9268-9274.
- (49) Lessard, B.; Tervo, C.; Marić, M. High-Molecular-Weight Poly(*tert*-butyl acrylate) by Nitroxide-Mediated Polymerization: Effect of Chain Transfer to Solvent. *Macromol. React. Eng.* **2009**, *3*, 245-256.
- (50) Lessard, B.; Marić, M. Nitroxide-Mediated Polymerization of Poly(ethylene glycol) Acrylate Comb-Like Polymers. *Macromolecules* **2008**, *41*, 7870-7880.
- (51) Lessard, B.; Schmidt, S. C.; Marić, M. Styrene/Acrylic Acid Random Copolymers Synthesized by Nitroxide-Mediated Polymerization: Effect of Free Nitroxide on Kinetics and Copolymer Composition. *Macromolecules* **2008**, *41*, 3446-3454.
- (52) Lessard, B.; Graffe, A.; Marić, M. Styrene/*tert*-Butyl Acrylate Random Copolymers Synthesized by Nitroxide-Mediated Polymerization: Effect of Free Nitroxide on Kinetics and Copolymer Composition. *Macromolecules* **2007**, *40*, 9284-9292.
- (53) Harrisson, S.; Couvreur, P.; Nicolas, J. SG1 Nitroxide-Mediated Polymerization of Isoprene: Alkoxyamine Structure/Control Relationship and α,ω -Chain-End Functionalization. *Macromolecules* **2011**, *44* (23), 9230-9238.
- (54) Vinas, J.; Chagneux, N.; Gignes, D.; Trimaille, T.; Favier, A.; Bertin, D. SG1-based Alkoxyamine bearing a N-Succinimidyl Ester: A Versatile Tool for Advanced Polymer Synthesis. *Polymer* **2008**, *49* (17), 3639-3647.
- (55) Moayeri, A.; Lessard, B.; Marić, M. Nitroxide Mediated Controlled Synthesis of Glycidyl Methacrylate-Rich Copolymers enabled by SG1-based Alkoxyamines bearing Succinimidyl Ester Groups. *Polym. Chem.* **2011**, *2*, 2084-2092.
- (56) Zhang, C.; Marić, M. Synthesis of Stimuli-Responsive, Water-Soluble Poly[2-(dimethylamino)ethyl methacrylate/styrene] Statistical Copolymers by Nitroxide Mediated Polymerization. *Polymers* **2011**, *3* (3), 1398-1422.
- (57) Marić, M.; Consolante, V. Versatility of a Succinimidyl-Ester Functional Alkoxyamine for Controlling Acrylonitrile Copolymerizations. *J. Appl. Polym. Sci.* **2013**, *127*, 3645-3656.
- (58) Georges, S.; Bria, M.; Zinck, P.; Visseaux, M. Polymyrcene Microstructure revisited from Precise High-Field Nuclear Magnetic Resonance Analysis. *Polymer* **2014**, *55*, 3869-3878.
- (59) Xie, J. Viscometric Constants for Small Polystyrenes and Polyisobutenes by Gel Permeation Chromatography. *Polymer* **1994**, *35* (11), 2385-2389.
- (60) Hattam, P.; Gauntlett, S.; Mays, J. W.; Hadjichristidis, N.; Young, R. N.; Fetters, L. J. Conformational Characteristics of some Model Polydienes and Polyolefins. *Macromolecules* **1991**, *24* (23), 6199-6209.
- (61) Pasch, H.; Trathnigg, B. *Multidimensional HPLC of Polymers*; Springer: Heidelberg, **2013**; 37-90.
- (62) Marque, S. R. A.; Le Mercier, C.; Tordo, P.; Fischer, H. Factors Influencing the C–O–Bond Homolysis of Trialkylhydroxylamines. *Macromolecules* **2000**, *33* (12), 4403-4410.
- (63) Charleux, B.; Nicolas, J.; Guerret, O. Theoretical Expression of the Average Activation-Deactivation Equilibrium Constant in Controlled/Living Free-Radical Copolymerization Operating via Reversible Termination. Application to a Strongly Improved Control in Nitroxide-Mediated Polymerization of Methyl Methacrylate. *Macromolecules* **2005**, *38* (13), 5485-5492.
- (64) Couvreur, L.; Lefay, C.; Belleney, J.; Charleux, B.; Guerret, O.; Magnet, S. First Nitroxide-Mediated Controlled Free-Radical Polymerization of Acrylic Acid. *Macromolecules* **2003**, *36* (22), 8260-8267.
- (65) Charleux, B.; Nicolas, J. Water-Soluble SG1-based Alkoxyamines: A Breakthrough in Controlled/Living Free-Radical Polymerization in Aqueous Dispersed Media. *Polymer* **2007**, *48* (20), 5813-5833.
- (66) Roberts, G.; Davis, T.; Heuts, J.; Ball, G. Monomer Substituent Effects in Catalytic Chain Transfer Polymerization: *tert*-Butyl Methacrylate and Dimethyl Itaconate. *Macromolecules* **2002**, *35* (27), 9954-9963.
- (67) Beuermann, S.; Buback, M. Rate Coefficients of Free-Radical Polymerization deduced from Pulsed Laser Experiments. *Prog. Polym. Sci.* **2002**, *27* (2), 191-254.
- (68) Tebben, L.; Studer, A. Nitroxides: Applications in Synthesis and in Polymer Chemistry. *Angew. Chem. Int. Ed.* **2011**, *50* (22), 5034-5068.
- (69) Gryn'ova, G.; Lin, C. Y.; Coote, M. L. Which Side-Reactions Compromise Nitroxide Mediated Polymerization? *Polym. Chem.* **2013**, *4* (13), 3744-3754.
- (70) Moad, G.; Rizzardo, E. Alkoxyamine-Initiated Living Radical Polymerization: Factors Affecting Alkoxyamine Homolysis Rates. *Macromolecules* **1995**, *28* (26), 8722-8728.
- (71) Beckwith, A. L. J.; Bowry, V. W.; Ingold, K. U. Kinetics of Nitroxide Radical Trapping. 1. Solvent Effects. *J. Am. Chem. Soc.* **1992**, *114* (13), 4983-4992.

- (72) Lefay, C.; Bellene, J.; Charleux, B.; Guerret, O.; Magnet, S. End-Group Characterization of Poly(acrylic acid) Prepared by Nitroxide-Mediated Controlled Free-Radical Polymerization. *Macromol. Rapid Commun.* **2004**, *25* (13), 1215-1220.
- (73) Harrisson, S.; Couvreur, P.; Nicolas, J. Use of Solvent Effects to Improve Control over Nitroxide-Mediated Polymerization of Isoprene. *Macromol. Rapid Commun.* **2012**, *33* (9), 805-810.
- (74) Fierens, S. K.; D'Hooge, D. R.; Van Steenberge, P. H. M.; Reyniers, M. F.; Marin, G. B. MAMA-SG1 Initiated Nitroxide Mediated Polymerization of Styrene: From Arrhenius Parameters to Model-based Design. *Chem. Eng. J.* **2015**, *278*, 407-420.
- (75) Runckel, W. J.; Goldblatt, L. A. Inhibition of Myrcene Polymerization during Storage. *Ind. Eng. Chem.* **1946**, *38* (7), 749-751.
- (76) Becer, C. R.; Paulus, R. M.; Hoogenboom, R.; Schubert, U. S. Optimization of the Nitroxide-Mediated Radical Polymerization Conditions for Styrene and *tert*-Butyl Acrylate in an Automated Parallel Synthesizer. *J. Polym. Sci., Part A: Polym. Chem.* **2006**, *44* (21), 6202-6213.
- (77) McHale, R.; Aldabbagh, F.; Zetterlund, P. B. The Role of Excess Nitroxide in the SG1 (*N*-*tert*-butyl-*N*-[1-diethylphosphono-(2,2-dimethylpropyl)] Nitroxide)-Mediated Polymerization of Methyl Methacrylate. *J. Polym. Sci., Part A: Polym. Chem.* **2007**, *45* (11), 2194-2203.
- (78) Hawker, C. J.; Barclay, G. G.; Dao, J. Radical Crossover in Nitroxide Mediated "Living" Free Radical Polymerizations. *J. Am. Chem. Soc.* **1996**, *118*, 11467-11471.
- (79) Noshay, A.; McGrath, J. E. A-B-A Triblock Copolymers. *Block Copolymers: Overview and Critical Survey*; Academic Press: New York, **1977**; 186-304.
- (80) Morton, M.; McGrath, J. E.; Juliano, P. C. Structure-Property Relationships for Styrene-Diene Thermoplastic Elastomers. *J. Polymer Sci.: Part C* **1969**, *26* (1), 99-115.
- (81) Fetters, L. J.; Lohse, D. J.; Colby, R. H. Part V. Mechanical Properties: Chain Dimensions and Entanglement Spacings. In *Physical Properties of Polymers Handbook*, 2nd Ed.; Mark, J. E., Ed.; Springer: New York, **2007**; 447-454.
- (82) Landel, R. F.; Nielsen, L. E. Stress-Strain Behavior and Strength. *Mechanical Properties of Polymers and Composites*, 2nd Ed.; Marcel Dekker: New York, **1994**; 233-336.
- (83) Adhikari, R. Influence of Uncoupled Diblock Molecules on Mechanical Properties of Styrene/Butadiene/Styrene Triblock Copolymers. *Nepal Journal of Science and Technology* **2011**, *12*, 49-56.
- (84) Tilley, R. J. D. Physical Properties. *Understanding Solids: The Science of Materials*, 2nd Ed.; John Wiley & Sons: Chichester, **2013**; 289-294.
- (85) Jones, D. R. H.; Ashby, M. F. Mechanical Behaviour of Polymers. *Engineering Materials 2: An Introduction to Microstructure, Processing and Design*, 2nd Ed.; Butterworth-Heinemann: Oxford, **1998**; 238-253.
- (86) Robinson, R. A.; White, E. F. T. Mechanical Properties of Styrene-Isoprene Block Copolymers. In *Block Polymers*; Aggarwal, S. L., Ed.; Plenum Press: New York, **1970**; 123-136.
- (87) Fukuda, T.; Terauchi, T.; Goto, A.; Ohno, K.; Tsujii, Y.; Miyamoto, T.; Kobatake, S.; Yamada, B. Mechanisms and Kinetics of Nitroxide-Controlled Free Radical Polymerization. *Macromolecules* **1996**, *29*, 6393-6398.
- (88) Odian, G. Chain Copolymerization. *Principles of Polymerization*, 4th Ed.; John Wiley & Sons: New Jersey, **2004**; 466-505.
- (89) Mayo, F. R.; Lewis, F. M. Copolymerization. I. A Basis for Comparing the Behavior of Monomers in Copolymerization; The Copolymerization of Styrene and Methyl Methacrylate. *J. Am. Chem. Soc.* **1944**, *66* (9), 1594-1601.
- (90) Fineman, M.; Ross, S. D. Linear Method for Determining Monomer Reactivity Ratios in Copolymerizations. *J. Polym. Sci., Part A: Polym. Chem.* **1950**, *5* (2), 259-262.
- (91) Kelen, T.; Tüdös, F. Analysis of the Linear Methods for Determining Copolymerization Reactivity Ratios. I. A New Improved Linear Graphic Method. *J. Macromol. Sci. Chem.* **1975**, *A9* (1), 1-27.
- (92) Tidwell, P. W.; Mortimer, G. A. An Improved Method of Calculating Copolymerization Reactivity Ratios. *J. Polym. Sci., Part A: Polym. Chem.* **1965**, *3*, 369-387.
- (93) Wiley, R. H.; Davis, B. Tracer Techniques for the Determination of Monomer Reactivity Ratios. IV. Monomer Reactivity Ratios for Styrene-Isoprene Copolymerization. *J. Polym. Sci., Part A: Polym. Chem.* **1963**, *1* (9), 2819-2830.
- (94) Zverev, M. P.; Margaritova, M. F. Copolymerization of Isoprene and Styrene. *Ukrain. Khim. Zh.* **1958**, *24*, 626-628.
- (95) Lewis, F. M.; Walling, C.; Cummings, W.; Briggs, E. R.; Wenisch, W. J. Copolymerization. VII. Copolymerizations of Some Further Monomer Pairs. *J. Am. Chem. Soc.* **1948**, *70* (4), 1527-1529.
- (96) Gilbert, R. D.; Williams, H. L. Reactivity Ratios of Conjugated Dienes Copolymerized in Emulsion at 5 °C. *J. Am. Chem. Soc.* **1952**, *74* (16), 4114-4118.

- (97) Crescentini, L.; Gechele, G. B.; Zanella, A. Butadiene/Styrene/2-Methyl-5-vinylpyridine Terpolymer. Composition-Conversion Data in Comparison with Calculated Values. *J. Appl. Polym. Sci.* **1965**, *9*, 1323-1340.
- (98) Meehan, E. J. Composition of Butadiene-Styrene Copolymers Prepared by Emulsion Polymerization. *J. Polym. Sci., Part A: Polym. Chem.* **1946**, *1* (4), 318-328.
- (99) Orr, R. J.; Williams, H. L. The Polymerization of Isoprene and 2,3-Dimethylbutadiene and Copolymerization with Styrene at -18°C . in Emulsion. *Can. J. Chem.* **1952**, *30*, 108-123.
- (100) Orr, R. J. Thermochemical Aspects of Butadiene-Styrene Copolymerization. *Polymer* **1961**, *2*, 74-82.
- (101) Mitchell, J. M.; Williams, H. L. Laboratory Study of Low Ratio Butadiene-Styrene Copolymers. *Can. J. Res.* **1949**, *27* (2), 35-46.
- (102) Qiu, J.; Charleux, B.; Matyjaszewski, K. Controlled/Living Radical Polymerization in Aqueous Media: Homogeneous and Heterogeneous Systems. *Prog. Polym. Sci.* **2001**, *26* (10), 2083-2134.
- (103) Kamachi, N.; Kajiwara, A. ESR Study on Radical Polymerizations of Diene Compounds. Determination of Propagation Rate Constants. *Macromolecules* **1996**, *29* (7), 2378-2382.
- (104) Matheson, M. S.; Auer, E.E.; Bevilacqua, E. B.; Hart, E. J. Rate Constants in Free Radical Polymerization. III. Styrene. *J. Am. Chem. Soc.* **1951**, *73* (4), 1700-1706.
- (105) Morton, M.; Salatiello, P. P.; Landfield, H. Absolute Propagation Rates in Emulsion Polymerization. III. Styrene and Isoprene. *J. Polym. Sci., Part A: Polym. Chem.* **1952**, *8* (3), 279-287.
- (106) Greszta, D.; Matyjaszewski, K. Mechanism of Controlled/Living Radical Polymerization of Styrene in the Presence of Nitroxyl Radicals. Kinetics and Simulations. *Macromolecules* **1996**, *29* (24), 7661-7670.
- (107) Kruse, T. M.; Souleimonova, R.; Cho, A.; Gray, M. K.; Torkelson, J. M.; Broadbelt, L. J. Limitations in the Synthesis of High Molecular Weight Polymers via Nitroxide-Mediated Controlled Radical Polymerization: Modeling Studies. *Macromolecules* **2003**, *36* (20), 7812-7823.
- (108) Zetterlund, P. B.; Saka, Y.; McHale, R.; Nakamura, T.; Aldabbagh, F.; Okubo, M. Nitroxide-Mediated Radical Polymerization of Styrene: Experimental Evidence of Chain Transfer to Monomer. *Polymer* **2006**, *47* (23), 7900-7908.
- (109) Nicolas, J.; Dire, C.; Mueller, L.; Belleney, J.; Charleux, B.; Marque, S. R. A.; Bertin, D.; Magnet, S.; Couvreur, L. Living Character of Polymer Chains Prepared via Nitroxide-Mediated Controlled Free-Radical Polymerization of Methyl Methacrylate in the Presence of a Small Amount of Styrene at Low Temperature. *Macromolecules* **2006**, *39* (24), 8274-8282.
- (110) Petton, L.; Ciolino, A. E.; Dervaux, B.; Du Prez, F. E. From One-pot Stabilization to *In Situ* Functionalization in Nitroxide Mediated Polymerization: An Efficient Extension towards Atom Transfer Radical Polymerization. *Polym. Chem.* **2012**, *3*, 1867-1878.
- (111) Nishizaki, H.; Yoshida, K. Effect of Molecular Weight on Various TGA Methods in Polystyrene Degradation. *J. Appl. Polym. Sci.* **1981**, *26*, 3503-3504.
- (112) Loadman, M. J. R. The Glass Transition Temperature of Natural Rubber. *J. Therm. Anal. Calorim.* **1985**, *30* (4), 929-941.
- (113) Rieger, J. The Glass Transition Temperature of Polystyrene: Results of a Round Robin Test. *J. Therm. Anal. Calorim.* **1996**, *46* (3), 965-972.
- (114) Georgopoulos, P.; Rangou, S.; Haenelt, T. G.; Abetz, C.; Meyer, A.; Filiz, V.; Handge, U. A.; Abetz, V. Analysis of Glass Transition and Relaxation Processes of Low Molecular Weight Polystyrene-*b*-Polyisoprene Diblock Copolymers. *Colloid Polym. Sci.* **2014**, *292* (8), 1877-1891.
- (115) Gedde, U. W. The Glassy Amorphous State. *Polymer Physics*; Kluwer Academic Publishers: Dordrecht, **1999**; 77-98.
- (116) Tonelli, A. E. Possible Molecular Origin of Sequence Distribution-Glass Transition Effects in Copolymers. *Macromolecules* **1974**, *7* (5), 632-634.
- (117) Fox, T. G.; Flory, P. J. 2nd-Order Transition Temperatures and Related Properties of Polystyrene .I. Influence of Molecular Weight. *J. Appl. Phys.* **1950**, *21*, 581-591.
- (118) Fox, T. G. Influence of Diluent and of Copolymer Composition on the Glass Temperature of a Polymer System. *Bull. Am. Phys. Soc.* **1956**, *1*, 123-125.
- (119) Michael, R. C. Glass Transition in Rubbery Materials. *Rubber Chemistry and Technology*, Vol. 85; ACS: Akron, **2012**; 3, 313-327.
- (120) Halasa, A. F.; Jusinas, C.; Hsu, W. L.; Zanzig, D. J. Random Low Vinyl Styrene-Isoprene Copolymers. *Eur. Polym. J.* **2010**, *46*, 2013-2018.

Chapter 2. Functionalization of poly(β -myrcene) by β -myrcene / glycidyl methacrylate nitroxide-mediated copolymerization

2.1. Preface

The thermoplastic elastomer desired by ArianeGroup has to provide a tough and stable join between composite matrices. The assembly can be done either by welding (use of polar thermoplastic composites) or by adhesive bonding (use of thermoset composites bearing functional groups). Accordingly, the functionalization of the targeted styrenic block copolymer TPE appears to be important. In the case of a welding, the functional units carried by the TPE would increase the miscibility at the welding interface to favor chains inter-diffusion with the polar thermoplastic composites. If adhesive bonding is implemented with thermoset composites, the incorporation of functional units into the TPE could be valuable to encourage covalent bonding at the interface.

This chapter presents an article published in the *Journal of Polymer Science, Part A: Polymer Chemistry* (Métafiot, A.; Gérard, J. -F.; Defoort, B.; Maric, M. Synthesis of β -Myrcene/Glycidyl Methacrylate Statistical and Amphiphilic Diblock Copolymers by SG1 Nitroxide-Mediated Controlled Radical Polymerization *J. Polym. Sci., Part A : Polym. Chem.* **2018**, 56 (8), 860). It first details attempts to copolymerize *My* with three different functional monomers, namely maleic anhydride (MA), *tert*-butyl acrylate (*t*BuA) and methyl methacrylate (MMA). *My*/MMA was the only binary system to be effectively controlled by NMP, stressing the possibility to synthesize via this RDRP technique well-tailored copolymers based on *My* and a methacrylate monomer. Accordingly, an in-depth study was conducted as regards the NMP of *My* with the epoxy functional glycidyl methacrylate (GMA).

2.2. Abstract

Bulk nitroxide-mediated polymerization (NMP) of β -myrcene (*My*) and glycidyl methacrylate (GMA) with varying GMA molar feed fraction ($f_{\text{GMA},0} = 0.10\text{-}0.91$) was accomplished at 120 °C, initiated by SG1-based alkoxyamine bearing a N-succinimidyl ester group (NHS-BlocBuilder). Low dispersity *My*/GMA copolymers ($\mathcal{D} < 1.56$) with slight number-average molecular weights (M_n s) deviations from predicted values ($M_{n,\text{theo}}$ with $M_n/M_{n,\text{theo}} > 70\%$) were obtained. The copolymerization was revealed to be statistical, confirmed via Fineman-Ross ($r_{My} = 0.80 \pm 0.31$ and $r_{GMA} = 0.71 \pm 0.15$) and Kelen-Tüdös ($r_{My} =$

0.48 ± 0.12 and $r_{\text{GMA}} = 0.53 \pm 0.18$) approaches. Glass transition temperature (T_g) of the statistical P(*My-stat-GMA*)s increased from $-77\text{ }^\circ\text{C}$ to $+43\text{ }^\circ\text{C}$ as the GMA molar fraction incorporated (F_{GMA}) increased from 0.10 to 0.90. High SG1 chain-end fidelity for *My*-rich and GMA-rich P(*My-stat-GMA*)s was assessed by phosphorus nuclear magnetic resonance (^{31}P NMR, SG1 fraction $> 69\text{ mol}\%$) and chain-extensions in toluene with *My*, GMA and styrene (S) (monomodal shift in M_n). Lastly, diblock P(*My-b-GMA*) was made and treated with morpholine to produce amphiphilic copolymer able to self-organize into micelles.

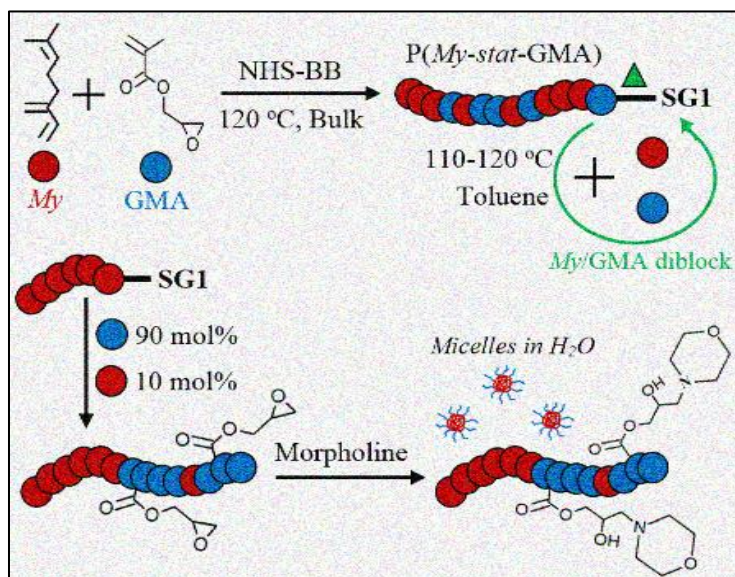


Table of contents graphic. Synthesis of well-defined *My*/GMA statistical and diblock copolymers by SG1 NMP. GMA units can be treated with morpholine to obtain 2-hydroxy-3-morpholinopropyl methacrylate hydrophilic groups.

2.3. Introduction

Elastomers based on 1,3-dienes exhibit unique and diverse properties. Their significant reversible elongation with low hysteresis combined with low modulus and poor abrasion make them suitable materials for automobile and aircraft tires, steam hoses and roofing membranes among others.¹ However, the incompatibility of hydrocarbon elastomers with polar entities considerably narrows their potential range of applications. Generally, the addition of functional units to non-polar polymers has been extensively explored in order to use them as coupling agents, adhesives, impact modifiers and compatibilizers, for instance, and thus enhance their service properties.² Post-polymerization modification was widely used to

prepare functional elastomers. Functionalization of poly(3-methylenehepta-1,6-diene) by reacting the pendant vinyl groups with various polar groups via a light-mediated thiol-ene method allowed the synthesis of functional butadiene-based materials with greater hydrophilicity.³ An epoxide functionalized poly(isobutylene-*co*-isoprene) derivative was also used to cleanly prepare a specific *exo*-diene, allowing subsequent functionalization by Diels-Alder cycloaddition and/or ring-opening of maleic anhydride adducts. This way, valuable multifunctional materials were achieved such as a graft copolymers with poly(ethylene oxide) (PEO) along with carboxylic acid moieties to name but one.^{4,5}

The insertion of polar groups in the elastomer can also be achieved directly during the polymerization process. Although coordination,⁶ anionic^{7,8} and cationic⁹ polymerizations are typically performed to synthesize polydienes, their sensitivity to impurities and to the presence of functional groups limits their use for functionalization of diene-based elastomers by direct polymerization.¹⁰ It is for instance commonly reported that functional groups can coordinate with selective catalysts and poison its activity during coordination polymerizations.⁹ An intriguing tool is reversible-deactivation radical polymerization (RDRP)¹¹⁻¹⁴ which is robust for the synthesis of well-tailored complex macromolecular architectures with controlled molecular weights. This technique appears to be well-suited for the synthesis of diene-based elastomers.¹⁵⁻¹⁸ Moreover, RDRP is desirable as a route towards well-defined functional polymers thanks to its great tolerance for functional units of monomers and reaction conditions. Well-defined glycidyl-methacrylate-based polymers were mediated by 2-cyanoprop-2-yl 1-dithionaphthalate (CPDN) RAFT agent and initiated by 2,2'-azobisisobutyronitrile (AIBN) in bulk and in benzene.¹⁹

Among RDRP techniques, nitroxide-mediated polymerization (NMP)^{12,13,20} under homogeneous conditions in bulk is one of the easiest systems to implement. 2,2,6,6-Tetramethylpiperidine-*N*-oxyl (TEMPO) nitroxide as trapping agent and benzoyl peroxide as free radical initiator served as the pioneering bicomponent initiating system used for polymerizing styrenic monomers in bulk.²¹ However, the high polymerization temperature needed ($T \sim 120-130$ °C) when using TEMPO combined with the inability to control effectively monomers other than styrenics²²⁻²⁴ triggered the development of new alkoxyamine structures. The synthesis of alkoxyamine unimolecular initiators like 2,2,5-trimethyl-4-phenyl-3-azahexane-3-oxyl (TIPNO)²⁵ and *N*-*tert*-butyl-*N*-[1-diethylphosphono-(2,2-dimethylpropyl)] nitroxide (DEPN or SG1)²⁶ increased the variety of monomers polymerizable by bulk NMP with lower temperatures accessible. TIPNO and its derivatives were used to control effectively homopolymerizations of acrylates such as *tert*-butylacrylate,²⁷⁻²⁹ acrylamides such as *N,N*-dimethylacrylamide^{29,30} and also 1,3-dienes such as isoprene (I).^{27,30} The NMP of I in bulk using TIPNO was effectively controlled with a dispersity $\bar{D} < 1.20$ and a linear relationship between the number-average molecular weight (M_n) and the conversion. Statistical copolymerizations of I in bulk with styrenics, acrylates and methacrylates were then performed in a

controlled manner.²⁴ Random and block copolymers based on associations of 1,3-dienes with functionalized vinyl monomers using TIPNO were successfully prepared.^{28,31-33}

Well-controlled 1,3-dienes polymerizations were reported for SG1-mediated NMP as well. Successful NMP of I in bulk at 115 °C using a range of SG1-based alkoxyamines was studied. Poly(isoprene)s (PIs) exhibiting $\bar{D} < 1.20$ and M_n close to the predicted one at approximately 40% conversion were achieved.³⁴ We reported recently the optimized NMP of β -myrcene (*My*),³⁵ an acyclic monoterpene 1,3-diene, in bulk, initiated by the SG1-based succinimidyl ester-terminated NHS-BlocBuilder,³⁶⁻³⁸ derived from the esterification of BlocBuilderTM initiator.³⁹ Moreover, SG1-type initiators led to the synthesis of well-defined poly(acrylate)s^{40,41} such as poly(*n*-butyl acrylate) and poly(methacrylate)s like poly(methyl methacrylate).^{42,43} Accordingly, these studies highlighted the ease of NMP based on the second generation of acyclic nitroxides to homopolymerize conjugated 1,3-dienes and to copolymerize them with functional monomers.

The copolymerization of ``renewable`` *My* with functional monomers has been rarely reported although it could provide a wide latitude of polymer properties. Trumbo studied the free radical copolymerization of *My* with methyl methacrylate and *p*-fluorostyrene at 65 °C initiated by AIBN.⁴⁴ To the best of our knowledge, the controlled/living copolymerization of *My* with polar monomers by ionic polymerization or RDRP has never been performed. Taken the robustness of NMP based on the second generation alkoxyamines to copolymerize 1,3-dienes with functionalized vinyl monomers into account, the synthesis of functional *My*-based copolymers by SG1-mediated NMP appears to be promising.

In the present study, we report on NHS-BlocBuilder-initiated copolymerization of *My* with glycidyl methacrylate (GMA) in a controlled manner at 120 °C in bulk. Copolymer composition and kinetics were studied according to the molar feed composition of GMA. The glass transition behavior of the resulting P(*My*-*stat*-GMA) statistical copolymers was explored. Their active feature was assessed by phosphorus nuclear magnetic resonance (³¹P NMR) and by their ability to initiate a fresh batch of monomer. Lastly, a P(*My*-*b*-GMA) diblock was achieved and modified using morpholine in order to synthesize readily an amphiphilic poly(β -myrcene-*block*-2-hydroxy-3-morpholinopropyl methacrylate) P(*My*-*b*-HMPMA) diblock copolymer.

2.4. Results and discussion

2.4.1. Attempts to copolymerize β -myrcene with various functional monomers by NMP

The insertion of functional groups into poly(β -myrcene) P(My) elastomer was first tried by nitroxide-mediated copolymerization with various polar monomers (Figure 1). Maleic anhydride (MA), bearing the reactive acid anhydride moiety, was first attempted. Acrylic acid (AA) was not copolymerized due to the sensitivity of the SG1 free nitroxide towards decomposition by some acids.⁴⁷ Although Charleux and coworkers demonstrated that active SG1-capped low M_n P(AA)s and P(AA-co-S)s exhibiting $\bar{D} < 1.4$ and M_n close to the targeted values can be produced using SG1-based alkoxyamine in 1,4-dioxane,^{48,49} Lessard *et al.* highlighted the possible degradation reactions by the organic acid with SG1 as well as the loss of the propagating macroradicals due to β -hydrogen transfer to SG1.^{47,50-52} To avoid this, *tert*-butyl acrylate (*t*BuA), bearing a *tert*-butyl protecting group, was used. The subsequent cleavage after polymerization of the protecting group with trifluoroacetic acid can be performed to yield carboxylic acid groups.⁵³ Lastly, methyl methacrylate (MMA) was used to see if My with a methacrylate can be done in a controlled manner as has been suggested by isoprene/MMA copolymerizations at quite high MMA content in the initial monomer mixture.⁵⁴

The experimental conditions of the various copolymerizations performed and the characterization of the resulting copolymers at the end of the experiments are summarized in Table 1. The complete kinetic study including the semi-logarithmic plot of overall conversion $\ln((1-X)^{-1})$ versus time, M_n versus X plot and \bar{D} versus X plot for every experiment is provided in the Supporting Information, Figures S1b, S2b and S3b. It should be added that the M_n values reported in this whole study directly came from GPC measurements, calibrated with PS linear standards, and no corrections were made by using Mark-Houwink-Sakurada coefficients. Even though trends of M_n versus X were meaningful and direct M_n comparisons between the experiments done were relevant due to the similar structures of the copolymers produced, the deviations of experimental M_n values from predicted ones have to be carefully scrutinized. They did not necessarily correspond to accurate values and were mostly discussed in comparison with deviations determined from other experiments.

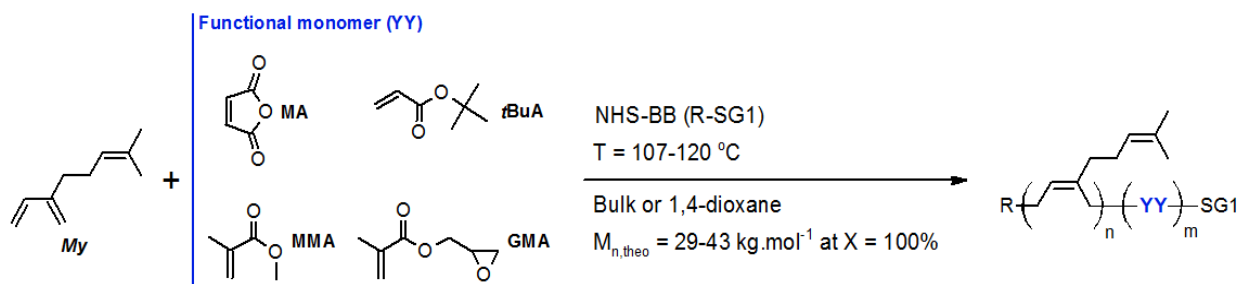


Figure 1. Copolymerization of My and YY (MA, *t*BuA, MMA or GMA) by NMP using NHS-BlocBuilder initiator.

Table 1. Experimental conditions and results for NHS-BB-initiated copolymerizations of *My* with MA, *t*BuA and MMA.

ID ^(a)	[NHS-BB] ₀ (M)	[<i>My</i>] ₀ (M)	[YY] ₀ ^(b) (M)	Solvent	[Solvent] ₀ (M)	T (°C)	M _{n,theo} (kg.mol ⁻¹)	X ^(c) (%)	M _n ^(d) (kg.mol ⁻¹)	Đ ^(d)
<i>My</i>/MA-90	0.015	2.98	0.35	1,4-dioxane	5.45	107	29.4	46.1	5.5	1.23
<i>My</i>/MA-50	0.017	2.11	2.18	1,4-dioxane	5.76	108	29.6	58.3	-(e)	-(e)
<i>My</i>/<i>t</i>BuA-90	0.020	5.33	0.57	-	-	115	40.0	64.9	16.7	1.31
<i>My</i>/<i>t</i>BuA-70	0.019	4.25	1.85	-	-	115	42.9	66.5	10.4	1.19
<i>My</i>/<i>t</i>BuA-50	0.021	3.14	3.11	-	-	115	39.3	85.2	6.4	1.25
<i>My</i>/MMA-50	0.028	3.54	3.51	-	-	110	29.8	59.2	8.4	1.24

a) Experimental identification given by *My*/YY-XX where YY refers to the functional comonomer and XX refers to the rounded % initial molar fraction of *My* in the mixture ($f_{My,0}$).

b) Initial molar concentration of YY in the mixture.

c) Overall monomer conversion $X = X_{My}f_{My,0} + X_{YY}f_{YY,0}$ determined by ¹H NMR in CDCl₃.

d) M_n and M_w determined by GPC calibrated with PS standards in tetrahydrofuran (THF) at 40 °C.

e) Undetectable polymer peak on the GPC chromatogram.

■ *My*/MA NMP.

Two *My*/MA copolymerizations in 1,4-dioxane under reflux (T = 107-108 °C) initiated by NHS-BB and with two distinct initial feed composition (*My*/MA-90 with $f_{My,0} = 0.89$ and *My*/MA-50 with $f_{My,0} = 0.49$) were first performed (Table 1). When adding 10 mol% of MA in the feed, it is of interest to note the early consumption of about one fifth of the monomers at the commencement of the reaction. Moreover, significant deviations of M_n from the theoretical predictions ($M_n/M_{n,theo} < 0.40$ all along the experiment, strong plateauing compared to *My*/*t*BuA-90, Figure S2) suggest the disruption of the NMP process via side reactions. To provide a better insight into the influence of MA on the control of the polymerization, a second reaction was conducted with a stoichiometric initial feed composition of monomers (*My*/MA-50, Table 1).

No polymerization occurred as signaled by the absence of polymer peak in the GPC chromatograms and the gravimetric conversion already reached 50% at $t = 0$ min. The reaction medium turned dark yellow/orange after only 30 minutes and was dark brown at the end of the reaction. These observations suggest a side product was formed at the initial stages of the polymerization, possibly followed by another

transformation that was indicated by the colour change. This incompatibility of *My* and MA to copolymerize might be explained by the formation of a Diels-Alder adduct. The Diels-Alder cycloaddition of isoprene with MA to yield 4-methyl-4-cyclohexene-1,2-dicarboxylic anhydride is well-known⁵⁵ and a similar mechanism was also reported for the *My*/MA system.⁵⁶ Figure S4b in the Supporting Information gives the individual *My* and MA conversions *versus* reaction time for both experiments. Interestingly, a similar trend in consumption for *My* and MA is noticeable regardless of the initial feed composition. This supports the assumption of the formation of a cyclic side product from a stoichiometric amount of *My* and MA.

■ *My*/tBuA NMP.

The polymerization of acrylates by NMP has become much more facile with second-generation alkoxyamines such as TIPNO and BlocBuilderTM. However, its main challenge is derived from selection of the proper conditions due to their elevated propagation rate constants (k_p) compared to styrenics.^{22,57} *My*/tBuA copolymerization, mediated by NHS-BB, was carried out in bulk at 115 °C and targeting about 40 kg.mol⁻¹ at X = 100% (Table 1). An investigation of the influence of the initial feed composition over the control of the polymerization was performed with $f_{My,0} = 0.90, 0.70$ and 0.50 (experiments *My*/tBuA-90, *My*/tBuA-70 and *My*/tBuA-50 respectively). Regardless of the initial feed composition, tBuA conversion was higher than *My* conversion (Figure S4b, Supporting Information) indicating the higher reactivity of this acrylate with a likely predominance of the propagating macro-radical to add tBuA monomer, whatever the terminal active unit ($---My^*$ or $---tBuA^*$). Relatively low dispersities lower than 1.40 were obtained, even at high overall conversion X > 60%, for every experiment (Figure S3). However, deviations of experimental M_n from $M_{n,theo}$ were greater as $f_{tBuA,0}$ increased. Although the copolymerization of *My* with 10 mol% of tBuA led to a satisfactory control of the NMP with a linear increase of M_n with conversion, the initial addition of 30 and 50 mol% of tBuA in the feed affected significantly the kinetics of the reaction. Indeed, experiment *My*/tBuA-70 exhibited M_n plateauing very early and remaining constant during the whole reaction and this observation was even more marked for experiment *My*/tBuA-50 with higher $f_{tBuA,0}$ (Figure S2). The predominance of chain transfer side reactions due to the presence of tBuA, terminating irreversibly the copolymer chains and thus lowering M_n values can be hypothesized. A secondary backbiting reaction, consisting of an intramolecular chain transfer event in which the propagating chain-end radical loops back and abstracts a hydrogen atom on its own backbone, may have occurred. It is now well-established that backbiting occurs during radical polymerization of acrylates, which can lead to propagation or chain-scission.^{58,59} More specifically, backbiting reactions in the presence of tBuA leading to the formation of mid-chains radicals was also reported.⁶⁰⁻⁶¹ Accordingly, uncontrol *My*/tBuA NMP might

be due to the occurrence of backbiting reactions, converting chain-end radicals to less reactive mid-chain radicals. With this assumption, the synthesis of branched P(*My-co-tBuA*) under these reaction conditions is probable. Interestingly, NMP of *tBuA* initiated by BlocBuilder™ with 4.5 mol% additional SG1 relative to initiator in bulk at 115 °C exhibited a linear increase of M_n with conversion.⁶² However, relatively high \bar{D} values (1.51-2.27) and a low chain end fidelity were observed, suggesting that substantial irreversible termination reactions took place as well. As $f_{tBuA,0}$ increased, the molar fraction of 1,2-content increased whereas the fraction of 1,4-addition decreased (Figure S5b, Supporting Information). While the SG1 NMP of *My* resulted in 1,4-rich-P(*My*) containing a minor proportion of 1,2- and 3,4-contents (< 20%),³⁵ it appears that 1,2-addition is encouraged due to the presence of *tBuA* likely as a terminal or penultimate unit of the propagating species.

■ *My*/MMA NMP.

Although some exceptions were reported using well-tailored alkoxyamines such as 2,2-diphenyl-3-phenylimino-2,3-dihydroindol-1-yloxy nitroxide (DPAIO),⁶³ the simplest way to control effectively the polymerization of methacrylate monomers by SG1-mediated NMP is to use a small concentration of controlling comonomer such as styrene.^{42,64} Benoit and coworkers reported the effective control of the bulk NMP of MMA initiated by 2,2,5-trimethyl-3-(1'-phenylethoxy)-4-phenyl-3-azahexane alkoxyamine and using isoprene at about 20 mol% in the feed.⁵⁴ In order to know if methacrylates can be readily copolymerized with *My* by NMP, MMA monomer was selected as a reference methacrylate. A stoichiometric feed composition of monomers ($f_{My,0} = 0.50$, experiment *My*/MMA-50, Table 1) was heated at 110 °C in the presence of NHS-BB initiator. As shown in Figure S1 by the linear relationship between $\ln((1-X)^{-1})$ versus reaction time t (correlation coefficient $R^2 > 0.98$), a first-order kinetic behavior was observed, assuming a quasi-constant concentration of the active propagating species during the polymerization. Linear trends can be noted regarding individual *My* and MMA conversions with respect to the polymerization time as well (Figure S4b, Supporting Information). Moreover, M_n values increased linearly with the overall conversion (Figure S2) and narrow molecular weight distributions were obtained ($\bar{D} \leq 1.32$, Figure S3). Consequently, the reversible dynamic equilibrium between the dormant SG1-terminated P(*My-co-MMA*) copolymers and active P(*My-co-MMA*) radicals was likely established. At $X > 20\%$, non-negligible deviations of the M_n from the predicted ones can be noted yet (Figure S2). This tendency of M_n to plateau at increasingly higher conversions is presumably due to irreversible terminations, commonly observed for copolymerizations of methacrylates using SG1-based alkoxyamine.^{52,65,66} Since the copolymerization was done in bulk, it can be assumed that the side reactions resulted mainly from β -hydrogen transfer to SG1⁵² or intramolecular chain transfer.⁶⁷

The satisfactory results regarding the SG1 nitroxide-mediated copolymerization of *My* with MMA in bulk prompted us to study more exhaustively the copolymerization of *My* with another methacrylic ester that contains functional groups, such as the epoxy-functional glycidyl methacrylate (GMA).

2.4.2. *My*/GMA statistical copolymerization

We reported previously the optimized NMP of *My* (experiment *My*/GMA-100 herein, Tables 2 and 3) performed at 120 °C in bulk and initiated by NHS-BB alkoxyamine, leading to M_n on average 90% of predicted $M_{n,theo}$, $\mathcal{D} < 1.3$ and a resulting SG1-capped P(*My*) able to reinitiate cleanly a second batch of styrene.³⁵ Accordingly, we attempted to copolymerize *My* and GMA, with initial *My* molar feed compositions $f_{My,0} = 0.10-0.90$, under the same reaction conditions. Notably, well-controlled NMP copolymerizations of isoprene (I) with small amounts of GMA (1-10 wt%) in toluene were also performed at 120 °C in a medium pressure reactor.⁶⁸ The formulations for the various *My*/GMA copolymerizations are summarized in Table 2.

Table 2. *My*/GMA copolymerization formulations for various compositions at 120 °C in bulk initiated by NHS-BB and targeting $M_{n,theo} = 30 \text{ kg}\cdot\text{mol}^{-1}$ at $X = 100\%$.

ID ^(a)	[NHS-BB] ₀ (M)	[<i>My</i>] ₀ (M)	[GMA] ₀ (M)	$f_{My,0}$	t (min)
<i>My</i>/GMA-0	0.036	0	7.52	0	– ^(b)
<i>My</i>/GMA-10	0.034	0.72	6.55	0.10	15
<i>My</i>/GMA-20	0.033	1.43	5.67	0.20	60
<i>My</i>/GMA-30	0.032	2.01	4.86	0.29	90
<i>My</i>/GMA-40	0.031	2.69	4.02	0.40	180
<i>My</i>/GMA-50	0.030	3.28	3.26	0.50	300
<i>My</i>/GMA-60	0.029	3.85	2.54	0.60	300
<i>My</i>/GMA-70	0.029	4.40	1.83	0.71	300
<i>My</i>/GMA-80	0.028	4.85	1.23	0.80	360
<i>My</i>/GMA-90	0.027	5.36	0.61	0.90	300
<i>My</i>/GMA-100^(c)	0.025	5.61	0	1	420

a) Experimental identification given by *My*/GMA-XX where XX refers to the rounded % initial molar fraction of *My* in the mixture ($f_{My,0}$).

b) Experiment stopped before the arbitrary time $t = 0$ min due to a highly viscous reaction medium.

c) *My* homopolymerization performed previously under the same experimental conditions.³⁵

■ Effect of feed composition on copolymer composition.

The influence of $f_{M_y,0}$ over the molar composition of the resulting P(*My-co-GMA*) copolymer was explored at relatively low overall conversion ($X \leq 23.2\%$ for every copolymerization). The compositions of the copolymers synthesized (F_{M_y} and $F_{GMA} = 1 - F_{M_y}$, Table 3 for the final compositions) during the experiments were determined by $^1\text{H NMR}$ (see Experimental Section for full information and Figure S6b in Supporting Information for the spectral assignments of $^1\text{H NMR}$ from experiment *My/GMA-50*). It should be noted that the terminal model was used, which assumes that the reactivity of an active center depends only on the nature of the terminal monomer unit of the growing chain.⁶⁹

Table S1b in the Supporting Information contains experimental data used to estimate the monomer reactivity ratios for low-conversion P(*My-co-GMA*)s via the Fineman-Ross (FR)⁷⁰ and the Kelen-Tudos (KT)⁷¹ approaches (equations used for the calculation of the reactivity ratios can be found in the Supporting Information). Figures 2a and 2b show the plots of the parameters for both linear methods, yielding $r_{M_y} = 0.80 \pm 0.31$ and $r_{GMA} = 0.71 \pm 0.15$ ($r_{M_y}r_{GMA} = 0.57 \pm 0.27$) via the FR approach and $r_{M_y} = 0.48 \pm 0.12$ and $r_{GMA} = 0.53 \pm 0.18$ ($r_{M_y}r_{GMA} = 0.25 \pm 0.17$) using the KT formula. The errors associated with the experimental data were derived from the standard errors of the slopes from FR and KT plots. Although monomer conversions considered were relatively low, the effect of possible composition drift during the copolymerization could not be taken into account by FR and KT approaches. Tidwell and Mortimer highlighted the defects of the linear methods and suggested the use of a non-linear least-squares (NLLS) procedure.⁷² This latter method is known to avoid the compositional drift, altering the chemical composition of the copolymer over the period of conversion. Therefore, the non-linear least-squares fitting to the data was also used to determine the reactivity ratios (Supporting Information). Since a starting point needs to be provided, the reactivity ratios calculated by the KT method were used as initial guesses. NLLS procedure applied to the Mayo-Lewis equation⁷³ showed good agreement with the other methods employed in this study, with $r_{M_y} = 0.49 \pm 0.13$ and $r_{GMA} = 0.50 \pm 0.13$ with 95% confidence bounds. These results have to be taken carefully into account since only 11 data points were used to implement the NLLS method. Regardless of the method applied, $r_{M_y} < 1$ and $r_{GMA} < 1$ showing the preference of $--M_y^*$ and $--GMA^*$ propagating species for adding the other monomer (GMA and *My* respectively) and each of these propagation steps proceed at a similar rate since $r_{M_y} \approx r_{GMA}$. Interestingly, $0.25 \leq r_{M_y}r_{GMA} \leq 0.57$ indicating that the behavior of *My/GMA* system cannot be considered as an ideal copolymerization ($r_{M_y}r_{GMA} = 1$, the relative rates of incorporation of the two monomers into the copolymer are independent of the identity of the unit at the end of the propagating species). As the product of the reactivity ratios decreases from one toward zero, there is an increasing tendency toward alternation, where each of the two types of propagating species preferentially adds the other monomer. Since $r_{M_y}r_{GMA} \geq 0.25$ is relatively far from zero, the

predominance of the statistical placement over alternating arrangement of *My* and GMA monomers along the copolymer chain can be assumed. Other diene/GMA were copolymerized by conventional free radical polymerization. P(*I-stat*-GMA) statistical copolymers were synthesized by benzoyl peroxide-initiated free radical polymerization in bulk at 80 °C and $r_1 = 0.195 \pm 0.005$ and $r_{\text{GMA}} = 0.135 \pm 0.005$ were determined graphically.⁷⁴ More recently, Contreras-Lopez and coworkers reported $r_1 = 0.119 \pm 0.048$ and $r_{\text{GMA}} = 0.248 \pm 0.161$, via the nonlinear method of Tidwell- Mortimer with 95% confidence intervals, for *I*/GMA copolymerization in bulk at 70 °C initiated by benzoyl peroxide.⁷⁵ Accordingly, lower reactivity ratios were calculated for *I*/GMA system with $r_{\text{I/GMA}}$ less than 0.03 indicating the stronger tendency to alternate compared to *My*/GMA system polymerized by bulk NMP at 120 °C. Two parameters may explain the difference in constants observed: the significantly higher reaction temperature for *My*/GMA copolymerization (120 °C) and the nature of the conjugated 1,3-diene and thus the effect of the lateral C6/C8 side group borne by *My* units.

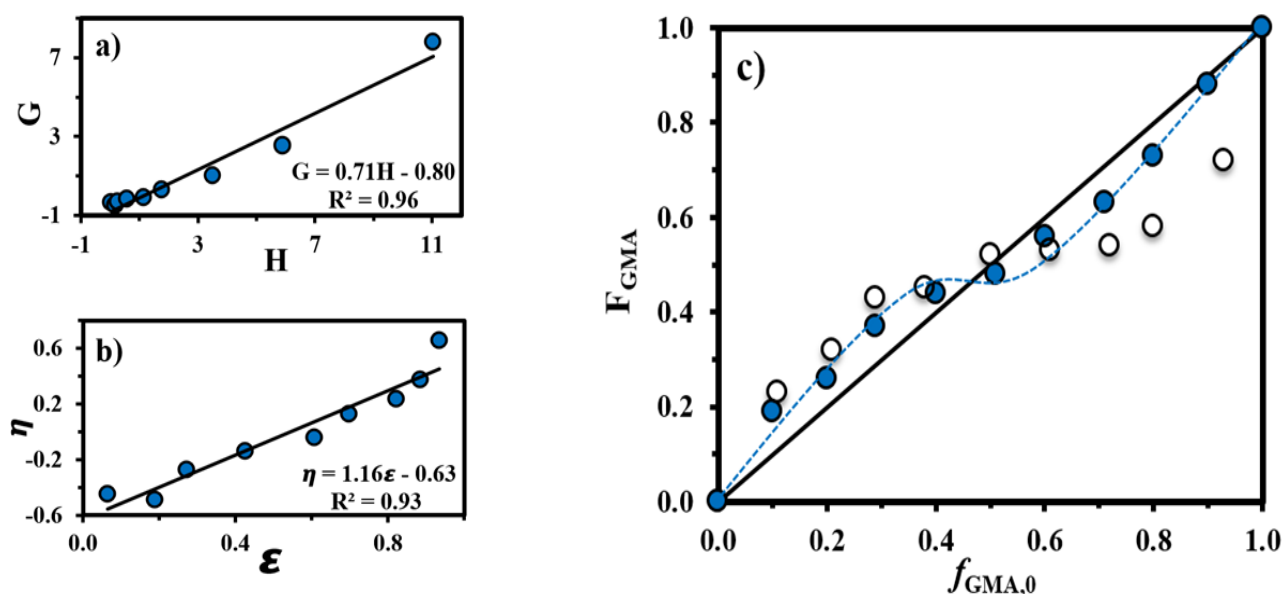


Figure 2. (a) FR and (b) KT plots (solid blue circles (●) corresponding to experimental data while solid lines refer to the trend lines) and (c) Mayo–Lewis plot of copolymer composition with respect to GMA (F_{GMA}) versus initial GMA feed composition $f_{\text{GMA},0}$ (experimental data indicated by the solid blue circles (●) while the blue dashed line is the associated trend line; open circles (○) refer to the data of Contreras-Lopez and coworkers for the *I*/GMA system initiated by benzoyl peroxide;⁷⁵ the straight line indicates the azeotropic composition ($f_{\text{GMA},0} = F_{\text{GMA}}$) for *My* and GMA copolymerizations done in bulk at 120 °C using NHS-BB. See Table S1b in the Supporting Information for the characterization of the samples used.

Figure 2c shows the curve of instantaneous copolymer composition (mole fraction of GMA) obtained for a given feed monomer composition regarding the *My*/GMA system as well as I/GMA system studied by Contreras-Lopez *et al.*.⁷⁵ A similar dependence of F_{GMA} over $f_{\text{GMA},0}$ can be noted for both systems with GMA-rich instantaneous copolymers produced at $f_{\text{GMA},0} \lesssim 0.45$ and diene-rich instantaneous copolymers formed at $f_{\text{GMA},0} \gtrsim 0.55$. The Mayo-Lewis plot exhibits an azeotropic point at $f_{\text{GMA},0} = 0.47$ for *My*/GMA system where the instantaneous composition of the copolymer is equal to the composition of the monomer feed. The greater deviations observed from the azeotropic composition for the I/GMA copolymerization were due to the lower reactivity ratios and thus the higher rates of cross-propagation measured.

■ Effect of feed composition on kinetics.

It is of interest to know if *My* and GMA monomers are generally more or less reactive in copolymerization than indicated by their respective rate of homopolymerization. Even though kinetic data regarding *My* polymerization are scarce, isoprene (I) can be chosen as a reference conjugated 1,3-diene. The propagation rate constant of free radical polymerization of I ($k_{p,I}$) in bulk initiated by di-*tert*-butyl peroxide under irradiation at 5 °C was estimated at $125 \pm 30 \text{ L}\cdot\text{mol}^{-1}\cdot\text{s}^{-1}$.⁷⁶ $k_{p,I} = 50 \text{ L}\cdot\text{mol}^{-1}\cdot\text{s}^{-1}$ was calculated by Morton *et al.* for the emulsion polymerization of I at 60 °C with diisopropylbenzene monohydroperoxide / tetraethylene pentamine (DIBHP/TEPA) catalyst system.⁷⁷ On the other hand, $k_{p,\text{GMA}}$ for the free radical polymerization of GMA at 50 °C was estimated through pulsed laser polymerization ($1\ 230 \text{ L}\cdot\text{mol}^{-1}\cdot\text{s}^{-1}$)⁷⁸ and through quantum chemistry simulations ($1\ 010 \text{ L}\cdot\text{mol}^{-1}\cdot\text{s}^{-1}$).⁷⁹ Consequently, it can be argued that GMA polymerizes at a rate of about ten times faster than *My* via a radical process.

The semi-logarithmic kinetic plots of $\ln((1-X)^{-1})$ (X = overall conversion) *versus* reaction time are illustrated in Figure 3a. The linear trend seen for every *My*/GMA copolymerization until the end of the experiment (squared linear regression coefficient, $R^2 \geq 0.95$) indicates the first-order kinetic behavior of the polymerizations, as described by Equation 2.

$$\ln([M]_0/[M]_t) = \ln([M]_0/([M]_0(1-X))) = \langle k_p \rangle [P^*] \text{time} \quad (2)$$

In Equation 2, $[M]_0$ and $[M]_t$ are the concentrations of monomers at time zero and subsequent later time t , respectively, $\langle k_p \rangle$ is the average propagation rate constant and $[P^*]$ is the concentration of propagating macro-radicals. Regardless of the *My*/GMA initial feed composition, at the early stages of the copolymerization (caption (d) in Table 3), the straight kinetic trends of the semi-logarithmic plots highlight

Table 3. Molecular characterization and M_y selectivity at the end of the experiments and kinetic data of P(M_y -stat-GMA) copolymers at 120 °C in bulk initiated by NHS-BB and targeting $M_{n,theo} = 30 \text{ kg.mol}^{-1}$ at $X = 1.0$.

ID	$F_{M_y}^{(a)}$	$X_{M_y}^{(b)}$ (%)	$X_{GMA}^{(b)}$ (%)	$X^{(b)}$ (%)	$M_n^{(c)}$ (kg.mol^{-1})	$\bar{D}^{(d)}$	$\langle k_p \rangle \langle K \rangle^{(d)}$ (10^{-5} s^{-1})	1,4- content ^(e) (%)	1,2- content ^(e) (%)
M_y/GMA-0^(f)	0	0	-	-	-	-	-	-	-
M_y/GMA-10	0.05	93.1	79.3	80.7	20.6	1.52	157.0 ± 0.9	47.3	39.2
M_y/GMA-20	0.16	98.9	86.1	88.7	21.9	1.51	47.7 ± 0.5	48.0	44.9
M_y/GMA-30	0.21	93.2	82.8	85.9	19.1	1.47	37.6 ± 0.3	58.8	38.1
M_y/GMA-40	0.34	88.3	92.2	90.6	20.0	1.55	31.2 ± 0.5	61.2	36.5
M_y/GMA-50	0.42	84.2	94.6	89.4	21.9	1.45	13.3 ± 0.8	69.4	26.5
M_y/GMA-60	0.57	85.9	93.8	89.1	20.1	1.34	15.1 ± 0.4	64.9	29.6
M_y/GMA-70	0.67	74.2	91.3	79.3	18.4	1.26	11.4 ± 0.3	70.0	23.1
M_y/GMA-80	0.78	78.2	95.8	81.7	20.3	1.30	8.2 ± 0.2	74.3	18.2
M_y/GMA-90	0.89	79.3	96.7	81.0	21.1	1.35	9.1 ± 0.2	81.0	10.5
M_y/GMA-100^(g)	1	66.0	0	66.0	14.9	1.26	4.3 ± 0.7	80.3	9.3

a) Molar fraction of M_y in the copolymer (F_{M_y}) as determined by $^1\text{H NMR}$ (Figure S6b in Supporting Information for the spectral assignments).

b) Individual X_{M_y} and X_{GMA} determined by $^1\text{H NMR}$. Average $X = X_{M_y}/F_{M_y,0} + X_{GMA}/F_{GMA,0}$ (further details in the experimental section).

c) M_n and M_w determined by GPC calibrated with PS standards in THF at 40 °C.

d) $\langle k_p \rangle \langle K \rangle$ corresponding to the product of the average propagation rate constant $\langle k_p \rangle$ and the average equilibrium constant $\langle K \rangle$ derived from the slopes $\langle k_p \rangle [P^\bullet]$ ($[P^\bullet]$ = concentration of propagating macroradicals) taken from the semi-logarithmic kinetic plots of $\ln((1-X)^{-1})$ versus time in the linear region generally from 0 to 65 min (0 to 30 min for M_y /GMA-30, 0 to 15 min for M_y /GMA-20, 0 to 10 min for M_y /GMA-10, 0 to 120 min for M_y /GMA-100 ; squared linear regression coefficient = $R^2 \geq 0.98$ for every experiment). $\langle k_p \rangle \langle K \rangle$'s estimated from $\langle k_p \rangle [P^\bullet]$ and $r = [\text{SG1}]_0 / [\text{NHS-BB}]_0$ (Equation 5). Error bars derived from the standard errors in the slope from the linear fits of $\ln((1-X)^{-1})$ versus time.

e) Determined by $^1\text{H NMR}$. 3,4-content% = $100 - 1,4\text{-content}\% - 1,2\text{-content}\%$ (Figure S6b in Supporting Information for further details).

f) No kinetic study led due to the very early ``caking`` (high viscosity) of the reaction medium.

g) Results from M_y homopolymerization performed previously under the same experimental conditions.³⁵

the lack of irreversible termination reactions so that $[P^*]$ was nearly constant.²² As expected for the NMP process, the homolytic decomposition of NHS-BB alkoxyamine into the propagating alkyl radical and the persistent radical SG1 \cdot allowed the establishment of a dynamic equilibrium between a low concentration of active propagating chains and a predominant concentration of SG1-capped dormant chains. These latter are unable to propagate or terminate, allowing thus the controlled growth of the macro-radicals. The reversible trapping can thus be assumed effective for GMA/My copolymerizations. It should be noted that deviations from the linear trend can be observed at the last stages of copolymerization, mostly for experiments My/GMA-40, My/GMA-50 and My/GMA-60 (Figure 3a). A decrease in $[P^*]$, which might result from irreversible termination reactions increasing the concentration of the persistent radical, could lead to the downward curvature trend seen for these reactions. $\ln((1-X)^{-1})$ versus time plot in the linear region allows the determination of the apparent rate constant, which can be defined as the product of the average propagation rate constant $\langle k_p \rangle$ with the concentration of propagating macro-radicals $[P^*]$, $\langle k_p \rangle [P^*]$. The apparent rate constant can be related to the average equilibrium constant $\langle K \rangle$ as the product $\langle k_p \rangle \langle K \rangle$ by making some assumptions regarding the equilibrium between dormant and active chains. It should be noted that an average propagation rate constant and average equilibrium constant were used since a statistical copolymerization is studied, consisting of a diene and a methacrylate, which likely have very different individual equilibrium constants. The $\langle K \rangle$ is defined in terms of the $[P^*]$, the concentration of free nitroxide $[N^*]$ and the concentration of dormant alkoxyamine terminated species $[P-N]$, as shown in Equation 3.

$$\langle K \rangle = ([P^*][N^*]) / [P-N] \quad (3)$$

The overall polymerization rate can be defined by the rate of chain propagation which is given by Equation 4.

$$R_p = -d[M]/dt = \langle k_p \rangle [P^*][M] \quad (4)$$

By assuming that the initial concentration of nitroxide $[N]_0$ is high so that $[N] = [N]_0$ in the early stages of polymerization and that $[P-N]$ is approximately equal to the initial concentration of initiator ($[P-N] = [NHS-BB]_0$), the following equation 5 can be obtained from Equation 3 with $r = [N]_0/[NHS-BB]_0$ (initial molar concentration ratio of SG1 free nitroxide to NHS-BlocBuilder initiator):

$$\langle k_p \rangle \langle K \rangle \approx (\langle k_p \rangle [P^*][N^*]_0) / [NHS-BB]_0 = \langle k_p \rangle [P^*] r \quad (5)$$

The reported $\langle k_p \rangle \langle K \rangle$ in Table 3 were measured during the early stages of the copolymerization, at low or moderate final conversion ($X \leq 45.2\%$) except for experiments My/GMA-40 and My/GMA-10

where the final overall conversions were 67% and 57%, respectively. In our study, a stoichiometric amount of SG1 free nitroxide and radical initiator just after initiation could be hypothesized since no extra SG1 was added in the initial feed. In any case, a linear growth of M_n versus X was observed (Figure 3c), making Equation 5 applicable. As $f_{GMA,0}$ increased, the $\langle k_p \rangle \langle K \rangle$'s increased with $\langle k_p \rangle \langle K \rangle = (9.1 \pm 0.2) 10^{-5} \text{ s}^{-1}$ at $f_{GMA,0} = 0.10$ to $\langle k_p \rangle \langle K \rangle = (157.0 \pm 0.9) 10^{-5} \text{ s}^{-1}$ at $f_{GMA,0} = 0.90$ (Table 3). These kinetic values are not surprising since $k_p K$ of pure My under identical reaction conditions³⁵ was estimated at $(4.3 \pm 0.7) 10^{-5} \text{ s}^{-1}$ while $\langle k_p \rangle \langle K \rangle = (66 \pm 4) 10^{-5} \text{ s}^{-1}$ was measured for GMA/S copolymerization with $f_{GMA,0} = 0.94$ initiated by NHS-BB at 90 °C in 50 wt% 1,4-dioxane solution.³⁶ The presumable large difference in the k_p between My ($k_{p,I} \sim 10^2 \text{ L.mol}^{-1}.\text{s}^{-1}$ for isoprene, a structurally similar 1,3-diene)^{76,77} and GMA ($k_{p,GMA} \sim 10^3 \text{ L.mol}^{-1}.\text{s}^{-1}$)^{78,79}, as discussed above, can partly explain the $\langle k_p \rangle \langle K \rangle$ increase with $f_{GMA,0}$ even though the contribution of the two individual activation-deactivation equilibrium constants cannot be neglected. The higher $\langle k_p \rangle \langle K \rangle$ values determined when using methacrylate-richer initial feeds agrees with previous studies, reporting similar kinetic trends for the *tert*-butyl methacrylate/S copolymerization at 90 °C in bulk initiated by BlocBuilderTM,⁸⁰ the GMA/S copolymerization at 90 °C in 1,4-dioxane initiated by NHS-BB³⁶ and the MMA/S binary system initiated by BlocBuilderTM in bulk at 90 °C.⁶⁴

A well-controlled RDRP exhibits linear M_n versus X and low dispersity with monomodal distributions. The general increase in $\langle k_p \rangle \langle K \rangle$ as a function of increasing $f_{GMA,0}$ suggested the polymerizations were becoming less controlled. This was reflected in faster polymerization rates (Table 3) and higher \mathcal{D} as shown in Figure 3b. While relatively low dispersities ($\mathcal{D} \leq 1.38$) were measured for My -rich initial feed composition ($f_{GMA,0} \leq 0.29$), higher \mathcal{D} values mainly ranging from 1.25 to 1.50 were obtained for experiments My/GMA -40, My/GMA -50 and My/GMA -60 with $f_{GMA,0} = 0.40$ -0.60. This tendency was amplified for GMA-rich feeds with broader molecular weight distributions measured, with values typically between 1.35 and 1.55 (Figure 3b). Independently of the initial molar composition, similar \mathcal{D} versus X trends can be observed. Disregarding the first inaccurate \mathcal{D} values for $X < 10\%$ (likely underestimation of the dispersity due to the low intensity of the polymer peaks on the GPC chromatograms), \mathcal{D} was quite elevated at the commencement of the copolymerization ($X = 15$ -25%) but became gradually lower as the overall conversion increased ($X = 25$ -70%). It can be assumed that the dynamic equilibrium between the propagating macro-radicals and the dormant SG1-terminated species was not being established sufficiently at the early stages of the polymerization for the persistent radical effect to be present. At the last stages of the copolymerization ($X = 70$ -95%), a broadening of the molecular weight distribution was apparent for every My/GMA experiment, probably underscoring the greater prevalence of termination reactions, resulting in a loss of the SG1 functionality on the chain end. Since a solvent free process was applied, it may be hypothesized that many of the irreversible terminations occurring resulted from β -hydrogen transfer

(disproportionation) from propagating P(*My-stat*-GMA) radical to SG1^{52,67} or intramolecular chain transfer to polymer.⁶⁷

Figure 3c gives M_n versus X for the various experiments. It should be first noted that M_n values have to be carefully compared to the theoretical ones since all GPC measurements were performed using linear poly(styrene) standards, which might not be very accurate for P(*My-stat*-GMA) samples. A similar linear growth of degree of polymerization with overall conversion for every *My*/GMA copolymerization with $M_n = 18.4\text{-}21.9 \text{ kg}\cdot\text{mol}^{-1}$ at $X > 80\%$ can be seen (Figure 3c). This can be explained by the active feature of the macro-radical chain end for a prolonged period of time, presumably due to the relatively low average equilibrium constant $\langle K \rangle$ obtained when polymerizing GMA with *My*. M_n values started slightly plateauing at $X \sim 40\%$ and non-negligible deviations from the predicted line can be observed at the final

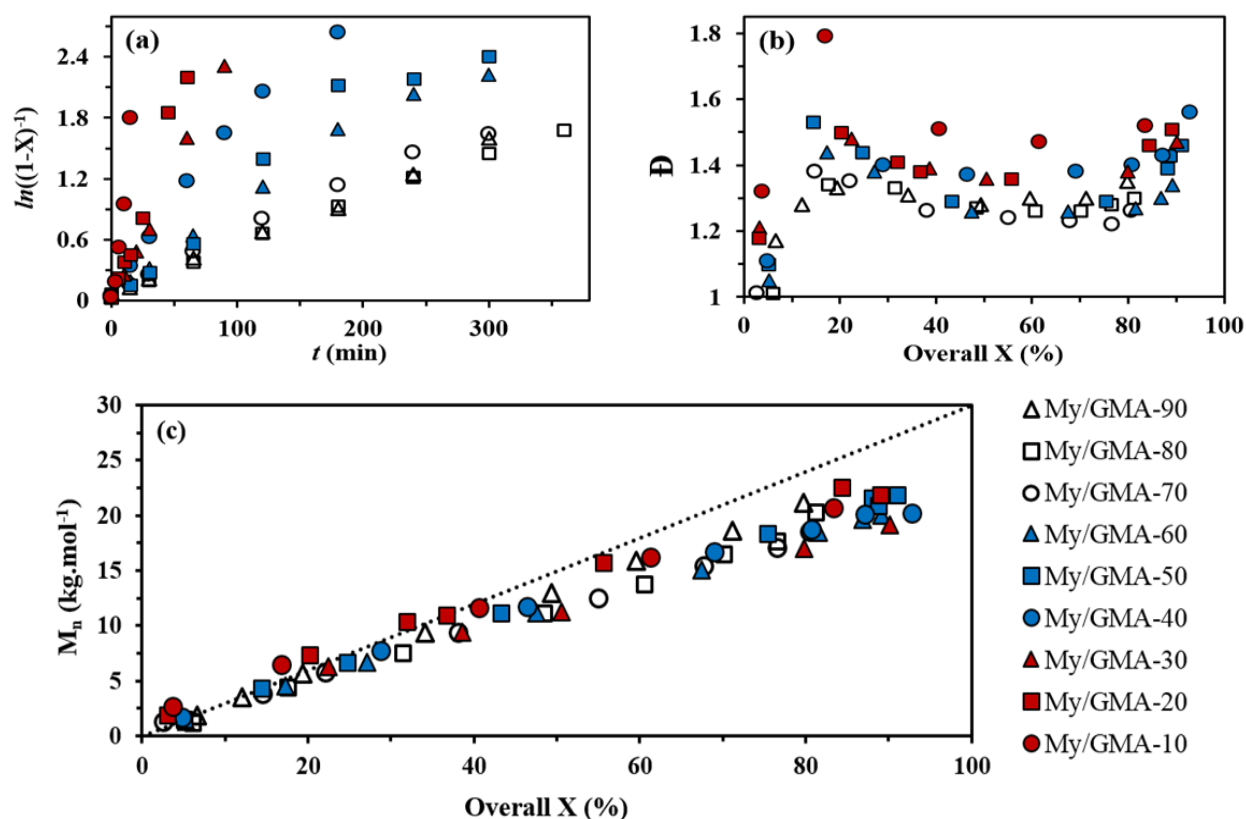


Figure 3. (a) Semi-logarithmic kinetic plots of $\ln((1-X)^{-1})$ (X = overall conversion) versus polymerization time t , (b) \bar{D} versus X and (c) M_n versus X for the various *My*/GMA copolymerizations in bulk at 120 °C initiated by NHS-BB. The dotted line indicates the theoretical M_n versus overall conversion based on the monomer to initiator ratio ($M_{n,theo} = 30 \text{ kg}\cdot\text{mol}^{-1}$ at $X = 100\%$ for every experiment). All experimental ID and characterization of experiments are listed in Table 2 and Table 3. The same legend at the bottom right of the figure is used for each of the three plots.

stages of the copolymerizations ($M_n/M_{n,theo} = 71-88\%$ at the end of the experiments, Table 3). It may be due to the occurrence of irreversible termination reactions, which were no longer retarded at $X > 40\%$.

The GPC traces for experiment *My*/GMA-50 exhibiting a nearly stoichiometric initial feed composition are shown in Figure 4. A monomodal shift of the GPC chromatograms can be observed with a slight tail at longer elution times, most likely resulting from irreversible termination reactions generating low M_n P(*My*-*stat*-GMA) chains. At $t = 15$ min, a minor population of longer chains was detectable at relatively short elution times (23-26 min, Figure 4). As discussed in a previous study reporting the NMP of *My*,³⁵ it may be caused by *My* auto-initiation,⁸¹ generating an excess of P^{*} and a fast auto-polymerization which makes the mediation by SG1 difficult. This second peak was easily detectable at the commencement of *My*-rich feed copolymerizations ($f_{My,0} = 0.60-0.90$) and hardly noticeable for experiments with higher $f_{GMA,0}$. This tends to confirm that this minor fraction of polymer consisted of high M_n P(*My*) chains resulting from *My* auto-polymerization.

Lastly, the influence of $f_{GMA,0}$ over the regioselectivity of *My* units in the final copolymer can be discussed (see Figure S6b in Supporting Information for the determination of 1,2-, 3,4- and 1,4-motif for experiment *My*/GMA-50). As already mentioned for *My*/*t*BuA system above, the molar fraction of 1,2-addition increased and that of 1,4-addition decreased with $f_{GMA,0}$ (and thus F_{GMA}). While *My* NMP produced P(*My*) exhibiting a large predominance of 1,4-content (~ 80 mol%) with a minor proportion of 1,2-units (< 10 mol%, experiment *My*/GMA-100, Table 3), the initial addition of 50 mol% of GMA resulted in P(*My*-*stat*-GMA) more than three times richer in 1,2-addition (28.5 mol%, experiment *My*/GMA-50, Table 3). For rich-GMA feeds ($f_{GMA,0} = 0.71-0.90$), the fraction of 1,2-content exhibited by the final copolymers was around 40 mol%. This change in regioselectivity for *My* units was likely due to the presence of GMA as a terminal or penultimate unit, which might bring about either steric hindrance or electronic effects.

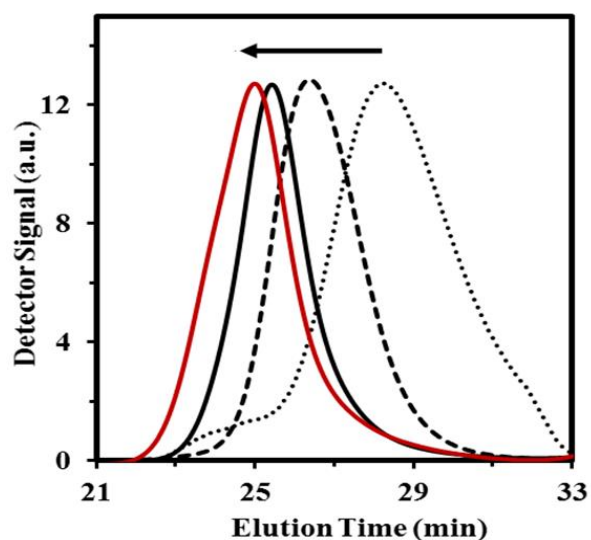


Figure 4. Normalized GPC traces of P(*My*-*stat*-GMA) with $f_{GMA,0} = 0.51$, initiated by NHS-BB at 120 °C in bulk targeting $M_{n,theo} = 30$ kg.mol⁻¹ at $X = 1$ (experiment *My*/GMA-50). Curves from right to left correspond respectively to the GPC chromatograms of samples taken at 15, 65, 120 and 300 min.

■ Active feature of *My*-rich and GMA-rich P(*My-stat*-GMA) copolymers.

A paramount feature of a NMP-based polymer is its ability to form a block copolymer via the re-activation of the dormant chains capped by the nitroxide group. Two extra statistical P(*My-stat*-GMA) copolymers were synthesized under the same previous experimental conditions (*My*/GMA-37 with $F_{My,1} = 0.37$ and *My*/GMA-78 with $F_{My,1} = 0.78$, Table 4A) in order to deem their degree of the active groups, in other words, the fraction of SG1-terminated P(*My-stat*-GMA) chains. Several strategies can be adopted to demonstrate whether a SG1-mediated (co)polymer is significantly active enough to re-initiate a second block.

Phosphorus nuclear magnetic resonance (^{31}P NMR) was first used to probe the chain end fidelity of the synthesized *My*/GMA copolymers. This quantitative approach allows to determine the living chain fraction (LF) by detecting the phosphorus-containing SG1 nitroxide end group with diethyl phosphite as an internal reference (see Experimental Section for further details).⁴² LF values for *My*-rich (*My*/GMA-78) and GMA-rich (*My*/GMA-37) macroinitiators were $82 \pm 5 \%$ and $71 \pm 7 \%$, respectively (Table 4A, standard deviation derived from the difference in macroinitiator M_n value obtained from PS calibration and PMMA calibration, ^{31}P spectra in Supporting Information, Figures S7b and S8b), indicating a satisfactory retention of the SG1 fragment. The lower ``living`` fraction exhibited by *My*/GMA-37 can be mainly attributed to the relatively high $\langle k_p \rangle / \langle K \rangle$ value ($\sim 40 \cdot 10^{-5} \text{ s}^{-1}$ for *My*/GMA-30 with $f_{GMA,0} = 0.70$, Table 3) and thus the more difficult mediation of the binary system, as witnessed by the broader molecular weight distribution ($D_1 = 1.39$), compared to *My*-rich NMP. Generally, these spectroscopic results are a clear indication of the active character of NMP-based P(*My-stat*-GMA) copolymers, which may allow efficient chain-extension to produce well-defined block copolymers.

To confirm the ^{31}P NMR quantitative analysis, *My*/GMA-78 and *My*/GMA-37 were used as macroinitiators in the polymerization of *My*, GMA and styrene (S) in 50 wt% toluene solution at $T = 110\text{--}120 \text{ }^\circ\text{C}$ (Table 4B). For every experiment, a high $M_{n,theo}$ was targeted ($80\text{--}85 \text{ kg}\cdot\text{mol}^{-1}$) to ensure a clear shift of the GPC peak. The final characterization of the chain-extended products is given in Table 4C.

Regarding *My*-rich macroinitiator *My*/GMA-78, a clean chain-extension with S was performed (experiment *My*/GMA-78-S) with a significant increase of M_n from 11.3 to $28.4 \text{ kg}\cdot\text{mol}^{-1}$ and D remaining low (< 1.40 , Table 4C). The monomodal nature of P[(*My-stat*-GMA)-*b*-S] was confirmed by GPC as indicated in Figure 5a'. Furthermore, the GMA chain-extension from the same *My*/GMA-78 macroinitiator was attempted in order to deem the crossover efficiency. It has to be noted that around 10 mol% of *My* with respect to GMA was initially added (Table 4B). Indeed, NMP of GMA with 10 mol% of *My* (experiment *My*/GMA-10, Table 2) allowed to slow down the reaction with a pseudo-control of the polymerization ($D \leq 1.52$ at $X > 20\%$, $M_n/M_{n,theo} > 80\%$ for every sample, Figures 3b and 3c) compared to the GMA

Table 4. Chain-extensions of **A)** *My*-rich and GMA-rich P(*My-stat*-GMA) macroinitiators (MI) with **B)** *My*, GMA and S monomers in 50 wt% toluene and **C)** molecular characterization of the resulting chain-extended products.

A. Macroinitiator ^(a)								
ID	$f_{My,0}$	$F_{My,1}$	LF ^(b) (%)	X_1 (%)	$M_{n,1}$ (kg.mol ⁻¹)	$M_{n,theo,X1}$ ^(c) (kg.mol ⁻¹)	\bar{D}_1	
<i>My</i> /GMA-37	0.30	0.37	71 ± 7	32.9	8.6	9.9	1.39	
<i>My</i> /GMA-78	0.80	0.78	82 ± 5	51.7	11.3	15.5	1.27	
B. Formulation of chain-extension								
ID	[MI] ₀ (M)	[<i>My</i>] ₀ (M)	[GMA] ₀ (M)	[S] ₀ (M)	[Toluene] ₀ (M)	$M_{n,theo}$ ^(d) (kg.mol ⁻¹)	T (°C)	<i>t</i> (min)
<i>My</i> /GMA-37- <i>My</i>	0.005	2.741	0	0	4.536	81.9	120	260
<i>My</i> /GMA-37-S	0.005	0	0	3.827	4.807	82.9	110	90
<i>My</i> /GMA-78-GMA/ <i>My</i>	0.005	0.259	2.612	0	5.081	85.6	110	60
<i>My</i> /GMA-78-S	0.006	0	0	3.660	4.813	80.5	110	100
C. Chain-extended copolymer ^(c)								
ID	X_2 (%)	$F_{My,2}$	$F_{S,2}$	$M_{n,2}$ (kg.mol ⁻¹)	$M_{n,theo,X2}$ ^(e) (kg.mol ⁻¹)	\bar{D}_2		
<i>My</i> /GMA-37- <i>My</i>	45.3	0.84	0	29.2	41.8	1.85		
<i>My</i> /GMA-37-S	37.1	0.06	0.81	35.4	36.2	1.46		
<i>My</i> /GMA-78-GMA/ <i>My</i>	30.8	0.35	0	29.1	34.2	1.50		
<i>My</i> /GMA-78-S	26.9	0.24	0.70	28.4	29.9	1.36		

a) The indexes “1” and “2” refer respectively to the final features of the P(*My-stat*-GMA) macroinitiator (MI) and the whole chain-extended diblock copolymer (macroinitiator + P(*My*), P(GMA) or PS segment added).

b) Living molar fraction of MI chains terminated by a SG1 unit, measured by ³¹P NMR (Figures S7b and S8b in Supporting Information).

c) Predicted $M_{n,1}$ at X_1 measured experimentally and calculated as follows: $M_{n,theo,X1} = (X_1/100)M_{n,theo,1}$ with $M_{n,theo,1} = 30$ kg.mol⁻¹ at $X = 100\%$.

d) Targeted number-average molecular weight of the whole chain-extended diblock copolymer (MI block + extended block) at $X = 100\%$.

e) Predicted $M_{n,2}$ of the whole chain-extended diblock copolymer (MI block + second block added) at X_2 measured experimentally and calculated as follows: $M_{n,theo,X2} = (X_2/100)(M_{n,theo} - M_{n,1}) + M_{n,1}$ (= Predicted M_n of the second block added at X_2 + experimental M_n of MI).

homopolymerization by NMP ineffectively controlled by the SG1 free nitroxide. This observation echoes the comprehensive work done by Benoit *et al.*, reporting the well-controlled bulk NMP of *tert*-butyl acrylate

and glycidyl methacrylate monomers at 120 °C in the presence of 10-20 mol% of isoprene and initiated by 2,2,5-trimethyl-3-(1'-phenylethoxy)-4-phenyl-3-azahexane.⁵⁴ This may suggest that the addition of a small amount of isoprene or β -myrcene could improve the NMP control for certain methacrylate and acrylate monomers, presumably by reducing the average equilibrium constant of the system. Table 4C shows the final features of the chain-extended polymer (experiment *My*/GMA-78-GMA/*My*) and the GPC traces in the course of the chain-extension are given in Figure 5a. Despite a slight broadening of the molecular weight distribution (\mathcal{D} from 1.27 to 1.50), the chain-extension was successful with a monomodal shift of the GPC chromatograms and the addition of a GMA-rich second block exhibiting about 18 kg.mol⁻¹. While the macroinitiator was poor in GMA ($F_{\text{GMA},1} = 0.22$), the chain-extension allowed to drastically alter the composition since the final diblock copolymer exhibited $F_{\text{GMA},2} = 0.65$ (Table 4C), as determined by ¹H NMR.

In order to deem the influence of the composition of the *My*/GMA statistical copolymer over its ability to re-initiate cleanly a second batch of monomer, a GMA-rich P(*My-stat*-GMA) (*My*/GMA-37, $F_{\text{GMA},1} = 0.63$, Table 4A) was used as a macroinitiator in the polymerization of *My* and S as described in Table 4B. For both experiments, a complete shift of the GPC peak (Figures 5b and 5b') corresponding to the addition of a P(*My*) segment exhibiting around 21 kg.mol⁻¹ (experiment *My*/GMA-37-*My*) and the addition of a PS segment with $M_n \sim 27$ kg.mol⁻¹ (experiment *My*/GMA-37-S, Table 4C) showed the effective synthesis of the diblock copolymer. The ¹H NMR spectrum of the final *My*/GMA-37-S diblock copolymer is given in Supporting Information, Figure S9b, illustrating the ternary composition of the chain-extended product synthesized. While a well-defined P[(*My-stat*-GMA)-*b*-S] was achieved ($\mathcal{D}_2 = 1.46$, $M_{n,2}/M_{n,theo,X2} \sim 98\%$, Table 4C), *My* chain-extension from *My*/GMA-37 was not as well controlled, as seen by the broader molecular weight distribution ($\mathcal{D}_2 = 1.85$) and the greater M_n deviation from the predicted one ($\sim 70\%$). This marked loss of control may be explained by the more elevated temperature used ($T = 120$ °C to perform a faster *My* polymerization)³⁵ as well as the higher conversion reached ($X_2 = 45.3\%$). Another reason can also be mentioned. The polymerization was run for a relatively long period of time ($t = 260$ min) under a mild toluene reflux. A slight but gradual evaporation of the toluene was apparent during the experiment which, along with the consumption of *My*, made the reaction medium more and more viscous. A non-negligible influence of the viscosity, increasing with polymerization time, over the loss of control of the chain-extension can thereby be hypothesized. Moreover, the GPC samples at $t = 90$ min and 200 min (not included herein) exhibited $M_n = 19.8$ kg.mol⁻¹, $\mathcal{D} = 1.40$ and $M_n = 25.9$ kg.mol⁻¹, $\mathcal{D} = 1.51$ respectively, which demonstrates that the loss of control predominantly occurred during the last hour of the reaction. Generally, at the end of every chain-extension experiment, no major shoulder on the low molar mass side was detected, which indicates a low fraction of unreacted macroinitiator. However, a slight tail can be observed for long elution times (25-29 min) most likely resulting from irreversible terminations.

This study allowed to assess the presence of an alkoxyamine chain end for SG1 NMP-based P(*My-stat-GMA*) copolymers by ^{31}P NMR and chain-extensions. Regardless of their composition, P(*My-stat-GMA*) can thus be used as efficient macroinitiators in order to form versatile and well-defined diblock copolymers.

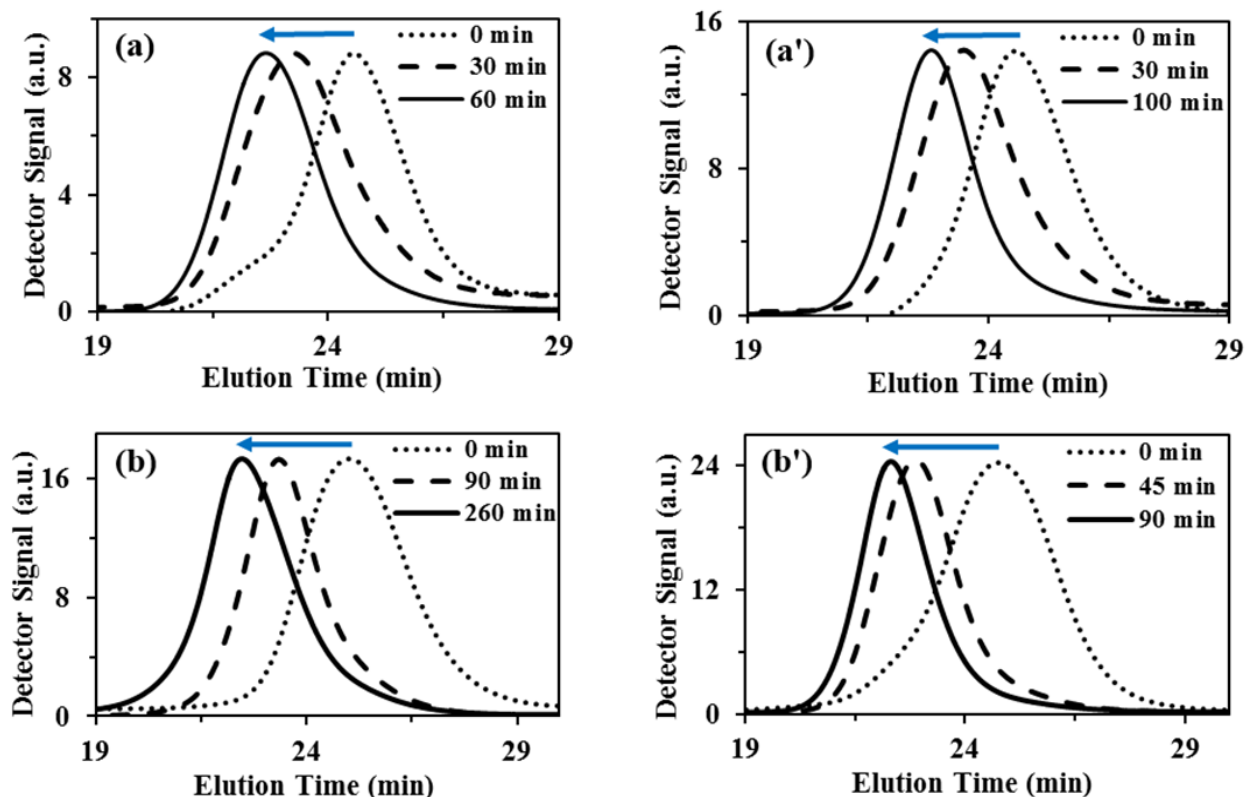


Figure 5. Normalized GPC traces for the chain-extensions of *My/GMA-78* with (a) GMA with 10 mol% of *My* (experiment *My/GMA-78-GMA/My*) and (a') S (experiment *My/GMA-78-S*) and for the chain-extensions of *My/GMA-37* with (b) *My* (experiment *My/GMA-37-My*) and (b') S (experiment *My/GMA-37-S*).

■ Glass transition behavior of *My/GMA* copolymers.

Glass transition temperatures (T_{gs}) were measured for the final P(*My-stat-GMA*) statistical copolymers exhibiting $F_{GMA} = 0.11-0.95$ (Table 3), by means of differential scanning calorimetry (see

Experimental Section for further details, All the DSC traces are given in Supporting Information, Figure S10b). T_g is plotted as a function of F_{GMA} in Figure 6. Each of the statistical copolymers showed a single T_g , which provided a concave glass transition temperature-composition curve. $T_{g,P(My)} = -77.0\text{ }^\circ\text{C}^{35}$ and $T_{g,P(GMA)} = +85.0\text{ }^\circ\text{C}^{82}$ corresponding to the T_g of P(My) and P(GMA) homopolymers have also been added in Figure 6 to serve as brackets for the copolymer T_g s. As expected, the concave trend reported indicates the non-ideal mixing of My and GMA, with the specific volume for P(My-stat-GMA) being larger than that for ideal mixing. This is likely due to the presence of the pendant flexible C6/C8 groups borne by the My units along the copolymer chain, which may alter the free volume. As it can be seen in Figure 6 for $F_{GMA} \geq 0.66$, the presence of a small fraction of My units in the chain reduced considerably P(My-stat-GMA)'s T_g , likely due to the plasticizing nature of P(My). A similar trend was observed with regards to NMP-based P(My-stat-S) copolymers.³⁵ Several theoretical and empirical approaches have been proposed for estimating the T_g of mixtures and random copolymers from knowledge of the properties of the pure components.⁸³⁻⁸⁶ Although different in detail, the proposed relationships are all based on the additivity of basic thermophysical properties. For the My/GMA system studied, they can be expressed by the Wood equation as given below (Equation 6):⁸⁶

$$W_{My} (T_g - T_{g,My}) + KW_{GMA} (T_g - T_{g,GMA}) = 0 \quad (6)$$

where T_g corresponds to the theoretical glass transition temperature of the copolymer containing the weight fractions W_{My} and W_{GMA} of the two monomers. The Fox relationship is obtained when the parameter $K = T_{g,My} / T_{g,GMA}$.⁸⁴ Interestingly, the Fox equation does not predict well the T_g versus composition relationship for the statistical My/GMA copolymers, as shown in Figure 6 (black dotted line) by the overestimation of the copolymer T_g s (+19.4 °C on average) when using this simple bulk additive approach. Alternatively, the Gordon-Taylor equation was used, relying still on Equation 6 but with $K = \Delta\beta_{GMA} / \Delta\beta_{My}$ where $\Delta\beta_{GMA}$ or $\Delta\beta_{My}$ is the difference between the expansion coefficients of the rubbery and glassy states of P(GMA) or P(My).⁸³ $K = 0.186 \pm 0.036$ was estimated via the use of a non-linear least-squares fitting of the data and the Gordon-Taylor fit is given in Figure 6 (blue dashed line). $K \ll 1$ indicates that the volume expansion coefficient for GMA in the rubbery phase is significantly lower than that of My, according to the Gordon-Taylor approach. This appears very consistent since, above the glass transition temperature, it can be assumed that the expansivity of My is much greater than that of GMA, notably due its long pendant side group. On the other hand, stronger intermolecular forces are generated by GMA units, which might reduce its expansivity. To the best of our knowledge, the coefficients of thermal expansions (CTEs) for P(My) and P(GMA) are not available, limiting thus the discussion. However, it is useful to compare the results obtained via the Gordon-Taylor method for My/GMA to another system such as I/MMA. The CTE for the

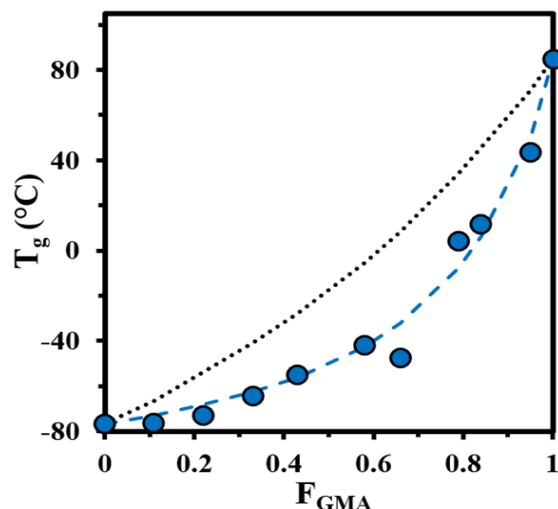


Figure 6. F_{GMA} effects on T_g in P(*My-stat-GMA*)s (solid blue circles, DSC traces given in the Supporting Information, Figure S10b). The Fox equation predictions represented by the black dotted line while the blue dashed line represents the experimental data fitted to the Gordon-Taylor equation.

unvulcanized natural rubber (*cis*-1,4-poly(isoprene)) in the rubbery state ($T = 0\text{-}20$ °C) was estimated to be $6.6 \cdot 10^{-4} \text{ K}^{-1}$ whereas the simulated value of its CTE in the glassy state was lower, $2.0 \cdot 10^{-4} \text{ K}^{-1}$ at $T = -73$ °C.^{87,88} Furthermore, the CTEs of atactic PMMA ($T_g \sim 105$ °C) in the rubbery state and in the glassy state are respectively $6.1 \cdot 10^{-4} \text{ K}^{-1}$ ($T = 160$ °C) and $1.8 \cdot 10^{-4} \text{ K}^{-1}$ ($T = 40$ °C).⁸⁷ Consequently, $K = \Delta\beta_{MMA} / \Delta\beta_I = 0.93$ can be estimated for MMA/I system, indicating in that case a similar expansivity of both units in the rubbery phase. For MMA/I pair, K is much closer to 1, showing a reduced expansivity of I units compared to *My* units in P(*My-stat-GMA* copolymers). This may be partly caused by the short methyl side groups borne by PI segments (100 mol% *cis*-1,4 motif) compared to the relatively longer C6/C8 pendant groups of P(*My*) segments (47-80 mol% 1,4-motif, stereoselectivity not determined).

The T_g values of the diblock copolymers synthesized via chain-extensions were explored as well. The DSC traces for P(*My-stat-GMA*) macroinitiators and the resulting chain-extended products are given in Figure 7. While *My*-rich macroinitiator *My/GMA-78* exhibited a single $T_g = -63.6$ °C relatively close to that of P(*My*) as predicted by Figure 6, two distinct T_g s were exhibited by the diblock copolymers *My/GMA-78-GMA/My* (-52.7 and $+15.8$ °C) and *My/GMA-78-S* (-27.1 and $+61.4$ °C). Such a thermal behavior is typical of the presence of two heterogeneous phases, highlighting herein the high degree of chemical incompatibility between *My/GMA-78* block and the chain-extended block. Interestingly, the lower T_g of these diblock copolymers (-52.7 and -27.1 °C) does not correspond exactly to that of the parent macroinitiator (-63.6 °C). This is particularly marked with *My/GMA-78-S* having a subzero T_g significantly

higher than that of *My*/GMA-78, which may reflect the partial mixing of the two segments. Likewise, the above-zero T_g s of *My*/GMA-78-GMA/*My* (+ 15.8 °C) and PS (~ 96 °C for $M_n \sim 17 \text{ kg.mol}^{-1}$) supported the possible partial miscibility between the soft and the hard blocks.⁸⁹

On the contrary, the two T_g s of the diblock *My*/GMA-37-*My* (- 78.1 °C and - 7.3 °C, Figure 7a) corresponded almost to those of the P(*My*) homopolymer (- 77 °C) and the initial *My*/GMA-37 macroinitiator (- 12.0 °C, Figure 7a).³⁵ Accordingly, a stronger incompatibility between the two blocks may be apparent, bringing about a much more distinct two-phase microstructure. This could result from the long hydrocarbon pendant groups of *My* units, increasing significantly the free volume and the steric hindrance around P(*My*) chains and thus reinforcing the heterogeneity of the two-phase system. Regarding *My*/GMA-37-S, only the upper T_g was observed at + 67.5 °C (Figure 7a). The disappearance of the parent macroinitiator T_g can be due to the large difference in M_n between the two blocks (8.6 and 26.8 kg.mol^{-1} for *My*/GMA-37 and PS respectively, Table 4) combined with the relatively short average chain length of *My*/GMA-37.

Generally, these DSC measurements suggest the possible microphase separation of the synthesized diblocks. In such instance, the use of a homopolymer as macroinitiator instead of a statistical copolymer and blocks exhibiting a higher degree of polymerization should favor a neater separation of the phases. The Flory-Huggins interaction parameter χ measuring the differences in the strength of pairwise interaction energies between species can be estimated for the *My*/GMA system using Equation 7 (Hildebrand and Scott method):^{90,91}

$$\chi_{My-GMA} = V_{m,GMA} (\delta_{My} - \delta_{GMA})^2 / RT \quad (7)$$

where $V_{m,GMA}$ is the molar volume of GMA ($136.4 \text{ cm}^3.\text{mol}^{-1}$) considered as the ``solvent`` (lower molecular weight), δ_{My} and δ_{GMA} are the solubility parameters of *My* and GMA respectively and R corresponds to the ideal gas constant ($8.314 \text{ J.mol}^{-1}.\text{K}^{-1}$). $\delta_{My} = 16.2 \text{ MPa}^{1/2}$ and $\delta_{GMA} = 19.3 \text{ MPa}^{1/2}$ were calculated, using the reported Hansen solubility parameters for *My* and GMA, which gives $\chi_{My-GMA} = 0.50$ at $T = 25 \text{ °C}$ (see Supporting Information for the calculations).^{92,93} In order to estimate the miscibility between the P(*My*) and P(GMA) blocks, a mixture of 1 g of P(*My*) and 1 g of P(GMA) with $M_{n,P(My)} = M_{n,P(GMA)} = 15 \text{ kg.mol}^{-1}$ can be arbitrarily considered as a basis. The Gibbs free energy of mixing ΔG_m for this binary P(*My*)/P(GMA) polymer mixture can be estimated using the equation developed by Flory and Huggins as given in Equation 8:⁹⁴

$$\Delta G_M = kT [(V/V_r) v_{P(GMA)} v_{P(My)} \chi_{My-GMA} (1-2/z) + N_c (v_{P(GMA)} \ln(v_{P(GMA)}) + v_{P(My)} \ln(v_{P(My)}))] \quad (8)$$

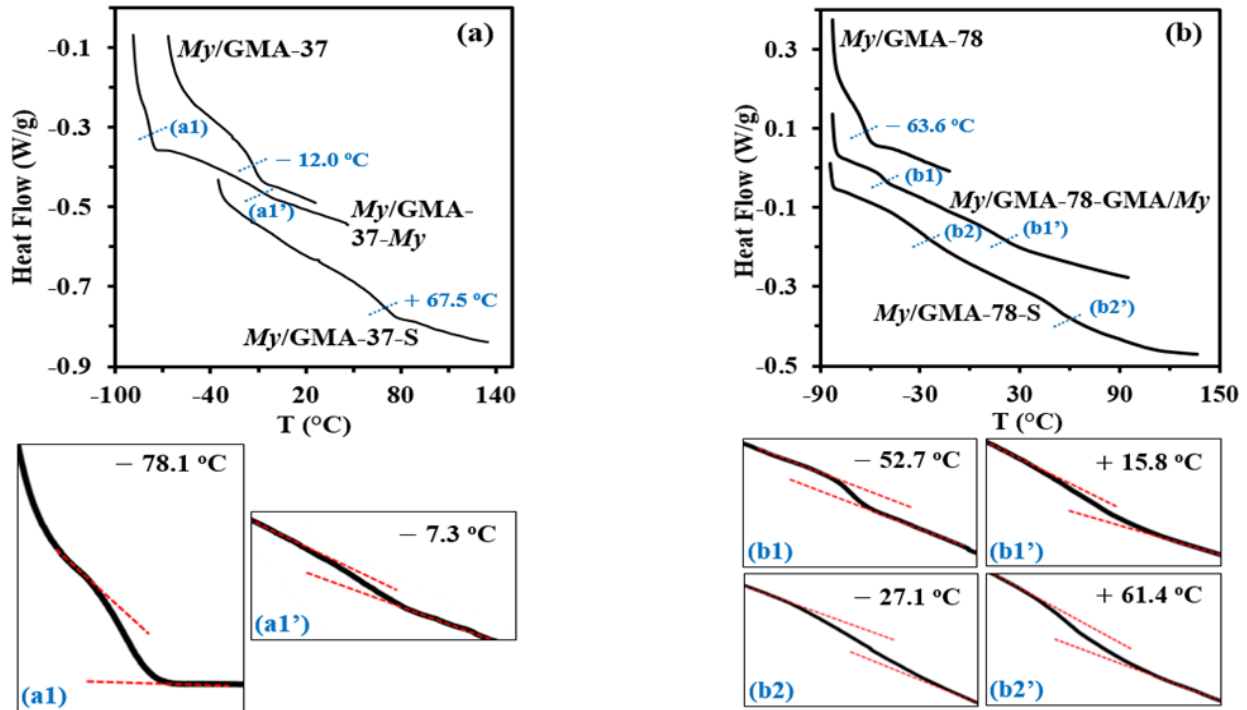


Figure 7. DSC traces of (a) *My/GMA-37*, *My/GMA-37-My* and *My/GMA-37-S* and (b) *My/GMA-78*, *My/GMA-78-GMA/My* and *My/GMA-78-S* diblock copolymers (dashed blue lines indicating the changes in slope observed; magnifications with T_g values given below for the changes in slope harder to observe, as indicated by the blue indexes in brackets).

where k is the Boltzmann's constant, V is the total volume of the mixture, V_r is the molar of a specific segment, v_i is the volume fraction of polymer ' i ', z is the lattice coordination number (usually between 6 and 12) and N_c is the number of chains per volume unit. $\Delta G_M(25\text{ °C}, z = 6) = 2.52\text{ J}$ was calculated when assuming that the number of lattice sites per chain is 6 (usually chosen for estimating polymer mixture miscibility).⁹⁵ Consequently, $\Delta G_M(25\text{ °C}, z = 6) > 0$ indicates that $P(My)/P(GMA)$ system with $M_{n,P(My)} = M_{n,P(GMA)} = 15\text{ kg.mol}^{-1}$ is not miscible at $T = 25\text{ °C}$, according to the Flory-Huggins theory. The upper limiting $M_{n,lim}$ number-average molecular weight value allowing the $P(My)/P(GMA)$ system to be miscible at $T = 25\text{ °C}$ can be calculated for $\Delta G_M(25\text{ °C}, z = 6) = 0$ as well. $M_{n,lim} \sim 1.2\text{ kg.mol}^{-1}$ was estimated, indicating that a homogeneous mixture of 1 g of $P(My)$ and 1 g of $P(GMA)$ with $M_{n,P(My)} = M_{n,P(GMA)} \leq 1.2\text{ kg.mol}^{-1}$ could be achieved at room temperature (see Supporting Information for the calculations). Even though this Flory-Huggins thermodynamic model does not account for a change of volume upon mixing to name but one limitation, it supports theoretically the possible phase separation of *My/GMA* diblock

copolymer. Obviously, direct experimental characterization using techniques such as transmission electron microscopy (TEM) or small-angle X-ray scattering (SAXS) should be done to unequivocally demonstrate whether a microphase separation is apparent. Regardless, in the context of the present study, the nature of the polymerization process (using statistical copolymer segments) influenced the thermal properties, not surprisingly showing some diffuse interfacial effects on the miscibility of the block copolymer segments.

2.4.3. Poly(β -myrcene-*block*-2-hydroxy-3-morpholinopropyl methacrylate) amphiphilic diblock copolymer

The well-controlled nitroxide-mediated copolymerization of *My* and GMA in bulk initiated by NHS-BB allowed the synthesis of epoxide functionalized *My*-based polymers. Once the polymer is produced, different chemical transformations of the epoxy groups can be performed to obtain a series of polymers with varied properties. In this study, we tried to synthesize an amphiphilic diblock copolymer in a three-step process: (1) NMP of *My*; (2) GMA chain-extension from NMP-based P(*My*) macroinitiator; (3) Post-polymerization treatment using morpholine to yield poly(β -myrcene-*block*-2-hydroxy-3-morpholinopropyl methacrylate) P(*My-b-HMPMA*) diblock copolymer. Morpholine as a nucleophilic reagent was selected relying on the conclusive results reported by Benaglia *et al.* demonstrating a complete conversion of the P(GMA) epoxy groups via a 10-fold amount of morpholine in DMSO at 80 °C.⁹⁶ The synthesis route is shown in Figure 8.

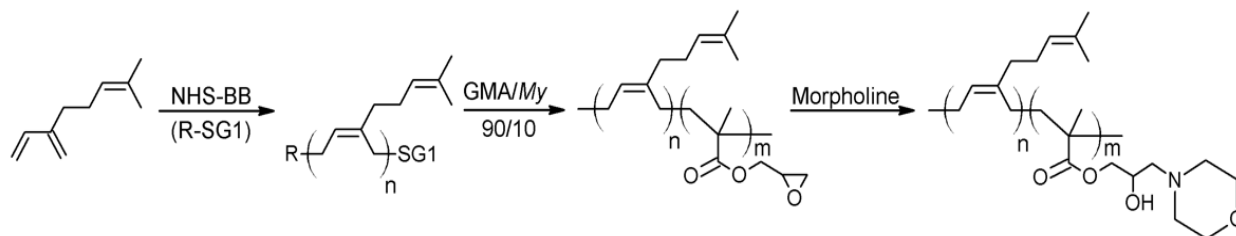


Figure 8. Synthetic route for P(*My-b-HMPMA*) diblock copolymer.

Firstly, NHS-BB-mediated P(*My*) exhibiting $M_n = 14.4 \text{ kg}\cdot\text{mol}^{-1}$ and $\text{Đ} = 1.51$ was synthesized in bulk at 120 °C after 6 h of polymerization. The chain-extension of this NMP-based polyterpene with 90 mol% of GMA and 10 mol% of *My* was then performed for 50 min at 110 °C in 50 wt% of toluene. The

resulting P(*My*-*b*-GMA) diblock copolymer had $M_n = 23.8 \text{ kg}\cdot\text{mol}^{-1}$, $\bar{D} = 1.89$ and $F_{My} = 0.58$ (^1H NMR spectrum in Figure 9a) and the epoxy groups, inert towards the previous polymerization process, were lastly treated with a 6-fold amount of morpholine in refluxing Me-THF for 3 h at 77 °C (complete experimental conditions and results for each step summed up in Supporting Information, Table S2b), relying on the comprehensive study led by Benaglia and coworkers.⁹⁶ This ring-opening reaction of the pendant epoxides proceeded quantitatively as shown by the ^1H NMR spectrum of the resulting P(*My*-*b*-HMPMA) diblock copolymer in Figure 9b. The final P(*My*-*b*-HMPMA) exhibited $M_n = 26.5 \text{ kg}\cdot\text{mol}^{-1}$, $\bar{D} = 1.91$, $F_{My} = 0.55$ and a monomodal distribution of the GPC trace (Supporting Information, Figure S11b). The slight increase of M_n after the treatment with morpholine may be explained by the occurrence of branching reactions, as reported previously.⁹⁶ It should be added that the hydrophilicity of the P(*My*) first segment may have been slightly increased due to the possible reaction of morpholine with the succinimidyl ester end-group (initiating group of NHS-BB alkoxyamine) of the diblock.

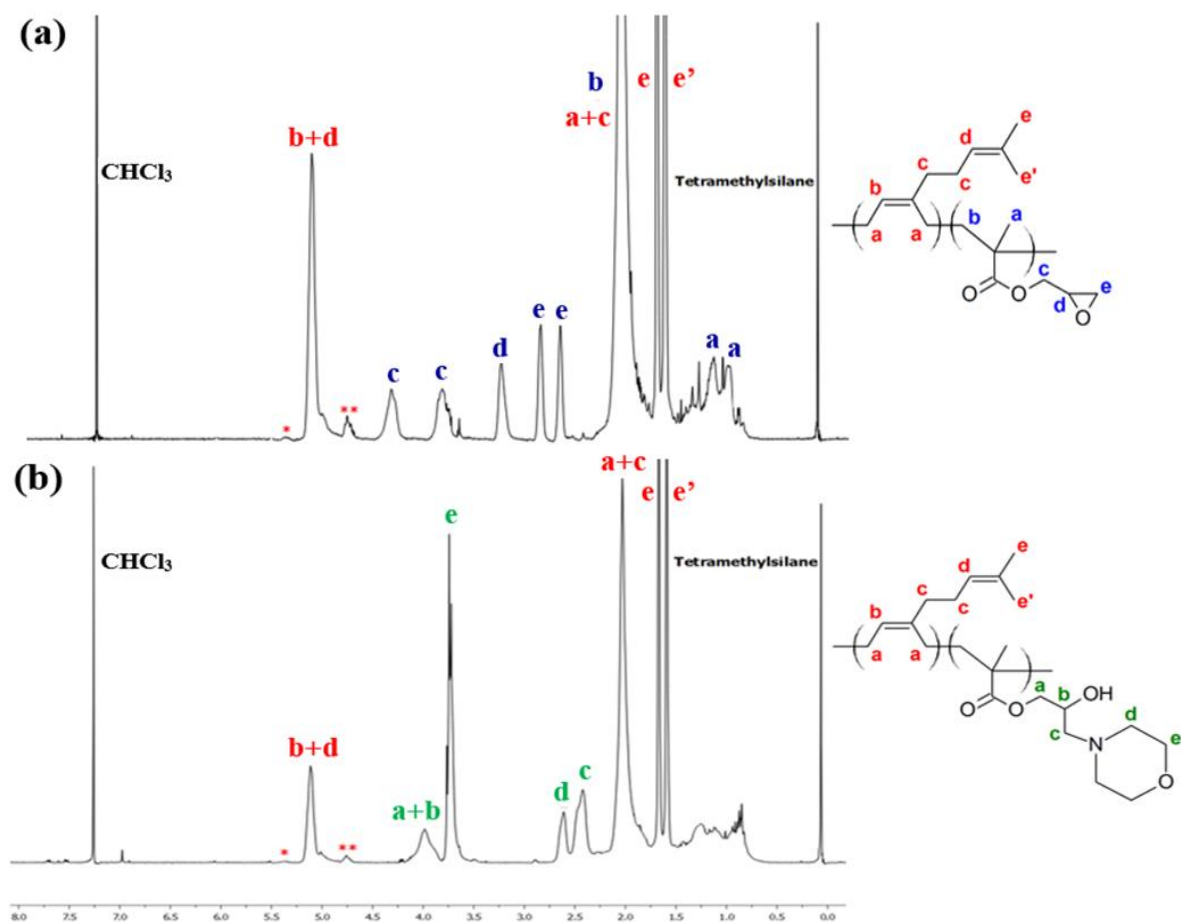


Figure 9. ^1H NMR spectra of (a) dry P(*My*-*b*-GMA) diblock copolymer and (b) dry P(*My*-*b*-HMPMA).

The assignments * and ** refer to olefinic and vinyl protons of 1,2- and 3,4-P(*My*) contents.

The behavior of this morpholine derivatized P(*My-b*-HMPMA) in water was then explored by dynamic light scattering (DLS) to determine if this diblock copolymer is able to self-assemble under specific conditions (Supporting Information, Figure S12b). The polymer was first dissolved in a minimum amount of THF, which is a good solvent for both P(*My*) and P(GMA) segments, and then added in a water solution (purified by reverse osmosis), followed by intense dispersion. The suspension was heated at 50 °C for 30 min and the THF was then eliminated by dialysis. A homogeneous clear aqueous solution was obtained. Regarding the samples used, two parameters were changed, [P(*My-b*-HMPMA)] = 0.4-1.4 mg.ml⁻¹ and the duration of the stirring (three days to ten days), as indicated in Table 5. Furthermore, the DLS measurements were carried out for every sample at three different temperatures, T_{DLS} = 25, 45 and 65 °C. It should be first noted that a monomodal distribution was observed for every sample, with a DLS polydispersity index relatively high for experiments conducted at room temperature (PDI = 0.24 on average at T = 25 °C) and more satisfactory at T = 45-65 °C (PDI = 0.10 on average). The relatively low PDI values make the Z-average size reliable and was reported in this study. Regardless of the preparation of the samples, as T_{DLS} increased from 25 to 45 °C, a marked drop of the Z-average diameter (Z_{ave}) was noticeable (105 nm drop on average). However, increasing T_{DLS} from 45 to 65 °C did not result in a further Z_{ave} decrease. The set of experiments III (Table 5) can be taken as an example. While large aggregates were detected at room temperature (> 300 nm), a second population of aggregates exhibiting a smaller hydrodynamic diameter (~ 130 nm) was obtained at 45 °C and 65 °C. Accordingly, a critical temperature (T_{cri}) between 25 and 45 °C might favor the formation of micelles exhibiting a lower hydrodynamic diameter. It was well-reported that the behavior of a polymeric micellar system toward temperature mostly depend on the nature of the hydrophilic block.⁹⁷ For P(*My-b*-HMPMA) diblock copolymer, the decrease of Z_{ave} at T ≥ 45 °C may be explained by the much lower salvation of the P(GMA) segments in the corona of the micelles. Four different preparations were performed before measuring the DLS samples, from a relatively high concentration (1.4 mg.ml⁻¹) with a short period of stirring (3 days, I, Table 5) to a low concentration (0.4 mg.ml⁻¹) combined with a long period of stirring (10 days, IV, Table 5). The influence of the concentration over Z_{ave} can be assessed by comparing the DLS results between the first (I) and the second (II) preparation, where samples were stirred for 3 days. Regardless of T_{DLS}, a clear decrease of Z_{ave} was effective when reducing [P(*My-b*-HMPMA)] from 1.4 to 1.0 mg.ml⁻¹. Generally, as the time of stirring increased and the concentration of the copolymer decreased, a clear reduction of Z_{ave} was observed. The aggregations of the micelles limited by reducing [P(*My-b*-HMPMA)] and/or stirring rigorously for 6 days or more. It can be assumed that stirring allowed to homogeneously disperse the particles in the water solution whereas a lower [P(*My-b*-HMPMA)] diminished statistically the formation of large aggregates.

Even though other experimental conditions could be used to characterize the self-assembly of P(*My-b*-HMPMA) exhibiting M_n = 26.5 kg.mol⁻¹ and F_{My} = 0.55, the study led herein suggests that micelles

having $Z_{\text{ave}} = 120\text{-}130$ nm can be formed in water at $T = 45\text{-}65$ °C and $[P(\text{My-}b\text{-HMPMA})] \leq 0.7$ mg.ml⁻¹, after a few days of stirring. It could also be argued that $Z_{\text{ave}} \geq 120$ nm is too high (50-80 nm expected) to form simple micelles in water for P(My-*b*-HMPMA) diblock exhibiting relatively low M_n .

Table 5. Dynamic light scattering analyses of P(My-*b*-HMPMA) in reverse osmosis water solution.

Preparation	$Z_{\text{ave}}^{(a)}$ (nm) / $\text{PDI}^{(b)}$			
	I. 1.4 mg.ml ⁻¹ (3 days ^(c))	II. 1.0 mg.ml ⁻¹ (3 days)	III. 0.7 mg.ml ⁻¹ (6 days)	IV. 0.4 mg.ml ⁻¹ (10 days)
$T_{\text{DLS}} = 25$ °C	341 ± 19 / 0.24	268 ± 21 / 0.16	309 ± 15 / 0.29	214 ± 15 / 0.27
$T_{\text{DLS}} = 45$ °C	266 ± 8 / 0.07	198 ± 6 / 0.10	129 ± 17 / 0.11	119 ± 12 / 0.13
$T_{\text{DLS}} = 65$ °C	275 ± 9 / 0.09	168 ± 12 / 0.09	134 ± 9 / 0.12	120 ± 16 / 0.11

a) Z-average diameter (cumulants mean) derived from three separate repeats. The error is given as the standard deviation from the three separate repeats.

b) Polydispersity Index (PDI) corresponding to the coefficient of the squared term ‘c’ when scaled as $2c/b^2$, where ‘b’ and ‘c’ are obtained from the cumulants analysis, which fits a polynomial to the log of the G_1 correlation function.

c) Time of stirring.

2.5. Conclusion

The possibility of synthesizing well-tailored *My*/methacrylate copolymers by NMP has been supported by the satisfactory copolymerization of *My* and MMA in bulk at 110 °C initiated by NHS-BB. The linear relationship between M_n and X combined with \bar{D} as low as 1.15-1.32 shown by this polymerization prompted us to study the NMP of *My* with GMA, a highly versatile monomer bearing an epoxy group. *My*/GMA NMP with $f_{\text{My},0} = 0.10\text{-}0.90$ was performed in bulk at 120 °C initiated by NHS-BB. $r_{\text{My}} = 0.80 \pm 0.31$ and $r_{\text{GMA}} = 0.71 \pm 0.15$ were determined by the FR approach whereas the KT method gave $r_{\text{My}} = 0.48 \pm 0.12$ and $r_{\text{GMA}} = 0.53 \pm 0.18$. The statistical nature of this copolymerization was confirmed using a NLLS procedure yielding $r_{\text{My}} = 0.49 \pm 0.13$ and $r_{\text{GMA}} = 0.50 \pm 0.13$. For $f_{\text{My},0} = 0.60\text{-}0.90$, well-defined P(*My-stat*-GMA) copolymers were achieved with M_n approximately 81% of $M_{n,\text{theo}}$ and $\bar{D} = 1.26\text{-}1.35$ at X as high as 79-89%. Even though broader molecular weight distributions ($\bar{D} = 1.35\text{-}1.55$) were

measured for GMA-rich initial feeds ($f_{My,0} = 0.10-0.49$) during the copolymerizations, the linear increase of M_n with X and the monomodal nature of the GPC peaks indicated the satisfactory mediation of these reactions by SG1. The more apparent loss of control observed for My /GMA copolymerizations exhibiting richer GMA initial concentrations was likely due to the significantly higher propagation rate as indicated by $\langle k_p \rangle \langle K \rangle = (157.0 \pm 0.9) 10^{-5} \text{ s}^{-1}$ at $f_{GMA,0} = 0.90$, about 36 times higher than that of My NMP under the same reaction conditions ($\langle k_p \rangle \langle K \rangle = (4.3 \pm 0.7) 10^{-5} \text{ s}^{-1}$). The faster kinetics presumably favored the occurrence of irreversible terminations which might be β -hydrogen transfer from propagating P(My -*stat*-GMA) radical to SG1 or intramolecular chain transfer to polymer. P(My -*stat*-GMA)s exhibiting $F_{GMA} = 0.11-0.95$ displayed a range of T_{gs} s from $-77 \text{ }^\circ\text{C}$ to $+43 \text{ }^\circ\text{C}$. My -rich and GMA-rich P(My -*stat*-GMA)s were cleanly chain-extended with My , S and GMA, indicating the high chain-end fidelity of these macroinitiators, which was also confirmed by the quantitative estimation of the SG1 end-group via ^{31}P NMR ($LF = 82 \pm 5 \%$ and $71 \pm 7 \%$ respectively). Most of the resulting diblock copolymers exhibited two distinct T_{gs} s, indicative of a possible microphase separation. Lastly, a NMP-based P(My -*b*-GMA) diblock copolymer was treated with morpholine, a nucleophilic reagent, to yield quantitatively P(My -*b*-HMPMA). This latter exhibited a higher degree of hydrophilicity, as shown by its total dissolution in water, compared to P(My -*b*-GMA). P(My -*b*-HMPMA) was able to self-organize into micelles in water, exhibiting $Z_{ave} = 120-130 \text{ nm}$ at $T = 45-65 \text{ }^\circ\text{C}$ and $[P(My-b-HMPMA)] \leq 0.7 \text{ mg.ml}^{-1}$. Thus, well-tailored statistical and diblock epoxide functionalized P(My)s can be readily synthesized by SG1-mediated NMP, opening the door to a multitude of post-polymerization treatments resulting in the achievement of multifunctional My -based polymers.

2.6. References

- (1) R. A. Shanks; I. Kong In *Advances in Elastomers I: Blends and Interpenetrating Networks*; P. M. Visakh; S. Thomas; A. K. Chandra; A. P. Mathew, Eds.; Springer-Verlag: Berlin, **2013**; Chapter 2, pp 11-45.
- (2) S. Shi; Q. Shi; J. Yin In *Reactive and Functional Polymers Research Advances*; M. I. Barroso, Ed.; Nova Science Publishers: New York, **2008**; Chapter 1, pp 1-77.
- (3) L. Li, S. Li and D. Cui, *Macromolecules* **2016**, *49*, 1242.
- (4) M. M. Abd Rabo Moustafa and E. R. Gillies, *Macromolecules* **2013**, *46*, 6024.
- (5) P. Wongthong, C. Nakason, Q. Pan, G. L. Rempel and S. Kiatkamjornwong, *Eur. Polym. J.* **2013**, *49*, 4035.
- (6) Z. Zhang; D. Cui; B. Wang; B. Liu; Y. Yang In *Molecular Catalysis of Rare-Earth Elements*; P. W. Roesky, Ed.; Springer: Berlin, **2010**; Chapter 2, pp 49-108.
- (7) M. Nishikawa; M. Maeda; H. Nakata; H. Takamatsu; M. Ishii In *Applications of Anionic Polymerization Research*; R. P. Quirk, Ed.; Oxford University Press: Washington, **1998**; Chapter 14, pp 186-196.
- (8) A. A. Arest-Yakubovich; I. P. Goldberg; V. L. Zolotarev; V. I. Aksenov; I. I. Ermakova; V. S. Ryakhovskiy In *Applications of Anionic Polymerization Research*; R. P. Quirk, Ed.; Oxford University Press: Washington, **1998**; Chapter 15, pp 197-206.
- (9) K. Nozaki In *Organometallic Reactions and Polymerization*; K. Osakada, Ed.; Springer: Berlin, **2014**; Chapter 6, pp 217-236.
- (10) S. R. Chowdhury; S. Sivaram In *Functional Polymers: Design, Synthesis, and Applications*; R. Shunmugam, Ed.; Apple Academic Press: Oakville, **2017**; Chapter 1, pp 3-56.

- (11) W. A. Braunecker and K. Matyjaszewski, *Prog. Polym. Sci.* **2007**, *32* (1), 93.
- (12) M. K. Georges, R. P. N. Veregin, P. M. Kazmaier and G. K. Hamer, *Macromolecules* **1993**, *26* (11), 2987.
- (13) R. P. N. Veregin, M. K. Georges, P. M. Kazmaier and G. K. Hamer, *Macromolecules* **1993**, *26* (20), 5316.
- (14) J. -S. Wang and K. Matyjaszewski, *J. Am. Chem. Soc.* **1995**, *117* (20), 5614.
- (15) J. Hui, Z. Dong, Y. Shi, Z. Fu and W. Yang, *RSC Adv.* **2014**, *4*, 55529.
- (16) J. Hua, X. Li, Y. -S. Li, L. Xu and Y. -X. Li, *J. Appl. Polym. Sci.* **2007**, *104* (6), 3517.
- (17) R. Wei, Y. Luo and Z. Li, *Polymer* **2010**, *51* (17), 3879.
- (18) L. Hlalele, D. R. D'Hooge, C. J. Dürr, A. Kaiser, S. Brandau and C. Barner-Kowollik, *Macromolecules* **2014**, *47* (9), 2820.
- (19) J. Zhu, D. Zhou, X. Zhu and G. Chen, *J. Polym. Sci., Part A: Polym. Chem.* **2004**, *42* (10), 2558.
- (20) D. H. Solomon, E. Rizzardo and P. Cacioli (Commonwealth Scientific And Industrial Research Organization). Eur. Pat. Appl. 0135280A3, August 13, **1986**.
- (21) T. Fukuda, T. Terauchi, A. Goto, K. Ohno, Y. Tsujii, T. Miyamoto, S. Kobatake and B. Yamada, *Macromolecules* **1996**, *29* (20), 6393.
- (22) J. Nicolas, Y. Guillauneuf, C. Lefay, D. Bertin, D. Gigmes and B. Charleux, *Prog. Polym. Sci.* **2013**, *38* (1), 63.
- (23) R. B. Grubbs, *Polym. Rev.* **2011**, *51* (2), 104.
- (24) M. Maric In Nitroxide Mediated Polymerization: From Fundamentals to Applications in Materials Science; D. Gigmes, Ed.; The Royal Society of Chemistry: Cambridge, **2016**; Chapter 4, pp 153-198.
- (25) D. Benoit, V. Chaplinski, R. Braslau and C. J. Hawker, *J. Am. Chem. Soc.* **1999**, *121*, 3904.
- (26) D. Benoit, S. Grimaldi, S. Robin, J. -P. Finet, P. Tordo and Y. Gnanou, *J. Am. Chem. Soc.* **2000**, *122* (25), 5929.
- (27) M. Rodlert, E. Harth, I. Rees and C. J. Hawker, *J. Polym. Sci., Part A: Polym. Chem.* **2000**, *38*, 4749.
- (28) C. Cheng, K. Qi, E. Khoshdel and K. L. Wooley, *J. Am. Chem. Soc.* **2006**, *128* (21), 6808.
- (29) N. L. Hill and R. Braslau, *Macromolecules* **2005**, *38* (22), 9066.
- (30) J. Ruehl, A. Nilsen, S. Born, P. Thoniyot, L. P. Xu, S. Chen and R. Braslau, *Polymer* **2007**, *48* (9), 2564.
- (31) J. K. Wegrzyn, T. Stephan, R. Lau and R. B. Grubbs, *J. Polym. Sci., Part A: Polym. Chem.* **2005**, *43* (14), 2977.
- (32) A. Sundararaman, T. Stephan and R. B. Grubbs, *J. Am. Chem. Soc.* **2008**, *130* (37), 12264.
- (33) Y. Cai, K. B. Aubrecht and R. B. Grubbs, *J. Am. Chem. Soc.* **2011**, *133* (4), 1058.
- (34) S. Harriison, P. Couvreur and J. Nicolas, *Macromolecules* **2011**, *44* (23), 9230.
- (35) A. Métafiot, Y. Kanawati, J. -F. Gérard, B. Defoort and M. Marić, *Macromolecules* **2017**, *50* (8), 3101.
- (36) A. Moayeri, B. Lessard and M. Marić, *Polym. Chem.* **2011**, *2*, 2084.
- (37) C. Zhang and M. Marić, *Polymers* **2011**, *3* (3), 1398.
- (38) V. Consolante and M. Marić, *J. Appl. Polym. Sci.* **2013**, *127*, 3645.
- (39) J. Vinas, N. Chagneux, D. Gigmes, T. Trimaille, A. Favier and D. Bertin, *Polymer* **2008**, *49* (17), 3639.
- (40) C. Farcet, J. Belleney, B. Charleux and R. Pirri, *Macromolecules* **2002**, *35* (13), 4912.
- (41) C. Farcet, B. Charleux and R. Pirri, *Macromolecules* **2001**, *34* (12), 3823.
- (42) J. Nicolas, C. Dire, L. Mueller, J. Belleney, B. Charleux, S. R. A. Marque, D. Bertin, S. Magnet and L. Couvreur, *Macromolecules* **2006**, *39* (24), 8274.
- (43) J. Nicolas, S. Brusseau and B. Charleux, *J. Polym. Sci., Part A: Polym. Chem.* **2010**, *48* (1), 34.
- (44) D. L. Trumbo, *Polym. Bull.* **1993**, *31*, 629.
- (45) P. Sarkar and A. K. Bhowmick, *RSC Adv.* **2014**, *4*, 61343.
- (46) S. Georges, M. Bria, P. Zinck and M. Visseaux, *Polymer* **2014**, *55*, 3869.
- (47) B. Lessard and M. Marić, *Macromolecules* **2008**, *41*, 7881.
- (48) C. Lefay, J. Belleney, B. Charleux, O. Guerret and S. Magnet, *Macromol. Rapid Commun.* **2004**, *25* (13), 1215.
- (49) L. Couvreur, B. Charleux, O. Guerret and S. Magnet, *Macromol. Chem. Phys.* **2003**, *204* (17), 2055.
- (50) B. Lessard, S. Schmidt and M. Maric, *Macromolecules* **2008**, *41*, 3446.
- (51) B. Lessard, A. Graffe and M. Maric, *Macromolecules* **2007**, *40*, 9284.
- (52) C. Dire, J. Belleney, J. Nicolas, D. Bertin, S. Magnet and B. Charleux, *J. Polym. Sci., Part A: Polym. Chem.* **2008**, *46* (18), 6333.
- (53) Q. Ma and K. L. Wooley, *J. Polym. Sci., Part A: Polym. Chem.* **2000**, *38* (S1), 4805.
- (54) D. Benoit, E. Harth, P. Fox, R. M. Waymouth and C. J. Hawker, *Macromolecules* **2000**, *33*, 363.

- (55) E. M. Glebov, L. G. Krishtopa, V. Stepanov, L. N. Krasnoperov, *J. Phys. Chem. A* **2001**, *105*, 9427.
- (56) C. H. Hornung, M. A. Alvarez-Diéguez, T. M. Kohl and J. Tsanaktsidis, *Beilstein J. Org. Chem.* **2017**, *13*, 120.
- (57) F. Chauvin, P. -E. Dufils, D. Gigmes, Y. Guillaeneuf, S. R. A. Marque, P. Tordo and D. Bertin, *Macromolecules* **2006**, *39* (16), 5238.
- (58) S. Liu, S. Srinivasan, M. C. Grady, M. Soroush and A. M. Rappe, *Int. J. Quant. Chem.* **2014**, *114*, 345.
- (59) J. Barth, M. Buback, P. Hesse and T. Sergeeva, *Macromolecules* **2010**, *43*, 4023.
- (60) B. Wenn and T. Junkers, *Macromol. Rapid Commun.* **2016**, *37*, 781.
- (61) E. Cadova, J. Dybal, J. Kriz, P. Vlcek, M. Janata and L. Toman, *Macromol. Chem. Phys.* **2008**, *209*, 1657.
- (62) B. Lessard, C. Tervo, M. Maric, *Macromol. React. Eng.* **2009**, *3*, 245.
- (63) Y. Guillaeneuf, D. Gigmes, S. R. A. Marque, P. Astolfi, L. Greci, P. Tordo and D. Bertin, *Macromolecules* **2007**, *40*, 3108.
- (64) B. Charleux, J. Nicolas and O. Guerret, *Macromolecules* **2005**, *38*, 5485.
- (65) B. Lessard, E. Ling, M. Morin and M. Marić, *J. Polym. Sci., Part A: Polym. Chem.* **2011**, *49*, 1033.
- (66) J. Nicolas, L. Mueller, C. Dire, K. Matyjaszewski and B. Charleux, *Macromolecules* **2009**, *42* (13), 4470.
- (67) G. Gryn'ova, C. Y. Lin and M. L. Coote, *Polym. Chem.* **2013**, *4* (13), 3744.
- (68) D. Contreras-Lopez, M. Albores-Velasco and E. Saldivar-Guerra, *J. Appl. Polym. Sci.* **2017**. DOI: 10.1002/app.45108
- (69) G. Odian In Principles of Polymerization, 4th ed.; G. Odian, Ed.; John Wiley & Sons: Hoboken, NJ, **2004**; Chapter 6, pp 466–505.
- (70) M. Fineman and S. D. Ross, *J. Polym. Sci.* **1950**, *5* (2), 259.
- (71) T. Kelen and F. Tüdös, *J. Macromol. Sci., Chem.* **1975**, *9* (1), 1.
- (72) P. W. Tidwell and G. A. Mortimer, *J. Polym. Sci., Part A: Gen. Pap.* **1965**, *3*, 369.
- (73) F. R. Mayo and F. M. Lewis, *J. Am. Chem. Soc.* **1944**, *66* (9), 1594.
- (74) K. A. Rusakova, I. M. Kuznetsova, N. A. Vargasova, M. F. Margaritova, S. G. Alekseyeva, Y. G. Urman and I. Y. Slonim, *Vysokomol. Soyed.* **1974**, *A16* 12, 2815.
- (75) D. Contreras-Lopez, E. Saldivar-Guerra and G. Luna-Barcenas, *Eur. Polym. J.* **2013**, *49*, 1760.
- (76) N. Kamachi and A. Kajiwara, *Macromolecules* **1996**, *29* (7), 2378.
- (77) M. Morton, P. P. Salatiello and H. Landfield, *J. Polym. Sci.* **1952**, *8* (3), 279.
- (78) S. Beuermann, M. Buback, T. P. Davis, N. Garcia, R. G. Gilbert, R. A. Hutchinson, A. Kajiwara, M. Kamachi, I. Lacik and G. T. Russell, *Macromol. Chem. Phys.* **2003**, *204* (10), 1338.
- (79) K. Liang, M. Dossi, D. Moscatelli and R. A. Hutchinson, *Macromolecules* **2009**, *42*, 7736.
- (80) B. Lessard, C. Tervo, S. De Wahl, F. J. Clerveaux, K. K. Tang, S. Yasmine, S. Andjelic, A. D'Alessandro and M. Marić, *Macromolecules* **2010**, *43* (2), 868.
- (81) W. J. Runckel and L. A. Goldblatt, *Ind. Eng. Chem.* **1946**, *38* (7), 749.
- (82) K. D. Safa and M. H. Nasirtabrizi, *Polymer Bulletin* **2006**, *57*, 293.
- (83) M. Gordon and J. S. Taylor, *J. Chem. Tech. and Biotech.* **1952**, *2* (9), 493.
- (84) T. G. Fox, *Bull. Am. Phys. Soc.* **1956**, *1*, 123.
- (85) E. A. Dimarzio and J. H. Gibbs, *J. Polym. Sci., Part A: Polym. Chem.* **1959**, *40* (136), 121.
- (86) L. A. Wood, *J. Polym. Sci., Part A: Polym. Chem.* **1958**, *28* (117), 319.
- (87) R. A. Orwoll In Physical Properties of Polymers Handbook; J. E. Mark, Ed.; Springer: New York, **2007**; Chapter 7, pp 93-101.
- (88) D. Guseva, P. Komarov and A. V. Lyulin, *J. Chem. Phys.* **2014**, *140*, 114903.
- (89) P. Claudy, J. M. Létoffé, Y. Camberlain and J. P. Pascault, *Polymer Bulletin* **1983**, *9*, 208.
- (90) P. J. Flory In Principles of Polymer Chemistry; P. J. Flory, Ed.; Cornell University Press; New York, **1975**; Chapter 13, pp 541-594.
- (91) J. B. Rosenholm, *Advances in Colloid and Interface Science* **2009**, *146*, 31.
- (92) E. Yara-Varon, A. S. Fabiano-Tixier, M. Balcels, R. Canela-Garayoa, A. Bily and F. Chemat, *RSC Adv.* **2016**, *6*, 27750.
- (93) C. M. Hansen In Hansen Solubility Parameters, A User's Handbook; C. M. Hansen, Ed.; CRC Press: New York, **2007**; Chapter 1, 1-26.
- (94) E. Manias; L. A. Utracki In Polymer Blends Handbook; L. A. Utracki; C. A. Wilkie, Eds.; Springer: Dordrecht, **2014**; Vol. 1, Part 1, Chapter 2, pp 171-289.
- (95) J. S. Higgins, J. E. Lipson and R. P. White, *Phil. Trans. R. Soc. A* **2010**, *368*, 1009.
- (96) M. Benaglia, A. Alberti, L. Giorgini, F. Magnoni and S. Tozzi, *Polym. Chem.* **2013**, *4*, 124.
- (97) M. Mertoglu, S. Garnier, A. Laschewsky, K. Skrabania and J. Storsberg, *Polymer* **2005**, *46* (18), 7726.

Chapter 3. Replacement of poly(styrene) by poly(isobornyl methacrylate) as the rigid domain of the β -myrcene-based block copolymers

3.1. Preface

This chapter presents a manuscript which will be shortly submitted to the journal *Polymer Chemistry* (Métafiot, A.; Gagnon, L.; Pruvost, S.; Hubert, P.; Gérard, J. -F.; Defoort, B.; Maric, M. β -Myrcene / Isobornyl Methacrylate SG1 Nitroxide-Mediated Controlled Radical Polymerization: Synthesis and Characterization of Gradient, Diblock and Triblock copolymers).

Despite the successful synthesis of NMP-based S-My-S triblocks (Chapter 1, section 1.4.3), poor mechanical properties were exhibited by these polymers at room temperature (tensile stress at break $\sigma_B < 0.8$ MPa, tensile elongation at break $\varepsilon_B < 200\%$). The use of P(My) as the soft segment of the triblocks, imparting ideally the elastomeric properties, can legitimately be a key factor of the brittleness of these copolymers. Indeed, the high entanglement molar mass of P(My) (22-31 kg.mol⁻¹) results in a relatively low entanglement density of the continuous flexible domain. However, another parameter which can affect the mechanical properties of the copolymer is the nature of the hard segment(s), as mentioned in the literature review (section C.1.4). The substitution of the PS blocks by harder blocks, exhibiting a higher T_g , can significantly increase the tensile strength of the material as well as its upper service temperature. Accordingly, it was decided herein to replace the PS outer segments by more rigid poly(isobornyl methacrylate) P(IBOMA) segments, displaying a $T_g \sim 190$ °C.

3.2. Abstract

β -Myrcene / isobornyl methacrylate (My/IBOMA) mixtures were copolymerized in bulk using the SG1-based BlocBuilderTM alkoxyamine functionalized with *N*-succinimidyl ester group, NHS-BlocBuilder, at $T = 100$ °C with initial IBOMA molar feed compositions $f_{IBOMA,0} = 0.10-0.90$. Copolymer reactivity ratios were $r_{My} = 1.90-2.16$ and $r_{IBOMA} = 0.02-0.07$ using Fineman-Ross, Kelen-Tudos and non-linear least-squares fitting to the Mayo-Lewis terminal model, and indicated the possibility of gradient My/IBOMA copolymers. A linear increase in molecular weight *versus* conversion and a low dispersity ($\mathcal{D} \leq 1.41$) were exhibited by

My/IBOMA copolymerization with $f_{\text{IBOMA},0} \leq 0.80$. *My*-rich and IBOMA-rich copolymers were shown to have a high degree of chain-end fidelity by performing subsequent chain-extensions with IBOMA and/or *My*, and by ^{31}P NMR analysis. IBOMA-*My*-IBOMA triblock copolymers containing a minor fraction of *My* or styrene (S) units in the outer hard segments ($M_n = 51\text{-}95 \text{ kg}\cdot\text{mol}^{-1}$, $\bar{D} = 1.91\text{-}2.23$ and $F_{\text{IBOMA}} = 0.28\text{-}0.36$) were then synthesized using SG1-terminated poly(ethylene-*stat*-butylene) dialkoxyamine. The micro-phase separation was suggested by the detection of two distinct T_g s at about $-60 \text{ }^\circ\text{C}$ and $+180 \text{ }^\circ\text{C}$, and confirmed by atomic force microscopy (AFM). A plastic stress-strain behavior (stress at break $\sigma_B = 3.90 \pm 0.22 \text{ MPa}$, elongation at break $\varepsilon_B = 490 \pm 31 \%$) associated to an upper service temperature of about $140 \text{ }^\circ\text{C}$ were also highlighted for these triblock polymers.

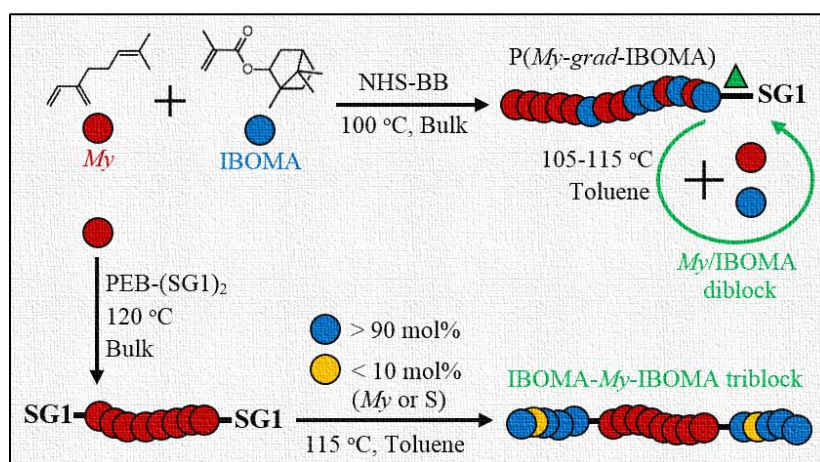


Table of contents graphic. Synthesis of well-defined *My*/IBOMA gradient and diblock copolymers by NMP at $100 \text{ }^\circ\text{C}$ in bulk, initiated by the alkoxyamine NHS-BB. Preparation of Co/IBOMA-*My*-IBOMA/Co triblock copolymers by NMP (Co = *My* or S comonomer, $< 10 \text{ mol}\%$), using PEB-(SG1) $_2$ difunctional initiator.

3.3. Introduction

The community of polymer researchers has long desired to elaborate polymerization techniques that couple the control of microstructure offered by living ionic polymerization¹⁻³ with the simplicity of industrial implementation made possible by other processes such as free radical polymerization⁴. Since the early 1980s, an easy-to-use synthetic technique now termed reversible-deactivation radical polymerization (RDRP)⁵⁻⁹ was developed, encompassing several novel controlled/pseudo-living radical polymerizations and allowing the preparation of tailor-made macromolecules with precise and predetermined molar masses,

compositions, topologies and functionalities. Among them, nitroxide-mediated polymerization (NMP)^{7,8,10} is conceptually and practically the simplest of these systems. Based on a reversible termination mechanism between the propagating free radical and the nitroxide used as a controlling agent, NMP establishes a thermal dynamic equilibration between dormant macro-alkoxyamines capped by the nitroxide moiety and actively propagating macroradicals¹¹. At a minimum, only an alkoxyamine, available from commercial sources and easily functionalizable, and the monomer(s) are necessary to implement a NMP process initiated via a mono-component pathway (i.e. unimolecular initiator). NMP relies on the elimination of oxygen prior to polymerization as the main experimental constraint^{6,12}.

The opportunity to prepare high-performance polymers by taking advantage of NMP's simplicity appears to be highly desirable from both practical and economical points of view. The synthesis of polymers having desirable mechanical properties such as a high tensile strength, a remarkable extensibility or a combination of both seems achievable by NMP. In particular, the development of styrenic-diene block copolymers, generally composed of a dispersed poly(styrene) PS or PS derivative phase in a continuous elastomer domain,^{13,14} looks specifically suited to the NMP process. Indeed, the NMP of conjugated dienes such as butadiene (B)^{15,16} and especially isoprene (I)¹⁷ was explored from the onset of the development of NMP, using 2,2,6,6-tetramethylpiperidinyl-1-oxy (TEMPO)⁷, the original stable free nitroxide. Well-tailored homopolymers and copolymers based on either B or I were produced as well¹⁸⁻²², mediated by the 2,2,5-trimethyl-4-phenyl-3-azahexane-3-oxyl nitroxide (TIPNO)^{18,23}, a more labile second-generation initiator. *N-tert*-Butyl-N-[1-diethylphosphono-(2,2-dimethylpropyl)] nitroxide (SG1)²⁴ showed also its effectiveness to control the polymerization of I²⁵⁻²⁷. Recently, we studied the well-controlled polymerization of β -myrcene²⁸, an acyclic monoterpene, initiated by unimolecular SG1-based succinimidyl ester-functionalized BlocBuilderTM alkoxyamine called NHS-BlocBuilder²⁹, demonstrating once again the facility of the NMP process to synthesize elastomers based on 1,3-dienes with low dispersity (\mathcal{D}) and substantial chain-end fidelity.

Well-tailored styrene (S)/I or B statistical, diblock and triblock polymers were thereby made by NMP^{18,30,31}. Surprisingly enough and to the best of our knowledge, no NMP-based styrenic-diene block copolymers were reported in the literature as possible alternative plastics with valuable mechanical properties or as thermoplastic elastomers. This observation prompted us to synthesize NMP-based block copolymers based on an unusual but promising monomer coupling, namely β -myrcene (*My*) / isobornyl methacrylate (IBOMA).

A naturally occurring monoterpene with a highly active diene structure, β -myrcene (*My*, 7-methyl-3-methylene-octa-1,6-diene), provides a classical chemistry similar to unsaturated hydrocarbons³². Its polymerization leads to a bio-sourced P(*My*) elastomer exhibiting an expected sub-zero glass transition temperature (T_g) of about -75 °C and a pseudo-plastic behavior³³. *My*-based thermoplastic elastomers were

notably produced by anionic polymerization, making P(*My*) a possible elastomer substitute to well-known poly(butadiene) PB and poly(isoprene) PI rubbers. In 1983, S-*My*-S triblock copolymers, initiated by *sec*-butyllithium at 30 °C in benzene solution, were made by sequential monomer addition (number-average molecular weight $M_n = 165\text{-}194 \text{ kg}\cdot\text{mol}^{-1}$, final S molar fraction $F_S = 0.23\text{-}0.58$) and exhibited tensile strengths at break $\sigma_B = 4.3\text{-}12.8 \text{ MPa}$ and elongations at break $\varepsilon_B = 670\text{-}1290\%$ ^{34,35}. Such triblocks exhibited the classical self-assembled morphologies in this case. More recently, Bolton *et al.* produced AMMS-*My*-AMMS (AMMS = α -methyl-*p*-methylstyrene) triblock polymers by sequential anionic polymerization³⁶, which showed ultimate tensile stress values ranging from 0.5 to 10.8 MPa and ε_B ranging from 525 to 1340%. Interestingly, the insertion of high T_g P(AMMS)s as outer hard blocks ($T_{g,P(\text{AMMS})} \sim 180 \text{ }^\circ\text{C}$) allowed the extension of the upper service temperature of these triblocks compared to that of traditional PS-based TPEs, which are limited to 90-100 °C.

Similarly, P(IBOMA), displaying a high $T_g \sim 190 \text{ }^\circ\text{C}$ ³⁷, can be used as the rigid domain of block copolymer TPEs to provide strength, hardness and an improved performance at high temperature. This was illustrated by Yu and coworkers, who prepared IBOMA-B-IBOMA triblock copolymers initiated by the *m*-diisopropenylbenzene / *tert*-butyllithium diadduct³⁸, which exhibited excellent stress-strain properties and an upper service temperature of 160 °C. With the development of alkoxyamine unimolecular initiators and SG1 nitroxide in the late 1990s, the polymerization of IBOMA, a bulky hydrophobic methacrylate, is no longer a barrier towards such block copolymers by NMP. Control of methacrylate polymerizations was accomplished by Charleux and coworkers via SG1-based initiators and a small fraction of co-monomer such as S^{39,40} or acrylonitrile⁴¹ (< 10 mol%).

In the present study, we report first the copolymerization of *My* and IBOMA in bulk at 100 °C, initiated by the succinimidyl ester-terminated NHS-BlocBuilder alkoxyamine. The active feature of these NMP-based *My*/IBOMA copolymers, ideally capped by a SG1 nitroxide moiety, was then assessed quantitatively via ³¹P NMR spectroscopy and qualitatively by chain-extensions with a fresh batch of IBOMA and/or *My*. After guaranteeing the efficient control of the SG1-mediated copolymerization of *My* with IBOMA, the second part of this investigation was focused on the preparation of P(*My*)-(SG1)₂ macroinitiators using telechelic poly(ethylene-*stat*-butylene) initiator terminated with SG1 nitroxide groups⁴² and their subsequent chain-extension with IBOMA-rich/*My* or S mixtures. The phase behavior, the thermal behavior, notably along with viscoelastic properties, and the stress-strain properties of the resulting triblock copolymers were elucidated to emphasize the possibility to produce valuable diene-based block copolymers from largely sustainable feedstocks, in a simple way by NMP.

3.4. Results and discussion

Two main parts are introduced thereafter and consist of the synthesis by nitroxide-mediated polymerization (NMP), via the SG1 nitroxide rate moderator, and the characterization of β -myrcene-rich (*My*-rich) and isobornyl methacrylate-rich (IBOMA-rich) copolymers. First, the nature of *My*/IBOMA copolymerization initiated by NHS-BlocBuilder (NHS-BB) was examined as well as its kinetics, its level of control and the ability of the resulting copolymers to re-initiate a second batch of monomer(s). Glass transition temperature (T_g) and decomposition temperature (T_{dec}) of the *My*/IBOMA copolymers were also investigated. Secondly, the preparation of relatively high M_n $P(My)-(SG1)_2$ was explored by using the PEB-(SG1)₂ dialkoxyamine. The possibility to synthesize triblock polymers by IBOMA/Co chain-extensions (Co = *My* or S co-monomer ~ 8-9 mol%, relative to IBOMA) from $P(My)-(SG1)_2$ was then presented. Figure 1 depicts the various polymerizations done in this study.

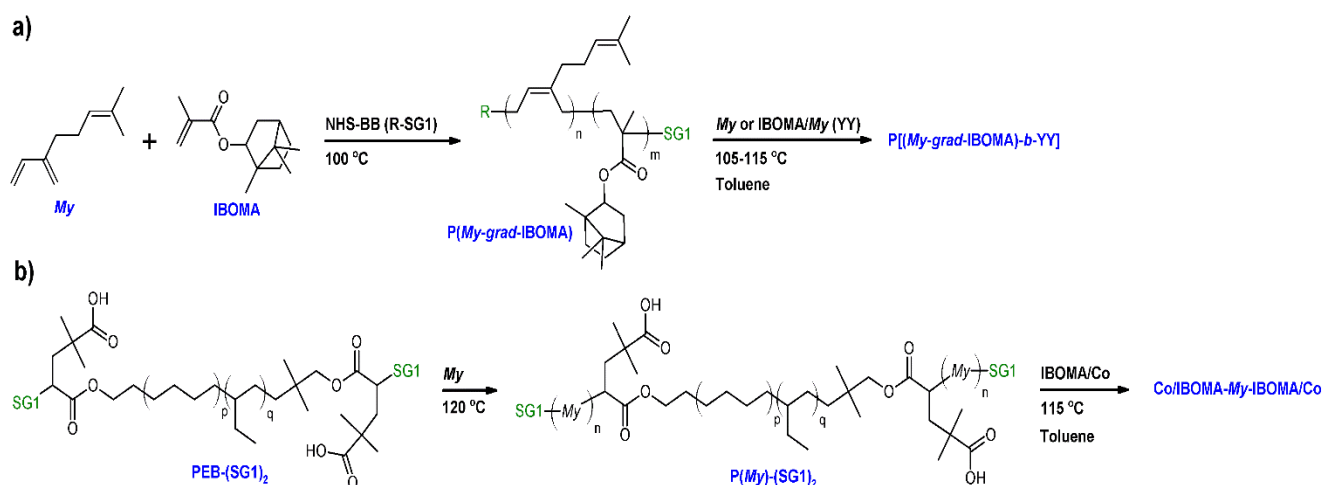


Figure 1. a) *My*/IBOMA gradient copolymerization in bulk initiated by NHS-BB and subsequent *My* or IBOMA/*My* (~ 93/7 mol%) chain-extension in toluene and b) synthesis of $P(My)-(SG1)_2$ from PEB-(SG1)₂ difunctional initiator ($n \gg p, q$) and subsequent IBOMA/Co chain-extension in toluene (Co = *My* or S co-monomer, 8-9 mol%).

3.4.1. β -Myrcene / isobornyl methacrylate copolymerization by NMP

▣ Preliminary polymerization temperature study.

Before exploring the effects of the initial mixture composition of the NMP-based *My*/IBOMA copolymerization over its kinetics and the composition of the resulting copolymers, the polymerization temperature was first studied. NMP of *My* in bulk initiated by NHS-BB at 120 °C was well-controlled, exhibiting minor deviations of M_n values from the predicted ones and low dispersities < 1.30 , even at *My* conversion $X_{My} > 50\%$ ²⁸. Interestingly, the copolymerization of *My* with methyl methacrylate (MMA, molar feed composition $f_{MMA,0} = 0.50$) and glycidyl methacrylate (GMA, $f_{GMA,0} = 0.11-0.95$) under the same experimental conditions also gave well-defined statistical copolymers⁴⁹. For both *My*/MMA and *My*/GMA systems, M_n increased linearly with overall conversion and $\mathcal{D} < 1.55$ at the end of the reactions. Accordingly, these encouraging results prompted us to study two *My*/IBOMA copolymerizations in bulk using NHS-BB initiator at 120 °C (experiments *My*/IBOMA-50-T120 with $f_{My,0} = 0.50$ and *My*/IBOMA-70-T120 with $f_{My,0} = 0.71$, Table 1). Although a linear increase of $M_{n,MHS}$ with the overall conversion X was observed in both cases, relatively broad molecular weight distributions were obtained throughout the reactions ($\mathcal{D} = 1.45-1.71$ for $X = 26-94\%$, Figure S1c, Supporting Information). This may be due to the likely high individual equilibrium constant of IBOMA, as typically reported for methacrylates^{24,50,51}, leading to a high concentration of propagating radicals that can promote self-termination. Consequently, it was decided to perform the two same experiments at 100 °C (experiments *My*/IBOMA-50 with $f_{My,0} = 0.50$ and *My*/IBOMA-70 with $f_{My,0} = 0.70$, Table 1) in order to know if a better control of the NMP can be obtained, by reducing likely the average activation-deactivation equilibrium constant $\langle K \rangle$ of this binary system. Regardless of $f_{My,0}$, similar $M_{n,MHS}$ values were measured for the experiments run at 100 and 120 °C (Figure S1c, Supporting Information). However, narrower molecular weight distributions were obtained ($\mathcal{D} \leq 1.29$ for $X = 9-65\%$) at 100 °C, for both experiments exhibiting $f_{My,0} = 0.50$ and 0.70. This apparent enhanced control of the NMP may be due to the reduction of disproportionation side reactions (β -hydrogen transfer from a propagating radical to SG1), commonly observed during the NMP of methacrylates^{52,53}, at 100 °C. Accordingly, a copolymerization temperature of 100 °C was selected for the *My*/IBOMA NMP. This reduction of temperature is consistent with the SG1-mediated methacrylate polymerizations performed previously with a fairly low temperature ($\sim 70-90$ °C), notably by Charleux *et al.*^{39,54} and Lessard *et al.*^{55,56}.

■ Effect of the feed composition on copolymer composition.

It is first of interest to determine the monomer sequences of P(*My-co*-IBOMA) copolymers via the determination of the copolymer-monomer feed composition relationship. To that end, *My*/IBOMA NMP, with different feed ratios ($f_{My,0} = 0.10-0.90$), was carried out at 100 °C in bulk, initiated by NHS-BB and targeting $M_{n,theo} = 30 \text{ kg}\cdot\text{mol}^{-1}$, as indicated in Table 1. The copolymer composition was determined through ¹H NMR analysis (F_{My} and $F_{IBOMA} = 1 - F_{My}$, Figure S4c in Supporting Information for the spectral

assignments from experiment *My*/IBOMA-50) for relatively low overall conversion samples ($X \leq 27.5\%$, Table S1c in Supporting Information gives the samples used for extracting the reactivity ratios). The terminal copolymerization model, where only the terminal monomer residue is considered, was applied⁵⁷.

The equations used for the calculation of the reactivity ratios can be found in the Supporting Information. By using the Fineman-Ross (FR) method⁵⁸ (Figure 2a), the reactivity ratios were determined: $r_{My} = 2.16 \pm 0.34$ and $r_{IBOMA} = 0.07 \pm 0.04$ ($r_{My} r_{IBOMA} = 0.15 \pm 0.19$). Similar values were calculated via the Kelen-Tudos (KT) approach⁵⁹ (Figure 2b): $r_{My} = 1.90 \pm 0.18$ and $r_{IBOMA} = 0.02 \pm 0.21$ ($r_{My} r_{IBOMA} = 0.04 \pm 0.15$). The errors associated were derived from the standard errors of the slopes from FR and KT plots. Even though the KT equation refines the linearization method by introducing an arbitrary positive constant to spread the data more evenly, it remains a rearrangement of the copolymer composition equation and a non-linear least-squares (NLLS) fit to the Mayo-Lewis equation⁶⁰ is likely one of the sounder methods to determine r_{My} and r_{IBOMA} . Consequently, the reactivity ratios determined by the KT method were used as the initial guesses for a NLLS fitting of the data (Supporting Information). At 95% confidence level and with a regression coefficient $R^2 = 0.91$, the statistical fit to the data yielded reactivity ratios $r_{My} = 2.07 \pm 0.58$ and $r_{IBOMA} = 0.05 \pm 0.08$. These latter results are similar from those obtained by FR and KT approaches, confirming the general trends with respect to *My*/IBOMA NMP at 100 °C in bulk and initiated by NHS-BB: $r_{My} > 1.50$, $r_{IBOMA} < 0.30$ and $r_{My} r_{IBOMA} < 0.50$. The large difference in reactivity between *My* and IBOMA can be first noted. Whatever the terminal unit of the propagating species ($---My^*$ or $---IBOMA^*$), the macro-radical showed a large preference for *My*. The insertion of IBOMA units at low conversions, either by self-propagation or cross-propagation, is not favored: IBOMA-terminated macro-radical has a strong tendency to alternate. Accordingly, it can be assumed that *My*/IBOMA copolymerization under these conditions produces copolymers that possess a gradient in composition consisting of *My* enrichment at the start of the polymer chain followed by the incremental IBOMA enrichment at the end of the chain due to *My* depletion. However, the gradient nature of this copolymerization was moderate as indicated by the presence of methacrylate units at the start of the copolymer chain synthesized ($X = 3-12\%$ and $F_{IBOMA} = 13-18\%$ at $t = 0-60$ min for experiment *My*/IBOMA-50 for instance). Even though samples exhibiting relatively low conversions were used, it can be assumed that the composition drift in the monomer feed was non-negligible, especially taking the difference between r_{My} and r_{IBOMA} into account and was the main source of error by relying on the instantaneous copolymer composition model⁶¹. To the best of our knowledge, no reactivity ratios were reported in the literature for diene/IBOMA systems, limiting thus the discussion. Nonetheless, for the *My*/GMA pair copolymerized under similar conditions (120 °C in bulk initiated by NHS-BB)⁴⁹, statistical copolymers were synthesized with $r_{My} = 0.48-0.80$ and $r_{GMA} = 0.50-0.71$. Such a difference compared to the *My*/IBOMA system highlights the likely influence of the bulky and rigid bicyclic

isobornyl groups over the reactivity of the methacrylate monomer (steric hindrance, hydrophobicity, reduction of polar interactions).

Table 1. Formulations for *My*, IBOMA and *My*/IBOMA polymerizations performed in bulk or in toluene at T = 100-120 °C, initiated by NHS-BB and targeting $M_{n,theo} = 30 \text{ kg.mol}^{-1}$ at X = 100%

ID ^(a)	[NHS-BB] ₀ (M)	[<i>My</i>] ₀ (M)	[IBOMA] ₀ (M)	<i>f</i> _{<i>My</i>,0}	T (°C)	Solvent	<i>t</i> (min)
<i>My</i>/IBOMA-50-T120	0.030	2.49	2.51	0.50	120	-	240
<i>My</i>/IBOMA-70-T120	0.029	3.76	1.57	0.71	120	-	200
<i>My</i>/IBOMA-0-Tol	0.015	0	2.08	0	100	Toluene ^(b)	140
<i>My</i>/IBOMA-0	0.033	0	4.40	0	100	-	4 ^(c)
<i>My</i>/IBOMA-10	0.032	0.45	4.04	0.10	100	-	108
<i>My</i>/IBOMA-20	0.032	0.91	3.73	0.20	100	-	240
<i>My</i>/IBOMA-30	0.031	1.45	3.33	0.30	100	-	300
<i>My</i>/IBOMA-40	0.031	1.94	2.92	0.40	100	-	280
<i>My</i>/IBOMA-50	0.031	2.51	2.52	0.50	100	-	340
<i>My</i>/IBOMA-60	0.028	3.07	2.10	0.59	100	-	380
<i>My</i>/IBOMA-70	0.029	3.70	1.61	0.70	100	-	480
<i>My</i>/IBOMA-80	0.028	4.46	1.08	0.81	100	-	380
<i>My</i>/IBOMA-90	0.027	5.09	0.55	0.90	100	-	400
<i>My</i>/IBOMA-100	0.026	5.80	0	1	100	-	500

a) Experimental identification given by *My*/IBOMA-XX where XX refers to the rounded % initial molar fraction of *My* in the mixture (*f*_{*My*,0}).

b) 50 wt% of toluene in the initial feed.

c) Highly viscous reaction medium after relatively short times for experiments having IBOMA-rich starting mixture.

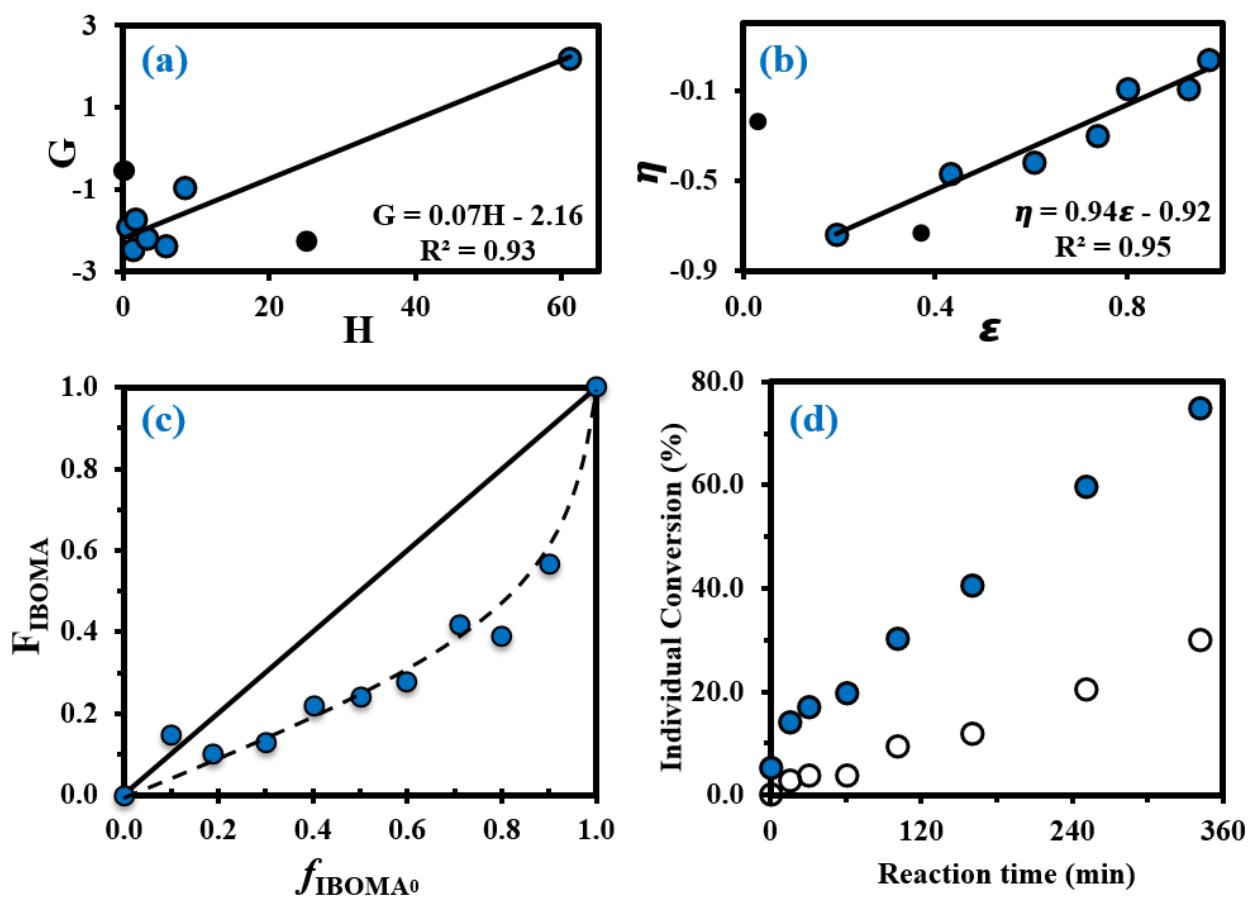


Figure 2. (a) Fineman-Ross (FR) and (b) Kelen-Tudos (KT) plots (solid black circles (●) corresponding to experimental outliers not taken into account for the calculations while solid lines refer to the linear trend lines) to determine the binary reactivity ratios for *My* and IBOMA for copolymerizations done in bulk at 100 °C initiated by NHS-BB (parameters *G*, *H*, η and ϵ defined in the Supporting Information). (c) Mayo–Lewis plot of *My*/IBOMA copolymerizations with respect to IBOMA, using the final molar composition F_{IBOMA} , and the initial monomer feed composition $f_{\text{IBOMA},0}$. The solid straight line indicates the azeotropic composition where $f_{\text{IBOMA},0} = F_{\text{IBOMA}}$ while the dashed line is the associated trend line of the experimental data (solid blue circles (●)). Table S1c in the Supporting Information lists the samples used for these plots. (d) Individual *My* (●) and IBOMA (○) conversions, determined by ¹H NMR in CDCl₃, versus reaction time *t* for the gradient copolymerization *My*/IBOMA-50 exhibiting $f_{M_y,0} = 0.50$.

The Mayo-Lewis plot with respect to IBOMA is shown in Figure 2c. Regardless of the $f_{\text{IBOMA},0}$, the copolymer compositions are always below the diagonal line where the copolymer composition equals the

feed composition ($F_{\text{IBOMA}} = f_{\text{IBOMA},0}$). Thus, the polymer formed at the early stages of the reaction was always richer in *My* than in IBOMA. The composition gradient of the *My*/IBOMA copolymers can be highlighted by determining the individual *My* and IBOMA conversions as a function of polymerization time, as illustrated in Figure 2d with equimolar amounts of each monomer in the initial feed ($f_{\text{My},0} = 0.50$). Throughout the first hour, essentially only *My* was reacting ($X_{\text{My}} = 19.8\%$ and $X_{\text{IBOMA}} = 3.7\%$ at $t = 60$ min) leading to essentially quasi P(*My*) propagating macro-radicals. Afterwards, while the consumption rate of *My* remained constant, IBOMA monomer reacted more significantly ($X_{\text{IBOMA}} = 30.2\%$ at $t = 340$ min) from a *My*-poor feed, resulting in an increase of the composition of IBOMA in the chain. Although this experiment was stopped at $X_{\text{My}} = 75.2\%$ and $X_{\text{IBOMA}} = 30.2\%$, the last stages of the copolymerization can be easily deduced with the gradual IBOMA enrichment of the chain due to the depletion of *My* monomer.

■ Effect of the feed composition on kinetics.

Since the P(*My-grad*-IBOMA) gradient copolymers were characterized by GPC with THF at 40 °C and linear PMMA standards were used for the calibration, the method developed by Benoit *et al.* regarding the universal calibration⁶² was employed. As detailed in the experimental section, Mark-Houwink-Sakurada (MHS) parameters for P(IBOMA) at 25 °C in THF eluent⁴⁵ and for 1,4-P(*My*) at 30 °C in THF eluent⁴⁶ were used and Figure S2c (Supporting Information) shows M_n values before ($M_{n,\text{GPC}}$) and after ($M_{n,\text{MHS}}$) the MHS correction *versus* overall conversion X for experiments *My*/IBOMA-30 and *My*/IBOMA-80. Interestingly, while minor variations can be observed for *My*-rich copolymers (experiment *My*/IBOMA-80 with $F_{\text{My}} \geq 0.66$ during the whole reaction), as F_{IBOMA} increases, $M_{n,\text{MHS}}$ becomes greater than $M_{n,\text{GPC}}$ (*My*/IBOMA-30 with $F_{\text{IBOMA}} \geq 0.44$ for $X = 25\text{-}47\%$). It can be thereby hypothesized that an underestimation of IBOMA-rich copolymer M_n values was done when calibrating with PMMA due to the specific hydrodynamic volume of this copolymer coil in THF.

Before exploring the kinetics of *My*/IBOMA copolymerization at various initial feed compositions, attention can be paid to the homopolymerization of *My* and IBOMA by NMP under the same conditions (experiments *My*/IBOMA-100 and *My*/IBOMA-0, Table 1). *My* NMP at 100 °C in bulk mediated by NHS-BB showed a satisfactory control with $M_{n,\text{MHS}}$ increasing linearly with conversion and $\mathcal{D} \leq 1.36$ (Figure S3c, Supporting Information), resulting in 1,4-rich P(*My*) (Table 2), even though non-negligible deviations of $M_{n,\text{MHS}}$ values from theoretical ones were measured. The NMP of IBOMA without neither co-monomer nor additional free nitroxide was also attempted under these conditions. Controlled polymerization of methacrylates is still challenging for NMP because of their very high equilibrium constant K resulting from slow recombination of nitroxides and sterically-hindered poly(methacrylate) radicals^{63,64}. This long-time obstacle was confirmed once again by the inability to implement the SG1-based NMP of IBOMA in bulk

at 100 °C in a controlled manner: the reaction medium polymerized spontaneously, giving P(IBOMA) chains exhibiting $M_{n,MHS} = 27.1 \text{ kg}\cdot\text{mol}^{-1}$ and $\mathcal{D} = 1.75$ (*My*/IBOMA-0, Table 2). Due to the early high viscosity of the medium after only a few minutes, it was decided to repeat the experiment in 50 wt% toluene (experiment *My*/IBOMA-0-Tol, Table 1) in vain. The polymerization stagnated at $X \sim 10\%$ with $M_{n,MHS} = 11.4\text{-}12.3 \text{ kg}\cdot\text{mol}^{-1}$ and $\mathcal{D} = 1.63\text{-}1.76$ (Figure S3c, Supporting Information), illustrating presumably the disproportionation between P(IBOMA) macro-radicals and SG1 nitroxide.

In order to produce IBOMA-rich polymers by SG1-mediated NMP, the controlling co-monomer approach, developed by Charleux and co-workers³⁹⁻⁴¹, was tried where the addition of a small concentration of a co-monomer exhibiting a much lower activation-deactivation equilibrium constant K with respect to the methacrylate enhances the control of the polymerization. It was herein decided to use *My* as a potential controlling co-monomer although its individual K has not been reported. 10-20 mol% of *My* had a marked impact on the outcome of *My*/GMA NMP initiated by NHS-BB in bulk. It gave a linear evolution of M_n with monomer conversion together with $\mathcal{D} \leq 1.52$ up to almost quantitative overall conversion⁴⁹. Previously, 10-20 mol% of isoprene, another conjugated 1,3-diene, allowed the well-controlled bulk NMP of *tert*-butyl acrylate and GMA¹⁸. In the present study, the addition of 10 mol% of *My* (experiment *My*/IBOMA-10, Table 1) into the IBOMA feed undoubtedly slowed down the reaction even though the features of a controlled system were only partially observed due to the upward curvature of the semi-logarithmic plot and $\mathcal{D} = 1.51\text{-}1.60$ at $X = 4\text{-}42\%$ (Figures 3a and 3b). Expectations were fully met by performing the NMP of IBOMA in the presence of 20 mol% of *My* as a co-monomer (*My*/IBOMA-20, Table 1) with $\mathcal{D} \leq 1.39$, M_n increasing linearly with X and a quasi-linearity of $\ln((1-X)^{-1})$ versus t during the reaction with $R^2 = 0.92$ (Figures 3a, 3b and 3c). It can be assumed that the addition of *My* in the IBOMA-rich feed induced a significant decrease of the average $\langle K \rangle$ and therefore enhanced the control of the polymerization.

For $f_{My,0} = 0.30\text{-}0.90$, linear $M_{n,MHS}$ increase with overall X and narrow molecular weight distributions ($\mathcal{D} \leq 1.41$) of the P(*My-grad*-IBOMA)s were observed (Figures 3b and 3c). These results presumably illustrate the effective mediation of the stable SG1 free nitroxide, capping the propagating chains and thus shifting the equilibrium toward deactivation¹². Although termination and transfer side reactions were still present, they were likely minimized due to the high number of reversibly terminated chains (dormant P(*My-grad*-IBOMA)-(SG1) chains). Nonetheless, as $f_{My,0}$ increased, the deviations of $M_{n,MHS}$ from $M_{n,theo}$ became more significant. Even though the principle of universal calibration was applied, the MHS coefficients did not match exactly the GPC conditions used (THF, 40 °C). The likely large differences in hydrodynamic volumes of the P(*My-grad*-IBOMA)s and that of the PMMA standards that was used to calibrate the GPC may partly explain the deviations. The copolymerization with $f_{My,0} = 59\text{-}90$ had a flatter slope compared to the others (Figure 3c), where the unreliability of the GPC calibration cannot be the sole reason. Chain transfer side reactions to the monomers, creating new chains and resulting in

Table 2. Molecular characterization and *My* selectivity at the end of the experiments and kinetic data of P(*My*), P(IBOMA) and P(*My-grad*-IBOMA) polymers initiated by NHS-BB and targeting $M_{n,theo} = 30$ kg.mol⁻¹ at X = 1.0.

ID	$F_{My}^{(a)}$	$X_{My}^{(b)}$ (%)	$X_{IBOMA}^{(b)}$ (%)	$X^{(b)}$ (%)	$M_{n,MHS}^{(c)}$ (kg.mol ⁻¹)	$\bar{D}^{(c)}$	$\langle k_p \rangle \langle K \rangle^{(d)}$ (10 ⁵ s ⁻¹)	1,4- ^(e) (%)	1,2- ^(e) (%)
<i>My</i> /IBOMA-50-T120	0.52	97.1	73.5	85.3	16.1	1.48	6.4 ± 0.4	58.8	37.5
<i>My</i> /IBOMA-70-T120	0.70	98.8	82.9	94.2	13.7	1.71	12.7 ± 0.2	63.6	30.1
<i>My</i> /IBOMA-0-Tol	0	0	14.1	14.1	12.3	1.72	2.3 ± 0.8	-	-
<i>My</i> /IBOMA-0	0	0	38.4	38.4	27.1	1.75	-(f)	-	-
<i>My</i> /IBOMA-10	0.14	86.5	36.8	41.8	18.3	1.57	3.5 ± 0.2	-(g)	-(g)
<i>My</i> /IBOMA-20	0.51	81.5	11.1	25.2	8.6	1.38	0.9 ± 0.4	68.2	29.5
<i>My</i> /IBOMA-30	0.45	83.6	31.6	47.2	10.9	1.35	3.0 ± 0.2	61.9	36.0
<i>My</i> /IBOMA-40	0.64	66.2	16.6	36.4	6.5	1.36	0.9 ± 0.5	70.1	26.2
<i>My</i> /IBOMA-50	0.57	75.2	30.2	52.7	9.4	1.28	2.5 ± 0.3	65.9	30.5
<i>My</i> /IBOMA-60	0.83	77.5	15.3	52.0	7.3	1.26	2.7 ± 0.2	67.4	29.9
<i>My</i> /IBOMA-70	0.77	77.9	35.0	65.0	7.5	1.29	1.7 ± 0.6	71.3	24.9
<i>My</i> /IBOMA-80	0.81	57.8	56.0	57.5	7.4	1.41	1.8 ± 0.5	85.6	10.5
<i>My</i> /IBOMA-90	0.86	29.7	67.4	33.5	5.9	1.34	1.3 ± 0.7	86.4	8.5
<i>My</i> /IBOMA-100	1.0	39.4	0	39.4	5.0	1.32	1.4 ± 0.4	86.6	7.0

a) Molar fraction of *My* in the copolymer (F_{My}), as determined by ¹H NMR in CDCl₃ of the final dry sample (Figure S4c in Supporting Information for the spectral assignments).

b) Individual monomer conversions X_{My} and X_{IBOMA} , determined by ¹H NMR in CDCl₃. Overall conversion $X = X_{My}f_{My,0} + X_{IBOMA}f_{IBOMA,0}$.

c) $M_{n,GPC}$ and $M_{w,GPC}$ determined by GPC calibrated with PMMA standards in THF at 40 °C. $M_{n,MHS}$ obtained from $M_{n,GPC}$ and corrected using the Mark-Houwink relationship (further details in the experimental section).

d) $\langle k_p \rangle \langle K \rangle$ derived from the slopes $\langle k_p \rangle [P\bullet]$ taken from the semilogarithmic kinetic plots of $\ln((1-X)^{-1})$ versus time in the linear region generally from 0 to 60 min (0 to 20 min for *My*/IBOMA-0-Tol and 0 to 120 min for *My*/IBOMA-80, *My*/IBOMA-90 and *My*/IBOMA-100; squared linear regression coefficient = $R^2 \geq 0.91$ for every experiment). $\langle k_p \rangle \langle K \rangle$'s estimated from $\langle k_p \rangle [P\bullet]$ and $r = [SG1]_0/[NHS-BB]_0$ (equation 5). Error bars derived from the standard errors in the slope from the linear fits of $\ln((1-X)^{-1})$ versus time.

e) *My* regioselectivity determined by ¹H NMR in CDCl₃. 3,4-content% = 100 - 1,4-content% - 1,2-content% (Figure S4c in Supporting Information for further details).

f) No kinetic study led due to the very early ``caking`` (high viscosity) of the reaction medium.

g) ¹H NMR peaks could not be detected.

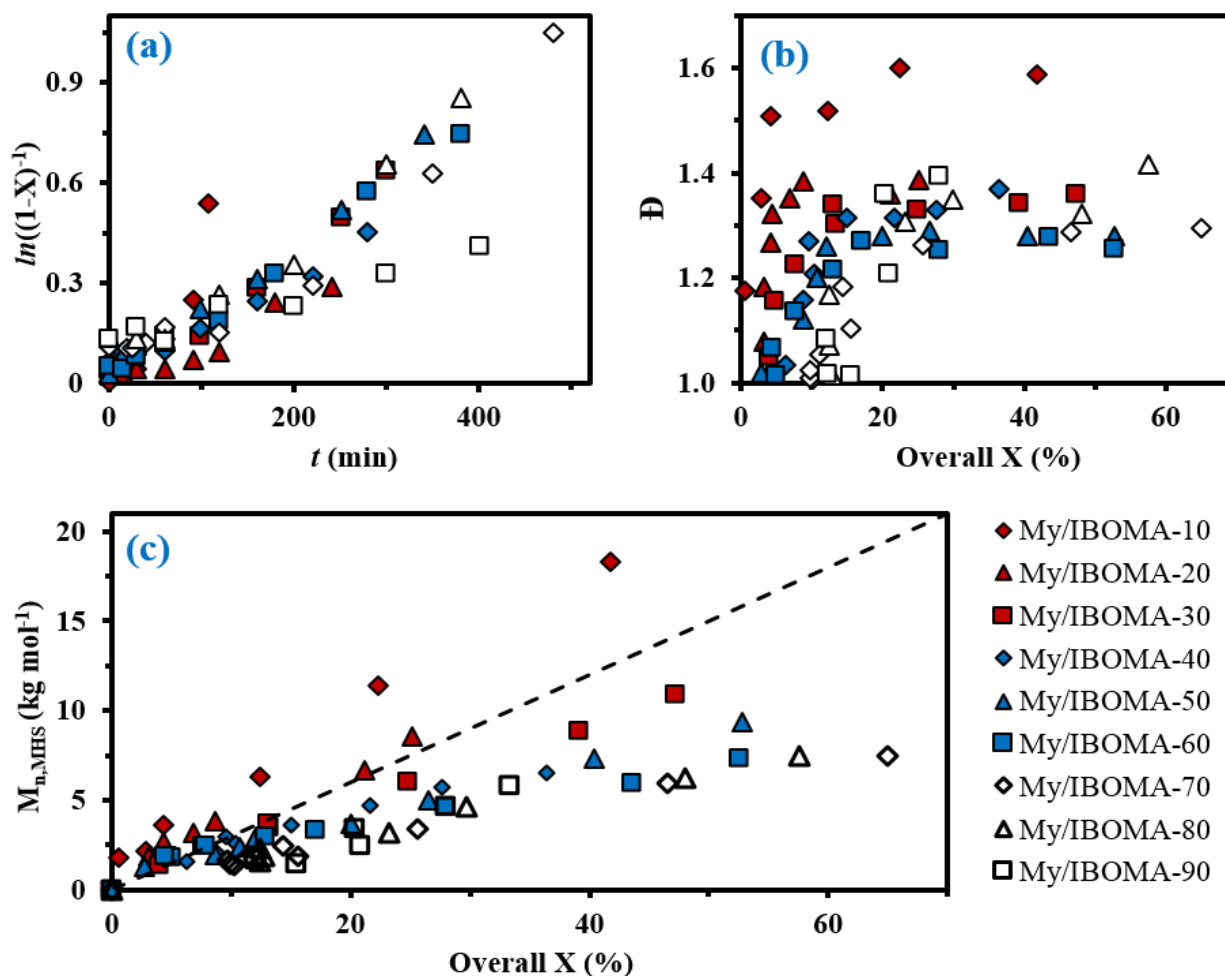


Figure 3. (a) Semi-logarithmic kinetic plots of $\ln((1-X)^{-1})$ (X = overall conversion) versus polymerization time t , (b) \bar{D} versus overall conversion X and (c) M_n determined by GPC relative to PMMA standards in THF at 40 °C, and corrected using the Mark-Houwink relationship, versus overall conversion X for the various *My/IBOMA* copolymerizations in bulk at 100 °C initiated by NHS-BB. The dashed line indicates the theoretical M_n versus overall conversion based on the monomer to initiator ratio ($M_{n,theo} \sim 30 \text{ kg}\cdot\text{mol}^{-1}$ at $X = 100\%$ for every experiment). All experimental ID and characterization of experiments are listed in Table 1 and Table 2. The same legend at the bottom right of the figure is used for each of the three plots.

shorter average chain length, may also explain the loss of control⁶⁵. The GPC chromatograms at different polymerization times are shown in Figure 4 for the experiment *My/IBOMA-50*. The monomodal shift of the curves to lower elution times with no major tails confirmed the well-controlled NMP of this monomer

pair. As reported previously²⁸, a minor peak, corresponding to high M_n polymers, was detectable mostly at the commencement of the copolymerization (20-25 min, Figure 4), presumably due to *My* auto-initiation⁶⁶.

Attention can also be paid to the kinetic plots of $\ln((1-X)^{-1})$ versus reaction time t (Figure 3a). For $f_{My,0} = 0.10-0.81$, all copolymerizations obeyed first order kinetics as described by Equation 3 and generated good fits to linear kinetic plots (squared linear regression coefficient $R^2 \geq 0.94$ for the whole experiments).

$$\ln([M]_0/[M]_t) = \ln([M]_0/([M]_0(1-X))) = \ln((1-X)^{-1}) = \langle k_p \rangle [P\bullet] \text{time} \quad (3)$$

In Equation 3, $[M]_0$ and $[M]_t$ are the concentrations of monomer at time zero and subsequent later time t , respectively, $\langle k_p \rangle$ is the average propagation rate constant and $[P\bullet]$ is the propagating radical concentration. Marked upward curvatures (Figure 3a) can be seen for experiments *My*/IBOMA-10 and *My*/IBOMA-20 having an initial feed rich in IBOMA ($f_{IBOMA,0} = 0.80-0.90$). It suggests an increase in $[P\bullet]$, which can be explained by the contribution of the likely high individual K of IBOMA, resulting from slow recombination of nitroxides and poly(methacrylate) radicals (decrease in the concentration of dormant chains) and leading to a high $[P\bullet]$. $\langle k_p \rangle [P\bullet]$ values were determined from the slopes of the semi-logarithmic plots of conversion versus time (figure 3a) in the linear regions where $[P\bullet]$ is expected to remain relatively constant (See Table 2, caption d). These slopes can be related to the equilibrium between the dormant and the active chains as shown in Equation 4.

$$K = ([P\bullet][SG1\bullet]) / [P-SG1] \quad (4)$$

where $[SG1\bullet]$ and $[P-SG1]$ are the concentrations of free nitroxide and dormant alkoxyamine terminated polymer, respectively. At the early stages of the copolymerization, it can be hypothesized that $[P-SG1] = [NHS-BB]_0$ (one initiating moiety generates a dormant chain) as well as $[SG1\bullet]_0 = [SG1\bullet]$ (large initial amount of free nitroxide being relatively constant in the course of the reaction). Equation 4 can therefore be rewritten in terms of $r = [SG1]_0/[NHS-BB]_0$.

$$\langle k_p \rangle \langle K \rangle \approx (\langle k_p \rangle [P\bullet][SG1]_0 / [NHS-BB]_0) = \langle k_p \rangle [P\bullet] r \quad (5)$$

Initially, we expected significant differences in $\langle k_p \rangle \langle K \rangle$ values between *My*-rich and IBOMA-rich initial feeds. Indeed, even though no kinetic constants for *My* are reported yet, $k_{p,I} = 125 \pm 30 \text{ L}\cdot\text{mol}^{-1}\cdot\text{s}^{-1}$ for the radical polymerization of isoprene, another similar conjugated 1,3-diene, initiated by di-*tert*-butyl peroxide at 5 °C, was reported⁶⁷. Comparatively, $k_{p,IBOMA} \sim 280 \text{ L}\cdot\text{mol}^{-1}\cdot\text{s}^{-1}$ at 5 °C can be estimated from the study led by Beuermann and coworkers using the pulsed-laser polymerization-GPC technique⁶⁸. IBOMA and *My* homopolymerizations performed herein (*My*/IBOMA-0 and *My*/IBOMA-100, Table 1)

confirmed the kinetic singularity of these two monomers polymerized by NMP. While a quasi-spontaneous polymerization was performed when an IBOMA solution was heated at 100 °C in the presence of NHS-BB, *My* polymerized slowly under identical experimental conditions and this reaction exhibited $k_pK = (1.4 \pm 0.4) 10^{-5} \text{ s}^{-1}$ (Table 2) consistent with the kinetic values reported as regards the NMP of dienes^{28,26}. Very interestingly, $\langle k_p \rangle \langle K \rangle$ was on average $(2.03 \pm 0.94) 10^{-5} \text{ s}^{-1}$ for the NMP of *My* with IBOMA with $f_{\text{IBOMA},0} = 0.10\text{-}0.90$ (Table 2), which was substantially close to the $\langle k_p \rangle \langle K \rangle$ value of the NMP of *My*. Accordingly, it can be assumed that the copolymerization kinetics was largely governed by the *My* kinetics, even when the initial mixture was rich in IBOMA. This behavior is illustrated in Figure 3a where all curves almost overlap regardless $f_{\text{IBOMA},0}$.

The molar fractions of 1,4-, 1,2- and 3,4-P(*My*) additions in the *My*/IBOMA copolymers were determined by ¹H NMR (Figure S4c in Supporting Information for the assignments). Interestingly, while the experiment *My*/IBOMA-100 led to a P(*My*) homopolymer rich in 1,4-content (86.6 mol%, Table 2), the fraction of 1,2-motif in the copolymers markedly increased when IBOMA-rich feeds were used (~ 30 mol% of 1,2-content for $f_{\text{IBOMA},0} = 0.41\text{-}0.80$). A very similar trend was observed for the systems *My*/GMA and *My*/*tert*-butyl acrylate copolymerized under the same conditions at 120 °C and 115 °C respectively⁴⁹. Therefore, it must be caused by the presence of a methacrylate radical as a terminal unit, which might have altered the steric and/or the electronic environment of the active end of the propagating species.

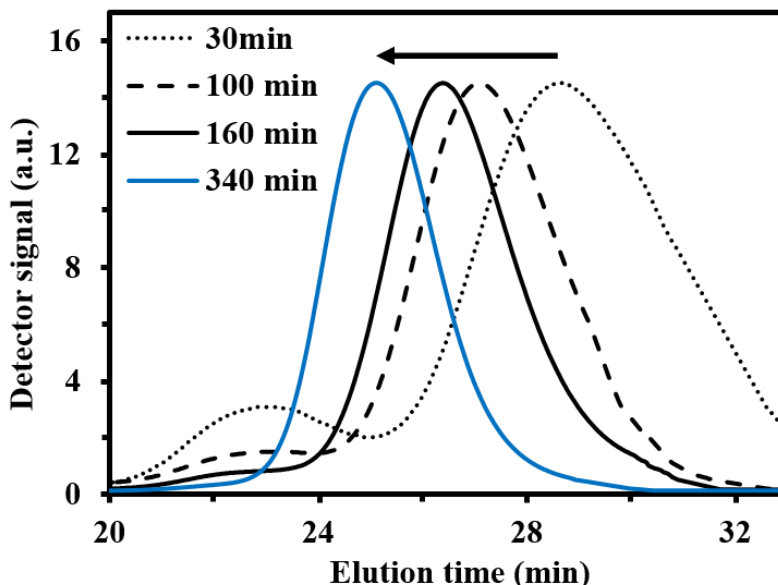


Figure 4. Normalized GPC traces of P(*My-grad-IBOMA*) with $f_{\text{My},0} = 0.50$, initiated by NHS-BB at 100 °C in bulk targeting $M_{n,\text{theo}} = 30 \text{ kg.mol}^{-1}$ at $X = 100\%$ (experiment *My*/IBOMA-50).

■ Glass transition and decomposition temperatures of P(*My-grad-IBOMA*).

Differential scanning calorimetry (DSC, see experimental section) was used to evaluate the nature and breadth of the gradient copolymer P(*My-grad-IBOMA*) glass transitions. Attention was first paid to the glass transition temperatures (T_g s) of the respective homopolymers, P(*My*) and P(*IBOMA*). The T_g of NMP-based P(*My*) was previously estimated at $-77.0\text{ }^\circ\text{C}$ ²⁸, highlighting its elastomeric nature. $T_{g,P(\text{IBOMA})} = 171\text{--}177\text{ }^\circ\text{C}$ was measured via the DSC curves of dry P(*IBOMA*)s from experiments *My/IBOMA-0* and *My/IBOMA-0-Tol*, performed in bulk and in 50 wt% toluene, respectively. This elevated T_g is explained by the limited P(*IBOMA*) segment flexibility caused by the steric hindrance of the bulky isobornyl group. Relying on previous studies^{37,38,69}, the relatively low T_g s observed herein for these rigid blocks suggest that P(*IBOMA*)s rich in isotactic triads ($> 50\text{ mol}\%$) were produced. Indeed, Yu *et al.* notably showed that syndiotactic P(*IBOMA*) ($> 50\text{ mol}\%$) exhibited a higher $T_g = 195\text{--}206\text{ }^\circ\text{C}$ ³⁸.

The glass transition behavior of P(*My-grad-IBOMA*) copolymer with cumulative *IBOMA* mole fractions ranging from 0.10 to 0.96 was also characterized using DSC heat curves (Figure S6c, Supporting Information). T_g versus *IBOMA* composition plot is given in Figure 5. A trend curve was included, which was obtained by fitting the Gordon-Taylor equation⁷⁰ (Equation 6) to the experimental data.

$$T_g = (T_{g,P(\text{My})} w_{\text{My}} + K T_{g,P(\text{IBOMA})} w_{\text{IBOMA}}) / (w_{\text{My}} + K w_{\text{IBOMA}}) \quad (6)$$

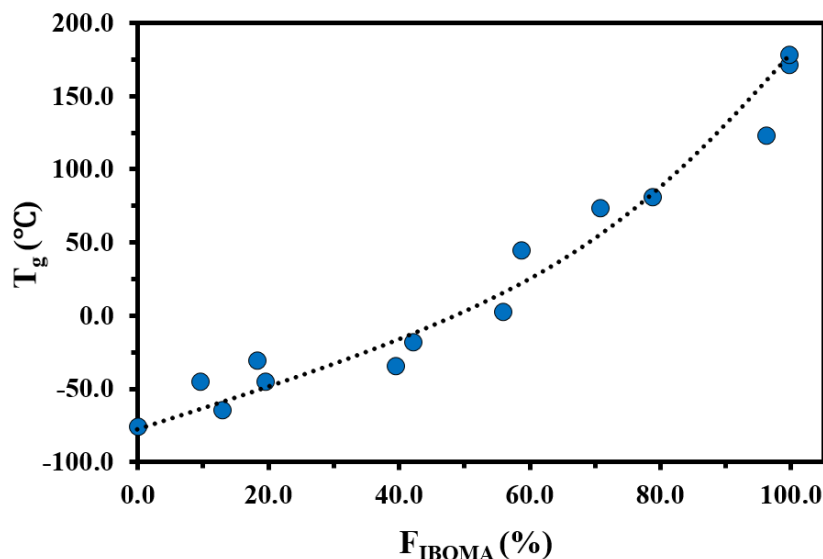


Figure 5. F_{IBOMA} effects on T_g in P(*My-grad-IBOMA*) gradient copolymers. The DSC traces can be found in the Supporting Information, Figure S6c. $T_g = -77.0\text{ }^\circ\text{C}$ for $F_{\text{IBOMA}} = 0$ was determined previously²⁸. The block dotted line represents the experimental data fitted to the Gordon-Taylor Equation.

where w_{My} and w_{IBOMA} are the weight fractions and $T_{g,P(My)}$ and $T_{g,P(IBOMA)}$ the glass transition temperatures of the respective homopolymers. T_g corresponds to the glass transition temperature of the gradient copolymer and $K = \Delta\beta_{IBOMA} / \Delta\beta_{My}$ with $\Delta\beta_{IBOMA}$ or $\Delta\beta_{My}$ being the difference between the expansion coefficients of the rubbery and glassy states of P(IBOMA) or P(My). This theory is based on two basic assumptions: the volume additivity (ideal volume of mixing) and a linear change in volume with temperature. With 95% confidence bounds, $K = 0.322 \pm 0.090$ ($R^2 = 0.94$) was determined via the use of a non-linear least-squares fitting of the data and indicated the larger expansivity of My units in the rubbery state than that of IBOMA units. A similar trend was reported for the system My/GMA ($K = 0.186 \pm 0.036$)⁴⁹, highlighting the plasticizing nature of P(My). The Gordon-Taylor fitting approach yielded a good representation of the experimental T_g data (Figure 5). A slight concave T_g versus IBOMA composition curve was obtained, pointing out deviations from an ideal mixing. As expected, P(My-grad-IBOMA)'s T_g increased from -65 to 123 °C with F_{IBOMA} ranging from 9.8 to 96.2 mol%. Interestingly, the presence of a minor fraction of My units considerably reduced the T_g of the copolymer ($T_g = 81$ °C for $F_{My} = 0.21$ in comparison to $T_{g,P(IBOMA)} \sim 174$ °C) while a moderate increase of the T_g was observed for a My-rich P(My-grad-IBOMA) containing a minority of IBOMA units ($T_g = -46$ °C for $F_{IBOMA} = 0.20$ and $T_{g,P(My)} = -77$ °C). Two explanations can be suggested: the long C6/C8 pendant groups of My units generating significant free volume; the gradient nature of the copolymer with a largely higher reactivity for My, resulting in the formation of short P(My) segments (elastomeric “knots”) and the isolation of the isobornyl rings.

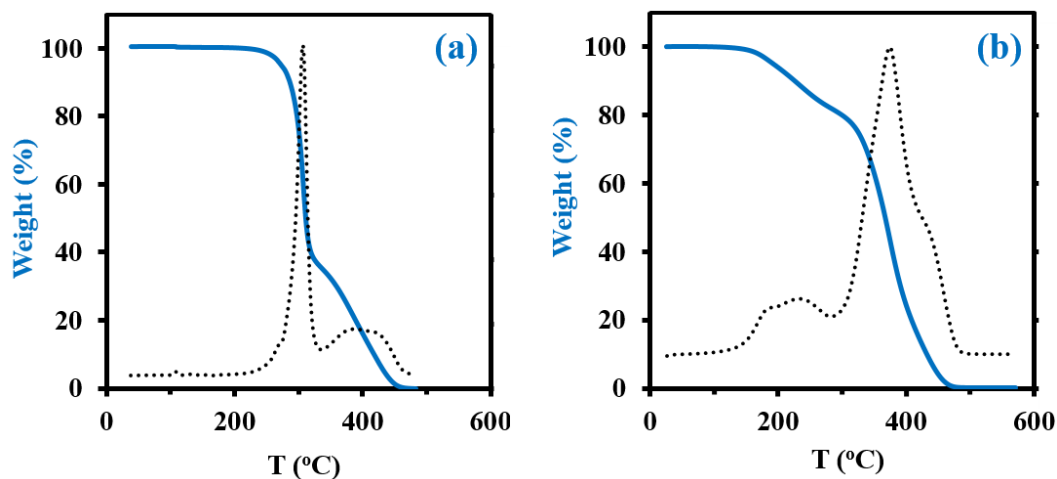


Figure 6. TGA traces (N_2 atmosphere, 10 °C.min⁻¹) of final gradient copolymers **a)** My/IBOMA-20 and **b)** My/IBOMA-80, previously precipitated in excess methanol and dried under vacuum at 50 °C. Sample weight versus temperature is represented by the solid blue line whereas the dotted line represents the derivative of weight relative to the temperature versus temperature in order to determine precisely the temperature at which weight loss is most apparent ($T_{dec,max}$).

Thermogravimetric analysis (TGA, experimental section) has been applied to decomposition study on the final dry samples taken from experiments *My*/IBOMA-20 and *My*/IBOMA-80, exhibiting 51 and 81 mol% of *My* units respectively (Table 2). Figure 6 represents the thermal decomposition curve of both gradient copolymers. Interestingly, the synthesized polymers exhibited markedly two step degradation pattern. A first weight loss was observed from 145 to 305 °C with a $T_{\text{dec,max}}$ of 242 °C (temperature at which the weight loss is most apparent, maximum of the derivative curve) for the sample richer in *My* (*My*/IBOMA-80, Figure 6b) and from 205 to 315 °C with $T_{\text{dec,max}} = 307$ °C for *My*/IBOMA-20 sample (Figure 6a). This early degradation peak was likely due to the loss of the side chains by cleavage of O-isobornyl bond, releasing camphene as a main product, as reported by Matsumoto and coworkers³⁷. This first weight loss was proportional to the IBOMA fraction possessed by the samples: while about 40% of mass loss was measured for *My*/IBOMA-20 with $F_{\text{IBOMA}} = 0.49$, only about 22 wt% of *My*/IBOMA-80, exhibiting $F_{\text{IBOMA}} = 0.19$, was lost (Figure 6). This observation supports the contribution of the IBOMA units to the premature P(*My-grad*-IBOMA) thermal decomposition. The second degradation step is similar for both samples, starting at 305-315 °C with $T_{\text{dec,max}} = 370$ -380 °C and decomposing totally the copolymers at about 450 °C (Figure 6), which could be mostly caused by the scission reactions of the main chain (depolymerization) resulting in the formation of monomer and oligomer radicals. We previously reported the decomposition behavior of SG1-mediated P(*My*), from 290 to 485 °C ($T_{\text{dec,max}} = 385$ °C)²⁸, matching closely the second degradation step of the two P(*My-grad*-IBOMA)s characterized.

■ Active feature of NMP-based P(*My-grad*-IBOMA).

Ideally, a majority of the P(*My-grad*-IBOMA) chain ends synthesized by NMP should possess the SG1 moiety. Indeed, the recombination of the propagating macro-radical with the controlling nitroxide should lead to a very low $[P\cdot]$, limiting the self-termination reaction. Afterwards, the final SG1-terminated P(*My-grad*-IBOMA) would be able to be re-activated via the thermal homolytic decomposition of this dormant species into the initiating macro-radical and the SG1 persistent radical. Two strategies were herein adopted to know if P(*My-grad*-IBOMA) chains were effectively capped by a SG1 group: ³¹P NMR analysis (see experimental section) allowing the detection of the phosphorus atom of the nitroxide group^{71,72}; IBOMA and/or *My* chain-extension from P(*My-grad*-IBOMA) macro-initiator by the same nitroxide mediated mechanism. Two samples were studied: *My*/IBOMA-82 and *My*/IBOMA-44 exhibiting respectively 82 and 44 mol% of *My* (Table 3A).

³¹P NMR was first performed to evaluate the living fraction (LF) of these two gradient copolymers initiated by NHS-BB alkoxyamine (Figure S5c in Supporting Information for the spectra). The proportion of chains containing a SG1 end group was 74 ± 9 mol% and 69 ± 3 mol% for *My*/IBOMA-44 and

Table 3. Chain-extensions of (A) P(*My-grad*-IBOMA) macroinitiators (MI) with (B) IBOMA and/or *My* in 50 wt% toluene and (C) molecular characterization of the resulting chain-extended products.

A. P(<i>My-grad</i> -IBOMA) macroinitiator ^(a)							
ID	$f_{My,0}$	$F_{My,1}$	LF ^(b) (%)	X ₁ (%)	M _{n,MHS,1} (kg.mol ⁻¹)	M _{n,theo,X1} ^(c) (kg.mol ⁻¹)	Đ ₁
<i>My</i> /IBOMA-44	0.30	0.44	74 ± 9	39.1	8.8	11.7	1.32
<i>My</i> /IBOMA-82	0.79	0.82	69 ± 3	64.2	13.6	19.3	1.51
B. Formulation of chain-extension							
ID	[MI] ₀ (M)	[<i>My</i>] ₀ (M)	[IBOMA] ₀ (M)	[Toluene] ₀ (M)	M _{n,theo} ^(d) (kg.mol ⁻¹)	T (°C)	<i>t</i> (min)
<i>My</i> /IBOMA-44- <i>My</i>	0.004	2.414	0	3.859	91.0	115	390
<i>My</i> /IBOMA-82-IBOMA/ <i>My</i>	0.004	0.147	1.857	5.216	122.0	105	210
C. Chain-extended diblock copolymer ^(a)							
ID	X ₂ (%)	F _{<i>My</i>,2}	M _{n,MHS,2} (kg.mol ⁻¹)	M _{n,theo,X2} ^(e) (kg.mol ⁻¹)	Đ ₂		
<i>My</i> /IBOMA-44- <i>My</i>	39.5	0.93	30.1	41.3	1.65		
<i>My</i> /IBOMA-82-IBOMA/ <i>My</i>	19.1	0.49	23.2	34.3	1.61		

a) The index “1” is associated to the characteristics of the P(*My-grad*-IBOMA) macroinitiators (MI) whereas the index “2” refers to the features of the whole chain-extended diblock copolymer (MI + P(*My*) or P(IBOMA-*co-My*) segment added).

b) Living molar fraction of MI chains capped by a SG1 group, measured by ³¹P NMR (Figure S5c in Supporting Information for the spectra). Standard deviation derived from the difference in macroinitiator M_n value between M_{n,GPC} and M_{n,MHS}.

c) Predicted M_{n,MHS,1} at X₁ measured experimentally and calculated as follows: M_{n,theo,X1} = (X₁/100)M_{n,theo,1} with M_{n,theo,1} = 30 kg.mol⁻¹ at X = 100%.

d) Targeted number-average molecular weight of the whole chain-extended diblock copolymer (MI block + extended block) at X = 100%.

e) Predicted M_{n,MHS,2} of the whole chain-extended diblock copolymer (MI block + second block added) at X₂, measured experimentally, and calculated as follows: M_{n,theo,X2} = (X₂/100)(M_{n,theo,2} - M_{n,MHS,1}) + M_{n,MHS,1} (= Predicted M_n of the second block added at X₂ + experimental M_{n,MHS} of MI).

My/IBOMA-82 copolymers, respectively (Table 3A). It is interesting to note that about two thirds of the *My*-rich *My*/IBOMA-82 chains remained SG1-capped despite a relatively high overall conversion (X₁ = 64.2%). It can thus be deduced that about 30% of these chains underwent irreversible terminations, becoming more prevalent at high conversion, resulting notably in a relatively broad molecular weight

distribution ($D_1 = 1.51$, Table 3A). A similar LF was measured for the IBOMA-rich gradient copolymer exhibiting a lower overall conversion ($X_1 = 39.1\%$). A moderate conversion was targeted for the synthesis of this macro-initiator since an IBOMA-rich ($f_{\text{IBOMA},0} = 0.70$) feed was polymerized, where disproportionation side reactions likely occur. It can be assumed that the synthesis of a high conversion P(*My-grad-IBOMA*) rich in IBOMA would have a relatively low LF, caused by the occurrence of terminations by H-transfer notably.

To further examine the capacity of these samples to re-initiate and produce diblock copolymers, two chain-extension experiments were done using *My/IBOMA-44* and *My/IBOMA-82* as macroinitiators (Table 3A). The reaction conditions and results of the chain-extensions are given in Tables 3B and 3C respectively. *My/IBOMA-44* macroinitiator ($F_{\text{IBOMA},1} = 0.56$, $M_{n,\text{MHS},1} = 8.8 \text{ kg}\cdot\text{mol}^{-1}$) was cleanly chain-extended at 115 °C in toluene with *My* to obtain a P[(*My-grad-IBOMA*)-*b-My*] diblock copolymer ($F_{\text{IBOMA},2} = 0.07$, $M_{n,\text{MHS},2} = 30.1 \text{ kg}\cdot\text{mol}^{-1}$, Table 3C) containing predominantly *My* units. The dispersity of this chain-extended product ($D_2 = 1.65$) was higher than that of the parent macro-initiator ($D_1 = 1.32$), which suggests that termination occurred during the reaction and/or some macroinitiator was not initiated. This latter assumption can be supported by the previous quantitative spectroscopic analysis, indicating that about 25 mol% of *My/IBOMA-44* was not terminated by SG1 (Table 3A), as well as the GPC traces of the chain-extension experiment (Figure 7b) showing that the tails of the final chain-extended copolymer overlapped to some degree with the associated macroinitiator trace. The asymmetrical last GPC trace at 390 min may also indicate the occurrence of irreversible terminations throughout the chain-extension, which generate “dead” species having lower M_n ($\sim 15\text{-}25 \text{ kg}\cdot\text{mol}^{-1}$). Generally, this successful *My* chain-extension from IBOMA-rich P(*My-grad-IBOMA*) copolymer prompted us to investigate the reversed situation where a *My*-rich macroinitiator can be re-activated to add an IBOMA-rich segment. With a fresh IBOMA/*My* mixture (93 mol% of purified IBOMA), *My/IBOMA-82* ($F_{\text{My},1} = 0.82$, $M_{n,\text{MHS},1} = 13.6 \text{ kg}\cdot\text{mol}^{-1}$, $D_1 = 1.51$, Table 3A) was extended at 105 °C in 50 wt% toluene (Table 3B). Due to the beneficial kinetic effects observed of the addition of 10-20 mol% of *My* over the control of the SG1-based NMP of IBOMA (Figure 3), 7 mol% of the acyclic monoterperene was initially introduced in the feed. After 210 min, the resulting chain-extended diblock exhibited $M_{n,\text{MHS},2} = 23.2 \text{ kg}\cdot\text{mol}^{-1}$, $D_2 = 1.61$ and the overall *My* molar composition was decreased from 82 to 49 mol% (Table 3C). Similarly to the first chain-extension, the GPC trace of the chain-extended product retained generally its mono-modal nature and had a clear shift to the left (Figure 7a), indicating a high-level of chain-end fidelity of the original macroinitiator.

These satisfactory results naturally paved the way to the preparation by NMP of well-defined 1,3-diene-based triblock copolymers composed of a flexible and bio-sourced P(*My*) mid-segment³² and two rigid P(IBOMA) outer segments, the latter coming from partially bio-based raw material source^{73,74}.

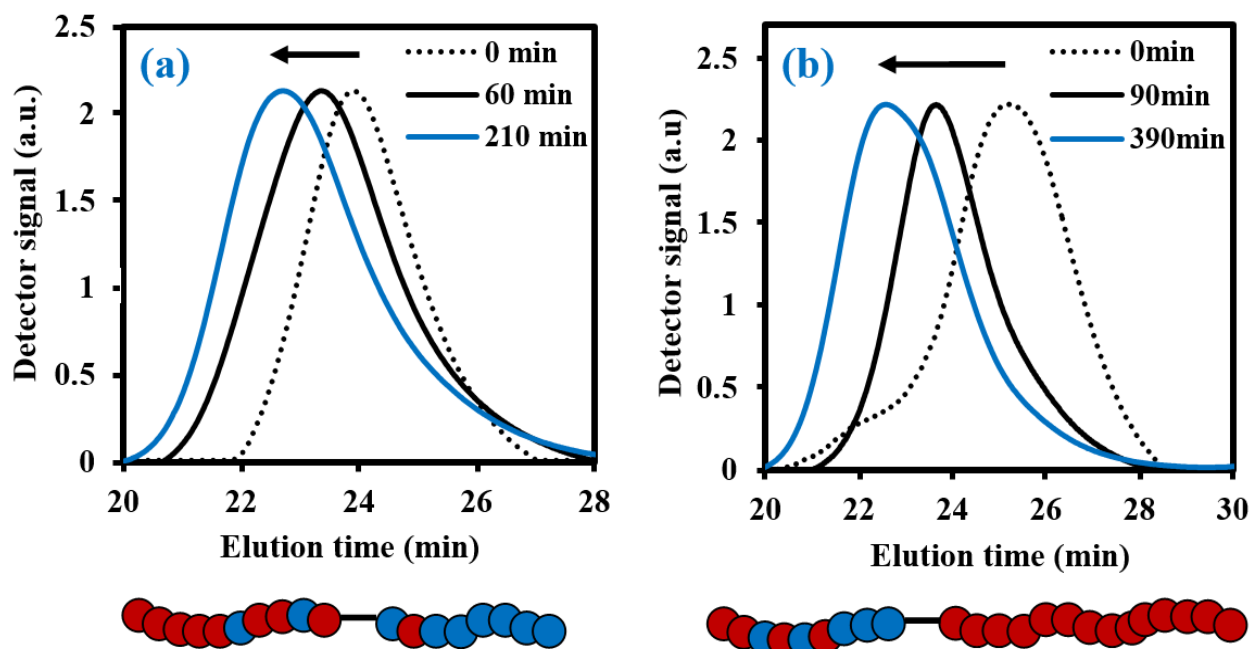


Figure 7. Normalized GPC traces for the chain-extensions of **a)** *My*/IBOMA-82 with a IBOMA/*My* (93/7 mol%) mixture (experiment *My*/IBOMA-82-IBOMA/*My*) and **b)** *My*/IBOMA-44 with *My* (experiment *My*/IBOMA-44-*My*) at T = 105-115 °C in 50 wt% toluene. Schematic representations of the final chain-extended copolymers, where solid red and blue circles represent *My* and IBOMA units respectively, are given below the GPC chromatograms.

3.4.2. Isobornyl methacrylate - β -myrcene - isobornyl methacrylate triblock copolymers by NMP

The synthesis by SG1-mediated NMP of triblock copolymers consisting of a soft P(*My*) middle block and two hard blocks, containing mostly IBOMA units, was aimed in this second part. A two-step approach was applied for preparing these triblock copolymers: (1) NMP of *My* initiated by the PEB-(SG1)₂ difunctional initiator (telechelic poly(ethylene-*stat*-butylene) copolymer terminated with SG1 groups)⁴²; (2) Chain-extension of the P(*My*)-(SG1)₂ macroinitiator with a IBOMA/Co mixture (Co = *My* or S comonomer, ~ 8-9 mol% relative to IBOMA). The synthesis route is depicted in Figure 1b. A triblock molecular architecture was targeted so that both ends of the rubbery mid-segment are theoretically anchored to a glassy domain⁷⁵, mimicking thus the traditional micro-structure of styrene block copolymers such as SIS or SBS (I = isoprene, B = butadiene).

■ Optimized synthesis of P(My)-(SG1)₂.

First of all, the preparation of a P(My) segment exhibiting a relatively high M_n and able subsequently to re-initiate a fresh batch of monomer(s) at each chain end was desired. In order to have sufficient mechanical properties, the targeted final triblock must have an entangled elastomeric phase, the physical chain entanglements must be contributing mainly to the network density and to the stress at small elongations⁷⁶. P(My) entanglement molecular weight ($M_{e,P(My)} = 22\text{-}31 \text{ kg}\cdot\text{mol}^{-1}$)⁷⁷ is significantly higher than that of comparable poly(diene)s such as poly(isoprene) PI ($M_{e,PI} = 4\text{-}6 \text{ kg}\cdot\text{mol}^{-1}$)⁷⁷ or poly(butadiene) PB ($M_{e,PB} = 2\text{-}4 \text{ kg}\cdot\text{mol}^{-1}$)⁷⁷. Accordingly, $M_n > 40 \text{ kg}\cdot\text{mol}^{-1}$ for P(My)-(SG1)₂ was desired to ensure a minimal entanglement density.

PEB-(SG1)₂ dialkoxyamine macroinitiator ($M_{n,MHS} = 5.7 \text{ kg}\cdot\text{mol}^{-1}$, $\mathcal{D} = 1.17$) was first produced, according to the method reported by Lessard *et al.*⁴². ¹H NMR of the final product revealed that about 84 mol% of the chain ends were capped by a SG1 unit. It can thus be deduced that a minor fraction of the synthesized macroinitiator consisted of monofunctional alkoxyamine terminated by SG1 only at one chain end and “dead” PEB chains. To know the optimal conditions for making high average chain length P(My) in a controlled manner, NMP of My initiated by various concentrations of PEB-(SG1)₂ at 120 °C in bulk was then studied. Four different theoretical M_n were thus targeted at quantitative conversion, namely 79.1, 105.0, 137.2 and 174.0 $\text{kg}\cdot\text{mol}^{-1}$ (Table S2c, Supporting Information), and kinetic studies were led (Figure S7c, Supporting Information) to assess the level of control. As $M_{n,theo}$ increased, higher dispersity values and greater deviations of $M_{n,MHS}$ from the theoretical molar masses were observed (Figures S7b and S7c), confirming likely the greater presence of irreversible terminations and chain transfer reactions to My and P(My) with $[My]_0$. Nonetheless, lowering the dialkoxyamine concentration resulted in the synthesis of higher $M_{n,MHS}$ P(My)s. Particularly, when targeting $M_{n,theo} = 137.2 \text{ kg}\cdot\text{mol}^{-1}$ at $X_{My} = 100\%$ (experiment My-137), a polyterpene exhibiting $M_{n,MHS} = 49.5 \text{ kg}\cdot\text{mol}^{-1}$ and $\mathcal{D} = 1.52$ was obtained at 51% conversion (Figures S7b and S7c), which consisted of the most satisfactory balance between a relatively high M_n and a moderate dispersity. It was then attempted to produce longer P(My) chains with a relatively narrow molecular weight distribution by using a low concentration of the dialkoxyamine initiator [PEB-(SG1)₂] ($M_{n,theo} = 169\text{-}173 \text{ kg}\cdot\text{mol}^{-1}$ at $X = 1.0$) combined with additional free SG1 nitroxide (9-18 mol% with respect to the initiator, experiments My-173_{SG1,9} and My-169_{SG1,18}, Table S2). An improved control of the NMP when using a slight excess of this potent nitroxide could have been expected since the dormant state should be favored (lower concentration of propagating macro-radicals, reduction of the overall polymerization rate)⁷⁸⁻⁸⁰. Despite apparent rate constants somewhat lower as $[SG1^*]_0$ increased (Figure S8a), similar \mathcal{D} versus X and $M_{n,MHS}$ versus X trends were determined (Figures S8b and S8c) indicating the ineffectiveness of adding SG1 free radical to the reaction mixture. This observation echoes a previous study

showing that the addition of 4.9-11.7 mol% of the SG1 mediator with respect to the initiator did not enhance the NMP of M_y at 120 °C in bulk initiated by NHS-BB²⁸. A last experiment in 50 wt% toluene, without extra SG1, was led, predicting $M_{n,theo} \sim 170 \text{ kg}\cdot\text{mol}^{-1}$ again (experiment M_y -170_{Tol}, Table S2). The use of a solvent was thought to help, as seen by the increase in viscosity at $X_{M_y} > 30\%$, when performing this reaction in bulk, which might account for the occurrence of diffusional limitations⁸¹, bringing about a loss of control. Interestingly, while the polymerization in toluene was slower (Figure S8a), similar molecular characteristics of the growing $P(M_y)$ were obtained compared to the previous mass polymerizations (Figures S8b and S8c). Higher \bar{D} values were even observed (Figure S8b), which may be assigned to chain-transfer side reactions to toluene^{82,83}.

Consequently, the $P(M_y)$ segment was prepared via the PEB-(SG1)₂-initiated NMP of M_y at 120 °C in bulk for 280-400 min ($X_{M_y} \sim 40$ -50%) targeting $M_{n,theo} \sim 140 \text{ kg}\cdot\text{mol}^{-1}$ and without any additional free nitroxide. Two 1,4-rich $P(M_y)$ s (experiments M_y -35 and M_y -52, Table 4A), exhibiting $M_{n,MHS} = 35$ -52 $\text{kg}\cdot\text{mol}^{-1}$ and acceptable $\bar{D} = 1.45$ -1.53, were synthesized this way. Attention was now shifted to the capacity of these $P(M_y)$ segments, ideally capped by two SG1 units, to form triblock copolymer with a mixture of IBOMA containing a minor fraction of co-monomer.

■ IBOMA/Co chain-extension from $P(M_y)$ -(SG1)₂.

IBOMA/ M_y chain-extension (7.8 mol% of M_y used as a co-monomer) from M_y -35 macroinitiator was first performed at 115 °C in toluene for 90 min (Table 4B). The shifts in the GPC traces, seen in Figure S9c (Supporting Information), clearly show the shift in elution time demonstrating the increase in M_n with time. The chain-extended product M_y -35-IBOMA/ M_y had an increase in M_n from 35.2 to 51.3 $\text{kg}\cdot\text{mol}^{-1}$ with a broadening of the molecular weight distribution going from 1.45 to 1.91. The monomodal nature of the GPC chromatograms confirmed that the M_y -35 chain ends were reversibly terminated in majority. Based on ¹H NMR analysis, the final triblock copolymer exhibited an overall $F_{IBOMA} = 0.26$ (Table 4C). More specifically, each chain-extended block was composed of a large fraction of IBOMA units (91 mol%) and a minority of M_y (9 mol%).

Afterwards, a second triblock copolymer, with a higher overall M_n as well as harder outer hard blocks, was targeted. To that end, M_y -52 macroinitiator ($M_{n,MHS,M_y} = 51.7 \text{ kg}\cdot\text{mol}^{-1}$, $\bar{D} = 1.53$, Table 4A) was reacted with a IBOMA/S mixture (8.7 mol% of S used as a controlling co-monomer, as previously reported^{23,39,84}) for 3 h in 50 wt% toluene at 115 °C (Table 4B). The resulting product M_y -52-IBOMA/S had $M_{n,MHS,CE} = 78.1 \text{ kg}\cdot\text{mol}^{-1}$ and $\bar{D} = 2.41$. Likewise, the final chain-extended product shifted to lower elution time compared to the macroinitiator (Figure S9b). In order to increase M_y -52-IBOMA/S M_n , a fractional precipitation using the non-solvent addition method was implemented, relying on the benzene (solvent) /

methanol (non-solvent) pair. Eventually, the fractionated triblock copolymer had $M_{n,MHS} = 94.7 \text{ kg.mol}^{-1}$ and $\bar{D} = 2.23$ (Table 4C), reflecting the removal of a fraction of relatively short chains. The rigid segments were constituted of about 88 mol% of methacrylate units and 12 mol% of S, as determined by $^1\text{H NMR}$.

Table 4. Chain-extensions of (A) P(My)-(SG1)₂ macroinitiators with (B) IBOMA/My and IBOMA/S mixtures at 115 °C in 50 wt% toluene and (C) features of the resulting triblock copolymers.

A. P(My)-(SG1) ₂ ^(a)								
ID	<i>t</i> (min)	X _{My} (%)	M _{n,MHS,My} (kg.mol ⁻¹)	M _{n,theo,XMy} ^(b) (kg.mol ⁻¹)	\bar{D}_{My}	1,4 ^(c) (%)	1,2 ^(c) (%)	
<i>My-35</i>	290	33.4	35.2	47.9	1.45	91.7	3.2	
<i>My-52</i>	360	49.1	51.7	68.6	1.53	88.2	5.0	
B. Formulation of chain-extension								
ID	[P(My)-(SG1) ₂] ₀ (M)	[IBOMA] ₀ (M)	[My] ₀ (M)	[S] ₀ (M)	[Toluene] ₀ (M)	M _{n,theo,CE} ^(d) (kg.mol ⁻¹)	T (°C)	<i>t</i> (min)
<i>My-35-IBOMA/My</i>	0.004	1.681	0.142	0	4.929	133.4	115	90
<i>My-52-IBOMA/S</i>	0.003	1.546	0	0.147	4.848	171.2	115	180
C. Chain-extended triblock copolymer ^(a)								
ID	X _{CE} (%)	F _{My}	F _{IBOMA}	F _S	M _{n,MHS,CE} (kg.mol ⁻¹)	M _{n,theo,XCE} ^(e) (kg.mol ⁻¹)	\bar{D}_{CE}	
<i>My-35-IBOMA/My</i>	28.6	0.72	0.28	0	51.3	63.3	1.91	
<i>My-52-IBOMA/S</i>	59.0	0.59	0.36	0.05	94.7	122.2	2.23	

a) The indexes “My” and “CE” refer, respectively, to the final characteristics of P(My)-(SG1)₂ and the whole chain-extended triblock copolymer.

b) Predicted $M_{n,MHS,My}$ at X_{My} measured experimentally and calculated as follows: $M_{n,theo,XMy} = (X_{My}/100)M_{n,theo,My}$ ($M_{n,theo,My} = 143.4$ and $139.8 \text{ kg.mol}^{-1}$ for experiments *My-35* and *My-52*, respectively).

c) See caption e) in Table 2.

d) Targeted number-average molecular weight of the whole chain-extended triblock copolymer at $X_{CE} = 100\%$.

e) Predicted $M_{n,MHS,CE}$ of the whole chain-extended triblock copolymer at X_{CE} , measured experimentally, and calculated as follows: $M_{n,theo,XCE} = (X_{CE}/100)(M_{n,theo,CE} - M_{n,MHS,My}) + M_{n,MHS,My}$.

A high $\bar{D} = 1.91\text{-}2.23$ was measured for these final triblock copolymers, which may be mainly caused by the difficulty to control the polymerization of a methacrylic ester-rich feed ($f_{\text{IBOMA},0} \geq 0.91$), although a small amount of *My* or *S* were added to possibly decrease the average activation-deactivation equilibrium constant $\langle K \rangle$. The inactivity of a fraction of PEB-(SG1)₂ and P(*My*)-(SG1)₂ macroinitiators may also contribute to the broadening of the molecular weight distribution. Besides, the very likely presence of PEB-SG1 monofunctional chains may have resulted in the synthesis of short diblock copolymer chains, assuming a similar activity between PEB-SG1 and PEB-(SG1)₂. All these hypotheses would lead to a non-negligible population of shorter than expected chains, as observed in Figure S9c (Supporting Information) by the tails on the low molecular weight edge of the GPC chromatograms (elution time $\sim 23\text{-}25$ min).

■ Characterization of the NMP-based Co/IBOMA-*My*-IBOMA/Co triblock copolymers.

The Co/IBOMA-*My*-IBOMA/Co triblock copolymers investigated were characterized by two discrete transition regions indicative of each polymer segment type (Figure 8a). A lower T_g of about -60 °C corresponded to the transition of the P(*My*) mid-segment while a largely upper transition at around $+180$ °C was assumed to indicate the softening of the IBOMA-rich segments. The lower T_g of these triblock polymers is about 15 °C higher than that of 1,4-rich P(*My*) homopolymer ($T_{g,P(\text{My})} = -77$ °C, Figure 5), which might be due to some partial compatibility of P(*My*) and IBOMA-rich regions. It is of interest to note that the upper T_g of the synthesized triblocks is similar to that of P(IBOMA) homopolymer ($T_{g,P(\text{IBOMA})} = 171\text{-}177$ °C, Figure 5) even though the outer hard blocks contained a non-negligible fraction of *S* (12 mol%) or *My* (9 mol%) units. A decrease of the upper T_g would have been expected due to the presence of softer units in the rigid segments (IBOMA/*My* system illustrated in Figure 5). This unaffected upper T_g can result from the extended blocks composition. For the IBOMA/*My* chain-extension, it can be assumed that the majority of the *My* units reacted at the early stages of the polymerization, considering the marked preference of the $\text{---}My\cdot$ macro-radical for *My* (Figure 2). This way, a *My*-rich segment including the middle block and the beginning of the two extended blocks may have been formed as well as two quasi neat P(IBOMA) outer blocks. The same hypothesis could be made for the IBOMA/*S* chain-extension, taking the higher reactivity of *S* for this system into account ($r_S = 0.57$, $r_{\text{IBOMA}} = 0.20$ reported with benzyl peroxide at 90 °C)⁸⁵.

These DSC results suggest a two-phase system, due to the immiscibility between P(*My*) and IBOMA-rich segments. To further examine immiscibility, the solubility parameters δ were compared to estimate the tendency towards micro-phase separation. Using the group contribution method developed by Hoftyzer and Van Krevelen⁸⁶, theoretical solubility parameters for P(IBOMA) and 1,4-P(*My*) (favored regioselectivity in our case) were determined (calculations can be found in the Supporting Information). $\delta_{P(\text{My})} = 16.7 \text{ MPa}^{1/2}$ and $\delta_{P(\text{IBOMA})} = 21.8 \text{ MPa}^{1/2}$ were calculated. Such a δ difference indicates a

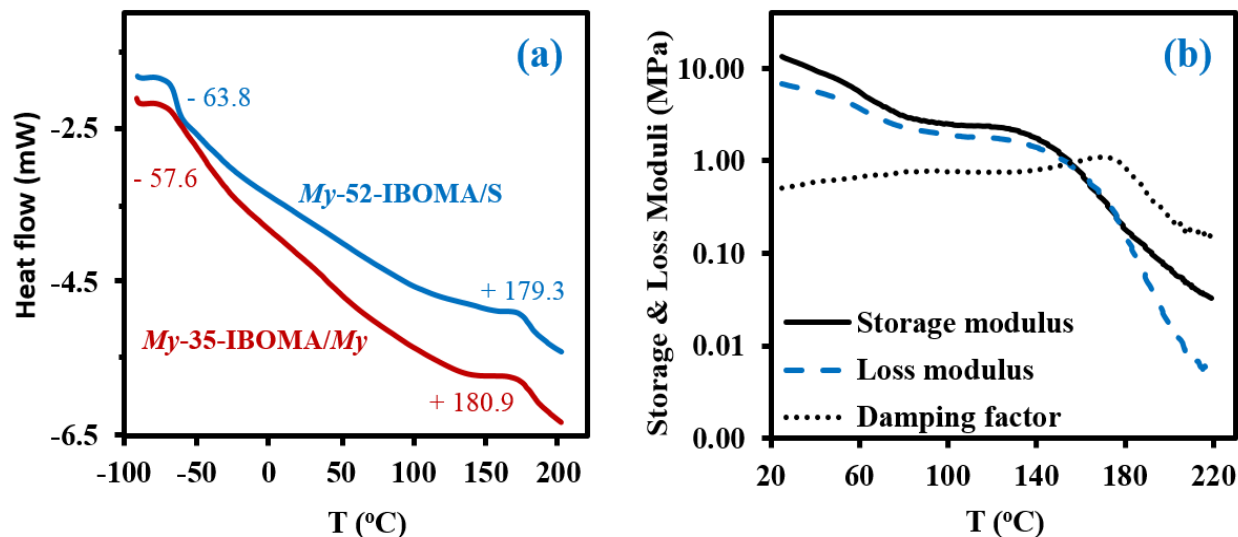


Figure 8. **a)** DSC traces (second heating run) of triblock copolymers *My-52-IBOMA/S* (blue) and *My-35-IBOMA/My* (red). The numbers near the changes in slope correspond to the T_g s determined via the inflection method. **b)** Dynamic mechanical analysis of the sample *My-52-IBOMA/S* by torsional oscillation, yielding the storage modulus, the loss modulus and the damping factor *versus* temperature (0.15 Hz, 1% strain, 5 °C.min⁻¹, N₂ atmosphere).

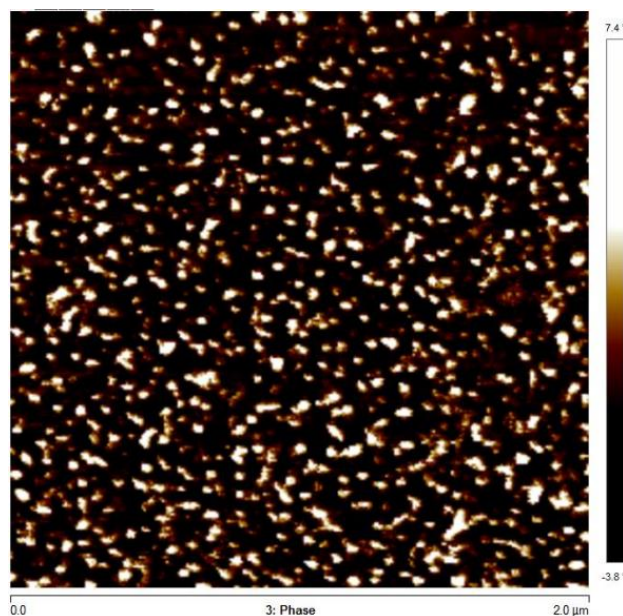


Figure 9. Atomic force microscopy (AFM, experimental section) phase image (2 μm x 2 μm) under tapping mode of operation of the surface morphology of triblock copolymer *My-35-IBOMA/My* cast film. The dark domain represents the *My* component (color-coded height scale given to the right of the image).

relatively high immiscibility between P(*My*) and P(IBOMA) segments and would suggest a strong bulk phase separation of P(*My*-*b*-IBOMA) block copolymer. Atomic force microscopy (AFM) was applied to the study of the surface morphology of *My*-35-IBOMA/*My* prepared by spin-coating a 3-4 wt% solution in chloroform. Figure 9 shows a 2 μm x 2 μm scan of the polymeric surface (two other AFM phase images of *My*-35-IBOMA/*My* in different regions are given in Supporting Information, Figure S10c). The nature of the light and dark domains was determined by quantifying the relative contribution of the light component (*ImageJ* software application, binary mode). This image contained 23-24% of light areas which is consistent with the molar fraction of P(IBOMA) in the characterized triblock ($F_{\text{IBOMA}} = 0.28$, Table 4). The light areas can thus be attributed to P(IBOMA) and the dark ones to the rubbery P(*My*) midblock material. The phase separation of the two component blocks appeared clear with the embedding of glassy P(IBOMA) aggregates (disperse phase) in the soft P(*My*) (continuous phase). A spherical or cylindrical morphology might be obtained. An in-depth analysis, using for instance small-angle X-ray scattering (SAXS), would be required to ascertain the block copolymer morphology. It is of importance to note that the *My*-35-IBOMA/*My* self-assembly was disordered with a random location of the rigid aggregates, which exhibited various sizes (27% of large aggregates exhibiting a surface area of $2650 \pm 740 \text{ nm}^2$ and 73% of smaller aggregates having a surface area of $930 \pm 480 \text{ nm}^2$, quantification via Nanoscope Analysis software). By assuming that cylinders were observed ($F_{\text{IBOMA}} = 0.28$, possibly elevated for spheres formation), the radius of the cylinders *R* can be estimated according to the following formula (7):

$$R = 1.0\alpha KM^{1/2} \quad (7)$$

where α is the chain expansion parameter ($\alpha = 1.25$ is generally assumed), *K* is the experimental constant related to the unperturbed root-mean-square end-to-end distance to the molecular weight ($K_{\text{P(IBOMA)}} \approx K_{\text{P(MMA)}} = 0.565 \text{ \AA}$ was hypothesized) and $M = M_{n,\text{P(IBOMA)}} \approx 16 \text{ kg}\cdot\text{mol}^{-1}$ in this case^{87,88}. Accordingly, $R \approx 8.9 \text{ nm}$ was estimated, suggesting that the surface area of the cylinders at the top/bottom (case where cylinders are perpendicular to AFM image, comparable to spheres) was equaled to about 250 nm^2 . This may suggest that the relatively small aggregates seen on the AFM image (average surface area of 930 nm^2) might not correspond to spheres but more likely to disoriented cylinders. For cylinders parallel to the AFM image having a mean length of 50 nm, a surface area of 2800 nm^2 was calculated, which is comparable to the size of the large aggregates observed experimentally. Several factors may explain the asymmetrical domain organization. First, the presence of *My* units in the P(IBOMA) hard blocks resulted presumably in attractive interactions at the soft/hard interfaces, increasing the miscibility between the domains. The relatively broad molecular weight distribution of the sample ($\text{Đ} = 1.91$) may also lead to a reduction of the segregation strength (decrease in χN , where χ is the Flory-Huggins interaction parameter and *N* is the

copolymer degree of polymerization⁸⁹). Lastly, the experimental approach can be discussed. The analyzed samples were not annealed prior to the AFM characterization. Indeed, due to the early thermal degradation of IBOMA-based polymers (Figure 6), it was decided to not heat the samples at $T > T_{g,P(IBOMA)}$ for a few hours or days. It may be argued that a stronger phase separation would have occurred after annealing, allowing a full relaxation of the P(IBOMA) chains.

Figure 8b shows the temperature dependence of the shear storage and loss moduli (G' and G'' respectively) as well as the damping factor ($\tan \delta = G''/G'$) from room temperature to 220 °C for the triblock copolymer *My*-52-IBOMA/S (Table 4C). The significant decrease of G' from about 13 to 5 MPa with temperature until 70 °C can be first noted. A quasi constant G' could have been expected in this temperature range due to the glassy state of the IBOMA units embedded in the soft rubbery P(*My*) phase. The presence of 12 mol% of S in the extended blocks can partly explain this behavior. Compared to P(IBOMA), the solubility parameter of PS, $\delta_{PS} = 18.4 \text{ MPa}^{1/2}$ (Hoftyzer and Van Krevelen approach), is closer to that of P(*My*), which may result in the partial homogeneity of the triblock copolymer. Moreover, short PS sequences softening at a relatively low temperature were likely contained by the outer blocks. It was notably reported⁹⁰ by DSC that $T_{g,PS} = 32\text{-}69 \text{ °C}$ for low $M_{n,PS} = 0.9\text{-}3.0 \text{ kg}\cdot\text{mol}^{-1}$. The rubbery plateau was then observed at $T = 70\text{-}140 \text{ °C}$ where G' slightly decreased from 3.6 to 2.2 MPa. At $T > 140 \text{ °C}$, the modulus dropped due to the softening of the P(IBOMA) phase, the flexible P(*My*) chains being no longer held together by the rigid domains. The maximum $\tan \delta$ peak appeared at 171 °C, which is consistent with the P(IBOMA)'s T_g measured previously ($T_{g,P(IBOMA)} = 171\text{-}177 \text{ °C}$, Figure 5). Generally, this dynamic mechanical analysis (DMA) suggests that *My*-52-IBOMA/S may have an upper service temperature $T \sim 140 \text{ °C}$ with $G' \geq 2.2 \text{ MPa}$ at $T \leq 140 \text{ °C}$.

Lastly, the mechanical properties at room temperature of *My*-52-IBOMA/S were determined by uniaxial tensile testing. The stress-strain curves are given in Figure 10 along with the mean Young's modulus E , yield stress σ_Y , tensile strength at break σ_B and tensile elongation at break ϵ_B values. The linear elastic region was apparent until 13-19% elongation, at which point the yield strength was observed. This low-strain region allowed the determination of $E = 2.32 \pm 0.28 \text{ MPa}$ and $\sigma_Y = 5.02 \pm 0.23 \text{ MPa}$ (Figure 10). Beyond the proportionality limit, the tensile strength decreased (23% on average) until about 130% elongation. This can be presumably explained by the onset of the plastic deformation, not allowing the total recovery of the strains (permanent deformation of the material). The plastic region was then markedly observed with a plateau, characteristic of the drawing of the *My*-52-IBOMA/S chains, ending at the fracture point ($\epsilon_B = 490 \pm 31 \%$). It has to be noted that the strain hardening phenomenon, consisting of the, was not observed. Consequently, no increase in stress was measured at the fracture orientation and alignment of polymer chains in the direction of the load which increases the strength and stiffness of the material ($\sigma_B = 3.90 \pm 0.22 \text{ MPa}$). A key-factor allowing the understanding of this behavior is presumably the

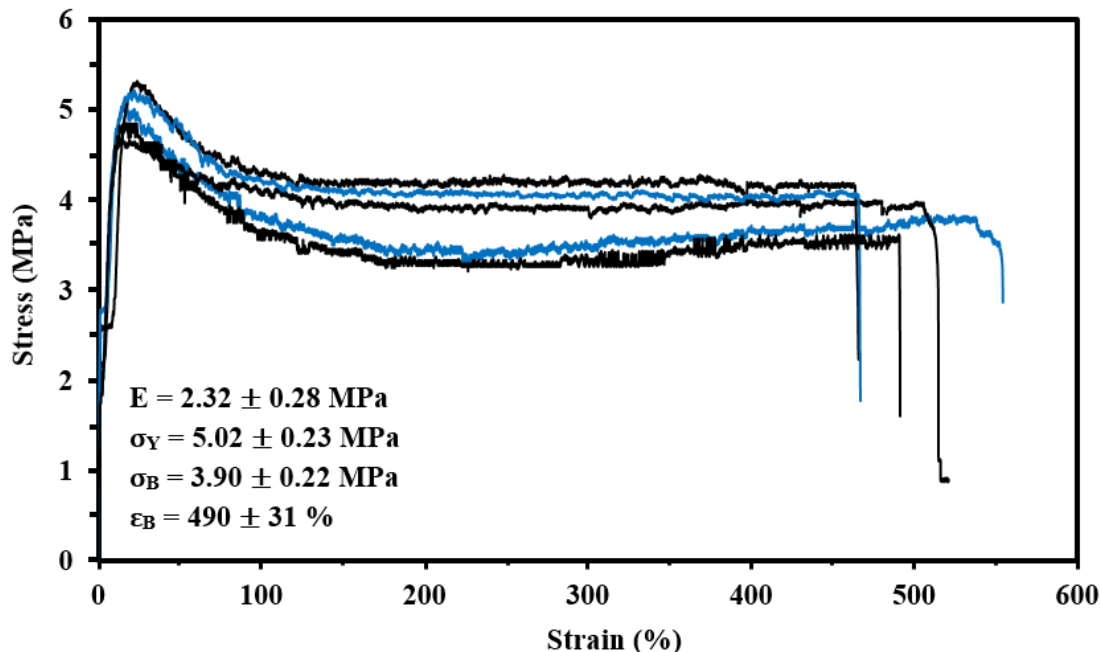


Figure 10. Tensile stress-strain curves of five *My*-52-IBOMA/S samples (same batch, color only used for differentiation) at room temperature and at a cross-head speed of $10 \text{ mm}\cdot\text{min}^{-1}$. The average Young's modulus E , yield stress σ_Y , tensile strength at break σ_B and tensile elongation at break ϵ_B , obtained from these curves are also given.

morphology of the triblock copolymer. The possible disorganized structure of *My*-52-IBOMA/S, not containing necessarily P(IBOMA) glassy spheres can be detrimental. In this case, the expected physical crosslinking structure does not exist, bringing about a decrease of the entropic contribution to strain hardening. By assuming that the strain hardening process is associated with the debonding of the entanglement network (chain disentanglement), it may be also caused by the P(*My*) continuous phase, not sufficiently entangled ($M_{n,MHS,My} = 51.7 \text{ kg}\cdot\text{mol}^{-1} < 3M_{e,P(My)}^{77}$), resulting in an unconstrained uncoiling of the chains. Generally, a flexible plastic was identified, having moderate elastic modulus and tensile strength at break combined with a good irreversible extensibility.

3.5. Conclusion

My/IBOMA NMP in bulk at $100 \text{ }^\circ\text{C}$ initiated by NHS-BB highlighted the gradient nature of this copolymerization with the largely higher reactivity of the monoterpene ($r_{My} = 1.90\text{-}2.16$) toward both propagating species ($---My^*$ and $---IBOMA^*$) compared of that of the bulky methacrylate ($r_{IBOMA} = 0.02\text{-}$

0.07). While the homopolymerization of IBOMA was not controlled, likely due to the high equilibrium constant of this methacrylate, the addition of 20 mol% of *My* as a co-monomer allowed the synthesis of a well-defined P(*My-grad*-IBOMA) copolymer with $\mathcal{D} \leq 1.39$ and $M_{n,MHS}$ close to the predicted one. More generally, well-controlled copolymerizations were performed for $f_{IBOMA,0} \leq 0.80$ and the resulting P(*My-grad*-IBOMA)s exhibited $\mathcal{D} \leq 1.41$, $M_{n,MHS} = 5.9\text{-}10.9 \text{ kg}\cdot\text{mol}^{-1}$ and monomodal GPC distributions at overall conversion $X = 25\text{-}65\%$. The deviations of experimental $M_{n,MHS}$ values from theoretical ones were greater with $f_{My,0}$, which may be caused by chain transfer side reactions to the monomers. Regardless of the initial feed composition, these copolymerizations had $\langle k_p \rangle \langle K \rangle = 2.0 \pm 0.9 \cdot 10^{-5} \text{ s}^{-1}$ relatively close to that of *My* homopolymerization ($1.4 \pm 0.4 \cdot 10^{-5} \text{ s}^{-1}$), stressing the strong influence of *My* kinetics over the copolymerization kinetics. P(*My-grad*-IBOMA) displayed a glass transition temperature between -65 and $+123 \text{ }^\circ\text{C}$ depending on the molar composition of IBOMA. A two-step thermal decomposition was observed by TGA, consisting of an early decomposition peak at $T_{dec,max} = 242\text{-}307 \text{ }^\circ\text{C}$, which results likely from the release of the isobornyl group, and a final decomposition peak at $T_{dec,max} = 370\text{-}380 \text{ }^\circ\text{C}$, due to the scission of the copolymer backbone. The chain-end fidelity of *My*-rich and IBOMA-rich P(*My-grad*-IBOMA)s was quantitatively deemed by ^{31}P NMR (69-74% of SG1-terminated chains) and confirmed via successful chain-extensions in toluene with IBOMA and/or *My* (monomodal shift of the GPC traces).

The satisfactory mediation of the *My*/IBOMA system by the SG1 nitroxide allowed subsequently the preparation of triblock copolymers, composed of a soft P(*My*) middle block and two outer IBOMA-rich segments. 1,4-P(*My*)-(SG1)₂ macro-initiator ($M_{n,MHS} = 35\text{-}52 \text{ kg}\cdot\text{mol}^{-1}$, $\mathcal{D} = 1.45\text{-}1.53$) was first synthesized using the PEB-(SG1)₂ dialkoxyamine initiator in bulk at $120 \text{ }^\circ\text{C}$, followed by the IBOMA/Co chain-extension (Co = *My* or S co-monomer, $< 9 \text{ mol}\%$) at $115 \text{ }^\circ\text{C}$ in toluene. Displaying two distinct T_{gs} at -58 and $+181 \text{ }^\circ\text{C}$, *My*/IBOMA-*My*-IBOMA/*My* triblock copolymer ($M_{n,MHS} = 51 \text{ kg}\cdot\text{mol}^{-1}$, $\mathcal{D} = 1.91$, $F_{IBOMA} = 0.28$) was studied by AFM, which revealed the micro-phase separation of the continuous P(*My*) domain and the disperse IBOMA-rich aggregates, despite an apparent disorganization. Lastly, rheological analysis as well as stress-strain tests were performed for the NMP-based S/IBOMA-*My*-IBOMA/S triblock copolymer ($M_{n,MHS} = 95 \text{ kg}\cdot\text{mol}^{-1}$, $\mathcal{D} = 2.23$, $F_{IBOMA} = 0.36$, $F_S = 0.05$). In comparison to traditional styrenic block copolymers, an extended upper service temperature at around $140 \text{ }^\circ\text{C}$ was observed by DMA. Furthermore, this triblock copolymer exhibited a tensile strength at break $\sigma_B \sim 4 \text{ MPa}$ and an elongation at break $\varepsilon_B \sim 500\%$, despite the absence of strain hardening.

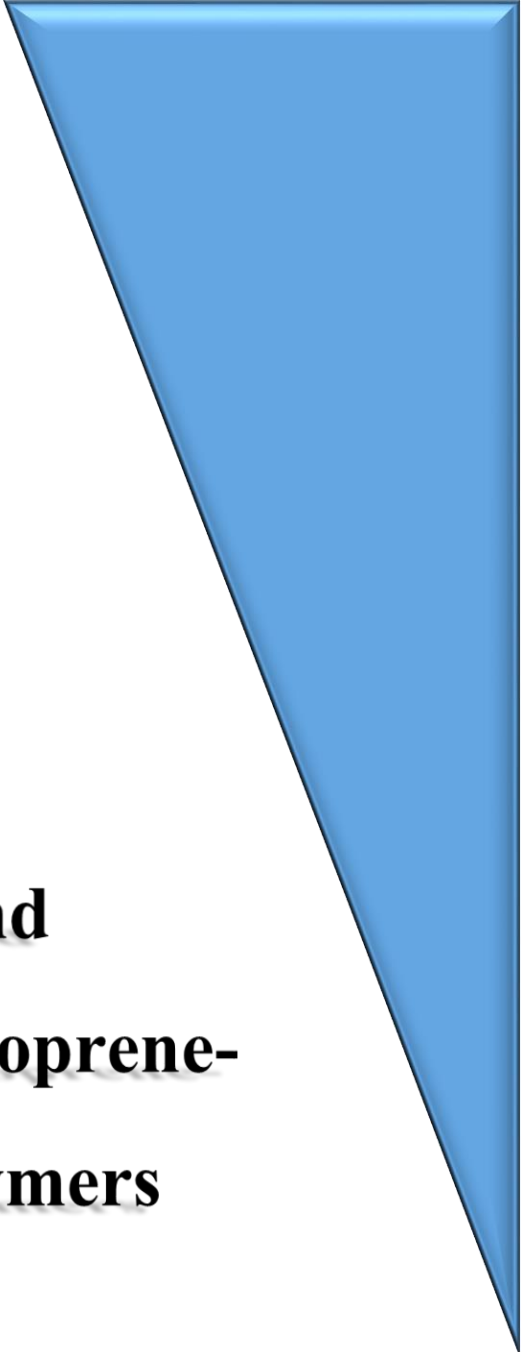
3.6. References

- (1) M. Szwarc, *Nature* **1956**, 178, 1168.
- (2) M. Szwarc, M. Levy and R. Milkovich, *J. Am. Chem. Soc.* **1956**, 78, 2656.

- (3) R. P. Quirk, Q. Zhuo; S. H. Jang; Y. Lee; G. Lizarraga In Applications of Anionic Polymerization Research; R. P. Quirk, Ed.; American Chemical Society: Washington, **1998**; Chapter 1, pp 2-27.
- (4) H. -G. Elias In Macromolecules: Synthesis, Materials, and Technology, 2nd Edition; H.-G. Elias, Ed.; Springer: New York, **1984**; Chapter 20, pp 681-736.
- (5) J. Chiefari, Y. Chong, F. Ercole, J. Krstina, J. Jeffery, T. Le, R. Mayadunne, G. Meijs, C. Moad, G. Moad, E. Rizzardo and S. Thang, *Macromolecules* **1998**, *31*, 5559.
- (6) W. A. Braunecker and K. Matyjaszewski, *Prog. Polym. Sci.* **2007**, *32* (1), 93.
- (7) M. K. Georges, R. P. N. Veregin, P. M. Kazmaier and G. K. Hamer, *Macromolecules* **1993**, *26* (11), 2987.
- (8) R. P. N. Veregin, M. K. Georges, P. M. Kazmaier and G. K. Hamer, *Macromolecules* **1993**, *26* (20), 5316.
- (9) J. -S. Wang and K. Matyjaszewski, *J. Am. Chem. Soc.* **1995**, *117* (20), 5614.
- (10) D. H. Solomon, E. Rizzardo and P. Cacioli (Commonwealth Scientific and Industrial Research Organization). Eur. Pat. Appl. 0135280A3, August 13, **1986**.
- (11) G. Moad; E. Rizzardo In Nitroxide Mediated Polymerization: From Fundamentals to Applications in Materials Science; D. Gigmes, Ed.; The Royal Society of Chemistry: Cambridge, **2016**; Chapter 1, pp 1-44.
- (12) J. Nicolas, Y. Guillauneuf, C. Lefay, D. Bertin, D. Gigmes and B. Charleux, *Prog. Polym. Sci.* **2013**, *38* (1), 63.
- (13) J. G. Drobny In Handbook of Thermoplastic Elastomers; J. G. Drobny, Ed.; Plastics Design Library: Norwich, **2007**; Chapter 5, 161-178.
- (14) R. C. Bening; W. H. Korcz; D. L. Handlin In Modern Styrenic Polymers: Polystyrenes and Styrenic Copolymers; J. Scheirs and D. Priddy, Eds.; John Wiley & Sons: Chichester, **2003**; Chapter 21, pp 463-500.
- (15) J. L. Pradel, B. Ameduri and B. Boutevin, *Macromol. Chem. Phys.* **1999**, *200*, 2304.
- (16) J. L. Pradel, B. Boutevin and B. Ameduri, *J. Polym. Sci., Part A: Polym. Chem.* **2000**, *38*, 3293.
- (17) B. Keoshkerian, M. Georges, M. Quinlan, R. Veregin and B. Goodbrand, *Macromolecules* **1998**, *31*, 7559.
- (18) D. Benoit, E. Harth, P. Fox, R. M. Waymouth and C. J. Hawker, *Macromolecules* **2000**, *33*, 363.
- (19) C. Cheng, K. Qi, E. Khoshdel and K. L. Wooley, *J. Am. Chem. Soc.* **2006**, *128*, 6808.
- (20) J. K. Wegrzyn, T. Stephan, R. Lau and R. B. Grubbs, *J. Polym. Sci., Part A: Polym. Chem.* **2005**, *43*, 2977.
- (21) A. Sundararaman, T. Stephan and R. B. Grubbs, *J. Am. Chem. Soc.* **2008**, *130*, 12264.
- (22) Y. Cai, K. B. Aubrecht and Grubbs, *J. Amer. Chem. Soc.* **2010**, *133*, 1058.
- (23) D. Benoit, V. Chaplinski, R. Braslau and C. J. Hawker, *J. Am. Chem. Soc.* **1999**, *121*, 3904.
- (24) D. Benoit, S. Grimaldi, S. Robin, J. -P. Finet, P. Tordo and Y. Gnanou, *J. Am. Chem. Soc.* **2000**, *122*, 5929.
- (25) H. Matsuoka, Y. Suetomi, P. Kaewsaiha and K. Matsumoto, *Langmuir* **2009**, *25*, 13752.
- (26) S. Harrisson, P. Couvreur and J. Nicolas, *Macromolecules* **2011**, *44*, 9230.
- (27) S. Harrisson, P. Couvreur P and J. Nicolas, *Macromol. Rapid Commun.* **2012**, *33*, 805.
- (28) A. Métafiot, Y. Kanawati, J. -F. Gérard, B. Defoort and M. Maric, *Macromolecules* **2017**, *50* (8), 3101.
- (29) J. Vinas, N. Chagneux, D. Gigmes, T. Trimaille, A. Favier and D. Bertin, *Polymer* **2008**, *49*, 3639.
- (30) M. K. Georges, G. K. Hamer and N. A. Listigovers, *Macromolecules* **1998**, *31*, 9087.
- (31) C. Detrembleur, V. Sciannamea, C. Koulic, M. Claes, M. Hoebeke and R. Jérôme, *Macromolecules* **2002**, *35*, 7214.
- (32) A. Behr and L. Johnen, *ChemSusChem* **2009**, *2* (12), 1072.
- (33) P. Sarkar and A. K. Bhowmick, *RSC Adv.* **2014**, *4*, 61343.
- (34) R. P. Quirk; T. -L. Huang In New Monomers and Polymers; B. M. Culbertson and C. U. Pittman, Eds.; Springer: New York, **1984**; Chapter 19, pp 329-355.
- (35) R. P. Quirk, US patent 4 374 957, February 22, **1983**.
- (36) J. M. Bolton, M. A. Hillmyer and T. R. Hoye, *ACS Macro Lett.* **2014**, *3*, 717.
- (37) A. Matsumoto, K. Mizuta and T. Otsu, *J. Polym. Sci., Part A: Polym. Chem.* **1993**, *31* (10), 2531.
- (38) J. M. Yu, P. Dubois and R. Jérôme, *Macromolecules* **1996**, *29*, 8362.
- (39) B. Charleux, J. Nicolas and O. Guerret, *Macromolecules* **2005**, *38*, 5485.
- (40) J. Nicolas, C. Dire, L. Mueller, J. Belleney, B. Charleux, S. R. A. Marque, D. Bertin, S. Magnet and L. Couvreur, *Macromolecules* **2006**, *39*, 8274.
- (41) J. Nicolas, S. Brusseau and B. Charleux, *J. Polym. Sci., Part A: Polym. Chem.* **2010**, *48*, 34.

- (42) B. Lessard, C. Aumand-Bourque, R. Chaudury, D. Gomez, A. Haroon, N. Ibrahimian, S. Mackay, M. -C. Noel, R. Patel, S. Sitaram, S. Valla, B. White and M. Maric, *Intern. Polymer Processing* **2011**, 26 (2), 197.
- (43) S. Georges, M. Bria, P. Zinck and M. Visseaux, *Polymer* **2014**, 55, 3869.
- (44) H. K. Mahabadi, *J. Appl. Polym. Sci.* **1985**, 30, 1535.
- (45) X. Q. Zhang and C. H. Wang, *J. Polym. Sci., Part B: Polym. Phys.* **1994**, 32, 1.
- (46) P. Hattam, S. Gauntlett, J. W. Mays, N. Hadjichristidis, R. N. Young and L. J. Fetters, *Macromolecules* **1991**, 24 (23), 6199.
- (47) H. Pasch; B. Trathnigg In *Multidimensional HPLC of Polymers*; H. Pasch; B. Trathnigg, Eds.; Springer: Heidelberg, 2013; Chapters 4 & 5, pp 37–90.
- (48) C. Petit, B. Luneau, E. Beaudoin, D. Gigmes and D. Bertin, *J. Chromatogr. A* **2007**, 1163, 128.
- (49) A. Métafiot, J. -F. Gérard, B. Defoort and M. Maric, *J. Polym. Sci., Part A: Polym. Chem.* **2018**, 56 (8), 860.
- (50) G. S. Ananchenko, M. Souaille, H. Fischer, C. LeMercier and P. Tordo, *J. Polym. Sci. A: Polym. Chem.* **2002**, 40, 3264.
- (51) S. Beuermann and M. Buback, *Prog. Polym. Sci.* **2002**, 27, 191.
- (52) C. Burguiere, M. Dourges, B. Charleux and J. P. Vairon, *Macromolecules* **1999**, 12, 3883.
- (53) J. Nicolas; E. Guégain; Y. Guillaneuf In *Nitroxide Mediated Polymerization: From Fundamentals to Applications in Materials Science*; D. Gigmes, Ed.; The Royal Society of Chemistry: Cambridge, **2016**; Chapter 7, pp 305-348.
- (54) C. Dire, B. Charleux, S. Magnet and L. Couvreur, *Macromolecules* **2007**, 40 (6), 1897.
- (55) B. Lessard and M. Maric, *J. Polym. Sci., Part A: Polym. Chem.* **2009**, 47, 2574.
- (56) A. Moayeri, B. Lessard and M. Maric, *Polym. Chem.* **2011**, 2, 2084.
- (57) M. Berger and I. Kuntz, *J. Polym. Sci., Part A: Polym. Chem.* **1964**, 2, 1687.
- (58) M. Fineman and S. D. Ross, *J. Polym. Sci.* **1950**, 5 (2), 259.
- (59) T. Kelen and F. Tudos, *J. Macromol. Sci., Chem.* **1975**, 9 (1), 1.
- (60) P. W. Tidwell and G. A. Mortimer, *J. Polym. Sci., Part A: Gen. Pap.* **1965**, 3, 369.
- (61) M. A. Dubé; E. Saldivar-Guerra; I. Zapata-Gonzales In *Handbook of Polymer: Synthesis, Characterization, and Processing*, 1st Edition; E. Saldivar-Guerra, E. Vivaldo-Lima, Eds.; John Wiley & Sons: Hoboken, **2013**; Chapter 6, pp 105-125.
- (62) H. Benoit, Z. Grubisic, P. Rempp, P. Decker and J. Zilliox, *J. Chim. Phys.* **1966**, 63, 1507.
- (63) R. B. Grubbs, *Polym. Rev.* **2011**, 51, 104.
- (64) G. S. Ananchenko, M. Souaille, H. Fischer, C. LeMercier and P. Tordo, *J. Polym. Sci. A: Polym. Chem.* **2002**, 40, 3264.
- (65) G. Gryn'ova, C. Y. Lin and M. L. Coote, *Polym. Chem.* **2013**, 4 (13), 3744.
- (66) W. J. Runckel and L. A. Goldblatt, *Ind. Eng. Chem.* **1946**, 38 (7), 749.
- (67) N. Kamachi and A. Kajiwara, *Macromolecules* **1996**, 29 (7), 2378.
- (68) S. Beuermann, M. Buback, T. P. Davis, N. Garcia, R. G. Gilbert, R. A. Hutchinson, A. Kajiwara, M. Kamachi, I. Lacik and G. T. Russel, *Macromol. Chem. Phys.* **2003**, 204, 1338.
- (69) N. Hadjichristidis, J. Mays, W. Ferry and L. J. Fetters, *J. Polym. Sci., Polym. Phys. Ed.* **1984**, 22, 1745.
- (70) M. Gordon and J. S. Taylor, *J. Chem. Tech. Biotech.* **1952**, 2, 493.
- (71) J. Nicolas, C. Dire, L. Mueller, J. Belleney, B. Charleux, S. R. A. Marque, D. Bertin, S. Magnet and L. Couvreur, *Macromolecules* **2006**, 39, 8274.
- (72) C. Lefay, J. Belleney, B. Charleux, O. Guerret and S. Magnet, *Macromol. Rapid Commun.* **2004**, 25, 1215.
- (73) J. W. Reed and W. L. Jolly, *J. Org. Chem.* **1977**, 42, 3963.
- (74) R. N. Cavalcanti; T. Forster-Carneiro; M. T. M. Gomes; M. A. Rostagno; J. M. Prado; M. A. A. Meireles In *Natural Product Extraction: Principles and Applications*; M. A. Rostagno, J. M. Prado, Eds.; The Royal Society of Chemistry: Dorchester, **2013**; Chapter 1, pp 1–57.
- (75) M. D. Gehlsen, K. Almdal and F. S. Bates, *Macromolecules* **1992**, 25 (2), 939.
- (76) S. Schlögl, M. -L. Trutschel, W. Chassé, G. Riess and K. Saalwächter, *Macromolecules* **2014**, 47, 2759.
- (77) L. J. Fetters; D. J. Lohse; R. H. Colby In *Physical Properties of Polymers Handbook*, 2nd ed.; J. E. Mark, Ed.; Springer: New York, **2007**; Chapter 25, pp 447–454.
- (78) S. Grimaldi, J. -P. Finet, F. Le Moigne, A. Zeghdaoui, P. Tordo, D. Benoit, M. Fontanille and Y. Gnanou, *Macromolecules* **2000**, 33 (4), 1141.
- (79) A. Goto and T. Fukuda, *Prog. Polym. Sci.* **2004**, 29, 329.
- (80) S. Robin, O. Guerret, J. -L. Couturier, R. Pirri and Y. Gnanou, *Macromolecules* **2002**, 35, 3844.

- (81) D. R. D'Hooge, M. -F. Reyniers and G. B. Marin, *Macromol. React. Eng.* **2013**, 7 (8), 362.
- (82) D. Gigmes, D. Bertin, C. Lefay and Y. Guillauneuf, *Macromol. Theory Sim.* **2009**, 18, 402.
- (83) B. Lessard, C. Tervo and M. Maric, *Macromol. React. Eng.* **2009**, 3, 245–256.
- (84) C. J. Hawker, E. Elce, J. L. Dao, W. Volksen, T. P. Russel and G. G. Barclay, *Macromolecules* **1996**, 29, 2686.
- (85) B. Zhang, Y. Ma, D. Chen, J. Xu and W. Yang, *J. Appl. Polym. Sci.* **2013**, 129 (1), 113.
- (86) D. W. van Krevelen; K. Te Nijenhuis In *Properties of Polymers*, 4th edition; D. W. van Krevelen, K. Te Nijenhuis, Eds.; Elsevier B. V.: Amsterdam, **2009**; Chapter 7, pp 189-227.
- (87) D. J. Meier, *J. Polym. Sci.* **1969**, 26C, 81.
- (88) D. J. Meier, *Polym. Preprints* **1970**, 11, 400.
- (89) F. S. Bates, *Annu. Rev. Phys. Chem.* **1990**, 41, 525.
- (90) L. -P. Blanchard, J. Hesse and S. L. Malhotra, *Can. J. Chem.* **1974**, 52, 3170.



**PART III. Synthesis by NMP and
characterization of isoprene-
based triblock copolymers**

Chapter 4. Synthesis of isoprene-based triblock copolymers by nitroxide-mediated polymerization (NMP)

4.1. Preface

The triblock copolymers based on β -myrcene (My) did not satisfy the mechanical requirements of the industrial application outlined previously. While S- My -S copolymers (S = styrene) exhibited poor stress-strain properties (tensile strength at break $\sigma_B < 0.8$ MPa, tensile elongation at break $\varepsilon_B < 200\%$) at room temperature, marked improvements were shown for IBOMA- My -IBOMA triblocks (IBOMA = isobornyl methacrylate) with $\sigma_B \sim 4$ MPa and $\varepsilon_B \sim 500\%$. However, despite a satisfactory extensibility of these latter, their lack of hardness was detrimental when compared to the tensile properties of traditional vulcanized rubbers or commercial thermoplastic elastomers. One main reason may explain such low strength of these materials: a poorly entangled elastomeric poly(β -myrcene) P(My) continuous phase. Indeed, for all these My -based triblock copolymers, the P(My) mid-segment exhibited $M_n \sim 52$ kg.mol⁻¹ at most, which is only about the double of its entanglement molecular weight ($M_{e,P(My)} = 22-31$ kg.mol⁻¹). Two solutions have been thus considered: (1) increase of the P(My) degree of polymerization; (2) replacement of P(My) by an elastomeric segment exhibiting a lower entanglement molar mass. The first option was disregarded since the synthesis of very high M_n P(My) by NMP under homogeneous conditions in bulk or in organic solvents might not have been feasible due to the limitations of this controlled polymerization. NMP in a dispersed medium or anionic polymerization would have been relevant but the time constraint of the doctoral thesis did not allow considering these alternatives. Consequently, it was decided to substitute P(My) by poly(isoprene) (PI), having a much lower entanglement molecular weight ($M_{e,PI} = 4-6$ kg.mol⁻¹). The synthesis of well-defined PI by NMP in bulk or in organic solvents was envisioned since it was already studied and optimized as regards the polymerization of My in a controlled manner. Moreover, the effective NMP of I was reported in the literature.

In comparison to the previous paper-based chapters, Chapter 4 is intentionally more technical and results-based. It first details the synthesis of the telechelic PI-(SG1)₂ mid-segment using poly(ethylene-*stat*-butylene)-(SG1)₂ difunctional initiator. Then, the successful S and IBOMA chain-extensions from PI-(SG1)₂ macro-initiator is presented as well as the characterization of the resulting well-tailored S-I-S and S/IBOMA-I-IBOMA/S triblock copolymers.

4.2. Abstract

The polymerization of isoprene initiated by the poly(ethylene-*stat*-butylene)-(SG1)₂ dialkoxyamine at 115 °C in 50 vol% pyridine for 14-17 h led, after fractionation, to *cis*-1,4-rich PI-(SG1)₂ poly(diene)s exhibiting $M_n = 54\text{-}61 \text{ kg}\cdot\text{mol}^{-1}$ and $\bar{D} = 1.47\text{-}1.59$. Well-defined PS-PI-PS triblock copolymers ($M_n = 94.6\text{-}109.4 \text{ kg}\cdot\text{mol}^{-1}$, $\bar{D} = 2.11\text{-}2.29$, $F_S = 0.30\text{-}0.49$) were synthesized via subsequent S chain-extensions from PI-(SG1)₂ macro-initiators. Generally, these triblock copolymers displayed two glass transition temperatures (T_g s), a sub-zero one from -61 to -65 °C and an upper one from 102 to 104 °C, suggesting the segregation into two different phases of the flexible PI and rigid PS blocks. A micro-phase separation, exhibiting possibly a cylindrical or lamellar morphology, was observed by AFM for a synthesized PS-PI-PS having $F_S = 0.30$. While a hard and brittle PS-PI-PS plastic containing 49 mol% of styrene units was mechanically characterized ($\sigma_B = 10.8 \pm 1.2 \text{ MPa}$, $\varepsilon_B = 21 \pm 7 \%$), softer and more extensible triblock copolymers having $F_S = 0.30\text{-}0.38$ were obtained with $\sigma_B = 2.8\text{-}4.1 \text{ MPa}$ and $\varepsilon_B = 376\text{-}449\%$. Despite a satisfactory extensibility, these latter diene-styrene block copolymers showed a relatively low tensile strength at break. Two axes were followed to increase σ_B , namely the hydrogenation of the PI mid-segment and the substitution of PS blocks by higher T_g rigid blocks.

The saturation of the soft mid-segment of the NMP-based PS-PI-PS polymers was attempted using the diimide-generating reagent *p*-toluenesulfonyl hydrazide (TSH), combined with tributylamine (TBA) to mitigate the participation of side reactions. A hydrogenation degree (HD) higher than 75% was determined via ¹H NMR and no significant chain degradation was observed after the post-polymerization modification as characterized by GPC. Generally, TGA evidenced higher thermal stability of the partially hydrogenated triblock copolymers under inert atmosphere compared to the parent PS-PI-PS. Moreover, the elastic modulus and the tensile strength at break of PS-PI-PS ($F_S = 0.49$) markedly increased after the chemical hydrogenation (HD = 76.3%) and its elongation at break decreased.

Lastly, IBOMA-I-IBOMA type triblock copolymer ($M_n = 94.0 \text{ kg}\cdot\text{mol}^{-1}$, $\bar{D} = 1.76$) containing a small fraction of S units in the outer blocks ($F_{\text{IBOMA}} = 0.35$, $F_S = 0.06$) was synthesized sequentially from telechelic PEB-(SG1)₂. Despite its poor micro-phase separation and its early thermal degradation (onset of decomposition ranging from 219 to 265 °C depending on the nature of the atmosphere), this copolymer displayed an upper service temperature higher than 150 °C due to the glass transition of the IBOMA-rich segments occurring at 180-185 °C. Furthermore, it exhibited at room temperature a remarkable elongation at break $\varepsilon_B = 1360 \pm 210 \%$ and a moderate tensile strength at break $\sigma_B = 11.4 \pm 0.6 \text{ MPa}$. The lower tensile stress value measured compared to these of commercial styrene-diene thermoplastic elastomers can be mainly explained by the very limited strain hardening of this experimental sample when highly stretched.

4.3. Results and discussion

The synthesis of isoprene-based triblock copolymers by NMP was performed in a very similar manner to *S-My-S* (Chapter 1, Section 1.4.3) and *IBOMA-My-IBOMA* (Chapter 3, Section 3.4.2) polymers produced previously. Therefore, $\text{PEB}-(\text{SG1})_2$ was first used to prepare telechelic $\text{PI}-(\text{SG1})_2$. Afterwards, chain-extensions were performed from these active $\text{PI}-(\text{SG1})_2$ macro-initiators to add PS or P(*IBOMA*) rigid blocks.

4.3.1. Preparation of SG1-terminated poly(isoprene) $\text{PI}-(\text{SG1})_2$

■ Optimized synthesis of $\text{PI}-(\text{SG1})_2$.

It was first aimed to synthesize a high M_n PI segment (elevated entanglement density desired) while having a high degree of chain-end fidelity at both chain ends (for the subsequent chain-extension). Whereas the NMP of *My* was not reported in the literature before this doctoral thesis, the NMP of isoprene (I) was well studied using the stable free nitroxide 2,2,6,6-tetramethylpiperidinyl-1-oxy (TEMPO) and the 2,2,5-trimethyl-4-phenyl-3-azahexane-3-oxy nitroxide (TIPNO), as mentioned in the literature review (Section D.2.3)¹⁻¹⁰. Specifically, Harrison *et al.* studied the NMP of isoprene initiated by various SG1-based alkoxyamines¹¹. They showed that a good control of the isoprene homopolymerization can be obtained when using the commercial BlocBuilder™ initiator as well as its derivative NHS-BlocBuilder. Accordingly, it appeared herein consistent to use $\text{PEB}-(\text{SG1})_2$ as the initiating system¹², which also showed its effectiveness to mediate the NMP of *My* (Chapters 1 and 3). 115 °C was selected as the reaction temperature since it was shown to provide a controlled polymerization at an acceptable polymerization rate¹¹. Lastly, a high target number-average molecular weight at quantitative conversion ($M_{n,\text{theo}} \sim 145 \text{ kg}\cdot\text{mol}^{-1}$ at $X_I = 100\%$) was chosen, allowing the synthesis of relatively long PI chains. Due to the low boiling point of isoprene ($T_{b,I} \sim 34 \text{ °C}$), 15 mL high-pressure reactors were used, each fitted with plunger valve and thermowell, and placed in an oil bath, as shown in Ph. 1.

Ph. 1. Polymerization of isoprene using four capacity pressure tubes placed in an oil bath.



Two first experiments (PI1, from 2 to 8 h, and PI2, from 11 to 17 h, experimental conditions in Table 1) were conducted in bulk since it corresponds to the easiest system to study, consisting solely of the monomer and the alkoxyamine initiator (mono-component initiating system)¹³. The kinetic study is given in Figure 1. Interestingly, two marked regimes can be distinguished. At a moderate isoprene conversion $X_I < 30\%$ (experiment PI1), a good control of the polymerization was observed with low dispersity values ($\mathcal{D} < 1.26$, Figure 1b) and experimental M_n values close to the theoretical ones (Figure 1a, GPC calibration curve based on linear PI standards). Nonetheless, at $X_I > 40\%$ (experiment PI2, reaction time $t = 15-17$ h), a clear loss of control was seen with significant deviations of the experimental M_n values from the predicted line (Figure 1a) and broader molecular weight distributions ($\mathcal{D} > 1.73$, Figure 1b). This unstable second regime was presumably due to the high viscosity of the reaction medium after the early stages of the polymerization. Since PI samples exhibiting relatively low $M_{n,PI} < 35 \text{ kg}\cdot\text{mol}^{-1}$ were produced in the controlled regime, it was attempted to improve the control of the isoprene polymerization at $X_I > 30\%$ via the use of a solvent.

Harrisson and coworkers reported an enhanced control over the SG1-based NMP of isoprene in pyridine compared to the same reaction in bulk¹⁴. Lower \mathcal{D} values were obtained, which can be likely caused by the stabilization of the polar SG1 free nitroxide as well as the disruption of intramolecular hydrogen bonding due to the presence of pyridine. Therefore, a third experiment was performed for 25 h with the initial addition of 50 v% pyridine relative to isoprene (PI3, Table 1). M_n , from 36.7 to 63.9 $\text{kg}\cdot\text{mol}^{-1}$ increased linearly with conversion with minor deviations from the theoretical line (Figure 1a). A broadening of the molecular weight distribution was also observed with conversion ($\mathcal{D} \geq 1.57$ at $X_I \geq 27\%$, Figure 1b). However, it is of interest to note that these conditions allowed the synthesis of a PI sample having a relatively high $M_n \sim 55 \text{ kg}\cdot\text{mol}^{-1}$ with $\mathcal{D} \sim 1.55$. The preparation of such a PI sample was not possible in

Table 1. Formulations for isoprene polymerizations performed in bulk or in pyridine at $T = 115 \text{ }^\circ\text{C}$, initiated by $\text{PEB}-(\text{SG1})_2$ and targeting $M_{n,\text{theo}} \sim 145 \text{ kg}\cdot\text{mol}^{-1}$ at $X_I = 100\%$.

ID	[PEB-(SG1) ₂] (M)	[I] (M)	[Pyridine] (M)	$M_{n,\text{target}}^{(a)}$ ($\text{g}\cdot\text{mol}^{-1}$)	T (°C)	$t^{(b)}$ (h)
PI1	0.0051	9.973	0 ^(c)	139	115	8
PI2	0.0050	10.208	0 ^(c)	145	115	17
PI3	0.0024	4.928	6.17	146	115	25

a) Rounded values including the number-average molecular weight of $\text{PEB}-(\text{SG1})_2$ ($M_{n,\text{PEB}(\text{SG1})_2} = 5.7 \text{ kg}\cdot\text{mol}^{-1}$).

b) Samples periodically taken at: 2 h, 4 h, 6 h and 8 h (PI1); 11 h, 13 h, 15 h and 17 h (PI2); 11 h, 13 h, 16 h, 19 h and 25 h (PI3).

c) Polymerization performed in bulk.

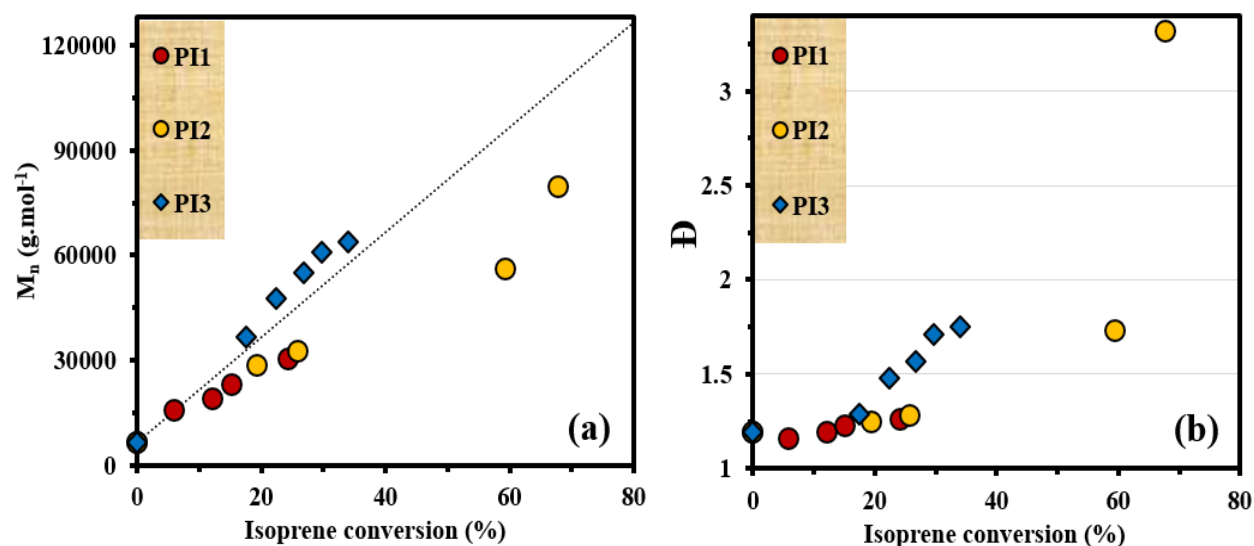


Figure 1. (a) M_n versus isoprene conversion X_I and (b) \bar{D} versus X_I for the isoprene homopolymerizations performed in bulk (experiments PI1 and PI2) and in pyridine (experiment PI3) at 115 °C and initiated by PEB-(SG1)₂. The dotted black line indicates the theoretical M_n versus overall conversion based on the monomer to initiator ratio ($M_{n,theo} \sim 145 \text{ kg.mol}^{-1}$ at $X_I = 100\%$ for every experiment). All experimental ID are listed in Table 1.

bulk. Consequently, it was decided to synthesize the PI-(SG1)₂ mid-segment by relying on the following experimental conditions: initiation of I with PEB-(SG1)₂ at 115 °C in 50 v% pyridine for about 13-16 h and targeting $M_{n,theo} \sim 145 \text{ kg.mol}^{-1}$ at quantitative conversion.

To produce subsequently well-defined isoprene-based triblock copolymers, three PI samples were synthesized under these optimized experimental conditions and exhibited satisfactory features with $M_{n,1} = 51.0\text{-}55.7 \text{ kg.mol}^{-1}$ and $\bar{D}_1 \leq 1.64$ (Table 2). As previously performed for one of the NMP-based IBOMA-My-IBOMA triblock copolymers (Chapter 3, Section 3.4.2), a benzene (solvent) / methanol (non-solvent) fractional precipitation^{15,16} was applied to the PI samples. It was aimed at eliminating the shorter PI chains, the majority of those being presumably irreversibly terminated (not capped by a SG1 unit). This way, longer PI chains can be obtained, exhibiting ideally a higher degree of chain-end fidelity. As expected, M_n increased (+ 3-6 kg.mol^{-1} , Table 2) and \bar{D} decreased (− 0.01-0.07, Table 2) after fractionation, indicating the effective removal of a population of relatively short PI chains.

▣ Characterization of the synthesized NMP-based PI.

Table 2. Molecular characterization of final NMP-based PI, initiated by PEB-(SG1)₂ at 115 °C in 50 v% pyridine and targeting $M_{n,theo} \sim 145 \text{ kg}\cdot\text{mol}^{-1}$ at $X_1 = 100\%$ (optimized experimental conditions).

ID	t (h)	X_1 (%)	Before fractionation		After fractionation ^(a)	
			$M_{n,1}$ ^(b) (kg.mol ⁻¹)	D_1 ^(b)	$M_{n,2}$ ^(b) (kg.mol ⁻¹)	D_2 ^(b)
PI4	14	24.2	51.0	1.48	54.3	1.47
PI5	16	27.9	55.7	1.62	59.8	1.59
PI6	17	28.5	55.1	1.64	61.0	1.57

a) Fractional precipitation using the non-solvent addition method, relying on the benzene (solvent) / methanol (non-solvent) pair (2 cycles).

b) M_n and M_w measured by GPC (Water Breeze, differential refractive index RI 2414 detector, 40 °C) with HPLC grade THF as the mobile phase (flow rate of 0.3 mL.min⁻¹). M_n values determined by calibration with linear narrow molecular weight distribution PI standards.

The ¹H NMR spectrum of PI4 is presented in Figure 3. This polymer may have four different types of microstructure, namely *cis*-1,4, *trans*-1,4, 1,2- and 3,4-poly(isoprene). The spectral assignments were in good accord with the literature^{17,18}. The olefinic protons' signal of *cis*- and *trans*-1,4-addition (C=CH) was observed at $\delta = 5.05$ -5.15 ppm. The signal at 4.55–4.75 ppm was attributed to olefinic protons of 3,4-addition (C=CH₂). The peaks at 4.80–5.00 ppm and 5.65–5.85 ppm indicated the olefinic protons of 1,2-addition (CH=CH₂). These peaks confirmed the formation of 1,4-PI (86 mol%) with the presence of minor fractions of 3,4-motif (6 mol%) and 1,2-motif (8 mol%). Furthermore, the sharp chemical shift from the methyl protons of *cis*-1,4 and *trans*-1,4 units (C-CH₃) was observed at 1.59 and 1.67 ppm, respectively. This way, the stereo-selectivity of PI4, containing about 71 mol% of *cis*-1,4 units, was elucidated. The predominance of the *cis*-1,4-microstructure (1,4-addition ≥ 83 mol%, *cis*-1,4-content ≥ 66 mol%) was also determined for the samples PI5 and PI6. P(My) homopolymers produced previously by SG1 NMP were also rich in *cis*-1,4-motif (1,4-addition ≥ 80 mol%, *cis*-1,4-content ≥ 67 mol%, Chapter 1, Section 1.4.1, Table 2).

Thermal analysis was also used to investigate the physical properties of the NMP-based PI as a function of temperature. Differential scanning calorimetry (DSC) was performed to determine the glass transition temperature (T_g). This latter characteristic temperature plays an important role in dictating whether a particular polymer is in the rubbery state at room temperature. Elastomers are amorphous in nature and thus should have a T_g much below the ambient temperature, preferably at sub-zero range¹⁹. Figure 2a shows the DSC thermogram of the sample PI4. A distinct baseline shift at around -60 °C was observed, corresponding to the T_g of PI4. This sub-zero T_g thereby implies a rubber-like behavior of the

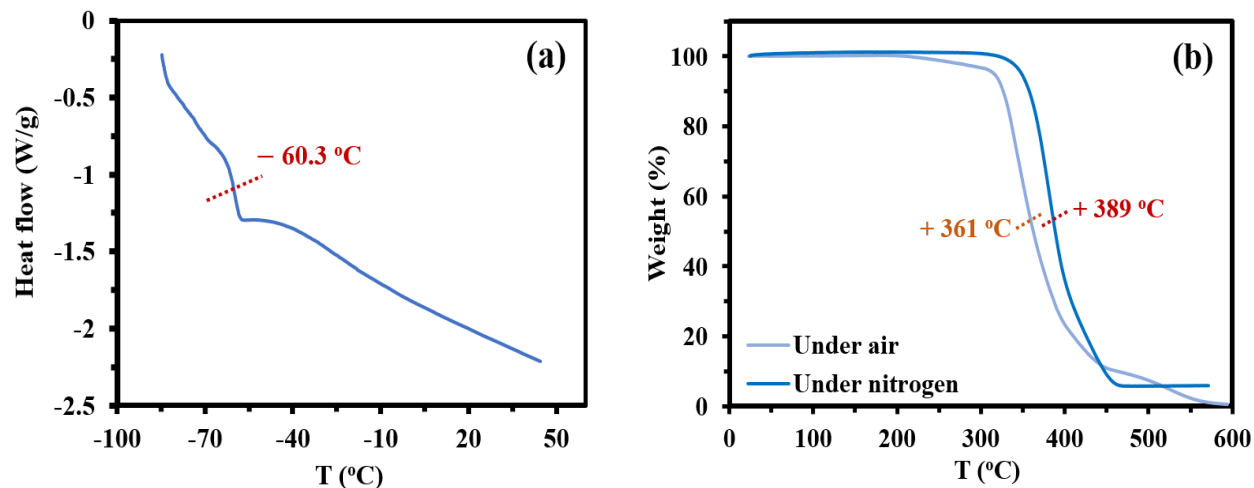


Figure 2. (a) DSC trace (second heating run) of the final dry PI4 sample ($T_{g,PI4} = -60.3\text{ }^{\circ}\text{C}$, determined via the inflection method) and (b) TGA traces ($10\text{ }^{\circ}\text{C}\cdot\text{min}^{-1}$) of final dry PI4 sample under air ($T_{dec,max,PI4} = 361\text{ }^{\circ}\text{C}$) and nitrogen ($T_{dec,max,PI4} = 389\text{ }^{\circ}\text{C}$) atmospheres.

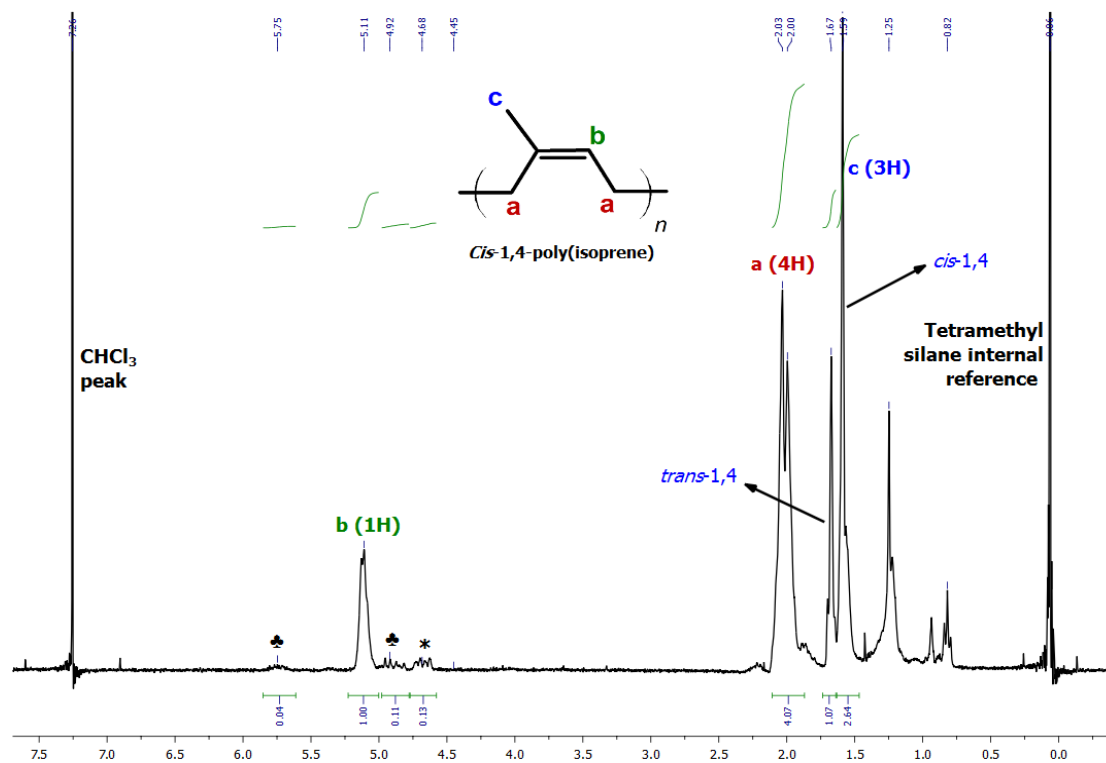


Figure 3. ^1H NMR spectrum of the final dry PI4 polymer in CDCl_3 (300 MHz, 32 scans, room temperature). *Signal at $\delta = 4.55\text{--}4.75\text{ ppm}$ corresponds to olefinic protons of 3,4-PI. *Signals at $\delta = 4.80\text{--}5.00\text{ ppm}$ and $5.65\text{--}5.85\text{ ppm}$ correspond to olefinic protons of 1,2-PI.

synthesized polymer. T_g s from -70.5 to -64.5 °C were reported for well-defined 1,4-rich PI prepared anionically ($\bar{D} \leq 1.22$)²⁰. Interestingly, a lower $T_g = -77$ °C was found for P(*My*) synthesized by NMP (Chapter 1, Section 1.4.5, Table 8). This might be due to the long and flexible C6/C8 pendant groups of the P(*My*) segment, generating free volume.

The maximum decomposition temperature ($T_{dec,max}$, temperature at which weight loss is most apparent) of PI4 under air and nitrogen atmospheres was determined via thermogravimetric analysis (TGA, Figure 2b) as well. PI4 showed a single degradation peak at $T_{dec,max} = 389$ °C under N₂ flow, which was very similar to that of P(*My*) ($T_{dec,max} = 385$ °C, Chapter 1, Section 1.4.5, Table 8). The thermal stability of PI4 was reduced under air with $T_{dec,max} = 361$ °C, highlighting the likely occurrence of oxidation reactions generating chain scissions.

4.3.2. NMP-based styrene-isoprene-styrene triblock copolymers

Ideally, the synthesis of well-defined PI terminated at each chain end by a SG1 moiety allows the addition of two outer blocks via chain-extension. Preliminary styrene (2.3 - 2.8 mol.L⁻¹) chain-extensions from NMP-based PI-(SG1)₂ samples ($M_n = 46.8$ - 61.0 kg.mol⁻¹, $\bar{D} = 1.41$ - 1.58 , 0.002 - 0.003 mol.L⁻¹) were performed in 50 wt% toluene (4.8 - 5.7 mol.L⁻¹) at $T = 110$ - 114 °C. Despite successful chain-extensions notably marked by the monomodal shift of the GPC chromatograms to lower elution times, indicating a high level of the chain end fidelity, a low fraction of styrene (S) was incorporated with a molar fraction of S in the final copolymer $F_S = 7.9$ - 14.1% . For purposes of developing relatively tough and strong triblock copolymers for the industrial issue, the addition of longer PS segments to the PI macro-initiator was targeted. Accordingly, bulk chain-extensions were considered to “push” the conversion of S to higher levels. It should be noted that well-tailored P(*I-b-S*) polymers can be obtained via a solvent-free process. For instance, anionic bulk polymerization to synthesize isoprene-styrene block copolymers (sequential polymerization) by reactive extrusion was reported^{21,22,23}.

The chain-extensions of PI4, PI5 and PI6 macro-initiators synthesized previously (Table 2) with S were performed in bulk at 115 °C (temperature kept under 120 °C to avoid S auto-initiation²⁴), at different reaction times (50 - 140 min) to prepare S-I-S copolymers with various F_S . The experimental conditions are given in Table 3A below. A marked broadening of the molecular weight distribution was observed for every experiment from $\bar{D}_{PI} = 1.47$ - 1.59 to $\bar{D}_{PS-PI-PS} = 2.19$ - 2.32 (Table 3B). Several factors may explain this increase in dispersity: dead chains from PI macro-initiators; rapid increase in S conversion at short times and high initial concentration of S bringing about irreversible terminations and chain-transfer reactions²⁵⁻²⁷. However, the addition of relatively long PS outer blocks was apparent since the resulting chain-

Table 3. Chain-extensions of (A) PI-(SG1)₂ macroinitiators with S at 115 °C in bulk and (B) features of the resulting S-I-S triblock copolymers.

A. Styrene chain-extension from PI-(SG1) ₂						
ID	[PI-(SG1) ₂] ₀ (M)	[S] ₀ (M)	M _{n,theo} ^(a) (kg.mol ⁻¹)	T (°C)	t (min)	
PS-PI4-PS	0.004	5.714	203	115	140	
PS-PI5-PS	0.003	4.147	204	115	50	
PS-PI6-PS	0.004	6.281	225	115	80	
B. Chain-extended PS-PI-PS triblock copolymer						
ID	Before fractionation				After fractionation ^(e)	
	X _S ^(b) (%)	F _S ^(c)	M _{n,1} ^(d) (kg.mol ⁻¹)	Đ ₁ ^(d)	M _{n,2} ^(d) (kg.mol ⁻¹)	Đ ₂ ^(d)
PS-PI4-PS	44.1	0.49	94.4	2.19	103.1	2.11
PS-PI5-PS	31.2	0.30	89.2	2.32	94.6	2.29
PS-PI6-PS	36.8	0.38	101.8	2.23	109.4	2.18

a) Rounded values including the number-average molecular weight of PI-(SG1)₂ macro-initiators (M_{n,PI-(SG1)₂} = 54.3-61.0 kg.mol⁻¹).

b) Styrene conversion X_S determined by ¹H NMR in CDCl₃.

c) Molar fraction of S in the copolymer (F_S) as determined by ¹H NMR in CDCl₃.

d) M_n and M_w determined by GPC calibrated with PI standards in THF at 40 °C.

e) Fractional precipitation using the non-solvent addition method was implemented, relying on the benzene (solvent) / methanol (non-solvent) pair (2 cycles).

extended products exhibited M_n = 89.2-101.8 kg.mol⁻¹ and F_S = 30-49% (Table 3B). As performed previously, the synthesized PS-PI-PS triblock copolymers were fractionated, resulting in an increase in M_n = 94.6-109.4 kg.mol⁻¹ and a slight decrease in Đ = 2.11-2.29 (Table 3B).

The thermal stability of the fractionated PS-PI4-PS copolymer was investigated using thermogravimetric analysis (TGA, Figure 4b). A higher decomposition temperature T_{dec,max} was determined for this triblock compared to the parent PI, whether under nitrogen (+ 31 °C) or under air (+ 38 °C) atmospheres. Such an observation agrees with the higher PS T_{dec,max} = 445 °C, determined previously (Chapter 1, Section 1.4.5, Table 8), compared to that of natural rubber. Under air, the early thermo-oxidative degradation of PS-PI4-PS, starting at 271 °C, was observed. The formation of a highly reactive peroxy radical intermediate (ROO•), then abstracting a labile hydrogen which gives rise to the hydroperoxide species (ROOH), likely occurred throughout this decomposition process in an O₂ environment²⁸. Thermal

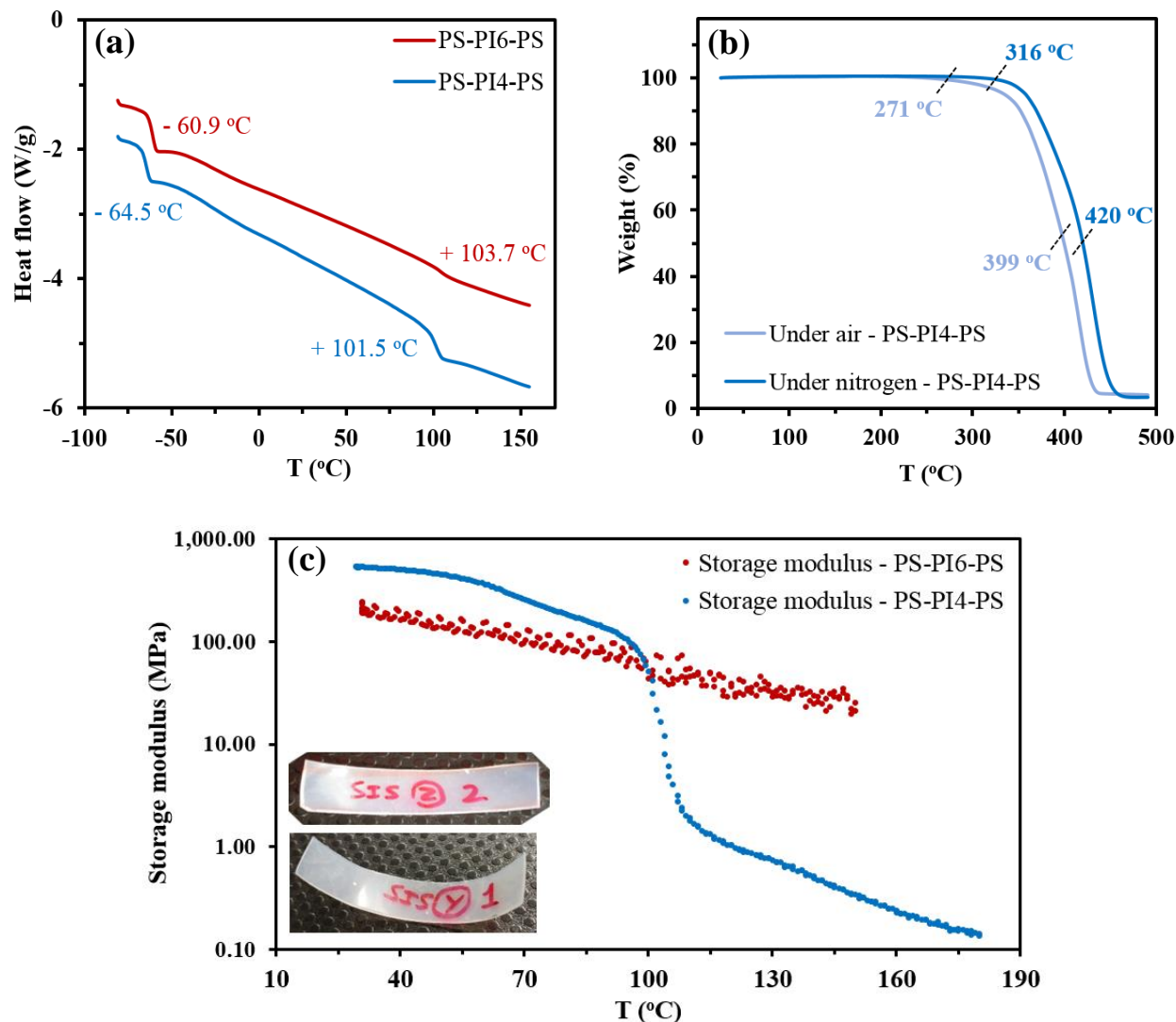


Figure 4. (a) DSC traces (second heating run) of final dry PS-PI4-PS and PS-PI6-PS. The numbers near the changes in slope correspond to the T_g s determined via the inflection method. (b) TGA traces ($10\text{ }^\circ\text{C}\cdot\text{min}^{-1}$) of final dry PS-PI4-PS samples under air and N_2 atmospheres. The characteristic temperatures $T_{\text{dec},1} = 271\text{--}316\text{ }^\circ\text{C}$ (onset of decomposition) and $T_{\text{dec,max}} = 399\text{--}420\text{ }^\circ\text{C}$ (temperature at which weight loss is most apparent) were determined. (c) Dynamic mechanical analysis of the samples PS-PI4-PS and PS-PI6-PS by torsional oscillation, yielding the storage modulus *versus* temperature (0.15 Hz , 1% strain, $5\text{ }^\circ\text{C}\cdot\text{min}^{-1}$, N_2 atmosphere, pictures of DMA test bars PS-PI4-PS (top) and PS-PI6-PS (bottom) prepared by dichloromethane casting).

characterization of block copolymers is commonly used to discriminate between homogeneous and phase-separated systems. The existence of two glass transitions is then taken as evidence for a phase-separated state²⁹. DSC measurements were carried out for the samples PS-PI4-PS and PS-PI6-PS (Figure 4a). A

subzero $T_{g,PI} \leq -61$ °C corresponding to the glass transition temperature of the flexible PI mid-block was clearly detected. At higher temperatures, $T_{g,PS} = 102-104$ °C was determined and corresponded to the rigid PS blocks (Figure 4a). A slight change in slope can be noted for the DSC trace of PS-PI6-PS at $T = 80-120$ °C, which can be due to the lower S molar fraction in this copolymer ($F_S = 38$ mol%) compared to that of PS-PI4-PS ($F_S = 49$ mol%). The difficult detection of the PS T_g was also reported in the case of S-B-S triblock copolymers (B = butadiene) for instance³⁰⁻³². It can also be noted that the T_g s of the synthesized PS-PI-PS samples were very similar to those of the respective PI and PS homopolymers, suggesting a strong heterogeneity of the micro-structure.

Atomic force microscopy was applied to the study of the surface morphology of PS-PI5-PS ($F_S = 0.30$, $M_n = 94.6$ kg.mol⁻¹, $D = 2.29$, Table 3B) to know if the two component blocks segregated into different phases with a typical microdomain structure. Figure 5 shows $2 \mu\text{m} \times 2 \mu\text{m}$ scans of the surface morphology of PS-PI5-PS in two different regions. A clear phase separation was observed with the dark area corresponding to the continuous PI domain whereas the light area corresponded to the discrete PS phase. The domain structure may be cylindrical (disordered cylinder phases), although a definite assignment requires further study. Despite a relatively low PS content (30 mol%) in this triblock copolymer, a lamellar microstructure might be suggested as notably supported by a few examples in the literature^{33,34}.

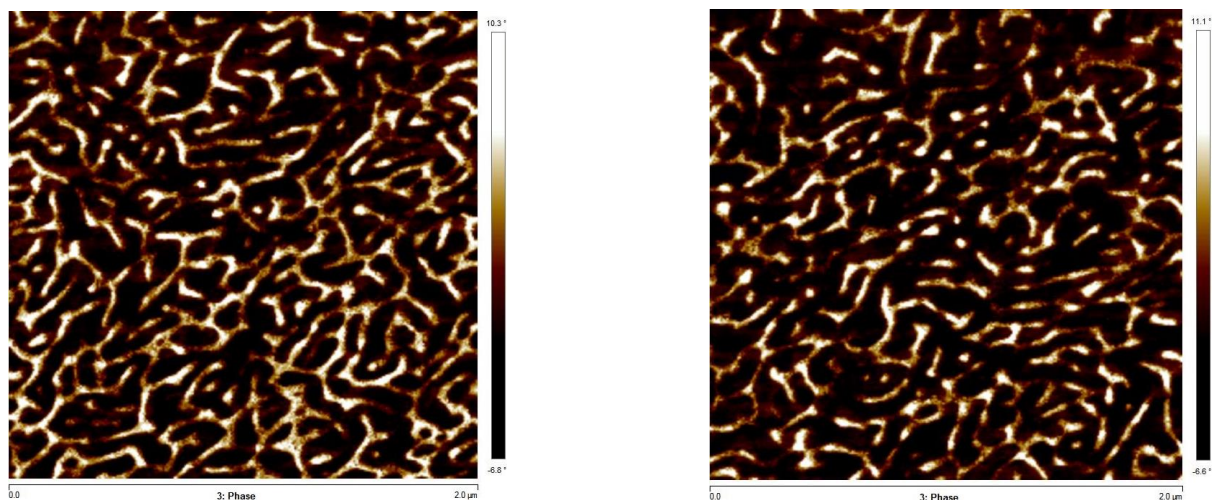


Figure 5. Atomic force microscopy (AFM, experimental section) phase images ($2 \mu\text{m} \times 2 \mu\text{m}$, two different regions shown for the same sample) under tapping mode of operation of the surface morphology of triblock copolymer PS-PI5-PS cast film (chloroform used). The dark domain represents the isoprene component (color-coded height scale given to the right of the image).

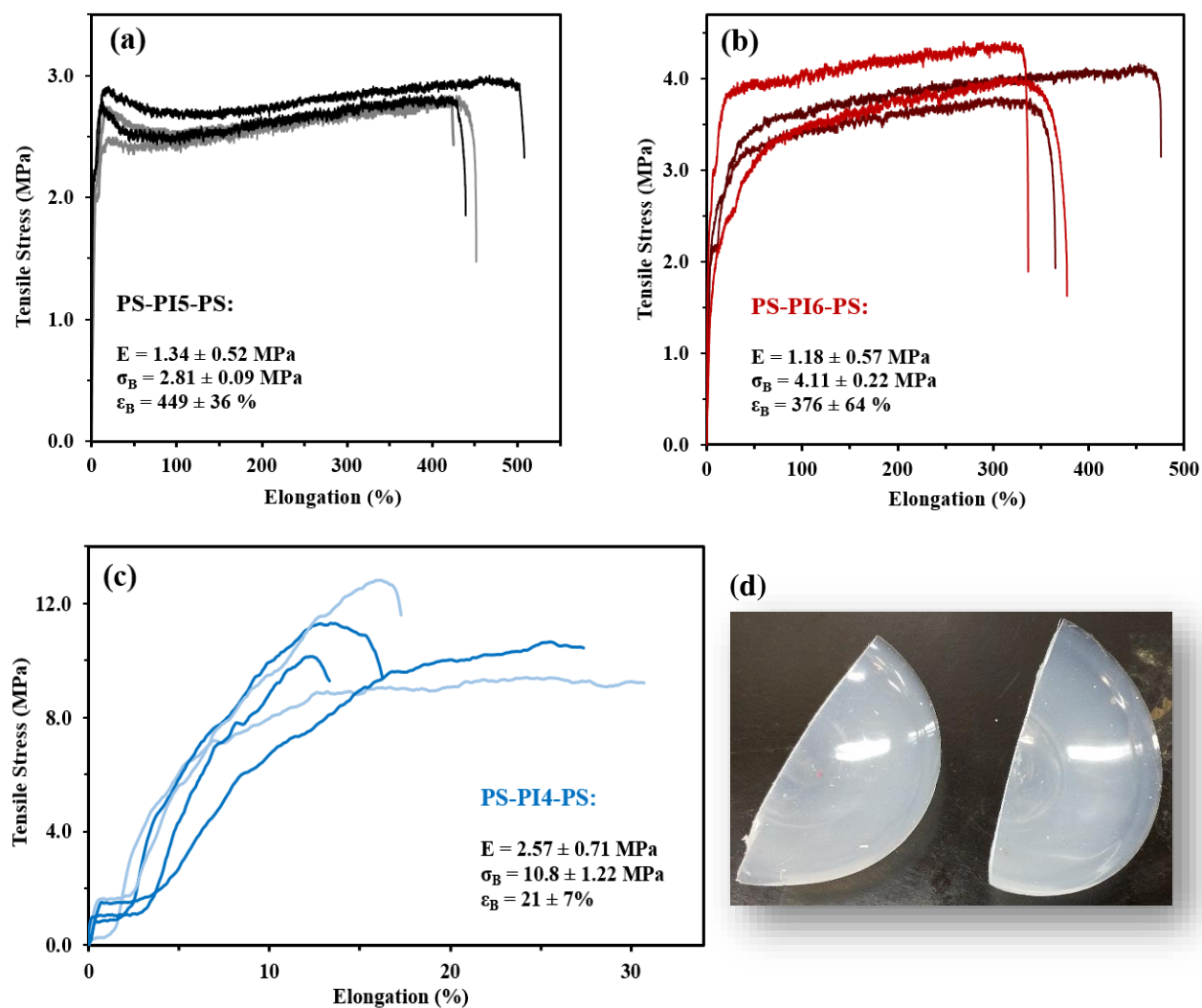


Figure 6. Uniaxial tensile stress-strain curves at room temperature and a cross-head speed of $10 \text{ mm}\cdot\text{min}^{-1}$ of (a) four PS-PI5-PS specimens ($F_s = 0.30$), (b) four PS-PI6-PS specimens ($F_s = 0.38$) and (c) five PS-PI4-PS specimens ($F_s = 0.49$), all prepared via a film casting process. (d) PS-PI4-PS cast films from dichloromethane solution, cut then into typical dog-bone shapes using a sharp blade. The average Young's modulus E , tensile stress at break σ_B and tensile elongation at break ϵ_B obtained from these curves are also given.

In comparison to the previous S-My-S synthesized by NMP (Chapter 1, Section 1.4.3, Figure 7'), the degree of immiscibility between the PI and PS phases seemed higher (stronger phase separation). This can be due to the lower solubility parameter of isoprene $\delta_I = 15.3 \text{ MPa}^{1/2}$ compared to that of β -myrcene $\delta_{My} = 16.2 \text{ MPa}^{1/2}$, calculated using the Hansen solubility parameters ($\delta_S = 19.1 \text{ MPa}^{1/2}$ for styrene)^{35,36}.

The viscoelastic behavior of PS-PI4-PS and PS-PI6-PS in the rubbery region was investigated as well (Figure 4c). The storage modulus G' for PS-PI4-PS stayed relatively constant up to 90 °C, at which point the PS phase softened. A drastic drop of G' was observed at $T \sim T_{g,PS} = 102$ °C (Figure 4a) since the block copolymer chains were no longer locked into position and all the chains were free to flow. A much more atypical behavior was seen for the sample PS-PI6-PS since G' gradually decreased with temperature without a sharp drop at $T \sim T_{g,PS}$ (Figure 4c). It might be explained by the possible specific three-dimensional network morphology of PS-PI6-PS. Considering the PS content of this sample ($F_S = 38\%$), a gyroid structure could have been obtained, which might offer a higher order-disorder phase transition temperature (T_{ODT}) relative to their one- and two-dimensional counterparts (lamellae and cylinders)³⁷. Such an explanation is highly hypothetical and an in-depth study should be led to understand these viscoelastic properties, starting with the elucidation of PS-PI6-PS micro-structure (AFM or TEM combined with SAXS for instance).

The tensile stress-strain plots of the synthesized PS-PI-PS polymers are presented in Figure 6. The tensile bar specimens were prepared by casting a solution of polymer in dichloromethane (~ 80 wt%) and driving off the solvent at room temperature (Figure 6d). The film samples were cut into typical dog-bone shapes using a sharp blade. As expected, tensile stress at break σ_B increased and elongation at break ϵ_B decreased as F_S increased. While PS-PI5-PS ($F_S = 30$ mol%) can be considered as a flexible plastic with a relatively high irreversible extensibility ($\epsilon_B = 449 \pm 36$ %, Figure 6a), a hard and brittle PS-PI4-PS plastic was characterized ($F_S = 49$ mol%) with $\sigma_B = 10.8 \pm 1.2$ MPa and $\epsilon_B = 21 \pm 7$ % (Figure 6c). Considering our industrial criterion, PS-PI6-PS appeared to be the most satisfactory triblock copolymer, which was as soft as PS-PI5-PS (similar Young's modulus E and ϵ_B) but tougher ($\sigma_B = 4.11 \pm 0.22$ MPa, Figure 6b). As reported previously for the NMP-based IBOMA- M_y -IBOMA type triblock copolymer containing 36 mol% of IBOMA (Chapter 3, Section 3.4.2, sample M_y -52-IBOMA/S, Figure 10), no strain hardening (strengthening of the material during large strain deformation) was observed for these samples, limiting thus their tensile strength at break. Such a behavior may be explained by their possible lamellar micro-structure, not allowing a large-scale orientation and alignment of the macromolecules in the direction of the load. It may be assumed that a PS-PI-PS sample exhibiting a spherical morphology (hard blocks forming discrete minority spheres embedded in a rubbery matrix) would have favored the strain hardening due to its isotropic nature. Generally, these isoprene-based triblock copolymers showed largely improved mechanical properties at room temperature compared to the NMP-based S - M_y - S samples (Chapter 1, Section 1.4.3, $M_n = 56.4$ -65.9 kg.mol⁻¹, $\bar{D} = 1.72$ -1.86, $F_S = 20.4$ -32.1 mol%), which exhibited $\sigma_B < 0.8$ MPa and $\epsilon_B < 190\%$ (Chapter 1, Section 1.4.3, Figure 7''). This is likely due to the soft PI domain of PS-PI-PS, being much more entangled ($M_{n,PI} = 54.3$ -61.0 kg.mol⁻¹ ~ $10M_{e,PI}$ with $M_{e,PI} = 4$ -6 kg.mol⁻¹, the

entanglement molar mass of PI) than the flexible P(*My*) matrix ($M_{n,P(My)} = 44.6 \text{ kg.mol}^{-1} \sim 2M_{e,P(My)}$ with $M_{e,P(My)} = 22\text{-}31 \text{ kg.mol}^{-1}$) of the S-*My*-S triblock copolymers.

Despite encouraging results, the PS-PI-PS triblock copolymers prepared by NMP exhibited a tensile strength at break below the industrial requirements. Two options were considered to increase σ_B : hydrogenation of the PI mid-segment; replacement of PS outer blocks by higher T_g hard blocks.

4.3.3. Hydrogenation of NMP-based styrene-isoprene-styrene triblock copolymers

Industrially, hydrogenation is conveniently performed with elemental hydrogen in the presence of a transition metal catalyst. On a laboratory scale, however, the equipment required to perform hydrogenations at moderate to high hydrogen pressure is often not readily available. For this reason, the inorganic reagent diimide (N_2H_2) has been widely used to prepare laboratory scale quantities of hydrogenated diene polymers (Literature Review, Section C.2.2 for further details)^{38,39}.

Hydrogenation of the unsaturated PI mid-segment of the triblocks synthesized by NMP was performed herein with diimide generated *in-situ* by thermolysis of *p*-toluenesulfonyl hydrazide (TSH). Since the by-products from TSH, particularly *p*-toluenesulfinic acid, can attack at olefinic sites (protonation of unsaturation) and degrading macromolecules, tributylamine (TBA) was added to eliminate these side reactions. The protonation of this high-boiling tertiary amine was expected to greatly decrease the propensity of the by-products to attack at the polymer backbone⁴⁰. The chemical hydrogenation performed for PS-PI4-PS and PS-PI6-PS is depicted in Figure 7, relying on Hillmyer's study⁴¹.

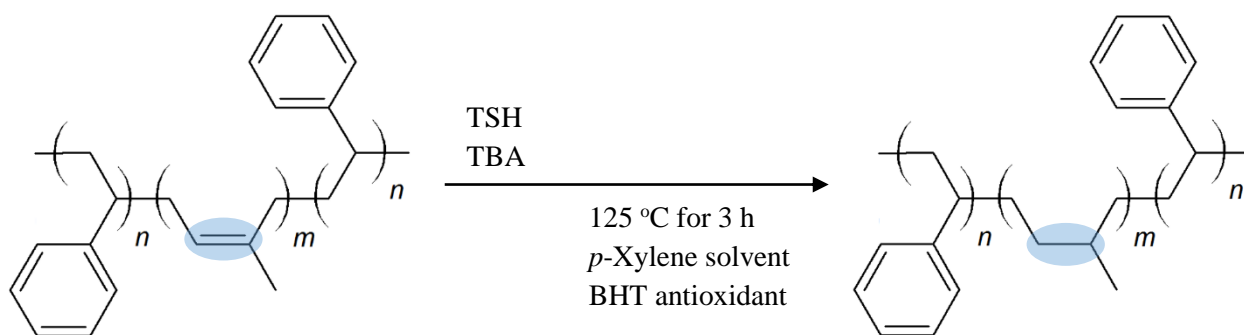


Figure 7. Chemical hydrogenation of the carbon-carbon double bond of the poly(isoprene) mid-segment using *p*-toluenesulfonyl hydrazide (TSH, 2.4 equivalent to the double bond) with tributylamine (TBA, 2.5 equivalent to the double bond). 0.1 wt% of butylated hydroxytoluene (BHT) relative to the polymer was added as well.

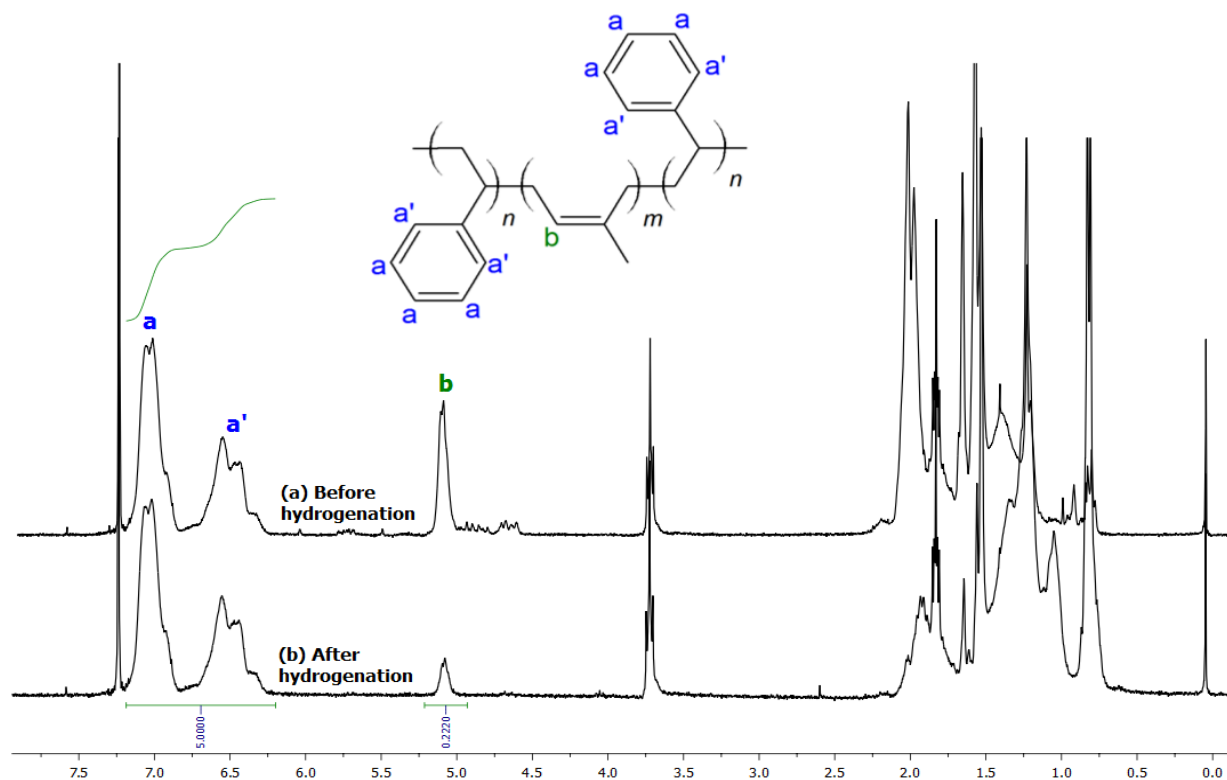


Figure 8. ^1H NMR spectra of the final dry PS-PI4-PS in CDCl_3 (300 MHz, 32 scans, room temperature) (a) before and (b) after hydrogenation. The styrene-isoprene-styrene triblock copolymer structure is given at the top of the spectra. A hydrogenation degree (HD) of 76.3% was determined.

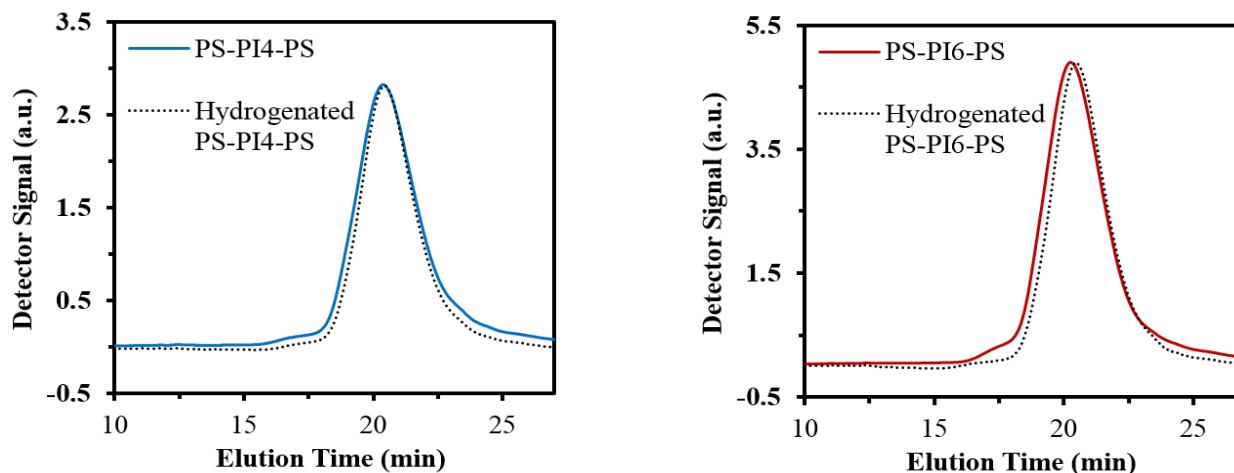


Figure 9. Normalized GPC traces of PS-PI4-PS before ($M_n = 103.1 \text{ kg}\cdot\text{mol}^{-1}$, $\bar{D} = 2.11$) and after ($M_n = 97.4 \text{ kg}\cdot\text{mol}^{-1}$, $\bar{D} = 2.27$) hydrogenation and of PS-PI6-PS before ($M_n = 109.4 \text{ kg}\cdot\text{mol}^{-1}$, $\bar{D} = 2.18$) and after ($M_n = 101.8 \text{ kg}\cdot\text{mol}^{-1}$, $\bar{D} = 2.23$) hydrogenation.

The unsaturated polymers were first dissolved in *p*-xylene (40 mL per gram of polymer) at 45 °C and then, TSH, TBA and a small amount of hydrogen-atom-donating butylated hydroxytoluene (BHT) was added to protect against oxidative degradation. The reaction mixture was stirred at 125 °C for 3 h and the polymer was precipitated in methanol. Prior to hydrogenation, the thermal stabilization of the chain-ends of PS-PI-PS was ensured via removal of the SG1 end-groups using thiophenol as described elsewhere⁴².

The ¹H NMR spectra of PS-PI4-PS before and after hydrogenation with TSH is given in Figure 8. The partial hydrogenation was evidenced by the diminution of the olefinic resonance at $\delta = 5.08$ ppm. A hydrogenation degree (HD) of 76.3% was determined spectroscopically. The TSH/TBA combination did not give complete saturation of the PI block, which is consistent with the literature reporting the incomplete hydrogenation of PI via this specific hydrogenation method⁴⁰. Figure 9 shows the GPC traces of the starting PS-PI4-PS and PS-PI6-PS polymers as well as the partially hydrogenated polymers. A slight broadening of the TSH-treated material molecular weight distribution was apparent, although the shape of the GPC traces did not change perceptibly. Furthermore, lower M_n were determined after hydrogenation for both isoprene-based triblock copolymers. A degradation of the PI mid-segment during the hydrogenation, which may involve TSH/TBA by-products reacting with unsaturated sites, can explain this change in M_n ⁴⁰. It can also be hypothesized that some chains decomposed due to thermal or oxidative reactions. It should be added that the molecular features obtained after hydrogenation must be carefully interpreted due to the change in the GPC response of the hydrogenated polymers, exhibiting a hydrodynamic volume different from the PS-PI-PS starting materials.

Thermal gravimetric analysis (TGA) was used to determine the thermal stability for both the original polymers and the hydrogenated ones. Regardless of the hydrogenation degree, similar TGA traces were obtained for PS-PI4-PS ($F_S = 0.49$) under air (Figure 10a). However, after hydrogenation (HD = 76.3%), this sample displayed an enhanced thermal stability under N₂ atmosphere since no weight loss occurred before 362 °C (305 °C for the parent polymer) and $T_{dec,max} = 436$ °C, slightly higher than that of the neat polymer (419 °C), was determined (Figure 10a'). With regard to PS-PI6-PS ($F_S = 0.38$), while a similar improvement of the thermal stability after hydrogenation (HD = 77.3%) was observed under inert atmosphere (Figure 10b'), higher onset and maximal decomposition temperatures ($T_{dec,1} = 302$ °C and $T_{dec,max} = 416$ °C respectively) of the hydrogenated sample were determined under air (Figure 10b). Generally, the greater thermal stability of the PS-PI-PS copolymers with the partial saturation of the isoprene units can be explained by the conversion of the weak π -bond within the original PI segment to a stronger C-H σ -bond⁴³.

The partially hydrogenated PS-PI4-PS triblock copolymer was tested via a stress-strain experiment at ambient conditions (Figure 11, must be discussed cautiously due to the poor reproducibility of the specimens after hydrogenation) and exhibited an elastic modulus ($E = 10.3 \pm 2.9$ MPa) about four times

higher than that of the parent PS-PI4-PS. Moreover, a marked increase of the tensile stress at break (from 10.8 to 16.5 MPa) and a reduction of the elongation at break (from 21 to 9%) were observed after the hydrogenation reaction. Accordingly, the tensile strength and the Young's modulus of this partially

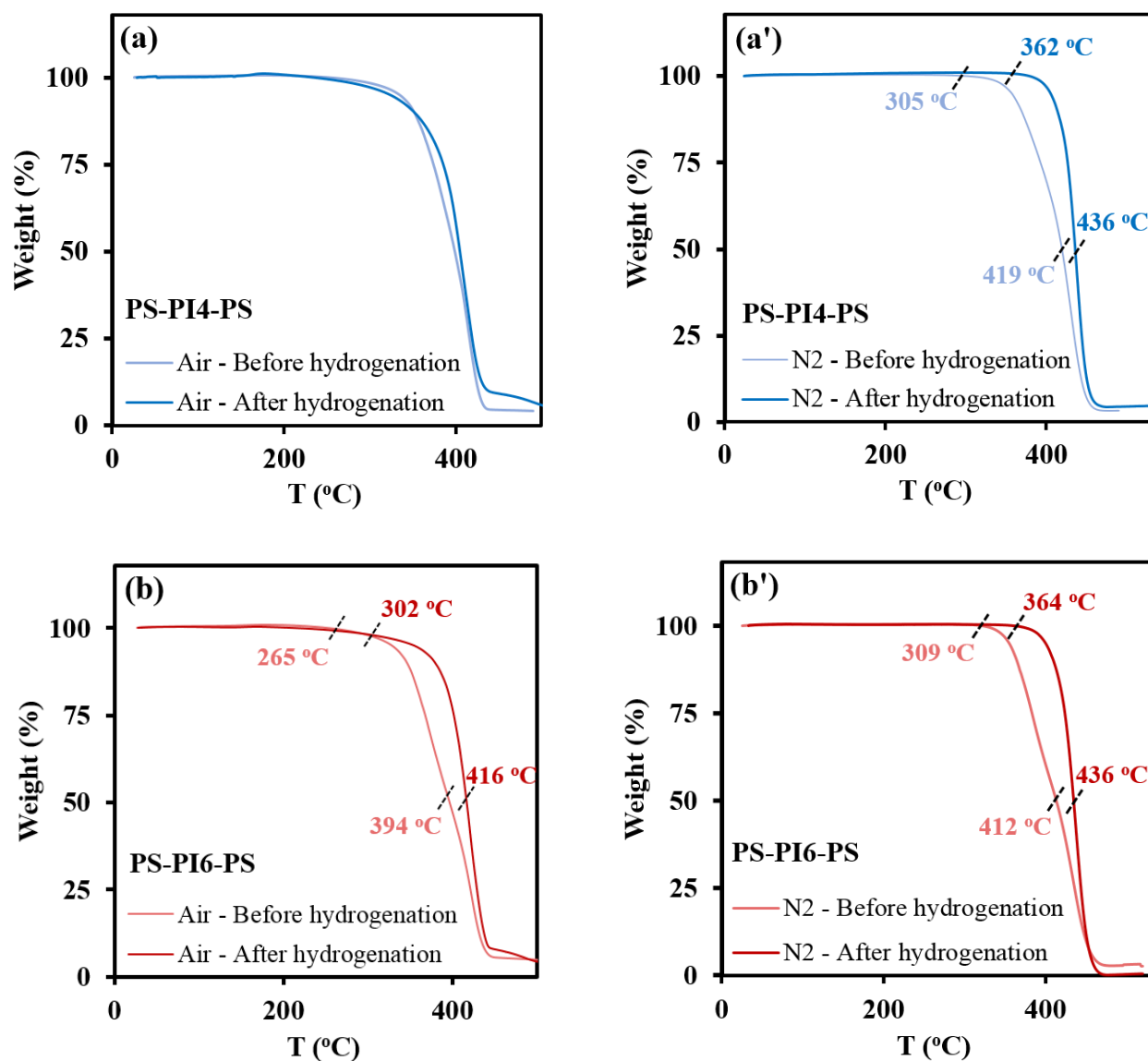


Figure 10. TGA traces ($10\text{ }^{\circ}\text{C}\cdot\text{min}^{-1}$) of final dry PS-PI4-PS (blue curves, (a) and (a')) and PS-PI6-PS (red curves, (b) and (b')) samples before and after hydrogenation (HD = 76.3% and 77.3% respectively) under air and N₂ atmospheres. The characteristic temperatures $T_{dec,1} = 265\text{-}364\text{ }^{\circ}\text{C}$ (onset of decomposition) and $T_{dec,max} = 394\text{-}436\text{ }^{\circ}\text{C}$ (temperature at which weight loss is most apparent) were determined.

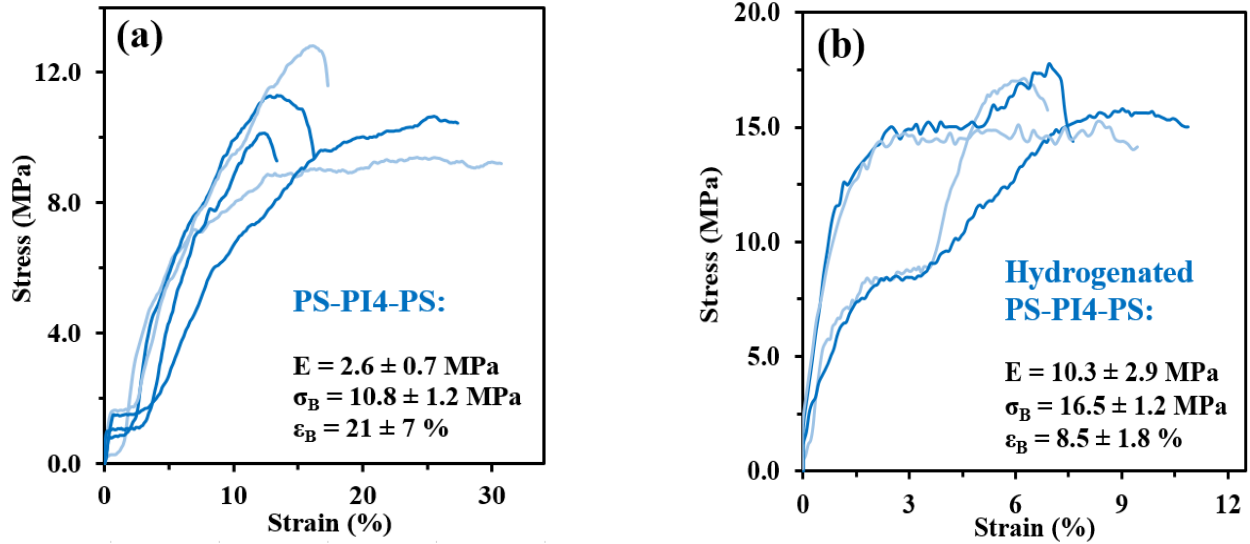


Figure 11. Uniaxial tensile stress-strain curves at room temperature and a cross-head speed of $10 \text{ mm}\cdot\text{min}^{-1}$ of (a) five PS-PI4-PS specimens ($F_s = 0.49$) and (b) four partially hydrogenated PS-PI4-PS specimens ($HD = 76.3\%$). The average Young's modulus E , tensile stress at break σ_B and tensile elongation at break ε_B obtained from these curves are also given in black.

hydrogenated triblock copolymer distinctly increased compared to the original one, although the content of the hard PS outer segments did not change. The replacement of about three quarters of isoprene repeat units ($HD = 76.3\%$) by ethylene/propylene units, forming segments intrinsically harder and/or tougher than PI⁴⁴⁻⁴⁶, can explain this change in stress-strain properties. The enhancement of the mechanical properties might also be attributed to the greater segregation of the microphase structure after hydrogenation, owing to the increase in the incompatibility between the PS and hydrogenated PI blocks⁴⁷. Such an assumption can be for instance supported by the overall Hansen solubility parameter of poly(ethylene) ($\delta_{PE} = 16.2 \text{ MPa}^{1/2}$, $M_{w,PE} = 35.0 \text{ kg}\cdot\text{mol}^{-1}$, calculated at T_{room} via extrapolation from values obtained at higher temperatures⁴⁸) being lower than that of poly(isoprene) ($\delta_{PI} = 16.7 \text{ MPa}^{1/2}$, trade name *Cariflex IR 305*, linear 1,4-*cis*-rich PI³⁵). Please note that the hydrogenated PS-PI6-PS sample was not tested mechanically due to time constraints.

4.3.4. NMP-based isobornyl methacrylate – isoprene - isobornyl methacrylate type triblock copolymer

The second strategy implemented to increase the tensile stress at break of the candidate triblock copolymer consisted of the replacement of the PS outer segments by higher T_g rigid segments. As mentioned in the literature review (Section C.1.4), higher tensile stresses are generally observed for diene-based block copolymers when replacing PS blocks by higher T_g blocks⁴⁹. Due to the improved stress-strain properties and extended upper service temperature of the M_y -based triblock copolymers after substituting PS by poly(isobornyl methacrylate) P(IBOMA) (Chapter 3, Section 3.4.2), the preparation of a IBOMA-I-IBOMA type triblock copolymer was herein undertaken.

In an identical way as the previous syntheses, *cis*-1,4-rich PI-(SG1)₂ macro-initiator, termed PI7, was initiated by PEB-(SG1)₂ difunctional initiator in 50 v% pyridine at 115 °C for 15 h and exhibited $M_n = 53.1 \text{ kg.mol}^{-1}$ and $\mathcal{D} = 1.46$ (Table 4A). The monomodal molecular weight distribution of PI7 is shown in Figure 12. The chain-extension of PI7 with a IBOMA/S mixture (91/9 mol%) in 50 wt% toluene was subsequently performed at 115 °C (Table 4B). A small fraction of S was added as a controlling co-monomer to enhance the control of this bulky methacrylate chain-extension. A monomodal shift in molecular weight as a function of elution time from macro-initiator to final chain-extended copolymer was observed in the GPC chromatogram (Figure 12), indicating the successful addition of IBOMA/S segments. The resulting PI7-P(IBOMA-*co*-S)₂ triblock copolymer ($M_n = 73.5 \text{ kg.mol}^{-1}$, $\mathcal{D} = 2.00$) was fractionated via the non-solvent addition technique using the benzene/methanol pair. After fractionation, the tail on the low molecular weight edge was partly removed (Figure 12) and the triblock copolymer exhibited higher $M_n = 94.0 \text{ kg.mol}^{-1}$ and narrower molecular weight distribution ($\mathcal{D} = 1.76$). Fractionated PI7-P(IBOMA-*co*-S)₂ possessed two outer rigid segments containing 85 and 15 mol% of IBOMA and S units respectively, as indicated in Table 4C.

The thermal stability of the synthesized triblock copolymer was assessed by thermogravimetric analysis. Figure 13b represents the thermal degradation curves of PI7-P(IBOMA-*co*-S)₂ under air and nitrogen atmospheres. As expected, the polymer degraded at higher temperatures under inert atmosphere. It was particularly marked at the commencement of the TGA analysis where PI7-P(IBOMA-*co*-S)₂ started degrading at 265 °C under N₂ compared to 219 °C under air. A distinct three-step degradation behavior was observed under both conditions: a first weight loss up to about 345 °C likely due to the release of the isobornyl group (as previously mentioned in Chapter 3, Figure 6); a second major weight loss up to 412-432 °C which may be mainly caused by the scission of isoprene-rich segments ($T_{\text{dec,max,PI}} = 361\text{-}389 \text{ °C}$, Figure 2b); a last and minor decomposition step up to around 500 °C which might be due to the scission of

Table 4. Chain-extension of (A) PI-(SG1)₂ macro-initiator with (B) IBOMA/S mixture at 115 °C in 50 wt% toluene and (C) characteristics of the resulting triblock copolymer.

A. PI-(SG1) ₂ Macro-initiator							
ID	M _n ^(a) (kg.mol ⁻¹)	Đ ^(a)	1,4- ^(b) (%)	Cis-1,4- ^(b) (%)			
PI7	53.1	1.46	89.3	72.4			
B. Formulation of chain-extension							
ID	[PI7] ₀ (M)	[IBOMA] ₀ ^(c) (M)	[S] ₀ ^(c) (M)	[Toluene] ₀ (M)	M _{n,theo} ^(d) (kg.mol ⁻¹)	T (°C)	t (min)
PI7-P(IBOMA-co-S) ₂	0.004	1.571	0.154	4.631	144.4	115	90
C. Chain-extended triblock copolymer							
ID	X ^(b) (%)	F _I ^(b)	F _{IBOMA} ^(b)	F _S ^(b)	M _n ^(a) (kg.mol ⁻¹)	M _{n,theo,X} ^(e) (kg.mol ⁻¹)	Đ ^(a)
PI7-P(IBOMA-co-S) ₂	57.8	0.59	0.35	0.06	94.0	105.9	1.76

a) M_n and M_w determined by GPC calibrated with PI standards in tetrahydrofuran (THF) at 40 °C.

b) Determined by ¹H NMR in CDCl₃.

c) Previously purified by passing through a column of basic alumina mixed with 5 wt% calcium hydride.

d) Targeted number-average molecular weight of the whole chain-extended triblock copolymer at quantitative conversion.

e) Predicted M_n of the whole chain-extended triblock copolymer at X, measured experimentally, and calculated as follows:

$$M_{n,theo,X} = (X/100)(M_{n,theo} - M_{n,PI7}) + M_{n,PI7}$$

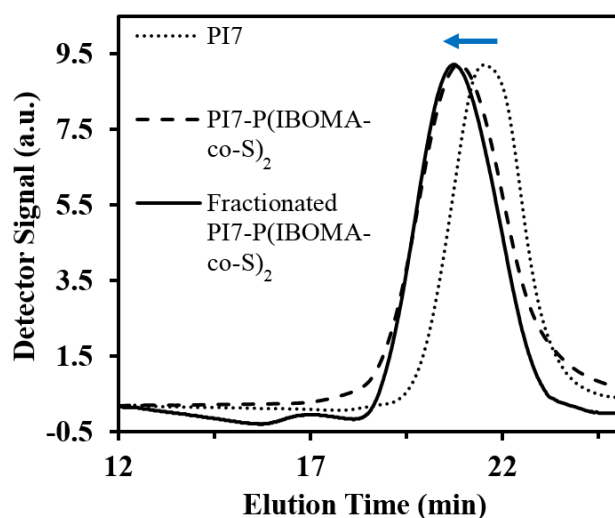


Figure 12. Normalized GPC traces (40 °C, HPLC grade THF as the mobile phase, flow rate of 0.3 mL.min⁻¹, PI standards) of macro-initiator PI7 (M_n = 53.1 kg.mol⁻¹, Đ = 1.46), chain-extended product PI7-P(IBOMA-co-S)₂ (M_n = 73.5 kg.mol⁻¹, Đ = 2.00) and fractionated PI7-P(IBOMA-co-S)₂ (M_n = 94.0 kg.mol⁻¹, Đ = 1.76).

the rigid IBOMA/S backbone.

Figure 13a shows the DSC trace of PI7-P(IBOMA-*co*-S)₂. The T_g of the soft PI block was clearly observed at - 63 °C, similar to that of PI homopolymer (- 60 °C, Figure 2a). Although harder to detect, the T_g of the IBOMA-rich segments was also determined at + 182 °C. It is consistent with the literature reporting the T_g of P(IBOMA) which ranged from 174 to 206 °C depending on the chain tacticity⁵⁰. The relatively low T_g of the PI7-P(IBOMA-*co*-S)₂ rigid segments herein may thus be caused by the high isotactic content of the P(IBOMA) sequences. A decrease of this upper T_g may also be due to the presence of S units, by assuming the formation of a homogeneous phase with IBOMA units. Generally, the T_g of these IBOMA-rich segments was much higher than that of the PS hard blocks (102-104 °C, Figure 4a), reflecting the reduced chain flexibility due to the steric hindrance of the large isobornyl side groups. Two questions can be raised following this DSC characterization: Did PI7-P(IBOMA-*co*-S)₂ phase separate as suggested by the detection of two T_gs? Did PI7-P(IBOMA-*co*-S)₂ exhibit extended service temperature compared to analogous S-I-S triblock copolymers?

The morphology of PI7-P(IBOMA-*co*-S)₂ was visualized by atomic force microscopy (AFM). Figure 14 presents a representative AFM topography and phase trace of this triblock copolymer. An unusual organization of the two phases at the micro-scale was observed with a possible core-shell type structure (dark domain) inserted in a continuous matrix (brighter domain). Although PI7-P(IBOMA-*co*-S)₂ exhibited F_I = 0.59, assigning the brighter domain to PI is not trivial. It could be for instance argued that, considering its elastic nature, PI, which was trapped between two rigid segments, tended to protrude out from the surface. These protrusions appeared as peaks in the 3D topography image (Figure 14). In this case, the darker domain would correspond to PI. Generally, this AFM study did not allow to distinctly determine a morphology (weakly aligned cylinders/lamellae might be present) and this system could be qualified as poorly ordered.

To further elucidate thermal behavior along with viscoelastic properties, the triblock was subjected to dynamic mechanical analysis (DMA). Figure 13c shows the dynamic elastic modulus (G') data as a function of temperature for PI7-P(IBOMA-*co*-S)₂. This sample had a modulus of approximately 100 MPa in order of magnitude from room temperature to about 150 °C. G' in the rubbery plateau was thus significantly higher than that of the analogous IBOMA-*My*-IBOMA type copolymer (1-10 MPa, Chapter 3, Figure 8b) and relatively similar to that of S-I-S triblock copolymers (100-1000 MPa, Figure 4c), previously synthesized by SG1-based NMP. This relatively high storage modulus observed at T < T_{g,hard block} for isoprene-based triblocks highlights the presence of a more entangled elastomeric continuous phase compared to *My*-based polymers. The softening of the IBOMA-rich segments was evidenced by the drop of G', starting at 155-160 °C. The maximum value of the damping factor appeared at 185 °C, which is consistent with the PI7-P(IBOMA-*co*-S)₂ upper T_g measured previously via DSC (182 °C, Figure 13a).

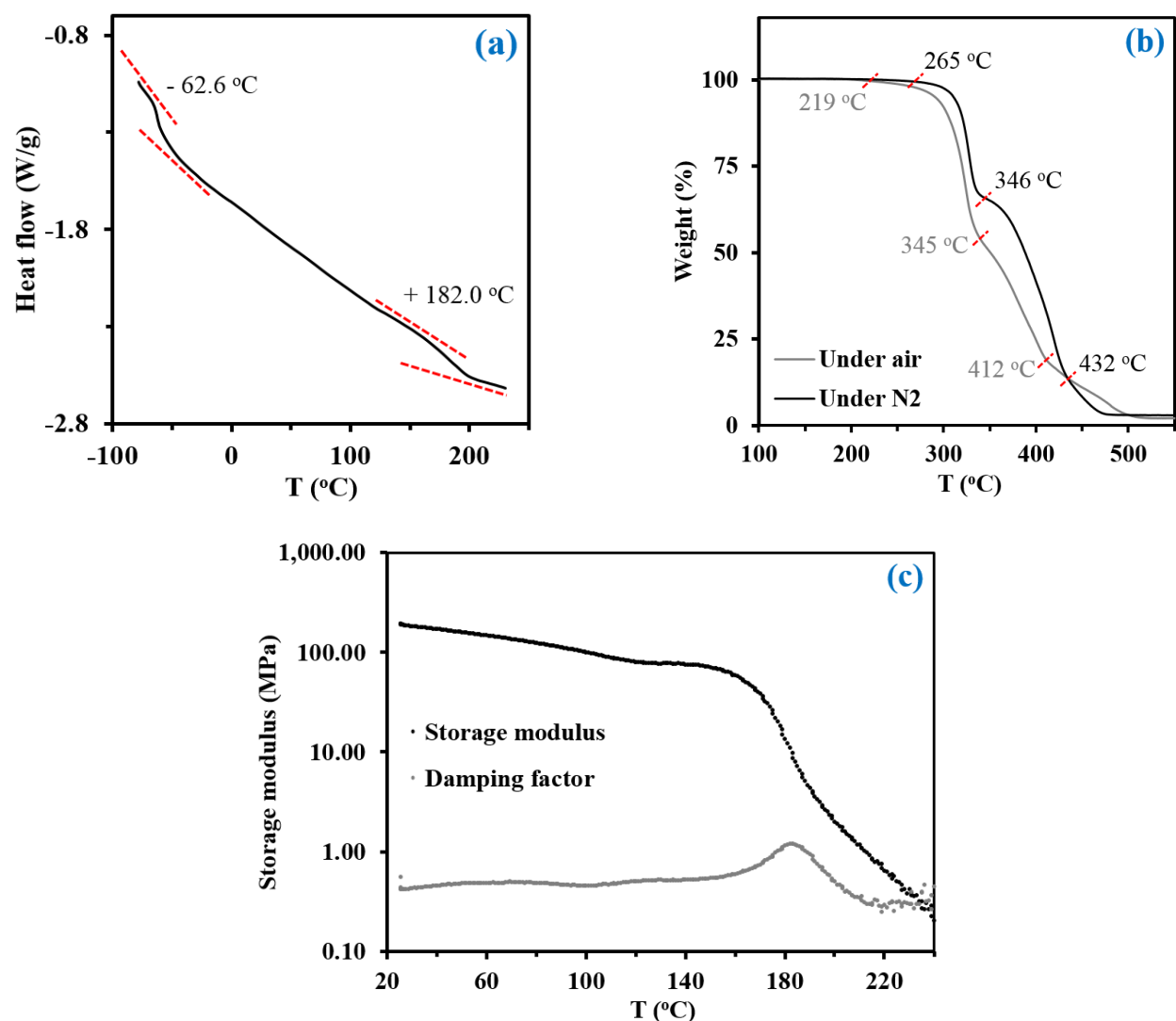


Figure 13. (a) DSC trace (second heating run) of fractionated PI7-P(IBOMA-*co*-S)₂. The numbers near the changes in slope correspond to the T_g s determined via the inflection method. (b) TGA traces (10 °C.min⁻¹) of fractionated PI7-P(IBOMA-*co*-S)₂ under air and N₂ atmospheres. The characteristic temperatures $T_{dec,1} = 219$ -265 °C (onset of decomposition) and $T \geq 345$ °C (temperatures between two degradation steps) were determined. (c) Dynamic mechanical analysis of fractionated PI7-P(IBOMA-*co*-S)₂ cast film (dichloromethane used) by torsional oscillation, yielding the storage modulus (G') and the damping factor *versus* temperature (0.15 Hz, 1% strain, 5 °C.min⁻¹, N₂ atmosphere).

Generally, the DMA test suggested that this IBOMA-I-IBOMA type triblock may well have an attractively high service temperature.

Tensile testing at room temperature for PI7-P(IBOMA-*co*-S)₂ was also performed to know if this NMP-based block copolymer can mechanically compete with industrial styrene/diene thermoplastic elastomers. The stress-strain curves of four PI7-P(IBOMA-*co*-S)₂ dog-bone specimens are given in Figure 15. The limit of elastic behavior was marked by a yield point at 20-30% elongation. It was followed by a non-reversible plastic deformation until the specimen failure at $\epsilon_B = 1356 \pm 214 \%$. Such a stretch capacity is comparable to commercial S-I-S and S-B-S (B = butadiene) thermoplastic elastomers as mentioned in the literature review (Section C.3.2, Table 8, $\epsilon_B = 880$ -1300%). Interestingly, a reduced extensibility was observed for S-I-S samples previously synthesized (Figure 6) with $\epsilon_B \leq 450 \%$, while they possessed a similar PI mid-segment ($M_n \sim 50$ -60 kg.mol⁻¹, $\bar{D} = 1.45$ -1.60). Accordingly, it might be due to the PS outer segments of S-I-S not being able to withstand mechanical stress at high elongation unlike the IBOMA-rich blocks of PI7-P(IBOMA-*co*-S)₂. This latter sample exhibited a tensile strength at break, $\sigma_B = 11.4 \pm 0.6$ MPa, largely higher than these of *My*-based block copolymers ($\sigma_B < 4$ MPa, Chapter 1, Section 1.4.3 and Chapter 3, Section 3.4.2) and S-I-S having $F_s \leq 0.38$ ($\sigma_B < 4.5$ MPa, Figure 6), stressing the beneficial combination of an entangled PI matrix with very rigid IBOMA-rich phase. However, it remained largely below the stress at break values of commercial thermoplastic elastomers such as S-I-S and S-B-S copolymers ($\sigma_B = 28$ -33 MPa, Literature Review, Section C.3.2). Despite a slight increase in tensile stress during the permanent deformation of the PI7-P(IBOMA-*co*-S)₂ specimens, no significant strain hardening was observed. The lack of strain hardening, also seen for the previous triblock copolymers made by NMP,

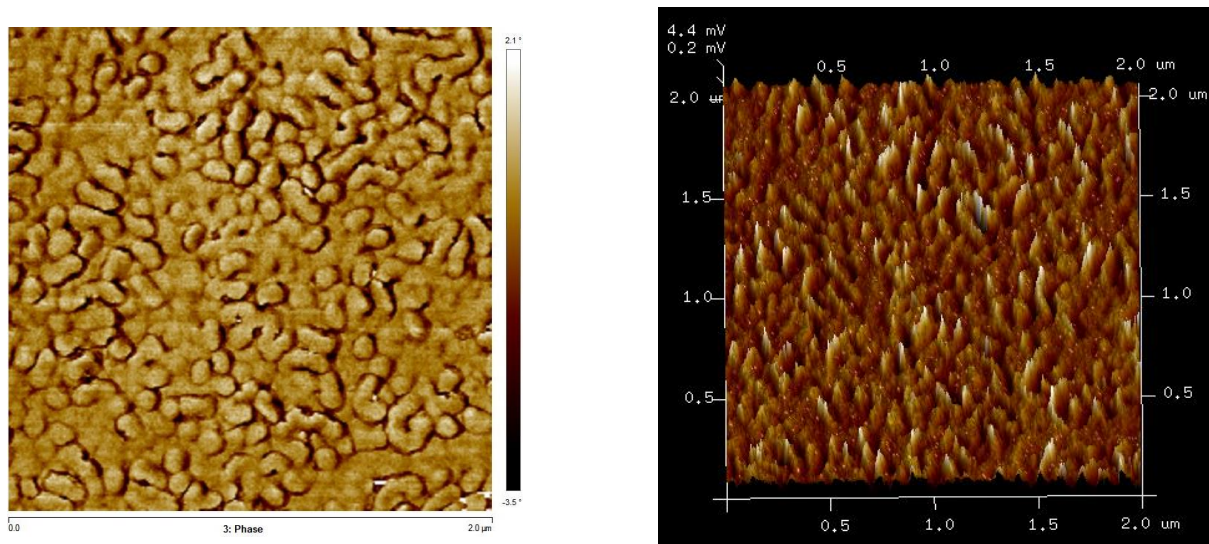


Figure 14. Atomic force microscopy (AFM, experimental section) phase image under tapping mode of operation (left) and 3D topography (right, same region) of the surface morphology of fractionated PI7-P(IBOMA-*co*-S)₂ cast film (chloroform used).

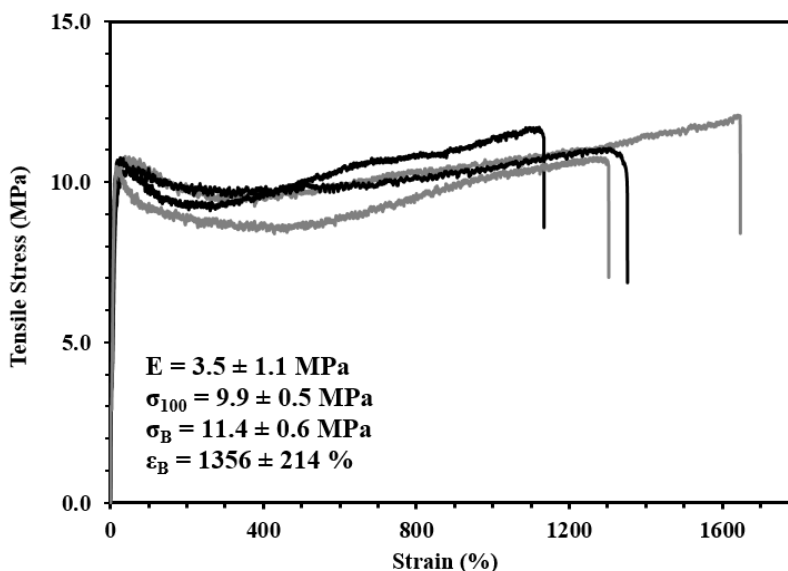


Figure 15. Uniaxial tensile stress-strain curves at room temperature and at a cross-head speed of $10 \text{ mm}\cdot\text{min}^{-1}$ of four fractionated PI7-P(IBOMA-co-S)₂ specimens (dichloromethane casting). The average Young's modulus E , tensile stress at 100% elongation σ_{100} and at break σ_B and tensile elongation at break ε_B obtained from these curves are also given.

can explain the relatively low σ_B of PI7-P(IBOMA-co-S)₂ compared to traditional styrene/diene thermoplastic elastomers. The poorly ordered micro-domain structure of PI7-P(IBOMA-co-S)₂, as suggested by the AFM analysis (Figure 14), might have been the main cause of this stress-strain behavior, hindering the orientation and the alignment of the macromolecules in the direction of the load.

It should be noted that hydrogenation of the IBOMA-I-IBOMA type copolymer was not performed due to time constraints.

4.4. Conclusion

Replacing the soft P(M_y) mid-segment ($M_{e,P(M_y)} = 22\text{-}31 \text{ kg}\cdot\text{mol}^{-1}$) of the candidate triblock copolymer by a more entangled PI segment ($M_{e,PI} = 4\text{-}6 \text{ kg}\cdot\text{mol}^{-1}$) resulted in a marked improvement of its stress-strain properties. In comparison to the NMP-based S- M_y -S which significantly lacked toughness ($\sigma_B < 1 \text{ MPa}$, $\varepsilon_B < 200\%$), synthesized S-I-S samples having $F_S \leq 0.38$ showed $\sigma_B = 2.8\text{-}4.1 \text{ MPa}$ and $\varepsilon_B = 380\text{-}450\%$. The influence of the hard segment type was also investigated via the substitution of PS blocks by harder IBOMA/S blocks (85/15 mol%). The resulting PI-P(IBOMA-co-S)₂ triblock copolymer exhibited

enhanced mechanical properties at room temperature with $\sigma_B = 11.4 \pm 0.6$ MPa and $\epsilon_B = 1356 \pm 214$ % and an extended upper service temperature, above 150 °C. The presence of IBOMA units in the outer segments remained problematic due to the thermal instability of the isobornyl ring lowering the degradation temperature of the triblock copolymer (onset of decomposition at 219 °C under air and 265 °C under N₂).

This latter IBOMA-I-IBOMA type block copolymer corresponded to the most conclusive material prepared by NMP in this doctoral thesis in terms of mechanical performance at ambient temperature. However, its tensile strength at break remained below the industrial requirement. Hydrogenation of the elastomeric mid-segment at normal pressure using diimide can be considered to increase σ_B as implemented for a S-I-S sample ($M_n = 103.1$ kg.mol⁻¹, $\bar{D} = 2.11$, $F_S = 0.49$). σ_B of the partially hydrogenated triblock copolymer (HD = 76.3%) increased of about 53% compared to the parent S-I-S, despite a reduced extensibility.

4.5. References

- (1) Pradel, J. L.; Ameduri, B.; Boutevin, B. Use of Controlled Radical Polymerization of Butadiene with AIBN and Tempo for the Determination of the NMR Characteristics of Hydroxymethyl Groups. *Macromol. Chem. Phys.* **1999**, *200*, 2304–2308.
- (2) Pradel, J. L.; Ameduri, B.; Boutevin, B. Controlled Radical Polymerization of 1,3-Butadiene. II. Initiation by Hydrogen Peroxide and Reversible Termination by Tempo. *J. Polym. Sci., Part A: Polym. Chem.* **2000**, *38*, 3293–3302.
- (3) Keoshkerian, B.; Georges, M.; Quinlan, M.; Veregin, R.; Goodbrand, B. Polyacrylates and Polydienes to High Conversion by a Stable Free Radical Polymerization Process: Use of Reducing Agents. *Macromolecules* **1998**, *31*, 7559–7561.
- (4) Benoit, D.; Harth, E.; Fox, P.; Waymouth, R. M.; Hawker, C. J. Accurate Structural Control and Block Formation in the Living Polymerization of 1,3-Dienes by Nitroxide-Mediated Procedures. *Macromolecules* **2000**, *33*, 363–370.
- (5) Cheng, C.; Qi, K.; Khoshdel, E.; Wooley, K. L. Tandem Synthesis of Core–Shell Brush Copolymers and their Transformation to Peripherally Cross-linked and Hollowed Nanostructures. *J. Am. Chem. Soc.* **2006**, *128*, 6808–6809.
- (6) Wegrzyn, J. K.; Stephan, T.; Lau, R.; Grubbs, R. B. Preparation of Poly(ethylene oxide)-block-poly(isoprene) by Nitroxide Mediated Free Radical Polymerization from PEO Macroinitiators. *J. Polym. Sci., Part A: Polym. Chem.* **2005**, *43*, 2977–2984.
- (7) Sundararaman, A.; Stephan, T.; Grubbs, R. B. Reversible Restructuring of Aqueous Block Copolymer Assemblies through Stimulus Induced Changes in Amphiphilicity. *J. Am. Chem. Soc.* **2008**, *130*, 12264–12265.
- (8) Cai, Y.; Aubrecht, K. B.; Grubbs, R. B. Thermally Induced Changes in Amphiphilicity Drive Reversible Restructuring of Assemblies of ABC Triblock Copolymers with Statistical Polyether Blocks. *J. Am. Chem. Soc.* **2010**, *133*, 1058–1065.
- (9) Ajellal, N.; Thomas, C. M.; Carpentier, J. -F. Controlled Radical Polymerization of Conjugated 1,3-Dienes with Methyl 1,3-Butadiene-1-phosphonate. *Polymer* **2008**, *49*, 4344–4349.
- (10) Luo, K.; Rzaev, J. Living Radical Polymerization of Bicyclic Dienes: Synthesis of Thermally Cross-linkable Block Copolymers. *Macromolecules* **2009**, *42*, 9268–9274.
- (11) Harrisson, S.; Couvreur, P.; Nicolas, J. SG1 Nitroxide-Mediated Polymerization of Isoprene: Alkoxyamine Structure/Control Relationship and α,ω -chain-end Functionalization. *Macromolecules* **2011**, *44*, 9230–9238.
- (12) Lessard, B.; Aumand-Bourque, C.; Chaudury, R.; Gomez, D.; Haroon, A.; Ibrahimian, N.; Mackay, S.; Noel, M. -C.; Patel, R.; Sitaram, S.; Valla, S.; White, B.; Maric, M. Poly(ethylene-co-butylene)-b-(styrene-ran-maleic anhydride)₂ compatibilizers via Nitroxide Mediated Radical Polymerization. *Intern. Polymer Processing* **2011**, *26* (2), 197.
- (13) Maric M. In Nitroxide Mediated Polymerization: From Fundamentals to Applications in Materials Science; Giggles, D., Ed.; The Royal Society of Chemistry: Cambridge, **2016**; Chapter 4, p. 153.

- (14) Harrison, S.; Couvreur, P.; Nicolas, J. Use of Solvent Effects to Improve Control over Nitroxide-Mediated Polymerization of Isoprene. *Macromol. Rapid Commun.* **2012**, *33*, 805–810.
- (15) Morey, D. R.; Tamblyn, J. W. The Fractional Precipitation of Molecular-Weight Species from High Polymers. Theories of the Process and Some Experimental Evidence. *J. Phys. Chem.* **1947**, *51* (3), 721–746.
- (16) Kotera, A. In *Polymer Fractionation*; Cantow, M. J. R., Ed.; Academic Press Inc.: New York, **1967**; Chapter B.1, pp. 44-66.
- (17) Suppaibulsuk, B.; Prasassarakich, P.; Rempel, G. L. Factorial Design of Nanosized Polyisoprene Synthesis via Differential Microemulsion Polymerization. *Polym. Adv. Technol.* **2010**, *21*, 467–475.
- (18) Sato, H.; Tanaka, Y. ¹H-NMR Study of Polyisoprenes. *J. Polym. Sci.: Polym. Chem.* **1979**, *17*, 3551–3558.
- (19) Sarkar, P.; Bhowmick, A. K. Synthesis, Characterization and Properties of a Bio-based Elastomer: Polymyrcene. *RSC Adv.* **2014**, *4*, 61343–61354.
- (20) Widmaier, J. M.; Meyer, G. C. Glass Transition Temperature of Anionic Polyisoprene. *Macromolecules* **1981**, *14*, 450-452.
- (21) Michaeli, W.; Grefenstein, A.; Frings, W. Synthesis of Polystyrene and Styrene Copolymers by Reactive Extrusion. *Adv. Polym. Tech.* **1993**, *12* (1), 25-33.
- (22) Yuan, X.; Guan, Y.; Li, S.; Zheng, A. Anionic Bulk Polymerization to Synthesize Styrene-Isoprene Diblock and Multiblock Copolymers by Reactive Extrusion. *J. Appl. Polym. Sci.* **2014**, DOI: 10.1002/APP.39429.
- (23) Wang, J. -M.; Yuan, X. -Y.; Shan, D.; Zheng, A. Styrene/Isoprene/Styrene Thermoplastic Elastomer Prepared by Anionic Bulk Polymerization in a Twin-Screw Extruder. *Int. Polym. Proc.* **2015**, *30* (1), 44-50.
- (24) Fukuda, T.; Terauchi, T.; Goto, A.; Ohno, K.; Tsujii, Y.; Miyamoto, T.; Kobatake, S.; Yamada, B. Mechanisms and Kinetics of Nitroxide-Controlled Free Radical Polymerization. *Macromolecules* **1996**, *29*, 6393-6398.
- (25) Gryn'ova, G.; Lin, C. Y.; Coote, M. L. Which Side-Reactions Compromise Nitroxide Mediated Polymerization? *Polym. Chem.* **2013**, *4* (13), 3744-3754.
- (26) Hawker, C. J.; Barclay, G. G.; Dao, J. Radical Crossover in Nitroxide Mediated “Living” Free Radical Polymerizations. *J. Am. Chem. Soc.* **1996**, *118*, 11467-11471.
- (27) Charleux, B.; Nicolas, J.; Guerret, O. Theoretical Expression of the Average Activation-Deactivation Equilibrium Constant in Controlled/Living Free-Radical Copolymerization Operating via Reversible Termination. Application to a Strongly Improved Control in Nitroxide-Mediated Polymerization of Methyl Methacrylate. *Macromolecules* **2005**, *38* (13), 5485-5492.
- (28) Peterson, J. D.; Vyazovkin, S.; Wight, C. A. Kinetics of the Thermal and Thermo-Oxidative Degradation of Polystyrene, Polyethylene and Poly(propylene). *Macromol. Chem. Phys.* **2001**, *202*, 775-784.
- (29) Stuhn, B. The Relation Between the Microphase Separation Transition and the Glass Transition in Diblock Copolymers. *J. Polym. Sci., Part B: Polym. Phys.* **1992**, *30*, 1013-1019.
- (30) Spaans, R. D.; Muhammad, M.; Williams, M. C. Probing the Interfacial Region of Microphase-Separated Block Copolymers by Differential Scanning Calorimetry. *J. Polym. Sci., Part B: Polym. Phys.* **1999**, *37*, 267-274.
- (31) Letoffe, J. -M.; Champion-Lapalu, L.; Martin, D.; Planche, J. -P.; Gerard, J. -F.; Claudy, P. Analyse Thermique de Bitumes Routiers modifiés par des Polymeres. *Bull. Lab. Ponts Chaussees* **2000**, *229*, 13-20.
- (32) Masson, J. -F.; Bundalo-Perc, S.; Delgado, A. Glass Transitions and Mixed Phases in Block SBS. *J. Polym. Sci., Part B: Polym. Phys.* **2005**, *43*, 276-279.
- (33) van den Berg, R.; de Groot, H.; van Dijk, M. A.; Denley, D. R. Atomic Force Microscopy of Thin Triblock Copolymer Films. *Polymer* **1994**, *35* (26), 5778-5781.
- (34) Khandpur, A. K.; Foerster, S.; Bates, F. S.; Hamley, I. W.; Ryan, A. J.; Bras, W.; Almdal, K.; Mortensen, K. Polyisoprene-Polystyrene Diblock Copolymer Phase Diagram near the Order-Disorder Transition. *Macromolecules* **1995**, *28* (26), 8796-8806.
- (35) Hansen, C. M. In *Hansen Solubility Parameters, A User's Handbook*, 2nd ed.; Hansen, C. M., Ed.; CRC Press: New York, **2007**; Chapter 1, pp 1-26.
- (36) Yara-Varon, E.; Fabiano-Tixier, A. S.; Balcells, M.; Canela-Garayoa, R.; Bily, A.; Chemat, F. Is it Possible to Substitute Hexane with Green Solvents for Extraction of Carotenoids? A Theoretical versus Experimental Solubility Study. *RSC Adv.* **2016**, *6*, 27750-27759.
- (37) Roy, R.; Park, J. K.; Young, W. -S.; Mastroianni, S. E.; Tureau, M. S.; Epps, T. H. Double-Gyroid Network Morphology in Tapered Diblock Copolymers. *Macromolecules* **2011**, *44*, 3910-3915.

- (38) Esneault, C. P.; Hahn, S. F.; Meyers, G. F. Development of Elastomers Based on Fully Hydrogenated Styrene-Diene Block Copolymers. In *Developments in Block Copolymer Science and Technology*; Hamley, I. W., Ed.; John Wiley & Sons: Chichester, **2004**; 341-362.
- (39) Parker, D. K. Emulsion Polymers (Noncatalytic Diimide Hydrogenation). In *Polymeric Materials Encyclopedia, 12 Volume Set*; Salamone, J. C., Ed.; CRC Press: New York, **1996**; 2048-2053.
- (40) Hahn, S. F. An Improved Method for the Diimide Hydrogenation of Butadiene and Isoprene Containing Polymers. *J. Polym. Sci., Part A: Polym. Chem.* **1992**, *30*, 397-408.
- (41) Wang, Y.; Hillmyer, M. A. Oxidatively Stable Polyolefin Thermoplastics and Elastomers for Biomedical Applications. *ACS Macro Lett.* **2017**, *6*, 613-618.
- (42) Nicolas, J.; Brusseau, S.; Charleux, B. A Minimal Amount of Acrylonitrile Turns the Nitroxide-Mediated Polymerization of Methyl Methacrylate into an Almost Ideal Controlled/Living System. *J. Polym. Sci., Part A: Polym. Chem.* **2010**, *48* (1), 34-47.
- (43) Piya-areetham, P.; Prasassarakich, P.; Rempel, G. L. Organic Solvent-Free Hydrogenation of Natural Rubber Latex and Synthetic Polyisoprene Emulsion Catalyzed by Water-Soluble Rhodium Complexes. *Journal of Molecular Catalysis A: Chemical* **2013**, *372*, 151-159.
- (44) Shubhra, Q. T. H.; Alam, A. K. M. M.; Quaiyyum, M. A. Mechanical Properties of Polypropylene Composites: A Review. *JTCM* **2011**, *26* (3), 362-391.
- (45) Carey, R. H.; Schulz, E. F.; Dienes, G. J. Mechanical Properties of Polyethylene. *Ind. Eng. Chem.* **1950**, *42* (5), 842-847.
- (46) Jordan, J. L.; Casem, D. T.; Bradley, J. M.; Dwivedi, A. K.; Brown, E. N.; Jordan, C. W. Mechanical Properties of Low Density Polyethylene. *J. dynamic behavior mater.* **2016**, *2*, 411-420.
- (47) Araki, Y.; Shimizu, D.; Hori, Y.; Nakatani, K.; Saito, H. Mechanical Properties and Microphase Structure of Hydrogenated S-SB-S Triblock Copolymers. *Polymer Journal* **2013**, *45*, 1140-1145.
- (48) Camacho, J.; Diez, E.; Diaz, I.; Ovejero, G. Hansen Solubility Parameter: From Polyethylene and Poly(vinyl acetate) Homopolymers to Ethylene-Vinyl Acetate Copolymers. *Polym. Int.* **2017**, *66*, 1013-1020.
- (49) Fetters, L. J.; Morton, M. Synthesis and Properties of Block Polymers. I. Poly- α -methylstyrene-polyisoprene-poly- α -methylstyrene. *Macromolecules* **1969**, *2* (5), 453-458.
- (50) Yu, J. M.; Dubois, P.; Jérôme, R. Poly[alkyl methacrylate-*b*-butadiene-*b*-alkyl methacrylate] Triblock Copolymers: Synthesis, Morphology, and Mechanical Properties at High Temperatures. *Macromolecules* **1996**, *29* (26), 8362-8370.

Chapter 5. *Characterization of commercial styrenic triblock copolymers*

5.1. Preface

The synthesis by nitroxide-mediated polymerization (NMP) to yield isoprene-based triblock copolymers exhibiting valuable stress-strain properties was highlighted in the previous chapter. However, the lack of toughness of these synthesized copolymers can be stressed when comparing with the mechanical features of commercial thermoplastic elastomers (TPE).

This technical chapter is dedicated to the thermal, mechanical and rheological characterization of commercial styrene-isoprene-styrene (S-I-S) and styrene-ethylene/butylene-styrene (SEBS) triblock copolymers, all synthesized industrially by living anionic polymerization. Although properties of sold products are generally reported by companies, in-house measurements were required in order to use the same testing machines throughout the doctoral thesis. The objective was not to find a marketed candidate TPE for the industrial problem. It was only aimed at targeting commercial styrenic block copolymer TPE satisfying the ArianeGroup mechanical requirements at room temperature. The group of styrenic block copolymers was selected to allow direct comparisons with the previous isoprene-based triblocks made by SG1-based NMP (Chapter 4).

5.2. Abstract

The relatively low tensile strength at break ($\sigma_B = 7.5 \pm 0.6$ MPa) of an initially supplied S-I-S possessing about 8 mol% of styrene (S₄-I-S₄) prompted us to study a second S-I-S richer in PS ($F_S \sim 0.16$, S₈-I-S₈, the subscripts state the mol% S in the polymer). Doubling the fraction of the rigid phase resulted in higher but not sufficient $\sigma_B = 12.7 \pm 0.7$ MPa. The preparation of tensile specimens by a solvent casting instead of compression molding allowed this latter copolymer to be tougher (σ_B and elongation at break ϵ_B increased by 13% and 25% respectively). Moreover, the partial hydrogenation (67 mol%) of S₈-I-S₈ enhanced its mechanical strength at low- and high-elongation regions. A styrene-butadiene-styrene (S-B-S) having its soft mid-segment completely hydrogenated and a high fraction of PS (48 mol%) showed the most conclusive stress-strain properties at ambient temperature with $\sigma_B = 25.0 \pm 2.1$ MPa and $\epsilon_B = 730 \pm 40$ %. However, its limited thermal stability would impose a welding with the tank and the skirts at $T \leq 275$ °C under inert atmosphere.

5.3. Results

5.3.1. Commercial S-I-S from *Sigma-Aldrich*[®]

A preliminary styrene-isoprene-styrene S-I-S provided by *Sigma-Aldrich*[®] (product number = 432393, experimental section) containing only 14 wt% of S units, as outlined in the specification sheet, was first characterized and the following features were determined in the laboratory:

- 8.4 mol% S was determined by ¹H NMR (triblock thus abbreviated S₄-I-S₄ for the study).
- M_n = 98.3 kg.mol⁻¹ and Đ = 1.29 were measured via GPC (Figure 1).
- DSC analysis gave T_{g,soft segment} = - 60 °C (Figure 2a) and the T_g of the PS blocks was not detected (presumably due to the low S molar fraction).
- As typically observed for styrene-based TPE, the storage modulus stayed relatively constant (G' = 0.1-0.3 MPa) until about 100 °C where the PS hard phase softened (Figure 3).
- Tensile stress at break σ_B = 7.5 ± 0.6 MPa and elongation at break ε_B = 4250 ± 230 % were determined via uniaxial tensile testing.

The relatively low σ_B of this commercial styrenic TPE was not satisfactory for the industrial application. Consequently, a similar S-I-S from *Sigma-Aldrich*[®] possessing a higher fraction of S units (22 wt% as specified, product number = 432415, experimental section) was subsequently tested and exhibited:

- 15.9 mol% S as determined by ¹H NMR (triblock abbreviated S₈-I-S₈).
- M_n = 97.2 kg.mol⁻¹ and Đ = 1.25 via GPC measurement (Figure 1).
- T_{g,soft segment} = - 61 °C (Figure 2a).

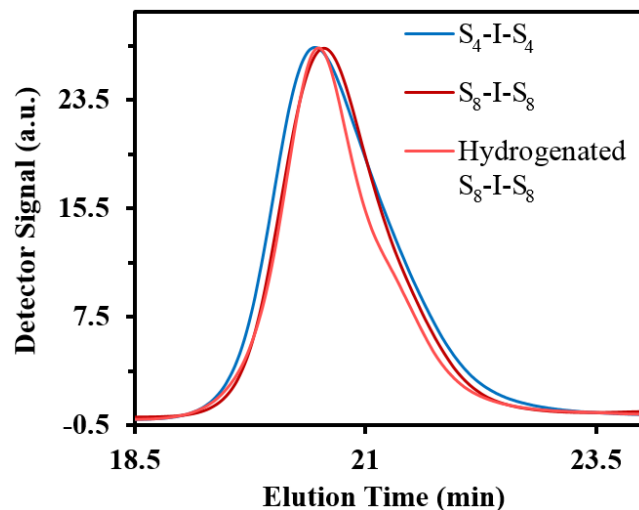


Figure 1. Normalized GPC traces (40 °C, THF as the mobile phase, PI standards) of S₄-I-S₄ (M_n = 98.3 kg.mol⁻¹, Đ = 1.29), S₈-I-S₈ (M_n = 97.2 kg.mol⁻¹, Đ = 1.25) and hydrogenated S₈-I-S₈ (M_n = 110.1 kg.mol⁻¹, Đ = 1.32).

- Well-ordered micro-phase separation revealing possibly a cylindrical/lamellar morphology as observed by AFM (Figure 5) despite a low $F_S \sim 0.16$.
- Higher Young's modulus $E = 0.19 \pm 0.04$ MPa, $\sigma_B = 12.7 \pm 0.7$ MPa and lower $\epsilon_B = 3740 \pm 140$ % compared to the mechanical properties of S_4 -I- S_4 at room temperature (Figure 4).
- Higher G' in the rubbery plateau (1-3 MPa) as well as at $T > T_{g,PS}$ (Figure 3).

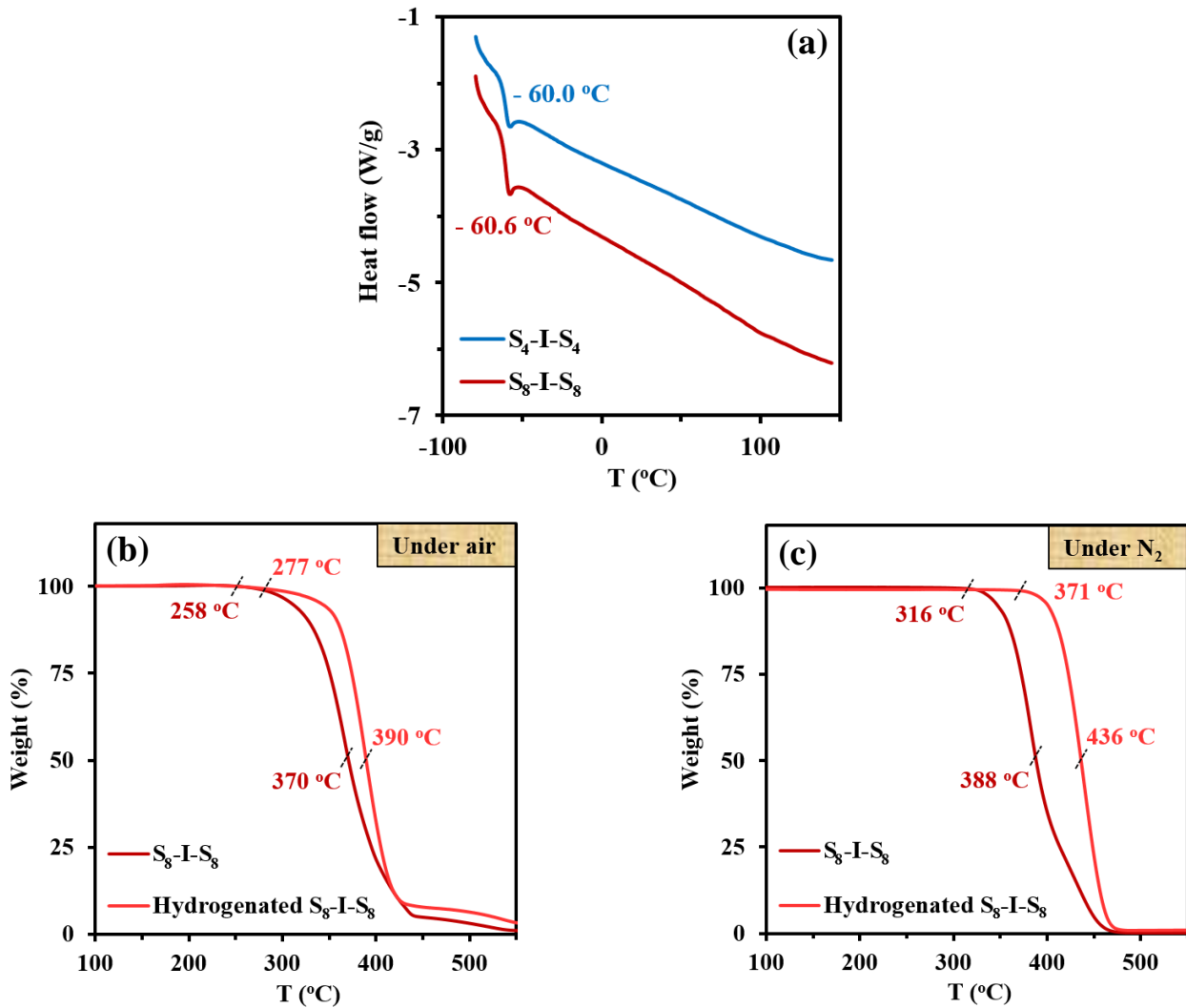


Figure 2. (a) DSC traces (second heating run) of S_4 -I- S_4 and S_8 -I- S_8 . The numbers near the changes in slope correspond to the T_g s determined via the inflection method. TGA traces (10 °C. min^{-1}) of S_8 -I- S_8 under (b) air and (c) N_2 atmospheres. The characteristic temperatures $T_{dec,1} = 258$ - 371 °C (onset of decomposition) and $T_{dec,max} = 370$ - 436 °C (temperature at which weight loss is most apparent) were determined.

Direct comparisons between these two commercial styrenic TPE and the S-I-S previously synthesized by NMP (Chapter 4, Section 4.3.2) can be made. While these two groups of triblock copolymers had a similar $M_n \sim 90\text{-}110 \text{ kg}\cdot\text{mol}^{-1}$, the dispersity of the polymers from *Sigma-Aldrich*[®] ($\mathcal{D} < 1.30$) was drastically lower than that of the experimental block copolymers ($\mathcal{D} \geq 2.11$). The narrow molecular weight distribution exhibited by the commercial S-I-S resulted from the use of living anionic polymerization, eliminating most of the transfer and termination reactions, and can partly explain the strong phase separation observed by AFM for $S_8\text{-I-S}_8$ (Figure 5) where a distinct morphology was identified. The more ambiguous and disordered phase separation of the NMP-based triblocks (Chapter 4, Figure 5) may in contrast be caused by the high dispersity of these samples, reducing the segregation strength. Another major difference between the commercial and the experimental S-I-S can be highlighted with regard to the stress-strain behavior. After the low-strain region, strain hardening took place for $S_4\text{-I-S}_4$ and $S_8\text{-I-S}_8$ samples, converting the soft plastic to a tough and stiffer material. While relatively low tensile strength values were displayed by $S_4\text{-I-S}_4$ ($\sigma_B \sim 0.5\text{-}1.7 \text{ MPa}$) and $S_8\text{-I-S}_8$ ($\sigma_B \sim 1.6\text{-}4.5 \text{ MPa}$) during the initial plastic deformation ($\varepsilon \sim 200\text{-}2000\%$, drawing of the chains), the subsequent alignment of the chains at $\varepsilon > 2000\%$ markedly increased σ_B . Such a tensile behavior was not observed for the samples prepared by controlled radical polymerization (Chapter 4, Figure 6). Despite a slight increase of the stress during the irreversible deformation for the NMP-based S-I-S having $F_S \leq 0.38$, no strain hardening occurred. It may be partly due to the presence in the tested specimens of a small fraction of short S-I-S chains ($M_n < 20 \text{ kg}\cdot\text{mol}^{-1}$), disrupting the orientation and alignment of the macromolecules in the direction of the load.

Although $S_8\text{-I-S}_8$ was tougher than $S_4\text{-I-S}_4$ with notably an enhanced tensile strength at low and high deformations, a higher σ_B was required. To improve the properties of the commercial $S_8\text{-I-S}_8$ triblock copolymer, two strategies were undertaken: (1) preparation of specimens via film casting instead of compression molding; (2) hydrogenation of the elastomeric block.

The way to prepare the samples prior to tensile testing or DMA analysis can significantly affect the results. When molding the specimens via hot press (compression-molded specimens), the relatively fast cooling phase after molding may hinder the equilibrium morphology to occur. For films prepared from direct casting, the solvent evaporates slowly thus allowing a stable organization of the macromolecules close to the thermodynamic equilibrium. Accordingly, a stronger phase separation may be expected for S-I-S cast film. For this study, dichloromethane casting allowed the preparation of dog-bone style tensile specimens and rectangular bars for DMA. Figure 3 shows G' versus T curves of $S_8\text{-I-S}_8$ prepared by hot press (HP, red curve) and via solvent casting (cast film, CF, black curve). Interestingly, G' of the cast film was higher throughout the analysis. In the rubbery plateau, while the storage modulus of the compression-molded bar decreased with T , G' stayed almost constant for the cast film. Another noteworthy observation can be made: while G' of the molded specimen started to significantly drop at $T \sim 85 \text{ }^\circ\text{C}$, G' of $S_8\text{-I-S}_8$ cast

film decreased only at $T \geq 95$ °C. This slightly higher upper service temperature can be due to a stronger segregation of the soft PI and hard PS phases when preparing the specimens via solvent casting (possible higher order-disorder transition temperature T_{ODT}). Figure 4 gives the stress-strain curves (in black) of five S_8 -I- S_8 cast film specimens. Compared to identical samples prepared by compression molding, improved mechanical properties were obtained with $\sigma_B = 14.3 \pm 2.1$ MPa and $\epsilon_B = 4690 \pm 325$ %.

The saturation of the PI mid-segment was also implemented to increase the tensile strength of S_8 -I- S_8 . As done for the NMP-based S-I-S (Chapter 4, Section 4.3.3), hydrogenation of the elastomeric segment was performed relying on the Hahn procedure (polymer allowed to react with *p*-toluenesulfonyl hydrazide in toluene for 3 h at 125 °C in the presence of tributylamine and BHT antioxidant). HD (hydrogenation degree) = 67 mol% was determined via ^1H NMR. Three partially hydrogenated specimens prepared from dichloromethane casting were tested mechanically (Figure 4, grey curves). The modulus of the initial slope increased ($E = 0.49 \pm 0.05$ MPa). An increase in stress was also observed in low-strain and high-strain regions after the chemical hydrogenation and $\sigma_B = 18.4 \pm 0.7$ MPa was measured at the complete breakup of the specimens. As previously observed for the partially hydrogenated S-I-S made by NMP (Chapter 4, Section 4.3.3), the greater stiffness of S_8 -I- S_8 , when having its mid-segment partly saturated, resulted in a

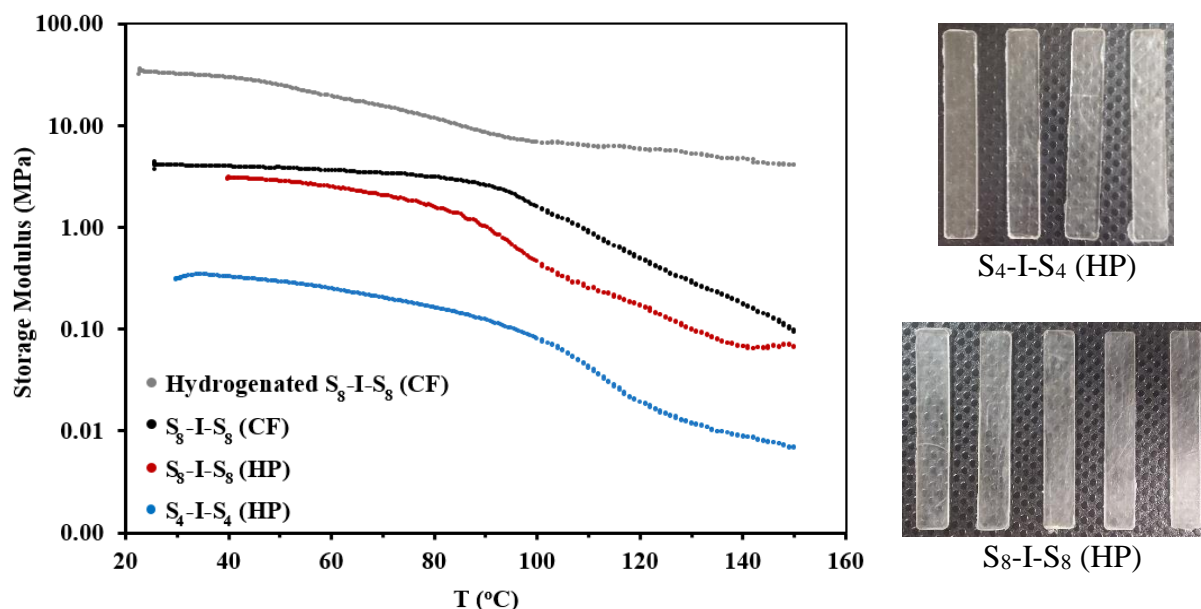
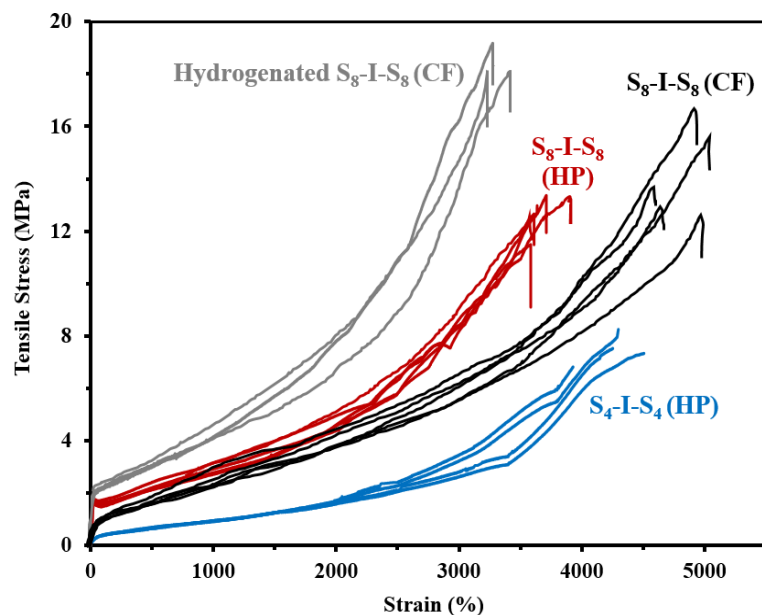


Figure 3. Dynamic mechanical analysis of S_4 -I- S_4 and (partially hydrogenated) S_8 -I- S_8 by torsional oscillation, yielding the storage modulus (G') versus temperature (0.15 Hz, 1% strain, 5 °C.min $^{-1}$, N_2 atmosphere). The rectangular bars were made either using hot press (HP) or from dichloromethane casting (cast film, CF).



S₄-I-S₄ (HP)



S₈-I-S₈ (HP)

Sample	E (MPa)	σ_B (MPa)	ϵ_B (%)
S ₄ -I-S ₄ (HP)	0.030 ± 0.002	7.5 ± 0.6	4250 ± 230
S ₈ -I-S ₈ (HP)	0.19 ± 0.04	12.7 ± 0.7	3740 ± 140
S ₈ -I-S ₈ (CF)	0.09 ± 0.02	14.3 ± 2.1	4690 ± 325
Hydrogenated S ₈ -I-S ₈ (CF)	0.49 ± 0.05	18.4 ± 0.7	3310 ± 95

Figure 4. Uniaxial tensile stress-strain curves at room temperature and at a cross-head speed of $10 \text{ mm} \cdot \text{min}^{-1}$ of S₄-I-S₄ and (partially hydrogenated) S₈-I-S₈ specimens. The average Young's modulus E, tensile stress at break σ_B and tensile elongation at break ϵ_B obtained from these curves are also given in the table below the curves. The dog-bone style tensile specimens were made using either hot press (HP) or from dichloromethane casting (cast film, CF).

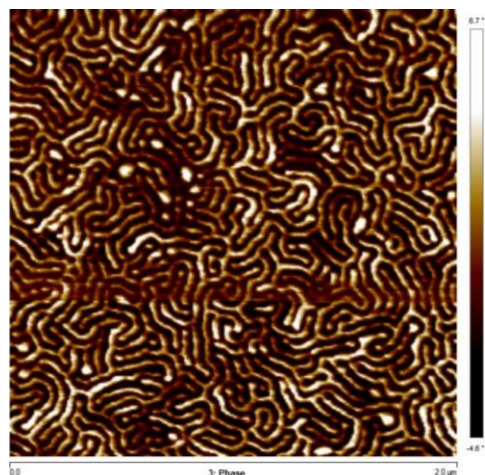


Figure 5. Atomic force microscopy (AFM) phase image ($2 \mu\text{m} \times 2 \mu\text{m}$) under tapping mode of operation of the surface morphology of S₈-I-S₈ cast film (chloroform used).

lower extensibility with $\epsilon_B = 3310 \pm 95 \%$. Furthermore, the TGA results before and after hydrogenation were of interest. Whereas the thermal stability of S₈-I-S₈ was slightly improved under air after incomplete hydrogenation (Figure 2b), the commencement of the thermal decomposition (+ 55 °C) as well as the maximal degradation at about 50 wt% loss (+ 48 °C) occurred at much higher temperatures under nitrogen (Figure 2c). Lastly, a hydrogenated S₈-I-S₈ cast film bar was tested via DMA (Figure 3, grey curve). A marked increase of G' was observed compared to the parent unsaturated S₈-I-S₈ cast film (black curve), either before or after the glass transition at T ~ 90-100 °C. Such a trend can be explained by the presence of ethylene/propylene sequences in the polymer chain after hydrogenation of the isoprene units, tending to decrease the mobility and the free volume of the triblock copolymer. Interestingly, at T > T_{g,PS} ~ 100 °C, no drop of G' was seen for the hydrogenated S₈-I-S₈ and it remained almost constant at about 4.5-6.5 MPa up to 150 °C.

The preparation of cast films as well as the hydrogenation of the flexible mid-segment allowed an enhancement of the TPE mechanical and thermal properties. Partially hydrogenated S₈-I-S₈ cast film exhibited conclusive properties for our industrial criterion. Since solvent casting process can be considered not adequate from an industrial point of view, attention was then paid to the characterization of a fully hydrogenated styrenic block copolymer TPE.

5.3.2. Commercial SEBS from *Kraton*[®]

Styrene-ethylene/butylene-styrene (SEBS) block copolymers are produced industrially in a two-step process: (1) synthesis of styrene-butadiene-styrene (SBS) by living anionic polymerization; (2) Conversion of SBS to SEBS through selective and quantitative hydrogenation of the rubbery mid-block using high-pressure H₂ and a catalyst. SEBS A1536 H (industrial specifications in the experimental section) from *Kraton*[®] was purchased and characterized in this study.

Preliminary ¹H NMR and GPC analyses gave F_S = 0.48, M_n = 87.5 kg.mol⁻¹ and Đ = 1.16. The tensile yield behavior of SEBS specimens prepared via compression molding is shown in Figure 6a. The effects of the complete hydrogenation of the polydiene segment were clearly observed with a high tensile strength at break $\sigma_B \sim 25$ MPa and a relatively low elongation at break $\epsilon_B \sim 700\%$ compared to traditional styrenic TPE. Despite a moderate extensibility, this stress-strain behavior meets the industrial requirements at room temperature. The TGA traces under air and nitrogen are given in Figure 6c below. Regardless of the atmosphere, the thermal stability displayed by this fully hydrogenated SBS was not as good as that of the partially hydrogenated S₈-I-S₈ characterized previously. This may be caused by the high molar fraction of styrene in the SEBS (F_S = 0.48) compared to that of S₈-I-S₈ (F_S ~ 0.16). G' *versus* T curve of SEBS

A1536 H is also shown in Figure 6b. An early drop of the storage modulus at about 70 °C was detected which might be due to the melting of weak crystalline segments of the ethylene/butylene block. Indeed,

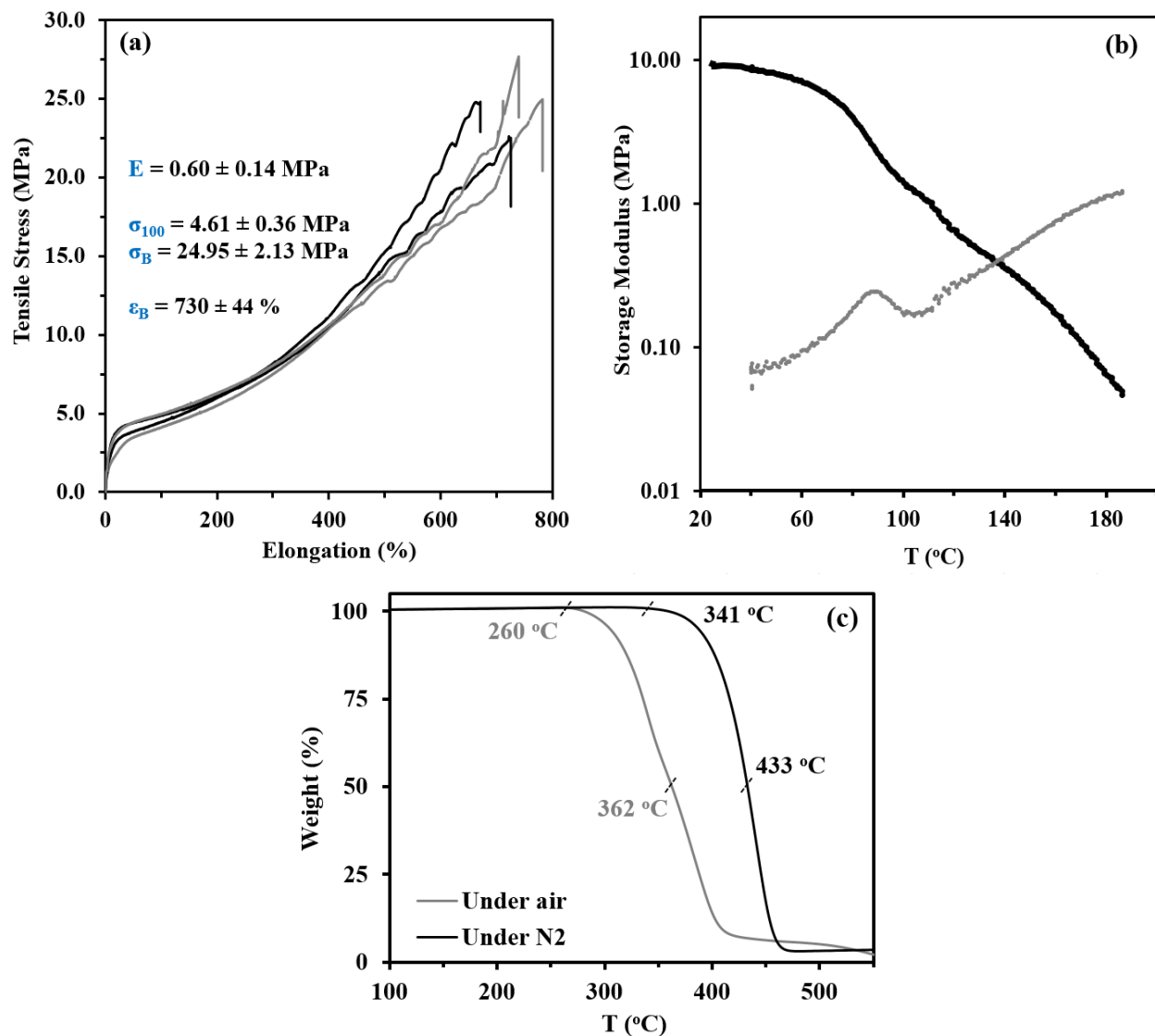


Figure 6. (a) Uniaxial tensile stress-strain curves at room temperature and a cross-head speed of 10 mm.min⁻¹ of four SEBS specimens prepared by hot press. The average Young's modulus E , tensile stress at 100% elongation σ_{100} and at break σ_B and tensile elongation at break ϵ_B obtained from these curves are also given. (b) Dynamic mechanical analysis of SEBS specimens prepared by hot press by torsional oscillation, yielding the storage modulus (G' , black curve) and the damping factor (grey curve) *versus* temperature (0.15 Hz, 1% strain, 5 °C.min⁻¹, N₂ atmosphere). (c) TGA traces (10 °C.min⁻¹) of SEBS under air (grey) and nitrogen (black) atmospheres. The characteristic temperatures $T_{dec,1} = 260$ -341 °C (onset of decomposition) and $T_{dec,max} = 362$ -433 °C (temperature at which weight loss is most apparent) were determined.

hydrogenation of common SBS copolymers can result in a predominantly PE mid-block that crystallizes. The damping factor ($\tan \delta = G''/G'$) is also given in Figure 6b (grey curve) and a local peak appeared at 89 °C, referring likely to the glass transition temperature of the PS outer blocks.

Generally, this commercial SEBS triblock copolymer satisfied the ArianeGroup specifications in terms of stress-strain properties at room-temperature. The high styrene content associated to the complete hydrogenation of the poly(butadiene) segment allowed this styrenic block copolymer to display a high mechanical strength while having a largely acceptable extensibility.

For purposes of welding the candidate TPE with the thermoplastic composite considered for the application (constituting the tank and the skirts of the launcher), the assembly must be heated at an elevated temperature ($T > 250$ °C) for a few minutes. Consequently, the TPE must be stable thermally and any degradation would make the welding process inefficient. To deem the ability of the purchased SEBS to resist high temperatures, isothermal TGA were led (Figure 7). Under air, While SEBS did not decompose at 200 °C for almost 90 min, the sample weight fell after 20 min at $T = 230$ °C (Figure 7a), thus not allowing the welding in an O_2 environment. Under nitrogen, the hydrogenated SBS was stable for 90 min at $T = 230$ -275 °C. However, a 10% weight loss was apparent when running the TGA at 290 °C (Figure 7b). Accordingly, the limited thermal stability of SEBS imposes the welding under inert atmosphere at $T \leq 275$ °C.

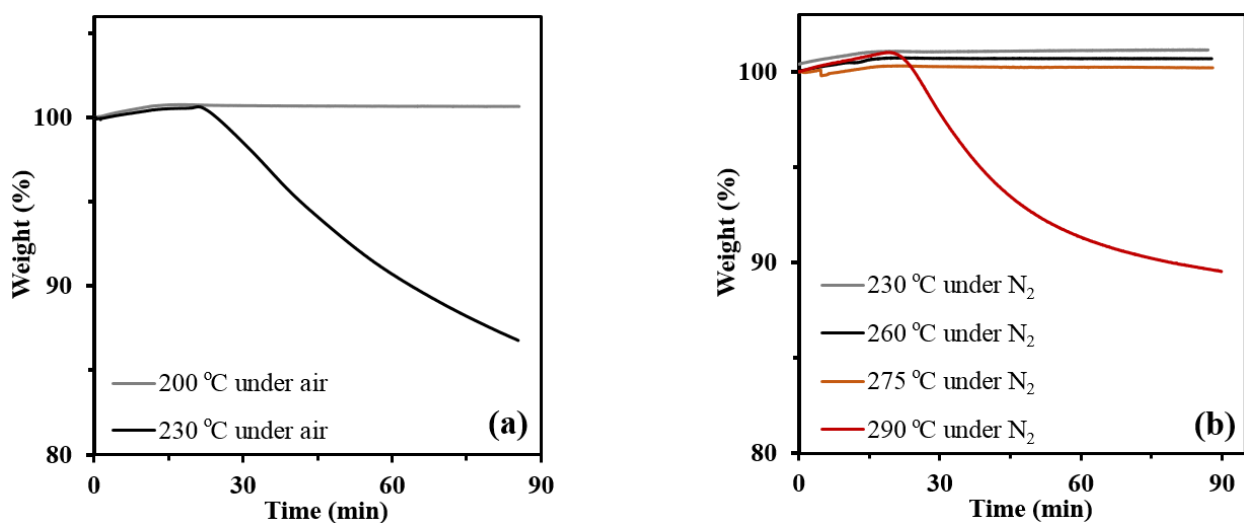


Figure 7. Isothermal TGA traces of the commercial SEBS A1536 H under (a) air ($T = 200$ -230 °C) and (b) N_2 ($T = 230$ -290 °C) atmospheres.

5.4. Conclusion

This chapter aimed to identify reference styrenic block copolymer TPE providing conclusive mechanical features at room temperature with respect to the ArianeGroup issue. Commercial S-I-S triblock copolymers ($M_n = 97\text{-}98 \text{ kg}\cdot\text{mol}^{-1}$, $\mathcal{D} = 1.25\text{-}1.29$) exhibiting a minor fraction of S ($\leq 16 \text{ mol}\%$) were first evaluated. Despite a remarkable extensibility with $\varepsilon_B = 4250 \pm 230 \%$, S-I-S having $F_S \sim 0.08$ was not strong enough with $\sigma_B = 7.5 \pm 0.6 \text{ MPa}$. A slightly less stretchable S-I-S ($\varepsilon_B = 3740 \pm 140 \%$) richer in S ($F_S \sim 0.16$), which micro-phase separated into lamellae (or cylinders), showed a higher tensile strength at break $\sigma_B = 12.7 \pm 0.7 \text{ MPa}$, although not sufficient for the considered application. Following these characterizations, the importance of the fraction of the rigid phase in the copolymer was highlighted. Mechanical properties in this family of TPE can be significantly tuned based on composition. While TPE displaying a spherical morphology (hard blocks forming discrete minority spheres embedded in a rubbery matrix) were initially privileged for this thesis due to their isotropic nature, it can be concluded herein that S-I-S having $F_S > 20 \text{ mol}\%$ (with likely a cylindrical/lamellar morphology) must be targeted in order to reach a satisfactory σ_B .

Unlike the NMP-based S-I-S previously synthesized ($M_n = 95\text{-}109 \text{ kg}\cdot\text{mol}^{-1}$, $\mathcal{D} = 2.18\text{-}2.29$, $F_S = 0.30\text{-}0.38$), these commercial samples prepared anionically showed a marked strain hardening in the high-strain region ($\varepsilon > 2000\%$), allowing the tensile stress to greatly increased. It may be explained by the narrower molecular weight distribution of these block copolymers ($\mathcal{D} < 1.30$) where all the chains, exhibiting a similar length, can straighten. The high level of control of these triblock copolymers was also evidenced by the strong phase-separation of S-I-S possessing $16 \text{ mol}\%$ S, in comparison to the more disordered PI and PS microdomains observed for the triblocks made by NMP.

Preparing commercial S-I-S specimens ($F_S \sim 0.16$) via dichloromethane casting instead of compression molding allowed to increase their toughness ($\sigma_B = 14.3 \pm 2.1 \text{ MPa}$, $\varepsilon_B = 4690 \pm 325 \%$) as well as their storage modulus at $T = 25\text{-}150 \text{ }^\circ\text{C}$. The incomplete hydrogenation of this latter triblock (saturation of $67 \text{ mol}\%$ of the soft segment) made it stronger ($\sigma_B = 18.4 \pm 0.7 \text{ MPa}$) and more stable thermally under an inert environment, with a starting decomposition at about $370 \text{ }^\circ\text{C}$. Moreover, the storage modulus of this hydrogenated S-I-S was significantly higher in the rubbery plateau ($G' = 35\text{-}10 \text{ MPa}$) and did not dramatically drop at $T > 100 \text{ }^\circ\text{C}$ (gradual decrease from 10 to 4 MPa), suggesting an extended upper service temperature compared to typical styrenic block copolymers.

Targeting a styrenic block copolymer TPE which has a relatively high molar fraction of S ($F_S > 20 \text{ mol}\%$) and its elastomeric mid-block hydrogenated appeared thereby to be relevant to meet the mechanical requirements at room temperature. A commercial and well-defined SEBS triblock copolymer ($M_n = 87.5 \text{ kg}\cdot\text{mol}^{-1}$, $\mathcal{D} = 1.16$), originating from the complete hydrogenation of SBS and possessing almost as much

styrene as ethylene/butylene units ($F_s = 0.48$), showed a satisfactory stress-strain behavior with $\sigma_B = 25.0 \pm 2.1$ MPa and $\varepsilon_B = 730 \pm 40$ %. Its acceptable thermal stability under inert atmosphere indicated seemingly a possible welding with the thermoplastic composite at $T \leq 275$ °C.

GENERAL CONCLUSION

This doctoral thesis aimed to synthesize a tough and stable thermoplastic elastomer (TPE), capable of providing a soft junction between polar composite matrices (tank and skirts of a launcher). The TPE, joined to the composites by adhesive bonding or welding, is used to transmit mostly shearing forces occurring at the joint and has to meet specific requirements, including:

- tensile behavior similar to that of vulcanized elastomers.
- minimal drop of its mechanical properties at $T \leq 80$ °C.
- no flowing nor degradation during the joining process ($T \sim 160$ - 180 °C for more than 10 h if adhesive bonding is employed, $T \sim 240$ - 280 °C for a few minutes in the case of a welding).

Styrenic triblock copolymers, consisting of a poly(diene) segment (continuous domain) and two poly(styrene) (PS) end segments (discrete domain), were initially targeted since most of the commercial ones satisfy the ArianeGroup mechanical requirements at room temperature (primary focus). Nitroxide-mediated polymerization (NMP) was selected mainly due to its simplicity to implement, its effectiveness for controlling the polymerization of 1,3-dienes, which also conveniently aligns with the expertise of Prof. Maric's laboratories. Furthermore, the robustness of NMP towards polar monomers and a large variety of vinyl monomers was of importance since two main modifications were proposed: (1) functionalization of the poly(diene) via direct diene/functional monomer copolymerization (to aid the joining with the polar composite matrices); (2) substitution of PS by higher glass transition temperature (T_g) polymer (to increase the tensile stress and the upper service temperature of the triblock copolymer).

Pending the acquirement of pressurized reactors to polymerize isoprene (low boiling point, $T_b \sim 34$ °C), β -myrcene (My), a non-volatile ($T_b \sim 167$ °C) and renewably-sourced 1,3-diene, was first considered as a promising building block for making the flexible segment of the TPE.

Poly(β -myrcene) $P(My)$ (number-average molecular weight $M_n = 23$ - 30 kg.mol⁻¹, dispersity $\mathcal{D} = 1.32$ - 1.38) were first produced by NMP at 120 °C in bulk using the NHS-BlocBuilder (NHS-BB) monofunctional initiator (possessing the SG1 controlling nitroxide group). The active feature of these poly(diene)s (chain end capped by a nitroxide moiety) allowed styrene (S) chain-extensions in toluene at 110 °C. The resulting **My -S diblock copolymers** ($M_n = 39$ - 49 kg.mol⁻¹, $\mathcal{D} = 1.50$ - 1.88 , molar fraction of S, $F_S = 0.27$ - 0.47) showed poor strain-stress properties (tensile stress at break $\sigma_B < 1$ MPa, elongation at break $\epsilon_B < 16\%$) with no plastic deformation. Two main reasons can explain this brittle behavior: a lack of

entanglement density of the soft domain caused by the high $P(My)$ entanglement molecular weight ($M_{e,P(My)} = 22-31 \text{ kg}\cdot\text{mol}^{-1}$); the diblock type molecular architecture where rubber $P(My)$ chains are attached to a rigid PS chain at only one end (not physically cross-linked). The synthesis of **S-My-S triblock copolymers** exhibiting a higher $P(My)$ M_n appeared thus essential and was made possible using the SG1-terminated poly(ethylene-*co*-butylene) (PEB-(SG1)₂) difunctional initiator. Telechelic $P(My)$ -(SG1)₂ macro-initiator capped by two SG1 units was first synthesized using PEB-(SG1)₂ in bulk at 120 °C, followed by the S chain-extension at 115 °C in toluene. Greater extensibility ($\epsilon_B = 90-180 \%$) was displayed by S-My-S ($M_n = 56-66 \text{ kg}\cdot\text{mol}^{-1}$ with $M_{n,P(My)} = 45 \text{ kg}\cdot\text{mol}^{-1}$, $\bar{D} = 1.72-1.86$ and $F_S = 0.20-0.32$) compared to My-S, in spite of a similar and low tensile stress ($\sigma_B < 0.8 \text{ MPa}$). Generally, these NMP-based My/S block copolymers displayed tensile properties largely below the industrial specifications.

PS outer segments ($T_g \sim 100 \text{ °C}$) were then replaced by higher T_g blocks, namely poly(isobornyl methacrylate) P(IBOMA) ($T_g \sim 190 \text{ °C}$) to enhance the tensile strength and the service temperature of the candidate material. The conditions used to produce S-My-S were applied on a similar way to the synthesis of **IBOMA-My-IBOMA type triblock copolymers** ($M_n = 51-95 \text{ kg}\cdot\text{mol}^{-1}$, $\bar{D} = 1.91-2.23$, $F_{IBOMA} = 0.28-0.36$), containing a minor fraction of My or S in the rigid segments. Indeed, due to the difficulty to homopolymerize methacrylate by NMP, My or S was added as a controlling co-monomer during the IBOMA chain-extension. Two distinct T_g s were detected at about -60 °C and $+180 \text{ °C}$, suggesting a two-phase system. The micro-phase separation of the continuous $P(My)$ domain and the disperse IBOMA-rich aggregates was confirmed by atomic force microscopy (AFM). Moderate mechanical strength ($\sigma_B = 3.9 \pm 0.2 \text{ MPa}$) and relatively high irreversible extensibility ($\epsilon_B = 490 \pm 30 \%$) were measured via tensile testing, which revealed a marked plastic region and the absence of strain hardening. A potential upper service temperature of these triblocks at about 140 °C was highlighted by the high and relatively constant storage modulus $G' \geq 2.2 \text{ MPa}$ at $T \leq 140 \text{ °C}$. Consequently, the substitution of PS by harder P(IBOMA) segments was beneficial, allowing the enhancement of the mechanical properties of the block copolymer at room temperature and presumably at higher temperatures.

Compared to the S-My-S triblocks, marked mechanical improvements were shown for IBOMA-My-IBOMA type copolymers, with notably a satisfactory extensibility ($\epsilon_B \sim 500\%$). However, the lack of tensile strength of these latter ($\sigma_B \sim 4 \text{ MPa}$) remained detrimental for the industrial application. A poorly entangled elastomeric $P(My)$ phase could be responsible of such a stress-strain behavior. The $P(My)$ mid-segment exhibited $M_n \sim 50 \text{ kg}\cdot\text{mol}^{-1}$ at most (difficulty to produce high molar mass polymers by NMP under homogeneous conditions), which was only about the double of its entanglement molecular weight ($M_{e,P(My)} = 22-31 \text{ kg}\cdot\text{mol}^{-1}$). It was thus decided to substitute $P(My)$ by poly(isoprene) (PI), having a much lower entanglement molecular weight ($M_{e,PI} = 4-6 \text{ kg}\cdot\text{mol}^{-1}$).

The polymerization of isoprene (I) in a high-pressure reactor initiated by PEB-(SG1)₂ at 115 °C in pyridine led to well-defined and active PI-(SG1)₂ poly(diene)s ($M_n = 54\text{-}61 \text{ kg}\cdot\text{mol}^{-1}$, $\bar{D} < 1.60$). **S-I-S triblock copolymers** ($M_n = 95\text{-}109 \text{ kg}\cdot\text{mol}^{-1}$, $\bar{D} = 2.11\text{-}2.29$, $F_S = 0.30\text{-}0.49$) were synthesized via subsequent S chain-extensions in bulk at 115 °C. The segregation into two different phases of PI and PS blocks was suggested by the observation of two T_{gs} , at about - 60 °C and + 100 °C. An AFM study for S-I-S having $F_S = 0.30$ revealed a micro-phase separation, exhibiting possibly a cylindrical or lamellar morphology. Whereas a rigid and brittle S-I-S sample containing 49 mol% S was identified ($\sigma_B \sim 11 \text{ MPa}$, $\varepsilon_B \sim 20\%$), softer and more extensible S-I-S plastics containing 30-38 mol% S were characterized with $\sigma_B = 2.8\text{-}4.1 \text{ MPa}$ and $\varepsilon_B = 380\text{-}450\%$. Accordingly, substituting the flexible P(My) middle block of the candidate triblock copolymer by a more entangled PI block brought about an enhancement of its stress-strain properties. Despite an acceptable elongation at break, these NMP-based S-I-S having $F_S \leq 0.38$ showed a low and unsatisfactory tensile strength at break.

Taking the positive results obtained for the My-based triblock copolymers after replacing PS by P(IBOMA) into account, a **IBOMA-I-IBOMA type triblock copolymer** ($M_n = 94.0 \text{ kg}\cdot\text{mol}^{-1}$, $\bar{D} = 1.76$, $F_{IBOMA} = 0.35$, $F_S = 0.06$, S as a controlling co-monomer) was developed in a similar way as S-I-S. It exhibited a remarkable $\varepsilon_B = 1360 \pm 210 \%$ and a moderate $\sigma_B = 11.4 \pm 0.6 \text{ MPa}$. Moreover, it displayed a potential upper service temperature higher than 150 °C due to the glass transition of the IBOMA-rich blocks occurring at 180-185 °C. Nonetheless, the presence of IBOMA units in the outer segments lowered the decomposition temperature of the triblock copolymer due to the thermal instability of the isobornyl ring (onset of decomposition at 220 °C under air and 265 °C under N₂). Generally, this IBOMA-I-IBOMA type triblock was the closest to the benchmarks established in this study. However, its tensile strength at break remained below the industrial requirement. Moreover, its early thermal degradation renders it unusable for a subsequent welding process where $T = 240\text{-}280 \text{ °C}$ must be applied.

The table below (page 255) gives a summary of the main features of the experimental and commercial block copolymers characterized during this PhD project.

With respect to the industrial issue, two main modifications were implemented to the synthesized polymers:

- Incomplete **hydrogenation** (~ 75%) of the elastomeric PI mid-segment of S-I-S at normal pressure using diimide-generating reagent *p*-toluenesulfonyl hydrazide (TSH). A higher thermal stability of the partially saturated triblock copolymers was evidenced under inert atmosphere compared to the original S-I-S. Furthermore, the tensile strength at break markedly increased after the chemical hydrogenation, despite a reduced extensibility.

- **Functionalization** of P(*My*): the introduction of functional groups into the soft segment was performed to encourage the joining process with the polar composite matrices. Bulk NMP of *My* and glycidyl methacrylate (GMA) initiated by NHS-BB was accomplished at 120 °C and led to the manufacture of well-tailored epoxide functionalized P(*My*). During the assembly, the presence of epoxy groups into the candidate material could either increase the miscibility at the interface to favor chains inter-diffusion (welding) or allow covalent bonding at the interface (adhesive bonding).

Generally, the various block copolymers produced by NMP in this project did not satisfy the ArianeGroup specifications, due in part to their lack of mechanical strength. This deficiency can be explained by the absence of strain hardening of these NMP-based triblock copolymers in the high-strain region, not allowing the tensile stress to be greatly increased. Such a tensile behavior may be due to the broad molecular weight distribution of the experimental triblocks ($\bar{M}_w = 1.72\text{-}2.29$), indicating the presence of a fraction of short chains in the characterized samples, which could act as a plasticizer and could disrupt the orientation and alignment of the chains in the direction of the load.

Nonetheless, this thesis represents a series of advances related to the development of novel polymers and molecular architectures via a controlled radical polymerization. Several new contributions to the field of NMP have resulted from this project, including in particular:

- Optimized NMP of *My* at 120 °C in bulk using the NHS-BB monofunctional initiator resulted in low dispersity ($\bar{M}_w = 1.1\text{-}1.4$) P(*My*)-SG1.
- Well-controlled statistical *My*/S ($r_{My} = 1.88\text{-}2.90$, $r_S = 0.25\text{-}0.47$) and *My*/GMA ($r_{My} = 0.48\text{-}0.80$, $r_{GMA} = 0.50\text{-}0.71$), and gradient *My*/IBOMA ($r_{My} = 1.90\text{-}2.16$, $r_{IBOMA} = 0.02\text{-}0.07$) nitroxide-mediated copolymerizations.
- Use of *My* (≤ 20 mol% in the initial feed) as a potential controlling co-monomer, allowing to enhance the control of GMA and IBOMA polymerizations by NMP.
- Preparation of an amphiphilic polymer able to self-organize into micelles in water, after treating a NMP-based *My*/GMA diblock copolymer with morpholine.
- Synthesis of telechelic P(*My*)-(SG1)₂ ($M_n = 35\text{-}52$ kg.mol⁻¹) and PI-(SG1)₂ ($M_n = 53\text{-}61$ kg.mol⁻¹) poly(diene)s using the PEB-(SG1)₂ dialkoxamine.
- Development of NMP-based IBOMA-*My*-IBOMA, S-I-S and IBOMA-I-IBOMA type triblock copolymers exhibiting valuable stress-strain properties ($\sigma_B = 2.8\text{-}11.4$ MPa, $\epsilon_B = 20\text{-}1360$ %).

	M_n (kg.mol ⁻¹)	\bar{D}	$F_{\text{hard}}^{(a)}$ (mol%)	σ_B (MPa)	ε_B (%)	Upper T_g (°C)	$T_{\text{dec,onset}}^{(b)}$ under N_2 (°C)
Experimental							
<i>My-S</i>	34-49	1.3-1.9	27-62	< 1	< 20	57-61	140-155
<i>S-My-S</i>	56-66	1.7-1.9	20-32	< 1	90-180	-	300-310
IBOMA- <i>My</i> - IBOMA ^(c)	95	2.2	41	3.9	490	179	260-280
<i>S-I-S</i>	95-109	2.1-2.3	30-49	2.8-10.8	20-450	102-104	305-315
Hydrogenated <i>S-I-S</i> ^(d)	97	2.3	49	16.5 (increase by 53%)	< 10 (decrease by 60%)	102	360 (increase of 45-55 °C)
IBOMA-I- IBOMA ^(c)	94	1.8	41	11.4	1360	182	265
Commercial							
<i>S₄-I-S₄</i> <i>Aldrich</i> [®]	98	1.3	8	7.5	4250	Not detected	-
<i>S₈-I-S₈</i> <i>Aldrich</i> [®]	97	1.3	16	12.7-14.3	3740- 4690	Not detected	315
Hydrogenated <i>S₈-I-S₈</i> <i>Aldrich</i> ^{® (e)}	110	1.3	16	18.4 (increase by 29%)	3310 (decrease by 29%)	-	370 (increase of 55 °C)
SEBS <i>Kraton</i> [®]	88	1.2	48	25.0	730	-	340

Overview table of the main experimental and commercial block copolymers characterized in this project. (a) Molar fraction of hard segment (S, IBOMA or both) in the copolymer. (b) Onset of decomposition. (c) P(IBOMA) outer segments possessed a small fraction of S units. (d) Hydrogenation degree (HD) = 76 mol%. (e) HD = 67 mol%.

CONCLUSION GÉNÉRALE

Cette thèse doctorale avait pour objectif de synthétiser un élastomère thermoplastique (TPE) permettant de fournir une jonction souple entre des matrices composites polaires (réservoir et jupettes d'un lanceur). Ce TPE, assemblé aux composites par collage ou par soudage, doit être utilisé afin de transmettre principalement des forces de cisaillement qui se produisent au niveau de la jonction. Il doit répondre à un cahier des charges précis, incluant :

- Un comportement en contrainte-taux d'extension semblable à celui d'élastomères vulcanisés.
- Une perte minimale des propriétés mécaniques à $T \leq 80$ °C.
- L'absence de fluage et de dégradation lors du procédé d'assemblage ($T \sim 160-180$ °C pendant plus de 10 h pour un collage, $T \sim 240-280$ °C pendant quelques minutes pour un soudage).

Les copolymères triblocs de type styrénique, constitués d'un segment poly(diène) (domaine continu) et de deux segments poly(styrène) (PS) (domaine isolé), furent ciblés. La polymérisation radicalaire contrôlée par des nitroxydes (NMP) fut sélectionnée pour sa facilité à mettre en œuvre, son efficacité à contrôler la polymérisation des 1,3-diènes et l'expertise des laboratoires du Professeur Maric. De plus, la robustesse de la NMP vis-à-vis des monomères polaires et d'une grande variété de monomères vinyliques fut primordiale puisque deux principales modifications furent proposées : (1) fonctionnalisation du poly(diène) par copolymérisation du diène avec un monomère fonctionnel, afin d'encourager l'assemblage ultérieur avec les matrices composites polaires ; (2) remplacement du PS par un polymère ayant une plus haute température de transition vitreuse (T_g), dans le but d'augmenter la résistance en traction et la température de service maximale du copolymère tribloc.

Dans l'attente de réacteurs haute pression permettant de polymériser l'isoprène (température d'évaporation $T_b \sim 34$ °C), le β -myrcène (*My*), un 1,3-diène biosourcé et non volatile ($T_b \sim 167$ °C), fut considéré dans un premier temps pour préparer le bloc souple du TPE.

Le poly(β -myrcène) P(*My*) (masse molaire moyenne en nombre $M_n = 23-30$ kg.mol⁻¹, dispersité $\mathcal{D} = 1,32-1,38$) fut tout d'abord produit par NMP en utilisant l'amorceur monofonctionnel NHS-BB (possédant un groupe nitroxyde SG1). Le caractère actif de ce poly(diène) (chaîne terminée par une unité nitroxyde) permit l'extension de chaîne avec du styrène (S). Les **copolymères diblocs My-S** ainsi formés ($M_n = 39-49$ kg.mol⁻¹, $\mathcal{D} = 1,50-1,88$, fraction molaire en styrène $F_S = 0,27-0,47$) montrèrent de faibles propriétés en traction uniaxiale (résistance à la rupture en traction $\sigma_B < 1$ MPa, allongement à la rupture en

traction $\varepsilon_B < 16\%$) avec notamment l'absence de déformation plastique. Le manque d'enchevêtrement du domaine flexible causé par la haute masse molaire d'enchevêtrement de $P(My)$ ($M_{e,P(My)} = 22-31 \text{ kg.mol}^{-1}$) peut expliquer ce comportement fragile. De plus, l'architecture moléculaire de type dibloc, où les chaînes souples $P(My)$ sont attachées aux chaînes rigides PS que d'un seul bout, pourrait empêcher la réticulation physique du réseau. La synthèse de **copolymères triblocs S-My-S**, ayant un segment central $P(My)$ plus long, apparaissait alors essentielle et fut possible par l'utilisation de l'amorceur bifonctionnel poly(éthylène-*ran*-butylène) terminé par des groupes nitroxyde SG1 (PEB-(SG1)₂). Un macro-amorceur téléchélique $P(My)$ -(SG1)₂ fut ainsi préparé via le PEB-(SG1)₂, suivi d'une extension de chaîne avec du styrène. Une plus grande extensibilité ($\varepsilon_B = 90-180\%$) fut mesurée pour S-My-S ($M_n = 56-66 \text{ kg.mol}^{-1}$ avec $M_{n,P(My)} = 45 \text{ kg.mol}^{-1}$, $\bar{D} = 1,72-1,86$ et $F_S = 0,20-0,32$) en comparaison à My-S. La résistance en traction de ces triblocs ($\sigma_B < 0,8 \text{ MPa}$) fut toutefois similaire à celle des copolymères diblocs. De manière générale, ces copolymères à base de My et S présentèrent des caractéristiques en traction bien en deçà des spécifications industrielles.

Les segments PS ($T_g \sim 100 \text{ }^\circ\text{C}$) furent par la suite remplacés par des segments poly(méthacrylate d'isobornyle) (P(IBOMA)) ayant une T_g plus haute ($\sim 190 \text{ }^\circ\text{C}$). Le but fut d'améliorer la résistance mécanique et d'étendre la température de service du matériau candidat. Les conditions expérimentales utilisées pour la fabrication des triblocs S-My-S furent employées de la même manière pour la synthèse de **copolymères triblocs de type IBOMA-My-IBOMA** ($M_n = 51-95 \text{ kg.mol}^{-1}$, $\bar{D} = 1,91-2,23$, $F_{IBOMA} = 0,28-0,36$), contenant une minorité d'unités My ou S dans ses blocs rigides. Deux T_g s distinctes furent détectées à environ $-60 \text{ }^\circ\text{C}$ et $+180 \text{ }^\circ\text{C}$, suggérant un système polymère ségrégué en deux phases. La micro-séparation de phase du domaine continu $P(My)$ et d'agrégats isolés, riches en unité IBOMA, fut confirmée par microscopie de force atomique (AFM). $\sigma_B = 3,9 \pm 0,2 \text{ MPa}$ et $\varepsilon_B = 490 \pm 30\%$ furent également mesurés par des tests de traction, qui montrèrent une déformation plastique permanente marquée et l'absence de durcissement à de hauts taux d'élongation. Une possible température de service maximale de l'ordre de $140 \text{ }^\circ\text{C}$ fut mise en évidence par la stabilité du module de conservation $G' \geq 2,2 \text{ MPa}$ à $T \leq 140 \text{ }^\circ\text{C}$. La substitution de PS par P(IBOMA), plus dur, fut ainsi concluante, permettant une amélioration des propriétés mécaniques à température ambiante et probablement à plus haute température.

Par rapport aux matériaux S-My-S, les copolymères de type IBOMA-My-IBOMA montrèrent de meilleures propriétés mécaniques, avec notamment $\varepsilon_B \sim 500\%$. Néanmoins, le manque de résistance mécanique ($\sigma_B \sim 4 \text{ MPa}$) constitua une lacune importante pour l'application industrielle. Une phase $P(My)$ faiblement enchevêtrée pourrait être à l'origine d'un tel comportement en traction. En effet, $M_n \sim 50 \text{ kg.mol}^{-1}$ fut au maximum obtenu pour le segment $P(My)$ (difficulté de produire des polymères de hautes masses molaires par NMP en masse ou dans un solvant), ce qui ne représente que le double environ de sa masse

molaire d'enchevêtrement. La substitution de P(My) par le poly(isoprène) (PI), dont la masse molaire d'enchevêtrement est bien plus faible ($M_{e,PI} = 4-6 \text{ kg.mol}^{-1}$), fut par conséquent décidée.

La polymérisation de l'isoprène dans un réacteur haute-pression, amorcée par PEB-(SG1)₂ dans de la pyridine, permet d'obtenir des poly(diène)s PI-(SG1)₂ bien définis et actifs ($M_n = 54-61 \text{ kg.mol}^{-1}$, $\bar{D} < 1,60$). Des **copolymères triblocs S-I-S** ($M_n = 95-109 \text{ kg.mol}^{-1}$, $\bar{D} = 2,11-2,29$, $F_S = 0,30-0,49$) furent synthétisés par la suite via l'extension de chaîne de PI-(SG1)₂ avec du styrène. La ségrégation des blocs PI et PS en deux phases différentes fut suggérée par la détection de deux T_{gs} , à environ - 60 °C et + 100 °C. L'étude AFM d'un S-I-S contenant 30 mol% de styrène révéla une séparation de phase, possiblement cylindrique ou lamellaire, à l'échelle du micromètre. Alors qu'un tribloc S-I-S riche en styrène ($F_S = 0,49$) fut dur et fragile ($\sigma_B \sim 11 \text{ MPa}$, $\epsilon_B \sim 20\%$), des matériaux S-I-S constitués de segments PS plus courts ($F_S = 0,30-0,38$) montrèrent une plus grande souplesse et une extensibilité plus importante avec $\sigma_B = 2,8-4,1 \text{ MPa}$ et $\epsilon_B = 380-450\%$. La substitution du segment P(My) du copolymère tribloc par un segment PI plus enchevêtré permit ainsi d'améliorer ses propriétés mécaniques en traction. Malgré une extensibilité acceptable, la résistance à la rupture en traction des triblocs S-I-S ayant $F_S \leq 0,38$ resta problématique.

Les résultats concluants obtenus pour les polymères à base de My, après le remplacement des blocs PS par des blocs P(IBOMA) plus rigides nous poussèrent à préparer de manière similaire un **copolymère tribloc de type IBOMA-I-IBOMA** ($M_n = 94,0 \text{ kg.mol}^{-1}$, $\bar{D} = 1,76$, $F_{IBOMA} = 0,35$, $F_S = 0,06$, S utilisé en tant que co-monomère lors de l'extension de chaîne). Ce dernier se caractérisa par une grande ductilité ($\epsilon_B = 1360 \pm 210 \%$) et par une résistance mécanique modérée ($\sigma_B = 11,4 \pm 0,6 \text{ MPa}$). Il présenta une température de service maximale potentielle supérieure à 150 °C, du fait de la transition vitreuse des blocs durs riches en IBOMA, se produisant à 180-185 °C. Toutefois, la température de décomposition de ce tribloc fut relativement basse (début de dégradation à 220 °C sous air et à 265 °C sous azote), à cause de l'instabilité thermique des groupes isobornyle. De manière générale, IBOMA-I-IBOMA représenta le copolymère à blocs synthétisé par NMP le plus concluant, malgré une résistance à la rupture en traction encore trop faible et une décomposition thermique précoce, ne permettant pas de réaliser un soudage pour lequel $T = 240-280 \text{ °C}$ doit être appliquée.

Le tableau ci-dessus (page 255) récapitule les principales caractéristiques des copolymères à blocs expérimentaux et commerciaux étudiés lors de ce projet.

Par rapport à la problématique industrielle, deux principales modifications furent réalisées sur les polymères synthétisés :

- L'**hydrogénation** incomplète (~ 75%) du segment PI de triblocs S-I-S à pression ambiante et en utilisant l'agent diimide. Une plus grande stabilité thermique des copolymères partiellement

saturés fut mise en évidence sous atmosphère inerte, en comparaison aux S-I-S originaux. De plus, σ_B augmenta significativement suite à cette hydrogénation chimique, en dépit d'une perte notable d'extensibilité.

- **Fonctionnalisation** de P(My) : l'incorporation de groupes fonctionnels au sein du segment souple fut entreprise pour favoriser l'assemblage avec les matrices composites polaires. La copolymérisation de My avec le méthacrylate de glycidyle, amorcée par NHS-BB à 120 °C, permit d'obtenir un polymère flexible bien défini et portant des unités époxydes. Lors du procédé d'assemblage, la présence de groupes époxydes au sein de l'élastomère pourrait soit augmenter la miscibilité à l'interface afin de favoriser l'inter-diffusion des chaînes (soudage), soit permettre la formation de liaisons covalentes à l'interface (collage).

De manière générale, les différents copolymères à blocs produits par NMP lors de ce projet doctoral ne satisfirent pas le cahier des charges d'ArianeGroup, du fait notamment de leur relativement faible résistance mécanique. Cette déficience peut s'expliquer par l'absence d'une phase de durcissement de ces copolymères à de hauts taux d'extension, ne permettant pas d'accroître significativement la résistance à la rupture en traction. La haute dispersité de ces matériaux préparés par NMP ($\mathcal{D} = 1,72-2,29$) pourrait être un facteur clé afin de comprendre ce comportement mécanique. Elle indique la présence de chaînes courtes au sein du réseau polymère, fragilisant la structure du copolymère et empêchant possiblement l'alignement de ses chaînes dans le sens de la traction.

Néanmoins, cette thèse apporta des contributions scientifiques dans le domaine de la NMP. Les avancées suivantes peuvent être citées en particulier :

- Synthèse optimisée de P(My) ($\mathcal{D} = 1,1-1,4$) en utilisant l'alcoxyamine NHS-BB.
- Copolymérisation contrôlée des couples My/S, My/GMA et My/IBOMA par NMP.
- Utilisation de My en tant que co-monomère (≤ 20 mol% dans le mélange initial) afin d'améliorer le contrôle de la polymérisation des monomères GMA et IBOMA par NMP.
- Préparation de poly(diène)s téléchéliques P(My)-(SG1)₂ ($M_n = 35-52$ kg.mol⁻¹) et PI-(SG1)₂ ($M_n = 53-61$ kg.mol⁻¹) en utilisant l'alcoxyamine PEB-(SG1)₂.
- Synthèse par NMP de copolymères de type IBOMA-My-IBOMA, S-I-S et IBOMA-I-IBOMA présentant des propriétés intéressantes en traction ($\sigma_B = 2,8-11,4$ MPa, $\varepsilon_B = 20-1360$ %).

PERSPECTIVES

Although the various diene-based block copolymers synthesized by nitroxide-mediated polymerization (NMP) in this study did not meet the industrial requirements, marked improvements were noticed when using poly(isoprene) (PI) as the soft middle segment and hard outer segments rich in isobornyl methacrylate (IBOMA). IBOMA-I-IBOMA type triblock copolymer ($M_n = 94 \text{ kg}\cdot\text{mol}^{-1}$, $\bar{D} = 1.76$, $F_{\text{IBOMA}} = 0.35$ with a minor fraction of styrene (S) units in the outer blocks) showed a satisfactory elongation at break ($\epsilon_B = 1360 \pm 210 \%$) combined to a relatively high upper service temperature at about $150 \text{ }^\circ\text{C}$. However, its low tensile strength at break ($\sigma_B = 11.4 \pm 0.6 \text{ MPa}$) and thermal stability (onset of decomposition $T_{\text{dec,onset}}$ at $220 \text{ }^\circ\text{C}$ and $265 \text{ }^\circ\text{C}$ under air and N_2 , respectively) were detrimental. This experimental isoprene-based copolymer can thus be used as a benchmark for the preparation of optimized triblock copolymers, with respect to the ArianeGroup specifications.

Three main modifications can be undertaken to synthesize the candidate TPE by NMP, namely:

1. Synthesis of PI in a dispersed medium: NMP under homogeneous conditions in bulk or in organic solvents displays a main challenge: the synthesis of high average molecular weight polymers. It was stressed in this project with the difficulty to produce in bulk or in pyridine a well-defined PI having a number-average molecular weight (M_n) higher than $60 \text{ kg}\cdot\text{mol}^{-1}$. The aim to increase the average chain length of the elastomeric mid-segment is to develop a more entangled matrix and thus a tougher resulting triblock copolymer. Performing isoprene NMP in an aqueous dispersed medium (suspension of stable nano- or micro-particles) may be a solution. It was found that compartmentalization of the polymerization in particles (acting as nano-reactors) can improve control over molar mass distributions and afford a higher degree of end functionality. Low dispersity can be maintained even at high conversions, allowing the synthesis of well-tailored polymers exhibiting high M_n ¹. NMP in mini-emulsion, using either a water-soluble or a lipophilic initiating system², could be for instance envisioned to prepare a “living” PI latex with $M_n > 60 \text{ kg}\cdot\text{mol}^{-1}$ and $\bar{D} < 1.3$.

2. Replacement of P(IBOMA) by a high glass transition temperature (T_g) and decomposition temperature (T_{dec}) polymer: the early thermal degradation of P(IBOMA), presumably due to the release of the isobornyl group, is problematic³. Its substitution by a polymer having a higher thermal stability while being at least as hard ($T_g \geq T_{g,\text{P(IBOMA)}} \sim 180\text{-}190 \text{ }^\circ\text{C}$ ³) would be valuable. For instance, the use of poly(α -methylene- γ -butyrolactone) P(MBL) ($T_g \sim 190\text{-}200 \text{ }^\circ\text{C}$, atactic^{4,5,6}) would be of interest since it is thermally stable under N_2 ($T_{\text{dec,onset}} \sim 340 \text{ }^\circ\text{C}$)⁶. Its high T_g would also ensure an extended upper service temperature

compared to traditional styrenic TPE as well as an elevated tensile strength at break σ_B . Furthermore, well-defined P(MBL) ($M_n = 22 \text{ kg.mol}^{-1}$, $\bar{D} = 1.21$) was synthesized via addition-fragmentation chain-transfer polymerization (RAFT)⁶, which indicates the propensity of MBL to be polymerized by a controlled radical process. Lastly, the addition of neat P(MBL) blocks to PI would be possible while IBOMA chain-extensions were performed with a small amount of styrene (S) to enhance the control of this bulky methacrylate NMP. It could be argued that the presence of styrene in the rigid segments can reduce the strength and the performance at high temperature of the triblock copolymer due to the relatively low T_g of PS ($\sim 95\text{-}100 \text{ }^\circ\text{C}$)⁷.

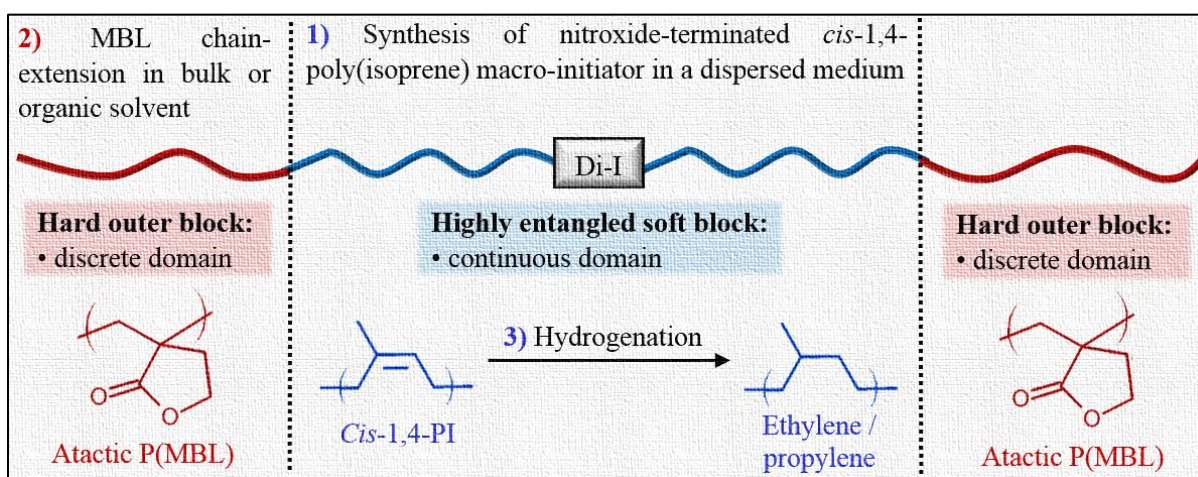
Please note that P(MBL) is herein mentioned as an example. P(MBL) derivatives, such as poly(γ -methyl- α -methylene- γ -butyrolactone) (P(MeMBL), $T_g = 210\text{-}220 \text{ }^\circ\text{C}$, MeMBL copolymerized with styrene via RAFT emulsion^{8,9,10}) or poly(α -methylene- γ,γ -dimethyl- γ -butyrolactone) (P(Me₂MBL), $T_g \sim 210 \text{ }^\circ\text{C}$, $T_{\text{dec,onset}} \sim 340 \text{ }^\circ\text{C}$ under N_2 , Me₂MBL controlled by RAFT⁶) could be used the same way. Other groups of polymers, produceable via a radical process and exhibiting high T_g and T_{dec} , can be considered. Poly(styrene) derivatives, including for instance poly(α -methyl-*p*-methylstyrene) ($T_g = 165\text{-}180 \text{ }^\circ\text{C}$, $T_{\text{dec,onset}} \sim 320 \text{ }^\circ\text{C}$ under N_2)¹¹, are of interest as well. It should be added that the incompatibility of these candidate rigid segments with the soft middle block is assumed, allowing a strong phase separation of the two phases (investigation of the solubility parameters required).

3. Hydrogenation of the PI middle block: As performed in this project for experimental and commercial S-I-S, the saturation of the soft segment appears paramount. The improved thermal stability and the higher tensile strength at break exhibited by the isoprene-based copolymer after hydrogenation are beneficial, despite a loss of extensibility. A higher upper service temperature could also result from hydrogenation, due to the stronger phase separation of the hydrogenated block copolymer (greater incompatibility between hard and soft blocks) compared to that of the parent one¹². The chemical hydrogenation using diimide reduction in this study led to incomplete replacement of isoprene units by ethylene/propylene units. Applied industrially, the catalytic hydrogenation of PI could be considered using a transition metal and high-pressure H_2 in order to saturate quantitatively the poly(diene) segment and enhance the mechanical and thermal properties of the triblock copolymer.

Accordingly, the preparation by NMP and after post-polymerization treatment of a fully hydrogenated MBL-I-MBL copolymer can be targeted in the future. A schematic representation of this latter triblock copolymer is given in the figure below (page 262). Compared to the IBOMA-I-IBOMA sample, higher M_n ($> 100 \text{ kg.mol}^{-1}$) and more importantly lower D (< 1.5) could be targeted for MBL-I-MBL due to the synthesis of the first PI mid-block by NMP in a dispersed medium followed by its chain-extension with MBL, presumably easier to control than IBOMA. The preparation of a narrow molecular

weight distribution triblock copolymer may be essential for the purposes of mimicking the mechanical properties of commercial styrenic TPE. Generally, the following properties could be expected for this well-tailored MBL-I-MBL triblock copolymer:

- *Stress-strain behavior at room temperature:* $\sigma_B > 20$ MPa, $\varepsilon_B > 600$ % with a marked strain hardening (low dispersity encouraging the orientation and the alignment of the chains).
- *Thermal behavior:* softening at $T \sim 170$ -180 °C, onset of decomposition at $T \sim 280$ -300 °C under air and at $T \sim 340$ -360 °C under inert atmosphere.
- *Mechanical performance at high temperature:* maximum service temperature ~ 170 -180 °C (minimal loss of the mechanical properties at $T < 170$ °C).



Summary outline of a potential linear triblock copolymer thermoplastic elastomer envisioned for further study. Di-I corresponds to a difunctional initiator.

Afterwards, the joining of the triblock copolymer TPE with the tank and the skirt (polar thermoplastic or thermoset composites) of the launcher, via a bonding or welding process, would presumably necessitate the introduction of functional groups into MBL-I-MBL. The copolymerization of isoprene with a small amount of a polar monomer could be envisioned, as performed in this study between β -myrcene and glycidyl methacrylate bearing an epoxide group. The functionalization of P(MBL) during the chain-extension would be another alternative.

(1) G. Delaittre In *Nitroxide Mediated Polymerization: From Fundamentals to Applications in Materials Science*; D. Gimes, Ed.; The Royal Society of Chemistry: Cambridge, 2016; Chapter 5, pp 199-263.

- (2) J. M. Asua, *Prog. Polym. Sci.* **2002**, *27*, 1283–1346.
- (3) A. Matsumoto, K. Mizuta and T. Otsu, *J. Polym. Sci., Part A: Polym. Chem.* **1993**, *31* (10), 2531-2539.
- (4) S. Agarwal, Q. Jin and M. Samarendra, *ACS Sym. Ser.* **2012**, *1105*, 197–212.
- (5) R. R. Gowda and E. Y.-X. Chen, In *Encyclopedia of Polymer Science and Technology*; A. Seidel, Ed.; Wiley: New York, **2013**; pp 1–37.
- (6) J. T. Trotta, M. Jin, K. J. Stawiasz, Q. Michaudel, W. -L. Chen and B. P. Fors, *J. Polym. Sci., Part A: Polym. Chem.* **2017**, *55*, 2730-2737.
- (7) J. Rieger, *J. Therm. Anal. Calorim.* **1996**, *46* (3), 965-972.
- (8) J. Suenaga, D. M. Sutherlin and J. K. Stille, *Macromolecules* **1984**, *17*, 2913-2916.
- (9) S. Xu, J. Huang, S. Xu and Y. Luo, *Polymer* **2013**, *54*, 1779-1785.
- (10) R. A. Cockburn, R. Siegmann, K. A. Payne, S. Beuermann, T. F. L. McKenna and R. A. Hutchinson, *Biomacromolecules* **2011**, *12*, 2319-2326.
- (11) J. M. Bolton, M. A. Hillmyer and T. R. Hoye, *ACS Macro Letters* **2014**, *3* (8), 717-720.
- (12) Y. Araki, D. Shimizu, Y. Hori, K. Nakatani and H. Saito, *Polymer Journal* **2013**, *45*, 1140-1145.

PERSPECTIVES

Les divers copolymères à blocs à base de diène synthétisés par polymérisation radicalaire contrôlée par des nitroxydes (NMP) ne satisfirent pas le cahier des charges d'ArianeGroup. Néanmoins, des améliorations importantes des propriétés de ces polymères furent constatées en utilisant le poly(isoprène) (PI) en tant que segment souple et des segments durs composés majoritairement de méthacrylate d'isobornyle (IBOMA). Le copolymère tribloc de type IBOMA-I-IBOMA ($M_n = 94 \text{ kg.mol}^{-1}$, $\bar{D} = 1,76$, $F_{\text{IBOMA}} = 0,35$ avec une minorité d'unités styrène (S) dans les blocs rigides) montra un allongement à la rupture en traction ($\varepsilon_B = 1360 \pm 210 \%$) satisfaisant ainsi qu'une potentielle température de service maximale d'environ $150 \text{ }^\circ\text{C}$. Sa faible résistance à la rupture en traction ($\sigma_B = 11,4 \pm 0,6 \text{ MPa}$) associée à son instabilité thermique (début de la dégradation $T_{\text{dec,onset}}$ à $220 \text{ }^\circ\text{C}$ sous air et $265 \text{ }^\circ\text{C}$ sous azote) furent toutefois préjudiciables. Ce copolymère à base d'isoprène peut ainsi être utilisé comme point de départ pour la préparation de copolymères à blocs plus performants, selon les exigences industrielles.

Trois principales modifications peuvent être considérées afin de produire par NMP le TPE candidat, à savoir :

1. Synthèse du PI en milieu dispersé : L'application de la technique NMP en masse ou dans des solvants organiques se confronte à la difficulté de produire des polymères de haute masse molaire moyenne. Cela fut mis en évidence dans cette étude en ce qui concerne la synthèse de PI bien définis ayant une masse molaire moyenne en nombre (M_n) maximale comprise entre 50 et 60 kg.mol^{-1} lorsque la NMP en masse ou dans la pyridine fut employée. Augmenter la longueur moyenne de chaîne du bloc souple permettrait d'obtenir une matrice plus enchevêtrée et de ce fait, un copolymère tribloc plus résistant et tenace. A cette fin, la polymérisation de l'isoprène par NMP dans un milieu dispersé (suspension de nano- et micro-particules) peut être envisageable. Il a été démontré que le compartimentage de ce type de polymérisation, où chaque particule agit comme un nano-réacteur, peut améliorer le contrôle par NMP avec une faible dispersité des chaînes (\bar{D}) et un degré de fonctionnalité élevé des bouts de chaînes (groupe nitroxyde permettant le réamorçage). Une distribution étroite des masses molaires peut être maintenue à de hautes conversions, ce qui permet la synthèse de polymères bien définis ayant un M_n élevé¹. La méthode NMP en mini-émulsion², en utilisant un amorceur hydrosoluble ou lipophile, pourrait par exemple être considérée afin de préparer un latex PI « vivant » ayant $M_n > 60 \text{ kg.mol}^{-1}$ et $\bar{D} < 1,3$.

2. Remplacement de P(IBOMA) par un polymère possédant de hautes températures de transition vitreuse (T_g) et de décomposition (T_{dec}) : La dégradation thermique précoce de P(IBOMA),

vraisemblablement due au détachement du groupe isobornyle, est problématique³. La substitution de P(IBOMA) par un polymère ayant une haute stabilité thermique, tout en étant au moins aussi dur ($T_g \geq T_{g,P(IBOMA)} \sim 180-190 \text{ °C}$ ³) serait bénéfique. Par exemple, le poly(α -méthylène- γ -butyrolactone) P(MBL) ($T_g \sim 190-200 \text{ °C}$, atactique^{4,5,6}) constituerait un substitut intéressant puisqu'il est stable sous atmosphère inerte ($T_{dec,onset} \sim 340 \text{ °C}$)⁶. Sa haute T_g assurerait une température de service maximale bien plus élevée que celle des TPE de référence de type styrénique ainsi qu'une importante résistance à la rupture en traction. De plus, MBL fut polymérisé de manière contrôlée par RAFT ($M_n = 22 \text{ kg.mol}^{-1}$, $\bar{D} = 1,21$)⁶, indiquant la prédisposition de P(MBL) à être synthétisé par polymérisation radicalaire contrôlée. Il peut être ajouté que l'addition de deux blocs P(MBL) purs serait possible alors que le monomère IBOMA fut toujours copolymériser avec une minorité de styrène afin d'améliorer le contrôle de l'extension de chaîne (homopolymérisation délicate des méthacrylates via NMP). Il se peut que la présence d'unités styrène au sein des segments rigides diminue la résistance mécanique et la performance à haute température du copolymère tribloc du fait de la relativement basse T_g du poly(styrène) PS ($\sim 95-100 \text{ °C}$)⁷.

P(MBL) est cité en tant qu'exemple. Des dérivés du P(MBL), tels que le poly(γ -méthyl- α -méthylène- γ -butyrolactone) (P(MeMBL), $T_g = 210-220 \text{ °C}$, MeMBL copolymérisé avec du styrène par émulsion RAFT^{8,9,10}) ou le poly(α -méthylène- γ,γ -diméthyl- γ -butyrolactone) (P(Me₂MBL), $T_g \sim 210 \text{ °C}$, $T_{dec,onset} \sim 340 \text{ °C}$ sous N₂, Me₂MBL contrôlé par RAFT⁶) pourraient être utilisés de la même manière. D'autres types de polymères, synthétisables par un procédé radicalaire et ayant des hautes T_g et T_{dec} , peuvent aussi être considérés comme les dérivés du poly(styrène). Le poly(α -méthyl-*p*-méthylstyrène) par exemple présente $T_g = 165-180 \text{ °C}$ et $T_{dec,onset} \sim 320 \text{ °C}$ sous atmosphère inerte¹¹. Il doit être noté que l'incompatibilité de ces potentiels blocs durs avec le bloc souple central est assumée, offrant une séparation de phase nette du copolymère (étude approfondie nécessitant l'usage des paramètres de solubilité).

3. Hydrogénation du segment souple PI : Comme réalisée dans cette étude pour des triblocs S-I-S expérimentaux et commerciaux, la saturation du poly(isoprène) apparait essentielle. La plus haute stabilité thermique et la plus grande résistance à la rupture en traction de ces copolymères après hydrogénation sont avantageux, malgré une perte notable de leur extensibilité. Une plus haute température de service maximale peut également être apparente, du fait d'une séparation de phase plus forte du copolymère tribloc hydrogéné (plus grande incompatibilité entre les domaines durs et flexibles)¹². L'hydrogénation chimique employée dans ce projet et utilisant le diimide, résulta en un remplacement partiel des unités isoprène en unités éthylène/propylène. Appliquée dans l'industrie, l'hydrogénation catalytique de PI en utilisant un métal de transition et du dihydrogène H₂ sous haute-pression permettrait de saturer complètement le bloc poly(diène) et d'améliorer ainsi les propriétés thermiques et mécaniques du copolymère tribloc.

Par conséquent, la préparation par NMP et après modification chimique post-polymérisation d'un copolymère MBL-I-MBL entièrement hydrogéné serait une option envisageable pour un travail futur. Une représentation schématique de ce polymère en question est donnée dans la figure ci-dessous. Par rapport au tribloc IBOMA-I-IBOMA, une plus grande masse molaire moyenne ($M_n > 100 \text{ kg.mol}^{-1}$) et surtout une plus faible dispersité ($\mathcal{D} < 1,5$) pourraient être atteintes pour MBL-I-MBL puisque le segment PI préliminaire serait synthétisé par NMP en milieu dispersé et que son extension de chaîne avec MBL serait probablement plus facilement contrôlable qu'avec IBOMA. La synthèse d'un copolymère tribloc ayant une faible dispersité pourrait être essentielle afin d'obtenir des propriétés mécaniques similaires à celles des TPE commerciaux traditionnels. De manière générale, les caractéristiques suivantes seraient attendues pour ce MBL-I-MBL bien défini :

- *Comportement en contrainte/déformation à température ambiante* : $\sigma_B > 20 \text{ MPa}$, $\epsilon_B > 600 \%$ dont le domaine plastique est suivi d'une phase de durcissement, provoquant un accroissement significatif de la résistance à la rupture (faible \mathcal{D} encourageant l'orientation et l'alignement des chaînes dans la direction de traction).
- *Comportement thermique* : écoulement caoutchoutique à $T \sim 170\text{-}180 \text{ }^\circ\text{C}$, décomposition débutant à $T \sim 280\text{-}300 \text{ }^\circ\text{C}$ sous air et $T \sim 340\text{-}360 \text{ }^\circ\text{C}$ sous atmosphère inerte.
- *Performance mécanique à haute température* : température de service maximale $T \sim 170\text{-}180 \text{ }^\circ\text{C}$ (perte minimale des propriétés mécaniques à $T < 170 \text{ }^\circ\text{C}$).

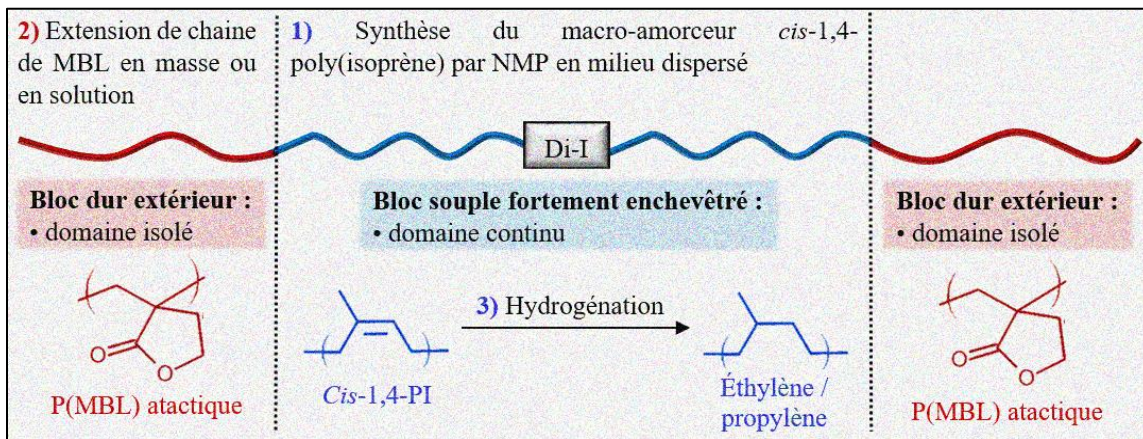


Schéma récapitulatif du copolymère tribloc linéaire envisageable pour un travail futur. Di-I correspond à un amorceur bifonctionnel.

Par la suite, l'assemblage du TPE candidat avec le réservoir et les jupettes du lanceur (composites thermoplastiques ou thermodurcissables relativement polaires) serait réalisé par collage ou par soudage.

Cela nécessiterait vraisemblablement l'incorporation de groupes fonctionnels au sein de MBL-I-MBL. La copolymérisation de l'isoprène avec une minorité d'un monomère polaire pourrait être une possibilité, comme cela fut réalisée dans cette étude entre le β -myrcène et le méthacrylate de glycidyle portant un groupe époxyde. La fonctionnalisation des blocs P(MBL) pendant l'extension de chaîne serait une alternative.

- (1) G. Delaittre In *Nitroxide Mediated Polymerization: From Fundamentals to Applications in Materials Science*; D. Gigmes, Ed.; The Royal Society of Chemistry: Cambridge, **2016**; Chapter 5, pp 199-263.
- (2) J. M. Asua, *Prog. Polym. Sci.* **2002**, *27*, 1283–1346.
- (3) A. Matsumoto, K. Mizuta and T. Otsu, *J. Polym. Sci., Part A: Polym. Chem.* **1993**, *31* (10), 2531-2539.
- (4) S. Agarwal, Q. Jin and M. Samarendra, *ACS Sym. Ser.* **2012**, *1105*, 197–212.
- (5) R. R. Gowda and E. Y.-X. Chen, In *Encyclopedia of Polymer Science and Technology*; A. Seidel, Ed.; Wiley: New York, **2013**; pp 1–37.
- (6) J. T. Trotta, M. Jin, K. J. Stawiasz, Q. Michaudel, W. -L. Chen and B. P. Fors, *J. Polym. Sci., Part A: Polym. Chem.* **2017**, *55*, 2730-2737.
- (7) J. Rieger, *J. Therm. Anal. Calorim.* **1996**, *46* (3), 965-972.
- (8) J. Suenaga, D. M. Sutherlin and J. K. Stille, *Macromolecules* **1984**, *17*, 2913-2916.
- (9) S. Xu, J. Huang, S. Xu and Y. Luo, *Polymer* **2013**, *54*, 1779-1785.
- (10) R. A. Cockburn, R. Siegmann, K. A. Payne, S. Beuermann, T. F. L. McKenna and R. A. Hutchinson, *Biomacromolecules* **2011**, *12*, 2319-2326.
- (11) J. M. Bolton, M. A. Hillmyer and T. R. Hoye, *ACS Macro Letters* **2014**, *3* (8), 717-720.
- (12) Y. Araki, D. Shimizu, Y. Hori, K. Nakatani and H. Saito, *Polymer Journal* **2013**, *45*, 1140-1145.

APPENDICES

a. Appendix for Chapter 1

a.1. Experimental section

■ **Materials.** β -Myrcene (M_y , ≥ 90 %), basic alumina (Al_2O_3 , Brockmann, Type I, 150 mesh), calcium hydride (CaH_2 , 90-95 % reagent grade) and 1,4-dioxane (≥ 99 %) were purchased from Sigma-Aldrich and used as received. Toluene (≥ 99 %), methanol (MeOH, ≥ 99 %) and tetrahydrofuran (THF, 99.9 % HPLC grade) were obtained from Fisher Scientific and used as received. 2-Methyl-2-[*N*-*tert*-butyl-*N*-(1-diethoxyphosphoryl)-2,2-dimethylpropyl]-aminoxy]-*N*-propionyloxy-succinimide, also known as NHS-BlocBuilder (NHS-BB), was prepared according to a published method¹ from 2-(*tert*-butyl[1-(diethoxyphosphoryl)-2,2-dimethylpropyl]aminoxy)-2-methylpropionic acid, also known as MAMA-SG1 (BlocBuilder™, BB, 99 %, purchased from Arkema and used without further purification), *N*-hydroxy-succinimide (NHS, 98 %, purchased from Aldrich and used as received) and *N,N'*-dicyclohexylcarbodiimide (DCC, 99 %, purchased from Aldrich and used as received). *N-tert*-Butyl-*N*-[1-diethylphosphono-(2,2-dimethylpropyl)] nitroxide (SG1, > 85 %) was kindly donated by Noah Macy of Arkema and used as received. Styrene (S, 99 %) was obtained from Fisher Scientific and was purified to remove the inhibitor (*p-tert*-butylcatechol) by passing through a column of basic alumina mixed with 5 weight % calcium hydride and then stored in a sealed flask under a head of nitrogen in a refrigerator until needed. The deuterated chloroform ($CDCl_3$, 99.8 %) used as a solvent for proton and carbon nuclear magnetic resonance (1H and ^{13}C NMR) was obtained from Cambridge Isotopes Laboratory.

■ **(Co-)Polymerization of β -myrcene (with styrene) by NMP.** The (co-)polymerizations were performed in a 25-mL three-necked round-bottom glass flask equipped with a reflux condenser, a thermal well and a magnetic stir bar. The flask was placed inside a heating mantle and the whole set-up mounted on top of a magnetic stirrer. Table 1 and Table 5 list the formulations studied for the various M_y/S (co-)polymerizations. For example, for the experiment M_y/S -20 (molar fraction of S in the initial feed $f_{S,0} = 0.20$), the reactor was sealed with the rubber septa after the addition of NHS-BB (0.204 g, 0.427 mmol) and the stir bar. M_y (10.514 g, 77.178 mmol) and previously purified S (2.043 g, 19.616 mmol) were then injected with a disposable needle into the reactor. For this experiment, the initial molar ratio of monomers and NHS-BB was calculated to give theoretically a M_y/S copolymer sample with target number-average molecular weight $M_{n,theo} = (M_{M_y}f_{M_y,0} + M_Sf_{S,0}) DP = 30 \text{ kg}\cdot\text{mol}^{-1}$ at complete overall conversion with $DP = ([M_y]_0 + [S]_0) / [NHS-BB]_0 = 231$, the average degree of polymerization.

A thermocouple connected to the temperature controller was placed inside the thermal well and connected through one of the necks. A mixture of ethylene glycol/distilled water (20/80 vol%) at a temperature of 5 °C was circulated (Fisher Scientific Isotemp 3016D Digital Refrigerated Bath) through the condenser connected to one of the necks of the reactor to prevent any evaporation loss of the monomers. A purge of ultra-pure nitrogen was then introduced to the reactor for 30 min to deoxygenate at room temperature the reactants prior to polymerization. The purge was vented through the reflux condenser. After purging, the reactor was heated at a rate of about 10 °C.min⁻¹ to the desired polymerization temperature (T = 120 °C for *My*/S-20) with continuous nitrogen purge. The time at which the reactor temperature reached 100 °C was taken arbitrarily as the commencement of the reaction (*t* = 0 min). Samples were then taken from the reactor periodically by a syringe until the end of the experiments or until the samples became too viscous to withdraw. Reactions were then stopped by removing the reactor from the heating mantle and letting the contents cool down to room temperature, while under continuous nitrogen purge. For each sample withdrawn during the polymerization, the crude polymer was precipitated with excess methanol. After filtration and recovery, the precipitated polymer was dried at 40 °C under vacuum in the oven overnight to remove unreacted monomers. Samples were analyzed by nuclear magnetic resonance (NMR) and gel permeation chromatography (GPC). Specifications of the GPC and the NMR are fully described in the Characterization section. At the end of the experiment, the overall NMR conversion for *My*/S-20 was 37.1 % (individual conversions: $X_{My} = 40.5$ % and $X_S = 28.9$ %) with $M_n = 9.9$ kg.mol⁻¹, molecular weight distribution $\bar{D} = 1.26$ and the molar composition of S in the final copolymer was $F_S = 0.15$ according to NMR spectroscopy. The exact same procedure was followed for all *My*/S copolymerizations and *My* homopolymerizations.

▀ ***Chain-extension of poly(myrcene) P(My) homopolymer macroinitiator and poly(myrcene-stat-styrene)***

P(My-stat-S) statistical copolymer macroinitiator with styrene and/or β -myrcene. P(*My*) homopolymers and P(*My-stat-S*) statistical copolymers were chain-extended with purified S and/or *My* at 110 °C or 120 °C in 50 wt% toluene solution or in bulk. The experimental setup and procedures were the same as the syntheses for the P(*My*) and P(*My-stat-S*) polymers described earlier. The entire set of formulations for the chain-extension experiments is shown in Table 3, from P(*My*) macroinitiators, and Table 7.B, from P(*My-stat-S*) macroinitiators. An example is given to illustrate the chain-extension of *My*/S statistical copolymer macroinitiator with purified S. To the reactor was added *My*/S-20 macroinitiator (1.00 g, $M_n = 9.9$ kg.mol⁻¹, $\bar{D} = 1.26$) and toluene (7.51 g, 81.51 mmol) solvent with magnetic stirring. After sealing the reactor, previously purified S (6.49 g, 62.31 mmol) was added via syringe and a purge of nitrogen was applied for 30 minutes. The reactor was then heated to 110 °C to commence polymerization while continuing the nitrogen purge. Samples were periodically removed by syringe and polymers were precipitated using excess methanol. After removal of the supernatant, the wet cake was dried under vacuum at 50 °C to obtain the *My*/S-20-S block copolymer. The chain-extended products were characterized by GPC, calibrated with poly(styrene) PS standards, at 40°C in THF eluent. For the specific example cited, the final S conversion was 53 % according to ¹H NMR spectroscopy with $M_n = 25.3$ kg.mol⁻¹ and dispersity $\bar{D} = 1.46$ determined by GPC.

■ **Characterization.** The overall monomer conversion X was determined by gravimetry X_{grav} and ^1H nuclear magnetic resonance (NMR) X_{NMR} (average deviation = 3.12 %, standard deviation = 2.48 %, see Supporting Information for X_{grav} and X_{NMR} values in the course of experiment *My*-6, Figure S1a) and calculated from formula 1:

$$X = (X_{\text{grav}} + X_{\text{NMR}}) / 2 \quad (1)$$

X_{grav} was calculated from the following formula:

$$X_{\text{grav}} = (m_{\text{v+p}} - m_{\text{v}}) / [(m_{\text{v+p+s}} - m_{\text{v}}) \times (100 - w_{\text{S}})] \quad (2)$$

in which m_{v} is the mass of the empty vial, $m_{\text{v+p+s}}$ is the mass of the vial containing the reaction solution just after the sample withdrawal (polymer, unreacted monomer(s) and solvent if used), $m_{\text{v+p}}$ is the mass of the vial containing the polymer after drying and w_{S} is the mass percentage of solvent relative to the initial masses of initiator and monomer(s). In order to prevent any overestimated X_{grav} , drying of the samples was performed first under intense air flow for 24 h and then under vacuum at 50 °C for 24 h to maximize the removal of non-polymer components. Average conversion X_{NMR} was then calculated from formula 3:

$$X_{\text{NMR}} = X_{M_y} f_{M_y,0} + X_{\text{S}} f_{\text{S},0} \quad (3)$$

where $f_{M_y,0}$ and $f_{\text{S},0}$ are the initial molar fractions of *My* and S respectively and X_{M_y} and X_{S} are the individual conversions of *My* and S respectively. X_{M_y} and X_{S} were determined with a Varian NMR Mercury spectrometer (^1H NMR, 300 MHz, 32 scans) using CDCl_3 deuterated solvent. The signal of the solvent ($\delta = 7.27$ ppm) was used as reference for chemical shifts. *My* conversion was calculated by comparing the integrated peaks corresponding to the four aliphatic protons of the monomers ($\delta = 2.15$ - 2.30 ppm), the eight aliphatic protons of the polymers ($\delta = 1.90$ - 2.15 ppm) and the six protons of the two methyl groups of both monomers and polymers ($\delta = 1.55$ - 1.75 ppm). S conversion was determined using the three vinyl protons ($\delta = 6.7$ - 6.8 , 5.7 - 5.8 and 5.2 - 5.3 ppm) of the monomers and the five aromatic protons of both monomers and polymers ($\delta = 6.9$ - 7.5 ppm). Please note that X was only used for homopolymerizations. In the case of the copolymerizations, X_{NMR} was considered since *My* and S have significantly different molar masses.

The regioselectivity of the *My* repetitive units in the various *My*-based polymers was also determined by using the same spectra (^1H NMR, 300 MHz Varian NMR Mercury spectrometer, CDCl_3 eluent, 32 scans). Comparing the three integrated peaks at $\delta = 4.70$ - 4.80 ppm (two vinyl protons of 3,4-addition and two vinyl protons of 1,2-addition), $\delta = 5.00$ - 5.25 ppm (two olefinic protons of 1,4-addition, one olefinic proton of 1,2-addition and one olefinic proton of 3,4-addition) and $\delta = 5.30$ - 5.50 ppm (one olefinic proton of 1,2-addition) allowed the three different types of configurations to be quantified². The two stereoisomers of 1,4-*P(My)*, *cis*-1,4-*P(My)* and *trans*-1,4-*P(My)*, were quantified using ^{13}C NMR (300 MHz Varian NMR Mercury spectrometer, CDCl_3 eluent at $\delta = 77.4$ ppm, 1000 scans) chemical shifts of specific nuclei: methylene carbon at $\delta = 37$ - 38 ppm (*trans*-, 37,6 ppm; *cis*-, 37,1 ppm) and the quaternary carbon at $\delta = 131$ - 132 ppm (*trans*-, 131,7 ppm; *cis*-, 131,3 ppm)³. Deconvolution (Mnova[®] software, GSD

options, 5 fitting cycles with high resolution, proportional line width new spectrum with factor 0.30) was applied to all ^{13}C NMR spectra in order to improve the quality of the integrations.

Two P(*My-stat-S*) copolymers were analyzed by ^{31}P NMR spectroscopy to determine the fraction of the chains terminated with SG1. The spectra were recorded in CDCl_3 using a 5 mm diameter Up NMR tube with 800 scans being performed in a 200 MHz Varian Gemini 2000 spectrometer operating at 81 MHz. The NMR tubes were carefully weighed and filled with polymer (mass of polymer = 0.0682 g and 0.1179 g for *My/S-07* with $M_n = 11.1 \text{ kg.mol}^{-1}$ and *My/S-55* with $M_n = 16.6 \text{ kg.mol}^{-1}$ respectively) and diethylphosphite as internal reference (0.0044 g and 0.0031 g respectively). In order to know if *My*-based polymers and diethylphosphite have similar relaxation times, *My/S-55* was run under the exact same conditions with only one scan and no dummy scans ($ss = 0$). A negligible difference ($< 1.9\%$) in integral values was measured between this spectrum and the standard one with multiple scans. It was thereby assumed that diethylphosphite and *My*-based polymers with moderate $M_n < 17 \text{ kg.mol}^{-1}$ relax at the same rate.

The number-average molecular weights ($M_{n,\text{GPC}}$) and the molecular weight distributions ($\mathcal{D} = M_w/M_n$) were measured using gel permeation chromatography (GPC, Water Breeze) with HPLC grade tetrahydrofuran (THF) as the mobile phase. A mobile phase flow rate of 0.3 mL.min^{-1} was applied and the GPC was equipped with 3 Waters Styragel[®] HR columns (HR1 with a molecular weight measurement range of $10^2 - 5 \times 10^3 \text{ g.mol}^{-1}$, HR2 with a molecular weight measurement range of $5 \times 10^2 - 2 \times 10^4 \text{ g.mol}^{-1}$ and HR4 with a molecular weight measurement range of $5 \times 10^3 - 6 \times 10^5 \text{ g.mol}^{-1}$) and a guard column was used. The columns were heated to $40 \text{ }^\circ\text{C}$ during the analysis. The molecular weights were determined by calibration with linear narrow molecular weight distribution PS standards (PSS Polymer Standards Service GmbH, molecular weights ranging from 682 g.mol^{-1} to $2,520,000 \text{ g.mol}^{-1}$) and the GPC was equipped with a differential refractive index (RI 2414) detector. The P(*My*) contribution to $M_{n,\text{GPC}}$ was converted using the appropriate Mark-Houwink-Sakurada (MHS) coefficients (MHS parameters determined at $40 \text{ }^\circ\text{C}$ with THF eluent for PS⁴: $K_{\text{PS}} = 15.8 \times 10^{-5} \text{ dL.g}^{-1}$ and $\alpha_{\text{PS}} = 0.706$; MHS parameters determined at $30 \text{ }^\circ\text{C}$ with THF eluent for 1,4-P(*My*)⁵, $K_{\text{P(My)}} = 7.46 \times 10^{-5} \text{ dL.g}^{-1}$ and $\alpha_{\text{P(My)}} = 0.772$). Therefore, Every M_n value reported in the Results & Discussion section was calculated using the following formula: $M_n = F_{\text{My}} \times M_{n,\text{MHS}} + F_{\text{S}} \times M_{n,\text{GPC}}$ where F_{My} and F_{S} are the respective molar fraction of *My* and S in the final polymer and $M_{n,\text{MHS}} = [(K_{\text{PS}}/K_{\text{P(My)}}) \times M_{n,\text{GPC}}^{\alpha_{\text{PS}}}]^{1/(\alpha_{\text{P(My)}}+1)}$ using the Mark-Houwink relationship⁶.

Thermogravimetric analysis (TGA) was carried out using Q500TM from TA Instruments under nitrogen flow at a ramp rate of $10 \text{ }^\circ\text{C.min}^{-1}$. Samples were heated in aluminum pans. This technique allowed the decomposition temperature (T_d) to be determined. Differential scanning calorimetry (DSC, Q2000TM from TA Instruments) was also performed under nitrogen atmosphere to measure the glass transition temperatures (T_g s) of P(*My*), P(*My-b-S*) and P(*My-stat-S*) polymers. Calibrations for temperature and heat flow were done using indium and benzoic acid standards respectively. The DSC was typically performed in the temperature range from $-90 \text{ }^\circ\text{C}$ to $+150 \text{ }^\circ\text{C}$ using three scans per cycle (heat/cool/heat) at a rate of $10 \text{ }^\circ\text{C.min}^{-1}$. To eliminate the thermal history, glass transition temperatures were reported from the second heating run. The reported T_g s were calculated using the injection method from the change in slope observed in the DSC traces.

The stress-strain behavior of the synthesized P(*My-b-S*) diblock copolymers was recorded using a MTS Insight™ material testing system with a 5 kN load cell at room temperature and a cross-head speed of 1 mm.min⁻¹. Dog-bone style tensile specimens (ASTM D638, *type V*, overall length = 63.5 mm, overall width = 9.53 mm) were made using a hot press (Carver hydraulic press, model #3925) at $T \sim T_{g,specimen} + 50\text{ }^{\circ}\text{C}$ where $T_{g,specimen}$ refers to the specimen's higher T_g , under a mean pressure of 5000 psi. The width (3.18 ± 0.5 mm) and the thickness (1.40 ± 0.3 mm) of the narrow section of each specimen were previously measured using a digital ruler. Each test was considered finished after the complete break-up of the specimen in two distinct parts. A minimum of five specimens was tested for each P(*My-b-S*) diblock copolymer sample and averaged results were reported. This mechanical characterization allowed the Young's modulus, the ultimate tensile strength and the elongation at break to be determined, using TestWorks 4 software. The Young's modulus was determined as the slope of the stress-strain curve at strains of 0-0.5 %.

■ References of the experimental section.

- (1) Harrison, S.; Couvreur, P.; Nicolas, J. SG1 Nitroxide-Mediated Polymerization of Isoprene: Alkoxyamine Structure/Control Relationship and α,ω -Chain-End Functionalization. *Macromolecules* **2011**, *44* (23), 9230-9238.
- (2) Sarkar, P.; Bhowmick, A. K. Synthesis, Characterization and Properties of a Bio-based Elastomer: Polymyrcene. *RSC Adv.* **2014**, *4*, 61343-61354.
- (3) Georges, S.; Bria, M.; Zinck, P.; Visseaux, M. Polymyrcene Microstructure revisited from Precise High-Field Nuclear Magnetic Resonance Analysis. *Polymer* **2014**, *55*, 3869-3878.
- (4) Xie, J. Viscometric Constants for Small Polystyrenes and Polyisobutenes by Gel Permeation Chromatography. *Polymer* **1994**, *35* (11), 2385-2389.
- (5) Hattam, P.; Gauntlett, S.; Mays, J. W.; Hadjichristidis, N.; Young, R. N.; Fetters, L. J. Conformational Characteristics of some Model Polydienes and Polyolefins. *Macromolecules* **1991**, *24* (23), 6199-6209.
- (6) Pasch, H.; Trathnigg, B. *Multidimensional HPLC of Polymers*; Springer: Heidelberg, **2013**; 37-90.

a.2. Supporting information

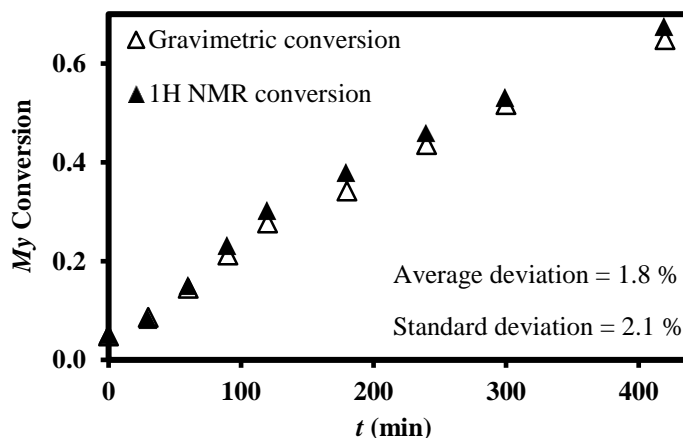


Figure S1a. Gravimetric conversion X_{grav} and ^1H NMR conversion X_{NMR} versus reaction time t for the polymerization *My-6*.

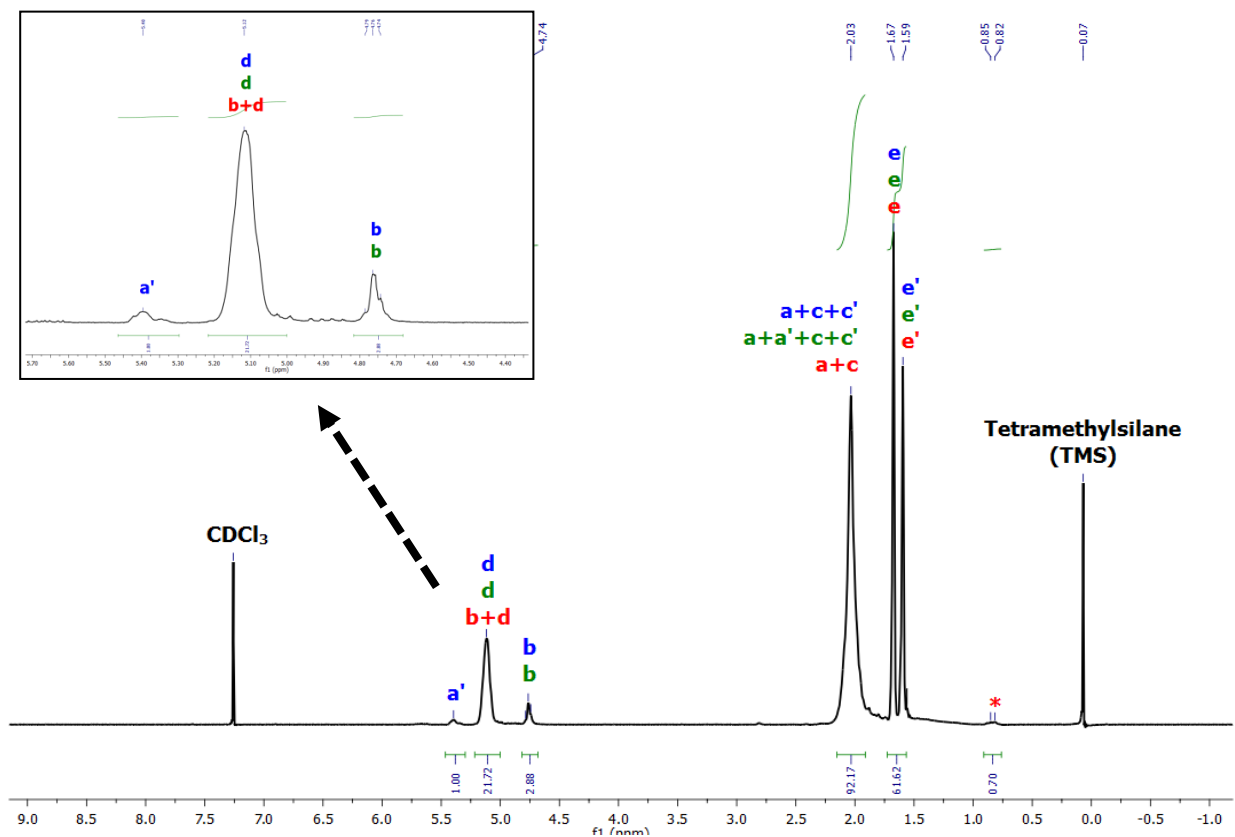
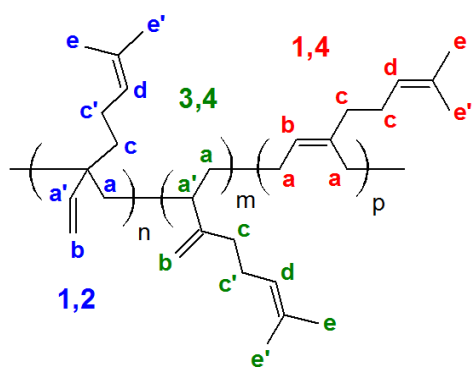


Figure S2a. ^1H NMR spectrum of P(My) My-2 in CDCl_3 (300 MHz) at room temperature.



P(My) My-2: ^1H NMR (CDCl_3 , 300 MHz, RT): $\delta = 5.50\text{-}5.30$ (t br, $1\text{H}^{1,2}$), $5.25\text{-}5.00$ (t br, $1\text{H}^{1,2}$, $1\text{H}^{3,4}$, $2\text{H}^{1,4}$), $4.80\text{-}4.70$ (d, $2\text{H}^{1,2}$ and s, $2\text{H}^{3,4}$), $2.20\text{-}1.85$ (m br, $6\text{H}^{1,2}$, $7\text{H}^{3,4}$, $8\text{H}^{1,4}$), 1.67 (s, $3\text{H}^{1,2}$, $3\text{H}^{3,4}$, $3\text{H}^{1,4}$), 1.59 (s, $3\text{H}^{1,2}$, $3\text{H}^{3,4}$, $3\text{H}^{1,4}$).

*Peak at $\delta = 0.90\text{-}0.75$ ppm may correspond to the protons at the chain ends.

The three different types of configuration, 1,4-, 1,2- and 3,4-P(My), were quantified by comparing the three integrated areas at $\delta = 5.50\text{-}5.30$ ppm (one olefinic proton of 1,2-addition), $\delta = 5.25\text{-}5.00$ ppm (two olefinic protons of 1,4-addition, one olefinic proton of 1,2-addition and one olefinic proton of 3,4-addition) and $\delta = 4.80\text{-}4.70$ ppm (two vinyl protons of 3,4-addition and two vinyl protons of 1,2-addition)¹. 1,4-content = 87.6 %, 1,2-content = 8.6 % and 3,4-content = 3.8 % were calculated for My-2.

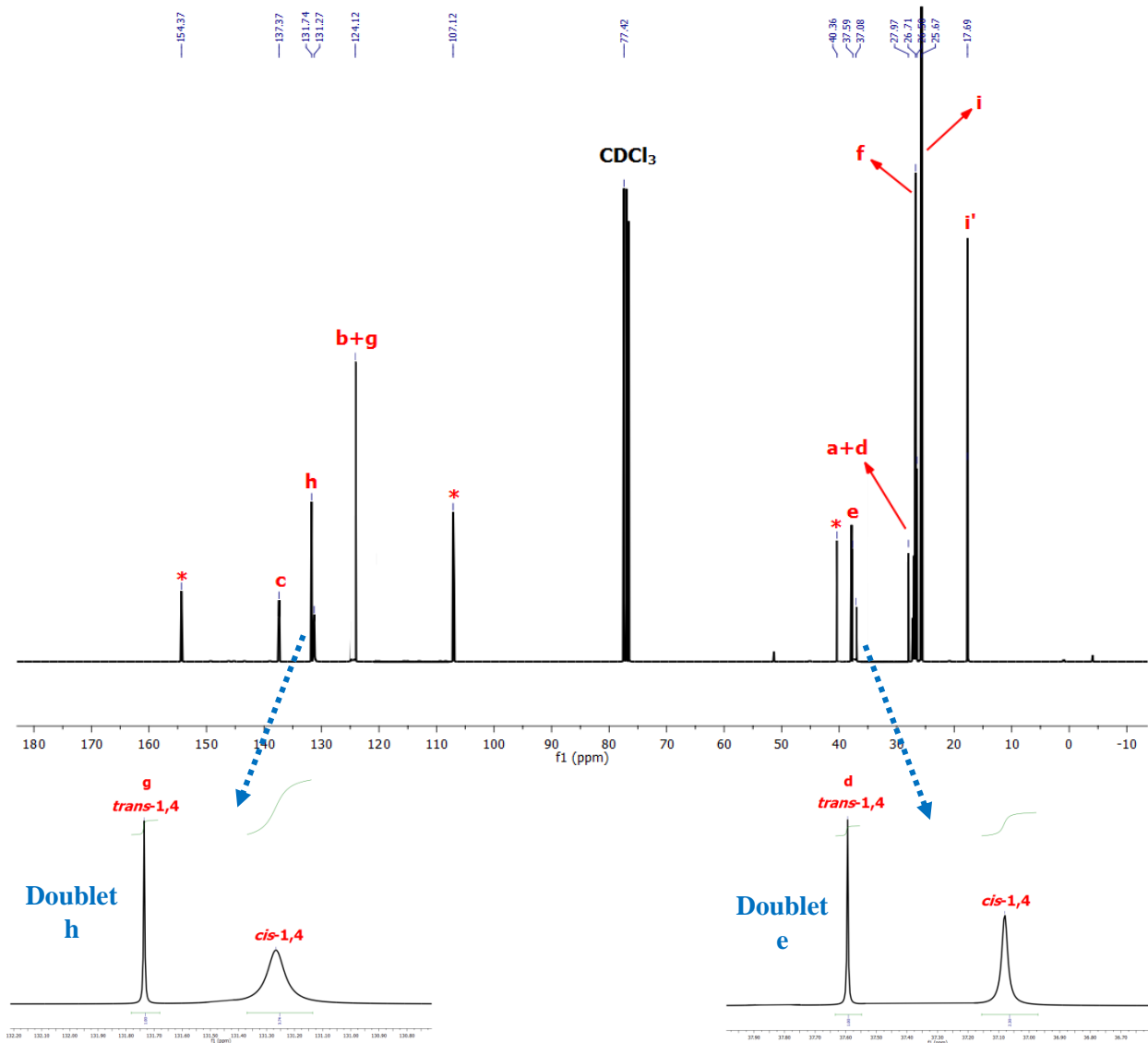
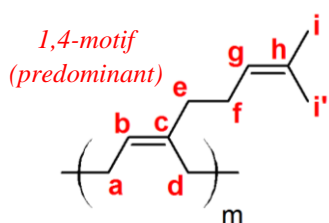


Figure S3a. ^{13}C NMR spectrum of P(My) macroinitiator My-12 in CDCl_3 (300 MHz) at room temperature. Deconvolution (Mnova[®] software, GSD options, 5 fitting cycles with high resolution, proportional line width new spectrum with factor 0.30) was applied.



P(My) Macroinitiator My-12: ^{13}C NMR (CDCl_3 , 300 MHz, RT): $\delta = 137.4$ (s, 1C), 131.8-131.1 (d (*cis*- and *trans*-), 1C), 124.1 (s, 2C), 37.7-36.9 (d (*cis*- and *trans*-), 1C), 28.0 (s, 1C), 26.7 (s, 1C), 26.5 (s, 1C), 25.7 (s, 1C), 17.7 (s, 1C).

*Signals at $\delta = 154.4$ (1), 107.1 (2) and 40.4 (3) ppm correspond to aliphatic carbon from 3,4-P(My) (1), vinylic carbons from 3,4- and 1,2-P(My) (2) and aliphatic carbons from 3,4- and 1,2-P(My) (3).

cis-1,4/*trans*-1,4 molar ratio was quantified by using the chemical shifts of methylene carbon at $\delta = 37$ -38 ppm and the quaternary carbon at $\delta = 131$ -132 ppm². *cis*-1,4-content = 74.3 % was calculated for My-12.

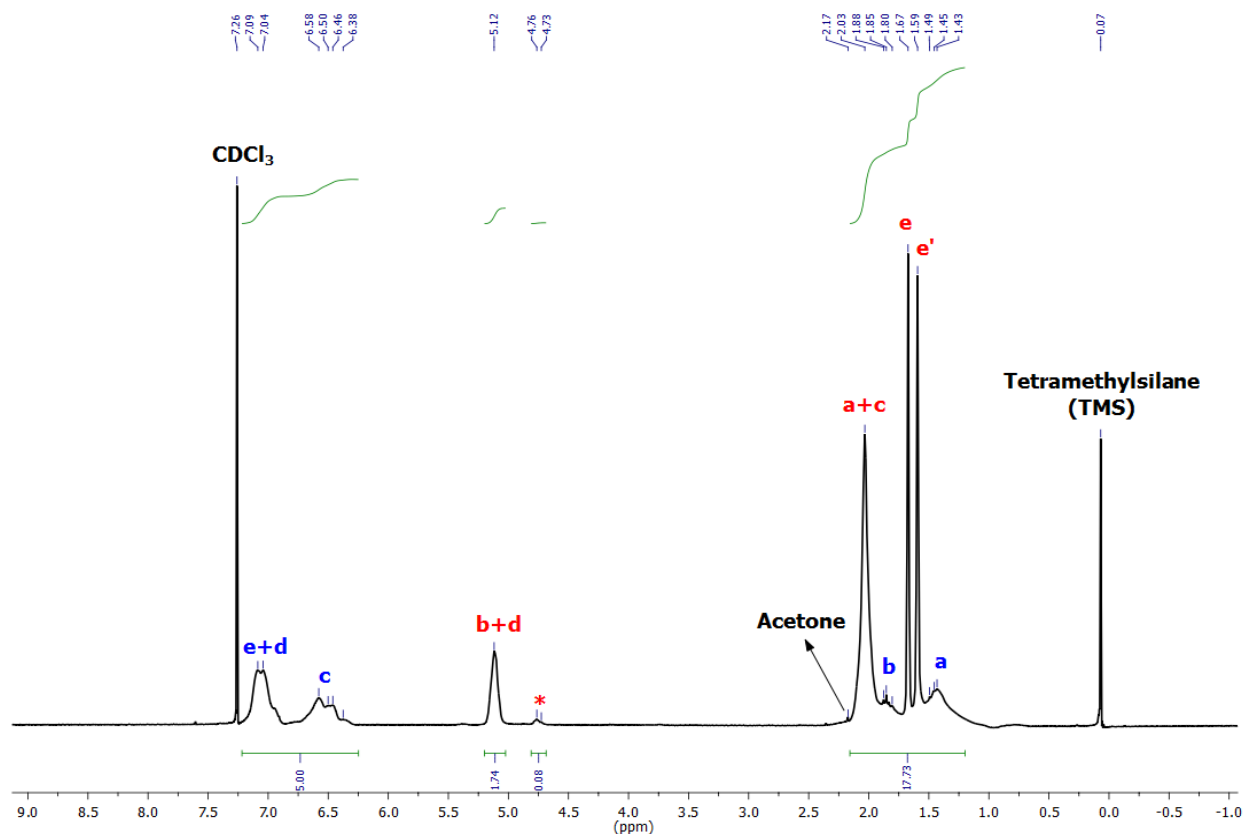
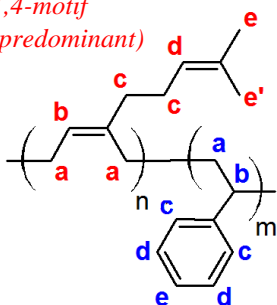


Figure S4a. ^1H NMR spectrum in CDCl_3 (300 MHz) at room temperature of dried $\text{P}(\text{My}-b\text{-S})$ diblock copolymer $\text{My}-11\text{-Sa}$ after recovery, using methanol as the precipitant.

1,4-motif
(predominant)



$\text{P}(\text{My}-b\text{-S})$ $\text{My}-11\text{-Sa}$: ^1H NMR (CDCl_3 , 300 MHz, RT): $\delta = 7.20\text{-}6.86$ (m br, 3H^{PS}), $6.80\text{-}6.25$ (m br, 2H^{PS}), $5.20\text{-}5.00$ (s br, $2\text{H}^{\text{P}(\text{My})}$), $2.20\text{-}1.90$ (m br, $8\text{H}^{\text{P}(\text{My})}$), $1.90\text{-}1.72$ (quint br, 1H^{PS}), 1.67 (s, $3\text{H}^{\text{P}(\text{My})}$), 1.59 (s, $3\text{H}^{\text{P}(\text{My})}$), $1.54\text{-}1.20$ (t br, 2H^{PS}).

*Signal at $\delta = 4.82\text{-}4.70$ ppm (s br, $2\text{H}^{\text{P}(\text{My})}$) corresponds to vinylic protons from 3,4- $\text{P}(\text{My})$.

The molar composition of S in the final $\text{P}(\text{My}-b\text{-S})$ copolymer (F_S) was calculated by comparing the two integrated areas corresponding to the five aromatic protons of PS ($\delta = 6.25\text{-}7.25$ ppm) and the three aliphatic protons of PS, the eight aliphatic protons and the six protons of the two methyl groups of $\text{P}(\text{My})$ ($\delta = 1.20\text{-}2.15$ ppm). $F_S = 0.47$ was calculated for $\text{My}-11\text{-Sa}$.

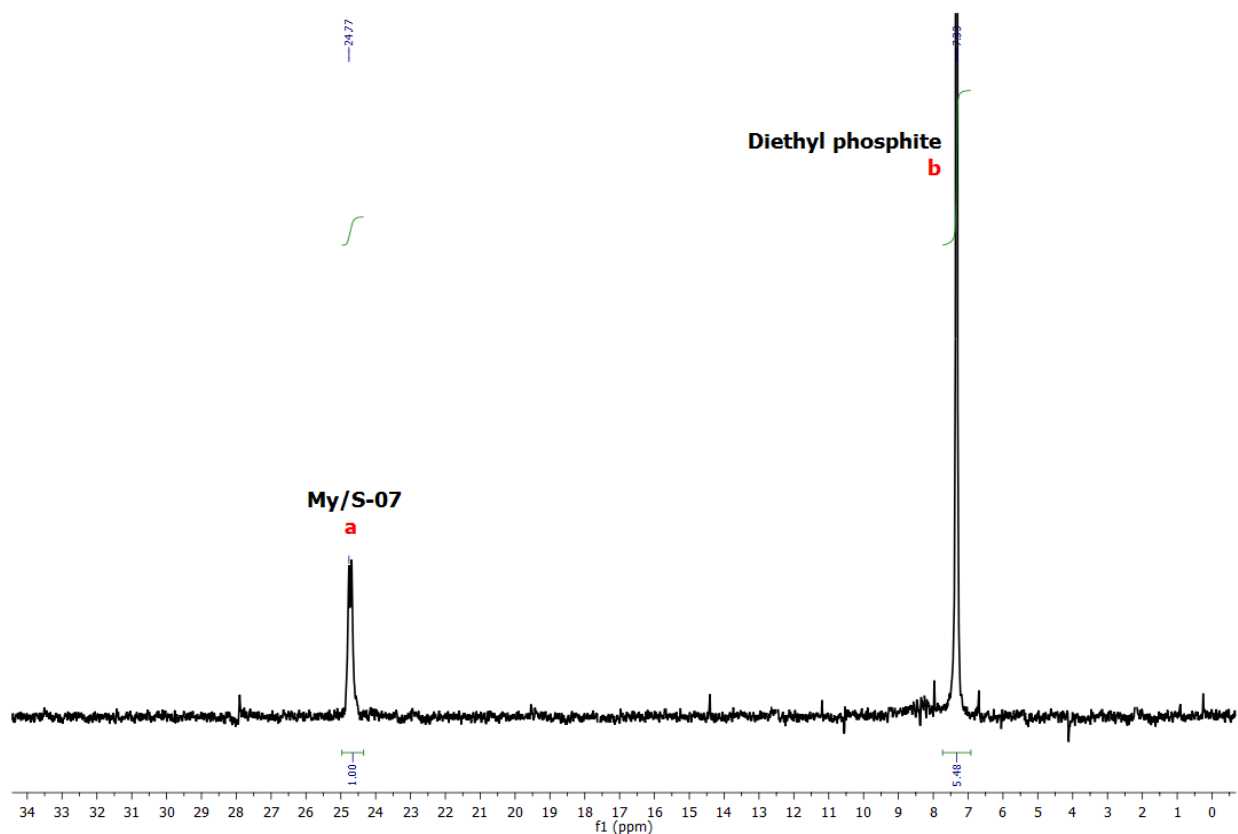
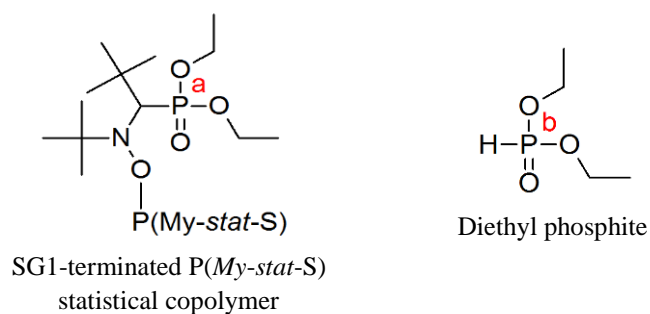


Figure S5a. 81 MHz ^{31}P NMR spectrum of dried P(*My-stat-S*)-SG1 macroinitiator *My/S-07* in CDCl_3 at room temperature.



The fraction of P(*My-stat-S*) chains terminated with SG1 was calculated by comparing the two integrated peaks corresponding to the phosphorus atom of the SG1 group ($\delta = 24.8$ ppm) and the phosphorus atom of diethyl phosphite ($\delta = 7.3$ ppm) used as an internal reference^{3,4}. Using the known amounts of diethyl phosphite (0.0044 g) and P(*My-stat-S*) copolymer (0.0682 g with $M_n = 11.1$ kg.mol⁻¹), the proportions of chains containing the SG1 moiety attached to the *My/S-07* terminal unit was estimated to 94 % \pm 6 mol% (standard deviation derived from the difference in M_n value between the GPC result and the corrected M_n using MHS equation). The calculation of the fraction of SG1 groups was done by considering similar relaxation times between diethyl phosphite and the polymer.

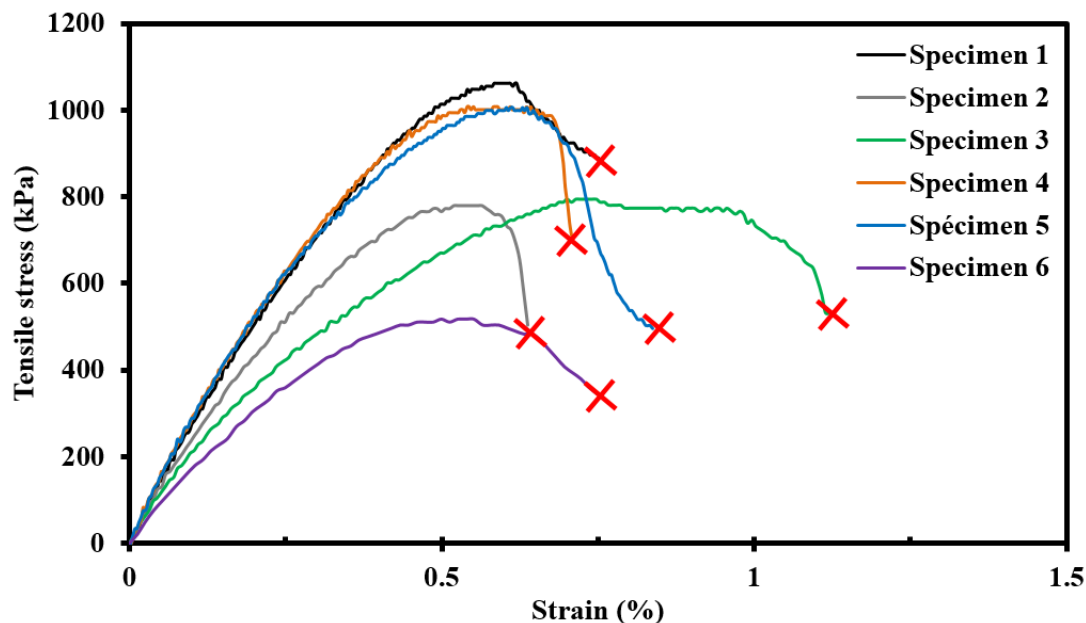


Figure S6a. Tensile stress-strain curves of six P(*My-b-S*) diblock copolymer specimens from *My-11-Sa* sample with $M_{n,P(My)} = 22.8 \text{ kg.mol}^{-1}$ and $M_{n,PS} = 26.2 \text{ kg.mol}^{-1}$ at room temperature and 1 mm.min^{-1} . The red crosses denote failure points.

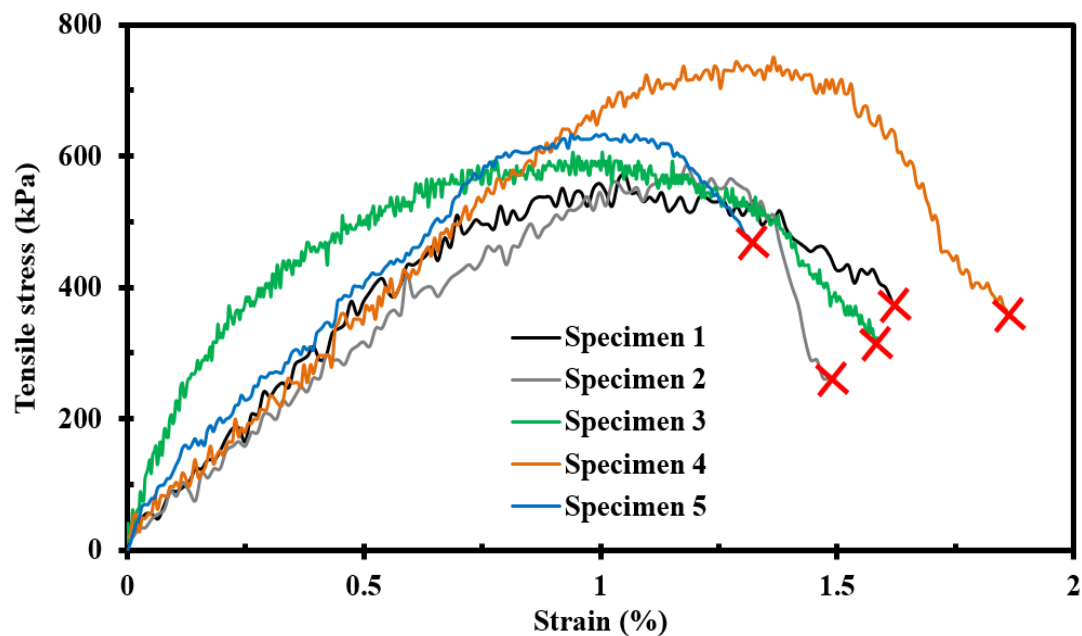


Figure S7a. Tensile stress-strain curves of five P(*My-b-S*) diblock copolymer specimens from *My-11-Sb* sample with $M_{n,P(My)} = 22.8 \text{ kg.mol}^{-1}$ and $M_{n,PS} = 15.7 \text{ kg.mol}^{-1}$ at room temperature and 1 mm.min^{-1} . The red crosses denote failure points.

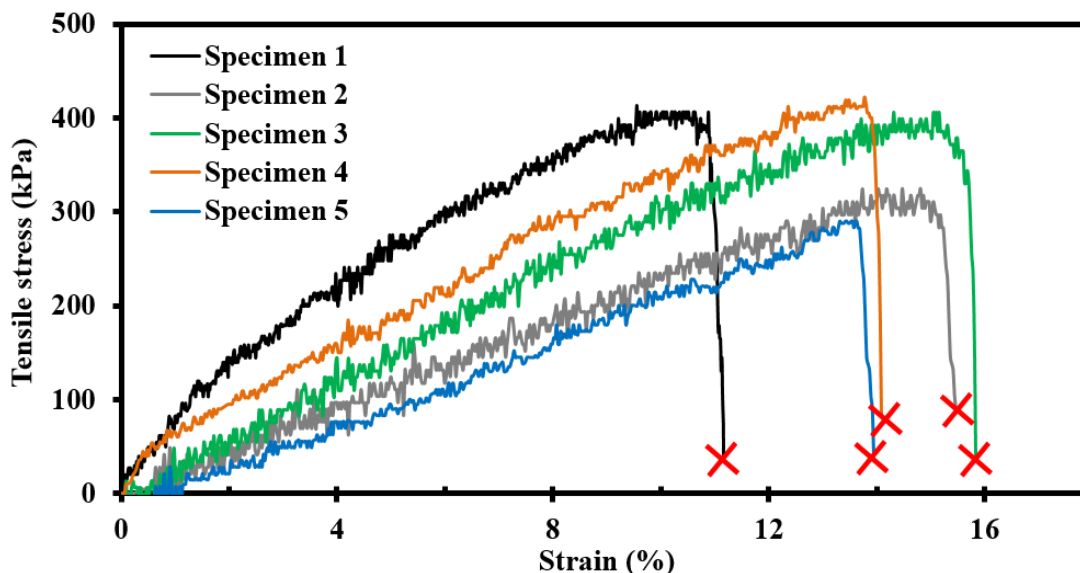


Figure S8a. Tensile stress-strain curves of five P(*My-b-S*) diblock copolymer specimens from *My-12-S* sample with $M_{n,P(My)} = 30.4 \text{ kg.mol}^{-1}$ and $M_{n,PS} = 12.2 \text{ kg.mol}^{-1}$ at room temperature and 1 mm.min^{-1} . The red crosses denote failure points.

Table S1a. Young's modulus (*E*), ultimate tensile strength and tensile elongation at break values for every specimen tested from experiments *My-11-Sa*, *My-11-Sb* and *My-12-S*.

Experiment	Specimen	<i>E</i> (MPa)	Ultimate tensile strength (MPa)	Tensile elongation at break (%)
<i>My-11-Sa</i>	1	336.4	1.06	0.75
	2	255.9	0.78	0.64
	3	228.3	0.79	1.12
	4	298.2	1.01	0.71
	5	288.9	1.01	0.84
	6	173.8	0.52	0.75
Average		263.6	0.86	0.80
Standard deviation		52.5	0.19	0.15
<i>My-11-Sb</i>	1	92.4	0.57	1.62
	2	83.6	0.59	1.48
	3	264.6	0.61	1.58
	4	82.6	0.75	1.86
	5	105.8	0.63	1.32
	Average		125.8	0.63
Standard deviation		69.9	0.06	0.18
<i>My-12-S</i>	1	8.0	0.41	11.02
	2	3.0	0.32	15.25
	3	3.7	0.41	15.67
	4	13.3	0.42	14.04
	5	2.5	0.29	13.73
	Average		6.1	0.37
Standard deviation		4.1	0.05	1.63

■ **Use of terminal models:** The experimental data used to determine the reactivity ratios r_{My} and r_S is given in Table S2a. Calculation of r_{My} and r_S was first done by linearization of the Mayo-Lewis equation⁵ (eg. the Fineman-Ross (FR) approach⁶) and by the Kelen-Tüdös (KT) approach⁷. The latter refines the linearization method by introducing an arbitrary positive constant α to spread the data more evenly so as to give equal weight to all data points. Accordingly, the KT approach minimizes the bias of the FR approach. The appropriate plot of the variables G and H, defined in Equation C1, will provide a linear relationship giving the reactivity ratios as the slope and intercept as shown in Equation C2.

$$G = (f_{S,0}/f_{My,0}) \times [(2F_S - 1) / F_S] ; H = (f_{S,0}/f_{My,0})^2 \times [(1 - F_S) / F_S] \quad (C1)$$

$$G = r_S \times H - r_{My} \quad (C2)$$

Equation C3 shows the additional variables used for the KT plot as illustrated in Equation C4.

$$\eta = G / (\alpha + H) ; \varepsilon = H / (\alpha + H) ; \alpha = \sqrt{H_{max}H_{min}} \quad (C3)$$

$$\eta = (r_S + r_{My} / \alpha)\varepsilon - r_{My} / \alpha \quad (C4)$$

In Equations C3 and C4, H_{max} and H_{min} refer to the minimum and maximum H values determined from the experimental data. $r_{My} = 1.88 \pm 0.12$ and $r_S = 0.25 \pm 0.04$ ($r_{My} \times r_S = 0.47 \pm 0.11$) were obtained via the FR method and $r_{My} = 2.19 \pm 0.07$ and $r_S = 0.34 \pm 0.19$ ($r_{My} \times r_S = 0.74 \pm 0.41$) were calculated via the KT method. The errors associated with the experimental data were derived from the standard errors of the slopes from FR and KT plots.

■ **Use of a NLLS model:** Although the KT method is more reliable than the FR method, it is still a linearization. Statistically, a NLLS fit to the Mayo-Lewis equation is probably the soundest method to determine the desired parameters⁸. Therefore, the reactivity ratios were also determined using a non-linear least-squares fitting of the data. The commercial software package Matlab R2016a was used to solve the Mayo-Lewis equation⁵ for My/S copolymerization (C5).

$$F_S = (r_S f_{S,0}^2 + f_{S,0} f_{My,0}) / (r_S f_{S,0}^2 + 2 f_{S,0} f_{My,0} + r_{My} f_{My,0}^2) \quad (C5)$$

Using the reactivity ratios determined by the KT method as initial guesses, the statistical fit to the data yielded reactivity ratios $r_{My} = 2.90 \pm 1.25$ and $r_S = 0.47 \pm 0.27$ at a confidence interval of 95 % and with a regression coefficient $R^2 = 0.968$.

Table S2a. Samples used for determination of reactivity ratios for *My*/S statistical copolymerization done at 110 °C in bulk with NHS-BB and targeting $M_{n,theo} = 30 \text{ kg}\cdot\text{mol}^{-1}$ at $X = 1.0$.

$f_{S,0}^{(a)}$	$F_S^{(b)}$	$X^{(c)}$	$M_n^{(d)}$ ($\text{kg}\cdot\text{mol}^{-1}$)	$\mathfrak{D}^{(d)}$
0.10	0.05	0.148	4.5	1.36
0.21	0.10	0.101	2.9	1.37
0.31	0.24	0.089	2.8	1.36
0.40	0.22	0.119	5.3	1.27
0.45	0.25	0.102	4.3	1.19
0.51	0.21	0.113	4.2	1.33
0.60	0.31	0.074	3.5	1.35
0.69	0.45	0.089	3.4	1.34
0.80	0.66	0.122	5.6	1.33
0.89	0.83	0.091	5.5	1.31
0.94	0.84	0.153	4.9	1.23

a) $f_{S,0}$ is the initial molar feed composition of styrene.

b) F_S is the molar composition of styrene in the P(*My-stat-S*) copolymer determined by ^1H NMR in CDCl_3 .

c) Overall monomer conversion X corresponding to the average value of the gravimetric conversion X_{grav} and the spectroscopic conversion X_{NMR} (further details in the experimental section).

d) M_n and M_w determined by GPC calibrated with PS standards in THF at 40 °C. Appropriate MHS coefficients and $F_{My} = 1 - F_S$ used to convert molecular weights based on PS to the fraction of *My* incorporated in the P(*My-stat-S*) copolymer.

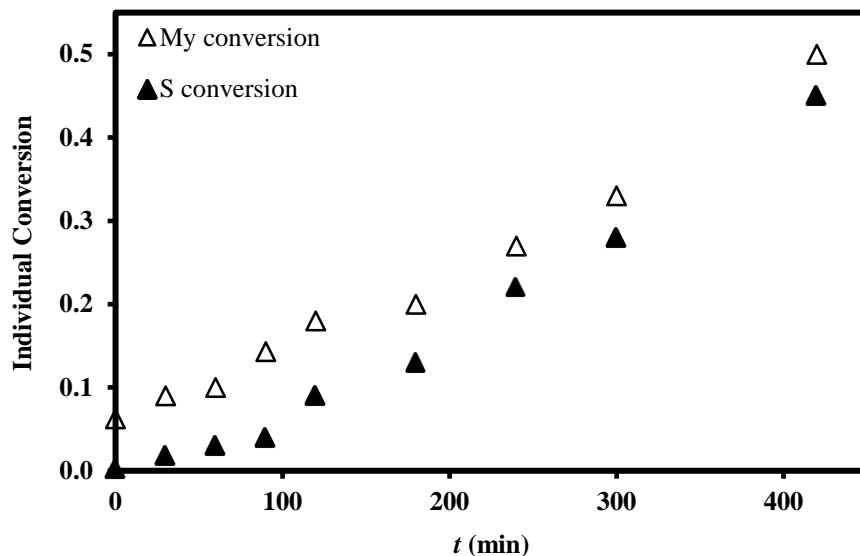


Figure S9a. Individual monomer conversions, determined by ^1H NMR in CDCl_3 , versus reaction time t for the statistical copolymerization $\text{My}/\text{S}-50$.

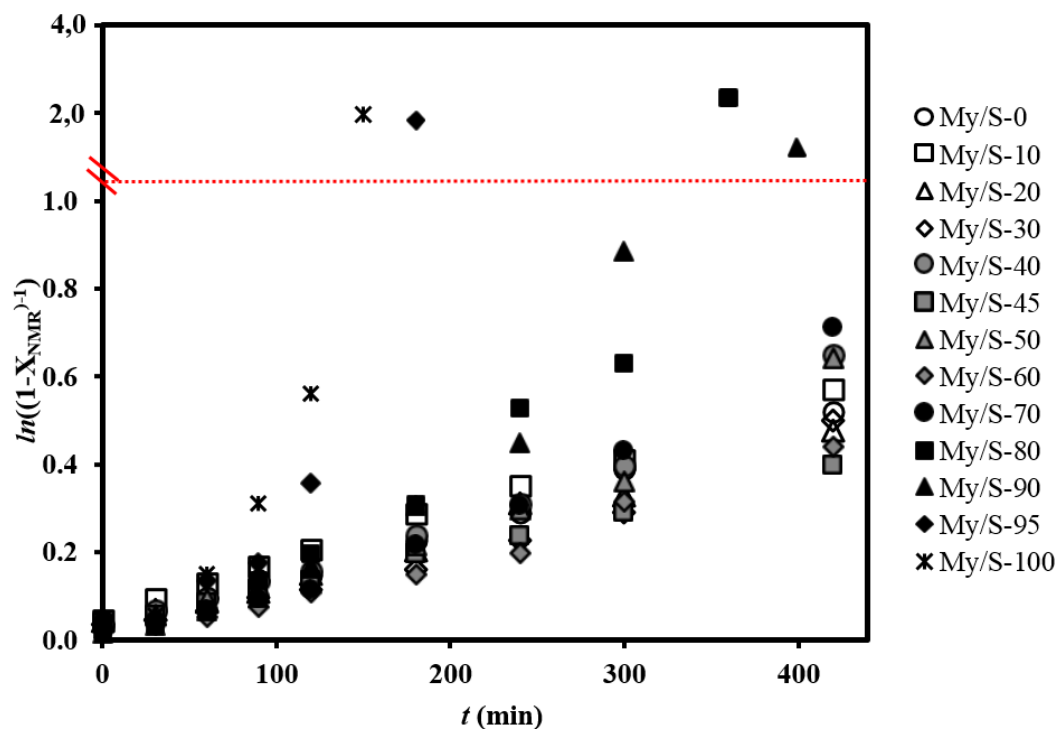


Figure S10a. Semi-logarithmic kinetic plots of $\ln((1-X_{\text{NMR}})^{-1})$ ($X_{\text{NMR}} = X_{\text{My}/\text{My},0} + X_{\text{S}/\text{S},0}$) versus polymerization time t for the homopolymerizations $\text{My}/\text{S}-0$ and $\text{My}/\text{S}-100$ and the various My/S statistical copolymerizations at 110°C in bulk initiated by NHS-BB and targeting $M_{n,\text{theo}} = 30 \text{ kg}\cdot\text{mol}^{-1}$ at $X = 1.0$. Note that the scale of the y-axis is discontinuous (red dotted line) in order to display the higher values.

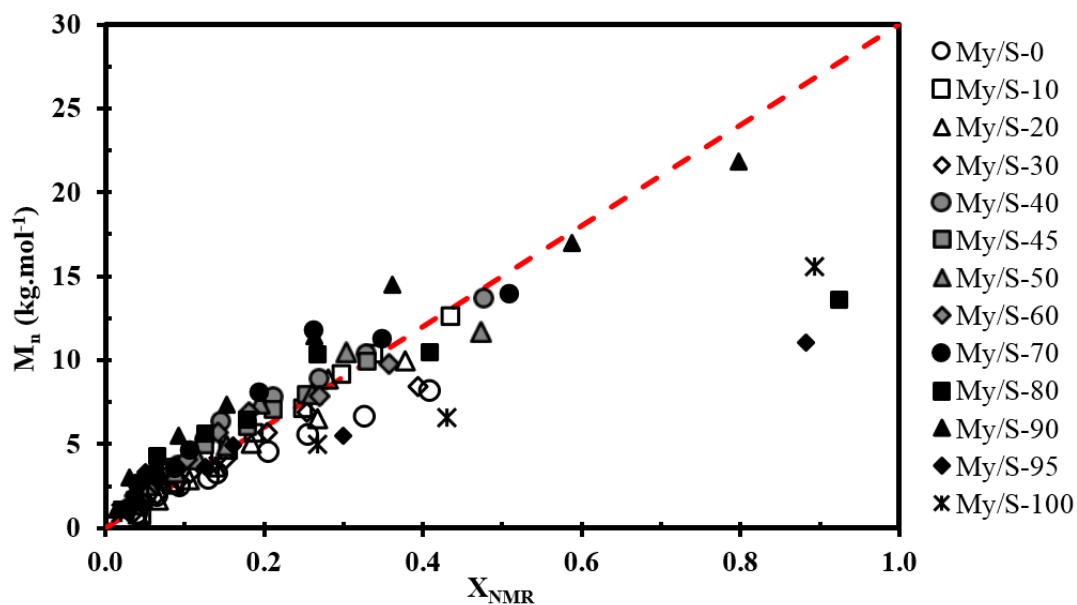


Figure S11a. M_n determined by GPC relative to PS standards in THF and corrected with appropriate MHS coefficients *versus* average NMR conversion X_{NMR} for the homopolymerizations $M_y/S-0$ and $M_y/S-100$ and the various M_y/S statistical copolymerizations at 110 °C in bulk initiated by NHS-BB and targeting $M_{n,\text{theo}} = 30 \text{ kg.mol}^{-1}$ at $X = 1.0$. The red dashed line indicate the theoretical M_n ($M_{n,\text{theo}}$) *versus* overall conversion based on the monomers to initiator ratio.

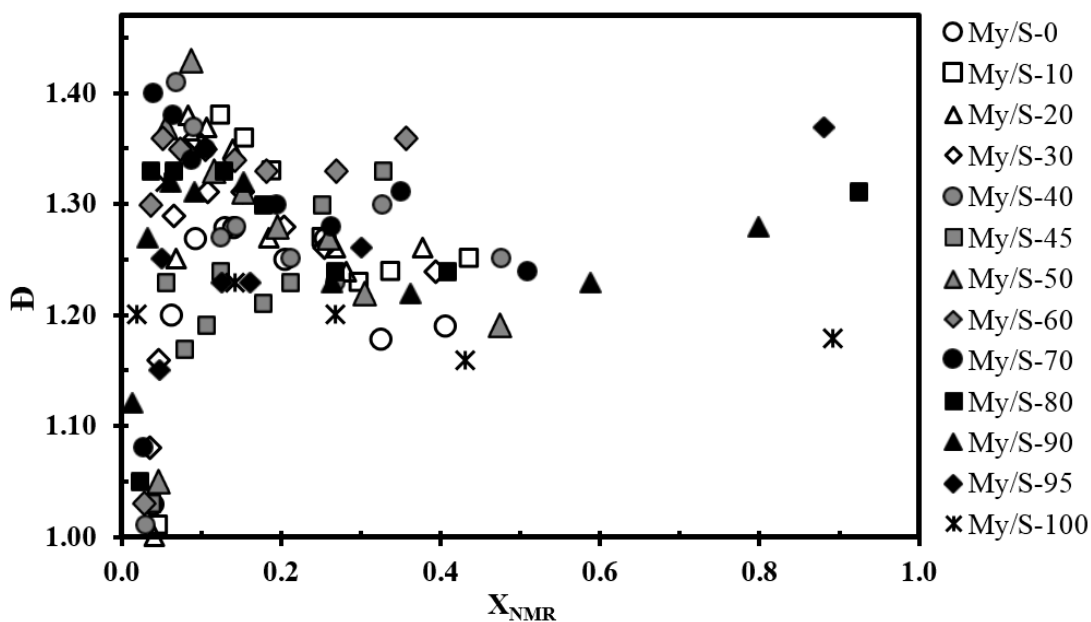


Figure S12a. \bar{D} *versus* average NMR conversion X_{NMR} for the homopolymerizations $M_y/S-0$ and $M_y/S-100$ and the various M_y/S statistical copolymerizations at 110 °C in bulk initiated by NHS-BB and targeting $M_{n,\text{theo}} = 30 \text{ kg.mol}^{-1}$ at $X = 1.0$.

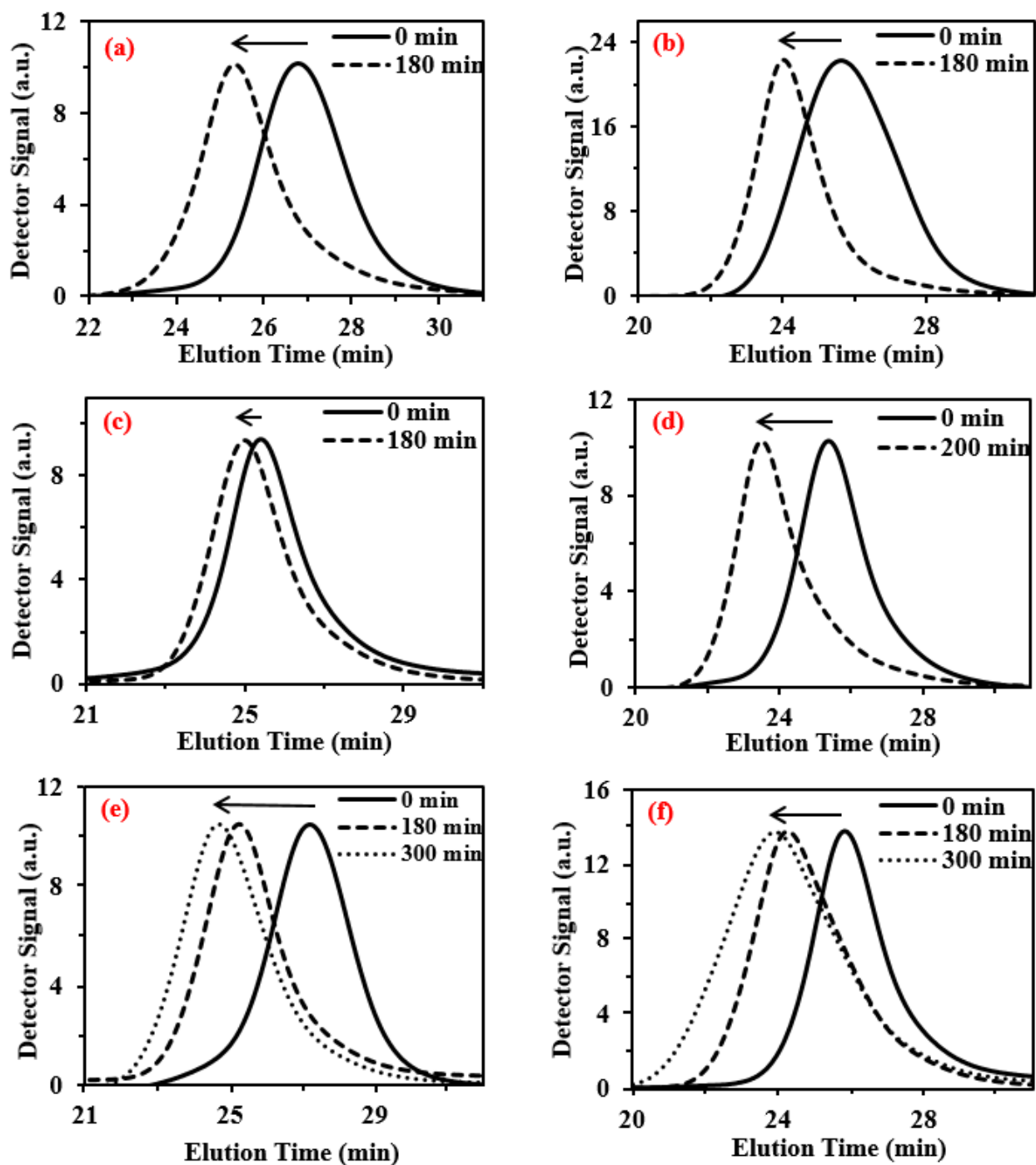


Figure S13a. Normalized GPC traces for *My* and *S* chain-extensions from *My*-rich *My/S-07* and *S*-rich *My/S-55* macroinitiators at 110 °C or 120 °C in bulk or in toluene. Chain-extensions **a)** *My/S-07-My.a*, **b)** *My/S-07-S*, **c)** *My/S-55-My.a*, **d)** *My/S-55-S*, **e)** *My/S-07-My.b* and **f)** *My/S-55-My.b*.

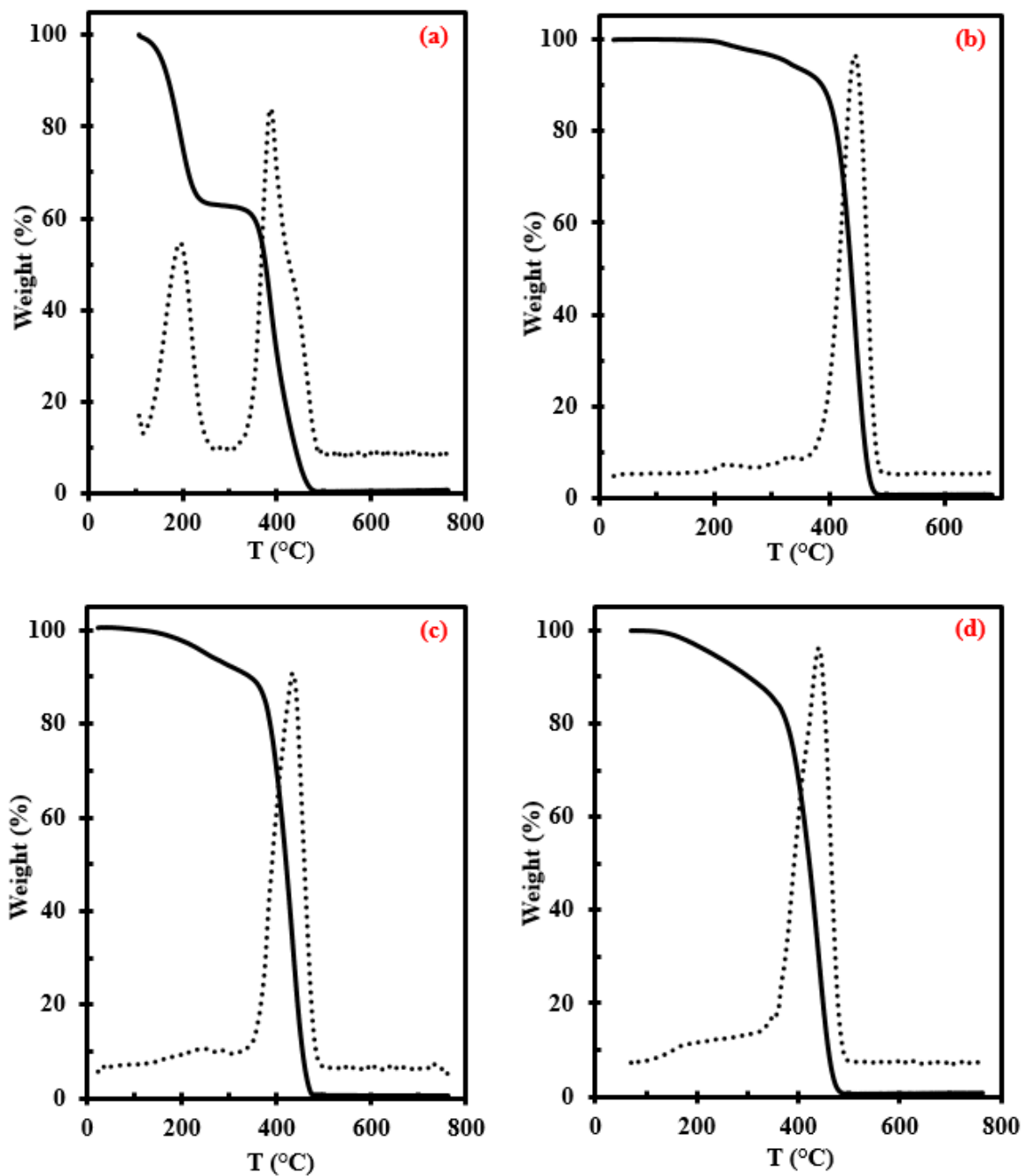


Figure S14a. TGA traces of **a)** P(My) My-12, **b)** PS My/S-100, **c)** P(My-b-S) My-10-S and **d)** P(My-b-S) My-11-Sa. Measurements performed under nitrogen flow at a ramp rate of $10\text{ }^{\circ}\text{C}\cdot\text{min}^{-1}$. Sample weight *versus* temperature is represented by the solid line whereas the dotted line represents the derivative of weight relative to the temperature *versus* temperature in order to determine precisely the temperature at which weight loss is most apparent ($T_{\text{dec,max}}$).

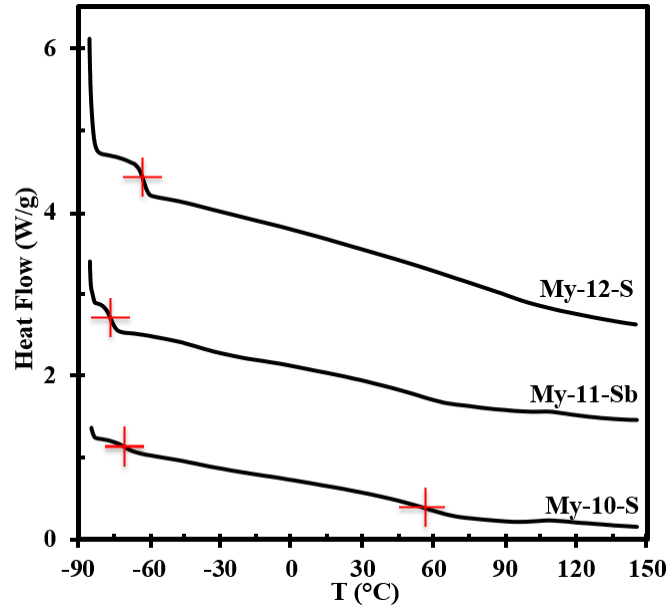


Figure S15a. DSC traces (second heating run) of P(*My-b-S*) diblock copolymers *My-10-S*, *My-11-Sb* and *My-12-S*. The red crosses indicate the changes in slope observed.

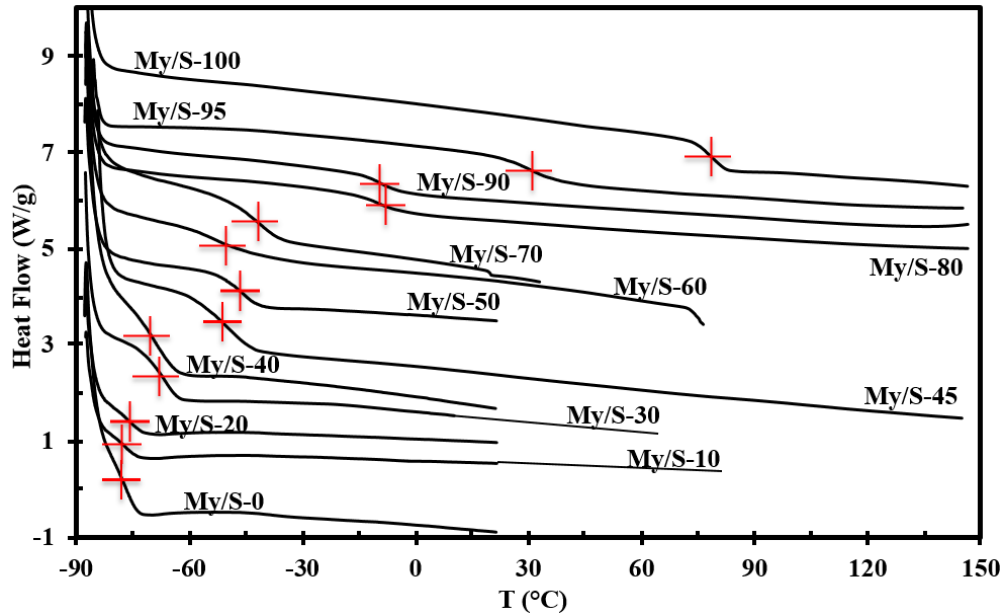


Figure S16a. DSC traces (second heating run) of P(*My*) *My/S-0*, PS *My/S-100* and P(*My-stat-S*) statistical copolymers. The red crosses indicate the changes in slope observed.

References of the supporting information:

- (1) Sarkar, P.; Bhowmick, A. K. Synthesis, Characterization and Properties of a Bio-based Elastomer: Polymyrcene. *RSC Adv.* **2014**, *4*, 61343-61354.
- (2) Georges, S.; Bria, M.; Zinck, P.; Visseaux, M. Polymyrcene Microstructure revisited from Precise High-Field Nuclear Magnetic Resonance Analysis. *Polymer* **2014**, *55*, 3869-3878.
- (3) Lefay, C.; Bellenev, J.; Charleux, B.; Guerret, O.; Magnet, S. End-Group Characterization of Poly(acrylic acid) Prepared by Nitroxide-Mediated Controlled Free-Radical Polymerization. *Macromol. Rapid Commun.* **2004**, *25* (13), 1215-1220.
- (4) Nicolas, J.; Dire, C.; Mueller, L.; Bellenev, J.; Charleux, B.; Marque, S. R. A.; Bertin, D.; Magnet, S.; Couvreur, L. Living Character of Polymer Chains Prepared via Nitroxide-Mediated Controlled Free-Radical Polymerization of Methyl Methacrylate in the Presence of a Small Amount of Styrene at Low Temperature. *Macromolecules* **2006**, *39* (24), 8274-8282.
- (5) Mayo, F. R.; Lewis, F. M. Copolymerization. I. A Basis for Comparing the Behavior of Monomers in Copolymerization; The Copolymerization of Styrene and Methyl Methacrylate. *J. Am. Chem. Soc.* **1944**, *66* (9), 1594-1601.
- (6) Fineman, M.; Ross, S. D. Linear Method for Determining Monomer Reactivity Ratios in Copolymerizations. *J. Polym. Sci., Part A: Polym. Chem.* **1950**, *5* (2), 259-262.
- (7) Kelen, T.; Tüdös, F. Analysis of the Linear Methods for Determining Copolymerization Reactivity Ratios. I. A New Improved Linear Graphic Method. *J. Macromol. Sci. Chem.* **1975**, *A9* (1), 1-27.
- (8) Tidwell, P. W.; Mortimer, G. A. An Improved Method of Calculating Copolymerization Reactivity Ratios. *J. Polym. Sci., Part A: Polym. Chem.* **1965**, *3*, 369-387.

b. Appendix for Chapter 2

b.1. Experimental section

■ **Materials.** β -Myrcene (M_y , $\geq 90\%$), basic alumina (Al_2O_3 , Brockmann, 150 mesh), calcium hydride (CaH_2 , 90-95% reagent grade), 1,4-dioxane ($\geq 99\%$) and 2-methyltetrahydrofuran (Me-THF, $\geq 99\%$ anhydrous) were purchased from Sigma-Aldrich and used as received. Toluene ($\geq 99\%$), methanol (MeOH , $\geq 99\%$), tetrahydrofuran (THF, 99.9% HPLC grade) and morpholine ($\geq 99\%$ ACS reagent) were obtained from Fisher Scientific and used as received. 2-Methyl-2-[*N*-*tert*-butyl-*N*-(1-diethoxyphosphoryl)-2,2-dimethylpropyl]-aminoxy]-*N*-propionyloxy-succinimide, also known as NHS-BlocBuilder (NHS-BB), was prepared according to a published method¹ from 2-(*tert*-butyl[1-(diethoxyphosphoryl)-2,2-dimethylpropyl]aminoxy)-2-methylpropionic acid, also known as MAMA-SG1 (BlocBuilder™, BB, 99%, purchased from Arkema and used without further purification), *N*-hydroxy-succinimide (NHS, 98%, purchased from Aldrich and used as received) and *N,N'*-dicyclohexylcarbodiimide (DCC, 99%, purchased from Aldrich and used as received). Styrene (S, 99%), methyl methacrylate (MMA, 99%), glycidyl methacrylate (GMA, 97%), *tert*-butyl acrylate (*t*BuA, 99%) and maleic anhydride (MA, 99%) were obtained from Fisher Scientific and were purified by passing through a column of basic alumina mixed with 5 weight % calcium hydride and then stored in a sealed flask under a head of nitrogen in a refrigerator until needed. The deuterated chloroform (CDCl_3 , 99.8%) was obtained from Cambridge Isotopes Laboratory. Diethyl phosphite (98%) was purchased from Sigma-Aldrich. The dialysis tube (cutoff 12 000-14 000 Dalton) was purchased from Medicell International Ltd.

■ ***My*/GMA copolymerization by NMP.** All copolymerizations were done in a 10-mL three-necked round-bottom glass flask equipped with a condenser, a thermal well and a magnetic Teflon stir bar. The flask was placed inside a heating mantle, and the whole setup mounted on top of a magnetic stirrer. All formulations for *My*/GMA copolymerizations are found in Table 2. For every reaction, the initial molar ratio of monomers and NHS-BB was calculated to give a *My*/GMA copolymer sample with target number-average molecular weight $M_{n,theo} = (M_{My}f_{My,0} + M_{GMA}f_{GMA,0})DP = 30 \text{ kg}\cdot\text{mol}^{-1}$ at complete overall conversion ($X = 1.0$) with $DP = ([My]_0 + [GMA]_0) / [NHS-BB]_0$, the average degree of polymerization. A specific formulation for an initial feed composition of GMA ($f_{GMA,0}$) equal to 0.50 is given as an example (experiment *My*/GMA-50, Table 2). NHS-BB (0.144 g, 0.301 mmol), *My* (4.407 g, 32,350 mmol) and previously purified GMA (4.571 g, 32,156 mmol) were added to the reactor and mixing commenced with the stir bar. A thermocouple was inserted through one of the reactor ports via a thermal well. A mixture of ethylene glycol/reverse osmosis water (30/70 vol%) was circulated via a chiller (Fisher Scientific Isotemp 3016D Digital Refrigerated Bath, 4 °C) through the condenser connected to the second neck of the reactor. The reactor was sealed and a purge of ultra-pure nitrogen was then introduced to the reactor for 30 min. The purge was vented through the reflux condenser. After purging, the reactor was heated via the heating mantle at a rate of about 10 °C.min⁻¹ to 120 °C with continuous nitrogen purge. $t = 0$ min was taken when the reactor temperature reached 100 °C. Samples were taken periodically until the end of the experiment or until the samples became too viscous to withdraw. For each

sample withdrawn, the crude polymer was precipitated with excess methanol and then dried first under intense air and at 50 °C under vacuum. Nuclear magnetic resonance (NMR) and gel permeation chromatography (GPC) were used to characterize the samples. For the specific example cited, the overall conversion was 89.4% (individual conversions: $X_{My} = 84.2\%$ and $X_{GMA} = 94.6\%$) at the end of the experiment ($t = 300$ min) and the molar composition of GMA in the final copolymer was $F_{GMA} = 0.58$ as determined by 1H NMR. The final product exhibited $M_n = 21.9$ kg.mol $^{-1}$ and $\bar{D} = 1.45$, as determined by GPC. All final *My*/GMA copolymer characteristics can be found in Table 3. The exact same procedure was followed for *My* homopolymerization (Supporting Information, Table S2b) and copolymerizations of *My* with MMA, *t*BuA and MA. The formulations used for these latter experiments are summarized in Table 1. Figure 1 sums up the various copolymerizations performed.

■ **Chain-extension of P(*My-stat-GMA*) macroinitiator with *My*, GMA and S.** All chain-extensions from P(*My-stat-GMA*) macroinitiators were performed in a very similar setup to that used for the *My*/GMA copolymerizations with the use of a 25-mL reactor. All formulations can be found in Table 4B. As a brief illustration, *My*/GMA-78-GMA/*My* was synthesized using a statistical P(*My-stat-GMA*) copolymer (*My*/GMA-78, $F_{My} = 0.78$, $M_n = 11.3$ kg.mol $^{-1}$, $\bar{D} = 1.27$, 1.011 g, 0.0895 mmol) that was added to the reactor along with toluene (7.615 g), *My* (0.603 g, 4.426 mmol) and previously purified GMA (5.967 g, 42.021 mmol). The contents were mixed and bubbled with nitrogen for 30 min, then heated to 110 °C and allowed to react for 60 min while maintaining a nitrogen purge. Samples were drawn periodically via syringe. The samples and the final block copolymer were precipitated in excess methanol and allowed to dry overnight in a vacuum oven at 50 °C. *My*/GMA-78-GMA/*My* exhibited $M_n = 29.1$ kg.mol $^{-1}$, $\bar{D} = 1.50$ (GPC) and $F_{GMA} = 0.65$ (1H NMR). The results of the chain-extensions from P(*My-stat-GMA*)s are given in Table 4C. The same procedure was applied for the synthesis of P(*My-b-GMA*) diblock copolymer from P(*My*) macroinitiator (Supporting Information, Table S2b).

■ **Synthesis of poly(β -myrcene-block-2-hydroxy-3-morpholinopropyl methacrylate) P(*My-b-HMPMA*).** A conventional reflux apparatus with a 10-mL three-necked round-bottom glass flask was used. P(*My-b-GMA*) diblock synthesized previously ($F_{My} = 0.58$, $M_n = 23.8$ kg.mol $^{-1}$, $\bar{D} = 1.89$, 0.210 g, 0.009 mmol, Table S2b in Supporting Information) was dissolved in Me-THF (~ 5.3 g) and then morpholine (0.330 g, 3.791 mmol, 6.4 eq. relative to GMA repeating units) was added. The reaction medium was vigorously mixed and deoxygenated via N $_2$ bubbling (explosive morpholine vapor/air may be formed above 35 °C) for 30 min before heating to 77 °C for three hours while maintaining a gentle nitrogen purge. The final product was precipitated in reverse osmosis water (formation of a dispersion which aggregated with time), decanted, filtered via a Büchner funnel and the resulting white polymer was dried at 50 °C under vacuum. A quantitative conversion of GMA units in HMPMA units was determined by 1H NMR (Figure 9). 91% of P(*My-b-HMPMA*) was produced, exhibiting $M_n = 26.5$ kg.mol $^{-1}$ and $\bar{D} = 1.91$ (Supporting Information, Figure S11b). The complete experimental conditions and results can be found in the Supporting Information, Table S2b. Dynamic Light Scattering (DLS) was eventually used to measure the hydrodynamic diameter of P(*My-b-HMPMA*) particles dispersed in water (in the range of 120-130 nm under optimized experimental conditions, Table 5).

■ **Characterization.** The (overall) monomer conversion X was determined by proton nuclear magnetic resonance (^1H NMR) and calculated from formula 1:

$$X = X_{My}f_{My,0} (+ X_{YY}f_{YY,0}) \quad YY = \text{MMA, GMA, } t\text{BuA or MA} \quad (1)$$

where $f_{My,0}$ and $f_{YY,0}$ are the initial molar fractions of My and YY , and X_{My} and X_{YY} are the individual conversions of My and YY , respectively. X_{My} and X_{YY} were determined with a Varian NMR Mercury spectrometer (^1H NMR, 300 MHz, 32 scans) using CDCl_3 . My conversion was calculated via the aliphatic protons of the monomer ($\delta = 2.15\text{-}2.30$ ppm, 4H), the aliphatic protons of the polymer ($\delta = 1.90\text{-}2.15$ ppm, 8H) and the protons of the two methyl groups of monomer and polymer ($\delta = 1.55\text{-}1.75$ ppm, 6H). MMA conversion was obtained via the vinyl protons of the monomer ($\delta = 6.10$ and 5.55 ppm, 2H) and the methoxy group of the polymer ($\delta = 3.63$ ppm, 3H). GMA conversion was determined using the peaks of the vinyl protons of the monomer ($\delta = 6.15$ and 5.60 ppm, 2H), the non-equivalent protons of the methylene bonded to the ester oxygen ($\delta = 4.20\text{-}4.50$ and $3.65\text{-}4.00$ ppm, 2H), the methine proton of the oxirane ring ($\delta = 3.05\text{-}3.30$ ppm, 1H) and the protons of the methylene of the ring ($\delta = 2.75\text{-}2.90$ and $2.55\text{-}2.70$ ppm, 2H) for both monomer and polymer. $t\text{BuA}$ conversion was calculated via the vinyl protons ($\delta = 5.70$ and 6.00 ppm, 2H) and the methyl protons ($\delta = 1.47$ ppm, 9H) of the monomer and the methyl protons of the polymer ($\delta = 1.42$ ppm, 9H). MA conversion was determined by comparing the peaks of the vinylic protons of the monomer ($\delta = 7.04$ ppm, 2H) and the methine protons of the polymer ($\delta = 2.90\text{-}3.55$ ppm, 2H). Styrene (S) conversion was determined using the vinyl protons of the monomer ($\delta = 6.70\text{-}6.80$, $5.70\text{-}5.80$ and $5.20\text{-}5.30$ ppm, 3H) and the aromatic protons of both monomer and polymer ($\delta = 6.90\text{-}7.50$ ppm, 5H). The NMR conversion from GMA to 2-hydroxy-3-morpholinopropyl methacrylate HMPMA repetitive units was calculated using the methine proton of the oxirane ring ($\delta = 3.05\text{-}3.30$ ppm, 1H) and the non-equivalent protons corresponding to the methylene of the ring ($\delta = 2.75\text{-}2.90$ and $2.55\text{-}2.70$ ppm, 2H) for P(GMA) and the methylene protons attached to the morpholine ring ($\delta = 3.55\text{-}3.80$ ppm, 4H and $2.55\text{-}2.70$ ppm, 4H) and the aliphatic protons neighbor of the tertiary amine ($\delta = 2.30\text{-}2.55$ ppm, 2H) for P(HMPMA).

The regioselectivity of the My repetitive units in the polymers was determined by comparing the three integrated peaks at $\delta = 4.70\text{-}4.80$ ppm (two vinyl protons of 3,4-addition and two vinyl protons of 1,2-addition), $\delta = 5.00\text{-}5.25$ ppm (two olefinic protons of 1,4-addition, one olefinic proton of 1,2-addition and one olefinic proton of 3,4-addition) and $\delta = 5.30\text{-}5.50$ ppm (one olefinic proton of 1,2-addition).^{2,3}

A 5 mm diameter Up NMR tube with 800 scans being processed in a 200 MHz Varian Gemini 2000 spectrometer operating at 81 MHz was used to perform ^{31}P NMR spectroscopy. Polymer (mass of polymer = 0.0528 g with $M_n = 11.3$ kg.mol $^{-1}$ for My /GMA-78 and 0.0405 g with $M_n = 8.6$ kg.mol $^{-1}$ for My /GMA-37), diethylphosphite as internal reference (0.0047 g and 0.0052 g respectively) and CDCl_3 were added to the NMR tube. My /GMA-37 was run under the exact same conditions with only one scan and no dummy scans ($ss = 0$). A negligible difference (< 2.6%) in integral values was measured between this spectrum and the standard one with multiple scans. It was thereby assumed that diethylphosphite and My -based polymers with moderate $M_n < 15$ kg.mol $^{-1}$ relax at the same rate.

The number-average molecular weights (M_n) and the dispersities ($D = M_w/M_n$) were measured using gel permeation chromatography (GPC, Water Breeze, differential refractive index RI 2414 detector, 40 °C) with HPLC

grade THF as the mobile phase (flow rate of 0.3 mL.min⁻¹). The GPC was equipped with 3 Waters Styragel® HR columns (HR1 with a molecular weight measurement range of 10² – 5 X 10³ g.mol⁻¹, HR2 with a molecular weight measurement range of 5 X 10² - 2 X 10⁴ g.mol⁻¹ and HR4 with a molecular weight measurement range of 5 X 10³ - 6 X 10⁵ g.mol⁻¹) and a guard column was used. M_n values were determined by calibration with linear narrow molecular weight distribution PS standards (PSS Polymer Standards Service GmbH, molecular weights ranging from 682 g.mol⁻¹ to 2,520,000 g.mol⁻¹).

Differential scanning calorimetry (DSC, Q2000TM from TA Instruments) was used under N₂ atmosphere. Indium was used as a standard to calibrate temperature while heat flow was calibrated via benzoic acid standard. A temperature range from - 90 °C to + 100 °C using three scans per cycle (heat/cool/heat) at a rate of 10 °C.min⁻¹ was typically set. For the T_g measurement, only the second heating run was taken into account to eliminate the thermal history. The reported T_{gs} were calculated using the inflection method from the change in slope observed in the DSC traces.

DLS measurements were performed with a Malvern Zetasizer Nano equipped with a 532 nm 50 mW green laser. The error is given as the standard deviation from three separate repeats. The samples were prepared by dissolving P(My-*b*-HMPMA) diblocks in THF and adding dropwise reverse osmosis water while stirring. The suspension was heated at 50 °C for 30 min and the THF was then eliminated by dialysis. To do this, the suspension was put in a dialysis tube which was placed in a beaker filled with reverse osmosis water under magnetic stirring for one or two days. The solution from the beaker was replaced by fresh reverse osmosis water a few times throughout the procedure. The sample in the dialysis bag was eventually isolated (removal of THF confirmed by ¹H NMR) and used for DLS measurements.

■ *References of the experimental section.*

- (1) J. Vinas, N. Chagneux, D. Gignes, T. Trimaille, A. Favier and D. Bertin, *Polymer* **2008**, *49* (17), 3639.
- (2) P. Sarkar and A. K. Bhowmick, *RSC Adv.* **2014**, *4*, 61343.
- (3) S. Georges, M. Bria, P. Zinck and M. Visseaux, *Polymer* **2014**, *55*, 3869.

b.2. Supporting information

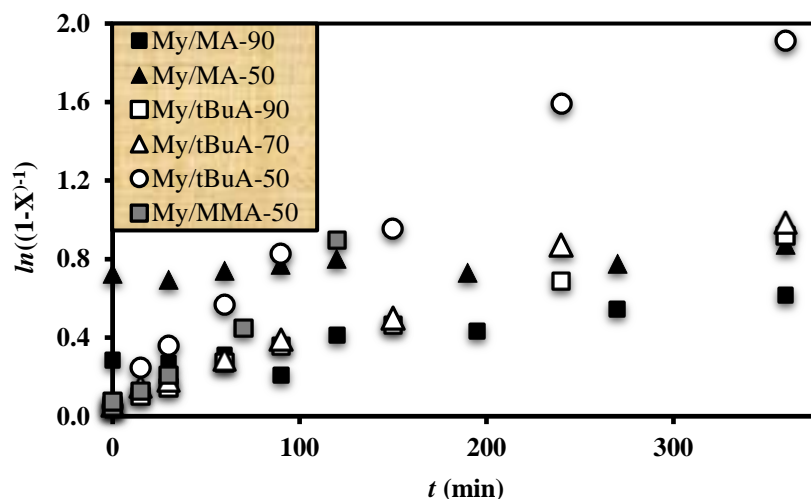


Figure S1b. Semi-logarithmic kinetic plots of $\ln((1-X)^{-1})$ ($X = X_{My}f_{My,0} + X_{YY}f_{YY,0}$) versus polymerization time t for the various My/YY copolymerizations initiated by NHS-BB ($YY = MA, tBuA$ or MMA).

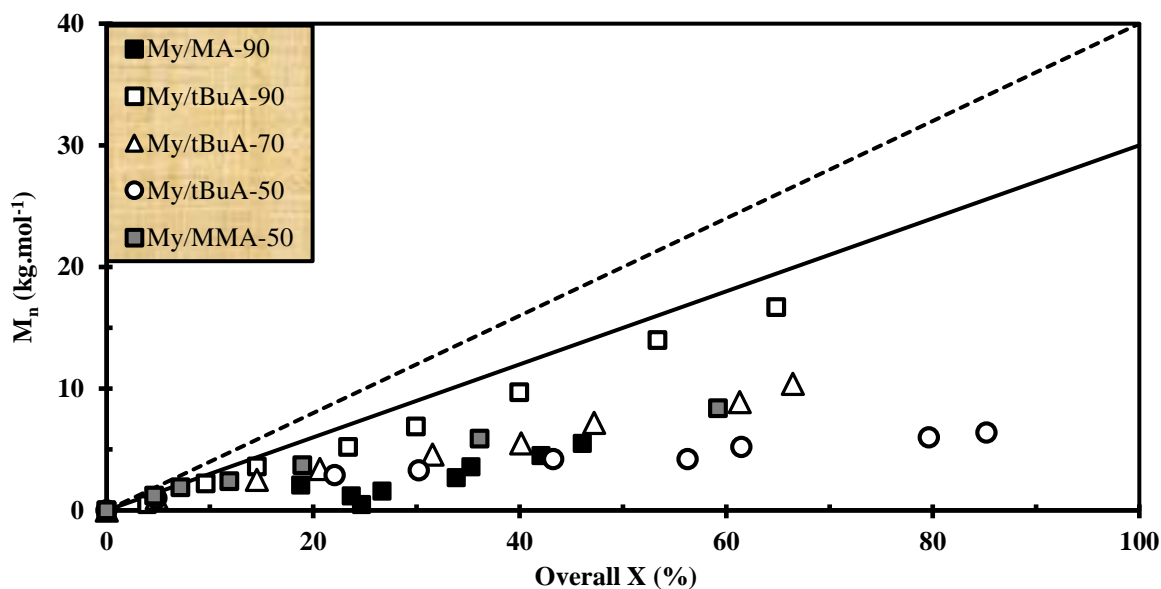


Figure S2b. M_n determined by GPC relative to PS standards in THF versus overall conversion X for the various My/YY copolymerizations initiated by NHS-BB ($YY = MA, tBuA$ or MMA). The dashed line indicates the theoretical M_n ($M_{n,theo}$) versus overall conversion based on the monomers to initiator ratio for $My/tBuA$ copolymerizations ($M_{n,theo} \sim 40 \text{ kg.mol}^{-1}$ at $X = 100\%$). The solid line refers to the predicted M_n for other polymerizations ($M_{n,theo} \sim 30 \text{ kg.mol}^{-1}$ at $X = 100\%$). No data were reported for experiment $My/MA-50$ since no polymer peak was detectable by GPC.

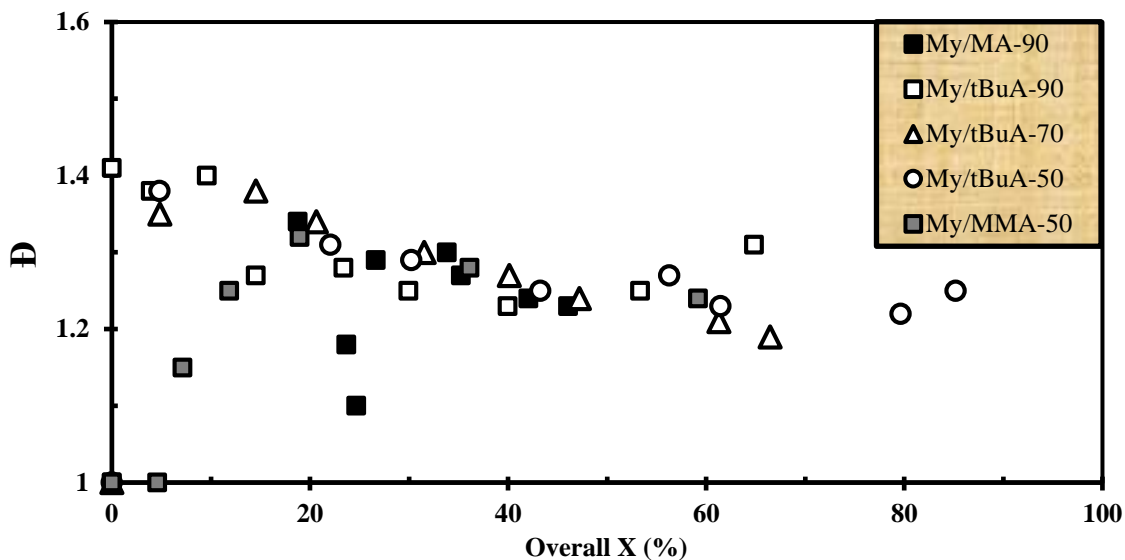
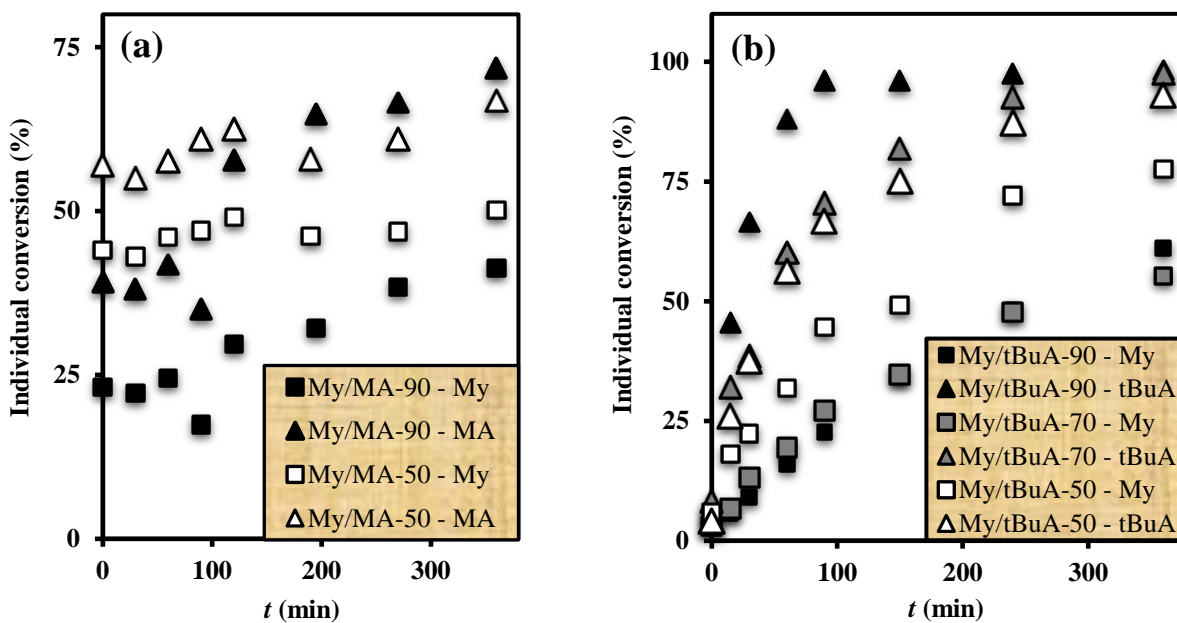


Figure S3b. \bar{D} versus overall conversion X for the various My/YY copolymerizations initiated by NHS-BB ($YY = MA, tBuA$ or MMA). No data were reported for experiment $My/MA-50$ since no polymer peak was detectable by GPC.



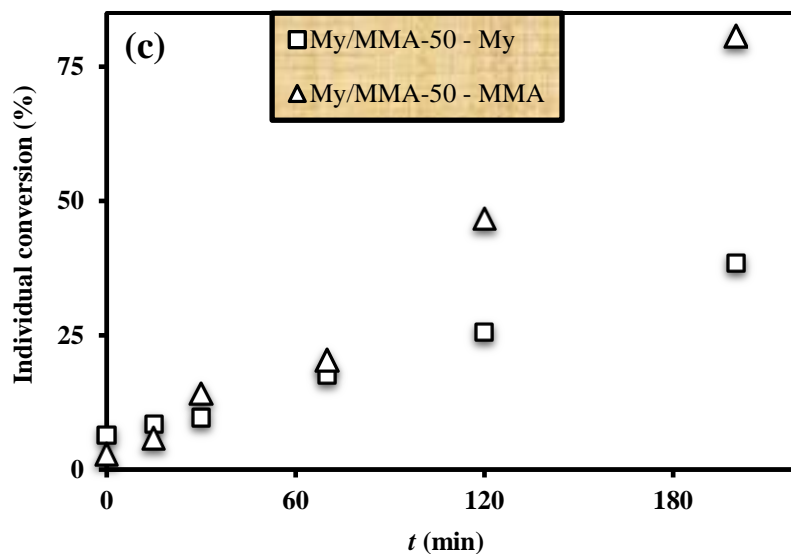


Figure S4b. ^1H NMR individual conversions X_{My} and X_{YY} ($YY = \text{MA}, t\text{BuA}$ or MMA) versus reaction time t for (a) My/MA , (b) $My/t\text{BuA}$ and (c) My/MMA copolymerizations.

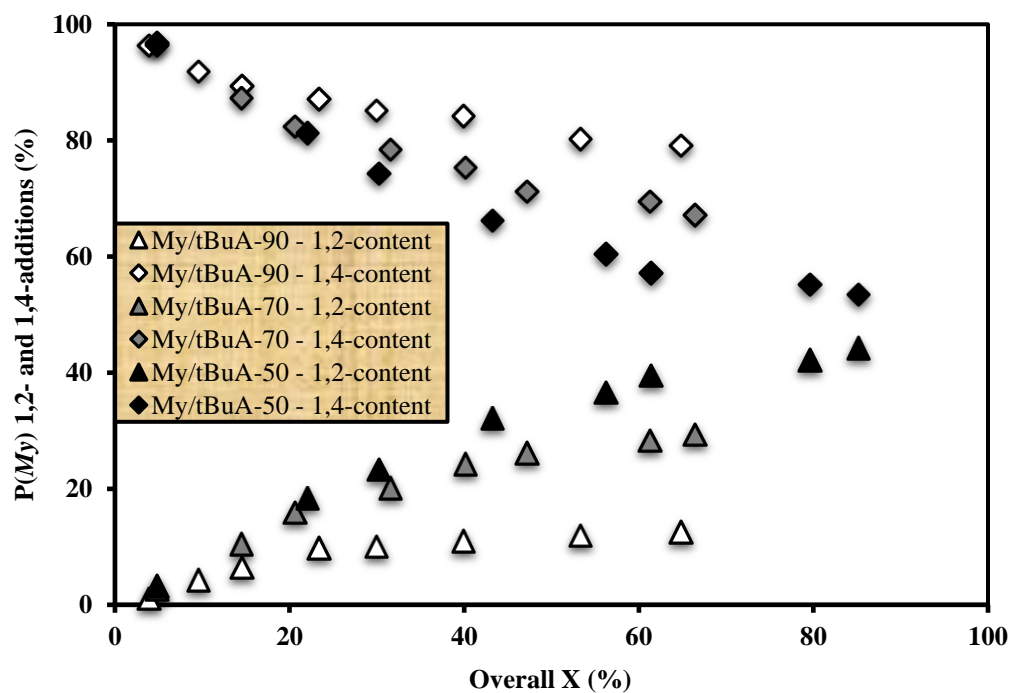


Figure S5b. Molar proportions of 1,2- and 1,4-additions of My repeat units in $P(My\text{-}co\text{-}t\text{BuA})$ copolymer versus overall conversion X for $My/t\text{BuA}$ copolymerizations.

■ **Use of terminal models:** Table S1b gives the experimental data used to determine the reactivity ratios r_{My} and r_{GMA} . It was assumed that the selected copolymers samples exhibited sufficiently low degree of conversion that the monomer composition was essentially unchanged. Calculation of r_{My} and r_{GMA} was first done by the Fineman-Ross (FR) approach¹ (rearrangement of the Mayo-Lewis copolymer equation into a linear form²) and by the Kelen-Tüdös (KT) approach³. The latter refines the linearization method by introducing an arbitrary positive constant α to spread the data more evenly so as to give equal weight to all data points. Accordingly, the KT approach minimizes the bias of the FR approach. The appropriate plot of the variables G and H, defined in Equation B1, will provide a linear relationship giving the reactivity ratios as the slope and intercept as shown in Equation B2.

$$G = (f_{GMA,0} / f_{My,0}) \times [(2F_{GMA} - 1) / F_{GMA}] ; H = (f_{GMA,0} / f_{My,0})^2 \times [(1 - F_{GMA}) / F_{GMA}] \quad (\text{B1})$$

$$G = r_{GMA} \times H - r_{My} \quad (\text{B2})$$

Equation B3 shows the additional variables used for the KT plot as illustrated in Equation B4.

$$\eta = G / (\alpha + H) ; \varepsilon = H / (\alpha + H) ; \alpha = \sqrt{H_{max}H_{min}} \quad (\text{B3})$$

$$\eta = (r_{GMA} + r_{My} / \alpha)\varepsilon - r_{My} / \alpha \quad (\text{B4})$$

In Equations B3 and B4, H_{max} and H_{min} stand for the highest and lowest values of the set of experimental points, respectively. $r_{My} = 0.80 \pm 0.31$ and $r_{GMA} = 0.71 \pm 0.15$ ($r_{My} \times r_{GMA} = 0.57 \pm 0.27$) were obtained via the FR method and $r_{My} = 0.48 \pm 0.12$ and $r_{GMA} = 0.53 \pm 0.18$ ($r_{My} \times r_{GMA} = 0.25 \pm 0.17$) were calculated via the KT method. The errors associated with the experimental data were derived from the standard errors of the slopes from FR and KT plots.

■ **Use of a NLLS model:** Still despite its improvements, the KT method does not overcome the shortcomings of the linear method: use of the differential form and errors that affect both variables. In order to handle rigorously the Mayo-Lewis equation, linearization has to be avoided. From a statistical point of view, a NLLS fit to the Mayo-Lewis equation is probably the soundest method to determine the desired parameters⁴. Therefore, the reactivity ratios were also determined using a non-linear least-squares fitting of the data. The commercial software package Matlab R2016a was used to solve the Mayo-Lewis equation¹ for My/GMA copolymerization (B5).

$$F_{GMA} = (r_{GMA} f_{GMA,0}^2 + f_{GMA,0} f_{My,0}) / (r_{GMA} f_{GMA,0}^2 + 2 f_{GMA,0} f_{My,0} + r_{My} f_{My,0}^2) \quad (\text{B5})$$

Using the reactivity ratios determined by the KT method as initial guesses, the statistical fit to the data yielded reactivity ratios $r_{My} = 0.49 \pm 0.13$ and $r_{GMA} = 0.50 \pm 0.13$ at 95 % confidence level and with a regression coefficient $R^2 = 0.99$ (SSE = 0.0042, RMSE = 0.0244).

Table S1b. Samples used for determination of reactivity ratios for *M_y*/GMA statistical copolymerization done at 120 °C in bulk with NHS-BB and targeting $M_{n,theo} = 30 \text{ kg.mol}^{-1}$ at $X = 100 \%$.

$f_{\text{GMA},0}^{(a)}$	$F_{\text{GMA}}^{(b)}$	$X^{(c)} (\%)$	t (min)	$M_n^{(d)}$ (kg.mol^{-1})	$\mathcal{D}^{(d)}$
0.10	0.19	17.4	30	4.8	1.33
0.20	0.26	16.6	30	3.7	1.34
0.29	0.37	14.9	15	3.2	1.38
0.40	0.44	16.1	15	4.0	1.44
0.51	0.48	13.8	15	3.8	1.52
0.60	0.56	23.2	15	6.1	1.43
0.71	0.63	21.0	10	5.9	1.48
0.80	0.73	19.8	5	7.0	1.49
0.90	0.88	16.9	3	6.2	1.79

a) $f_{\text{GMA},0}$ is the initial molar feed composition of glycidyl methacrylate.

b) F_{GMA} is the molar composition of glycidyl methacrylate in the $P(M_y\text{-stat-GMA})$ copolymer determined by ^1H NMR in CDCl_3 .

c) Overall monomer conversion $X = X_{M_y}f_{M_y,0} + X_{\text{GMA}}f_{\text{GMA},0}$ determined by ^1H NMR in CDCl_3 .

d) M_n and M_w determined by GPC calibrated with PS standards in THF at 40 °C.

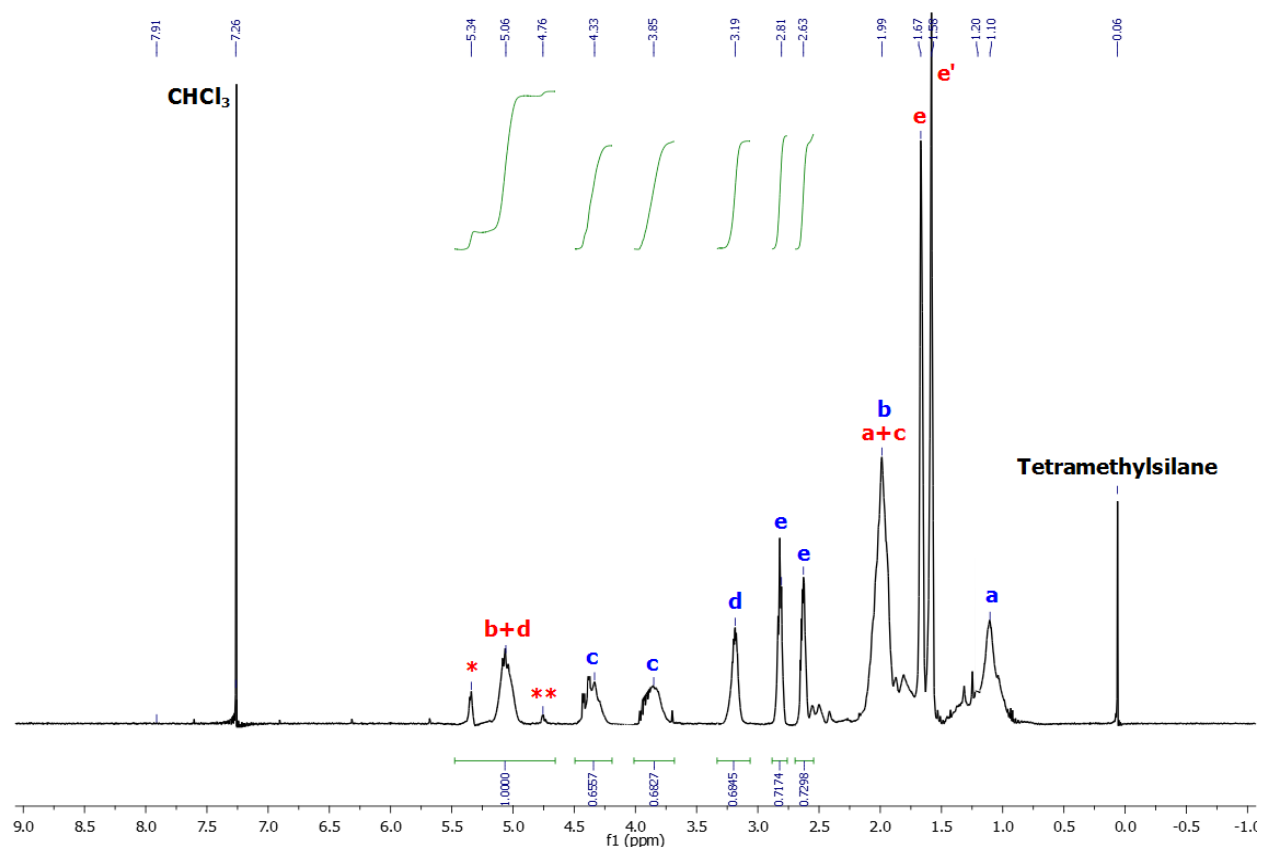
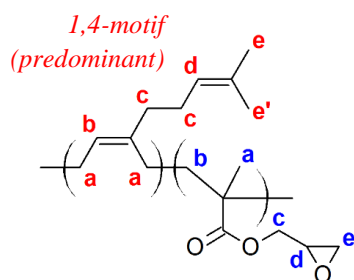


Figure S6b. ^1H NMR spectrum in CDCl_3 (300 MHz) at room temperature of dried $\text{P}(\text{My}\text{-stat}\text{-GMA})$ statistical copolymer $\text{My}/\text{GMA}\text{-50}$ after recovery, using methanol as the precipitant.



$\text{P}(\text{My}\text{-stat}\text{-GMA})$ $\text{My}/\text{GMA}\text{-50}$: ^1H NMR (CDCl_3 , 300 MHz, RT): $\delta = 5.20\text{-}5.00$ (s br, $2\text{H}^{\text{P}(\text{My})}$), $4.45\text{-}4.20$ (s br, $1\text{H}^{\text{P}(\text{GMA})}$), $3.90\text{-}3.65$ (s br, $1\text{H}^{\text{P}(\text{GMA})}$), $3.30\text{-}3.10$ (s, $1\text{H}^{\text{P}(\text{GMA})}$), $2.90\text{-}2.80$ (s, $1\text{H}^{\text{P}(\text{GMA})}$), $2.70\text{-}2.55$ (s, $1\text{H}^{\text{P}(\text{GMA})}$), $2.20\text{-}1.90$ (m br, $8\text{H}^{\text{P}(\text{My})}$), $2.00\text{-}1.80$ (m, $2\text{H}^{\text{P}(\text{GMA})}$), 1.67 (s, $3\text{H}^{\text{P}(\text{My})}$), 1.59 (s, $3\text{H}^{\text{P}(\text{My})}$), $1.30\text{-}0.70$ (m, $3\text{H}^{\text{P}(\text{GMA})}$).

*Signal at $\delta = 5.45\text{-}5.30$ ppm (t br, $1\text{H}^{1,2\text{-P}(\text{My})}$) corresponds to one olefinic proton of $1,2\text{-P}(\text{My})^5$.

**Signal at $\delta = 4.80\text{-}4.65$ ppm (d, $2\text{H}^{1,2\text{-P}(\text{My})}$) and s, $2\text{H}^{3,4\text{-P}(\text{My})}$) corresponds to two vinyl protons of $3,4\text{-addition}$ and two vinyl protons of $1,2\text{-addition}$ of My units⁵.

The molar composition of GMA in the final $\text{P}(\text{My}\text{-stat}\text{-GMA})$ copolymer (F_{GMA}) was calculated by comparing the two integrated areas corresponding to $\delta = 5.45\text{-}4.65$ ppm (two protons of $\text{P}(\text{My})$) and $\delta = 4.45\text{-}2.55$ ppm (five protons of $\text{P}(\text{GMA})$). $F_{\text{GMA}} = 0.58$ was calculated for final $\text{My}/\text{GMA}\text{-50}$ sample.

The three different types of configuration, 1,4-, 1,2- and 3,4-P(*My*), were quantified by comparing the three integrated areas at $\delta = 5.45\text{-}5.30$ ppm (one olefinic proton of 1,2-addition), $\delta = 5.20\text{-}5.00$ ppm (two olefinic protons of 1,4-addition, one olefinic proton of 1,2-addition and one olefinic proton of 3,4-addition) and $\delta = 4.80\text{-}4.65$ ppm (two vinyl protons of 3,4-addition and two vinyl protons of 1,2-addition)⁵. 1,4-content = 69.4 %, 1,2-content = 26.5 % and 3,4-content = 4.1 % were calculated for *My*/GMA-50 sample.

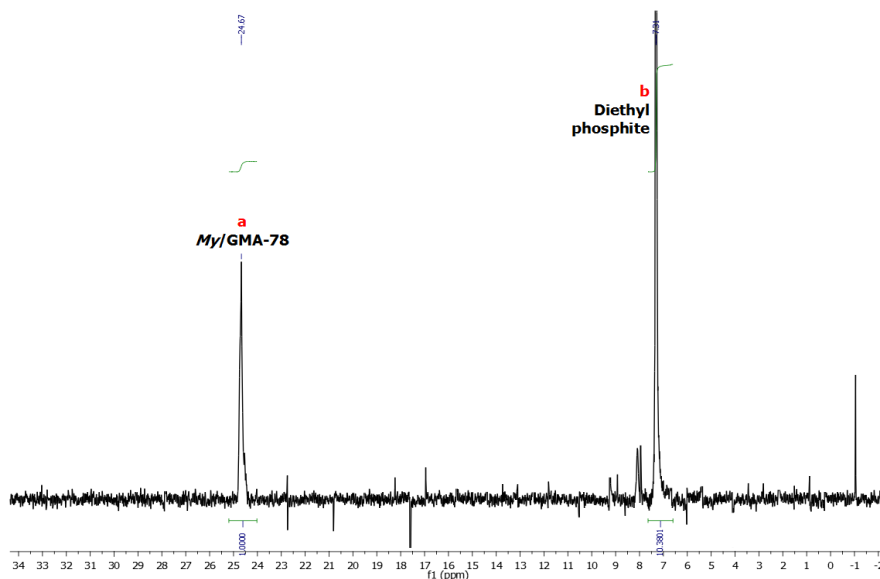


Figure S7b. 81 MHz ^{31}P NMR spectra of dried P(*My*-stat-GMA)-SG1 macroinitiator *My*/GMA-78 in CDCl_3 at room temperature.

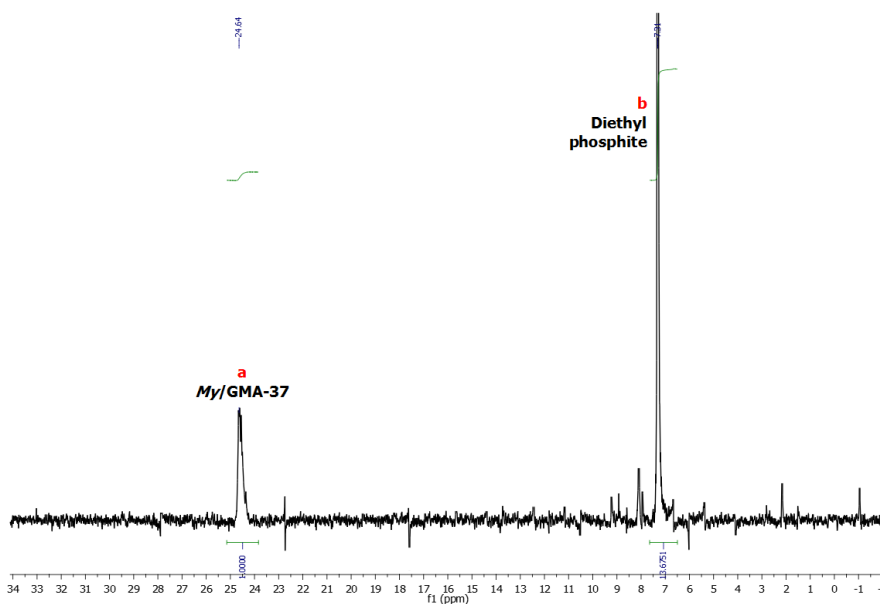
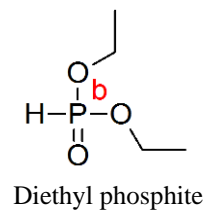
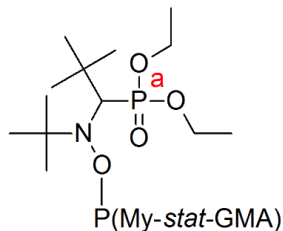


Figure S8b. 81 MHz ^{31}P NMR spectra of dried P(*My*-stat-GMA)-SG1 macroinitiator *My*/GMA-37 in CDCl_3 at room temperature.



SG1-terminated P(My-stat-GMA) statistical copolymer

The fraction of P(My-stat-GMA) chains terminated with SG1 was calculated by comparing the two integrated peaks corresponding to the phosphorus atom of the SG1 group ($\delta = 24.6$ ppm) and the phosphorus atom of diethyl phosphite ($\delta = 7.3$ ppm) used as an internal reference^{6,7}. Using the known amounts of diethyl phosphite (0.0055 g and 0.0063 g for *My*/GMA-78 and *My*/GMA-37 respectively) and P(My-stat-GMA) copolymer (0.0528 g with $M_n = 11.3$ kg.mol⁻¹ and 0.0405 g with $M_n = 8.6$ kg.mol⁻¹ respectively), the proportions of chains containing the SG1 moiety was estimated to 82 ± 5 mol% and 71 ± 7 mol% for *My*/GMA-78 and *My*/GMA-37 copolymers respectively (standard deviation derived from the difference in M_n value between the GPC result from PS calibration and from PMMA calibration). The calculation of the fraction of SG1 groups was done by considering similar relaxation times between diethyl phosphite and the polymer.

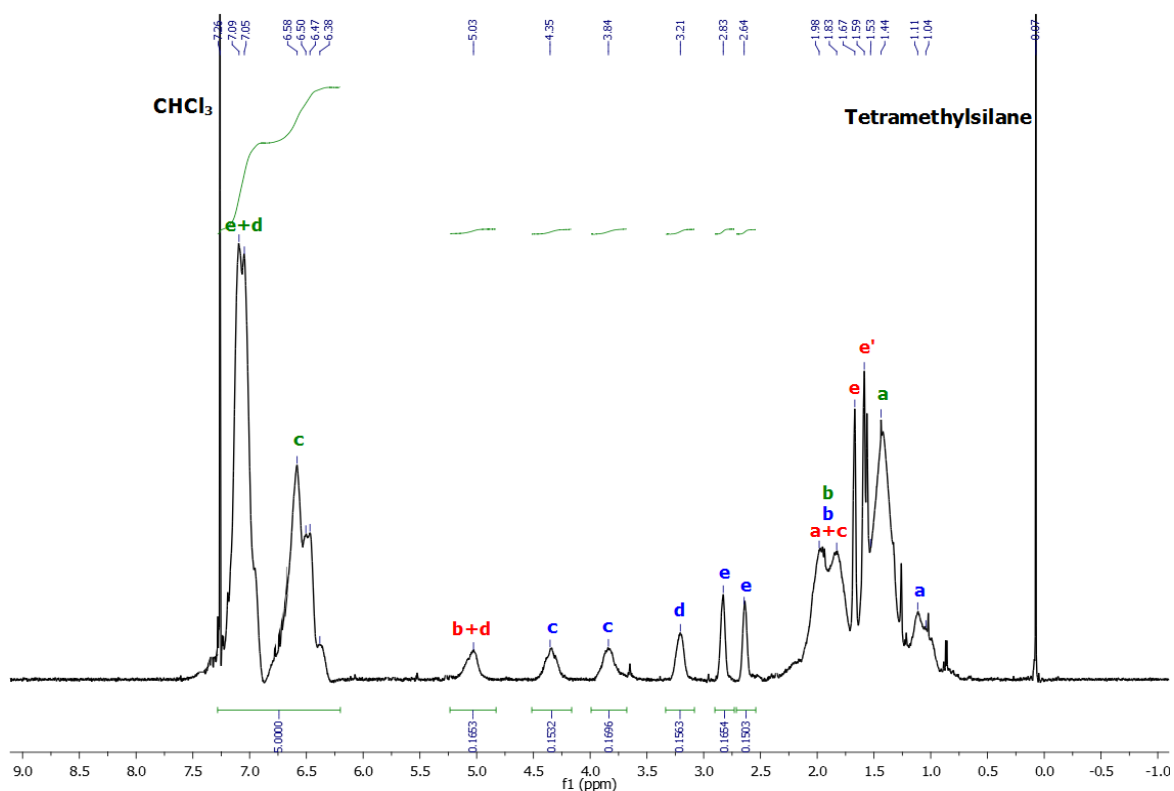
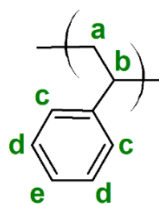


Figure S9b. ¹H NMR spectrum in CDCl₃ (300 MHz) at room temperature of dried P[(*My*-stat-GMA)-*b*-S] diblock copolymer *My*/GMA-37-S after recovery, using methanol as the precipitant.



Please see page 297 for NMR assignments corresponding to P(GMA) (blue indexes) and P(*My*) (red indexes).

PS: ^1H NMR (CDCl_3 , 300 MHz, RT): $\delta = 7.20\text{-}6.86$ (m br, 3H), $6.80\text{-}6.25$ (m br, 2H), $1.90\text{-}1.72$ (quint br, 1H), $1.54\text{-}1.20$ (t br, 2H).

The molar composition of *My*, GMA and S in the final P[(*My*-*stat*-GMA)-*b*-S] diblock copolymer was calculated by comparing three integrated areas:

- $\delta = 7.20\text{-}6.25$ ppm, five aromatic protons of PS.
- $\delta = 5.45\text{-}4.65$ ppm, two olefinic protons of P(*My*).
- $\delta = 4.45\text{-}2.55$ ppm, five protons of P(GMA).

$F_{My,2} = 0.06$ and $F_{S,2} = 0.81$ were calculated for *My*/GMA-37-S.

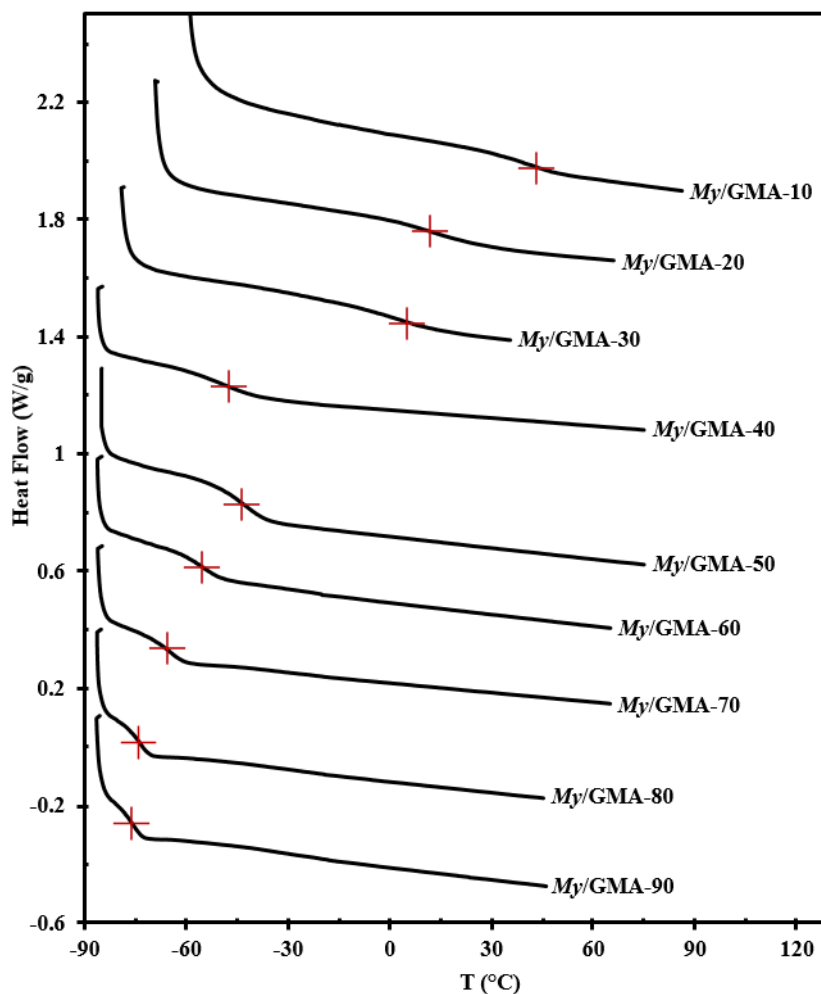


Figure S10b. DSC traces (second heating run) of P(*My*-*stat*-GMA) statistical copolymers. The red crosses indicate the changes in slope observed.

Theoretical estimation of ΔG_M for a mixture of P(My) and P(GMA):

■ **Introduction:** The Gibbs free energy (ΔG_M) describes the thermodynamics of the system and is a function of entropy (ΔS_M), enthalpy (ΔH_M) and temperature (T). ΔG_M is represented by the following Equation E1:

$$\Delta G_M = \Delta H_M - T\Delta S_M \quad (\text{E1})$$

When mixing two different polymers, the change in free energy will indicate whether the polymers are miscible ($\Delta G_M < 0$) or a phase separation occurs ($\Delta G_M > 0$). A statistical thermodynamic model was developed for the mixture of polymers and the free energy of mixing was given by Equation E2:

$$\Delta G_M = kT [(V/V_r)v_1v_2\chi(1 - 2/z) + N_c(v_1 \ln(v_1) + v_2 \ln(v_2))] \quad (\text{E2})$$

where $k = 1.38 \cdot 10^{-23} \text{ J.K}^{-1}$ is the Boltzmann's constant, V is the total volume of the mixture, V_r is the molar of a specific segment, v_i is the volume fraction of polymer i , z is the lattice coordination number (usually between 6 and 12), N_c is the number of chains per volume unit and χ is the Flory-Huggins parameter, which can be calculated from Equation E3:

$$\chi = V_{m,1} (\delta_1 - \delta_2)^2 / RT \quad (\text{E3})$$

where $V_{m,1}$ is the molar volume of the polymer with higher molar amount or, if equal composition, the one with smaller molecular weight monomer (for My/GMA system, $V_{m,1} = V_{m,GMA} = 136.4 \text{ cm}^3 \cdot \text{mol}^{-1}$), $R = 8.31 \text{ J} \cdot \text{mol}^{-1} \cdot \text{K}^{-1}$ is the ideal gas constant, δ_i is the solubility parameter of the polymer i ^{8,9}.

■ **Estimation of δ_{My} , δ_{GMA} and χ_{My-GMA} :** δ_{My} and δ_{GMA} were calculated using the Hansen solubility parameters (HSPs) δ_D (atomic dispersion forces), δ_P (molecular polar forces arising from dipole moments) and δ_H (hydrogen-bonds between molecules)¹⁰. HSPs are based on the concept that the total cohesive energy density is approximated by the sum of the energy densities required to overcome δ_D , δ_P and δ_H . The solubility parameters δ_{My} and δ_{GMA} can thus be determined as described in Equation E4:

$$\delta = (\delta_D^2 + \delta_P^2 + \delta_H^2)^{0.5} \quad (\text{E4})$$

$\delta_{My} = (16.0^2 + 1.6^2 + 2.2^2)^{0.5} = 16.23 \text{ MPa}^{1/2}$ was calculated, using HSPs reported by Chemat and coworkers¹¹.

$\delta_{GMA} = (16.3^2 + 8.5^2 + 5.7^2)^{0.5} = 19.25 \text{ MPa}^{1/2}$ was calculated using tabulated HSPs¹⁰.

Thus, $\chi_{My-GMA} = [136.4 (19.25 - 16.23)^2] / (8.31 \times 298.15) = 0.50$ was estimated at $T = 25 \text{ }^\circ\text{C}$.

■ **Estimation of ΔG_M :** Let us take a mixture of 1 g of P(My) and 1 g of P(GMA) with $M_{n,P(My)} = M_{n,P(GMA)} = 15 \text{ kg.mol}^{-1}$. The total volume of the mixture V can be calculated as follows:

$$V = V_{P(GMA)} + V_{P(My)} = m_{P(GMA)} / \rho_{P(GMA)} + m_{P(My)} / \rho_{P(My)} = 1 / 0.805 + 1 / 0.895 = 2.36 \text{ cm}^{-3}$$

(m = mass, ρ = density, $\rho_{P(My)} = 0.895 \text{ g.cm}^{-3}$)

The volume fractions of P(GMA) and P(My) are then determined: $v_{P(GMA)} = V_{P(GMA)} / V = 0.526$ and thus $v_{P(My)} = 0.474$. The ratio V/V_r corresponds to the number of molecules (N) in the mixture:

$$\begin{aligned} V/V_r &= V / (V_{P(GMA)} / N_{0,P(GMA)}) = V / (V_{P(GMA)} / (n_{0,P(GMA)} \times N_a)) = (V \times \rho_{P(GMA)} \times N_a) / M_{GMA} \\ &= (2.36 \times 0.805 \times 6.025 \cdot 10^{23}) / 142.15 \\ &= 8.052 \cdot 10^{21} \end{aligned}$$

Where N_a is the Avogadro constant and M_{GMA} , the molecular weight of GMA monomer.

$$\begin{aligned} \text{Moreover: } N_c &= N_{P(GMA)} + N_{P(My)} = N_a (m_{P(GMA)} / M_{n,P(GMA)} + m_{P(My)} / M_{n,P(My)}) \\ &= 6.025 \cdot 10^{23} (1/15000 + 1/15000) \\ &= 8.033 \cdot 10^{19} \end{aligned}$$

ΔG_M at $T = 25 \text{ }^\circ\text{C}$ can then be estimated using Equation E2 and assuming $z = 6$:

$$\begin{aligned} \Delta G_M (25 \text{ }^\circ\text{C}, z = 6) &= 1.38 \cdot 10^{-23} \times 298.15 (8.052 \cdot 10^{21} \times 0.526 \times 0.474 \times 0.50 (1 - 2/6) + \\ &\quad 8.033 \cdot 10^{19} (0.526 \ln(0.526) + 0.474 \ln(0.474))) \\ &= 2.52 \text{ J} \end{aligned}$$

$\Delta G_M (25 \text{ }^\circ\text{C}, z = 6) > 0$ indicates that this specific mixture of polymers is not miscible at $T = 25 \text{ }^\circ\text{C}$. The upper limiting M_n for the P(My)/P(GMA) miscible system at $T = 25 \text{ }^\circ\text{C}$ can be eventually calculated for $\Delta G_M (25 \text{ }^\circ\text{C}, z = 6) = 0$:

$$\begin{aligned} M_{n,\text{lim}} &= - (N_a \times m_{P(GMA)} (v_{P(GMA)} \ln(v_{P(GMA)}) + v_{P(My)} \ln(v_{P(My)}))) / ((1/3) \times (V/V_r) \times v_{P(GMA)} v_{P(My)} \chi_{My-GMA}) \\ &= - (6.025 \cdot 10^{23} \times 1.0 (0.526 \ln(0.526) + 0.474 \ln(0.474))) / ((1/3) \times 8.052 \cdot 10^{21} \times 0.526 \times 0.474 \times 0.50) \\ &= 1246 \text{ g.mol}^{-1} \sim 1.2 \text{ kg.mol}^{-1} \end{aligned}$$

Consequently, a mixture of 1 g of P(My) and 1 g of P(GMA) would be miscible at $T = 25 \text{ }^\circ\text{C}$ if $M_{n,P(My)} = M_{n,P(GMA)} < 1.2 \text{ kg.mol}^{-1}$, according to this thermodynamic model.

Table S2b. Experimental conditions and results for (1) the NMP of M_y , (2) the GMA chain-extension from $P(M_y)$ macroinitiator and (3) the post-polymerization treatment with morpholine.

(1) NMP of M_y								
$[NHS-BB]_0$	$[M_y]_0$	$M_{n,theo}$	T (°C)	t (min)	X_{M_y} (%)	$M_n^{(a)}$	$\mathcal{D}^{(a)}$	
(M)	(M)	($kg \cdot mol^{-1}$)				($kg \cdot mol^{-1}$)		
0.016	5.928	50.5	120	360	35.2	14.4	1.51	

(2) GMA extension from $P(M_y)$ macroinitiator										
$[P(M_y)]_0$	$[GMA]_0$	$[M_y]_0$	$[Toluene]_0$	$M_{n,theo}^{(b)}$	T (°C)	t (min)	$X_{ove}^{(c)}$	$M_n^{(a)}$	$\mathcal{D}^{(a)}$	$F_{M_y}^{(d)}$
(M)	(M)	(M)	(M)	($kg \cdot mol^{-1}$)	(°C)	(min)	(%)	($kg \cdot mol^{-1}$)		
0.007	2.310	0.257	5.042	69.8	110	50	41.2	23.8	1.89	0.58

(3) Post-polymerization treatment with morpholine								
$[P(M_y-b-GMA)]_0$	$[Morpholine]_0$	$[Me-THF]_0$	T (°C)	t (min)	$X_{epoxy}^{(e)}$	$M_n^{(a)}$	$\mathcal{D}^{(a)}$	
(M)	(M)	(M)			(%)	($kg \cdot mol^{-1}$)		
0.0014	0.5641	9.1518	77	180	~ 100	26.5	1.91	

- a) M_n and M_w determined by GPC calibrated with PS standards in tetrahydrofuran (THF) at 40 °C.
b) $M_{n,theo}$ corresponds to the targeted number-average molecular weight of the whole chain-extended diblock copolymer (macroinitiator block + extended block) at $X = 100\%$.
c) X_{ove} refers to the overall conversion $X = X_{M_y} f_{M_y,0} + X_{GMA} f_{GMA,0}$ determined by 1H NMR in $CDCl_3$.
d) Molar fraction of M_y in the copolymer (F_{M_y}) as determined by 1H NMR in $CDCl_3$.
e) X_{epoxy} corresponds to the conversion of GMA to HMPMA units, as determined by 1H NMR in $CDCl_3$.

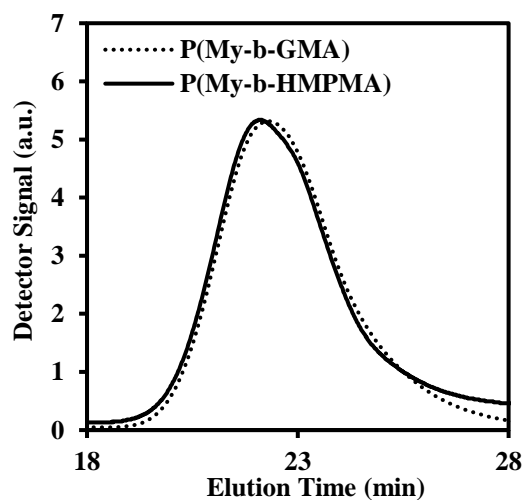


Figure S11b. Normalized GPC traces of dry $P(M_y-b-GMA)$ diblock copolymer (dotted curve, $M_n = 23.8 \text{ kg} \cdot \text{mol}^{-1}$, $\mathcal{D} = 1.89$) and dry $P(M_y-b-HMPMA)$ diblock copolymer after treatment with morpholine (solid curve, $M_n = 26.5 \text{ kg} \cdot \text{mol}^{-1}$, $\mathcal{D} = 1.91$). The GPC values were determined using PS standards in THF at 40 °C.

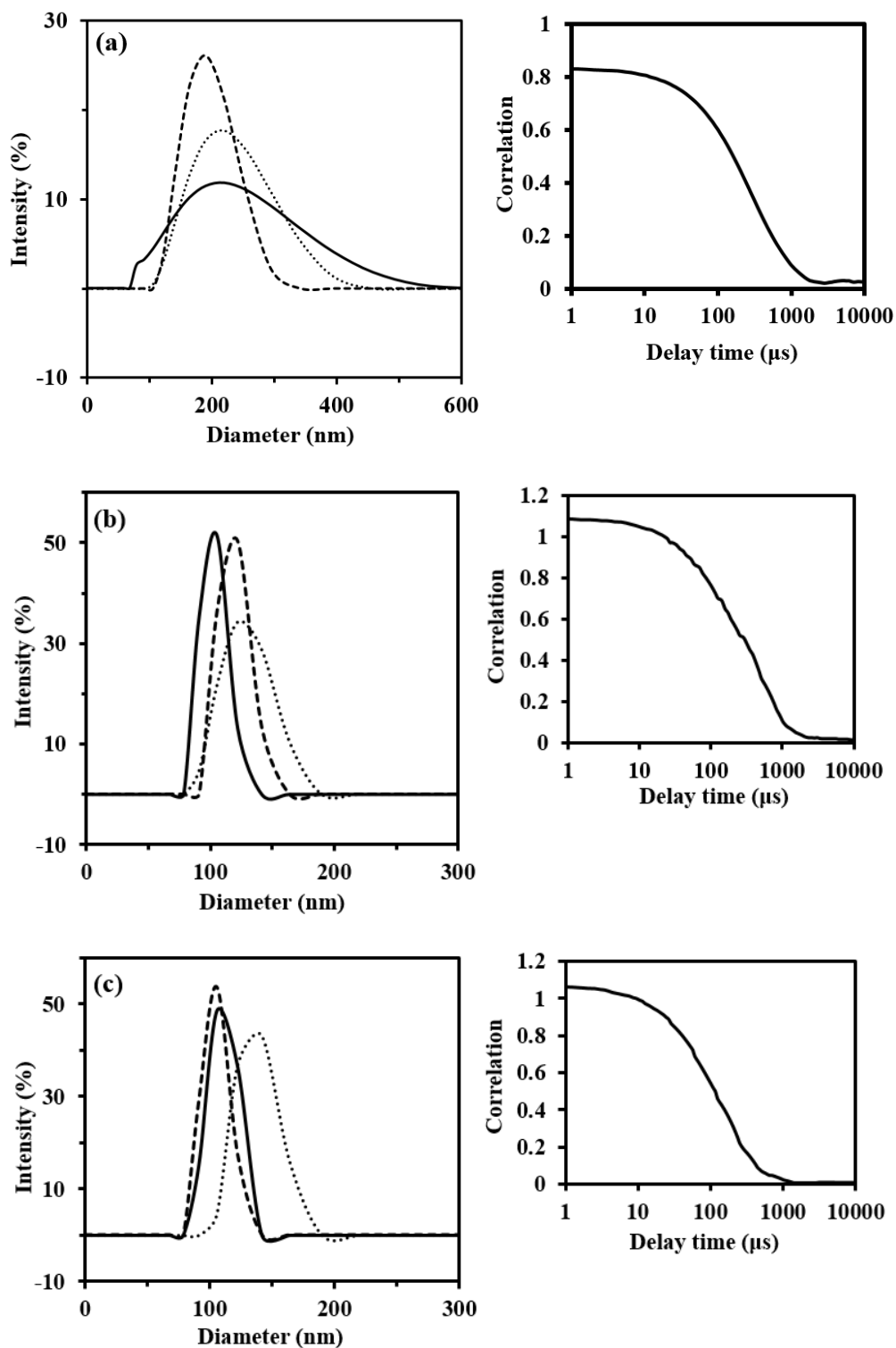


Figure S12b. DLS measurements at (a) 25 °C, (b) 45 °C and (c) 65 °C of 0.4 mg.ml⁻¹ of P(My-b-HMPMA) diblock copolymer in reversed osmosis water, stirred for 10 days before analysis. The correlation functions are also given to the right of the particle size distribution plots.

References of the supporting information:

- (1) M. Fineman and S. D. Ross, *J. Polym. Sci.* **1950**, 5 (2), 259.
- (2) F. R. Mayo and F. M. Lewis, *J. Am. Chem. Soc.* **1944**, 66 (9), 1594.
- (3) T. Kelen and F. Tüdös, *J. Macromol. Sci., Chem.* **1975**, 9 (1), 1.
- (4) P. W. Tidwell and G. A. Mortimer, *J. Polym. Sci., Part A: Gen. Pap.* **1965**, 3, 369.
- (5) P. Sarkar and A. K. Bhowmick, *RSC Adv.* **2014**, 4, 61343.
- (6) C. Lefay, J. Belleney, B. Charleux, O. Guerret and S. Magnet, *Macromol. Rapid Commun.* **2004**, 25 (13), 1215.
- (7) J. Nicolas, C. Dire, L. Mueller, J. Belleney, B. Charleux, S. R. A. Marque, D. Bertin, S. Magnet and L. Couvreur, *Macromolecules* **2006**, 39 (24), 8274.
- (8) P. J. Flory In *Principles of Polymer Chemistry*; P. J. Flory, Ed.; Cornell University Press; New York, **1975**; Chapter 13, pp 541-594.
- (9) G. Odian In *Principles of Polymerization*, 4th ed.; G. Odian, Ed.; John Wiley & Sons: Hoboken, NJ, **2004**; Chapter 6, pp 466–505.
- (10) C. M. Hansen In *Hansen Solubility Parameters, A User's Handbook*, 2nd ed.; C. M. Hansen, Ed.; CRC Press: New York, **2007**; Chapter 1, 1-26.
- (11) E. Yara-Varon, A. S. Fabiano-Tixier, M. Balcells, R. Canela-Garayoa, A. Bily and F. Chemat, *RSC Adv.* **2016**, 6, 27750.
- (12) V. Kholodovych; W. J. Welsh In *Physical Properties of Polymers Handbook*; J. E. Mark, Ed.; Springer: New York, **2007**; 611-618.

c. Appendix for Chapter 3

c.1. Experimental section

■ **Materials.** β -Myrcene (M_y , $\geq 90\%$), basic alumina (Al_2O_3 , Brockmann, Type I, 150 mesh), calcium hydride (CaH_2 , 90–95% reagent grade), thiophenol (97%) and benzene ($\geq 99\%$, ACS reagent) were purchased from Sigma-Aldrich and used as received. Toluene ($\geq 99\%$), methanol (MeOH , $\geq 99\%$), methylene chloride (CH_2Cl_2 , 99.9% certified ACS), chloroform (CHCl_3 , 99.8%) and tetrahydrofuran (THF, 99.9% HPLC grade) were obtained from Fisher Scientific and used as received. 2-Methyl-2-[*N*-*tert*-butyl-*N*-(1-diethoxyphosphoryl)-2,2-dimethylpropyl]-aminoxy]-*N*-propionyloxysuccinimide, also known as NHS-BlocBuilder (NHS-BB), was prepared according to a published method¹ from 2-(*tert*-butyl[1-(diethoxyphosphoryl)-2,2-dimethylpropyl]aminoxy)-2-methylpropionic acid, also known as MAMA SG1 (BlocBuilder-MATM, (BB), 99%, provided by Arkema and used without further purification), *N*-hydroxysuccinimide (NHS, 98%, purchased from Aldrich and used as received), and *N,N'*-dicyclohexylcarbodiimide (DCC, 99%, purchased from Aldrich and used as received). Telechelic poly(ethylene-*stat*-butylene) difunctional initiator PEB-(SG1)₂ terminated with *N*-*tert*-Butyl-*N*-[1-diethylphosphono-(2,2-dimethylpropyl)] nitroxide (SG1) was produced relying on a published synthesis route², from hydroxyl terminated poly(ethylene-*stat*-butylene) (PEB-(OH)₂, KratonTM D2205) obtained from Kraton, acryloyl chloride (98%) acquired from Sigma-Aldrich and BlocBuilderTM. Styrene (S, 99%) was obtained from Fisher Scientific and isobornyl methacrylate (IBOMA, Visiomer® Terra) was obtained from Evonik, and both S and IBOMA were purified by passing through a column of basic alumina mixed with 5 wt% calcium hydride and then stored in a sealed flask under a head of nitrogen in a refrigerator until needed. The deuterated chloroform (CDCl_3 , 99.8%) used as a solvent for nuclear magnetic resonance (NMR) was obtained from Cambridge Isotopes Laboratory. Diethyl phosphite (98%) was purchased from Sigma-Aldrich.

■ **My/IBOMA Copolymerization by NMP.** The copolymerizations, depicted in Figure 1a, were done in a 10 mL three-necked round-bottom glass flask equipped with a vertical reflux condenser (inserted in the middle neck), a thermal well, and a magnetic stir bar. The reactor was placed inside a heating mantle, and the whole setup mounted on top of a magnetic stirrer. Table 1 gives the formulations for the various *My*/IBOMA copolymerizations studied. For example, for the experiment *My*/IBOMA-50 (molar fraction of IBOMA in the initial feed $f_{\text{IBOMA},0} = 0.50$), the reactor was sealed with rubber septa after the addition of NHS-BB (0.102 g, 0.213 mmol) and the magnetic stir bar. *My* (2.381 g, 17.478 mmol) and previously purified IBOMA (3.897 g, 17.529 mmol) were then injected with a disposable needle into the reactor. The initial molar ratio of monomers and NHS-BB was calculated to give theoretically a copolymer sample with target number-average molecular weight $M_{n,\text{theo}} = (M_{My}f_{My,0} + M_{\text{IBOMA}}f_{\text{IBOMA},0})\text{DP} \sim 30 \text{ kg}\cdot\text{mol}^{-1}$ at complete overall conversion with $\text{DP} = ([My]_0 + [\text{IBOMA}]_0)/[\text{NHS-BB}]_0 = 164$, the average degree of polymerization. A thermocouple connected to the temperature controller was placed inside the thermal well and connected through one of the necks. A mixture of ethylene glycol/distilled water (20/80 vol%) at a temperature of 3 °C was circulated (Fisher Scientific Isotemp 3016D digital refrigerated bath) through the condenser

connected to one of the necks of the reactor to prevent any evaporative loss of the monomers. A purge of ultrapure nitrogen was then introduced to the reactor for 30 min to deoxygenate at room temperature the reactants prior to polymerization. The purge was vented through the reflux condenser. After purging, the reactor was heated at a rate of about $10\text{ }^{\circ}\text{C}\cdot\text{min}^{-1}$ to $100\text{ }^{\circ}\text{C}$ with continuous nitrogen purge. The time at which the reactor temperature reached $90\text{ }^{\circ}\text{C}$ was taken arbitrarily as the commencement of the reaction ($t = 0\text{ min}$). Samples were then taken from the reactor periodically by a syringe until the end of the experiments or until the samples became too viscous to withdraw. Reactions were then stopped by removing the reactor from the heating mantle and letting the contents cool down to room temperature, while under continuous nitrogen purge. For each sample withdrawn during the polymerization, the crude polymer was precipitated with excess methanol. After filtration and recovery, the precipitated polymer was dried at $50\text{ }^{\circ}\text{C}$ under vacuum in the oven overnight to remove unreacted monomers. Samples were analyzed by nuclear magnetic resonance (NMR) and gel permeation chromatography (GPC). At the end of the experiment ($t = 340\text{ min}$), the overall conversion for *My*/IBOMA-50 was 52.7% (individual conversions: $X_{My} = 75.2\%$ and $X_{IBOMA} = 30.2\%$) as determined by ^1H NMR, with a number-average molecular-weight $M_{n,MHS} = 9.4\text{ kg mol}^{-1}$ and a dispersity $\bar{D} = 1.28$, as determined by GPC. The molar composition of IBOMA in the final copolymer was $F_{IBOMA} = 0.43$ according to ^1H NMR spectroscopy. The exact same procedure was followed for all *My*/IBOMA copolymerizations. *My*/IBOMA copolymer characteristics can be found in Table 2.

■ **Chain-extension of *My*/IBOMA copolymers with *My*, IBOMA and *S*.** All chain-extensions from P(*My*-*grad*-IBOMA) macroinitiators were performed in a very similar setup to that used for the *My*/IBOMA copolymerizations with the use of a 10-mL reactor. The formulations can be found in Table 3B. As a brief illustration, *My*/IBOMA-82-IBOMA/*My* was synthesized using a gradient P(*My*-*grad*-IBOMA) copolymer (*My*/IBOMA-82, $F_{My} = 0.82$, $M_{n,MHS} = 13.6\text{ kg}\cdot\text{mol}^{-1}$, $\bar{D} = 1.51$, 0.367 g, 0.027 mmol) that was added to the reactor along with toluene (3.24 g), *My* (0.135 g, 0.991 mmol) and previously purified IBOMA (2.787 g, 12.530 mmol). The reaction medium was mixed and bubbled with ultrapure nitrogen for at least 30 min, then heated to $105\text{ }^{\circ}\text{C}$ and allowed to react for 210 min while maintaining a N_2 purge. $t = 0\text{ min}$ was selected once the reaction medium reached $90\text{ }^{\circ}\text{C}$. Samples were drawn periodically via syringe at 0, 60, 120 and 210 min. The samples and the final diblock copolymer were precipitated in excess methanol and allowed to dry overnight in a vacuum oven at $50\text{ }^{\circ}\text{C}$. *My*/IBOMA-82-IBOMA/*My* exhibited $M_{n,MHS} = 23.2\text{ kg}\cdot\text{mol}^{-1}$, $\bar{D} = 1.61$ (GPC) and $F_{My} = 0.49$ (^1H NMR). The results of the chain-extensions from P(*My*-*grad*-IBOMA)s are given in Table 3C.

■ **Synthesis of Co/IBOMA-*My*-IBOMA/Co (Co = *My* or *S* co-monomer) triblock copolymers by NMP.** A two-step process was implemented in a similar reactor apparatus used for the above-mentioned copolymerizations and chain-extensions: 1) *My* homopolymerization initiated by PEB-(SG1)₂ dialkoxyamine; 2) IBOMA/Co chain-extension from P(*My*)-(SG1)₂ macroinitiator. The entire set of formulations is given in Table 4. For example, the synthesis of S/IBOMA-*My*-IBOMA/S triblock polymer (Co = S), characterized then mechanically and rheologically, can be detailed. To the 50-mL reactor was added PEB-(SG1)₂ difunctional initiator ($M_{n,GPC} = 5.7\text{ kg}\cdot\text{mol}^{-1}$, $\bar{D} = 1.17$, 0.912 g, 0.140 mmol) and *My* (21.005 g, 143.671 mmol) with magnetic stirring (experiment *My*-52, Table 4A). After sealing

the reactor, a purge of nitrogen was applied for 30 min. The reactor was then heated to 120 °C to commence polymerization while continuing the nitrogen flow. $t = 0$ min was selected once the reaction medium reached 100 °C. At $t = 360$ min, the polymerization was stopped, the polymer was precipitated in excess methanol and dried overnight in a vacuum oven at 50 °C. ^1H NMR was performed to ensure the complete elimination of methanol and unreacted My in the dry polymer, and to determine the conversion (49.1%). $P(My)$ synthesized exhibited $M_{n,MHS} = 51.7 \text{ kg}\cdot\text{mol}^{-1}$ and $\bar{D} = 1.53$ as determined by GPC. The chain-extension of $P(My)$ -(SG1)₂ macroinitiator with a IBOMA/S mixture was then done by reacting $P(My)$ -(SG1)₂ (1.50 g, 0.029 mmol), purified IBOMA (3.32 g, 14.94 mmol) and purified S (0.15 g, 1.42 mmol) in toluene (~ 4.3 g) under continuous nitrogen flow and magnetic stirring for 3 h at 115 °C (experiment My -52-IBOMA/S, Table 4B). The resulting polymer sample ($M_{n,MHS} = 78.1 \text{ kg}\cdot\text{mol}^{-1}$, $\bar{D} = 2.41$) was precipitated in excess methanol and dried under vacuum at 50 °C overnight. Lastly, fractionation was performed using a methanol (non-solvent) / benzene (solvent) pair (2 cycles) to remove the low molecular weight species. The final fractionated triblock polymer exhibited $M_{n,MHS} = 94.7 \text{ kg}\cdot\text{mol}^{-1}$, $\bar{D} = 2.23$, $F_{IBOMA} = 0.34$ and $F_S = 0.07$. Final Co/IBOMA- My -IBOMA/Co copolymer characteristics can be found in Table 4C.

■ **Characterization.** Monomer conversion was determined with a Varian NMR Mercury spectrometer (^1H NMR, 300 MHz, 32 scans) using CDCl_3 . In the case of a copolymerization between two monomers A and B, the overall monomer conversion X was calculated from formula 1:

$$X = X_A f_{A,0} + X_B f_{B,0} \quad (1)$$

where $f_{A,0}$ and $f_{B,0}$ are the initial molar fractions of A and B, and X_A and X_B are the individual conversions of A and B, respectively. My conversion was calculated by comparing the integrated peaks of the aliphatic protons of the monomer ($\delta = 2.30$ - 2.15 ppm, 4H), the aliphatic protons of the polymer ($\delta = 2.15$ - 1.90 ppm, 8H) and the protons of the two methyl groups of both monomer and polymer ($\delta = 1.75$ - 1.55 ppm, 6H). IBOMA conversion was obtained using the NMR peaks of the vinyl protons of the monomer ($\delta = 6.05$ and 5.50 ppm, 2H) and the aromatic proton of both monomer and polymer ($\delta = 4.65$ - 4.20 ppm, 1H). Styrene (S) conversion was determined using the vinyl protons of the monomer ($\delta = 6.80$ - 6.70 , 5.80 - 5.70 and 5.30 - 5.20 ppm, 3H) and the aromatic protons of both monomer and polymer ($\delta = 7.50$ - 6.90 ppm, 5H). The same ^1H NMR spectra (300 MHz Varian NMR Mercury spectrometer, CDCl_3 eluent, 32 scans) allowed to determine the regioselectivity of the My repetitive units in the polymers by comparing the three integrated peaks at $\delta = 4.70$ - 4.80 ppm (two vinyl protons of 3,4-addition and two vinyl protons corresponding to 1,2-addition), $\delta = 5.00$ - 5.25 ppm (two olefinic protons corresponding to 1,4-addition, one olefinic proton corresponding to 1,2-addition and one olefinic proton from 3,4-addition) and $\delta = 5.30$ - 5.50 ppm (one olefinic proton from 1,2-addition).^{3,4}

Phosphorus nuclear magnetic resonance (^{31}P NMR) was performed using a 5 mm diameter Up NMR tube with 840 scans being processed in a 200 MHz Varian Gemini 2000 spectrometer operating at 81 MHz. 0.0352 g of My -rich My /IBOMA-82 ($M_{n,MHS} = 13.6 \text{ kg}\cdot\text{mol}^{-1}$) and 0.0676 g of IBOMA-rich My /IBOMA-44 ($M_{n,MHS} = 8.8 \text{ kg}\cdot\text{mol}^{-1}$) were characterized in CDCl_3 with the addition of diethylphosphite as internal reference (0.0027 g and 0.0072 g respectively). To confirm similar relaxation rates between diethylphosphite and the copolymer samples, My /IBOMA-

82 and *M_y/IBOMA-44* were run under the exact same conditions with only one scan and no dummy scans (*ss* = 0). Slight differences (< 3.2%) in integral values were measured between these spectra and the standard ones with multiple scans. Moderate *M_n* IBOMA/*M_y* copolymers were thus assumed to relax at the same rate compared to that of diethylphosphite.

The number-average molecular weights (*M_{n,GPC}*) and the dispersities ($\mathcal{D} = M_{w,GPC}/M_{n,GPC}$) were measured using gel permeation chromatography (GPC, Water Breeze, differential refractive index RI 2414 detector, 40 °C) with HPLC grade THF as the mobile phase (flow rate of 0.3 mL.min⁻¹). The GPC was equipped with 3 Waters Styragel® HR columns (HR1 with a molecular weight measurement range of 10² – 5 x 10³ g.mol⁻¹, HR2 with a molecular weight measurement range of 5 x 10² - 2 x 10⁴ g.mol⁻¹ and HR4 with a molecular weight measurement range of 5 x 10³ - 6 x 10⁵ g.mol⁻¹) and a guard column was used. *M_{n,GPC}* values were determined by calibration with 10 linear narrow molecular weight distribution P(MMA) standards (Varian Polymer Standards, molecular weights ranging from 875 to 1,677,000 g.mol⁻¹). The P(*M_y*) and P(IBOMA) contributions to *M_{n,GPC}* were converted using Mark–Houwink–Sakurada (MHS) coefficients (MHS parameters determined at 35 °C with THF eluent for P(MMA)⁵: $K_{P(MMA)} = 12.2 \times 10^{-5} \text{ dL.g}^{-1}$ and $\alpha_{P(MMA)} = 0.690$; MHS parameters determined at 25 °C with THF eluent for P(IBOMA)⁶: $K_{P(IBOMA)} = 3.8 \times 10^{-5} \text{ dL.g}^{-1}$ and $\alpha_{P(IBOMA)} = 0.748$; MHS parameters determined at 30 °C with THF eluent for P(*M_y*) containing 90 and 10 mol% of 1,4- and 3,4-content respectively⁷: $K_{P(M_y)} = 7.5 \times 10^{-5} \text{ dL.g}^{-1}$ and $\alpha_{P(M_y)} = 0.772$). Therefore, the converted *M_n* values were calculated according to the Mark-Houwink relationship⁸ and the molar composition of the copolymer samples (determined by ¹H NMR) as given in equation 2 in the case of *M_y/IBOMA* copolymers:

$$M_{n,MHS} = F_{M_y} [(K_{P(MMA)}/K_{P(M_y)}) M_{n,GPC}^{\alpha_{P(MMA)}+1}]^{1/(\alpha_{P(M_y)}+1)} + (1-F_{M_y}) [(K_{P(MMA)}/K_{P(IBOMA)}) M_{n,GPC}^{\alpha_{P(MMA)}+1}]^{1/(\alpha_{P(IBOMA)}+1)} \quad (2)$$

Thermogravimetric analysis (TGA) was carried out using a Q500TM from TA Instruments under nitrogen flow at a ramp rate of 15 °C.min⁻¹. Samples were heated in aluminum pans. Differential scanning calorimetry (DSC, Q2000TM from TA Instruments) was used under N₂ atmosphere. Indium was used as a standard to calibrate temperature while heat flow was calibrated via a benzoic acid standard. Three scans per cycle (heat/cool/heat) at a rate of 10 °C.min⁻¹ was set with a temperature range ranging for instance from – 90 °C to + 220 °C for the characterization of the triblock copolymers. Only the second heating run was taken into account to eliminate the thermal history. The reported *T_gs* were calculated using the inflection method from the change in slope observed in the DSC traces.

The stress-strain features of the Co/IBOMA-*M_y*-IBOMA/Co triblock polymer (Co = S) were determined using a MTS Insight material testing system with a 5 kN load cell at room temperature and a cross-head speed of 10 mm.min⁻¹. Dog-bone style tensile specimens (ASTM D638 type V for reference, overall length = 63.5 mm, overall width = 9.53 mm) were prepared by solvent casting. To cast the film, the polymer sample was fully dissolved in dichloromethane (~ 80 wt%) for an hour with continuous stirring using a magnetic stir bar. The solution was cast into a level Teflon Petri dish at room temperature for approximately two days. Then, the drying was completed after placing the film in the oven at 50 °C under vacuum until constant weight was measured. The film samples were cut into typical dog-bone shapes using a sharp blade. Specimens with defects (nicked sides, cracks, air bubbles) on their surface were

discarded and were not used in mechanical testing. For each specimen, the thickness and the width were measured at five different points along the small center portion with a digital caliper (Marathon, CO 030150F128) and the average film thickness and width were used for all calculations. The samples tested exhibited a mean thickness from 0.55 to 0.69 mm and a mean width from 3.11 to 3.32 mm. Each test was considered finished after the complete breakup of the specimen at the narrow section (films that broke near the grips were discarded). 6 specimens were tested, and averaged results were reported using TestWorks 4 software. The Young's modulus was determined as the slope of the stress-strain curve at strains of 0–0.5%.

The mechanical response of Co/IBOMA-*My*-IBOMA/Co (Co = S) to torsional oscillation at 0.15 Hz and 1% strain over a temperature range of 25 to 230 °C was measured at a rate of 5 °C.min⁻¹ under N₂ using the CDT 450 convection heated measuring chamber mounted on the Anton Paar Modular Compact Rheometer MCR302. The solid rectangular fixture (SFR) was used, consisting of an upper and a lower holder with insets. Rectangular bars (thickness = 1.05 ± 0.04 mm; width = 8.91 ± 0.13 mm; length = 46.13 ± 0.24) were made by solvent casting, following the above protocol used for preparing the tensile bars. Prior to the torsion tests, dynamic amplitude sweeps at 0.15 Hz and varying strain from 0.01 to 100% were conducted at various temperatures to ensure the material was kept within the linear viscoelastic regime. Please note that, before the rheological characterization, the removal of the SG1 groups of Co/IBOMA-*My*-IBOMA/Co chain-ends was performed as described elsewhere^{9,10}.

The micro-phase behavior of Co/IBOMA-*My*-IBOMA/Co (Co = *My*) triblock polymer was studied by Atomic Force Microscopy (AFM). AFM images were collected in tapping mode using an AFM Bruker Multimode 8 equipped with Nanoscope V controller. The scanning speed for image acquisition was 0.5 Hz. The used cantilevers are Bruker TAP 300A with a radius of curvature of the tip of 8 nm. Data analyses were processed using the Nanoscope Analysis software (version 1.5). The samples were prepared as follows: the polymer (~ 0.5 g) was fully dissolved in chloroform (~ 10 mL) and one or two drops was spin coated on a silicon wafer, previously rinsed with acetone and cleaned by UV-O₃ for 30 min. Lastly, the coated film was dried at 50 °C under vacuum overnight.

■ *References of the experimental section.*

- (1) J. Vinas, N. Chagneux, D. Gigmes, T. Trimaille, A. Favier and D. Bertin, *Polymer* **2008**, *49*, 3639.
- (2) B. Lessard, C. Aumand-Bourque, R. Chaudury, D. Gomez, A. Haroon, N. Ibrahimian, S. Mackay, M. -C. Noel, R. Patel, S. Sitaram, S. Valla, B. White and M. Maric, *Intern. Polymer Processing* **2011**, *26* (2), 197.
- (3) P. Sarkar and A. K. Bhowmick, *RSC Adv.* **2014**, *4*, 61343.
- (4) S. Georges, M. Bria, P. Zinck and M. Visseaux, *Polymer* **2014**, *55*, 3869.
- (5) H. K. Mahabadi, *J. Appl. Polym. Sci.* **1985**, *30*, 1535.
- (6) X. Q. Zhang and C. H. Wang, *J. Polym. Sci., Part B: Polym. Phys.* **1994**, *32*, 1.
- (7) P. Hattam, S. Gauntlett, J. W. Mays, N. Hadjichristidis, R. N. Young and L. J. Fetters, *Macromolecules* **1991**, *24* (23), 6199.
- (8) H. Pasch; B. Trathnigg In *Multidimensional HPLC of Polymers*; H. Pasch; B. Trathnigg, Eds.; Springer: Heidelberg, 2013; Chapters 4 & 5, pp 37–90.
- (9) J. Nicolas, S. Brusseau and B. Charleux, *J. Polym. Sci., Part A: Polym. Chem.* **2010**, *48*, 34.
- (10) C. Petit, B. Luneau, E. Beaudoin, D. Gigmes and D. Bertin, *J. Chromatogr. A* **2007**, *1163*, 128.

c.2. Supporting information

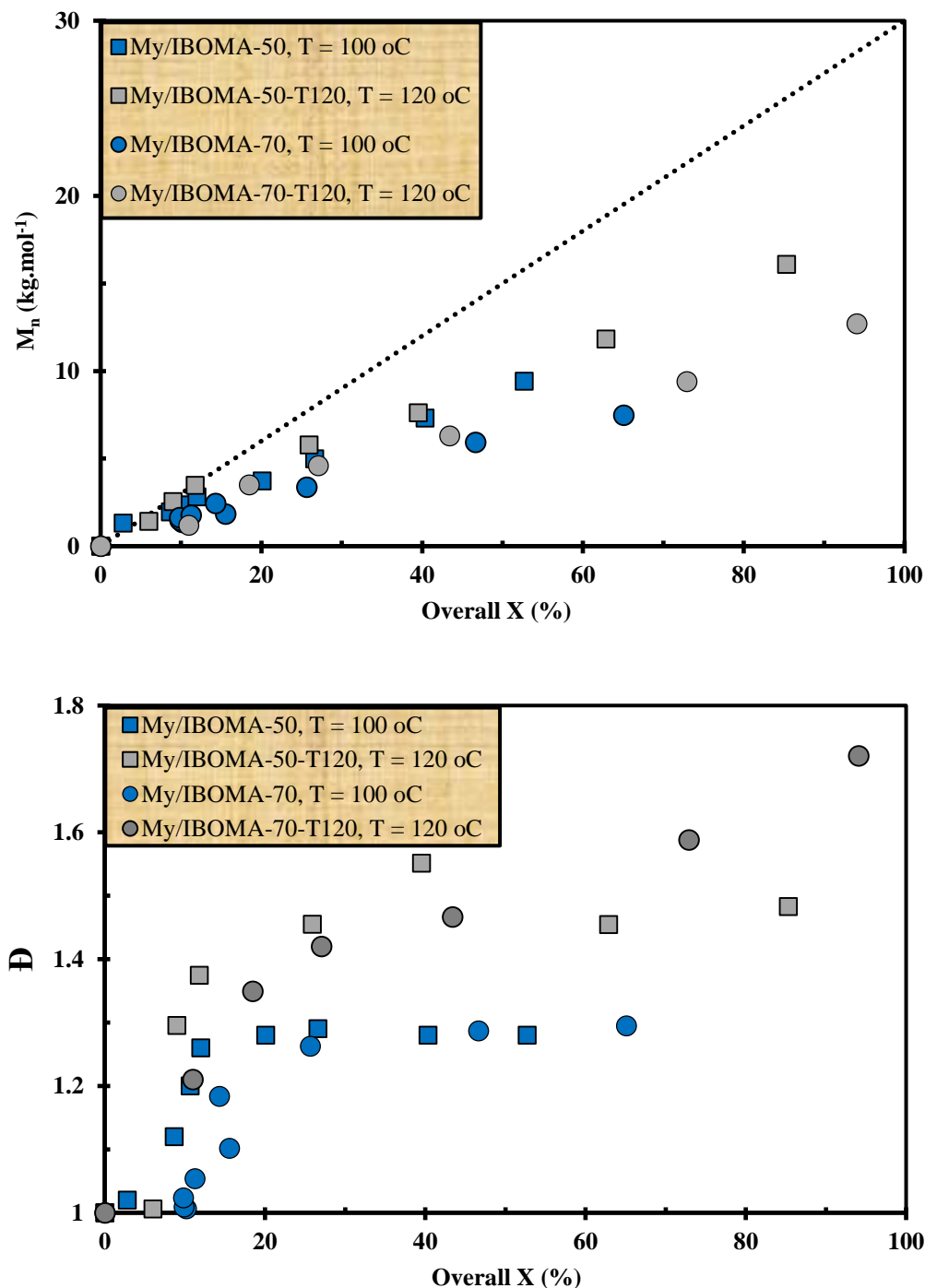


Figure S1c. $M_{n,\text{MHS}}$ determined by GPC relative to PMMA standards in THF at 40 °C and corrected via MHS parameters *versus* overall conversion X (**top**, the dotted line indicates the theoretical M_n ($M_{n,\text{theo}}$) *versus* overall conversion based on the monomers to initiator ratio) and \bar{D} *versus* overall conversion X (**bottom**) for M_y/IBOMA copolymerizations performed at $T = 100\text{-}120$ °C, and exhibiting $f_{M_y,0} = 0.50\text{-}0.71$.

■ **Use of terminal models:** Table S1c gives the experimental data used to determine the reactivity ratios r_{My} and r_{IBOMA} . It was assumed that the selected copolymers samples exhibited sufficiently low degree of conversion that the monomer composition was essentially unchanged. Calculation of r_{My} and r_{IBOMA} was first done by the Fineman-Ross (FR) approach¹ (rearrangement of the Mayo-Lewis copolymer equation into a linear form²) and by the Kelen-Tüdös (KT) approach³. The latter refines the linearization method by introducing an arbitrary positive constant α to spread the data more evenly so as to give equal weight to all data points. Accordingly, the KT approach minimizes the bias of the FR approach. The appropriate plot of the variables G and H, defined in Equation B1, will provide a linear relationship giving the reactivity ratios as the slope and intercept as shown in Equation B2.

$$G = (f_{IBOMA,0} / f_{My,0}) \times [(2F_{IBOMA} - 1) / F_{IBOMA}] ; H = (f_{IBOMA,0} / f_{My,0})^2 \times [(1 - F_{IBOMA}) / F_{IBOMA}] \quad (\text{B1})$$

$$G = r_{IBOMA} \times H - r_{My} \quad (\text{B2})$$

Equation B3 shows the additional variables used for the KT plot as illustrated in Equation B4.

$$\eta = G / (\alpha + H) ; \varepsilon = H / (\alpha + H) ; \alpha = \sqrt{H_{max}H_{min}} \quad (\text{B3})$$

$$\eta = (r_{IBOMA} + r_{My} / \alpha)\varepsilon - r_{My} / \alpha \quad (\text{B4})$$

In Equations B3 and B4, H_{max} and H_{min} stand for the highest and lowest values of the set of experimental points, respectively. $r_{My} = 2.16 \pm 0.34$ and $r_{IBOMA} = 0.07 \pm 0.04$ ($r_{My} \times r_{IBOMA} = 0.15 \pm 0.19$) were obtained via the FR method and $r_{My} = 1.90 \pm 0.18$ and $r_{IBOMA} = 0.02 \pm 0.21$ ($r_{My} \times r_{IBOMA} = 0.04 \pm 0.15$) were calculated via the KT method. The errors associated with the experimental data were derived from the standard errors of the slopes from FR and KT plots.

■ **Use of a NLLS model:** Still despite its improvements, the KT method does not overcome the shortcomings of the linear method: use of the differential form and errors that affect both variables. In order to handle rigorously the Mayo-Lewis equation, linearization has to be avoided. From a statistical point of view, a NLLS fit to the Mayo-Lewis equation is probably the soundest method to determine the desired parameters⁴. Therefore, the reactivity ratios were also determined using a non-linear least-squares fitting of the data. The commercial software package Matlab R2016a was used to solve the Mayo-Lewis equation¹ for $My/IBOMA$ copolymerization (B5).

$$F_{IBOMA} = (r_{IBOMA} f_{IBOMA,0}^2 + f_{IBOMA,0} f_{My,0}) / (r_{IBOMA} f_{IBOMA,0}^2 + 2 f_{IBOMA,0} f_{My,0} + r_{My} f_{My,0}^2) \quad (\text{B5})$$

Using the reactivity ratios determined by the KT method as initial guesses, the statistical fit to the data yielded reactivity ratios $r_{My} = 2.07 \pm 0.58$ and $r_{IBOMA} = 0.05 \pm 0.08$ at 95 % confidence level and with a regression coefficient $R^2 = 0.91$ (SSE = 0.0174, RMSE = 0.0499).

Table S1c. Samples used for determination of reactivity ratios for M_y /IBOMA gradient copolymerization done at 100 °C in bulk with NHS-BB and targeting $M_{n,theo} = 30 \text{ kg.mol}^{-1}$ at $X = 100\%$.

$f_{\text{IBOMA},0}^{(a)}$	$F_{\text{IBOMA}}^{(b)}$	$X^{(c)} (\%)$	t (min)	$M_{n,MHS}^{(d)}$ (kg.mol^{-1})	$D^{(d)}$
0.10	0.15	27.5	60	4.1	1.27
0.19	0.10	12.5	30	1.6	1.07
0.30	0.13	13.2	60	1.8	1.10
0.41	0.22	17.0	120	2.7	1.27
0.50	0.24	20.1	100	3.7	1.28
0.60	0.28	10.4	30	3.0	1.21
0.70	0.42	13.2	60	3.5	1.30
0.80	0.39	21.2	180	6.6	1.36
0.90	0.57	12.4	60	7.0	1.52

a) $f_{\text{IBOMA},0}$ is the initial molar feed composition of isobornyl methacrylate.

b) F_{IBOMA} is the molar composition of isobornyl methacrylate in the $P(M_y\text{-grad-IBOMA})$ copolymer determined by $^1\text{H NMR}$ in CDCl_3 .

c) Overall monomer conversion $X = X_{M_y}f_{M_y,0} + X_{\text{IBOMA}}f_{\text{IBOMA},0}$ determined by $^1\text{H NMR}$ in CDCl_3 .

d) $M_{n,GPC}$ and $M_{w,GPC}$ determined by GPC calibrated with PMMA standards in THF at 40 °C. $M_{n,MHS}$, obtained from $M_{n,GPC}$ and corrected using the Mark-Houwink relationship.

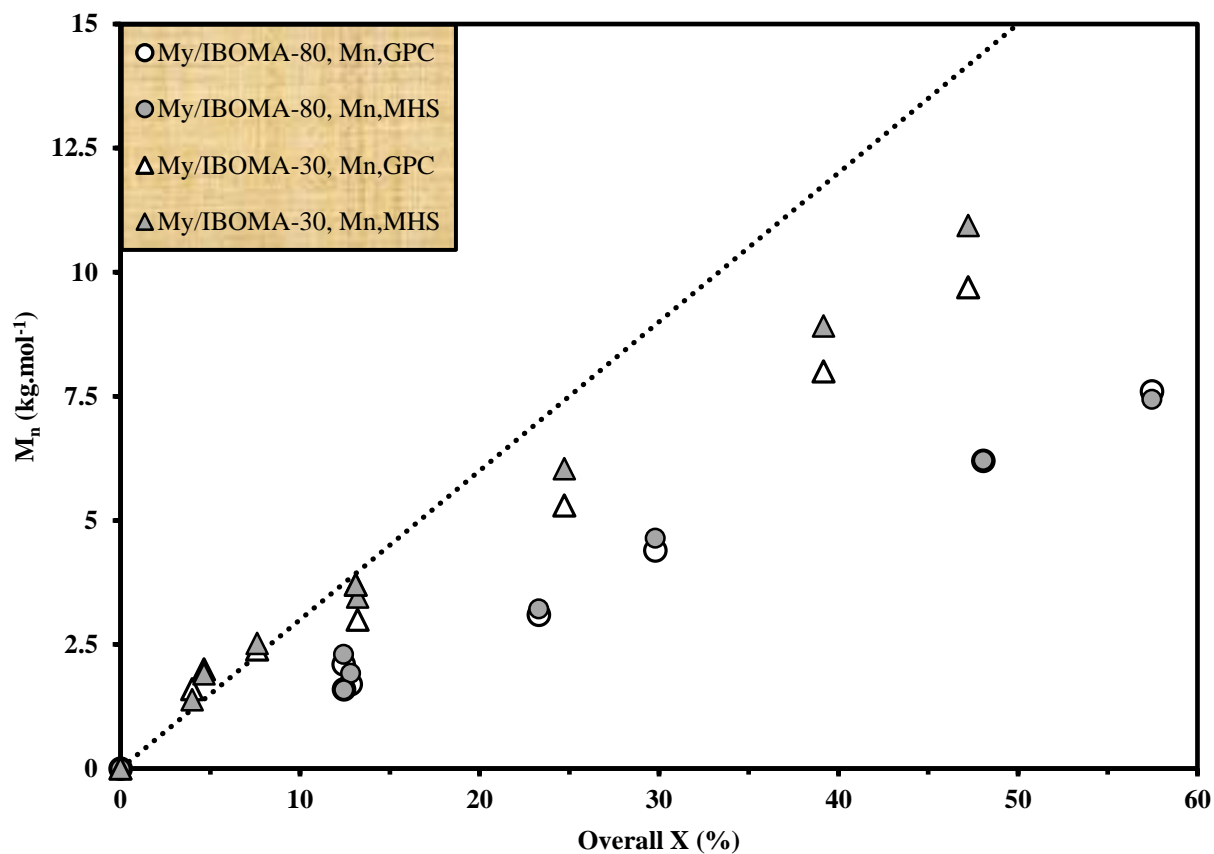


Figure S2c. $M_{n, \text{GPC}}$ determined by GPC relative to PMMA standards in THF at 40 °C and $M_{n, \text{MHS}}$, obtained from $M_{n, \text{GPC}}$ and corrected using the Mark-Houwink relationship, *versus* overall conversion X for experiments My/IBOMA-80 ($f_{My,0} = 0.81$) and My/IBOMA-30 ($f_{My,0} = 0.30$) at 100 °C. The dotted line indicates the theoretical M_n ($M_{n, \text{theo}}$) *versus* overall conversion based on the monomers to initiator ratio ($M_{n, \text{theo}} = 30 \text{ kg.mol}^{-1}$ at X = 100%).

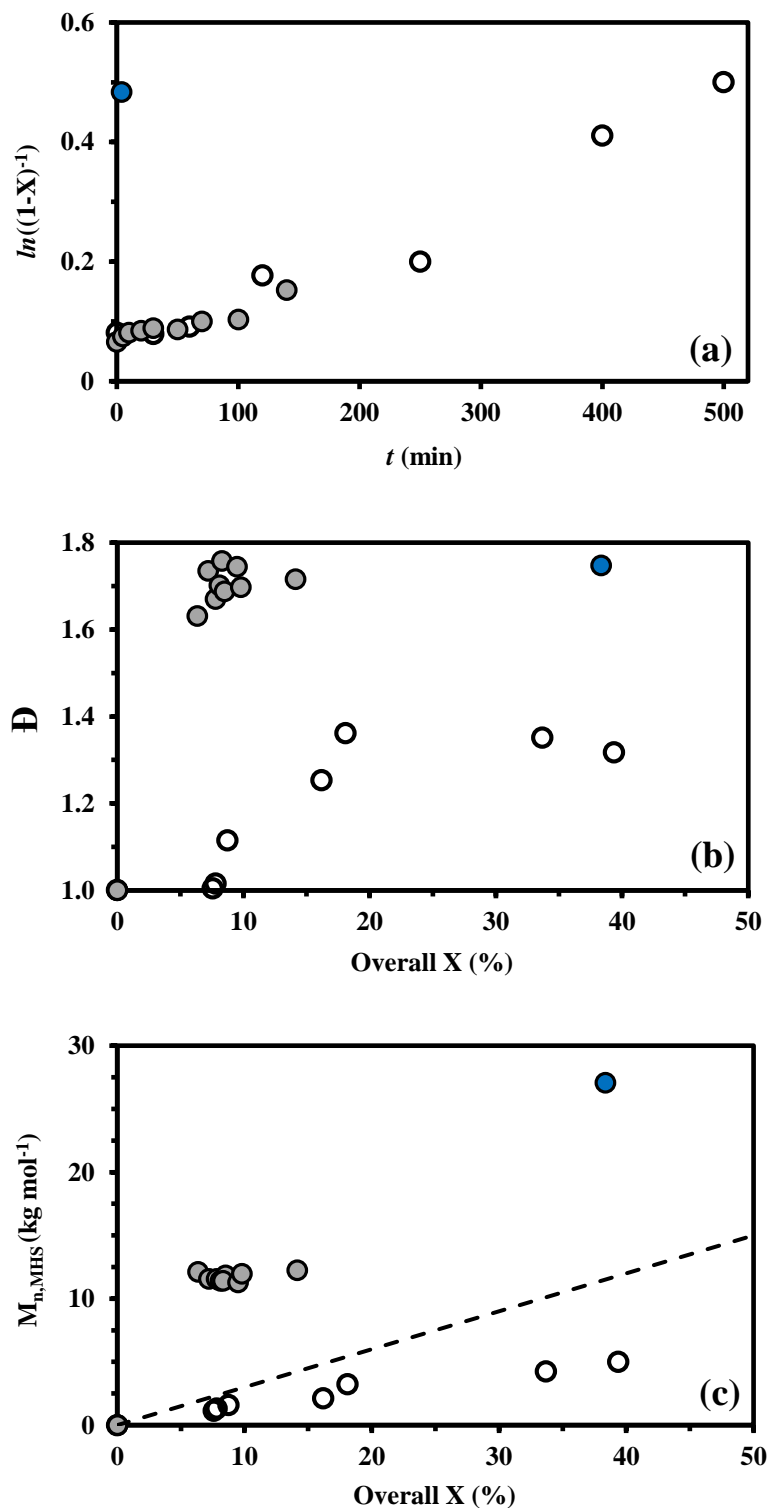


Figure S3c. (a) $\ln((1-X)^{-1})$ (X = overall conversion) versus reaction time t , (b) \bar{D} versus overall conversion X and (c) $M_{n,MHS}$ versus overall conversion X for *My*/IBOMA-100 ($f_{My,0} = 1.00$, open circles (\circ)), *My*/IBOMA-0 ($f_{My,0} = 0$, solid blue circles (\bullet)) and *My*/IBOMA-0-Tol ($f_{My,0} = 0$, in toluene, solid grey circles (\bullet)). The dashed line indicates the theoretical M_n versus overall conversion based on the monomer to initiator ratio.

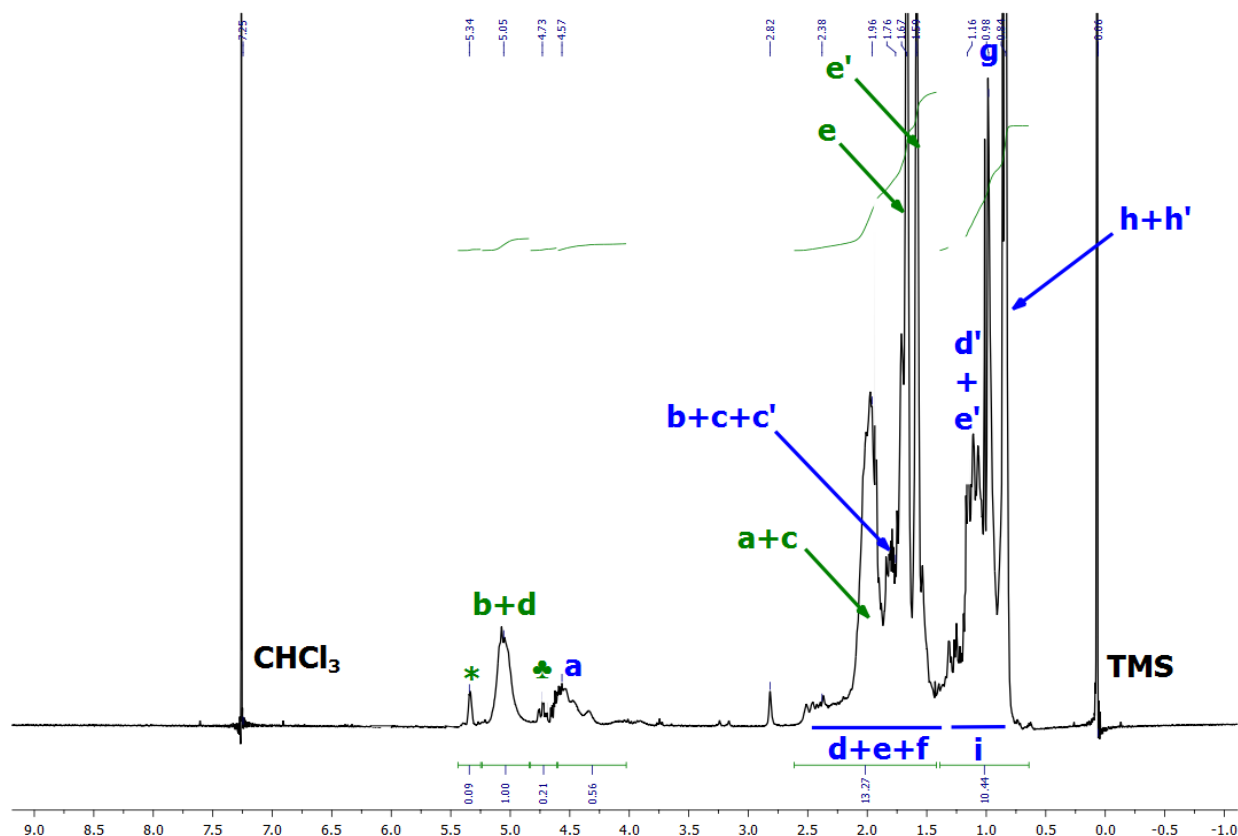
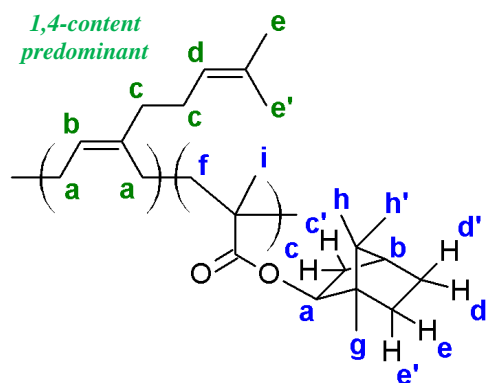


Figure S4c. ^1H NMR spectrum in CDCl_3 (300 MHz, tetramethylsilane TMS as internal reference) at room temperature of the final dried $\text{P}(\text{My-grad-IBOMA})$ gradient copolymer from experiment My/IBOMA-50 after recovery, using methanol as the precipitant.



$\text{P}(\text{My-grad-IBOMA})$ My/IBOMA-50 : ^1H NMR (CDCl_3 , 300 MHz, RT): $\delta = 5.20\text{-}4.90$ (s br, $2\text{H}^{\text{P}(\text{My})}$), $4.65\text{-}4.00$ (m br, $1\text{H}^{\text{P}(\text{IBOMA})}$), $2.60\text{-}1.40$ (m br, $7\text{H}^{\text{P}(\text{IBOMA})}$), $2.20\text{-}1.90$ (m br, $8\text{H}^{\text{P}(\text{My})}$), 1.67 (s, $3\text{H}^{\text{P}(\text{My})}$), 1.59 (s, $3\text{H}^{\text{P}(\text{My})}$), $1.40\text{-}0.70$ (m br, $14\text{H}^{\text{P}(\text{IBOMA})}$).

*Signal at $\delta = 5.45\text{-}5.30$ ppm (t br, $1\text{H}^{1,2\text{-P}(\text{My})}$) corresponds to one olefinic proton of $1,2\text{-P}(\text{My})^5$.

*Signal at $\delta = 4.80\text{-}4.65$ ppm (d, $2\text{H}^{1,2\text{-P}(\text{My})}$) and (s, $2\text{H}^{3,4\text{-P}(\text{My})}$) corresponds to two vinyl protons of $3,4\text{-addition}$ and two vinyl protons of $1,2\text{-addition}$ of My units⁵.

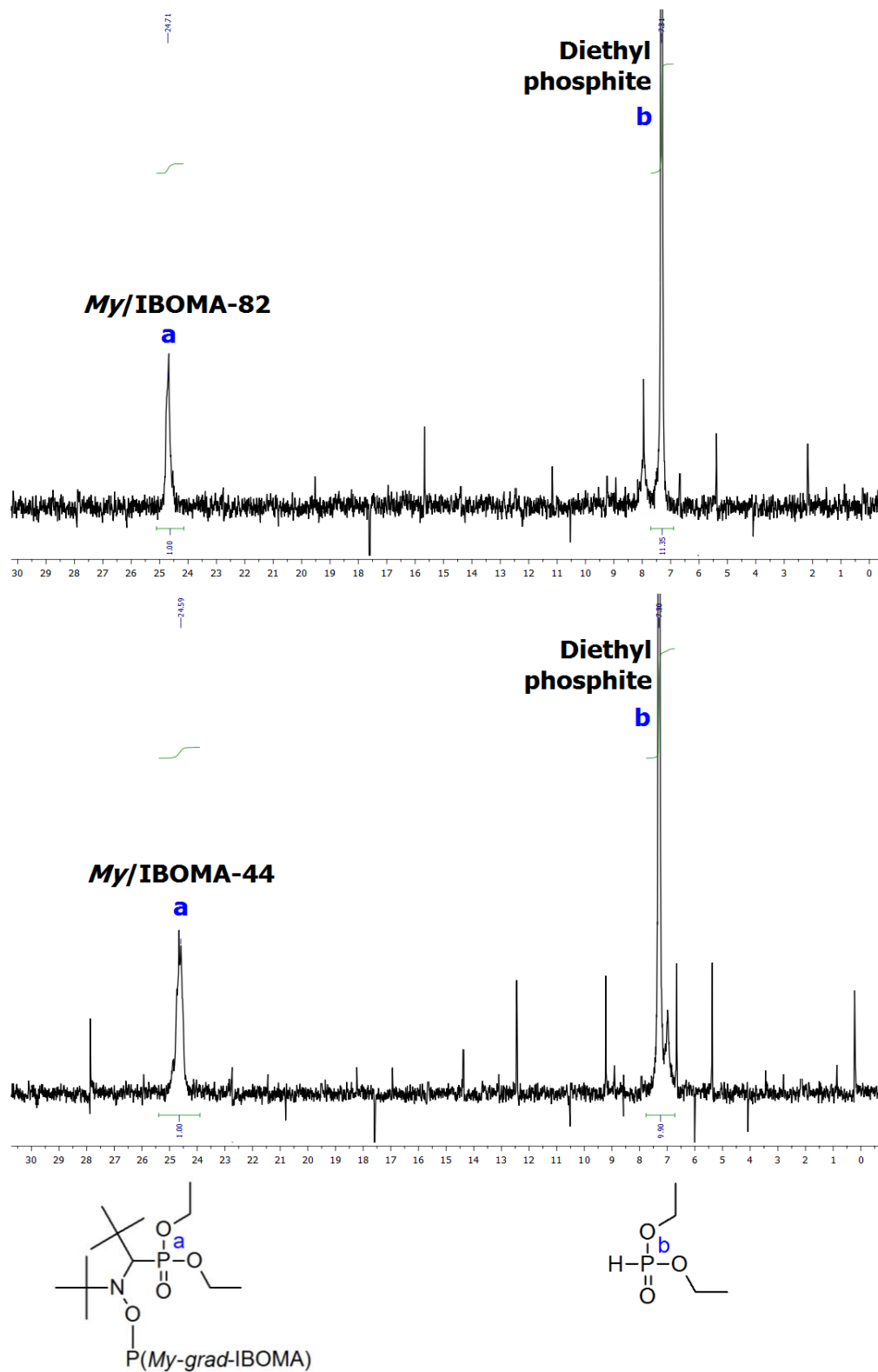


Figure S5c. 81 MHz ^{31}P NMR spectra of dried P(*My-grad-IBOMA*)-SG1 macroinitiators *My/IBOMA-82* (top) and *My/IBOMA-44* (down, chemical structure in bottom left) in CDCl_3 at room temperature with diethyl phosphite as an internal reference (structure in bottom right).

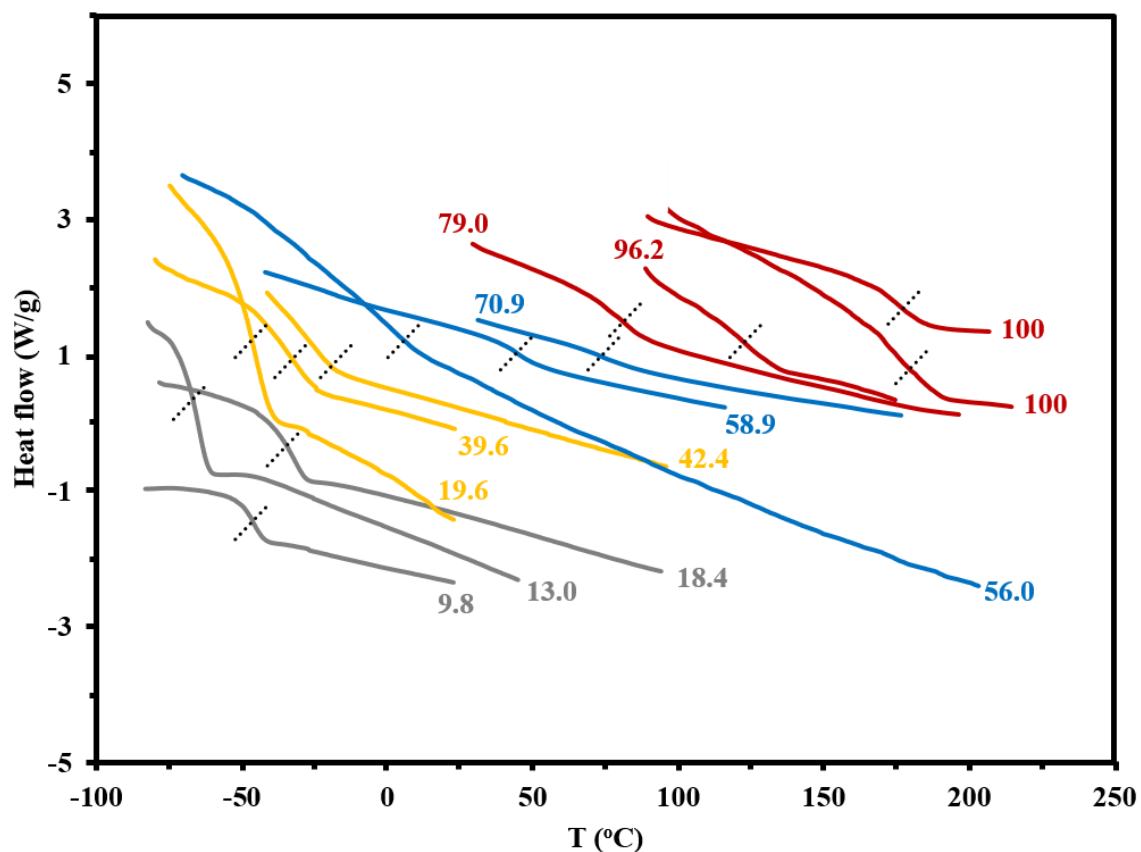


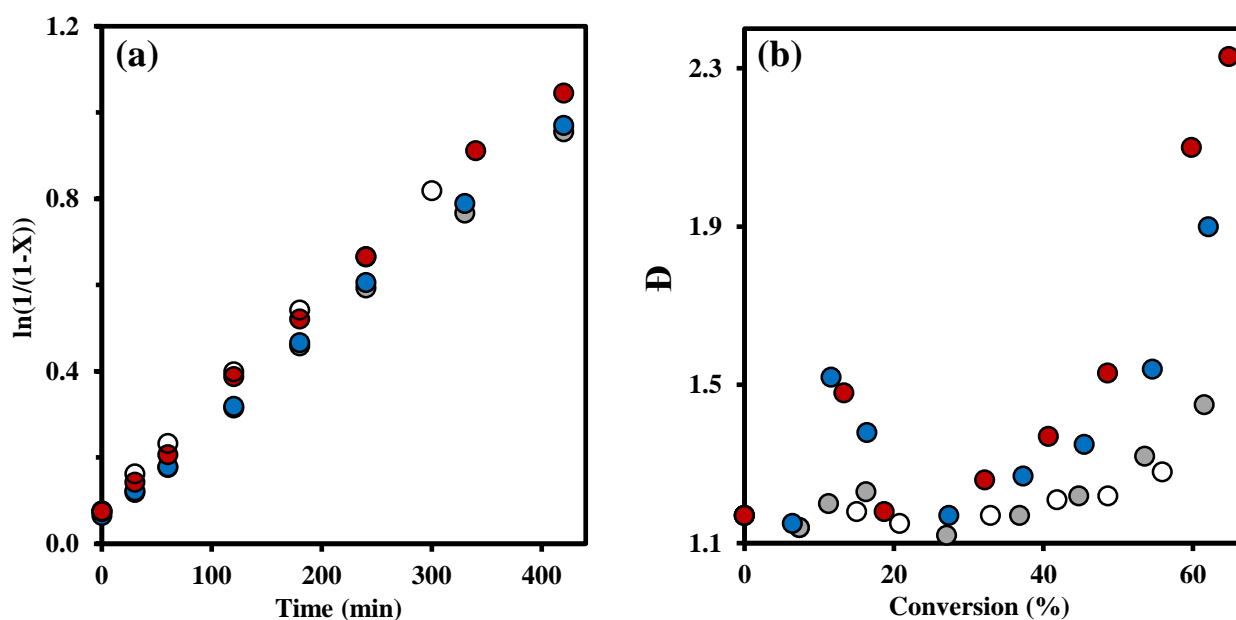
Figure S6c. DSC traces (second heating run) of P(*My-grad-IBOMA*) gradient copolymers. The black dotted lines indicate the changes in slope observed. The numbers alongside each DSC curve refer to the molar fraction of IBOMA (F_{IBOMA} in percentage) in the copolymer. Please note that the P(*My-grad-IBOMA*) copolymers characterized by DSC do not necessarily correspond to the final copolymers presented in Table 2.

Table S2c. Experimental conditions for *My* polymerizations initiated by PEB-(SG1)₂ at 120 °C in bulk or at 115 °C in toluene.

ID ^(a)	[PEB-(SG1) ₂] ₀ (M)	[<i>My</i>] ₀ (M)	[SG1] ₀ (M)	Solvent	[Solvent] ₀ (M)	M _{n,theo} ^(b) (kg.mol ⁻¹)	<i>t</i> (min)
<i>My</i> -79	0.011	5.928	0	-	0	79.1	300
<i>My</i> -105	0.008	5.831	0	-	0	105.0	420
<i>My</i> -137	0.006	5.791	0	-	0	137.2	420
<i>My</i> -174	0.005	6.178	0	-	0	174.0	420
<i>My</i> -173 _{SG1,9}	0.005	6.122	0.0005	-	0	172.5	420
<i>My</i> -169 _{SG1,18}	0.005	5.975	0.0011	-	0	168.5	480
<i>My</i> -170 _{Tol}	0.002	2.414	0	Toluene	4.573	170.1	420

a) Experimental identification given by *My*-XX where XX refers to the rounded M_{n,theo} targeted.

b) given for X = 100% and calculated as follows: $M_{n,theo} = M_{My} ([My]_0 / [PEB-(SG1)_2]_0) + M_{n,PEB-(SG1)_2}$ with $M_{My} = 136.23 \text{ g.mol}^{-1}$ and $M_{n,PEB-(SG1)_2} = 5.7 \text{ kg.mol}^{-1}$.



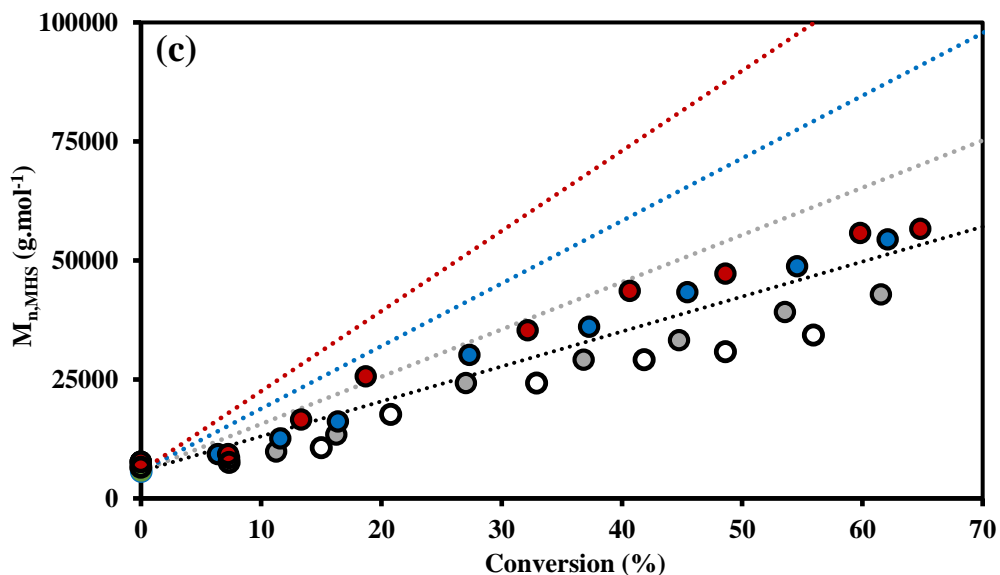
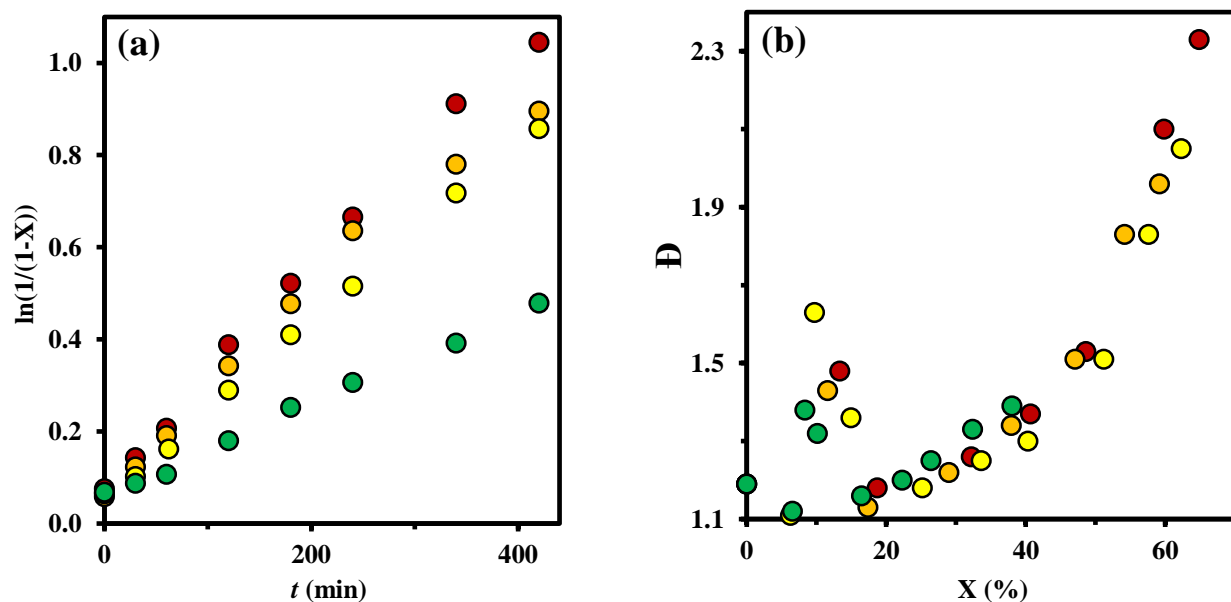


Figure S7c. (a) Semi-logarithmic kinetic plots of $\ln((1-X)^{-1})$ ($X = M_y$ conversion) versus polymerization time t , (b) D versus X , and (c) $M_{n,MHS}$ versus X for the experiments M_y -79 (open circles), M_y -105 (solid grey circles), M_y -137 (solid blue circles) and M_y -174 (solid red circles). The dotted lines indicate the theoretical M_n versus overall conversion based on the monomer-to-initiator ratio for each reaction (black, grey, blue and red predicted lines for experiments M_y -79, M_y -105, M_y -137 and M_y -174 respectively). All experimental ID are listed in Table S2c above.



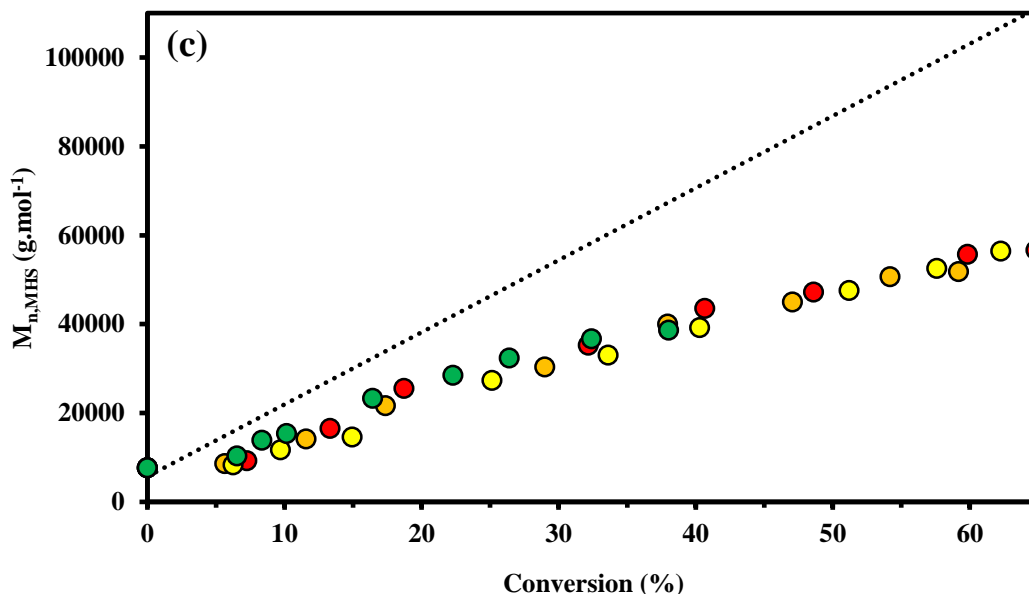


Figure S8c. (a) Semi-logarithmic kinetic plots of $\ln((1-X)^{-1})$ ($X = My$ conversion) versus polymerization time t , (b) \bar{D} versus X , and (c) $M_{n,MHS}$ versus X for the experiments $My-174$ (solid red circles), $My-173_{SG1,9}$ (solid orange circles), $My-169_{SG1,18}$ (solid yellow circles) and $My-170_{Tol}$ (solid green circles). The dotted line indicates the average theoretical M_n versus overall conversion based on the monomer-to-initiator ratio (average $M_{n,theo} = 171.3$ kg.mol $^{-1}$ at $X = 1.0$). All experimental ID are listed in Table S2c above.

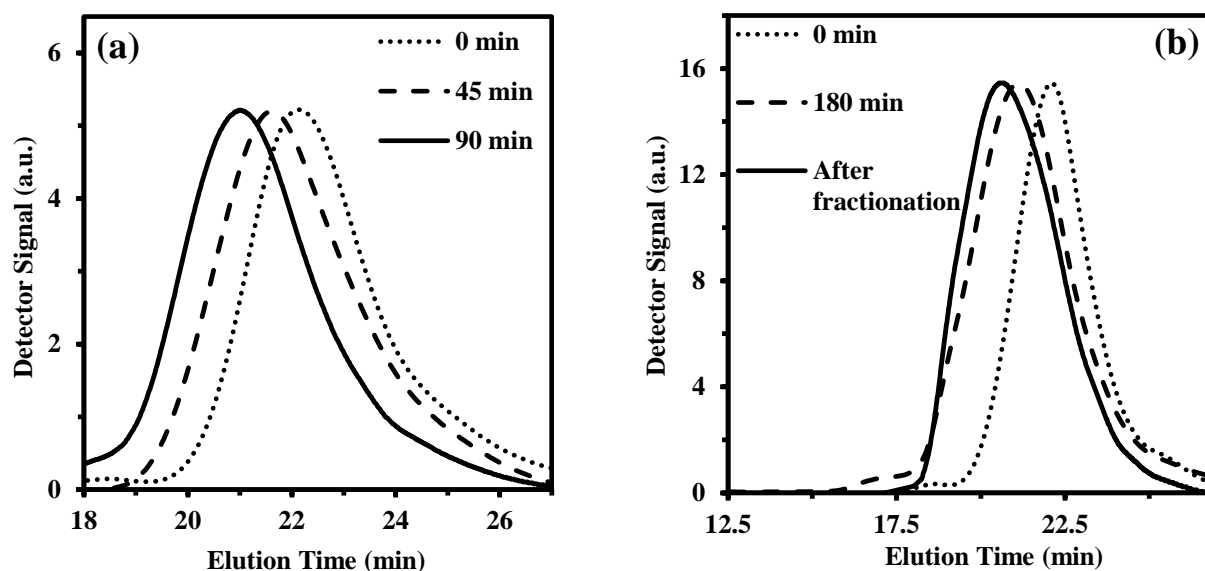


Figure S9c. Normalized GPC traces for the chain-extensions of (a) $My-35$ with a IBOMA/ My (92/8 mol%) mixture (experiment $My-35-IBOMA/My$) and (b) $My-52$ with a IBOMA/S (91/9 mol%) mixture (experiment $My-52-IBOMA/S$) at $T = 115$ °C in 50 wt% toluene. Fractionation of the final $My-52-IBOMA/S$ sample was performed using a methanol (non-solvent) / benzene (solvent) pair (2 cycles).

■ **Calculation of theoretical solubility parameter via the method of Hoftyzer and Van Krevelen⁶:** Relying on the group contribution principle, the solubility parameter components can be determined using the following equations:

$$\delta_d = \sum F_{di} / V_m \quad ; \quad \delta_p = (\sum F_{pi}^2)^{0.5} / V_m \quad ; \quad \delta_h = (\sum E_{hi} / V_m)^{0.5} \quad \text{(H1)}$$

where δ_d , δ_p and δ_h are the contributions of dispersion forces, polar forces and hydrogen bonding, respectively. F_{di} and F_{pi} are the molar attraction constants for dispersion and polar forces. E_{hi} is the cohesive energy for hydrogen bonding and V_m is molar volume of the structural unit of the polymer. The corresponding equation for determination of solubility parameter (δ) is the following:

$$\delta = (\delta_d^2 + \delta_p^2 + \delta_h^2)^{0.5} \quad \text{(H2)}$$

■ **Solubility parameter of 1,4-P(My):** Addition of the group contributions for 1,4-P(My) gives:

	F_{di} (MPa ^{1/2} .mol ⁻¹)	F_{pi}^2 (MPa.mol ⁻²)	E_{hi} (J.mol ⁻¹)	V_m (cm ³ .mol ⁻¹)
2 -CH ₃	+ 420	0	0	+ 33.5
4 -CH ₂ -	+ 270	0	0	+ 16.1
2 =CH-	+ 200	0	0	+ 13.5
2 =C<	+ 70	0	0	- 5.5
Total	2 460	0	0	147.4

Thus: $\delta_{P(My)} = (16.69^2 + 0^2 + 0^2)^{0.5} = 16.69 \text{ MPa}^{1/2}$

■ **Solubility parameter of P(IBOMA):** Addition of the group contributions for P(IBOMA) gives:

	F_{di} (MPa ^{1/2} .mol ⁻¹)	F_{pi}^2 (MPa.mol ⁻²)	E_{hi} (J.mol ⁻¹)	V_m (cm ³ .mol ⁻¹)
4 -CH ₃	+ 420	0	0	+ 33.5
4 -CH ₂ -	+ 270	0	0	+ 16.1
3 >C<	- 70	0	0	- 19.2
2 >CH-	+ 80	0	0	- 1.0
1 -CO-	+ 290	+ 592 900	+ 2 000	+ 10.8
1 -O-	+ 100	+ 160 000	+ 3 000	+ 3.8
Total	3 100	752 900	5 000	153.4

Thus: $\delta_{P(IBOMA)} = (20.21^2 + 5.66^2 + 5.71^2)^{0.5} = 21.75 \text{ MPa}^{1/2}$

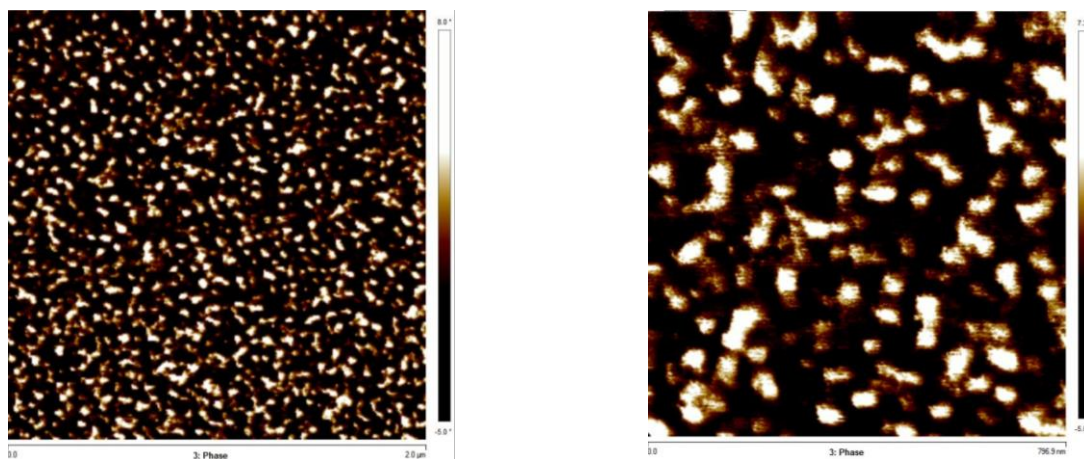


Figure S10c. Atomic force microscopy phase images (left image, 2 μm x 2 μm ; right image, 0.8 μm x 0.8 μm) under tapping mode of operation of the surface morphology of triblock copolymer *My*-35-IBOMA/*My* cast film. The dark domain represents the *My* component (color-coded height scale given to the right of the image).

References of the supporting information:

- (1) M. Fineman and S. D. Ross, *J. Polym. Sci.* **1950**, 5 (2), 259.
- (2) F. R. Mayo and F. M. Lewis, *J. Am. Chem. Soc.* **1944**, 66 (9), 1594.
- (3) T. Kelen and F. Tüdös, *J. Macromol. Sci., Chem.* **1975**, 9 (1), 1.
- (4) P. W. Tidwell and G. A. Mortimer, *J. Polym. Sci., Part A: Gen. Pap.* **1965**, 3, 369.
- (5) P. Sarkar and A. K. Bhowmick, *RSC Adv.* **2014**, 4, 61343.
- (6) D. W. van Krevelen; K. Te Nijenhuis In Properties of Polymers, 4th edition; D. W. van Krevelen, K. Te Nijenhuis, Eds.; Elsevier B. V.: Amsterdam, **2009**; Chapter 7, pp 189-227.

d. Appendix for Chapter 4: Experimental section

■ **Materials.** Basic alumina (Al_2O_3 , Brockmann, Type I, 150 mesh), calcium hydride (CaH_2 , 90–95% reagent grade), 2,6-di-*tert*-butyl-4-methylphenol (BHT, $\geq 99\%$), *p*-toluenesulfonyl hydrazide (TSH, 97%), thiophenol (97%), pyridine ($\geq 99\%$, ACS reagent), tributylamine (TBA, $\geq 98.5\%$) and benzene ($\geq 99\%$, ACS reagent) were purchased from Sigma-Aldrich and used as received. Toluene ($\geq 99\%$), methanol (MeOH , $\geq 99\%$), methylene chloride (CH_2Cl_2 , 99.9% certified ACS), *p*-xylene (99.9%), chloroform (CHCl_3 , 99.9%) and tetrahydrofuran (THF, 99.9% HPLC grade) were obtained from Fisher Scientific and used as received. Telechelic poly(ethylene-*stat*-butylene) difunctional initiator PEB-(SG1)₂ terminated with *N-tert*-butyl-N-[1-diethylphosphono-(2,2-dimethylpropyl)] nitroxide (SG1) was produced relying on a published synthesis route¹, from hydroxyl terminated poly(ethylene-*stat*-butylene) (PEB-(OH)₂, Kraton™ D2205) obtained from Kraton, acryloyl chloride (98%) acquired from Sigma-Aldrich and BlocBuilder™ (99%, provided by Arkema). Styrene (S, 99%) was obtained from Fisher Scientific, isoprene (I, 99%) was obtained from Sigma-Aldrich and isobornyl methacrylate (IBOMA, Visiomer® Terra) was obtained from Evonik, and they were purified by passing through a column of basic alumina mixed with 5 wt% calcium hydride and then stored in a sealed flask under a head of nitrogen in a refrigerator until needed. The deuterated chloroform (CDCl_3 , 99.8%) used as a solvent for nuclear magnetic resonance (NMR) was obtained from Cambridge Isotopes Laboratory.

■ **Synthesis of PI-(SG1)₂.** In a typical procedure, PEB-(SG1)₂ ($0.0024 \text{ mol.L}^{-1}$, $M_n = 5.7 \text{ kg.mol}^{-1}$) was placed in a 48 mL ChemGlass high-pressure reactor containing a magnetic stir bar and fitted with a plunger valve and thermowell. Previously purified isoprene (4.928 mol.L^{-1}) and pyridine (6.17 mol.L^{-1}) were added and the reactor was subjected to three cycles of freeze-thaw degassing, then backfilled with nitrogen. The reactor was placed in an oil bath at 115 °C for 11 h and then cooled to room temperature. The contents of the reactor were transferred to a pre-weighed flask and weighed. Unreacted isoprene was removed in the oven under vacuum at 30 °C and the residual poly(isoprene) and any unreacted PEB-(SG1)₂ (mass neglected) were weighed to calculate isoprene conversion gravimetrically. When kinetic studies were led, identical pressure tubes were prepared, degassed and allowed to react for various periods in order to trace the evolution of M_n , \bar{D} and isoprene conversion with time.

■ **S or IBOMA/S chain-extension from PI-(SG1)₂.** The chain-extension of PI-(SG1)₂ macroinitiator with S in bulk can be detailed (experiment PS-PI4-PS, similar protocol for IBOMA/S chain-extension). PI-(SG1)₂ (0.004 mol.L^{-1}) and previously purified S (5.714 mol.L^{-1}) were added in a 25-mL three-necked round-bottom glass flask equipped with a condenser, a thermal well and a magnetic Teflon stir bar. The reactor was sealed, a vigorous stirring was performed and a purge of ultra-pure nitrogen was then introduced to the reactor for 30 min. The reactor was then heated to 115 °C and allowed to react for 140 min while maintaining a nitrogen purge. The resulting polymer sample ($M_n = 94.4 \text{ kg.mol}^{-1}$, $\bar{D} = 2.19$) was precipitated in excess methanol and dried under vacuum at 50 °C overnight. Lastly, fractionation was performed using a methanol (non-solvent) / benzene (solvent) pair (2 cycles) to remove the low molecular weight species. The final fractionated triblock polymer exhibited $M_n = 103.1 \text{ kg.mol}^{-1}$, $\bar{D} = 2.11$ and $F_s = 0.49$.

■ **Hydrogenation of the synthesized S-I-S triblock copolymers.** PI mid-segment of the triblock copolymer was saturated using the method developed by Hahn², which does not require the use of high-pressure H₂. The unsaturated polymer was first dissolved in *p*-xylene (35-40 mL per gram of polymer) at 50 °C, and then *p*-toluenesulfonyl hydrazide (TSH, 2.4 equiv. to the double bond), tributylamine (TBA, 2.5 equiv. to the double bond) and small amount of 2,6-di-*tert*-butyl-4-methylphenol (BHT) were added. The reaction mixture was stirred at 125 °C for 3 hours under nitrogen atmosphere, and then allowed to cool to room temperature. The polymer was precipitated by adding cold methanol to the solution, and the methanol was decanted after stirring for 1 hour. The polymer was purified by repeating the precipitation using *p*-xylene/methanol system, and then dried under vacuum at 50 °C overnight. The dry and partially hydrogenated S-I-S was characterized by ¹H NMR, GPC, TGA and tensile testing.

■ **Characterization.** Isoprene conversion was determined by gravimetry. IBOMA conversion was obtained using the ¹H NMR peaks of the vinyl protons of the monomer ($\delta = 6.05$ and 5.50 ppm, 2H) and the aromatic proton of both monomer and polymer ($\delta = 4.65$ - 4.20 ppm, 1H). Styrene (S) conversion was determined using the vinyl protons of the monomer ($\delta = 6.80$ - 6.70 , 5.80 - 5.70 and 5.30 - 5.20 ppm, 3H) and the aromatic protons of both monomer and polymer ($\delta = 7.50$ - 6.90 ppm, 5H). The hydrogenation degree (HD) was also determined by ¹H NMR via the PS aromatic protons ($\delta = 7.50$ - 6.90 ppm, 5H) and the PI olefin peak ($\delta = 5.05$ ppm, 1H).

The number-average molecular weights (M_n) and the dispersities ($\mathcal{D} = M_w/M_n$) were measured using gel permeation chromatography (GPC, Water Breeze, differential refractive index RI 2414 detector, 40 °C) with HPLC grade THF as the mobile phase (flow rate of $0.3 \text{ mL}\cdot\text{min}^{-1}$). The GPC was equipped with 3 Waters Styragel[®] HR columns (HR1 with a molecular weight measurement range of $10^2 - 5 \times 10^3 \text{ g}\cdot\text{mol}^{-1}$, HR2 with a molecular weight measurement range of $5 \times 10^2 - 2 \times 10^4 \text{ g}\cdot\text{mol}^{-1}$ and HR4 with a molecular weight measurement range of $5 \times 10^3 - 6 \times 10^5 \text{ g}\cdot\text{mol}^{-1}$) and a guard column was used. M_n values were determined by calibration with 10 linear narrow molecular weight distribution PI standards (Polymer Standards Service, molecular weights ranging from 1,030 to 1,040,000 $\text{g}\cdot\text{mol}^{-1}$).

Please see the characterization section of Chapter 3 for the detailed protocols of DSC, TGA, DMA, AFM analyses and tensile testing (identical procedures).

■ **References of the experimental section.**

- (1) B. Lessard, C. Aumand-Bourque, R. Chaudury, D. Gomez, A. Haroon, N. Ibrahimian, S. Mackay, M. -C. Noel, R. Patel, S. Sitaram, S. Valla, B. White and M. Maric, *Intern. Polymer Processing* **2011**, 26 (2), 197.
- (2) Hahn, S. F. An Improved Method for the Diimide Hydrogenation of Butadiene and Isoprene Containing Polymers. *J. Polym. Sci., Part A: Polym. Chem.* **1992**, 30, 397-408.

e. Appendix for Chapter 5: Experimental section

■ **Materials.** 2,6-Di-*tert*-butyl-4-methylphenol (BHT, $\geq 99\%$), *p*-toluenesulfonyl hydrazide (TSH, 97%), tributylamine (TBA, $\geq 98.5\%$), polystyrene-*block*-polyisoprene-*block*-polystyrene with 14 wt% styrene (abbreviated S₄-I-S₄, specification sheet below, product number = 432393) and 22 wt% styrene (abbreviated S₈-I-S₈, specification sheet below, product number = 432415) were purchased from Sigma-Aldrich and used as received. Methanol (MeOH, $\geq 99\%$), methylene chloride (CH₂Cl₂, 99.9% certified ACS), *p*-xylene (99.9%), chloroform (CHCl₃, 99.9%) and tetrahydrofuran (THF, 99.9% HPLC grade) were obtained from Fisher Scientific and used as received. Styrene-*block*-ethylene/butylene-*block*-styrene A1536 H (SEBS, specification sheet below) was obtained from Kraton. The deuterated chloroform (CDCl₃, 99.8%) used as a solvent for nuclear magnetic resonance (NMR) was obtained from Cambridge Isotopes Laboratory.

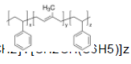
■ Specification sheets of the commercial triblock copolymers.

SIGMA-ALDRICH
sigma-aldrich.com
3050 Spruce Street, Saint Louis, MO 63103, USA
Website: www.sigmaaldrich.com
Email USA: techserv@si-al.com
Outside USA: eurtechserv@si-al.com

Product Specification

Product Name:
Polystyrene-*block*-polyisoprene-*block*-polystyrene - styrene 14 wt. %

Product Number: 432393
CAS Number: 25038-32-8
MDL: MFCD00217755
Formula: [CH₂CH(C₆H₅)]_x[CH₂CH=C(CH₃)C(CH₃)₂CH₂]_y[CH₂CH(C₆H₅)]_z



TEST	Specification
Appearance (Form)	Beads
Infrared spectrum	Conforms to Structure
Viscosity at 25 Degrees Celsius (25%, Toluene)	800 - 1600 cps
Volatile Matter	≤ 0.5 %
Total Extractables	≤ 1.0 %
Antioxidant, Irganox 565	0.08 - 0.30 %
Mole Weight (g/mol)	207 - 237
WHPS	≤ 2.3 %
Melt Index (g/10 minutes) 200 Degrees Celsius, 5.0kg	8.5 - 18.5

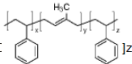
Specification: PRD.0.ZQ5.10000047999

SIGMA-ALDRICH
sigma-aldrich.com
3050 Spruce Street, Saint Louis, MO 63103, USA
Website: www.sigmaaldrich.com
Email USA: techserv@si-al.com
Outside USA: eurtechserv@si-al.com

Product Specification

Product Name:

Product Number: 432415
CAS Number: 25038-32-8
MDL: MFCD00217755
Formula: [CH₂CH(C₆H₅)]_x[CH₂CH=C(CH₃)C(CH₃)₂CH₂]_y[CH₂CH(C₆H₅)]_z



TEST	Specification
Appearance (Color)	White
Appearance (Form) Rubbery Beads	Conforms to Requirements
Infrared spectrum	Conforms to Structure
Loss on Drying Specification: Report Result	
% Volatiles	
Viscosity C= 25%, Toluene at 25 Degrees Celsius	750 - 1250 cps

Specification: PRD.0.ZQ5.10000033812

K0489 North America 3/6/2017		KRATON™ A1536 H Polymer		Data Document	
Identifier : K489DDJ17U					
Description					
Kraton A1536 H is a linear triblock copolymer based on styrene and ethylene/butylene. It is supplied from North America in the physical form identified below.					
<ul style="list-style-type: none"> • Kraton A1536 HU - supplied to customers as an undusted powder • Kraton A1536 HS - supplied to customers as a dusted powder 					
Kraton A1536 H is used in compound formulations and as a modifier of thermoplastics. It may also find use in formulating adhesives, sealants, coatings and modified bitumens.					
Sales Specifications					
Property	Test Method	Units	Sales Specification Range	Notes	
Ash, S	BAM 908	%w	0.35 TO 0.70	c	
Polystyrene Content	KM 03	%m	37.0 TO 44.0	b	
Antioxidant	KM 08	%m	0.07 TO 0.13	a	
Total Extractables	KM 05	%m	<= 1.6		
Volatile Matter	KM 04	%m	<= 1.0		
a Non-staining phenolic antioxidant. b Measured on the polymer before hydrogenation. c Silica dusted					
Typical Properties (These are typical values and may not routinely be measured on finished product)					
Property	Test Method	Units	Typical Value	Notes	
Melt Index 260°C, 5kg	ASTM D-1238	gms/10min.	7		
Hardness	ASTM 2240	Shore A (10s)	65	b	
300% Modulus	BAM 1245	psi	935	c	
Tensile Strength	BAM 1245	psi	> 5000	c	
Elongation at Break	BAM 1245	%	660	c	
Polystyrene Content	Anal. HNMR	%w	42		
b Measured on compression molded slabs. c Measured on solution cast film from toluene.					

■ **Hydrogenation of commercial S-I-S.** Please see the characterization section of the Chapter 4 for the detailed protocol (“Hydrogenation of the synthesized S-I-S triblock copolymers”).

■ **Characterization.** The hydrogenation degree (HD) of the TSH-treated S-I-S was determined by ¹H NMR, using the PS aromatic protons ($\delta = 7.50\text{-}6.90$ ppm, 5H) and the PI olefin peak ($\delta = 5.05$ ppm, 1H).

The number-average molecular weights (M_n) and the dispersities ($\mathcal{D} = M_w/M_n$) were measured using gel permeation chromatography (GPC, Water Breeze, differential refractive index RI 2414 detector, 40 °C) with HPLC grade THF as the mobile phase (flow rate of 0.3 mL.min⁻¹). The GPC was equipped with 3 Waters Styragel® HR columns (HR1 with a molecular weight measurement range of 10² – 5 x 10³ g.mol⁻¹, HR2 with a molecular weight measurement range of 5 x 10² - 2 x 10⁴ g.mol⁻¹ and HR4 with a molecular weight measurement range of 5 x 10³ - 6 x 10⁵ g.mol⁻¹) and a guard column was used. M_n values were determined by calibration with 10 linear narrow molecular weight distribution PI standards (Polymer Standards Service, molecular weights ranging from 1,030 to 1,040,000 g.mol⁻¹).

The stress-strain features of the commercial triblock copolymers were determined using a MTS Insight material testing system with a 5 kN load cell at room temperature and a cross-head speed of 10 mm.min⁻¹. Dog-bone style tensile specimens (ASTM D638 type V for reference, overall length = 63.5 mm, overall width = 9.53 mm) were prepared either by solvent casting or by hot press. To cast the film, the polymer sample was fully dissolved in dichloromethane (~ 80 wt%) for an hour with continuous stirring using a magnetic stir bar. The solution was cast into

a level Teflon Petri dish at room temperature for approximately two days. Then, the drying was completed after placing the film in the oven at 50 °C under vacuum until constant weight was measured. The film samples were cut into typical dog-bone shapes using a sharp blade. When using a hot press (Carver hydraulic press, model #3925), $T \sim T_{g,specimen} + 50\text{ °C}$ where $T_{g,specimen}$ refers to the specimen's higher T_g , under a mean pressure of 5000 psi was set. Specimens with defects (nicked sides, cracks, air bubbles) on their surface were discarded and were not used in mechanical testing. For each specimen, the thickness and the width were measured at five different points along the small center portion with a digital caliper (Marathon, CO 030150F128) and the average thickness and width were used for all calculations. Each test was considered finished after the complete breakup of the specimen at the narrow section (samples that broke near the grips were discarded). The averaged results were reported using TestWorks 4 software. The Young's modulus was determined as the slope of the stress–strain curve at strains of 0–0.5%.

The mechanical response of SIS and SEBS copolymers to torsional oscillation at 0.15 Hz and 1% strain over a temperature range of 20 to 180 °C was measured at a rate of 5 °C.min⁻¹ under N₂ using the CDT 450 convection heated measuring chamber mounted on the Anton Paar Modular Compact Rheometer MCR302. The solid rectangular fixture (SFR) was used, consisting of an upper and a lower holder with insets. Rectangular bars were made either by solvent casting or by hot press, following the above protocols used for preparing the tensile bars. Prior to the torsion tests, dynamic amplitude sweeps at 0.15 Hz and varying strain from 0.01 to 100% were conducted at various temperatures to ensure the material was kept within the linear viscoelastic regime.

Please see the characterization section of Chapter 3 for the detailed protocols of DSC, TGA and AFM analyses (identical procedures).

FOLIO ADMINISTRATIF

THESE DE L'UNIVERSITE DE LYON OPEREE AU SEIN DE L'INSA LYON

NOM : **MÉTAFIOT**

DATE de SOUTENANCE : **19/10/2018**

Prénoms : **Adrien**

TITRE : **Synthesis of 1,3-Diene-based Block Copolymers by Nitroxide-Mediated Polymerization for Application as Robust Joining between Composite Matrices**

NATURE : **Doctorat**

Numéro d'ordre : **2018LYSEI076**

Ecole doctorale : **MATÉRIAUX de Lyon (n° 34)**

Spécialité : **Synthèse et Caractérisation des Polymères**

RÉSUMÉ : L'objectif de ce projet fut consacré à la synthèse d'un élastomère thermoplastique (TPE) innovant, utilisable en tant que joint entre des matrices composites. La polymérisation radicalaire contrôlée par des radicaux nitroxyde (NMP) fut choisie afin de produire des TPE copolymères à blocs de type styrénique. Le β -myrcène (*My*) fut dans un premier temps sélectionné pour synthétiser le bloc souple poly(β -myrcène) P(*My*). La NMP du *My* en masse à 120 °C en utilisant l'amorceur BlocBuilder™ fonctionnalisé avec l'ester succinimidyl (NHS-BB) fut très bien contrôlée, permettant l'extension de chaîne du macro-amorceur *cis*-1,4-P(*My*) avec du styrène (S). Les copolymères diblocs P(*My-b-S*) obtenus ayant une masse molaire moyenne en nombre modérée ($M_n < 50 \text{ kg.mol}^{-1}$) montrèrent un comportement fragile en test de traction uniaxiale (résistance à la rupture en traction $\sigma_B < 1,1 \text{ MPa}$, allongement à la rupture en traction $\varepsilon_B < 16\%$). L'incorporation d'unités fonctionnelles au sein du segment souple fut réalisée en parallèle via la NMP du *My* avec du méthacrylate de glycidyle (GMA) afin de favoriser possiblement le processus de soudage / collage entre le TPE et les composites thermoplastiques envisagés. Un amorceur bifonctionnel, le poly(éthylène-co-butylène)-(SG1)₂ (SG1 = groupe nitroxyde), permit par la suite de synthétiser des copolymères triblocs S-*My*-S ayant une plus haute masse molaire moyenne $M_n = 56-66 \text{ kg.mol}^{-1}$ et une plus grande extensibilité ($\sigma_B < 0,8 \text{ MPa}$, $\varepsilon_B < 200\%$). Les segments PS furent remplacés par des segments ayant une température de transition vitreuse (T_g) plus élevée, à savoir des blocs poly(méthacrylate d'isobornyle) P(IBOMA) afin d'augmenter la résistance mécanique et la température de service du TPE candidat. Des triblocs de type IBOMA-*My*-IBOMA, dont les domaines furent micro-structurés, montrèrent de meilleures propriétés mécaniques ($\sigma_B = 3,9 \text{ MPa}$, contrainte à la limite d'élasticité $\sigma_Y = 5,0 \text{ MPa}$, $\varepsilon_B = 490\%$) et une température de service maximale d'environ 140 °C. Toutefois, ces TPE à base de *My* ne satisfirent pas le cahier des charges industriel à température ambiante, ce qui nous poussa à substituer le bloc flexible P(*My*) par du poly(isoprène) PI, ayant une masse molaire d'enchevêtrement bien plus faible. Des macro-amorceurs 1,4-PI bien définis et actifs furent d'abord étendus avec du styrène, ce qui permit d'obtenir des triblocs S-I-S auto-assemblés ($M_n = 95-109 \text{ kg.mol}^{-1}$, fraction molaire en styrène $F_S = 0,30-0,49$, dispersité $\bar{D} = 2,11-2,29$). $\sigma_B = 4,1 \pm 0,2 \text{ MPa}$ et $\varepsilon_B = 376 \pm 64 \%$ furent mesurés pour un S-I-S ayant $F_S = 0,38$. Un tribloc de type IBOMA-I-IBOMA fut par la suite synthétisé ($M_n = 94 \text{ kg.mol}^{-1}$, $\bar{D} =$

1,76, $F_{IBOMA} = 0,35$) et montra de meilleures propriétés en contrainte-déformation ($\sigma_B = 11,4 \pm 0,6$ MPa, $\varepsilon_B = 1356 \pm 214$ %). Enfin, des copolymères à blocs à base d'isoprène furent hydrogénés à pression ambiante en utilisant l'agent diimide, ce qui permit notamment d'améliorer la stabilité thermique et la résistance à la rupture de ces matériaux.

MOTS-CLÉS : élastomère thermoplastique, polymérisation contrôlée par des nitroxydes, β -myrcène, isoprène

Laboratoires de recherche : **Ingénierie des Matériaux polymères – UMR 5223 CNRS**
Département de Génie Chimique, Université McGill

Directeur de thèse : **Jean-Francois GÉRARD**

Co-directeurs de thèse : **Milan MARIC et Pascal HUBERT**

Président de jury :

Composition du jury :

Gigmes, Didier	Directeur de Recherche CNRS	Université Aix Marseille	Rapporteur
Fretigny, Christian	Directeur de Recherche CNRS	ESPCI	Rapporteur
Duchet, Jannick	Professeur des Universités	INSA Lyon	Examinatrice
Defoort, Brigitte	Docteur HDR	ArianeGroup	Examinatrice
Mortaigne, Bruno	Docteur	DGA – Ministère de la défense	Examineur
Gérard, Jean-François	Professeur des Universités	INSA Lyon	Directeur de thèse
Maric, Milan	Professeur	Université McGill	Invité
Hubert, Pascal	Professeur	Université McGill	Invité